

Copyright
By
Nathan Paul Dickerson
2005

Wireless Corrosion Sensors for Reinforced Concrete Structures

by

Nathan Paul Dickerson, B.S.C.E.

Thesis

Presented to the Faculty of the Graduate School of

The University of Texas at Austin

in Partial Fulfillment

of the Requirements

for the Degree of

Master of Science in Engineering

The University of Texas at Austin

August 2005

Wireless Corrosion Sensors for Reinforced Concrete Structures

**APPROVED BY
SUPERVISING COMMITTEE:**

Sharon L. Wood

Dean P. Neikirk

Dedication

To my wife, Katy, for her love and support.

Acknowledgements

First and foremost, I would like to thank Dr. Sharon L. Wood for her leadership and guidance on this research. In addition to being knowledgeable and insightful, she is attentive to the needs of her students and concerned about their personal development.

I would like to thank the National Science Foundation for funding the project and making my education possible through grant number CMS-0329808 to the University of Texas at Austin.

Dr. Dean P. Neikirk, Matthew Andringa, and Prem Nainani are also due thanks for their help with the electrical aspects of the project. A special thank you goes to Matthew Andringa for development of the signal processing method and computer algorithm used extensively on the data for this thesis. Thanks to Ryan King and Laura Wendling for their help in sensor fabrication and testing. I am grateful to Randy Poston and Scott Witthoft at WDP & Associates, Inc. for guidance and advice on corrosion rates, and especially for allowing me to use their linear polarization resistance equipment.

I also appreciate the cooperation and support of all students and staff members at Ferguson Structural Engineering Laboratory and the Construction Materials Research Group. Discussing and assisting with each other's projects was a highlight of my time at UT.

May 2005

Wireless Corrosion Sensors for Reinforced Concrete Structures

Nathan Paul Dickerson, M.S.E.

The University of Texas at Austin, 2005

SUPERVISOR: Sharon L. Wood

Corrosion of embedded reinforcing steel and the resulting deterioration of concrete structures is a worldwide problem. As part of a health monitoring scheme for reinforced concrete structures, early detection of corrosion would allow remedial or preventative measures before structural damage occurs. Embedded wireless corrosion sensors that are successful in detecting threshold amounts of corrosion have been developed and tested. The sensors consist of sealed circuits with exposed steel sensing wires for direct detection of corrosion. Batteries are not necessary for the sensor because power and communication are achieved through inductive coupling with an external transmitter/receiver. The low-cost sensors are fabricated from inexpensive and readily available materials,

and require no maintenance. Corrosion is detected by measuring the impedance response of the sensor. An automated signal processing routine can be used to evaluate the measured response and detect if a threshold amount of corrosion has occurred.

Table of Contents

LIST OF TABLES	xiv
LIST OF FIGURES	xix
CHAPTER 1 INTRODUCTION	1
1.1 Introduction	1
1.2 Scope of Research	2
CHAPTER 2 WIRELESS CORROSION SENSOR DEVELOPMENT	4
2.1 Introduction	4
2.2 Sensor Concept.....	4
2.2.1 Required Attributes	4
2.2.2 Conceptual Design	6
2.3 First Generation Sensors	10
2.3.1 Basic Sensor Design.....	10
2.3.2 Basic Sensor Testing	13
2.3.3 Conclusions	22
CHAPTER 3 EXPLORATION OF SENSOR DESIGN PARAMETERS	24
3.1 Introduction	24
3.2 Parametric Studies.....	24
3.2.1 Parametric Study I.....	25
3.2.2 Parametric Study II.....	25
3.2.3 Parametric Study III	26
3.2.4 Trial Sensors.....	27
3.3 Sensor Components.....	27
3.3.1 Practical Considerations	27

3.3.2	Capacitance	28
3.3.3	Inductance	28
3.3.4	Resistance.....	31
3.3.5	Steel Sensing Wire	32
3.3.6	Reference Circuit.....	35
3.4	Impedance Measurement.....	40
3.4.1	Read Distance.....	40
3.4.2	Reader Coil.....	43
3.5	Environmental Influence	49
3.5.1	Temperature	50
3.5.2	Surrounding Environment.....	51
3.6	Conclusions	53
3.6.1	Resistance Model of Steel Sensing Wire	54
3.6.2	Signal Processing	55
3.6.3	Summary of Recommendations for Sensor Redesign.....	56
CHAPTER 4 SECOND GENERATION SENSOR DESIGN.....		58
4.1	Introduction	58
4.2	Design Considerations.....	58
4.3	Concentric Sensor	59
4.3.1	Circuits	59
4.3.2	Materials.....	60
4.3.3	Fabrication.....	62
4.3.4	Response.....	62
4.4	Coplanar Sensor	66
4.4.1	Circuits	66
4.4.2	Materials.....	67
4.4.3	Fabrication.....	68

4.4.4	Response.....	68
4.5	Conclusions	73
CHAPTER 5 SECOND GENERATION SENSOR TESTING.....		74
5.1	Introduction	74
5.2	Concrete Prisms.....	74
5.2.1	Construction	75
5.2.2	Design of Experiments	76
5.2.3	Measured Response during First Twelve Weeks	80
5.2.4	Interpretation and Evaluation	102
5.3	Reinforced Concrete Slabs	104
5.3.1	Construction	104
5.3.2	Design of Experiments	109
5.3.3	Measured Response during First Twelve Weeks	113
5.3.4	Interpretation and Evaluation	133
CHAPTER 6 CONCLUSIONS.....		134
6.1	Summary	134
6.2	Recommendations	135
APPENDIX A PARAMETRIC STUDY I		137
A.1	Introduction	137
A.2	Sensors	138
A.3	Inductor Diameter	140
A.4	Number of Turns	144
A.5	Read Distance.....	146
A.6	Surrounding Environment.....	148

A.7 Capacitor Type	152
APPENDIX B PARAMETRIC STUDY II	154
B.1 Introduction	154
B.2 Sensors	155
B.3 Sensing Wire Material.....	157
B.4 Sensing Wire Diameter	158
B.5 Surrounding Environment	158
APPENDIX C PARAMETRIC STUDY III	169
C.1 Introduction	169
C.2 Sensor Circuit.....	170
C.3 Response of Individual Sensors	171
C.4 Response of Sensor Pairs	174
C.4.1 Sensor Pair 1: 5C_1 and 5C_2	174
C.4.2 Sensor Pair 2: 5C_2 and 5C_3	177
C.4.3 Sensor Pair 3: 5C_1 and 5C_3	180
C.4.4 Sensor Pair 4: 5C_3 and 5D_4	183
C.5 Conclusions	184
APPENDIX D SIGNAL PROCESSING.....	186
D.1 Introduction	186
D.2 Curve Fitting	188
D.2.1 Baseline	189
D.2.2 Phase Dip.....	190
D.3 Example	191
D.3.1 Measured Response.....	191

D.3.2	Baseline	192
D.3.3	Phase Dips	193
D.3.4	Complete Curve Fit	196
APPENDIX E SECOND GENERATION SENSOR FABRICATION		198
E.1	Concentric Sensor	198
E.2	Coplanar Sensor	212
APPENDIX F SECOND GENERATION SENSOR CALIBRATION		214
F.1	Introduction	214
F.2	Concentric Sensor B10.....	215
F.2.1	Surrounding Environment	216
F.2.2	Read Distance.....	223
F.2.3	Reader Configuration	237
F.3	Concentric Sensor B60.....	241
F.3.1	Surrounding Environment	242
F.3.2	Read Distance.....	249
F.3.3	Reader Configuration	263
F.4	Coplanar Sensor A10	267
F.4.1	Surrounding Environment	268
F.4.2	Read Distance.....	274
F.4.3	Reader Configuration	288
F.5	Coplanar Sensor A60	292
F.5.1	Surrounding Environment	293
F.5.2	Read Distance.....	299
F.5.3	Reader Configuration	313

APPENDIX G CONCRETE PRISM SENSOR MONITORING RESULTS.....	318
APPENDIX H CONCRETE PRISM EXAMINATIONS	342
H.1 Prism A26	344
H.2 Prism A29	345
H.3 Prism A30	347
H.4 Prism B25	348
H.5 Prism B30	351
APPENDIX I REINFORCED CONCRETE SLAB #1 MONITORING RESULTS ..	353
APPENDIX J REINFORCED CONCRETE SLAB #2 MONITORING RESULTS..	383
REFERENCES	413
VITA	415

List of Tables

Table 3-1 Experimental Reader Coils	44
Table 3-2 Summary of Temperature Effects on Sensor 4a	51
Table 4-1 Circuit Parameters for Concentric Sensor	59
Table 4-2 Circuit Parameters for Coplanar Sensor	66
Table 5-1 Environmental Cycles for Control Conditions	77
Table 5-2 Environmental Cycles with Varying Moisture Conditions.....	78
Table 5-3 Environmental Cycles with Varying Thermal Conditions	79
Table 5-4 Environmental Cycles with Varying Moisture and Thermal Conditions.....	80
Table 5-5 Prisms with Broken Sensing Wires	82
Table 5-6 Variation of Characteristic Frequency for Sensors Embedded in Prisms – Intact Wires	99
Table 5-7 Variation of Pseudo-Quality Factor for Sensors Embedded in Prisms – Intact Wires	100
Table 5-8 Variation of Phase Dip for Sensors Embedded in Prisms – Intact Wires	101
Table 5-9 Variation of Measured Response of Sensors Embedded in Prisms – Broken Wires.....	102
Table 5-10 Variation of Characteristic Frequency for Sensors Embedded in Slab #1 – Intact Wires.....	128
Table 5-11 Variation of Pseudo-Quality Factor for Sensors Embedded in Slab #1 – Intact Wires.....	129
Table 5-12 Variation of Phase Dip for Sensors Embedded in Slab #1 – Intact Wires	130
Table 5-13 Variation of Characteristic Frequency for Sensors Embedded in Slab #2 – Intact Wires.....	131
Table 5-14 Variation of Pseudo-Quality Factor for Sensors Embedded in Slab #2 – Intact Wires.....	132
Table 5-15 Variation of Phase Dip for Sensors Embedded in Slab #2 – Intact Wires	133
Table A-1 Sensors with 0.75-in. Nominal Diameter Inductors.....	139
Table A-2 Sensors with 1.0-in. Nominal Diameter Inductors.....	139
Table A-3 Sensors with 1.25-in. Nominal Diameter Inductors.....	140
Table A-4 Maximum Read Distance.....	147

Table B-1 Sensing Wire Material and Size	156
Table C-1 Parametric Study III Sensors.....	171
Table C-2 Summary of Interrogation Results for Sensor Pair 1: 5C_1 and 5C_2	176
Table C-3 Summary of Interrogation Results for Sensor Pair 2: 5C_2 and 5C_3	179
Table C-4 Summary of Interrogation Results for Sensor Pair 3: 5C_1 and 5C_3	182
Table C-5 Summary of Interrogation Results for Sensor Pair 1: 5C_1 and 5C_2	184
Table D-1 Fitting Coefficients for Baseline	192
Table D-2 Fitting Coefficients for Phase Dips.....	193
Table F-1 Effect of Surrounding Environment on Sensor B10 with Intact Sensing Wire	217
Table F-2 Effect of Surrounding Environment on Sensor B10 with Cut Sensing Wire.....	218
Table F-3 Effect of Varying Concentration of Salt Water on Sensor B10 with Cut Sensing Wire.....	220
Table F-4 Effect of Read Distance on Sensor B10 with Intact Sensing Wire	224
Table F-5 Variation of Measured Response of Sensor B10 with Intact Sensing Wire for Sensing Circuit with Varying Read Distance	228
Table F-6 Variation of Measured Response of Sensor B10 with Intact Sensing Wire for Reference Circuit with Varying Read Distance.....	228
Table F-7 Effect of Read Distance on Sensor B10 with Cut Sensing Wire.....	229
Table F-8 Variation of Measured Response of Sensor B10 with Cut Sensing Wire for Reference Circuit with Varying Read Distance	233
Table F-9 Variation of Measured Response of Sensor B10 with Cut Sensing Wire for Sensing Circuit with Varying Read Distance	233
Table F-10 Experimental Reader Coils used in Calibration Testing	237
Table F-11 Effect of Reader Configuration on Sensor B10 with Intact Sensing Wire for a 1-in. Read Distance.....	238
Table F-12 Effect of Reader Configuration on Sensor B10 with Cut Sensing Wire for a 1-in. Read Distance.....	239
Table F-13 Maximum Read Distances for Sensor B10 with Intact Sensing Wire	239
Table F-14 Variation of Measured Response of Sensor B10 with Intact Sensing Wire for Sensing Circuit with Different Reader Coils	240

Table F-15 Variation of Measured Response of Sensor B10 with Intact Sensing Wire for Reference Circuit with Different Reader Coils	240
Table F-16 Variation of Measured Response of Sensor B10 with Cut Sensing Wire for Reference Circuit with Different Reader Coils	241
Table F-17 Effect of Surrounding Environment on Sensor B60 with Intact Sensing Wire	244
Table F-18 Effect of Surrounding Environment on Sensor B60 with Cut Sensing Wire.....	245
Table F-19 Effect of Varying Concentration of Salt Water on Sensor B60 with Cut Sensing Wire	246
Table F-20 Effect of Read Distance on Sensor B60 with Intact Sensing Wire...	250
Table F-21 Variation of Measured Response of Sensor B60 with Intact Sensing Wire for Sensing Circuit with Varying Read Distance	254
Table F-22 Variation of Measured Response of Sensor B60 with Intact Sensing Wire for Reference Circuit with Varying Read Distance	254
Table F-23 Effect of Read Distance on Sensor B60 with Cut Sensing Wire	255
Table F-24 Variation of Measured Response of Sensor B60 with Cut Sensing Wire for Reference Circuit with Varying Read Distance	259
Table F-25 Variation of Measured Response of Sensor B60 with Cut Sensing Wire for Sensing Circuit with Varying Read Distance	259
Table F-26 Effect of Reader Configuration on Sensor B60 with Intact Sensing Wire for a 1-in. Read Distance.....	264
Table F-27 Effect of Reader Configuration on Sensor B60 with Cut Sensing Wire for a 1-in. Read Distance.....	264
Table F-28 Maximum Read Distances for Sensor B60 with Intact Sensing Wire	265
Table F-29 Variation of Measured Response of Sensor B60 with Intact Sensing Wire for Sensing Circuit with Different Reader Coils.....	265
Table F-30 Variation of Measured Response of Sensor B60 with Intact Sensing Wire for Reference Circuit with Different Reader Coils	266
Table F-31 Variation of Measured Response of Sensor B60 with Cut Sensing Wire for Reference Circuit with Different Reader Coils	266
Table F-32 Effect of Surrounding Environment on Sensor A10 with Intact Sensing Wire	269
Table F-33 Effect of Surrounding Environment on Sensor A10 with Cut Sensing Wire.....	270
Table F-34 Effect of Varying Concentration of Salt Water on Sensor A10 with Cut Sensing Wire	271
Table F-35 Effect of Read Distance on Sensor A10 with Intact Sensing Wire ..	275
Table F-36 Variation of Measured Response of Sensor A10 with Intact Sensing Wire for Sensing Circuit with Varying Read Distance	279

Table F-37 Variation of Measured Response of Sensor A10 with Intact Sensing Wire for Reference Circuit with Varying Read Distance	279
Table F-38 Effect of Read Distance on Sensor A10 with Cut Sensing Wire.....	280
Table F-39 Variation of Measured Response of Sensor A10 with Cut Sensing Wire for Reference Circuit with Varying Read Distance	284
Table F-40 Variation of Measured Response of Sensor A10 with Cut Sensing Wire for Sensing Circuit with Varying Read Distance	284
Table F-41 Effect of Reader Configuration on Sensor A10 with Intact Sensing Wire for a 1-in. Read Distance.....	289
Table F-42 Effect of Reader Configuration on Sensor A10 with Cut Sensing Wire for a 1-in. Read Distance.....	289
Table F-43 Maximum Read Distances for Sensor A10 with Intact Sensing Wire	290
Table F-44 Variation of Measured Response of Sensor A10 with Intact Sensing Wire for Sensing Circuit with Different Reader Coils.....	290
Table F-45 Variation of Measured Response of Sensor A10 with Intact Sensing Wire for Reference Circuit with Different Reader Coils	291
Table F-46 Variation of Measured Response of Sensor A10 with Cut Sensing Wire for Reference Circuit with Different Reader Coils	291
Table F-47 Effect of Surrounding Environment on Sensor A60 with Intact Sensing Wire	294
Table F-48 Effect of Surrounding Environment on Sensor A60 with Cut Sensing Wire.....	295
Table F-49 Effect of Varying Concentration of Salt Water on Sensor A60 with Cut Sensing Wire	296
Table F-50 Effect of Read Distance on Sensor A60 with Intact Sensing Wire ..	300
Table F-51 Variation of Measured Response of Sensor A60 with Intact Sensing Wire for Sensing Circuit with Varying Read Distance	304
Table F-52 Variation of Measured Response of Sensor A60 with Intact Sensing Wire for Reference Circuit with Varying Read Distance	304
Table F-53 Effect of Read Distance on Sensor A60 with Cut Sensing Wire.....	305
Table F-54 Variation of Measured Response of Sensor A60 with Cut Sensing Wire for Reference Circuit with Varying Read Distance	309
Table F-55 Variation of Measured Response of Sensor A60 with Cut Sensing Wire for Sensing Circuit with Varying Read Distance	309
Table F-56 Effect of Reader Configuration on Sensor A60 with Intact Sensing Wire for a 1-in. Read Distance.....	314
Table F-57 Effect of Reader Configuration on Sensor A60 with Cut Sensing Wire for a 1-in. Read Distance.....	314
Table F-58 Maximum Read Distances for Sensor A60 with Intact Sensing Wire	315

Table F-59 Variation of Measured Response of Sensor A60 with Intact Sensing Wire for Sensing Circuit with Different Reader Coils	315
Table F-60 Variation of Measured Response of Sensor A60 with Intact Sensing Wire for Reference Circuit with Different Reader Coils	316
Table F-61 Variation of Measured Response of Sensor A60 with Cut Sensing Wire for Reference Circuit with Different Reader Coils	316
Table G-1 Change in Moisture Content of Concrete Prisms with Time	318
Table G-2 Initial Weight of Concrete Prisms.....	319
Table H-1 Environmental Cycles for Concrete Prisms	343
Table H-2 Prisms with Broken Sensing Wires.....	343

List of Figures

Figure 2-1 EAS Tag	6
Figure 2-2 Idealized LC Circuit	7
Figure 2-3 Typical Phase Response of Sensor	8
Figure 2-4 Sensor Circuit Diagram	9
Figure 2-5 Basic Sensor Circuit Diagram	11
Figure 2-6 Basic Sensor Configuration	11
Figure 2-7 Photograph of a Basic Sensor	12
Figure 2-8 Phase Response of Basic Sensor	12
Figure 2-9 Arrangement of Sensors in a Slab	14
Figure 2-10 Phase Response of a Basic Sensor Embedded in a Slab [15].....	15
Figure 2-11 Characteristic Frequency of Basic Sensor Embedded in a Slab with Time [15].....	16
Figure 2-12 Photographs of Corrosion in Test Slabs	17
Figure 2-13 Phase Response of Sensor 1a During Immersion Testing.....	18
Figure 2-14 Phase Response of Basic Sensor 4a During Corrosion Testing of Concrete Prisms.....	21
Figure 3-1 Effect of Capacitor Type on Sensor Phase Response.....	28
Figure 3-2 Parameters Affecting Inductance	29
Figure 3-3 Effect of Inductor Diameter on Phase Dip	30
Figure 3-4 Effect of Number of Magnet Wire Turns on Phase Dip.....	31
Figure 3-5 Effect of Wire Diameter on Phase Response of Sensors.....	32
Figure 3-6 Effect of Steel Sensing Wire on Phase Response of Sensors	32
Figure 3-7 Effect of Wire Diameter and Material on Phase Dip	33
Figure 3-8 Sensor Circuit Diagram Including Wire Resistance.....	34
Figure 3-9 Possible Arrangements of Sensing Wire	35
Figure 3-10 Effect of Sensing Wire Geometry on Sensor Phase Response.....	35
Figure 3-11 Sensor Circuit Diagram with Sensing Wire Added in Series.....	36
Figure 3-12 Effect of the State of Sensing Wire on Sensor Phase Response.....	37
Figure 3-13 Sensor Circuit Diagram Including Reference Circuit	38
Figure 3-14 Arrangement of Sensor Pairs Tested in Parametric Study III	39
Figure 3-15 Definition of Read Distance	41
Figure 3-16 Effect of Read Distance on Phase Dip with Varying Inductor Diameter	42
Figure 3-17 Effect of Read Distance on Phase Dip with Varying Number of Magnet Wire Turns	43
Figure 3-18 Reader Coil Photographs	45
Figure 3-19 Baseline Phase Response of Reader Coils Attached Directly to Impedance Analyzer.....	47

Figure 3-20 Baseline Phase Response of Reader Coils Attached to Impedance Analyzer with 3-ft Cable	48
Figure 3-21 Effect of Temperature on Phase Response of Sensor 4a	50
Figure 3-22 Effect of Surrounding Environment on Phase Dip for Completely Sealed Sensors of Varying Diameter	52
Figure 3-23 Complete Sensor Circuit Diagram.....	55
Figure 4-1 Circuit Diagram for Second Generation Sensors	60
Figure 4-2 Configuration of Concentric Sensor	61
Figure 4-3 Photograph of Concentric Sensor	61
Figure 4-4 Concentric Sensor Phase Response	63
Figure 4-5 Phase Response of Concentric Sensor in 3.5% Salt Water	64
Figure 4-6 Pseudo-Quality Factor for Concentric Sensor with 26-gage Steel Sensing Wire in Varying Concentrations of Salt Water	65
Figure 4-7 Configuration of Coplanar Sensor.....	67
Figure 4-8 Photograph of Coplanar Sensor.....	68
Figure 4-9 Coplanar Sensor Phase Response.....	70
Figure 4-10 Phase Response of Coplanar Sensor in 3.5% Salt Water	71
Figure 4-11 Pseudo-Quality Factor for Coplanar Sensor with 26-gage Steel Sensing Wire in Varying Concentrations of Salt Water	72
Figure 5-1 Diagram of Concentric Sensor Prism	75
Figure 5-2 Diagram of Coplanar Sensor Prism.....	76
Figure 5-3 Prism B21 Interrogation History	83
Figure 5-4 Prism B30 Interrogation History	85
Figure 5-5 Prism B30 Prior to Internal Examination	86
Figure 5-6 Sensor B30 After Internal Investigation.....	86
Figure 5-7 Prism B19 Interrogation History	87
Figure 5-8 Prism B20 Interrogation History	88
Figure 5-9 Cracking After Oven Drying Stage	89
Figure 5-10 Sensor B23 Phase Response.....	91
Figure 5-11 Prism B23 Interrogation History	93
Figure 5-12 Prism B25 Interrogation History	95
Figure 5-13 Interior of Prism B25 After Removal of Bottom Cover.....	96
Figure 5-14 End of Wire Loop in Prism B25.....	96
Figure 5-15 Corrosion Along Wire in Prism B25	97
Figure 5-16 Discolored Sensor B25 Showing Corrosion at Wire Exit	97
Figure 5-17 Diagram of Reinforced Concrete Slab	105
Figure 5-18 Slab Cross-Section Showing Plastic Chairs and Clear Cover	106
Figure 5-19 Slab #1 Prior to Placing Concrete	106
Figure 5-20 Slab Cross-Section Showing Dimensions	107
Figure 5-21 Orientation of Sensors Embedded in Slabs	107

Figure 5-22 Slab #1 Sensor Layout.....	108
Figure 5-23 Slab #2 Sensor Layout.....	108
Figure 5-24 Slab Experiment Set-up.....	110
Figure 5-25 Slab #1 Crack Map	110
Figure 5-26 Slab #2 Crack Map	111
Figure 5-27 Half-Cell Potential Measurement Points.....	112
Figure 5-28 Linear Polarization Resistance Measurement Points	113
Figure 5-29 Slab #1 Half-Cell Potential Contour Plots.....	116
Figure 5-30 Slab #2 Half-Cell Potential Contour Plots.....	117
Figure 5-31 Slab #1 Corrosion Risk History Inside of Salt Water Bath	118
Figure 5-32 Slab #1 Corrosion Risk History Outside of Salt Water Bath	118
Figure 5-33 Slab #2 Corrosion Risk History Inside of Salt Water Bath	119
Figure 5-34 Slab #2 Corrosion Risk History Outside of Salt Water Bath	119
Figure 5-35 Slab #1 Corrosion Rate Contour Plots.....	122
Figure 5-36 Slab #2 Corrosion Rate Contour Plots.....	123
Figure 5-37 Slab #1 Corrosion Rate History Inside of Salt Water Bath	124
Figure 5-38 Slab #1 Corrosion Rate History Outside of Salt Water Bath	124
Figure 5-39 Slab #2 Corrosion Rate History Inside of Salt Water Bath	125
Figure 5-40 Slab #2 Corrosion Rate History Outside of Salt Water Bath	125
Figure A-1 Sensor Circuit Diagram for Parametric Study I.....	138
Figure A-2 Phase Dip vs. Inductor Diameter for 1-Turn Inductor.....	141
Figure A-3 Phase Dip vs. Inductor Diameter for 2-Turn Inductor.....	141
Figure A-4 Phase Dip vs. Inductor Diameter for 3-Turn Inductor.....	142
Figure A-5 Phase Dip vs. Inductor Diameter for 4-Turn Inductor.....	142
Figure A-6 Phase Dip vs. Inductor Diameter for 5-Turn Inductor.....	142
Figure A-7 Phase Dip vs. Inductor Diameter for 6-Turn Inductor.....	143
Figure A-8 Phase Dip vs. Inductor Diameter for 7-Turn Inductor.....	143
Figure A-9 Phase Dip vs. Inductor Diameter for 8-Turn Inductor.....	143
Figure A-10 Phase Dip vs. Inductor Diameter for 9-Turn Inductor.....	144
Figure A-11 Phase Dip vs. Number of Turns for 0.75-in. Diameter Inductor	145
Figure A-12 Phase Dip vs. Number of Turns for 1.0-in. Diameter Inductor	145
Figure A-13 Phase Dip vs. Number of Turns for 1.25-in. Diameter Inductor	145
Figure A-14 Phase Dip for 7-Turn Inductor at Different Read Distances	147
Figure A-15 Phase Dip for 1.25-in. Diameter Inductor at Different Read Distances	148
Figure A-16 Phase Dip for 7-Turn Inductor in Different Environments	150
Figure A-17 Phase Dip for 4-Turn Inductor in Different Environments	151
Figure A-18 Phase Dip for 1.25-in Inductor in Different Environments	151
Figure A-19 Effect of Capacitor Type on Phase Response of Sensors	152

Figure B-1 Sensor Circuit Diagram for Parametric Study II	155
Figure B-2 Phase Response of Sensors used in Parametric Study II	156
Figure B-3 Phase Dips for Intact Sensing Wires.....	157
Figure B-4 Phase Dips for Cut Sensing Wires.....	158
Figure B-5 Phase Response of Sensor 5D_C1 in Different Environments.....	161
Figure B-6 Phase Response of Sensor 5D_C2 in Different Environments.....	162
Figure B-7 Phase Response of Sensor 5D_C3 in Different Environments.....	163
Figure B-8 Phase Response of Sensor 5D_C4 in Different Environments.....	164
Figure B-9 Phase Response of Sensor 5D_C1 in Varying Concentrations of Salt Water	165
Figure B-10 Phase Response of Sensor 5D_C2 in Varying Concentrations of Salt Water	167
Figure C-1 Sensor Circuit Diagram for Parametric Study III	170
Figure C-2 Sensor 5C_1 Individual Response	172
Figure C-3 Sensor 5C_2 Individual Response	172
Figure C-4 Sensor 5C_3 Individual Response	173
Figure C-5 Sensor 5D_4 Individual Response at 0-in. Read Distance	173
Figure C-6 Response of Sensor Pair 1 in Stacked Arrangement with Lower- Frequency Sensor Closer to Reader Coil	176
Figure C-7 Response of Sensor Pair 1 in Stacked Arrangement with Higher Frequency Sensor Closer to Reader Coil	177
Figure C-8 Response of Sensor Pair 1 in Side-by-Side Arrangement	177
Figure C-9 Response of Sensor Pair 2 in Stacked Arrangement with Lower Frequency Sensor Closer to Reader Coil	179
Figure C-10 Response of Sensor Pair 2 in Stacked Arrangement with Higher Frequency Sensor Closer to Reader Coil	180
Figure C-11 Response of Sensor Pair 2 in Side-by-Side Arrangement	180
Figure C-12 Response of Sensor Pair 3 in Stacked Arrangement with Lower Frequency Sensor Closer to Reader Coil	182
Figure C-13 Response of Sensor Pair 3 in Stacked Arrangement with Higher Frequency Sensor Closer to Reader Coil	183
Figure C-14 Response of Sensor Pair 3 in Side-by-Side Arrangement	183
Figure C-15 Response of Sensor Pair 4 in Concentric Arrangement.....	184
Figure D-1 Definition of Terms for Signal Processing	186
Figure D-2 First Generation Basic Sensor Phase Response.....	187
Figure D-3 Second Generation Concentric Sensor Phase Response.....	187
Figure D-4 Measured Phase Response of Sensor B10.....	192
Figure D-5 Baseline Curve Fit	193
Figure D-6 Lorentzian Function for Sensing Circuit Phase Dip.....	194
Figure D-7 Curve Fit of Sensing Circuit Phase Dip.....	194

Figure D-8 Curve Fit of Reference Circuit Phase Dip	195
Figure D-9 Completed Curve Fit	196
Figure D-10 Comparison of Measured Phase Response and Fitted Curve	197
Figure E-1 Slices of PVC Pipe	198
Figure E-2 Piece of PC Component Board	198
Figure E-3 Holes Drilled in PVC Slices.....	199
Figure E-4 Winding Inductor Coil – Wind Toward Open Hole.....	199
Figure E-5 Winding Inductor Coil – Wind Five Complete Turns	200
Figure E-6 Winding Inductor Coil – Secure Wire with Hot Glue	200
Figure E-7 Winding Inductor Coil – Cut and Insert Wire.....	201
Figure E-8 Winding Inductor Coil – Cut Wires to Length and Strip Ends	201
Figure E-9 Preparation for Soldering Reference Circuit.....	202
Figure E-10 Soldering Reference Circuit Capacitor	203
Figure E-11 Arrangement of Sensing Circuit Capacitor Before Soldering	203
Figure E-12 Finished Soldering of Sensing Circuit Capacitor.....	204
Figure E-13 Reference Inductor and PC Component Board Connected Before Soldering	204
Figure E-14 Finished Reference Circuit.....	205
Figure E-15 Holes in Reference Circuit Inductor for Sensing Circuit Wires	206
Figure E-16 Placing Reference Circuit Over Sensing Circuit Inductor Wires ...	206
Figure E-17 Inductor Wires of Sensing Circuit Ready for PC Component Board	207
Figure E-18 Soldering Sensing Circuit Inductor Wires to PC Component Board	207
Figure E-19 Holes for Steel Sensing Wire	208
Figure E-20 Steel Sensing Wire	209
Figure E-21 Steel Sensing Wire in Position and Ready for Soldering.....	209
Figure E-22 Cleaning Steel Sensing Wires Before Soldering.....	209
Figure E-23 Completed Sensor Circuits Ready for Potting with Epoxy.....	211
Figure E-24 Completed Concentric Sensor.....	212
Figure E-25 Completed Coplanar Sensor.....	213
Figure F-1 Phase Response of Sensor B10	216
Figure F-2 Phase Response of Sensor B10 in Varying Concentrations of Salt Water	221
Figure F-3 Effect of Read Distance on Response of Sensor B10 with an Intact Sensing Wire for Readings in Air	225
Figure F-4 Effect of Read Distance on Response of Sensor B10 with an Intact Sensing Wire for Readings in Tap Water.....	226
Figure F-5 Effect of Read Distance on Response of Sensor B10 with an Intact Sensing Wire for Readings in 3.5% Salt Water	227

Figure F-6 Effect of Read Distance on Response of Sensor B10 with a Cut Sensing Wire for Readings in Air	230
Figure F-7 Effect of Read Distance on Response of Sensor B10 with a Cut Sensing Wire for Readings in Tap Water.....	231
Figure F-8 Effect of Read Distance on Response of Sensor B10 with a Cut Sensing Wire for Readings in 3.5% Salt Water	232
Figure F-9 Sensor B10 Reference Circuit Response for a Cut Sensing Wire with Increasing Concentration of Salt Water at Three Read Distances	235
Figure F-10 Sensor B10 Sensing Circuit Response for a Cut Sensing Wire with Increasing Concentration of Salt Water at Three Read Distances	236
Figure F-11 Phase Response of Sensor B60	242
Figure F-12 Phase Response of Sensor B60 in Varying Concentrations of Salt Water	247
Figure F-13 Effect of Read Distance on Response of Sensor B60 with an Intact Sensing Wire for Readings in Air	251
Figure F-14 Effect of Read Distance on Response of Sensor B60 with an Intact Sensing Wire for Readings in Tap Water.....	252
Figure F-15 Effect of Read Distance on Response of Sensor B60 with an Intact Sensing Wire for Readings in 3.5% Salt Water	253
Figure F-16 Effect of Read Distance on Response of Sensor B60 with a Cut Sensing Wire for Readings in Air	256
Figure F-17 Effect of Read Distance on Response of Sensor B60 with a Cut Sensing Wire for Readings in Tap Water.....	257
Figure F-18 Effect of Read Distance on Response of Sensor B60 with a Cut Sensing Wire for Readings in 3.5% Salt Water	258
Figure F-19 Sensor B60 Reference Circuit Response for a Cut Sensing Wire with Increasing Concentration of Salt Water at Three Read Distances	261
Figure F-20 Sensor B60 Sensing Circuit Response for a Cut Sensing Wire with Increasing Concentration of Salt Water at Three Read Distances	262
Figure F-21 Phase Response of Sensor A10	268
Figure F-22 Phase Response of Sensor A10 in Varying Concentrations of Salt Water	272
Figure F-23 Effect of Read Distance on Response of Sensor A10 with an Intact Sensing Wire for Readings in Air	276
Figure F-24 Effect of Read Distance on Response of Sensor A10 with an Intact Sensing Wire for Readings in Tap Water.....	277
Figure F-25 Effect of Read Distance on Response of Sensor A10 with an Intact Sensing Wire for Readings in 3.5% Salt Water	278
Figure F-26 Effect of Read Distance on Response of Sensor A10 with a Cut Sensing Wire for Readings in Air	281
Figure F-27 Effect of Read Distance on Response of Sensor A10 with a Cut Sensing Wire for Readings in Tap Water.....	282

Figure F-28 Effect of Read Distance on Response of Sensor A10 with a Cut Sensing Wire for Readings in 3.5% Salt Water	283
Figure F-29 Sensor A10 Reference Circuit Response for a Cut Sensing Wire with Increasing Concentration of Salt Water at Three Read Distances	286
Figure F-30 Sensor A10 Sensing Circuit Response for a Cut Sensing Wire with Increasing Concentration of Salt Water at Three Read Distances	287
Figure F-31 Phase Response of Sensor A60	293
Figure F-32 Phase Response of Sensor A60 in Varying Concentrations of Salt Water	297
Figure F-33 Effect of Read Distance on Response of Sensor A60 with an Intact Sensing Wire for Readings in Air	301
Figure F-34 Effect of Read Distance on Response of Sensor A60 with an Intact Sensing Wire for Readings in Tap Water.....	302
Figure F-35 Effect of Read Distance on Response of Sensor A60 with an Intact Sensing Wire for Readings in 3.5% Salt Water	303
Figure F-36 Effect of Read Distance on Response of Sensor A60 with a Cut Sensing Wire for Readings in Air	306
Figure F-37 Effect of Read Distance on Response of Sensor A60 with a Cut Sensing Wire for Readings in Tap Water.....	307
Figure F-38 Effect of Read Distance on Response of Sensor A60 with a Cut Sensing Wire for Readings in 3.5% Salt Water	308
Figure F-39 Sensor A60 Reference Circuit Response for a Cut Sensing Wire with Increasing Concentration of Salt Water at Three Read Distances	311
Figure F-40 Sensor A60 Sensing Circuit Response for a Cut Sensing Wire with Increasing Concentration of Salt Water at Three Read Distances	312
Figure G-1 Prism A21 Sensor Interrogation History	320
Figure G-2 Prism A22 Sensor Interrogation History	321
Figure G-3 Prism A23 Sensor Interrogation History	322
Figure G-4 Prism A24 Sensor Interrogation History	323
Figure G-5 Prism A25 Sensor Interrogation History	324
Figure G-6 Prism A26 Sensor Interrogation History	325
Figure G-7 Prism A27 Sensor Interrogation History	326
Figure G-8 Prism A28 Sensor Interrogation History	327
Figure G-9 Prism A29 Sensor Interrogation History	328
Figure G-10 Prism A30 Sensor Interrogation History	329
Figure G-11 Prism B19 Sensor Interrogation History	330
Figure G-12 Prism B20 Sensor Interrogation History	331
Figure G-13 Prism B21 Sensor Interrogation History	332
Figure G-14 Prism B22 Sensor Interrogation History	333
Figure G-15 Prism B23 Sensor Interrogation History	334
Figure G-16 Prism B24 Sensor Interrogation History	335

Figure G-17 Prism B25 Sensor Interrogation History	336
Figure G-18 Prism B26 Sensor Interrogation History	337
Figure G-19 Prism B27 Sensor Interrogation History	338
Figure G-20 Prism B28 Sensor Interrogation History	339
Figure G-21 Prism B29 Sensor Interrogation History	340
Figure G-22 Prism B30 Sensor Interrogation History	341
Figure H-1 Prism A26 Before Internal Examination	344
Figure H-2 Interior of Prism A26 Showing Location of Broken Wire	345
Figure H-3 Corrosion in Prism A26.....	345
Figure H-4 Prism A29 Before Internal Examination	346
Figure H-5 Interior of Prism A29.....	346
Figure H-6 Prism A29 Corrosion	347
Figure H-7 Prism A30 Before Internal Examination	347
Figure H-8 Interior of Prism A30 Showing Location of Broken Wire	348
Figure H-9 Prism B25 Before Internal Examination	348
Figure H-10 Interior of Cover Concrete of Prism B25	349
Figure H-11 Corrosion of Steel Sensing Wire in Prism B25	350
Figure H-12 Discoloration of Sensor B25 and Corrosion at Wire/Epoxy Interface	350
Figure H-13 Prism B30 Before Internal Examination	351
Figure H-14 Location of Broken Wire of Sensor B30.....	351
Figure H-15 Corrosion at Wire/Epoxy Interface of Sensor B30.....	352
Figure I-1 Temperature Data at Sensor Interrogations for Slab #1	353
Figure I-2 Sensor A01 Interrogation History	354
Figure I-3 Sensor A02 Interrogation History	355
Figure I-4 Sensor A03 Interrogation History	356
Figure I-5 Sensor A04 Interrogation History	357
Figure I-6 Sensor A05 Interrogation History	358
Figure I-7 Sensor A06 Interrogation History	359
Figure I-8 Sensor A07 Interrogation History	360
Figure I-9 Sensor A08 Interrogation History	361
Figure I-10 Sensor B01 Interrogation History	362
Figure I-11 Sensor B02 Interrogation History	363
Figure I-12 Sensor B03 Interrogation History	364
Figure I-13 Sensor B04 Interrogation History	365
Figure I-14 Sensor B05 Interrogation History	366
Figure I-15 Sensor B06 Interrogation History	367
Figure I-16 Sensor B07 Interrogation History	368
Figure I-17 Sensor B08 Interrogation History	369
Figure I-18 Sensor B09 Interrogation History	370

Figure I-19 Point 1 Corrosion Risk History	371
Figure I-20 Point 1 Corrosion Rate History	371
Figure I-21 Point 3 Corrosion Risk History	372
Figure I-22 Point 3 Corrosion Rate History	372
Figure I-23 Point 9 Corrosion Risk History	373
Figure I-24 Point 9 Corrosion Rate History	373
Figure I-25 Point 11 Corrosion Risk History	374
Figure I-26 Point 11 Corrosion Rate History	374
Figure I-27 Point 13 Corrosion Risk History	375
Figure I-28 Point 13 Corrosion Rate History	375
Figure I-29 Point 15 Corrosion Risk History	376
Figure I-30 Point 15 Corrosion Rate History	376
Figure I-31 Point 17 Corrosion Risk History	377
Figure I-32 Point 17 Corrosion Rate History	377
Figure I-33 Point 19 Corrosion Risk History	378
Figure I-34 Point 19 Corrosion Rate History	378
Figure I-35 Point 21 Corrosion Risk History	379
Figure I-36 Point 21 Corrosion Rate History	379
Figure I-37 Point 23 Corrosion Risk History	380
Figure I-38 Point 23 Corrosion Rate History	380
Figure I-39 Point 29 Corrosion Risk History	381
Figure I-40 Point 29 Corrosion Rate History	381
Figure I-41 Point 31 Corrosion Risk History	382
Figure I-42 Point 31 Corrosion Rate History	382
Figure J-1 Temperature Data at Sensor Interrogations for Slab #2.....	383
Figure J-2 Sensor A51 Interrogation History	384
Figure J-3 Sensor A52 Interrogation History	385
Figure J-4 Sensor A53 Interrogation History	386
Figure J-5 Sensor A54 Interrogation History	387
Figure J-6 Sensor A55 Interrogation History	388
Figure J-7 Sensor A56 Interrogation History	389
Figure J-8 Sensor A57 Interrogation History	390
Figure J-9 Sensor A58 Interrogation History	391
Figure J-10 Sensor B51 Interrogation History	392
Figure J-11 Sensor B52 Interrogation History	393
Figure J-12 Sensor B53 Interrogation History	394
Figure J-13 Sensor B54 Interrogation History	395
Figure J-14 Sensor B55 Interrogation History	396
Figure J-15 Sensor B56 Interrogation History	397
Figure J-16 Sensor B57 Interrogation History	398
Figure J-17 Sensor B58 Interrogation History	399

Figure J-18 Sensor B59 Interrogation History	400
Figure J-19 Point 1 Corrosion Risk History	401
Figure J-20 Point 1 Corrosion Rate History	401
Figure J-21 Point 3 Corrosion Risk History	402
Figure J-22 Point 3 Corrosion Rate History	402
Figure J-23 Point 9 Corrosion Risk History	403
Figure J-24 Point 9 Corrosion Rate History	403
Figure J-25 Point 11 Corrosion Risk History	404
Figure J-26 Point 11 Corrosion Rate History	404
Figure J-27 Point 13 Corrosion Risk History	405
Figure J-28 Point 13 Corrosion Rate History	405
Figure J-29 Point 15 Corrosion Risk History	406
Figure J-30 Point 15 Corrosion Rate History	406
Figure J-31 Point 17 Corrosion Risk History	407
Figure J-32 Point 17 Corrosion Rate History	407
Figure J-33 Point 19 Corrosion Risk History	408
Figure J-34 Point 19 Corrosion Rate History	408
Figure J-35 Point 21 Corrosion Risk History	409
Figure J-36 Point 21 Corrosion Rate History	409
Figure J-37 Point 23 Corrosion Risk History	410
Figure J-38 Point 23 Corrosion Rate History	410
Figure J-39 Point 29 Corrosion Risk History	411
Figure J-40 Point 29 Corrosion Rate History	411
Figure J-41 Point 31 Corrosion Risk History	412
Figure J-42 Point 31 Corrosion Rate History	412

CHAPTER 1

Introduction

1.1 INTRODUCTION

Corrosion of embedded reinforcing steel and the resulting deterioration of concrete structures is a worldwide problem. Structures exposed to marine environments or deicing salts are particularly at risk. Corrosion damage reduces the service life of structures and can create serious safety hazards. Visual inspections are not effective in identifying the initiation of corrosion because most of the damage remains concealed until cracking and spalling of the concrete occur. Traditional techniques for determining the presence, extent, and rate of corrosion are expensive and difficult to interpret. Often, existing techniques are used only after corrosion damage becomes visible, when it is too late to take less expensive preventative measures.

Structural health monitoring is an emerging field for assessing the condition of structures throughout their service life. A complete health monitoring scheme for a structure includes early detection and warning for all possible modes of failure or distress. Detection schemes for structures might include cracking, yielding, fatigue, vibration, overload history, damage due to extreme events, such as earthquakes, collisions, or fires, instability, and material deterioration or other environmental conditions leading to distress. The purpose of structural health monitoring is to determine the state of the structure through non-destructive means, which includes the use of smart materials, sensors and sensing networks, and non-destructive testing.

Early detection of corrosion is a subset of structural health monitoring for reinforced concrete structures and goes hand-in-hand with recent trends to focus on durability of concrete materials and concrete structures to obtain longer service life. The continuing development of a new class of sensors for early detection of corrosion is presented in this thesis. To be practical for ordinary structures, the sensors must be inexpensive. The sensors would be installed in new construction or in new portions of rehabilitated structures and positioned adjacent to reinforcing steel before concrete placement. During routine inspections of the structure, the sensors would be interrogated to determine if a corrosion threshold has been reached. If corrosion is detected, an owner can take action to arrest the corrosion and prolong the service life of the structure.

1.2 SCOPE OF RESEARCH

The objective of this research was to develop and test an improved wireless corrosion sensor. This thesis explores the sensor design process and provides data to demonstrate the performance and limitations of the sensors. Recommendations for improvement of the original prototype sensors are made and the second generation wireless corrosion sensors are presented. Presentation of results from sensor calibration and testing leads to formulation of conclusions regarding the performance of sensors for detecting corrosion. Issues requiring further development and requirements for successful implementation are also discussed.

Chapter 2 presents the required attributes and conceptual design of the wireless corrosion sensors. Tests of original prototype sensors demonstrate the success of using a steel wire as the sensing mechanism to directly detect a threshold of corrosion. However, deficiencies in sensor performance and environmental effects were identified, which led to the goals for improvement.

The parameters that influence sensor performance are identified and discussed in Chapter 3. The components used to fabricate sensors, factors due to wireless measurement of the impedance response, and environmental factors influence sensor performance. Recommendations for the design of second generation sensors are made based on extensive parametric testing.

Second generation sensors are discussed in Chapter 4. Results from calibration tests are presented that show the sensitivity of the sensors to the conductivity of the environment. Second generation sensors exhibit transition behavior similar to that of the original prototype sensors. Signal processing is used to determine the characteristic frequencies and pseudo-quality factors of each sensor circuit response. Calibration tests confirm that the state of the steel sensing wire can be ascertained in the presence of a conductive environment despite the transition behavior.

Tests to evaluate the performance of second generation sensors embedded in concrete are discussed and evaluated in Chapter 5. Sensors embedded in concrete prisms confirm the success of the sensors in detecting threshold amounts of corrosion in the steel sensing wires. Thermal effects and use of the pseudo-quality factor for evaluating the state of the steel sensing wire are also presented. Although half-cell potential and linear polarization resistance measurements indicate the likelihood of corrosion activity in the salt water bath area of the reinforced concrete slabs, no conclusions may be made regarding the performance of sensors embedded in reinforced concrete slabs because those tests are still ongoing.

A summary of the most pertinent results from this thesis and recommendations for future research are provided in Chapter 6.

CHAPTER 2

Wireless Corrosion Sensor Development

2.1 INTRODUCTION

The key impetus for sensor development is the need for an inexpensive and reliable method for early detection of corrosion in reinforced concrete structures. Research by Grizzle [9] and Simonen [15] on wireless corrosion sensors provided the basis for sensor development. Previous tests identified important technical issues for further research and confirmed the feasibility of a practical wireless corrosion sensor. Although this thesis presents the design of the second generation sensors, which exhibit improved performance and more reliable results than the original prototypes, the conceptual design of the sensors has remained the same. This chapter provides background on the design and testing of the first generation sensors that leads naturally to the formulation of requirements for the second generation sensors.

2.2 SENSOR CONCEPT

2.2.1 Required Attributes

During the first stage of design, a set of required attributes was developed for the prototype corrosion sensors. Not only did these attributes control the conceptual design of the sensors, they also limited the type and amount of information that the sensors can provide. Required attributes of the sensors are related to power and mode of communication, cost, durability, and reliability of sensor readings.

2.2.1.1 Power and Communication

In the development of any sensor, power demands and mode of communication are primary concerns, as both have a dramatic impact on the cost and performance of the resulting system. The decision was made to rely on wireless communication, such that the sensors are easy to place at the construction site and are self-contained. Use of a battery within the sensor was also dismissed, such that the life of the sensor would not be limited by the life of the battery. By eliminating on-board power and wired communication, the sensor can only be expected to transmit limited information.

2.2.1.2 Cost

As with any new technology, if the cost of implementation is out of proportion with the derived benefits, the technology will not be practical. In the case of corrosion, which can be widely distributed within a single structure, a dense sensor network is preferable. Installation of hundreds of sensors in a single structure might be possible. Therefore, the sensors must have a low initial unit cost and low lifetime costs. The focus throughout sensor development was producing a sensor that is inexpensive enough to be used in common structures. Elimination of batteries and use of inexpensive, commercially available materials for fabrication results in sensors with extremely low initial unit costs.

2.2.1.3 Durability

The service life of the sensor must be at least as long as the service life of the monitored structure. In order to achieve long life for the sensors, non-sensing elements must be sealed and protected from the environment. Sensors must be tough enough to survive the construction process, which might involve temperature fluctuations, rough handling, unexpected impact forces, and concrete placement and vibration. In addition, the existence of sensors within a structure

should not reduce the durability of the structure itself. Again, elimination of batteries substantially improves the service life of sensors. Durability of sensors through construction and the impact of the sensors on the durability of the monitored structure must be evaluated through testing.

2.2.1.4 Reliability

Any sensor that does not provide reliable information is useless. While producing a reliable sensor requires a valid sensing mechanism and good design, true reliability can only be assessed through testing. A comprehensive testing program including specific applications and diverse environmental conditions is necessary to demonstrate sensor reliability.

2.2.2 Conceptual Design

2.2.2.1 Technology

Motivation for the wireless corrosion sensor concept came from electronic article surveillance (EAS) tags. EAS tags (Fig. 2-1) are passive devices used to control shoplifting in retail stores. The tags are affixed to nearly every product for sale. EAS tags are mass-produced and very inexpensive. The technology that enables EAS tags to function without battery power is the same basic technology used for the wireless corrosion sensor.

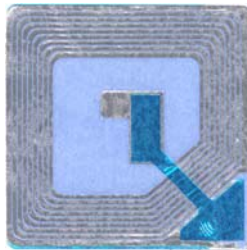


Figure 2-1 EAS Tag

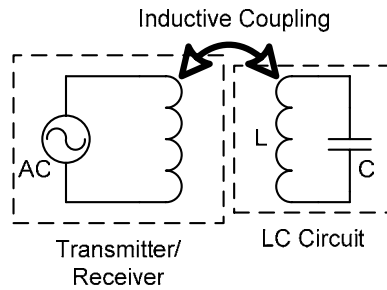


Figure 2-2 Idealized LC Circuit

In its most basic form, the sensor can be idealized as a simple LC circuit (Fig. 2-2). An external, magnetically coupled reader coil provides the power and communication for the sensor. Power is supplied by magnetic induction and communication is provided by measuring impedance response of the sensor through the external reader coil. The transmitter/receiver generates a frequency sweep at the external reader coil in the RF band and the characteristic or resonant frequency of the sensor can be determined from the measured impedance response. The characteristic frequency corresponds to the frequency at which the phase of the impedance is a minimum (Fig. 2-3). For the simple LC circuit, the characteristic frequency, f , is given by:

$$f = \frac{1}{2\pi} \sqrt{\frac{1}{L \cdot C}} \quad (2-1)$$

where L is the inductance and C is the capacitance of the circuit. Any change in the inductance or capacitance of the sensor circuit results in a change in the characteristic frequency.

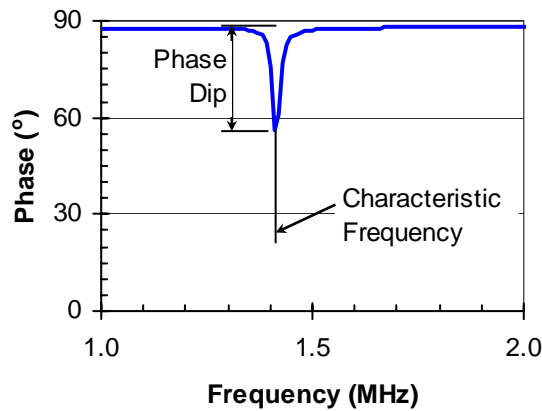


Figure 2-3 Typical Phase Response of Sensor

Visually, the quality of the phase response is best characterized by the amplitude of the phase dip (called simply phase dip throughout the remainder of this thesis). The phase dip (Fig. 2-3) is a qualitative measure that indicates the level of coupling efficiency between the sensor and the reader coil. Greater coupling efficiency results in larger phase dips. A coupling efficiency of zero would result in no distinguishable minimum in the phase response. Further interpretation of phase response will be discussed in Chapters 3 and 4.

For EAS tags, stationary transmitters and receivers are positioned near the exits of retail stores and generate a constant frequency signal over a narrow band. If a product with an intact EAS tag is taken through the exit by a shoplifter, the frequency signal is disrupted and an alarm sounds. When the cashier completes a purchase, the tag is disabled, allowing the customer to exit the store with a purchased item without sounding the alarm. Wireless corrosion sensors embedded in concrete can be interrogated using a reader coil attached to a portable transmitter/receiver. The condition of the sensor is detected by changes in the characteristic frequency.

2.2.2.2 Sensing Mechanism

Adding a steel sensing wire to the LC circuit (Fig. 2-4) provides a means for detecting corrosion. Although the wire is not connected to the reinforcing steel, it is exposed to the same levels of oxygen, moisture, and chlorides as the adjacent reinforcement. Therefore, the onset of corrosion in the wire is a measure of the onset of corrosion in the reinforcement. Because the wire is much smaller in diameter than the reinforcement, the wire will break before appreciable structural damage has occurred. Therefore, the steel wire can be considered as a switch and the phase response of the sensor varies dramatically depending on the state of the switch. By idealizing the sensing mechanism as a state switch, the sensor provides binary information about the state of the switch. The sensor exhibits one response for an intact steel sensing wire and a different response for a broken steel sensing wire.

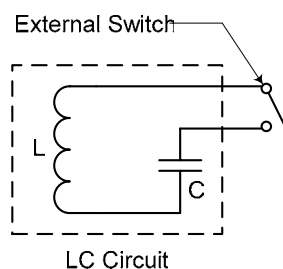


Figure 2-4 Sensor Circuit Diagram

It must be noted that the rate of corrosion in the reinforcement will not be directly related to the rate of corrosion in the steel sensing wire due to the complex nature of corrosion within a structure. The locations of the anode and cathode and electrical pathways will be much different for the reinforcing steel compared with the small steel sensing wires. The steel wire does, however, provide a mechanism for detecting threshold amounts of corrosion at the location of the sensor. While the steel sensing wire provides a direct measure of corrosion

within the wire, detection of a corrosion threshold in the sensor is not directly related to the same amount of corrosion in the reinforcing steel adjacent to the sensor. It is an indicator; however, that a sufficient concentration of chloride ions to cause corrosion has penetrated the concrete to the level of the reinforcement.

2.3 FIRST GENERATION SENSORS

Although a few different versions of prototype first generation sensors were developed and tested by Simonen [15], the discussion in this section will focus on only one version, termed the “basic” sensor. All of the first generation sensors were designed to produce a detectable shift in characteristic frequency between the initial state (wire intact) and final state (wire broken).

2.3.1 Basic Sensor Design

The basic sensor design is shown in Fig. 2-5. An external switch and capacitor were added in parallel with the simple LC circuit. The configuration of the basic sensor is shown in Fig. 2-6 along with a photograph of a typical basic sensor in Fig. 2-7. Sensor components include an inductor made from five turns of 24-gage copper magnet wire around a PVC pipe with a nominal diameter of 1.25 in., two 150-pF capacitors, and an external steel sensing wire. The sensor components were soldered together inside plastic Petri dishes and then potted. Several different potting materials were used before a suitable material was found. Marine epoxy appeared to be the best material for bonding to and protecting the sensor circuit components from the concrete environment.

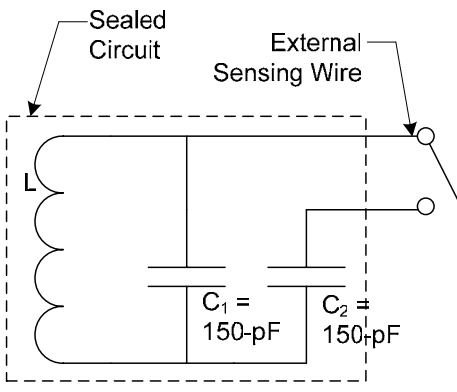


Figure 2-5 Basic Sensor Circuit Diagram

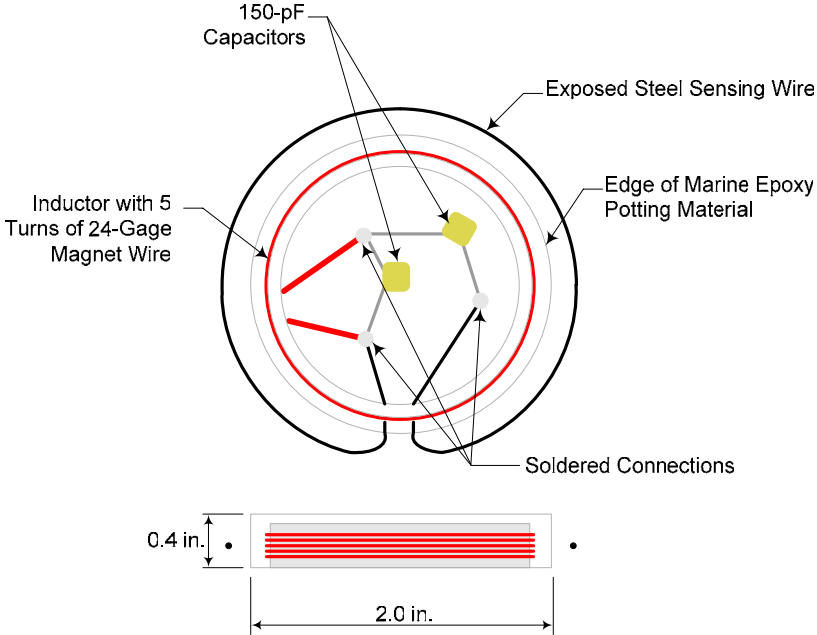


Figure 2-6 Basic Sensor Configuration



Figure 2-7 Photograph of a Basic Sensor

The characteristic frequencies for the sensor were selected arbitrarily based on observed characteristic frequencies of EAS tags. The basic sensor responds at an initial characteristic frequency of about 6.0 MHz with the steel sensing wire intact (switch closed) as shown in Fig. 2-8a. The final characteristic frequency of the basic sensor with a broken steel wire (switch open) is about 8.5 MHz as shown in Fig. 2-8b. The steel wire sizes chosen for the prototype sensors were 26 and 21 gage. Accelerated corrosion testing of wires in simulated concrete solutions were conducted by Grizzle [9] and Simonen [15]. The time to broken steel sensing wires increased for larger diameters.

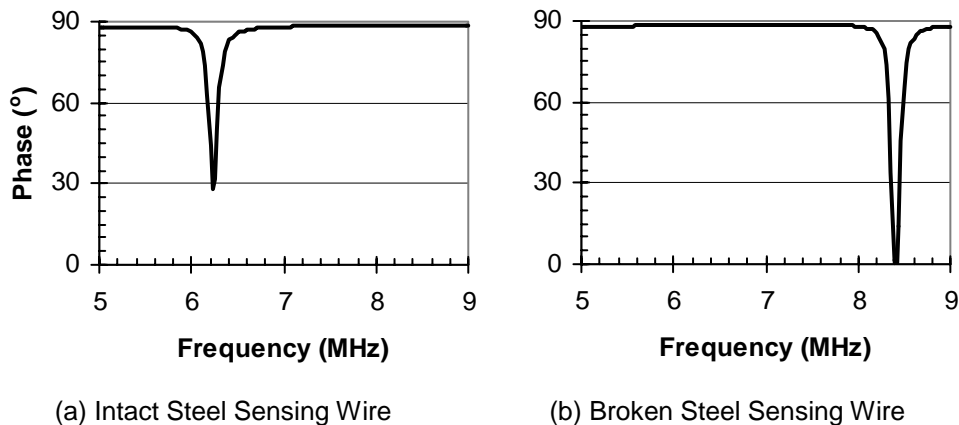


Figure 2-8 Phase Response of Basic Sensor

2.3.2 Basic Sensor Testing

Several types of tests were developed to determine the basic sensor response. Preliminary tests of the sensor in air were used to verify the frequency shift from the initial state (steel sensing wire intact) to the final state (steel sensing wire cut) as shown in Fig. 2-8. Corrosion testing of large-scale reinforced concrete slabs, small concrete prisms, and sensors alone in various environments were used to assess sensor behavior.

2.3.2.1 Reinforced Concrete Slabs

Test specimens consisted of four reinforced concrete slabs [15]. The specimens were specifically designed to accelerate corrosion of the reinforcement by using very permeable, low-strength concrete and concrete cover to the top longitudinal reinforcement of only 1 in. Top longitudinal reinforcing steel consisted of two #5 bars at a spacing of 12 in. Eight sensors were positioned at the level of the top layer of longitudinal reinforcement centered about midspan in each slab (Fig. 2-9). Sixteen basic sensors and sixteen “improved” sensors were embedded within the four slabs. The improved sensors are not discussed in detail in this thesis, but are described in the thesis by Simonen [15].

The sensors were interrogated for the first time in September 2004, which was approximately one month after the concrete had been placed and before the specimens were loaded. All basic sensors of the design shown in Fig. 2-7 responded at the initial characteristic frequency, indicating that the steel sensing wire survived the construction process intact. The slabs were positioned on top of a reaction beam and subjected to sustained point loads at the ends. The region between the supports was subjected to constant negative moment of sufficient magnitude to crack the concrete on the top surface. The average crack width in the constant moment region was 0.013 in. After loading, salt water ponds were

placed on the top surface of each specimen and slabs were subjected to wet and dry cycles using 3.5% salt water by weight. For two days every two weeks, the top surface of the specimens was allowed to dry.

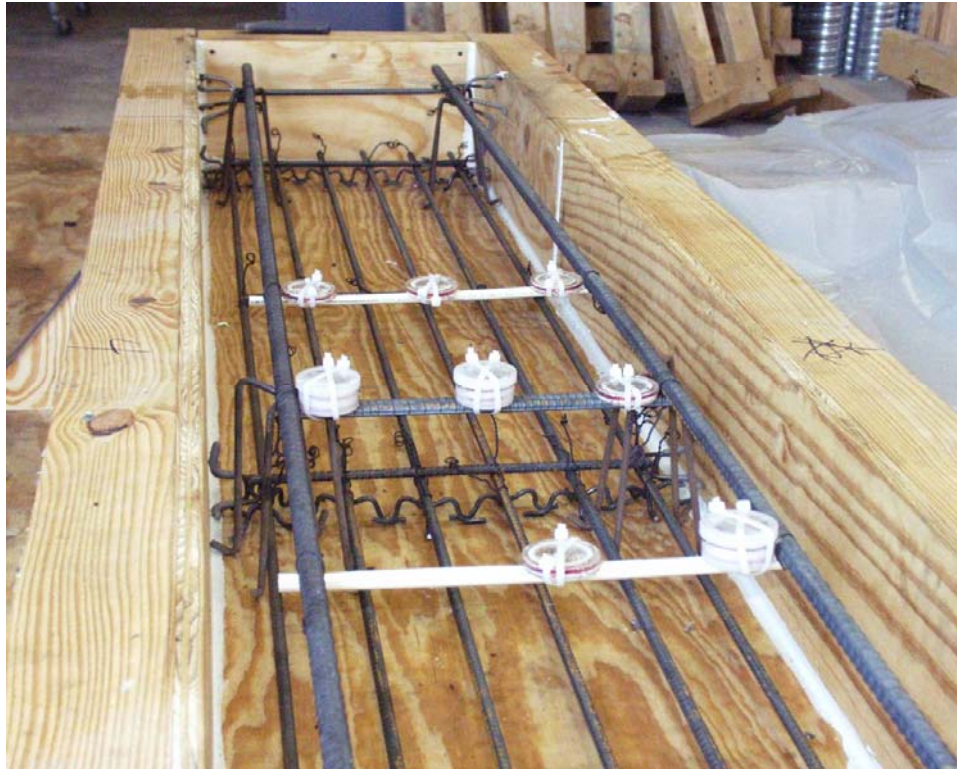


Figure 2-9 Arrangement of Sensors in a Slab

The sensors were interrogated once per month to evaluate the state of corrosion in the sensors. All data were acquired using a Hewlett-Packard 4194A Impedance/Gain-Phase Analyzer. Representative data from a basic sensor are shown in Fig. 2-10a. The amplitude of the phase dip of the impedance response was considerably less than had been observed when the sensors were interrogated in air (Fig. 2-8a). This behavior was expected, however, because the reader coil was placed adjacent to the sensor coil when the tests were conducted in air, while

the two coils were separated by the concrete cover in the slabs, which reduced the coupling efficiency of the system.

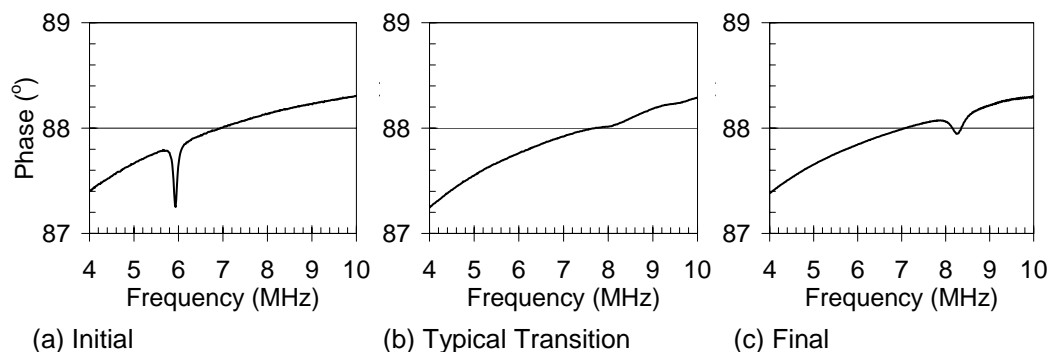


Figure 2-10 Phase Response of a Basic Sensor Embedded in a Slab [15]

When the sensors were interrogated after the first month of wet and dry cycles, most of the basic sensors appeared to have malfunctioned. A dip in the phase angle response at the initial characteristic frequency was not observed (Fig. 2-10b). Although it seemed unlikely that corrosion had progressed significantly in one month, the concrete cover was removed from the constant moment region of one of the slabs to evaluate the condition of the reinforcement. It was impossible to determine whether the steel sensing wires were intact because they were damaged removing the concrete, but it seemed unlikely that any had fractured due to corrosion. A very small amount of corrosion was observed on the steel wires and on the surface of the reinforcement in the immediate vicinity of the cracks. This level of corrosion was much less than that expected to break the steel sensing wires. Sensors in the three remaining specimens were monitored for several more months.

The variation of the characteristic frequencies with time is shown in Fig. 2-11 for one basic sensor. The frequency response of the sensor could not be detected in the readings two and three months after the initial interrogation.

However, after four months, the signal reappeared for some of the sensors, and the characteristic frequencies corresponded to the final state, indicating that the external switch had fractured (Fig. 2-10c). The gap in the data from the sensors shown in Fig. 2-11 was not expected.

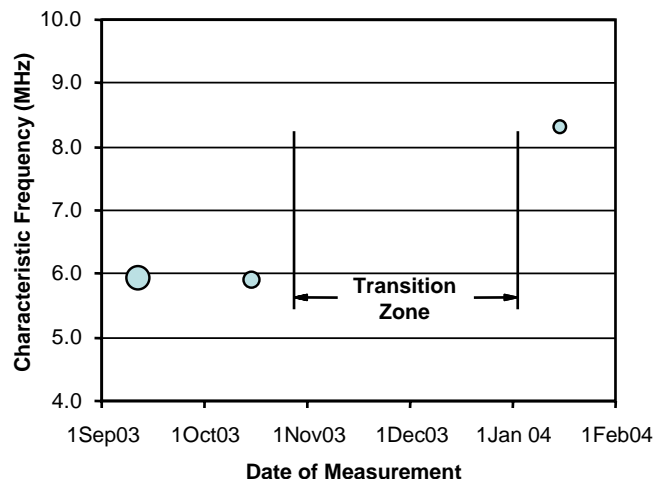


Figure 2-11 Characteristic Frequency of Basic Sensor Embedded in a Slab with Time [15]

Cores were taken from one of the remaining three slabs in late January 2004 to remove three sensors and the concrete cover was removed throughout the constant moment region. Photographs of the observed corrosion are presented in Fig. 2-12. Corrosion levels were modest, but the response of the sensors was consistent with the objective to detect corrosion before structural damage occurs. Chloride contents taken from near the surface of the slabs and near the reinforcing steel in the ponding area from both the cores and the slab varied between 0.08 and 0.13% by mass of cement. The chloride threshold for initiation of corrosion in reinforced concrete varies depending on the amount of available moisture and oxygen and the source of the chlorides. ACI 222 [2] recommends limits for new construction of 0.20% by mass of cement for acid-soluble chlorides in reinforced concrete with dry conditions and 0.10% with wet conditions to minimize the risk

of chloride-induced corrosion. However, studies indicate that chloride contents of 0.20% to 0.40% are required to initiate corrosion in reinforced concrete subjected to environmental chloride exposure [8].



(a) Corrosion on Reinforcement Adjacent to a Basic Sensor at a Crack Location

(b) Corrosion on Reinforcement in a Core with Bottom of Sensor Exposed

Figure 2-12 Photographs of Corrosion in Test Slabs

2.3.2.2 Sensor-Only Immersion

While testing the sensors in concrete is necessary to establish performance in the intended environment, the sensor and the corrosion of the sensing wire are not visible during those tests. One hypothesis for the behavior of the sensors in the large-scale slab tests was that as the steel sensing wire corroded, the resistance of the wire changed, resulting in a transition between the initial (very little resistance) and final (very large resistance) states. Therefore, sensor-only immersion was used to determine whether the sensor behavior in the large-scale slab tests was reproducible. This way, the corrosion of the steel sensing wire could be visually inspected at any point during testing. Sensors were subjected to wet cycles of three weeks in a simulated concrete solution with 3.5% sodium

chloride by weight and dry cycles of one week. Sensors were interrogated often, usually twice a week, to try to capture the transition behavior.

Testing began in March 2004 and concluded in June 2004. The hypothesized transition behavior was not observed in any of the sensors. Behavior of the basic sensor labeled 1a during the testing period is shown in Fig. 2-13a. As originally expected, the sensor responded at the initial characteristic frequency during every interrogation until a wire break occurred. Once the wire fully corroded, the sensor responded at the final characteristic frequency.

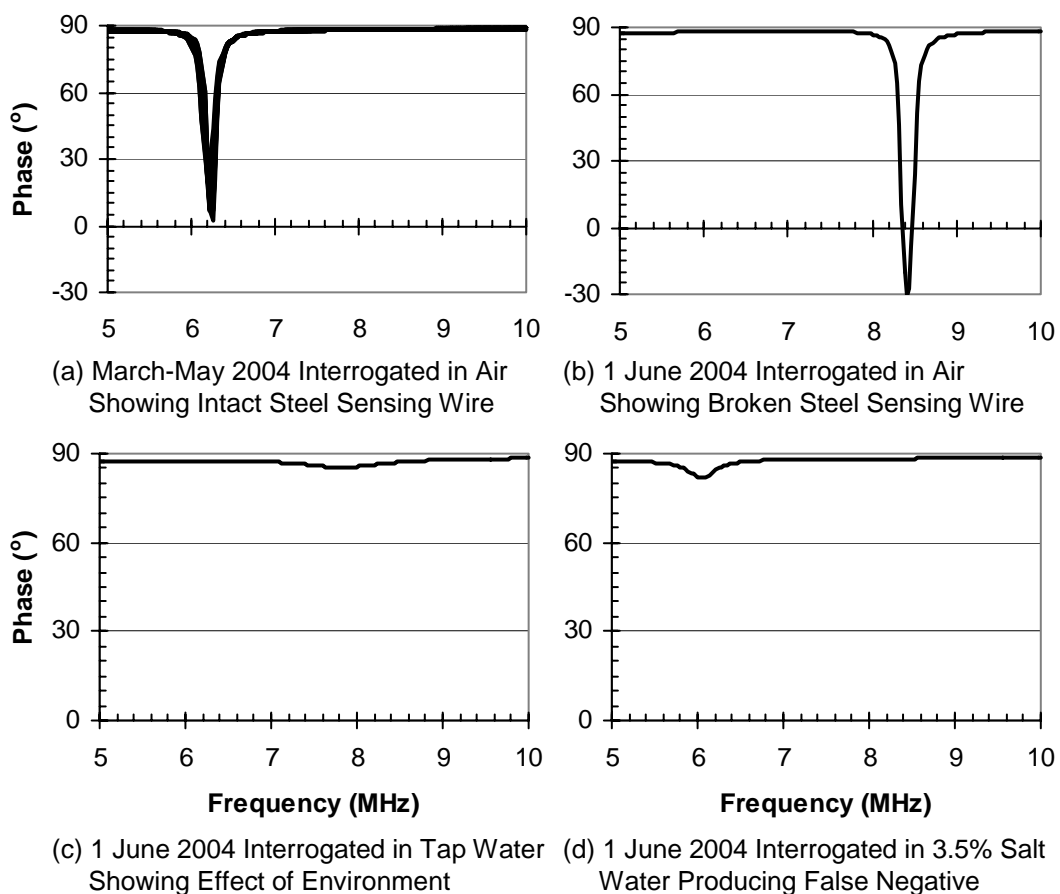


Figure 2-13 Phase Response of Sensor 1a During Immersion Testing

Because no transition behavior was observed, a new hypothesis that environmental factors contributed to the behavior of the sensors in the slab tests was formed. As shown in Fig. 2-13, sensor 1a was interrogated in various environments after the wire fully corroded: air (b), immersed in tap water (c), and immersed in 3.5% salt water (d). Clearly, the presence of a conductive environment around the sensor at the time of interrogation affects the sensor response. Although the response changed with immersion in tap water, the characteristic frequency still indicates that the wire has broken. When immersed in salt water, however, the characteristic frequency indicates that the wire is still intact, producing a false negative reading.

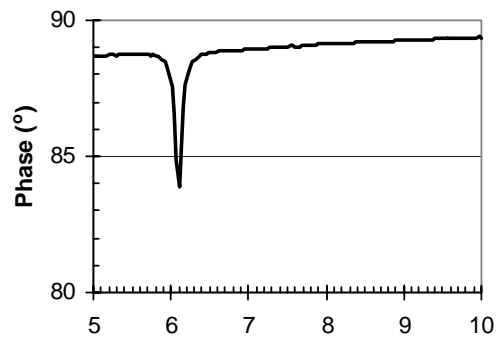
2.3.2.3 Concrete Prisms

To test the influence of moisture and chloride ions, several sensors were embedded in concrete prisms and subjected to wet and dry cycles using complete immersion. Prisms were 4-in. diameter cylinders with 1 in. of concrete cover over the sensor. Specimens were subjected to oven drying to accelerate the corrosion process. To evaluate performance under extreme temperatures, specimens were exposed to oven and freezer cycles for 24 hours at a time with 230 °F and -15 °F temperatures, respectively. Cycles began in April 2004, with three weeks wet followed by sensor interrogation and then one week dry followed by sensor interrogation. Oven and freezer cycles occurred during dry cycles. The performance of three basic sensors, one in salt water, one in tap water, and one control specimen in air are compared in this section.

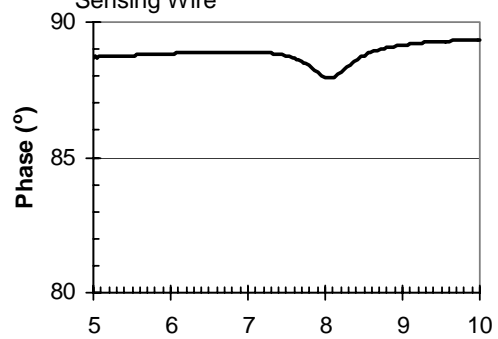
The first basic sensor, labeled 4a, was subjected to wet cycles with 3.5% salt water. The sensor responded at the initial characteristic frequency of 6.04 to 6.13 MHz during every interrogation including wet, dry, oven dry, and frozen until November 2004 (Fig. 2-14a). During the interrogation at the end of the wet

cycle, the sensor responded at 8.05 MHz, indicating a fully corroded (broken) wire. The amplitude of the phase response was small and wide as shown in Fig. 2-14b, but still indicated the wire break under wet conditions. After the following dry cycle, the sensor responded at 8.20 MHz with a well-defined phase dip as shown in Fig. 2-14c. Wet and dry cycles have continued to the present and still show the same performance during each interrogation. Although the amplitude of the phase dip after wet cycles may only be 10 to 20% of the amplitude after dry cycles, the characteristic frequency of the sensor has only varied by about 5%. Chloride content of one prism subjected to the same wet and dry cycles as sensor 4a was 0.4%, which is above the recommended limit for initiation of corrosion in reinforced concrete. After the most recent wet cycle, the interrogation was made while the prism was still immersed in salt water and the response was similar to the previous response shown in Fig. 2-14b.

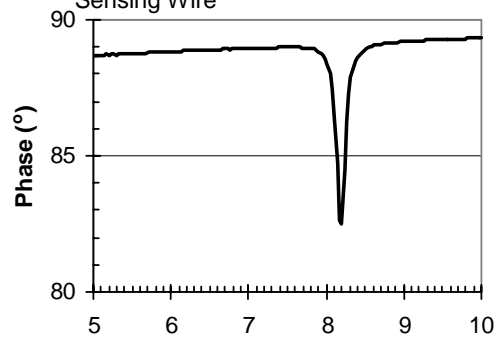
The second basic sensor, labeled 5a, was subjected to wet cycles with tap water. The sensor has responded at the initial characteristic frequency of 6.19 to 6.28 MHz at every interrogation including wet, dry, oven dry, and frozen through January 2005. So far, the sensor has shown no indication of corrosion or environmental effects. The third basic sensor, labeled 3a, was the control specimen stored in air at room temperature. The sensor has responded at the initial characteristic frequency of 6.13 MHz at every interrogation through January 2005.



(a) April-November 2004 Typical Sensor Response in Wet, Dry, and Frozen Conditions Showing Intact Steel Sensing Wire



(b) November 2004 Interrogation of Wet Concrete Prism Showing Broken Steel Sensing Wire



(c) November 2004 Interrogation of Dry Concrete Prism Showing Broken Steel Sensing Wire

Figure 2-14 Phase Response of Basic Sensor 4a During Corrosion Testing of Concrete Prisms

2.3.3 Conclusions

Although sensor behavior is much more complex than originally assumed, through testing of the original prototype sensors some valuable attributes are apparent. The steel sensing wires do indeed corrode and correspond to corrosion of reinforcing steel at the location of the sensor. The sensors are small, wireless, inexpensive, and easy to fabricate and install. They are sufficiently durable to survive the construction process and require no on-board power or maintenance. In the absence of environmental effects, the sensors respond at an initial characteristic frequency with the steel sensing wire intact and shift to the final characteristic frequency when the wire has corroded through.

Several deficiencies make the basic sensor unreliable. The amplitude of the phase dip of the impedance response diminishes rapidly with increasing distance between the interrogation antenna and the sensor. Environmental factors also affect the phase response, such as the presence of water or an electrically conductive environment. The response of a sensor with a cut or fully corroded wire may disappear or be too weak to decipher if saturated conditions are present with modest concentrations of salt. Under saturated conditions with a sufficient concentration of chlorides, sensors may give a false negative reading. This means that a sensor with a cut or completely corroded wire responds at the initial characteristic frequency during interrogation, indicating a wire that is intact (corrosion is below the threshold of the sensor).

Improved sensors with an additional reference circuit were developed to ensure that a characteristic frequency could be always be detected. This solved the problem described in Section 2.3.2.1; however, it also complicated the response of the sensor. The reference circuit affects the response of the sensor circuit and vice versa due to mutual inductance. Also, when immersed in salt

water of sufficient concentration, the improved sensors still produced false negative readings.

Deficiencies of the prototype sensors provided the goals for improving the sensors. Three goals were established for redesigning the sensors:

- 1) Determine the important parameters that influence sensor response,
- 2) Minimize the sensitivity of the sensor response to the conductivity of the environment, and
- 3) Improve the quality of sensor readings by increasing the amplitude of the phase dip.

To achieve these three goals, Chapter 3 presents the results of extensive testing to explore the parameters that control sensor response. Three parametric studies that were conducted to achieve these goals are described in Appendices A, B, and C. The resulting second generation sensors are presented in Chapter 4.

CHAPTER 3

Exploration of Sensor Design Parameters

3.1 INTRODUCTION

The first generation sensors were designed using two primary assumptions: (1) response at a given characteristic frequency is governed by only the inductance and capacitance of the sensor circuit, and (2) the response of conceptual sensors is binary and only the shift in characteristic frequency is necessary to determine the state of the sensor. However, from test results summarized in Chapter 2, it is clear that sensor response is much more complicated. Environmental effects and deficiencies in sensor performance have been identified. Further exploration into the parameters that affect sensor response is necessary before improvements can be made in the design.

This chapter provides results from an extensive set of parametric tests and trials using various sensor and reader configurations. Factors influencing sensor response are identified and explored. All comparisons are qualitative assessments based on the phase response of the sensor, using characteristic frequency and phase dip. Interpretation of phase response using further quantitative signal processing is presented. The factors that influence sensor response can be divided into three categories: (1) internal components used to fabricate the sensor, (2) factors due to wireless measurement of the impedance response, and (3) external environmental factors.

3.2 PARAMETRIC STUDIES

In order to identify the parameters most important to sensor response, several experiments were devised using sensors that were not embedded in

concrete. Experiments were carried out with the goals of reducing the sensitivity to environmental effects, increasing the read range, and decreasing the size of the sensors. Three distinct parametric studies were used to explore the factors influencing sensor response. In addition, several trial sensors were fabricated using various configurations of inductors, capacitors, and sensing wires. Descriptions of studies are provided in the following sections. The Solartron Impedance Analyzer was used for sensor interrogations in all tests.

3.2.1 Parametric Study I

In Parametric Study I, 27 completely sealed sensors were constructed using a single inductor with varying diameters and number of magnet wire turns. Three different nominal diameters of PVC pipe were used (0.75, 1.0, and 1.25 in.) and the number of 24-gage copper magnet wire turns varied between 1 and 9. The intent was to keep the characteristic frequency nearly constant at approximately 4 MHz, so different values of capacitance were required in the different sensors. Because different capacitors were used to construct the sensors, the effects of capacitor type could not be eliminated from the results. Sensors were interrogated using a 2-in. diameter reader coil with a single turn of 24-gage copper magnet wire. Interrogations were conducted with varying read distance in three different environments: air, tap water, and salt water with 3.5% sodium chloride by weight. Complete results from Parametric Study I are reported in Appendix A. Selected results are presented throughout this chapter.

3.2.2 Parametric Study II

In Parametric Study II, four trial sensors were constructed using nominally identical inductors and capacitors, but four different wire materials and gages were used as the sensing mechanism. Two different diameters of steel wire, 21-gage and 26-gage, and two diameters of copper magnet wire, 18-gage and 24-

gage were used for sensing wires. The circuit model for the trial sensors was the same as that for the first generation basic sensor. The inductor was fabricated using 2.0-in. nominal diameter PVC pipe with 5 turns of 18-gage copper magnet wire. Capacitors were 2,700 pF and 33,000 pF, which resulted in an initial effective circuit capacitance of 35,700 pF with an intact sensing wire and a final effective circuit capacitance of 2,700 pF with a cut sensing wire. Therefore, the initial characteristic frequency was approximately 0.4 MHz and the final characteristic frequency was approximately 1.8 MHz. Sensors were interrogated using a 4-in. diameter reader coil with a single turn of 24-gage copper magnet wire. Interrogations were conducted with varying read distance in air, water, and varying concentrations of salt water. Complete results from Parametric Study II are reported in Appendix B and selected results are presented in this chapter.

3.2.3 Parametric Study III

In Parametric Study III, three completely sealed sensors were constructed using nominally identical inductors, but with different values of capacitance. A single inductor constructed using 1.25-in. nominal diameter PVC pipe and 5 turns of 18-gage copper magnet wire was used for each sensor. Because each sensor had a different value of capacitance, the characteristic frequency of each sensor was different. A fourth trial sensor with a larger 2.0-in. nominal diameter PVC pipe inductor was also included in the study. Sensors were interrogated using a 4-in. diameter reader coil with 20 turns of 18-gage copper magnet wire. In addition to interrogating the sensors separately, sensors were interrogated in pairs with various arrangements including stacked, side-by-side, and concentric. Complete results from Parametric Study III are reported in Appendix C and selected results are presented in this chapter.

3.2.4 Trial Sensors

Selected trial sensors are used throughout this chapter. Descriptions and results from each are presented on a case-by-base basis.

3.3 SENSOR COMPONENTS

Sensor response is governed chiefly by the components used for fabrication. Components shown to influence sensor response include capacitors, inductors, and steel sensing wires. Along with determining the characteristic frequency of the sensor, the composition and quality of these components affects sensor phase response. The resonant sensor concept described in Chapter 2 requires that each sensor have at least one capacitor and one inductor. Using mass-produced capacitors and hand-wound inductor coils is a practical necessity for sensor fabrication and has consequences for sensor design. Adding a steel wire to the sensor circuit to act as a sensing mechanism and including more than one resonant circuit in the sensor for reference further complicates sensor response. By identifying the influence of each parameter on the phase response of the sensor, advances may be made in sensor design.

3.3.1 Practical Considerations

In order to achieve a low-cost sensor, the materials and methods used for fabrication must be readily available and inexpensive. Because of the developmental nature of the sensors, each is fabricated by hand using commercially available materials purchased in small quantities from local suppliers. Construction materials include capacitors, copper magnet wire, PC component boards, and PVC pipe, which is used as a form for the inductors. Some practical limitations result from the use of commercially available materials and hand fabrication. These limitations affect the range of characteristic frequencies that can be achieved and also the quality of the phase response.

Capacitance, inductance, and resistance of the circuit clearly influence sensor response. However, the use of PC component boards to facilitate soldering of components, solder chemistry, and soldering quality appear to have little effect on the phase response.

3.3.2 Capacitance

The range of available small-sized capacitors is roughly 1 to 50,000 pF. Although many different types of capacitors are sold, high-quality COG or NP0 ceramic capacitors seem to be best suited for sensor circuit fabrication. The effect of capacitor type on the quality of the sensor phase response is discussed in Appendix A. As shown in Fig. 3-1, the phase dip for a sensor constructed with a high-quality ceramic capacitor is deep and narrow (a), while the phase dip for a low-quality ceramic capacitor is wide and shallow (b).

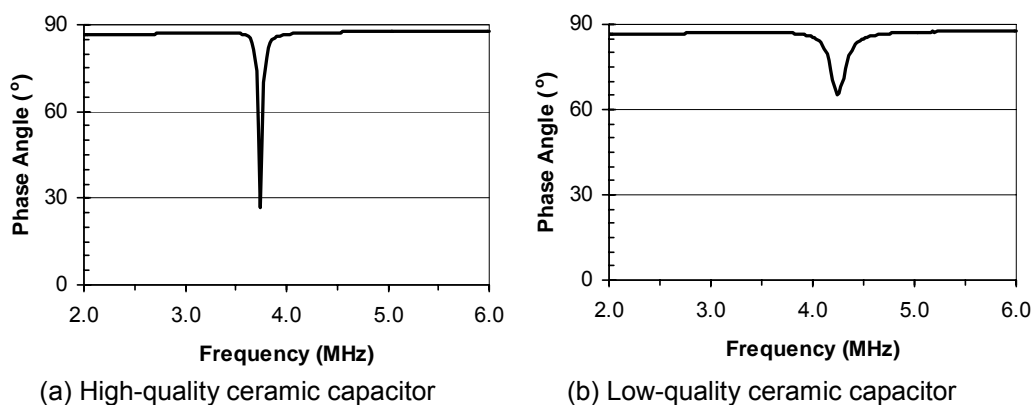


Figure 3-1 Effect of Capacitor Type on Sensor Phase Response

3.3.3 Inductance

Inductance of the sensor and, in turn, coupling efficiency with the reader coil have a substantial impact on phase response. Inductors are fabricated by winding copper magnet wire into a coil around slices of PVC pipe. The outside

diameter of the PVC pipe, the diameter of the magnet wire, and the number of turns in the coil influence the inductance. The inductance of a coil with constant radius may be approximated using EQ. (3-1) from Lee [11]:

$$L = \frac{(a \cdot N)^2}{22.9 \cdot \ell + 25.4 \cdot a} \quad (3-1)$$

where L is inductance in μH , a is radius of the coil in cm, N is number of turns, and ℓ is length of the coil in cm (Fig. 3-2).

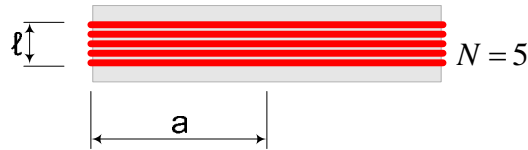


Figure 3-2 Parameters Affecting Inductance

It is evident from EQ. (3-1) that inductance is dominated by radius and number of turns, while the length of the coil has a very small impact on impedance. Therefore, the diameter of PVC pipe and number of magnet wire turns will have a much greater influence on inductance than the diameter of magnet wire. Inductor diameter and number of turns were investigated in Parametric Study I. In order to check the feasibility of reducing the size of the sensors, two inductor diameters were chosen that were smaller than the inductor diameter used in first generation sensors.

Results from Parametric Study I illustrate the effect of diameter and number of wire turns on phase response. For a range of practical PVC pipe sizes, Fig. 3-3 shows the relative magnitude of phase dip with increasing inductor diameter for sensors interrogated in air with a read distance of 0.5-in. Data are shown for sensors with seven turns of 24-gage magnet wire up to 1.25-in. nominal diameter. Although one goal of sensor design is to produce the smallest sensor possible, larger diameter coils provide greater coupling efficiency and larger

phase dips. PVC pipe comes in discrete sizes and must be large enough to allow soldering of the circuit components inside of the pipe. PVC pipe with 0.75-inch nominal diameter was considered the smallest practical size to allow soldering of the circuit components. The phase dips for sensors constructed with the small diameter inductors are poor. Although not shown in Fig. 3-3, PVC pipe with 2-in. nominal diameter was considered to be the largest practical coil diameter and results in the best possible coupling efficiency and largest phase dips for the sensor.

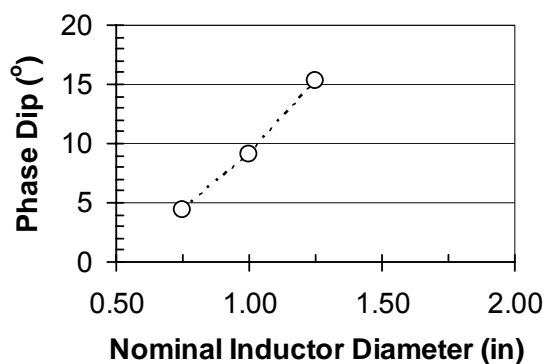


Figure 3-3 Effect of Inductor Diameter on Phase Dip

The sensitivity of the phase response to the number of turns in the inductor coil is shown in Fig. 3-4. In this case, the data are plotted for three nominal inductor diameters: 0.75, 1.0, and 1.25 in. This trend shows that coupling efficiency rapidly increases as the number of turns increases, but levels off at four or five turns. Therefore, an inductor with five turns was considered the most favorable for the sensor coil to produce a good quality phase dip while minimizing fabrication time and sensor size.

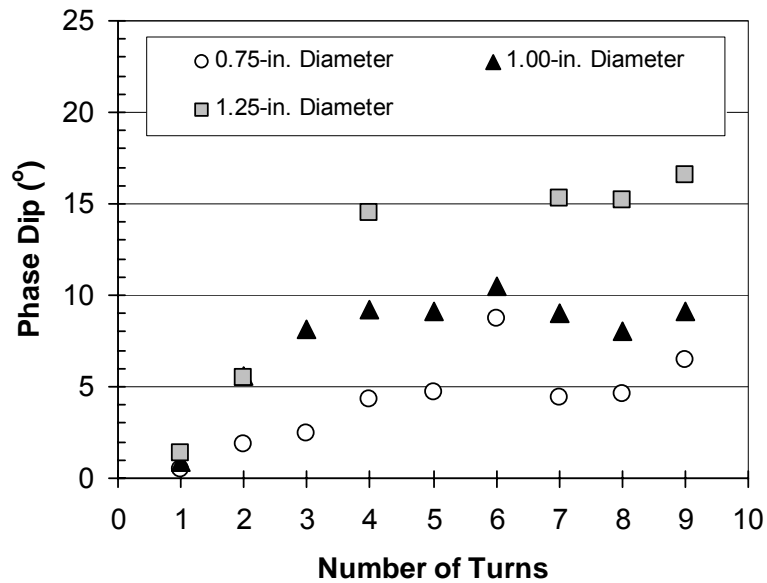


Figure 3-4 Effect of Number of Magnet Wire Turns on Phase Dip

3.3.4 Resistance

Although the effect of coil length and, therefore, magnet wire diameter on inductance is small, the size of the magnet wire does play an important role in the quality of phase response due to the inherent resistance of the wire. Larger diameter wire has lower resistance, and therefore, produces larger phase dips. The response of inductors fabricated using 18 and 24-gage copper magnet wire is shown in Fig. 3-5. These represented the practical limits of wire studied in this investigation. Magnet wire of 18-gage was considered the largest practical wire diameter that would still allow hand-winding of inductor coils. Clearly, the sensor with 18-gage magnet wire used in the inductor (Fig. 3-5b) gives a larger phase dip than the sensor with 24-gage magnet wire (Fig. 3-5a).

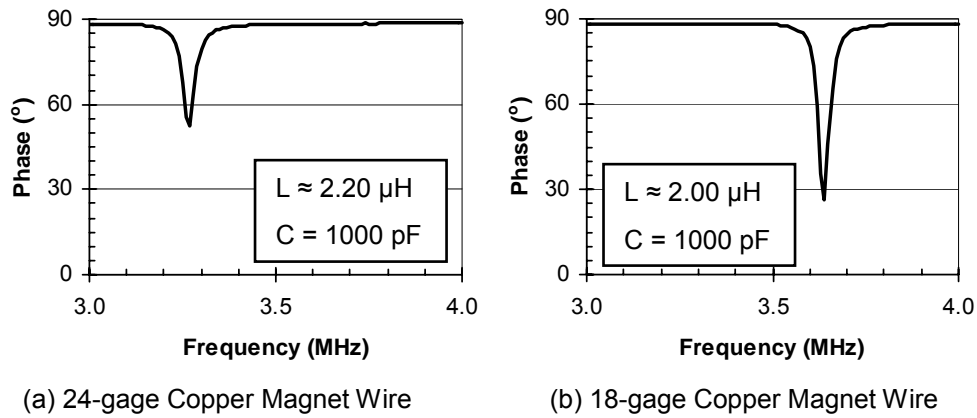


Figure 3-5 Effect of Wire Diameter on Phase Response of Sensors

3.3.5 Steel Sensing Wire

Results from Parametric Study II illustrate the effect of wire material on sensor response. The same length of wire was added to four nominally identical circuits. The phase response with a length of 18-gage copper wire is shown in Fig. 3-6a and the response with a nominally identical length of 21-gage steel wire is shown in Fig. 3-6b.

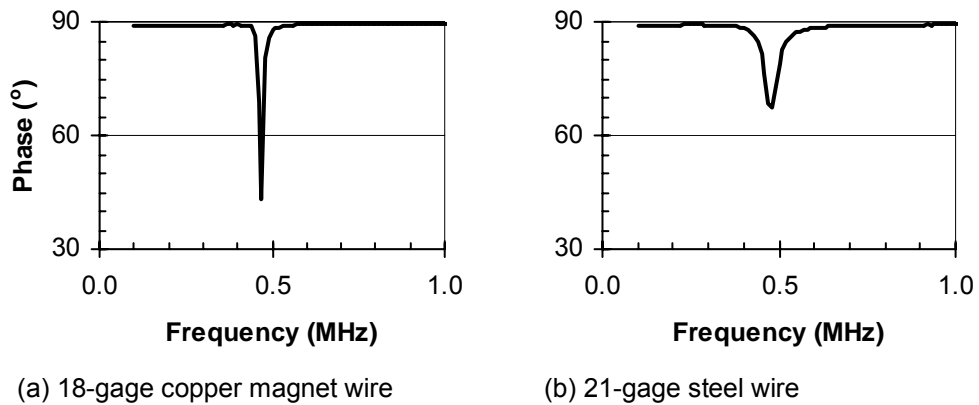


Figure 3-6 Effect of Steel Sensing Wire on Phase Response of Sensors

The phase dips of all four wire sizes are compared in Fig. 3-7. The phase dip of the circuit with 24-gage copper magnet wire is only slightly smaller than the circuit with 18-gage copper magnet wire. Using 21-gage steel wire reduces the phase dip by approximately one half from the 18-gage copper wire and using 26-gage steel wire reduces the phase dip by approximately three fourths. The smallest diameter steel wire (26-gage) was selected for laboratory tests in order to minimize the time to a corrosion threshold. In practice, steel wires with larger diameters would be used to detect higher corrosion thresholds and improve sensor response.

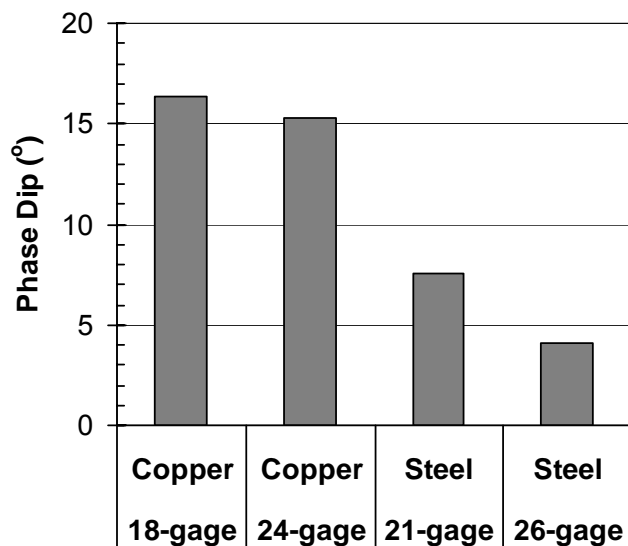


Figure 3-7 Effect of Wire Diameter and Material on Phase Dip

It is believed that the increased resistance of the steel wire, compared with the copper wire, causes these changes in the impedance response. The sensing circuit is therefore more accurately modeled as an RLC circuit (Fig. 3-8), which replaces the original simplified LC circuit (Fig. 2-2).

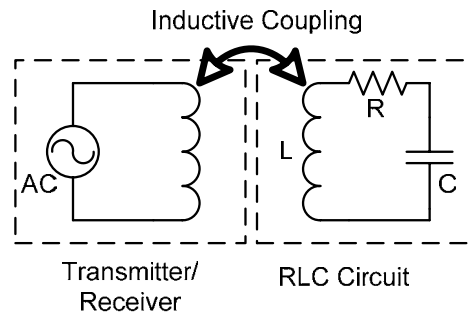


Figure 3-8 Sensor Circuit Diagram Including Wire Resistance

First generation corrosion sensors used two orientations of steel sensing wire: a circumferential loop (Fig. 3-9a) and an exposed loop (Fig. 3-9b). For small wire sizes used in first generation sensor testing, the exposed loop configuration did not survive construction as well as the circumferential loop. Therefore, the exposed loop was not used in further sensor development. During parametric tests, the circumferential loop was observed to reduce the performance of the sensor. In this configuration, the steel wire loop is magnetically coupled with the sensor coil. If the inductance of the steel wire is sufficiently large, the steel loop can shield the response of the sensor coil. An alternate geometry with a doubled half-loop steel wire was introduced to eliminate this coupling (Fig. 3-9c). The difference in phase response of the same sensor with circumferential and doubled half-loop geometries of steel wire is shown in Fig. 3-10.

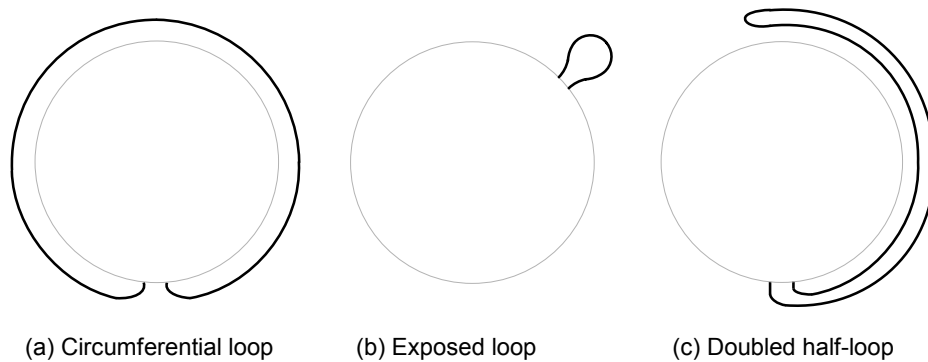


Figure 3-9 Possible Arrangements of Sensing Wire

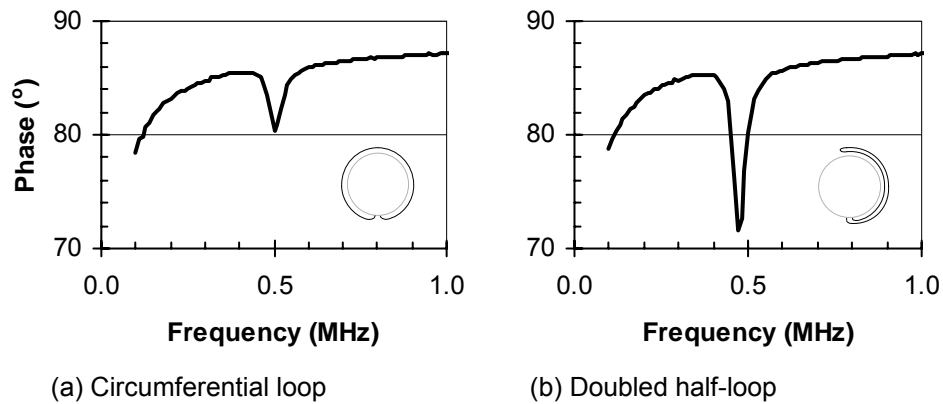


Figure 3-10 Effect of Sensing Wire Geometry on Sensor Phase Response

3.3.6 Reference Circuit

Tests using first generation sensors revealed “transition” behavior, in which no characteristic frequency could be detected for sensors that were embedded in concrete saturated with salt water. To eliminate the possibility of obtaining no characteristic frequency response, an additional reference circuit was added to the sensor that was completely sealed and separate from the basic sensing circuit. These sensors were termed “improved” sensors. However, the presence of the reference circuit in the improved sensor affected the response of

the sensing circuit. Because the circuits were placed in a stacked arrangement for the improved sensor, sensor response was also dependent on the location of the reader coil; either adjacent to the reference circuit or the sensing circuit. In addition, the transition behavior observed in basic sensors was also observed in the sensing circuit response of improved sensors. This showed that further exploration in behavior of sensors with multiple resonant circuits was necessary.

In the case of a sensor circuit with the steel sensing wire in series with the inductor and capacitor, as shown in Fig. 3-11, the sensor only responds at the characteristic frequency with the sensing wire intact. The response of the sensor circuit with an intact wire (switch closed) is shown in Fig. 3-12a. When the steel sensing wire corrodes and fractures (open switch), the phase dip disappears from the impedance response of the sensor (Fig. 3-12b). While the state of the switch can be determined easily by comparing the phase response in Fig. 3-12a and b, the lack of a characteristic frequency with an open switch creates a number of practical problems. An investigator would not know if the sensor had reached a corrosion threshold, if no sensor was at the location being interrogated, or if the sensor had malfunctioned. Therefore, a second circuit must be added to the sensor to provide a reference frequency that is not sensitive to the state of the switch.

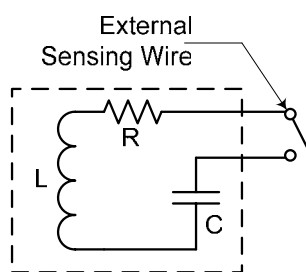


Figure 3-11 Sensor Circuit Diagram with Sensing Wire Added in Series

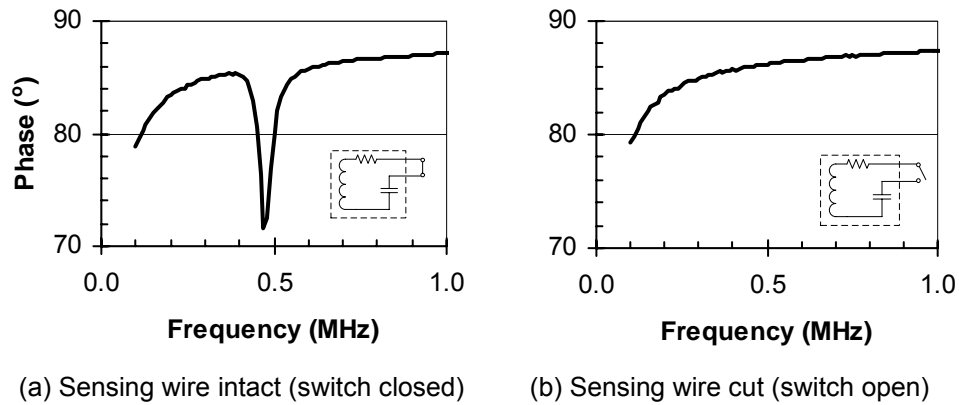


Figure 3-12 Effect of the State of Sensing Wire on Sensor Phase Response

The addition of the reference circuit complicates sensor response. Mutual inductance between the sensing circuit and reference circuit can result in a shift in both characteristic frequencies, a reduction of phase dip of both circuits, or even complete shielding of the sensing or reference phase dips. The mutual inductance between the sensing circuit and reference circuit depends on the individual inductance of each circuit, their characteristic frequencies, the location of each coil relative to the other, and the location of each coil relative to the reader coil. A complete circuit model for the sensor from Fig. 3-11 with an added reference circuit is shown in Fig. 3-13.

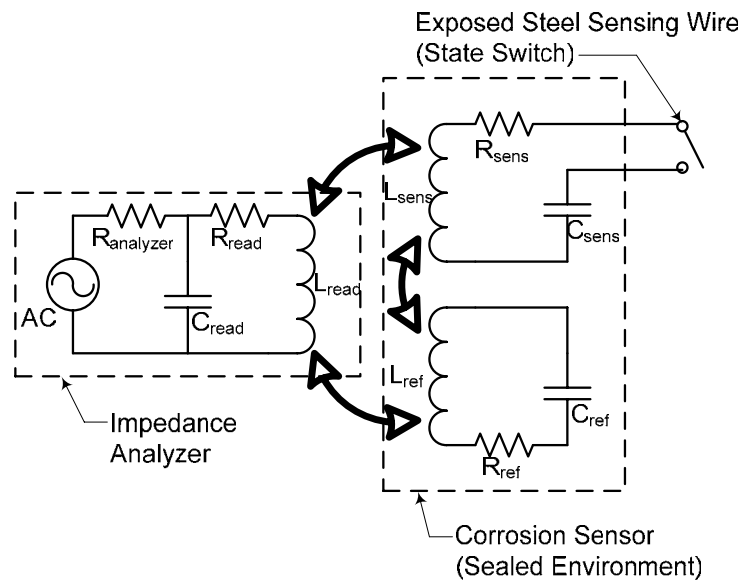


Figure 3-13 Sensor Circuit Diagram Including Reference Circuit

To improve the design of sensors with reference circuits, Parametric Study III was devised to explore the behavior of multiple sensor circuits interrogated simultaneously. Results from Parametric Study III show the effect of two resonant circuits within a single sensor and are presented in Appendix C. Of the four sensor circuit arrangements tested in the study (Fig 3-14), the concentric and side-by-side arrangements appear to be the most promising for further sensor development.

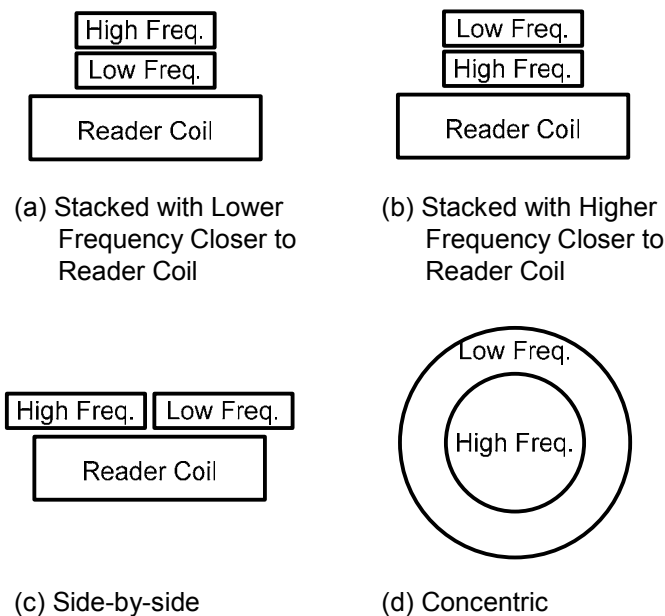


Figure 3-14 Arrangement of Sensor Pairs Tested in Parametric Study III

The concentric arrangement of inductor coils resulted in the greatest amount of mutual inductance and shielding of the higher frequency circuit. The side-by-side arrangement of inductor coils results in virtually no mutual inductance or shielding. In the stacked arrangements, the lower frequency circuit had a much larger shielding effect on the higher frequency circuit when it was closer to the reader coil than the higher frequency had on the lower frequency.

Because the sensing circuit includes a steel wire that significantly reduces the quality of the phase response from that circuit, the reference circuit should be placed in the position that reduces or eliminates shielding of the sensing circuit response. Therefore, the sensing circuit is best suited for lower frequencies when a reference circuit is present and the sensing circuit should always be closer to the reader coil for best response from the sensing circuit. In further sensor development, the sensing circuit should always be assigned a lower characteristic frequency than the reference circuit. This differs from the original improved

sensor [15], which had a sensing frequency that was higher than the reference frequency.

3.4 IMPEDANCE MEASUREMENT

As discussed in Chapter 2, power and communication are provided for the sensors through wireless inductive coupling between the sensor and the reader coil, which is connected to an impedance analyzer. The primary factor that influences the quality of the measured impedance response of the sensor and, therefore, the phase dip, is the coupling efficiency between the two sensor circuits and the reader coil. As discussed in Section 3.3, the components used to fabricate the sensor influence coupling efficiency and the size of the phase dip. To a larger extent, the effect of measuring the impedance response of the sensor wirelessly affects the quality of the response. Although the impedance analyzer used to interrogate the sensors is suspected of having a major influence on the measured impedance, exploration of analyzer design is outside the scope of this research. Two factors affecting the wireless measurement of impedance response were explored as part of this research: read distance and reader coil design.

3.4.1 Read Distance

For corrosion sensors to be commercially viable, read distances through concrete of at least 6 to 8 in. are required. Interrogation of first generation sensors through concrete resulted in very small phase dips for embedment depths of only 1 in. (Fig. 2-10). Maximum read distance for the combination of reader coil used in the first generation sensor tests (2.0-in. diameter with a single turn of 24-gage copper magnet wire) and the basic sensor was approximately 1.5 in. Therefore, one of the most important goals for redesign of the sensors was to increase the practical range of read distances.

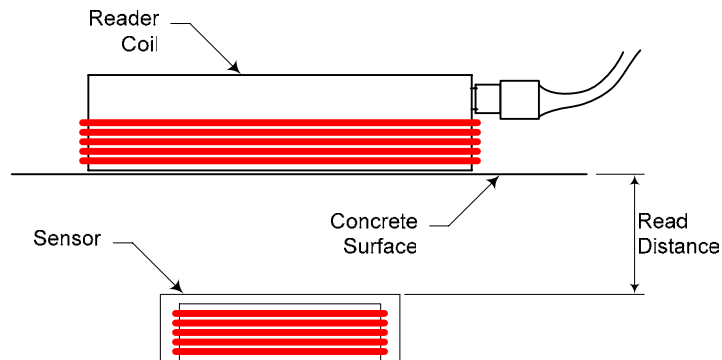


Figure 3-15 Definition of Read Distance

For the purposes of this research, read distance is defined as the distance between the adjacent edges of the sensor and the reader coil (Fig. 3-15). Read distance has the greatest effect on phase dip of all the parameters considered. Phase dips are greatly reduced with increasing read distance. For a given reader coil diameter and number of magnet wire turns, and a given inductor diameter and number of turns, phase dip may be reduced by as much as 80% with only a 0.5-in. increase in read distance. The maximum read distance was defined as the read distance where phase dips become less than 0.1° in air. This limit was selected because it is about two times the amplitude of the noise produced in readings with the Solartron Impedance Analyzer. Noise is the variation in baseline phase angle with varying frequency without any external sensor circuit present.

Results from Parametric Study I and II show the tremendous effect of read distance on the measured phase dip of sensors. Fig. 3-16 and 3-17 extend the discussion from the inductor comparison of Section 3.3.3 to include varying read distances. Fig. 3-16 shows phase dip plotted against inductor diameter for four different read distances: 0.0, 0.5, 1.0, and 1.5 in. All data shown in Fig. 3-16 are for sensors interrogated in air. For the 2.0-in. nominal inductor diameter, data from Parametric Study II correspond to a sensor with 5-turns of 18-gage magnet wire. The remaining data correspond to sensors with 7-turns of 24-gage magnet

wire from Parametric Study I. Fig. 3-17 shows phase dip on a log scale plotted against number of turns for the same four read distances. In this figure, sensors with a constant 1.25-in. nominal inductor diameter with 24-gage copper magnet wire were interrogated in air.

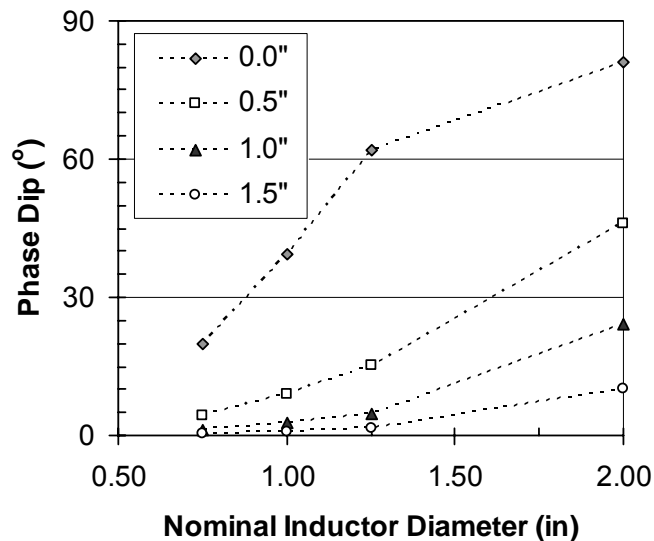


Figure 3-16 Effect of Read Distance on Phase Dip with Varying Inductor Diameter

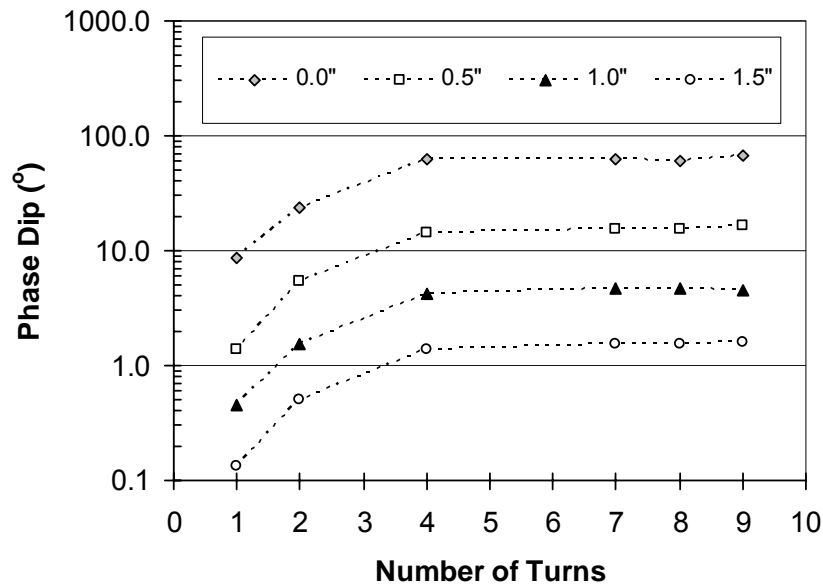


Figure 3-17 Effect of Read Distance on Phase Dip with Varying Number of Magnet Wire Turns

For a given reader coil diameter and number of turns, larger diameter inductors provide larger phase dips and greater coupling efficiency, which results in larger maximum read distances. Inductors fabricated with nominal diameters less than 1.25 in. (used in first generation basic sensors) generally resulted in substantially reduced phase dips. This would make the smaller diameter inductors unsuitable for use in the sensing circuit because the phase dip would be further reduced when a steel wire is added to the circuit. Inductors fabricated using 2.0-in. nominal diameter PVC pipe are best suited for the sensing circuit, because they give the largest phase dips and the largest maximum read distance.

3.4.2 Reader Coil

In addition to read distance, the configuration of the reader coil affects coupling efficiency and the amplitude of phase dips. The reader coil is simply an

inductor attached to the impedance analyzer directly or with a cable. Reader coils were constructed by hand-winding copper magnet wire around a suitable round form – plastic concrete cylinder molds worked well. The original reader coil used in tests by Andringa [5], Grizzle [9], and Simonen [15] was constructed using a 2-in. diameter Petri dish lid with a single turn of 24-gage copper magnet wire. In order to determine the effect of reader coil diameter and number of magnet wire turns on the measured phase response of sensors, seven other reader coils were constructed and tested. Figure 3-18 shows a photograph, and Table 3-1 gives the details of each reader coil. Reader coils were labeled based on diameter and number of magnet wire turns, where the first number is the nominal diameter of the form in inches, the next letter designates the type of reader coil: “t” for constant diameter coils and “s” for flat spiral coils, and the last digits indicate the number of magnet wire turns and magnet wire gage, if necessary.

Table 3-1 Experimental Reader Coils

Reader Coil	Diameter (in.)	Number of Turns	Magnet Wire Gage
2t01*	2	1	24
3t01	3	1	24
4t01-24	4	1	24
4t01-18	4	1	18
4t05	4	5	18
4t20	4	20	18
6t10	6	10	18
3s	3	**	18

* Original reader coil

** Flat spiral configuration

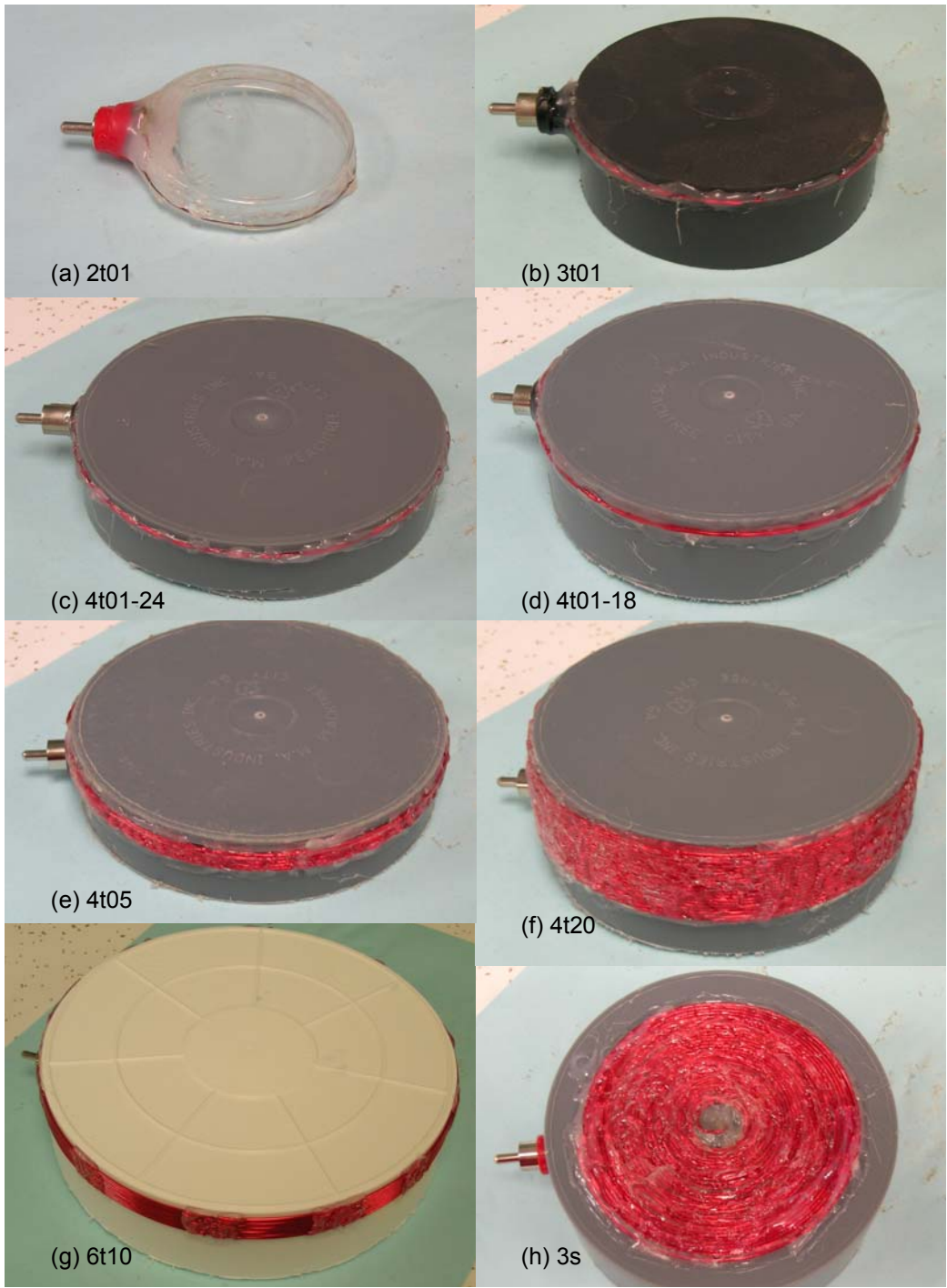
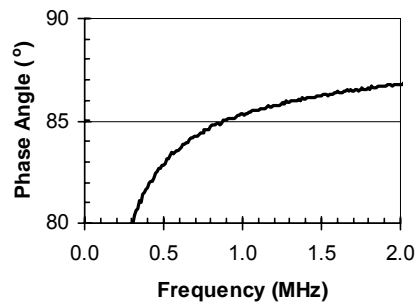


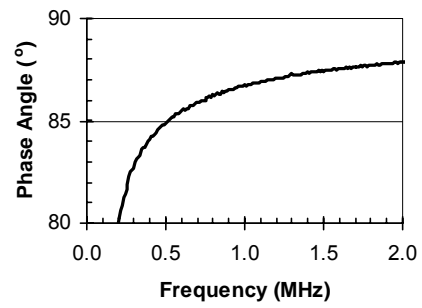
Figure 3-18 Reader Coil Photographs

Because the impedance response of the sensor is measured through the reader coil, the electrical properties of the reader coil influence the measured response of each sensor. Each reader coil has an effective inductance, resistance, and capacitance that may interfere with the response of the sensor if it is not designed properly. An ideal reader coil would give a baseline phase response of 90° for all frequencies. Because practical reader coils are hand-wound with copper magnet wire that has a finite resistance and an effective capacitance due to the electrical connections, the baseline phase responses of reader coils used to interrogate sensors are not ideal.

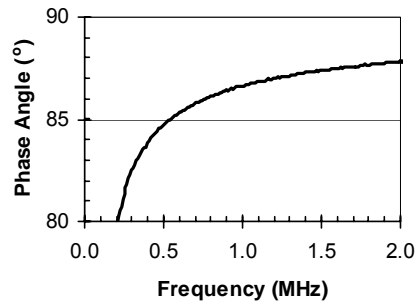
In order to compare the baseline response of reader coils experimentally, a frequency range from 100 kHz to 2.1 MHz was selected. In Fig. 3-19, the baseline phase response of each reader coil attached directly to the Solartron Impedance Analyzer without any sensor present is shown. Reader coils 4t20 and 6t10 had the best baseline phase response with the reader coil directly attached. Fig. 3-20 shows the baseline phase response of each reader coil attached to the Solartron Impedance Analyzer with a 3-ft long cable. The cable will be necessary for field interrogation of sensors and for laboratory tests on large-scale slabs. With the cable present, reader coils 3s and 4t20 exhibit some unstable behavior for frequencies above 1.5 MHz. Reader coil 6t10 also shows a declining baseline phase angle for frequencies near 2.0 MHz and above. Therefore, reader coil 4t05 is the best reader coil for interrogations when the reader coil is attached with a cable. All of these conclusions apply only for the range of frequencies tested.



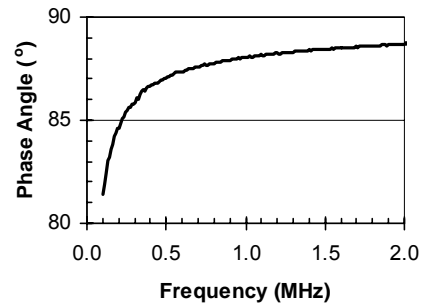
(a) 2t01



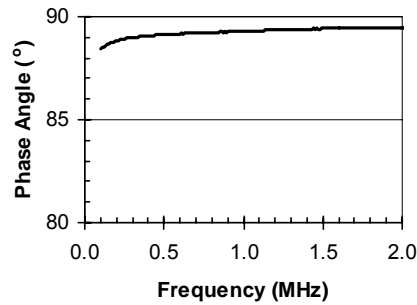
(b) 3t01



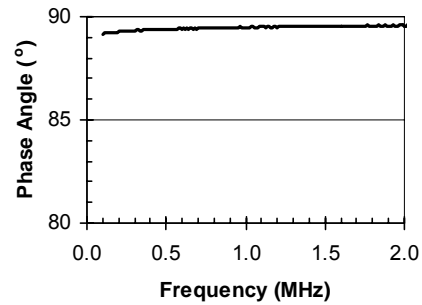
(c) 4t01-24



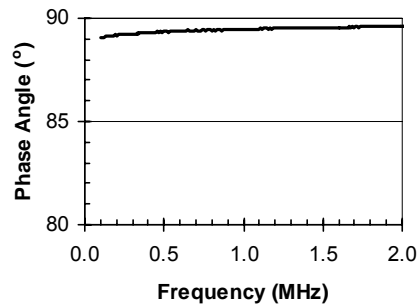
(d) 4t01-18



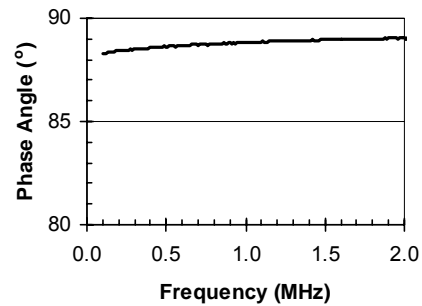
(e) 4t05



(f) 4t20

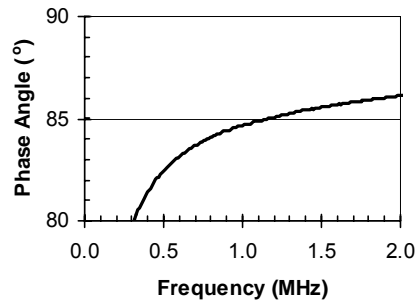


(g) 6t10

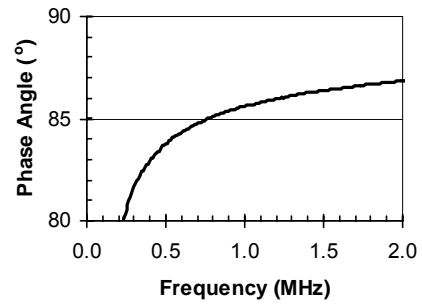


(h) 3s

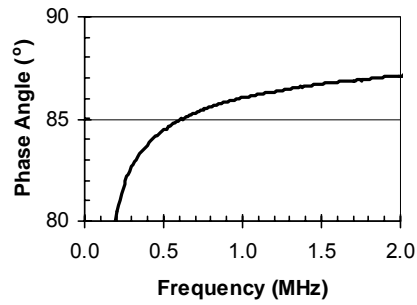
Figure 3-19 Baseline Phase Response of Reader Coils Attached Directly to Impedance Analyzer



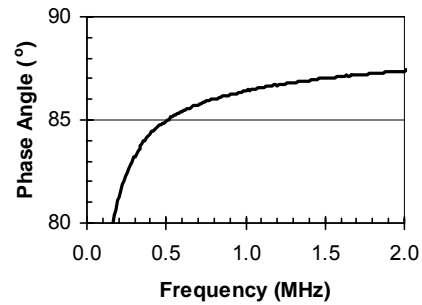
(a) 2t01



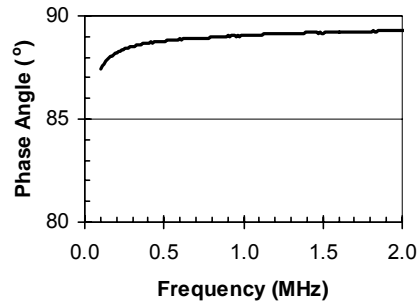
(b) 3t01



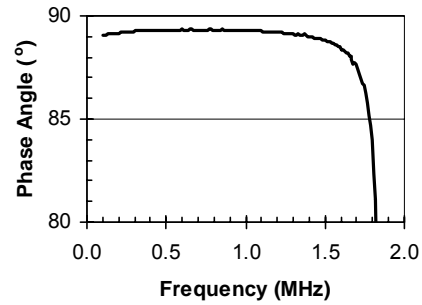
(c) 4t01-24



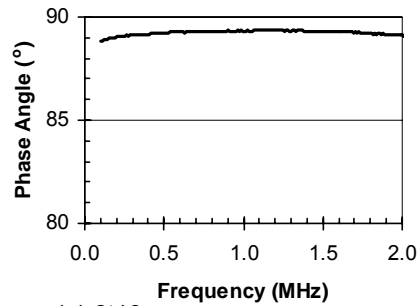
(d) 4t01-18



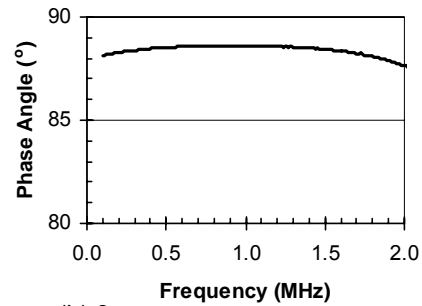
(e) 4t05



(f) 4t20



(g) 6t10



(h) 3s

Figure 3-20 Baseline Phase Response of Reader Coils Attached to Impedance Analyzer with 3-ft Cable

For lower frequencies (in the 100 kHz range), smaller reader coils with fewer turns show a very curved baseline response (Fig. 3-19). At higher frequencies, the differences among reader coil baseline responses are less pronounced. In general, reader coils with a larger inductance result in a baseline response closer to 90° for a wider range of frequencies, but this behavior changed when the coils were connected to the Solartron Impedance Analyzer with the cable. Overall, reader coil 4t20 was selected as the best for interrogations with the reader coil directly attached to the impedance analyzer. Reader coil 4t05 was the best for interrogations with the reader coil attached to the impedance analyzer with a 3-ft cable.

The reader coil also affects the amplitude of the phase dip at different read distances. For a given sensor inductor diameter, there is a different optimum reader coil diameter to produce the deepest phase dip at each read distance as shown by Nainani [12]. In general, larger diameter reader coils resulted in greater maximum read distances. This indicates that the coupling of larger diameter reader coils with smaller sensor inductor coils allows a greater read range. However, larger diameter reader coils also resulted in smaller phase dips for small read distances, indicating reduced coupling for reader coils and sensor inductor coils with different diameters. This effect will be discussed further in Chapter 4.

3.5 ENVIRONMENTAL INFLUENCE

From tests of first generation sensors described in Chapter 2, external environmental factors play a role in sensor response. Two types of environmental factors were explored as part of this research: temperature and conductivity of the surrounding environment.

3.5.1 Temperature

The effect of temperature on the phase response of first generation sensors is evident from tests on small concrete prisms with basic sensors embedded with 1 in. of concrete cover. In Fig. 3-21a, the phase response of sensor 4a is shown at room temperature (approximately 70 °F). The phase response of the same sensor after 24 hours in an oven at 230 °F is shown in Fig. 3-21b and after 24 hours in a freezer at -15 °F in Fig. 3-21c.

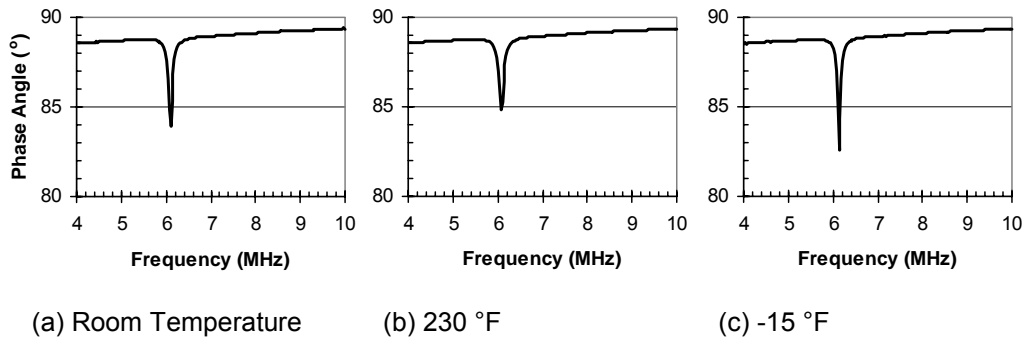


Figure 3-21 Effect of Temperature on Phase Response of Sensor 4a

The change in response of sensor 4a due to temperature is summarized in Table 3-2. Because the electrical properties of sensor components change slightly with temperature, the response of sensors also depends on temperature. However, the changes in characteristic frequency and phase dip for a very large temperature range are small. Therefore, temperature is expected to have a minor effect on sensor response. Temperature changes should not impact the ability to interrogate the sensors or the ability to determine the state of the steel sensing wire.

Table 3-2 Summary of Temperature Effects on Sensor 4a

Temperature (°F)	Characteristic Frequency (MHz)	Phase Dip (°)
-15	6.13	6.2
70	6.10	4.9
230	6.07	4.0

3.5.2 Surrounding Environment

Results of first generation sensor testing by Simonen [15] showed that environmental factors such as moisture and chlorides may influence sensor response. In Chapter 2, tests of first generation sensors confirmed that a conductive surrounding environment can result in “transition” behavior of sensors that is similar to measurements from basic sensors embedded in reinforced concrete slabs that were saturated with salt water. Parametric Study I concluded that the effect of a conductive environment on a completely sealed sensor is minimal. However, the presence of a sensing wire exposed to the environment in Parametric Study II gives evidence that sensor behavior can be more complex for broken sensing wires in the presence of a conductive environment.

For sensor circuits that are completely sealed by an impervious potting material, very little difference in phase dip occurs as the conductivity of the surrounding environment increases. A slight reduction in phase dip occurs with the change from air to tap water. This reduction is generally about 5-10% of the phase dip in air. Although the tap water may have some effect, the small decrease in phase dip may be due to the test method. In order to test the sensors in water, a beaker must be placed over the reader coil to contain the water. The thickness of the glass bottom of the beaker increases the read distance slightly. This increased read distance for readings in tap water probably results in the majority of the

reduction in phase dip. A larger reduction in phase dip occurs with the change from tap water to salt water. This reduction is generally about 20-40% of the phase dip in tap water. So, while the increased conductivity of salt water does have a slightly parasitic effect on readings, the reduction in phase dip is not sufficient to shield sensor response completely. In general, the maximum read distance in salt water was about 0.5-in. less than the maximum read distance in air and tap water.

Fig. 3-22 shows phase dip plotted against inductor diameter for completely sealed sensors with 7 turns of magnet wire interrogated at 0.5-in. read distance in air, tap water, and salt water. Clearly, the difference between interrogations in air and tap water is much smaller than the difference between interrogations in tap water and salt water.

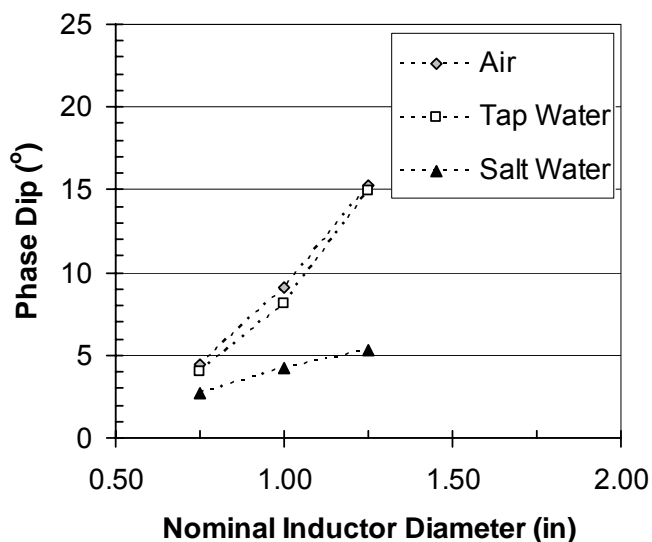


Figure 3-22 Effect of Surrounding Environment on Phase Dip for Completely Sealed Sensors of Varying Diameter

For sensors with exposed steel sensing wires, the response of sensors with intact wires is similar to the behavior of completely sealed sensors, where the

presence of a conductive environment only reduces the phase dips slightly. Transition behavior occurred with broken sensing wires exposed to conductive environments for all trial sensors constructed and tested as part of this research. Results from two trial sensors are presented in Appendix B.

Initially, reducing the inductance and increasing the capacitance of the sensor circuit while maintaining the characteristic frequency in the same 4-10 MHz range as the first generation sensors was proposed to reduce or eliminate environmental effects. However, the required values of inductance were too small to be practical and would diminish the maximum read distance and the size of phase dips. Therefore, a lower frequency range in the 100 kHz to 4 MHz range was selected so that larger values of capacitance could be used with inductors of similar values of inductance as those used in first generation sensors. Although environmental effects could not be eliminated, the differences in phase response between an intact wire and a broken wire for the same sensor interrogated with the same conductive surrounding environment were accentuated. Also, the threshold of conductivity at which the sensing characteristic frequency reappears for broken steel sensing wires was raised. This is expected to make the sensors less sensitive to a concrete environment saturated with salt water.

3.6 CONCLUSIONS

Exploration into sensor design parameters identified the factors with the greatest influence on sensor performance. Practical recommendations for sensor redesign may be derived from this information. In addition, results of sensor testing led to three major conclusions:

- 1) Read distance can be improved by using larger diameter inductors in the sensors and optimizing the reader coils, but the goals to minimize sensor size and increase the read distance are contradictory. Further

improvement to maximum read distance by increasing the diameter of the sensor inductor or reader coil is impractical. Further research into interrogation equipment is needed to make the maximum read distance at least 6 in. through concrete.

- 2) An appropriate circuit model for the sensor includes a variable resistor for the external sensing wire rather than a switch. This would account for sensor response in the presence of an electrically conductive environment.
- 3) Because the state of the steel sensing wire cannot be detected using the characteristic frequencies of the sensor alone, further signal processing of the sensor phase response is necessary to determine the difference between an intact sensing wire and a broken sensing wire.

3.6.1 Resistance Model of Steel Sensing Wire

The steel sensing wire is detrimental to the quality of the measured phase response because of the inherent resistance of the material. However, the use of a steel sensing wire is central to the corrosion sensor concept and cannot be avoided. The presence of an electrically conductive environment can complete the circuit when the sensing wire is not intact. Therefore, an appropriate circuit model for the sensor would include a variable resistor for the external sensing wire rather than a switch. When the steel sensing wire is intact, the resistance is small and does not change significantly as corrosion occurs. Once a threshold of corrosion occurs that is adequate to break the wire, the increase in resistance is significant, but varies depending on the conductivity of the surrounding environment. For further sensor development, the full circuit diagram including the interrogation equipment and sensor is shown in Fig. 3-23. Using this model for the sensor circuit, it may be possible to obtain analog information about the

state of the sensor and/or the conductivity of the environment rather than binary information as proposed in the conceptual design of first generation sensors.

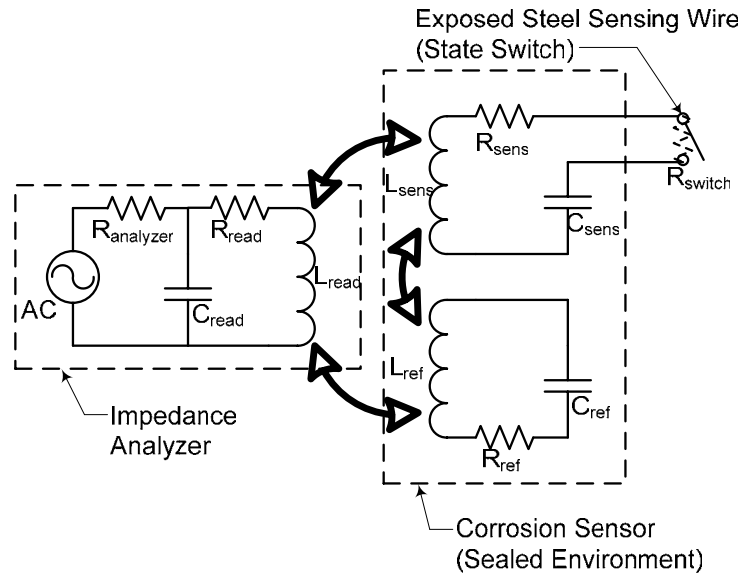


Figure 3-23 Complete Sensor Circuit Diagram

3.6.2 Signal Processing

For the range of characteristic frequencies examined in the tests described in this chapter, the effect of an electrically conductive environment on sensor response is a property of the sensing mechanism. It is not possible to design a sensor that is not influenced by the conductivity of the surrounding environment. The sensor can, however, be designed to be more or less sensitive to a particular conductivity by adjusting the capacitance and inductance of the sensor, but in the field, the environment around the sensor cannot be controlled and transition behavior should be expected. Fortunately, even though a phase dip appears at the sensing characteristic frequency beyond a certain threshold of conductivity of the surrounding environment, the shape of the phase response is different for an intact

wire than for a broken wire. Further signal processing may be used to determine the difference between an intact sensing wire and a broken sensing wire.

The signal processing algorithms are still being developed and tested, so further advances are expected in time. Currently, signal processing algorithms involve curve-fitting of the baseline using a fifth order inverse polynomial, fitting the phase dips with Lorentzian line-shapes, and calculating the pseudo-quality factor for each phase dip. An example of the signal processing method used to evaluate the response of the second generation sensors in this thesis is provided in Appendix D. The pseudo-quality factor is believed to be sufficiently sensitive to distinguish between a phase dip due to current through an intact sensing wire and a phase dip due to current through a conductive environment. This factor represents the coupling efficiency between the reader coil and the sensor circuits for a particular read distance and, with future development, may even be used to determine the resistance, temperature, or other properties of the sensor circuits. In order to verify that the pseudo-quality factor is a valid quantitative measure of the state of the steel sensing wire, additional testing will be necessary.

3.6.3 Summary of Recommendations for Sensor Redesign

The following items should be considered in corrosion sensor redesign:

- 1) Use only high-quality ceramic capacitors for sensor fabrication.
- 2) Use 18-gage copper magnet wire for inductor fabrication.
- 3) Only 5-turns of magnet wire are necessary to achieve a good balance between fabrication time and quality of sensor response.
- 4) Larger diameter inductors improve sensor performance, but sensors should be as small as possible. The maximum nominal inductor diameter should be 2 in.

- 5) Larger diameter inductors are recommended for circuits with steel sensing wires because the quality of sensor response is reduced due to the presence of the steel wire.
- 6) The sensing circuit for new sensors should be simplified to include only a single capacitor and a steel sensing wire in series with a single inductor (Fig. 3-11).
- 7) A reference circuit is required for new sensors and should resonate at a higher frequency than the sensing circuit.
- 8) Concentric and side-by-side arrangements of sensing circuit and reference circuit inductors should be considered for new sensors.
- 9) The reader coil should be optimized to achieve the maximum possible read distance and the best possible baseline response in the required range of characteristic frequencies.
- 10) Lower values of inductance and higher values of capacitance should raise the threshold conductivity of the surrounding environment at which the sensing circuit will respond at its characteristic frequency with a broken steel sensing wire. This is expected to make the sensor less sensitive to concrete saturated with salt water and reduce the possibility of transition behavior. Lower characteristic frequencies in the range of 100 kHz to 1 MHz may be used to achieve this goal.
- 11) Testing is necessary to determine the maximum read distance and environmental effects of temperature and conductivity of the surrounding environment.
- 12) In addition to visual interpretation of the phase response, quantitative signal processing should be used to evaluate sensor performance.

CHAPTER 4

Second Generation Sensor Design

4.1 INTRODUCTION

Second generation sensors were designed using an iterative process of trial sensor fabrication and preliminary testing. The trial sensors were selected based on the goals of reducing the sensor size, improving read range, and reducing the sensitivity to environmental effects. Two trial sensors with the best performance observed in preliminary tests were selected for thorough calibration testing and embedded in concrete for corrosion testing. In this chapter, the design of each second generation sensor is discussed, important design considerations are presented, and a summary of results from second generation sensor calibration is presented.

4.2 DESIGN CONSIDERATIONS

Second generation sensors were developed using the recommendations from exploration of sensor design parameters and the experience gained from building and testing several trial sensors. The major features of second generation sensor design that are different from first generation sensors include: (1) simplified circuit with a single inductor and capacitor in series with the steel sensing wire, (2) reference circuit with a higher characteristic frequency than the sensing circuit, and (3) larger capacitances and lower characteristic frequencies in both circuits. The use of alternative arrangements for sensing and reference circuits within the sensors is expected to improve sensor performance, as are the improved reader coil designs. Using a computer algorithm for signal processing of the phase response of the sensors will make more quantitative evaluation of

sensor behavior possible. Based on the recognition that sensor response is not simply binary, the sensor calibration process should involve testing in environments with varying conductivity to determine if the state of the steel sensing wire can be determined in the presence of a conductive environment.

4.3 CONCENTRIC SENSOR

The concentric sensor is so named because the smaller inductor coil of the reference circuit fits inside the larger inductor coil of the sensing circuit. With this orientation of coils, strong mutual inductance between the sensing and reference circuits would be expected. Therefore, when the steel sensing wire is intact, neither circuit response is independent of the other. This produces a dramatic change in the phase response of the sensor between intact wire and broken wire states.

4.3.1 Circuits

The concentric sensor design consists of a simple RLC reference circuit that is completely sealed and an RLC sensing circuit with an exposed steel sensing wire, which acts as a variable resistor. A complete circuit diagram including the impedance analyzer is provided in Fig. 4-1. Approximate values of inductance and capacitance are given in Table 4-1.

Table 4-1 Circuit Parameters for Concentric Sensor

	Sensing Circuit	Reference Circuit
Approximate Inductance (L)	3.0 μ H	2.0 μ H
Capacitance (C)	33,000 pF	6,800 pF

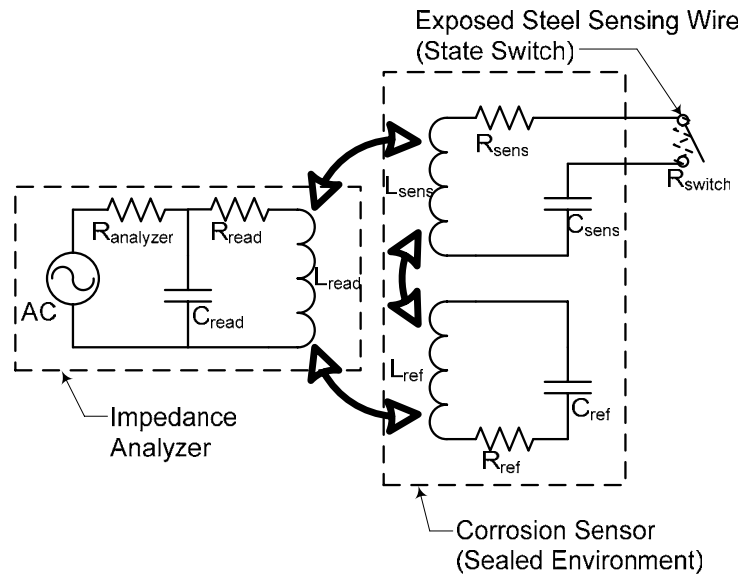


Figure 4-1 Circuit Diagram for Second Generation Sensors

4.3.2 Materials

As shown in Fig. 4-2, the sensing circuit components include an inductor made from five turns of 18-gage copper magnet wire around a 0.5-in. slice of PVC pipe with a nominal diameter of 2 in., a 33,000-pF ceramic capacitor, and a steel sensing wire. The reference circuit components include an inductor made from five turns of 18-gage copper magnet wire around a 0.5-in. slice of PVC pipe with a nominal diameter of 1.25 in., and a 6,800-pF ceramic capacitor. The sensors are potted using marine epoxy to seal and protect the sensor components from the environment within the concrete. Steel wire sizes chosen for testing of the concentric sensor were 26 and 21 gage. A photograph of a completed concentric sensor with a 21-gage steel sensing wire is shown in Fig. 4-3.

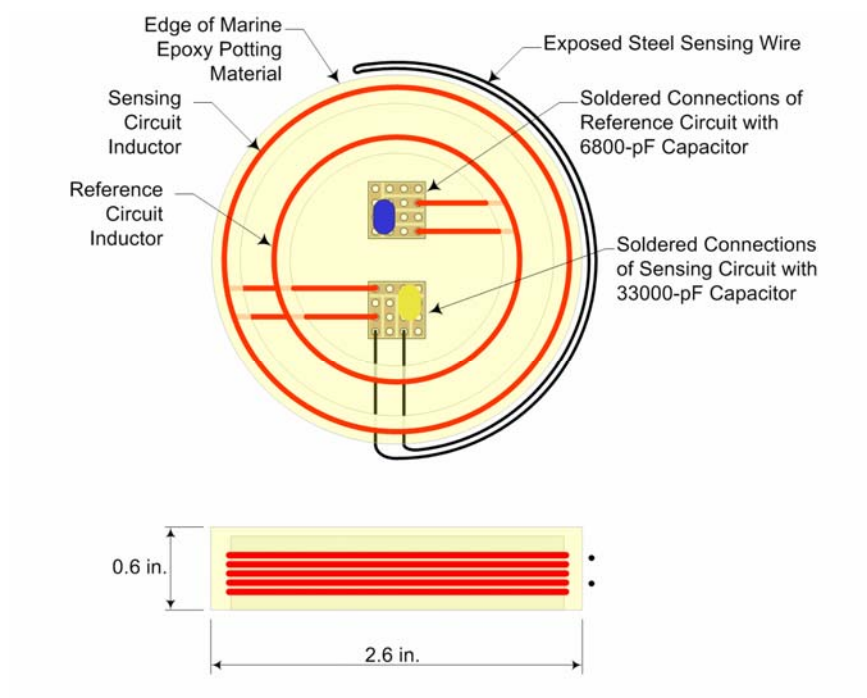


Figure 4-2 Configuration of Concentric Sensor



Figure 4-3 Photograph of Concentric Sensor

4.3.3 Fabrication

Detailed instructions for fabrication of concentric sensors are provided in Appendix E. Fabrication was done completely by hand, requiring only simple tools. For this project, forty concentric sensors were fabricated. The 30 sensors with 26-gage steel sensing wires were labeled B01 through B30 and the 10 sensors with 21-gage steel sensing wires were labeled B51 through B60.

4.3.4 Response

Preliminary tests of sensors not embedded in concrete were used to calibrate sensor response. The calibration technique involved testing representative sensors with intact and cut sensing wires in three different environments: air, tap water, and varying concentrations of salt water. Tests were carried out using different reader coils and with varying read distances. Complete results from calibration testing are presented in Appendix F. Selected results are discussed in this section.

Sensor response is compared in Appendix F using characteristic frequencies, phase dips, and pseudo-quality factors. The method of obtaining these values is provided in Appendix D. In this section, conclusions about the reliability of characteristic frequencies and pseudo-quality factors are presented that enable the interpretation of sensor response for sensors embedded in concrete.

4.3.4.1 Baseline Response in Air

The concentric sensor initially responds at two different characteristic frequencies. The reference frequency is about 1.6 MHz and the sensing frequency is about 0.5 MHz. Because the inductor coils are concentric, the mutual inductance between the reference and sensing circuits is strong. Therefore, the lower characteristic frequency and larger inductance of the sensing circuit shields the reference circuit response when the steel sensing wire is intact. As shown in

Fig. 4-4a, the reference circuit phase dip is smaller than the sensing circuit phase dip, even though the reference circuit does not include the added resistance of the steel wire. When the steel sensing wire is broken, the sensing frequency disappears and no longer shields the reference circuit response, as shown in Fig. 4-4b. In this state, the sensor responds at a single characteristic frequency of about 1.4 MHz.

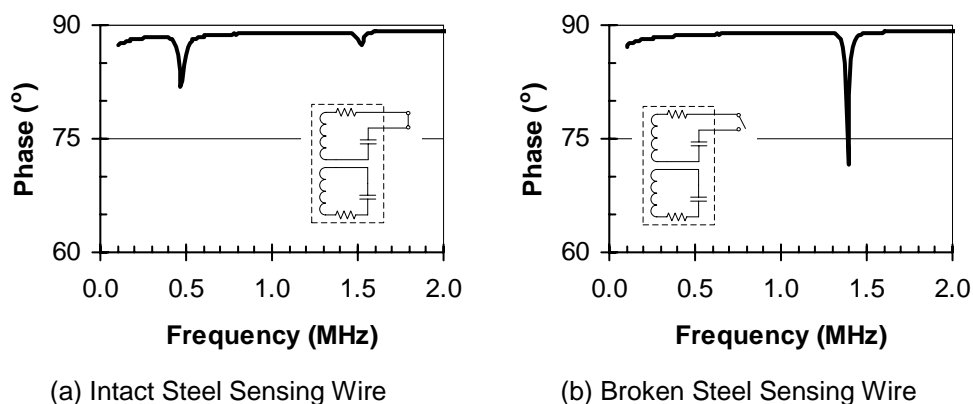


Figure 4-4 Concentric Sensor Phase Response

4.3.4.2 Influence of Surrounding Environment

The presence of a conductive environment has little effect on the response of concentric sensors with intact steel sensing wires. The sensor responds at two different characteristic frequencies. When the steel sensing wire is intact, the pseudo-quality factor for the sensing circuit should always be greater than 6 for sensors with 26-gage steel sensing wires. For sensors with intact 21-gage steel sensing wires, the pseudo-quality factor for the sensing circuit should always be greater than 10.

Sensors with cut or broken steel sensing wires have a more complex response in the presence of a conductive environment. As shown in Appendix F, tests of concentric sensors in varying concentrations of salt water resulted in

transition behavior. The sensing circuit characteristic frequency appears for concentrations of salt water greater than 0.5%. The phase response of a concentric sensor in a 3.5% concentration of salt water is shown in Fig. 4-5 for both intact and broken steel sensing wires. Visually, the responses are very similar. However, the pseudo-quality factor of the sensing circuit can be used to evaluate sensor response and determine the state of the steel sensing wire. The steel sensing wire can be assumed to be broken even if the characteristic frequency of the sensing circuit is present if the corresponding pseudo-quality factor is less than 5 for sensors with 26-gage steel sensing wires. For 21-gage steel sensing wires, the sensing wire can be assumed to be broken even if the characteristic frequency of the sensing circuit is present if the corresponding pseudo-quality factor is less than 6. If the characteristic frequency of the sensing circuit is not present, then the sensing wire is broken. Pseudo-quality factors for the sensing circuit of a concentric sensor with a 26-gage steel sensing wire are shown plotted against salt water concentration in Fig. 4-6.

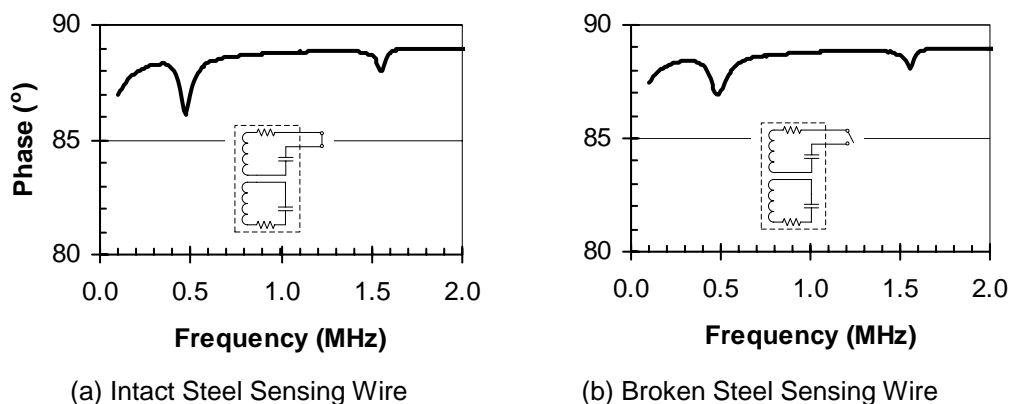


Figure 4-5 Phase Response of Concentric Sensor in 3.5% Salt Water

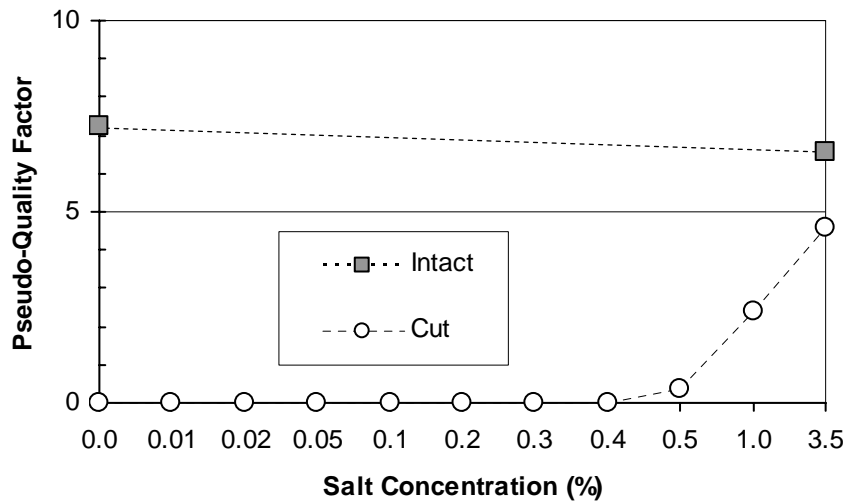


Figure 4-6 Pseudo-Quality Factor for Concentric Sensor with 26-gage Steel Sensing Wire in Varying Concentrations of Salt Water

4.3.4.3 Influence of Read Distance and Reader Configuration

The ability to obtain a reading from sensors is directly related to the read distance (defined in Chapter 3). Phase dips are greatly reduced with increasing read distance. Maximum read distances for concentric sensors with different reader coils are given in Appendix F. For the 4-in. diameter reader coil with 5 turns of 18-gage copper magnet wire attached to the impedance analyzer with a 3-ft cable used for all interrogations of sensors embedded in concrete, the maximum read distance of concentric sensors with 26 and 21-gage steel sensing wires was 3 in. Maximum read distance is defined as the read distance at which the phase dip is at least 0.1° for interrogations in air.

When interrogated at different read distances and using different reader coils, the characteristic frequencies do not change and the variation in pseudo-quality factors is small. Therefore, if the measured phase dip is greater than 0.1° ,

the characteristic frequencies and pseudo-quality factors are reliable at all read distances and with different reader configurations.

4.4 COPLANAR SENSOR

The coplanar sensor is so named because the inductor coils of the sensing and reference circuits are arranged side-by-side in the same plane. With this orientation of coils, virtually no mutual inductance occurs between the sensing and reference circuits. Therefore, when the steel sensing wire is intact, the two circuits are independent. In this design, the phase response of the reference circuit should not change between the intact wire and broken wire states. The sensing circuit responds at its characteristic frequency with an intact sensing wire, but completely disappears with a broken sensing wire.

4.4.1 Circuits

The coplanar sensor design consists of a simple RLC reference circuit that is completely sealed and an RLC sensing circuit with an exposed steel sensing wire, which acts as a variable resistor. A complete circuit diagram including the impedance analyzer is provided in Fig. 4-1. Approximate values of inductance and capacitance are given in Table 4-2.

Table 4-2 Circuit Parameters for Coplanar Sensor

	Sensing Circuit	Reference Circuit
Approximate Inductance (L)	2.0 μ H	2.0 μ H
Capacitance (C)	33,000 pF	6,800 pF

4.4.2 Materials

As shown in Fig. 4-7, the sensing circuit components include an inductor made from five turns of 18-gage copper magnet wire around a 0.5-in. slice of PVC pipe with a nominal diameter of 1.25 in., a 33,000-pF ceramic capacitor, and a steel sensing wire. The reference circuit components include an inductor made from five turns of 18-gage copper magnet wire around a 0.5-in. slice of PVC pipe with a nominal diameter of 1.25 in., and a 6,800-pF ceramic capacitor. The sensors are potted using marine epoxy to seal and protect the sensor components from the environment within the concrete. Steel wire sizes chosen for testing of the coplanar sensor were 26 and 21 gage. A photograph of a completed coplanar sensor with a 21-gage steel sensing wire is shown in Fig. 4-8.

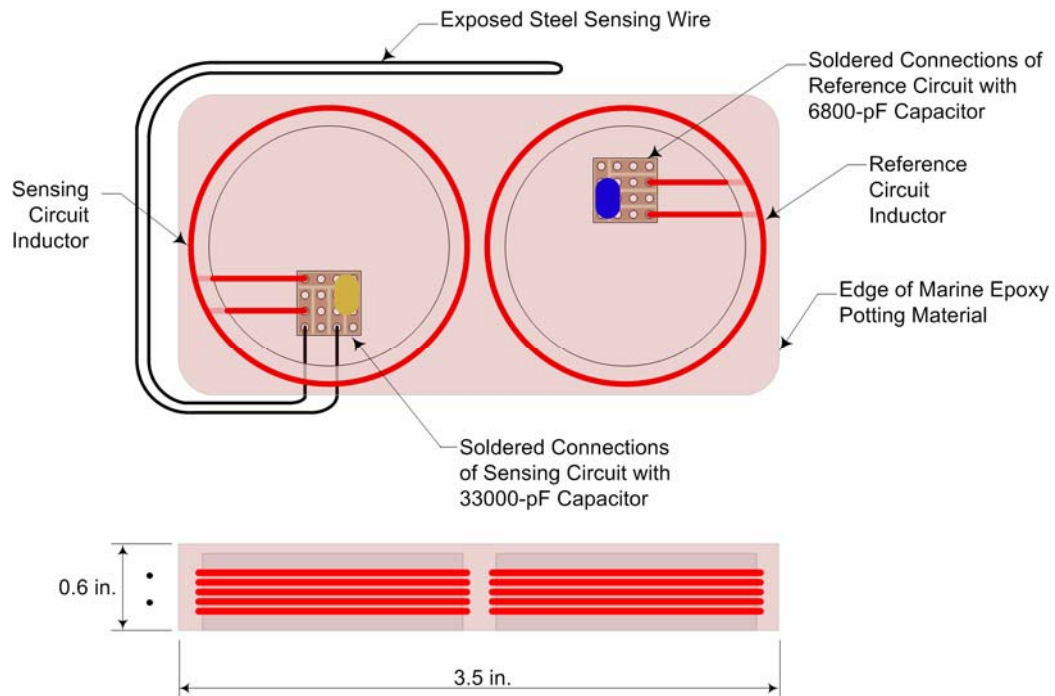


Figure 4-7 Configuration of Coplanar Sensor



Figure 4-8 Photograph of Coplanar Sensor

4.4.3 Fabrication

Detailed instructions for fabrication of coplanar sensors are provided in Appendix E. Fabrication was done completely by hand, requiring only simple tools. For this project, thirty-five coplanar sensors were fabricated. The 25 sensors with 26-gage steel sensing wires were labeled A01 through A15 and A21 through A30. The 10 sensors with 21-gage steel sensing wires were labeled A51 through A60.

4.4.4 Response

Preliminary tests of sensors not embedded in concrete were used to calibrate sensor response. The calibration technique involved testing representative sensors with intact and cut sensing wires in three different environments: air, tap water, and varying concentrations of salt water. Tests were carried out using different reader coils and with varying read distances. Complete

results from calibration testing are presented in Appendix F. Selected results are discussed in this section.

Sensor response is compared in Appendix F using characteristic frequencies, phase dips, and pseudo-quality factors. The method of obtaining these values is provided in Appendix D. In this section, conclusions about the reliability of characteristic frequencies and pseudo-quality factors are presented that enable the interpretation of sensor response for sensors embedded in concrete.

4.4.4.1 Baseline Response in Air

The concentric sensor initially responds at two different characteristic frequencies. The reference frequency is about 1.4 MHz and the sensing frequency is about 0.6 MHz. Because the inductor coils are side-by-side, the mutual inductance between the reference and sensing circuits is essentially zero. Therefore, the characteristic frequencies of sensor circuits are independent. As shown in Fig. 4-9a, the sensing circuit phase dip is smaller than the reference circuit phase dip due to the added resistance of the steel wire. The sensing circuit phase dip is smaller for coplanar sensors than it was for the concentric sensors because of the smaller diameter inductor used in the coplanar sensors. When the steel sensing wire is cut, the sensing frequency disappears and the reference circuit response remains essentially unchanged, as shown in Fig. 4-9b. In this state, the sensor responds at a single characteristic frequency of about 1.4 MHz.

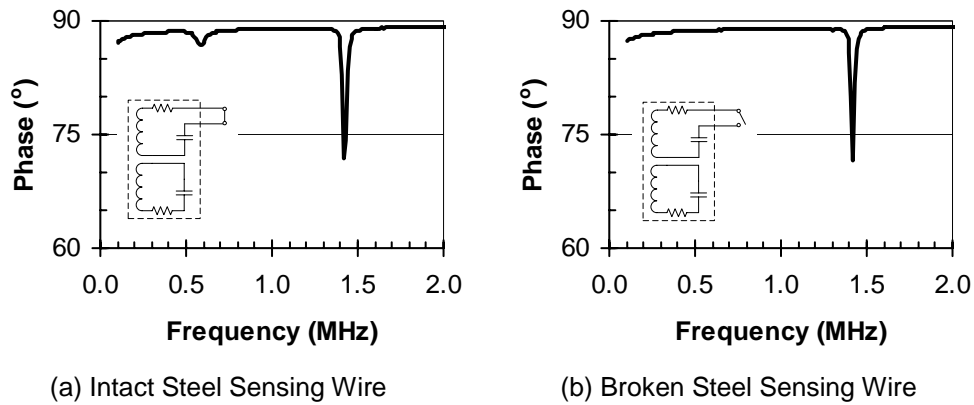


Figure 4-9 Coplanar Sensor Phase Response

4.4.4.2 Influence of Surrounding Environment

The presence of a conductive environment has little effect on the response of coplanar sensors with intact steel sensing wires. The sensor responds at two different characteristic frequencies. When the steel sensing wire is intact, the pseudo-quality factor for the sensing circuit should always be greater than 4.5 for sensors with 26-gage steel sensing wires. For sensors with intact 21-gage steel sensing wires, the pseudo-quality factor for the sensing circuit should always be greater than 7.

Sensors with cut or broken steel sensing wires have a more complex response in the presence of a conductive environment. As shown in Appendix F, tests on coplanar sensors in varying concentrations of salt water resulted in transition behavior. The sensing circuit characteristic frequency appears for concentrations of salt water greater than 0.5%. The phase response of a coplanar sensor in a 3.5% concentration of salt water is shown in Fig. 4-10 for both intact and broken steel sensing wires. Visually, the responses are very similar. However, the pseudo-quality factor of the sensing circuit can be used to evaluate sensor response and determine the state of the steel sensing wire. The steel

sensing wire can be assumed to be broken even if the characteristic frequency of the sensing circuit is present if the corresponding pseudo-quality factor is less than 4 for sensors with 26-gage steel sensing wires. For 21-gage steel sensing wires, the sensing wire can be assumed to be broken even if the characteristic frequency of the sensing circuit is present if the corresponding pseudo-quality factor is less than 5. If the characteristic frequency of the sensing circuit is not present, then the sensing wire is broken. Pseudo-quality factors for the sensing circuit of a coplanar sensor with a 26-gage steel sensing wire are shown plotted against salt water concentration in Fig. 4-11.

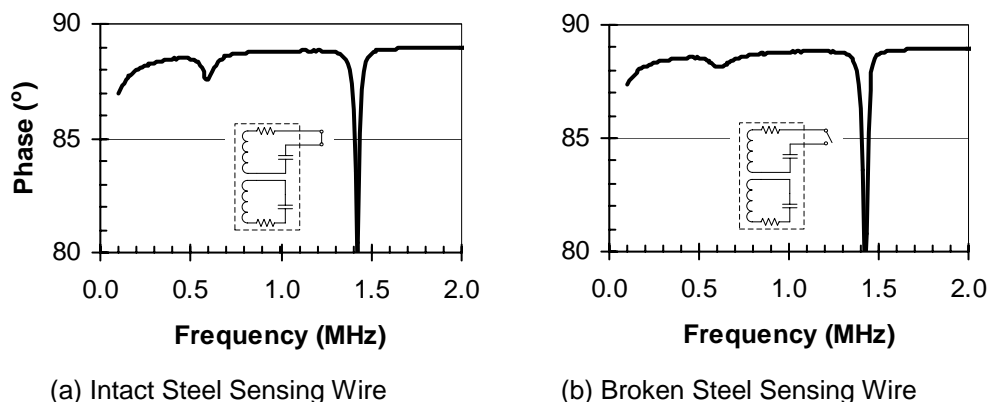


Figure 4-10 Phase Response of Coplanar Sensor in 3.5% Salt Water

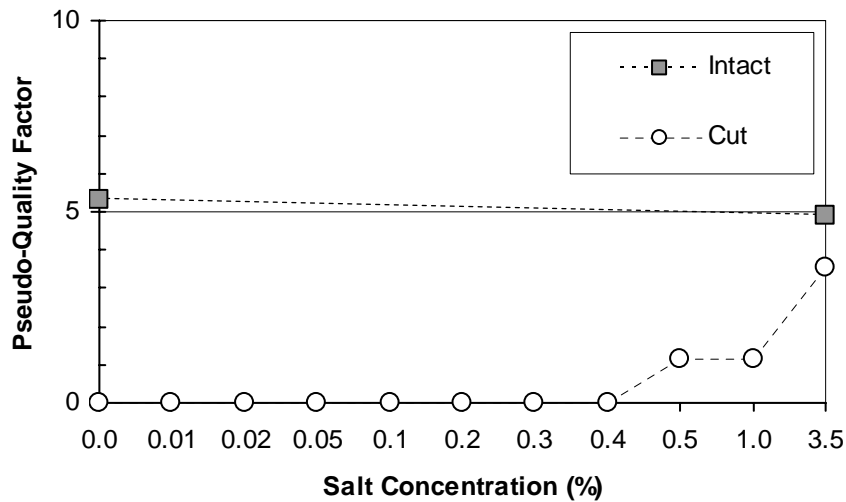


Figure 4-11 Pseudo-Quality Factor for Coplanar Sensor with 26-gage Steel Sensing Wire in Varying Concentrations of Salt Water

4.4.4.3 Influence of Read Distance and Reader Configuration

The ability to obtain a reading from sensors is directly related to the read distance (defined in Chapter 3). Phase dips are greatly reduced with increasing read distance. Maximum read distances for coplanar sensors with different reader coils are given in Appendix F. For the 4-in. diameter reader coil with 5 turns of 18-gage copper magnet wire attached to the impedance analyzer with a 3-ft cable used for all interrogations of sensors embedded in concrete, the maximum read distance of coplanar sensors with 26-gage steel sensing wires was 2-in. and the maximum read distance of coplanar sensors with 21-gage steel sensing wires was 3-in. Maximum read distance is defined as the read distance at which the phase dip is at least 0.1° for interrogations in air.

When interrogated at different read distances and using different reader coils, the characteristic frequencies do not change and the variation in pseudo-quality factors is small. Therefore, if the measured phase dip is greater than 0.1° ,

the characteristic frequencies and pseudo-quality factors are reliable at all read distances and with different reader configurations.

4.5 CONCLUSIONS

Overall, second generation sensors are vastly improved from first generation sensors. The amplitude of phase dips for the sensing circuits have been increased. A signal processing method has been applied to quantify sensor response using the characteristic frequencies and pseudo-quality factors. The pseudo-quality factor may be used to identify the state of the steel sensing wire in the presence of a conductive environment. Also, the reference circuit arrangement improves the readability of the sensors. Maximum read distances have been improved, although not to the required level.

Concentric sensors with 21-gage steel sensing wires performed the best in calibration tests with regard to maximum read distance and environmental effects. The use of smaller 26-gage steel sensing wires resulted in poorer performance of the sensor. The smaller wires were used in laboratory tests in order to decrease the time required for the wires to corrode and fracture. In practical applications, 21-gage or larger wires should be used to give reliable performance.

Coplanar sensors did not provide the same quality of readings. The phase dips of the sensing circuits were smaller and the range between pseudo-quality factors for intact steel sensing wires and broken steel sensing wires were also small. The likelihood of missing the response of the sensing circuit is increased for the coplanar sensors compared with concentric sensors.

CHAPTER 5

Second Generation Sensor Testing

5.1 INTRODUCTION

A testing program is currently underway to evaluate the performance of the second generation sensors. Sensors have been embedded in small-scale concrete prisms and large-scale reinforced concrete slabs. In addition to interrogating sensors at regular intervals, use of visual inspection and other corrosion monitoring techniques is continuing. After a corrosion threshold is detected, the chloride content will be determined from samples of concrete powder drilled from the specimens and cover concrete will be removed to allow observation of the state of corrosion within specimens. Accelerated corrosion tests began in January 2005. Because the tests are ongoing, only results obtained through 6 April 2005 are included in this thesis.

5.2 CONCRETE PRISMS

Sensors embedded in small concrete prisms may be tested more easily than sensors embedded in large-scale structures. Prisms can be placed in environments with controlled temperature and/or moisture conditions that would be difficult to create for large-scale specimens. In addition, the use of small prisms with shallow concrete cover allows for testing under an accelerated schedule. Corrosion may take years or decades to develop in a bridge deck with 2 in. or more of concrete cover subjected to only small temperature variations and intermittent salt and moisture exposure. However, results from accelerated corrosion tests of concrete prisms using sensors with small diameter steel sensing wires can be acquired in only a few months.

5.2.1 Construction

Sensors were embedded in concrete using 4-in. diameter plastic cylinder molds with 1 in. of cover above and below the sensor as shown in Fig. 5-1 and 5-2. Plastic chairs were attached to the bottom of the cylinder molds with a single metal screw and supported the sensors 1 in. above the bottom of the form. The sensors were secured to the chairs using plastic zip ties. Twelve concentric sensors (B19-B30) and ten coplanar sensors (A21-A30) were embedded in the prisms. All of the sensors used in concrete prisms were fabricated with 26-gage steel sensing wires. Prisms were cast on 16 December 2004 and allowed to cure for three weeks. At that time, the metal screws and plastic molds were removed. In a few of the prisms, the metal screw broke off and could not be removed, but this is not expected to influence testing.

The concrete mix was a standard Texas Department of Transportation class C substructure concrete with a minimum specified 28-day compressive strength of 3600 psi. A 3/8-in. maximum size aggregate and 6-in. slump were specified for the mix. Plastic sheets were draped over the specimens for moist curing. The actual strength of the concrete at 140 days was 5800 psi, determined by the average of three compression tests of 6 in. x 12 in. concrete cylinders.

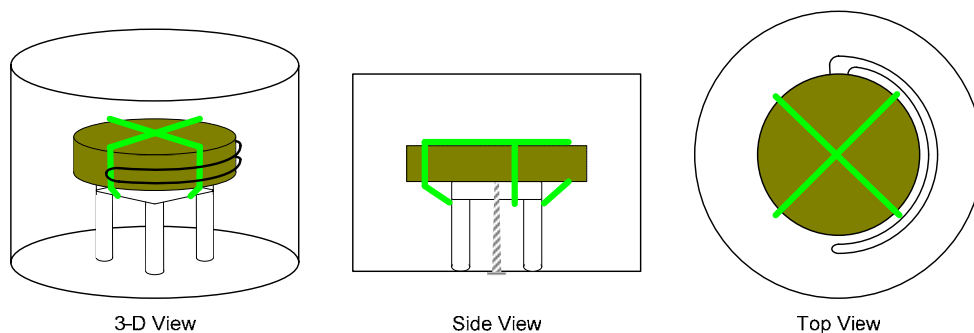


Figure 5-1 Diagram of Concentric Sensor Prism

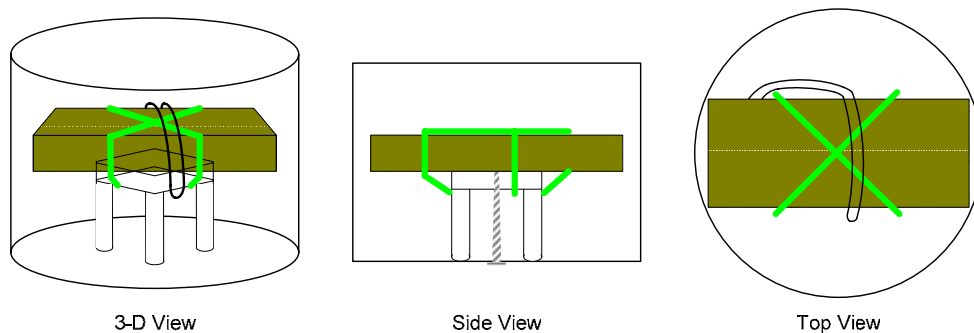


Figure 5-2 Diagram of Coplanar Sensor Prism

Due to the size of coplanar sensors, the plastic cylinder mold was deformed slightly with the sensors in place, which resulted in oblong concrete prisms. Because very little cover concrete remained at the edges of the sensor, the orientation of the steel sensing wires was adjusted to extend in a double half-loop over the top of the sensor near the middle (Fig. 5-2) rather than around the sides of the sensor as originally intended.

5.2.2 Design of Experiments

The concrete prisms were subjected to a variety of different environmental conditions during this set of experiments and the response of the sensors was evaluated periodically. Four different combinations of environmental conditions were selected for study: (a) control, (b) moisture cycles, (c) thermal cycles, and (d) combined moisture and thermal cycles. The duration of all environmental cycles was two weeks, which was selected to minimize the time needed to develop corrosion in the steel sensing wires subjected to moisture variations. All of the environmental cycles were divided into two, one-week stages. The second week of the combined moisture and thermal cycles was further subdivided into two stages. The four environmental conditions are defined in Tables 5-1 through 5-4.

All sensors were interrogated at the end of each stage during each two-week cycle using the Solartron impedance analyzer. A 4-in. diameter reader coil with 5 turns of 18-gage copper magnet wire was used for all readings. The reader coil was connected to the analyzer using a 3-ft cable. This analyzer and reader coil configuration was chosen to match the configuration used for interrogating sensors embedded in the reinforced concrete slabs. The weight of each prism was also recorded at the end of each stage to evaluate the variations in moisture content. Testing began on 10 January 2005.

5.2.2.1 Control Conditions

Control specimens are necessary to establish the baseline response of sensors that are not subjected to varying environmental conditions. Four prisms were used as control specimens (Table 5-1). Concentric sensors were embedded in two specimens (B21, B22) and coplanar sensors were embedded in the other two specimens (A21, A22). Control specimens were stored in air at room temperature throughout the tests. The temperature varied between approximately 68 and 72 °F.

Table 5-1 Environmental Cycles for Control Conditions

Concentric Sensors	Coplanar Sensors	First Week	Second Week
B21 B22	A21 A22	Air / 68-72 °F / 7 days	Air / 68-72 °F / 7 days

5.2.2.2 Varying Moisture Conditions

Eight prisms were subjected to cycles of varying moisture conditions (Table 5-2). During the first week of the cycle, the specimens were completely submerged in water, and the specimens dried in air during the second week. The

tests were designed to cause corrosion of the steel sensing wire. Two prisms with concentric sensors (B29, B30) and two with coplanar sensors (A29, A30) were submerged in salt water, while the other four specimens (A27, A28, B27, B28) were submerged in tap water. All tests were conducted at room temperature, which was approximately 68-72 °F.

Water with 3.5% salt content by weight was originally taken from ASTM G 109 [7] and has been shown through previous research to be adequate for accelerating corrosion of embedded reinforcement [14]. Prisms subjected to wet periods with tap water are not expected to have accelerated corrosion. Tap water specimens were used to confirm that an accelerated corrosion process occurs in specimens subjected to wet periods in salt water, thereby establishing confidence that steel wires used as a sensing mechanism corrode under the same conditions as mild reinforcing steel.

Table 5-2 Environmental Cycles with Varying Moisture Conditions

Concentric Sensors	Coplanar Sensors	First Week	Second Week
B27 B28	A27 A28	Tap Water / 68-72 °F / 7 days	Air / 68-72 °F / 7 days
B29 B30	A29 A30	Salt Water / 68-72 °F / 7 days	Air / 68-72 °F / 7 days

5.2.2.3 Varying Thermal Conditions

Two prisms with concentric sensors were subjected to thermal cycles (Table 5-3). These specimens were stored at room temperature in air for the first week of each cycle. Specimen B19 was stored in an oven at 230 °F for the second week of the cycle, while Specimen B20 was stored in a freezer at -15 °F for the second week. Temperatures chosen for thermal testing represent extremes

beyond those expected for use of sensors in service conditions. For normal use of sensors, thermal behavior is expected to fall within a much smaller range of temperatures.

Table 5-3 Environmental Cycles with Varying Thermal Conditions

Concentric Sensors	Coplanar Sensors	First Week	Second Week
B19	-	Air / 68-72 °F / 7 days	Oven / 230 °F / 7 days
B20	-	Air / 68-72 °F / 7 days	Freezer / -15 °F / 7 days

5.2.2.4 Varying Moisture and Thermal Conditions

Prisms were subjected to combined moisture and thermal cycles for two reasons: (1) increase transport of chlorides into the concrete during wet periods by drying the specimens at elevated temperatures, and (2) determine if the response of sensors under varying thermal conditions is affected by corrosion of the steel sensing wires. More chloride ions in the concrete should lead to more widespread corrosion and possibly an increase in corrosion rate, although this effect may be reduced due to a reduction in the available moisture.

Eight prisms were used for combined moisture and thermal cycles, including four with concentric sensors and four with coplanar sensors (Table 5-4). Two of the prisms with concentric sensors (B25, B26) and two of the prisms with coplanar sensors (A25, A26) were subjected to a wet period of seven days in 3.5% salt water at room temperature followed by seven days of oven drying at 230 °F. One prism with a concentric sensor (B23) and one prism with a coplanar sensor (A23) were subjected to a wet period of seven days in 3.5% salt water at room temperature, four days of oven drying at 230 °F, and three days in a freezer at -15 °F. The other two prisms (A24, B24) were subjected to a wet period of seven

days in tap water at room temperature, four days of oven drying at 230 °F, and three days in a freezer at -15 °F. All prisms were completely submerged during wet periods.

Table 5-4 Environmental Cycles with Varying Moisture and Thermal Conditions

Concentric Sensors	Coplanar Sensors	First Week	Second Week
B23	A23	Salt Water / 68-72 °F / 7 days	Oven / 230 °F / 4 days Freezer / -15 °F / 3 days
B24	A24	Tap Water / 68-72 °F / 7 days	Oven / 230 °F / 4 days Freezer / -15 °F / 3 days
B25 B26	A25 A26	Salt Water / 68-72 °F / 7 days	Oven / 230 °F / 7 days

5.2.3 Measured Response during First Twelve Weeks

The measured phase response of the test specimens between 10 January and 4 April 2005 are summarized in this section. The response is presented in the form of the measured characteristic frequency and pseudo-quality factor for both the sensing and reference circuits. Representative results from each environmental condition are discussed in Sections 5.2.3.1 through 5.2.3.4 and all data are presented in Appendix G. Appendix G also includes the variations in moisture content of the specimens. Photographs of crack patterns and corrosion of steel sensing wires in prisms with broken wires are provided in Appendix H. Section 5.2.3.5 provides a statistical summary of variations in key parameters with time.

When the last set of data was recorded on 4 April 2005, the steel sensing wires had fractured in nine of the twenty-two sensors. Table 5-5 gives a summary of the response of these sensors and identifies the mechanism that likely caused

the wire breaks. Sensors with broken wires are discussed in more detail in Sections 5.2.3.1 through 5.2.3.4. For the purpose of discussion, each two-week cycle is specified in sequential order and the end of each stage during the cycle is labeled with a letter as follows: (a) end of first week (7 days into 14-day cycle), (b) end of oven stage for specimens A23, A24, B23, and B24 (11 days into 14-day cycle), and (c) end of second week (14 days into 14-day cycle).

All specimens were interrogated at the end of the first week and the end of the second week. The four specimens that were subjected to both oven and freezer stages during the second week (A23, A24, B23, B24) had an additional interrogation 11 days into the two-week cycle at the time of transition from oven to freezer. Specimens were patted dry and weighed, then interrogated immediately after removal from tap water or salt water at the end of the first week stage. Specimens subjected to oven drying were all removed from the oven at the same time, weighed, and interrogated within a 30 minute period. At the end of freezer stages, specimens were removed one at a time, weighed, and immediately interrogated. The first week stage was extended to two weeks during the fifth cycle, therefore, no interrogations of sensors were made on 14 March.

Table 5-5 Prisms with Broken Sensing Wires

Specimen	Date of Detection	Cycle Stage*	Likely Cause of Wire Break
A23	21 Jan	1b	Concrete cracking due to differential thermal expansion
A24	21 Jan	1b	Concrete cracking due to differential thermal expansion
A25	7 Feb	2c	Concrete cracking due to differential thermal expansion
A26	28 Mar	5c	Corrosion of steel sensing wire
A29	7 Mar	4c	Corrosion of steel sensing wire
A30	28 Mar	5c	Corrosion of steel sensing wire
B23	21 Jan	1b	Concrete cracking due to differential thermal expansion
B25	4 Apr	6a	Corrosion of steel sensing wire
B30	4 Apr	6a	Corrosion of steel sensing wire

* a - end of first week (all specimens)

b - end of oven dry stage (specimens A23, A24, B23, and B24)

c - end of second week (all specimens)

5.2.3.1 Control Conditions

Concrete prisms used as control specimens exhibited no change in sensor response. The characteristic frequency of the sensing circuit for concentric sensor B21, for example, was 0.46 MHz for all twelve measurements (Fig. 5-3). Similarly, the characteristic frequency of the reference circuit was 1.53 MHz for all measurements. The pseudo-quality factors for both circuits varied slightly during the recording period, but the coefficients of variation were less than 1% in both cases.

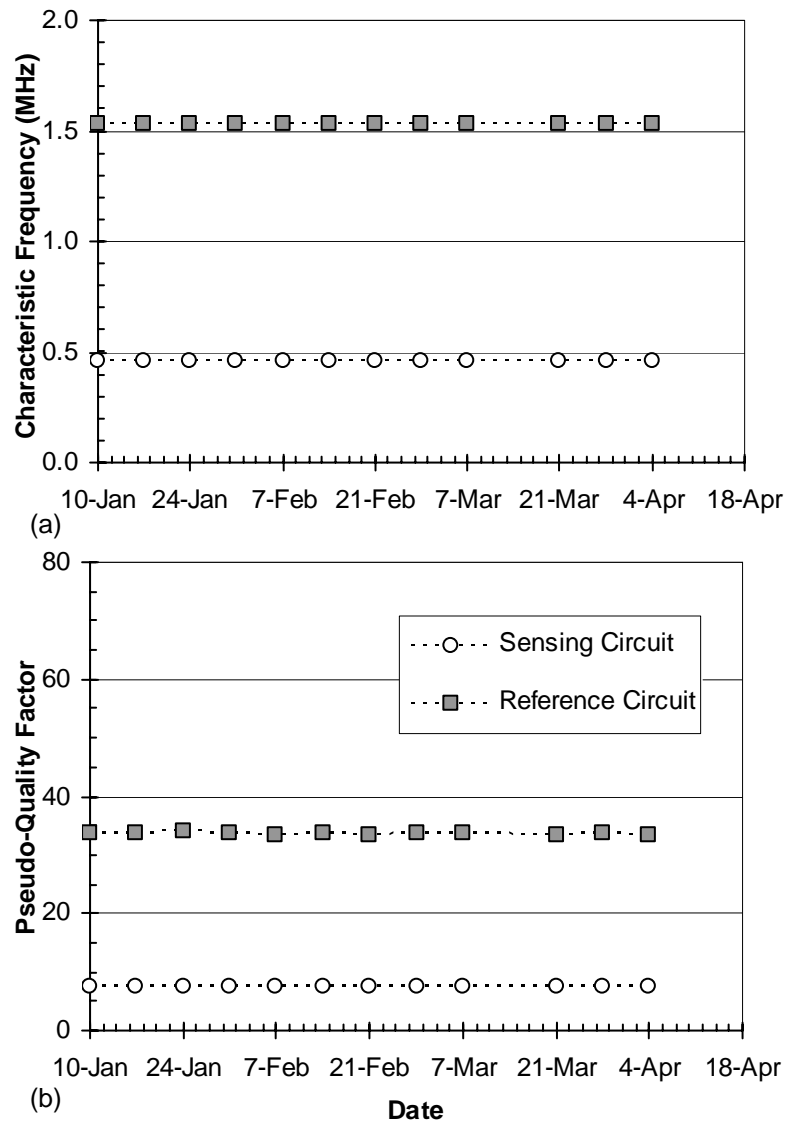


Figure 5-3 Prism B21 Interrogation History

5.2.3.2 Varying Moisture Conditions

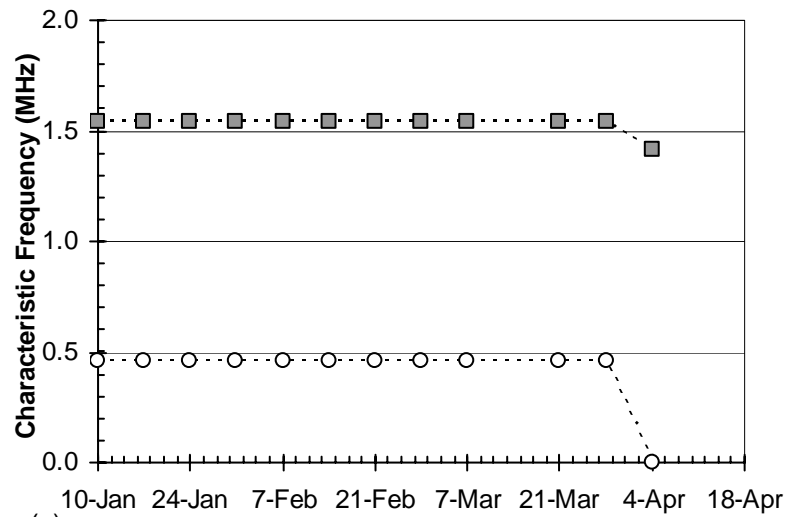
To date, no broken wires have been detected in any of the specimens that were submerged in tap water. However, wires have broken in one of the

concentric sensor prisms (B30) and both of the coplanar sensor prisms (A29, A30) that were submerged in salt water.

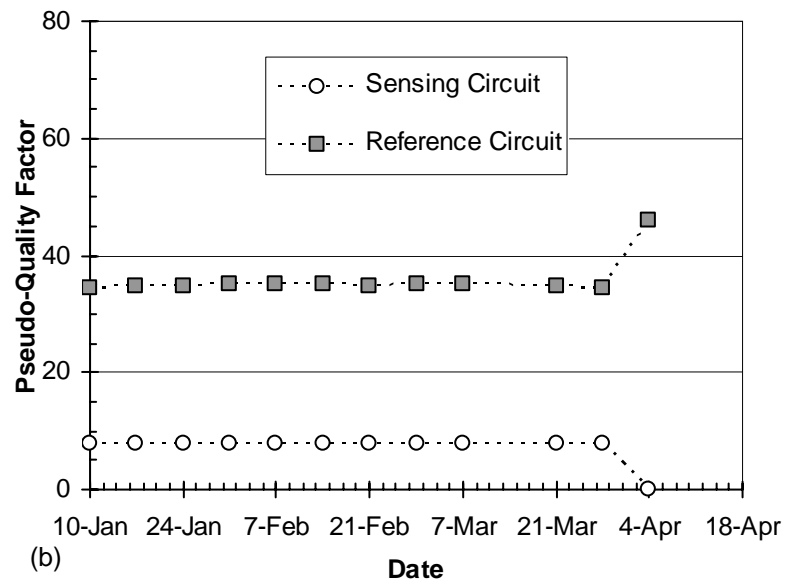
At the end of the sixth wet period in salt water, 12 weeks into testing, a broken wire was detected in prism B30. The interrogation history for this prism is shown in Fig. 5-4. A clear shift in the reference characteristic frequency from 1.54 MHz to 1.41 MHz occurs at the interrogation on 4 April, along with a complete disappearance of the sensing characteristic frequency (represented by 0 MHz). The pseudo-quality factor for the reference circuit also jumps from 34.8 to 46.1, while the sensing circuit pseudo-quality factor cannot be calculated due to no detectable characteristic frequency (again, represented by 0).

A photograph of prism B30 before removal of the concrete cover is shown in Fig. 5-5. Internal examination of the specimen revealed the location of the break in the steel sensing wire (Fig. 5-6) and localized rust staining at that location. The wire break occurred near the 180° bend at the end of the wire loop. Corrosion was also observed on one wire at the location where the steel sensing wires exit the body of the sensor. The remaining steel wire was examined and no other corrosion was observed.

Internal examination of prisms A29 and A30 revealed similar locations of broken steel sensing wires near the 180° bend at the end of the wire loop and localized rust staining at those locations. The remaining length of wire away from the location of the break was free from visible corrosion in both of those sensors.



(a)



(b)

Figure 5-4 Prism B30 Interrogation History



Figure 5-5 Prism B30 Prior to Internal Examination



(a) Entire Steel Sensing Wire Exposed

(b) Visible Corrosion on Broken Wire

Figure 5-6 Sensor B30 After Internal Investigation

5.2.3.3 Varying Thermal Conditions

The steel sensing wires in the two prisms with concentric sensors are still intact. The characteristic frequencies and pseudo-quality factors for both the sensing circuit and the reference circuit are plotted for each interrogation in Fig. 5-7 for prism B19 and Fig. 5-8 for prism B20.

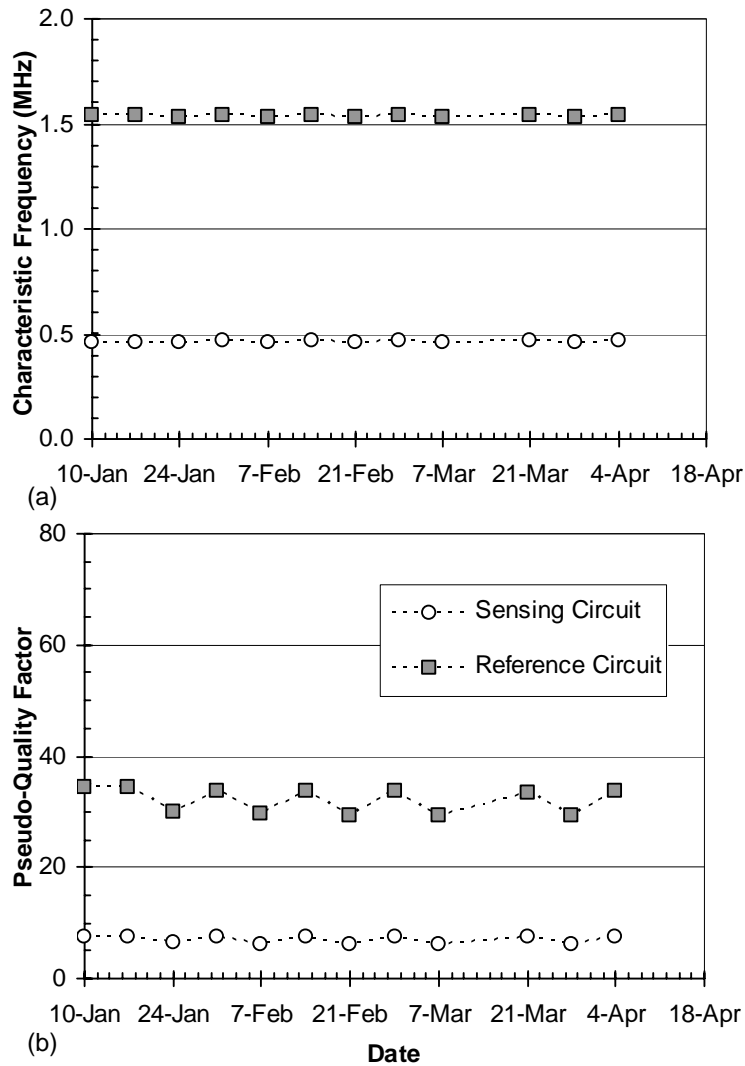


Figure 5-7 Prism B19 Interrogation History

Although the pseudo-quality factor of sensors at extreme cold temperatures is slightly higher than at room temperature and the pseudo-quality factor of sensors at extreme hot temperatures is slightly lower than at room temperature, no permanent change in sensor response was observed with freezer or oven exposure. For a temperature range of 245 °F, the range of pseudo-quality

factor was 6.2 to 8.4 for the sensing circuits and 29.1 to 37.0 for the reference circuits. This variation was expected based on the changing properties of circuit components with temperature and previous testing of sensors subjected to varying temperatures.

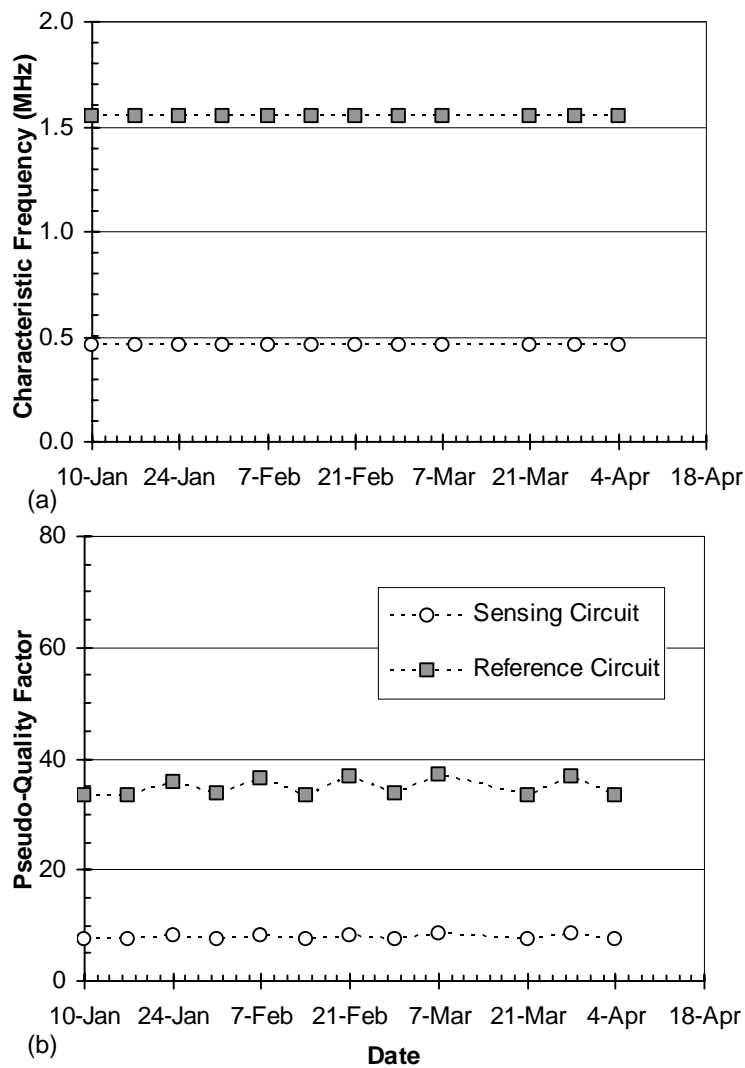


Figure 5-8 Prism B20 Interrogation History

5.2.3.4 Varying Moisture and Thermal Conditions

The response of concentric sensors in prisms B24 and B26 indicate that the steel sensing wires of those sensors are still intact. All of the coplanar sensors and two concentric sensors subjected to combined moisture and thermal variations have indicated broken wires during interrogations to date.

Broken wires were detected in three of the prisms (A23, A24, B23) just 11 days after testing began. The broken wires were detected at the end of the first four days in the oven. Another broken wire was detected in prism A25 just 28 days after testing began at the end of the second stage in the oven. As shown in Fig. 5-9, severe concrete cracking occurred during heating in the oven due to differential thermal expansion between the concrete and the plastic chair supporting the sensor, the marine epoxy of the sensor itself, and the plastic zip ties. The coefficient of thermal expansion is several times greater for plastic and epoxy than for concrete.

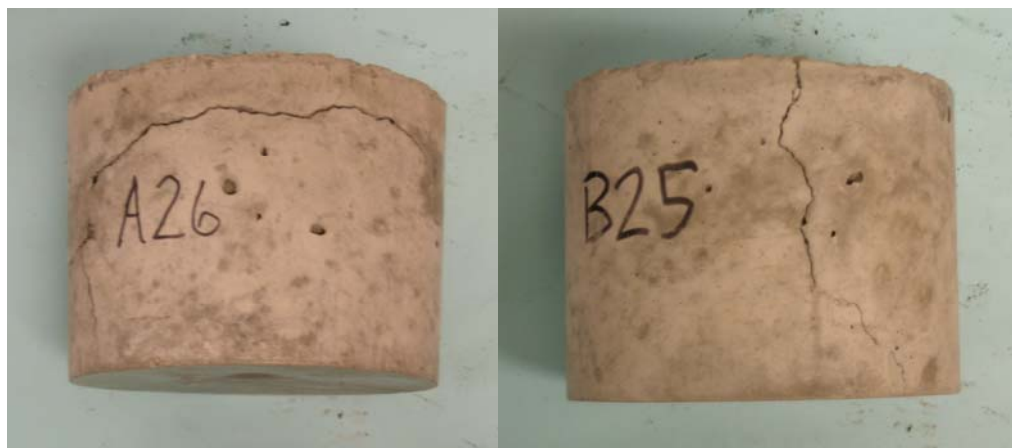


Figure 5-9 Cracking After Oven Drying Stage

Because the wires broke so early in the testing process, corrosion did not have time to develop in the steel sensing wire. Therefore, it was concluded that the wires must have broken because they crossed a crack that formed due to

differential thermal expansion. Rather than removing the concrete cover immediately after detecting that the steel wire had broken, specimens A23, A24, A25, and B23 were subjected to continuing environmental cycles. Sensors A23, A24, and A25 have responded at only the reference characteristic frequency for all interrogations after first detection of the broken wire. Sensor B23, however, exhibited response that was consistent with a transition zone following the first stage in the freezer.

The behavior of the sensor embedded in prism B23 provides evidence for the variable resistance model of the steel sensing wire. Fig. 5-10 shows the phase response as a function of frequency for sensor B23 before the start of environmental testing (a), at the end of the first wet stage in salt water (b), at the end of the first oven drying stage (c), and at the end of the first freezer stage (d). In the first two plots (Fig. 5-10a and b), both the sensing circuit and reference circuit phase dips are present and the sensing circuit response is shielding the reference response, indicating that the steel sensing wire is intact. The steel sensing wire broke during the first oven drying period as evidenced by the response of sensor B23 at only the reference frequency (Fig. 5-10c). When the sensor was interrogated at the end of the first freezer stage, the response of the sensing circuit reappeared and once again shielded the response of the reference circuit (Fig. 5-10d). When the concrete and sensor contracted in the freezer, the ends of the broken sensing wire must have come back into contact. The resistance in this case is higher than the intact wire, but current was still able to flow through the circuit. When the specimen returned to room temperature, the sensor responded as in Fig. 5-10c, indicating that the ends of the wire were no longer in contact, creating infinite resistance, or an open circuit. During all further interrogations, the sensor exhibited a response similar to that in Fig. 5-10c,

even after freezer cycles. This indicates that the crack became large enough such that the ends of steel wire did not come back into contact during further cycles.

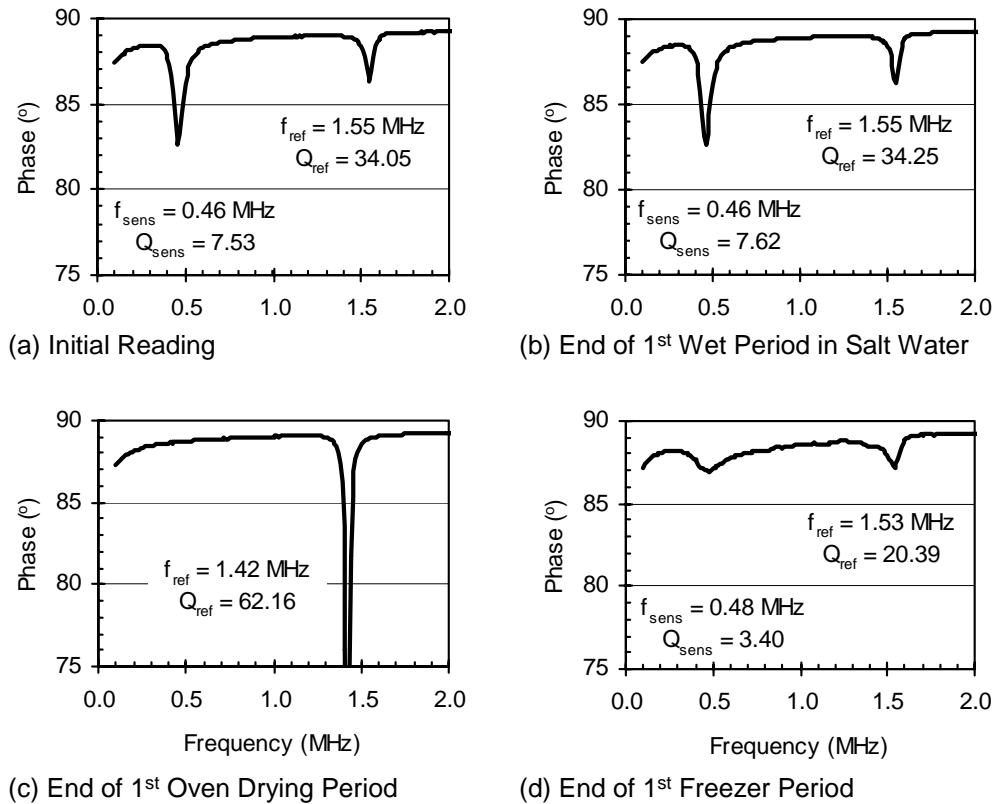


Figure 5-10 Sensor B23 Phase Response

Using the pseudo-quality factor, a distinction can be made between the response of a sensor with an intact wire (Fig. 5-10b) and a sensor with broken wire ends in contact (Fig. 5-10d). The increased resistance in the case of the broken wire ends in contact produces pseudo-quality factors for both the sensing and reference circuits that are roughly one-half of that with an intact wire. For the sensing circuit response, the pseudo-quality factor was 3.4 when the ends of the wire were in contact at the end of the freezer stage. This is less than 6, which is the minimum pseudo-quality factor observed for interrogations of concentric

sensors with intact 26-gage steel sensing wires, as shown in Chapter 4 and Appendix F. It is also less than the maximum pseudo-quality factor (5) observed for interrogations of concentric sensors in a conductive environment (Fig. 4-6). Conclusively, the steel sensing wire may be identified as broken despite the presence of the sensing circuit response in prism B23. The same type of comparison may be used for changing resistance of the wire due to steel section loss from corrosion or due to a conductive environment.

The interrogation history of prism B23 is shown in Fig. 5-11. The pseudo-quality factor for both intact and broken wire conditions changes with temperature as seen in thermal specimens. The pseudo-quality factor for the reference circuit of sensor B23 with broken, but touching, wires is about one-third less than the smallest pseudo-quality factor (29.2) calculated for any of the concentric sensors embedded in concrete prisms. The spike in pseudo-quality factor for the reference circuit occurs at the end of every freezer period except the first, when the ends of the steel sensing wire came into contact.

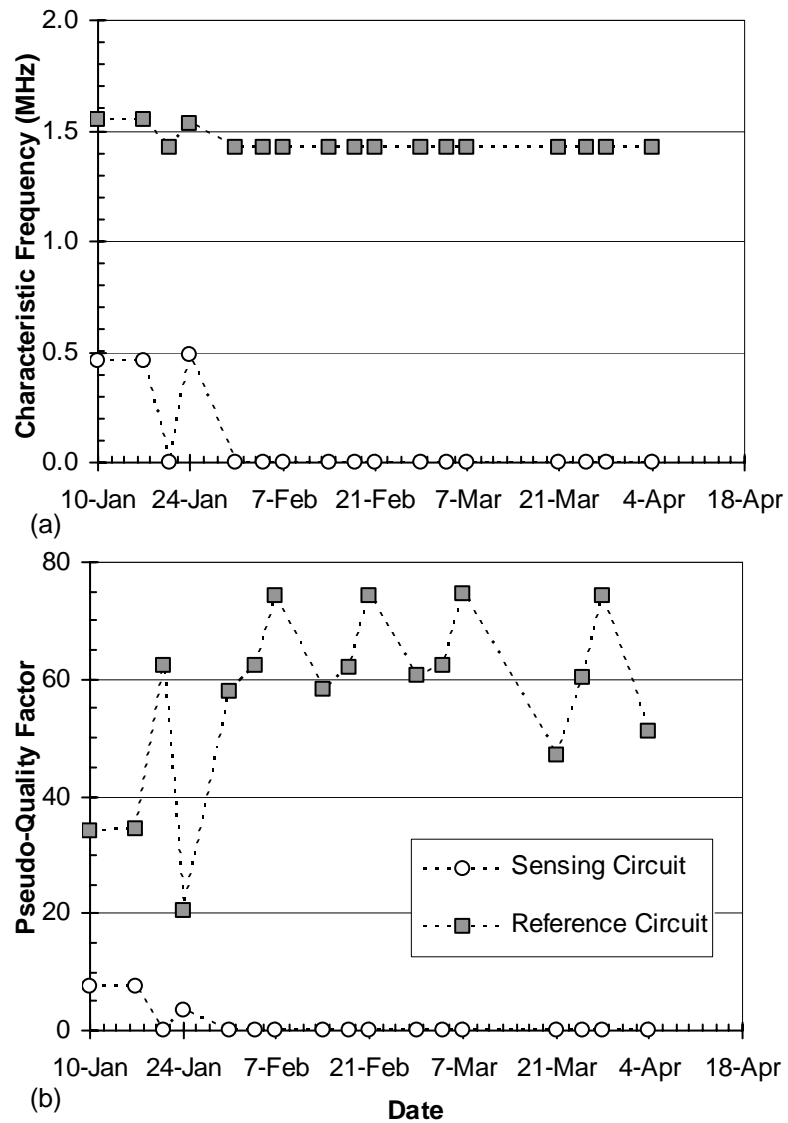


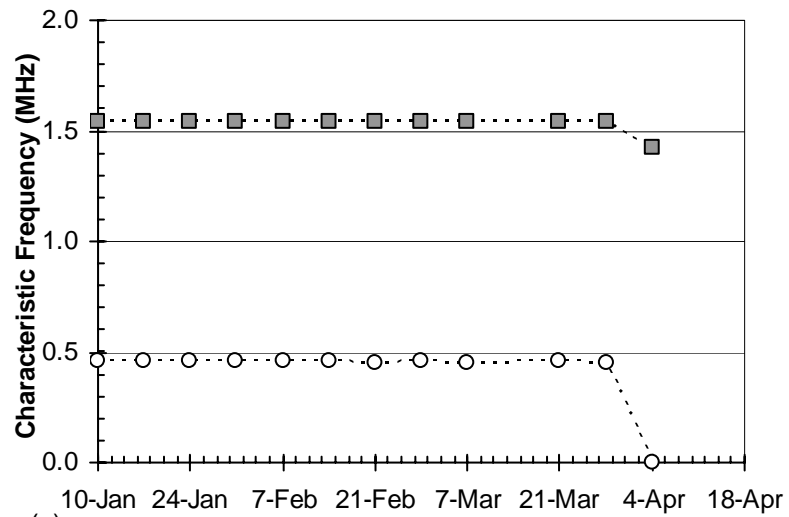
Figure 5-11 Prism B23 Interrogation History

A broken wire was detected in prism B25 at the end of the sixth wet period in salt water, 12 weeks into testing. The interrogation history for this prism is shown in Fig. 5-12. Like the other concentric sensor prisms subjected to

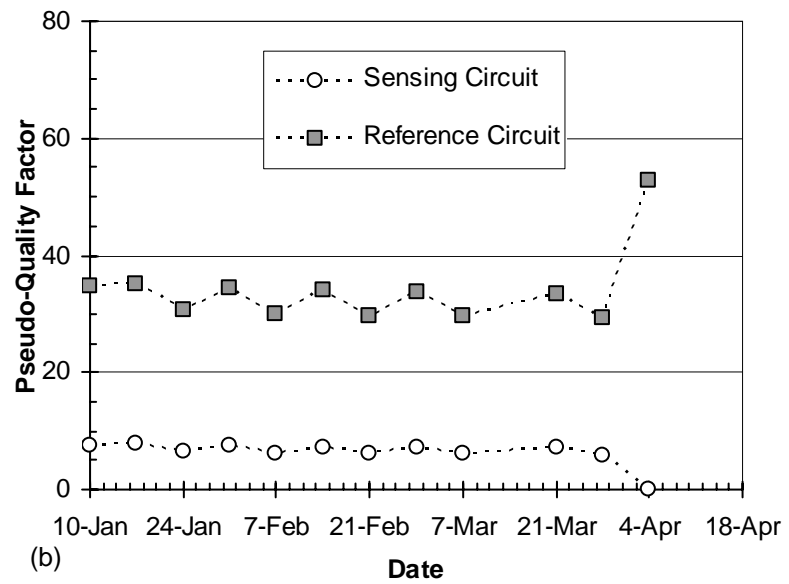
thermal cycles, the pseudo-quality factor changes with temperature. However, this prism was subjected to wet periods immersed in salt water to cause corrosion, as well. The interrogation on 4 April showed a similar response to prism B30, where the sensing characteristic frequency disappeared, the reference frequency shifted down, and the pseudo-quality factor of the reference circuit increased substantially. All of these indicate detection of a broken wire.

Internal examination of the specimen revealed more extensive corrosion than in any other previous prism examinations. As shown in Fig. 5-13 through 5-16, corrosion product is visible migrating away from the steel sensing wire at the 180° bend near the end of the wire loop and along the length of the wire for roughly one-third of the total loop length. The probable location of the broken wire was the end of the wire loop, but enough corrosion occurred elsewhere along the wire to cause a break in other locations as well. The examination also showed the discoloration of the sensor epoxy body and PVC due to high temperature exposure during the oven drying period.

One coplanar sensor prism, A26, also had a broken steel sensing wire due to corrosion. This was the only combined corrosion and thermal specimen with a coplanar sensor for which enough cycles to initiate corrosion occurred prior to detection of the broken wire. Internal examination of the specimen revealed the location of the break in the steel sensing wire, again near the 180° bend near the end of the wire loop and localized rust staining at that location. Some corrosion was also visible where the wires exit the sensor body, but the wire was not broken at that location. When the remainder of the steel wire was removed, no other corrosion was observed.



(a)



(b)

Figure 5-12 Prism B25 Interrogation History

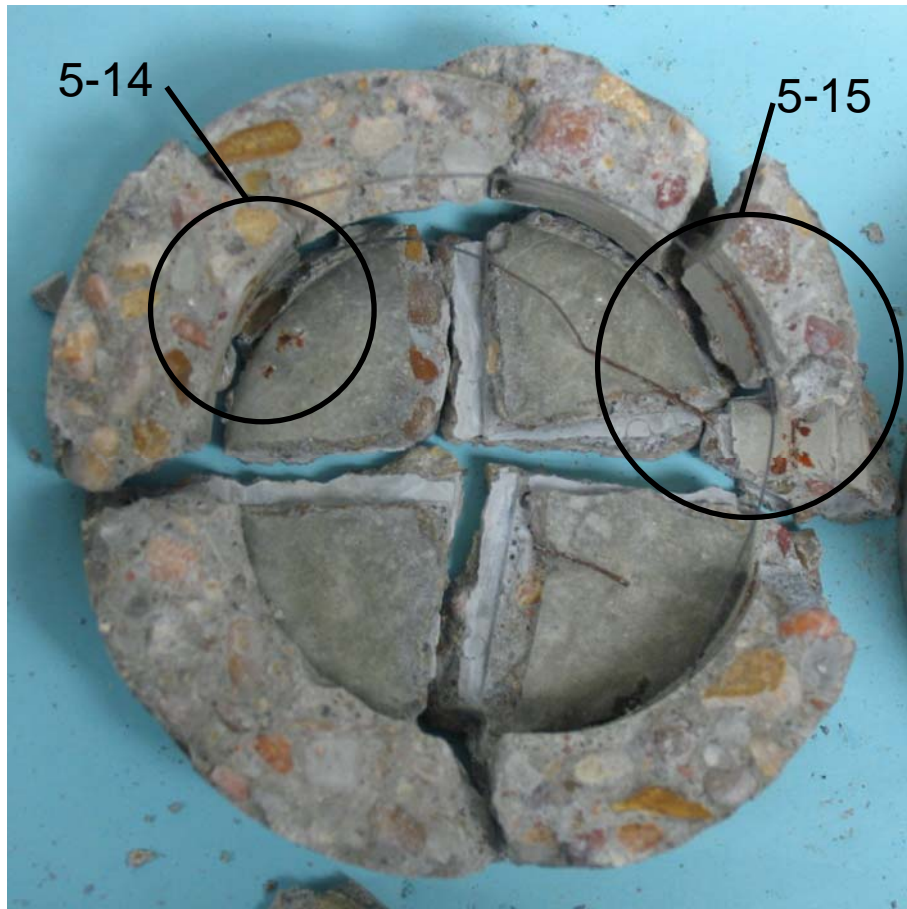


Figure 5-13 Interior of Prism B25 After Removal of Bottom Cover



Figure 5-14 End of Wire Loop in Prism B25



Figure 5-15 Corrosion Along Wire in Prism B25

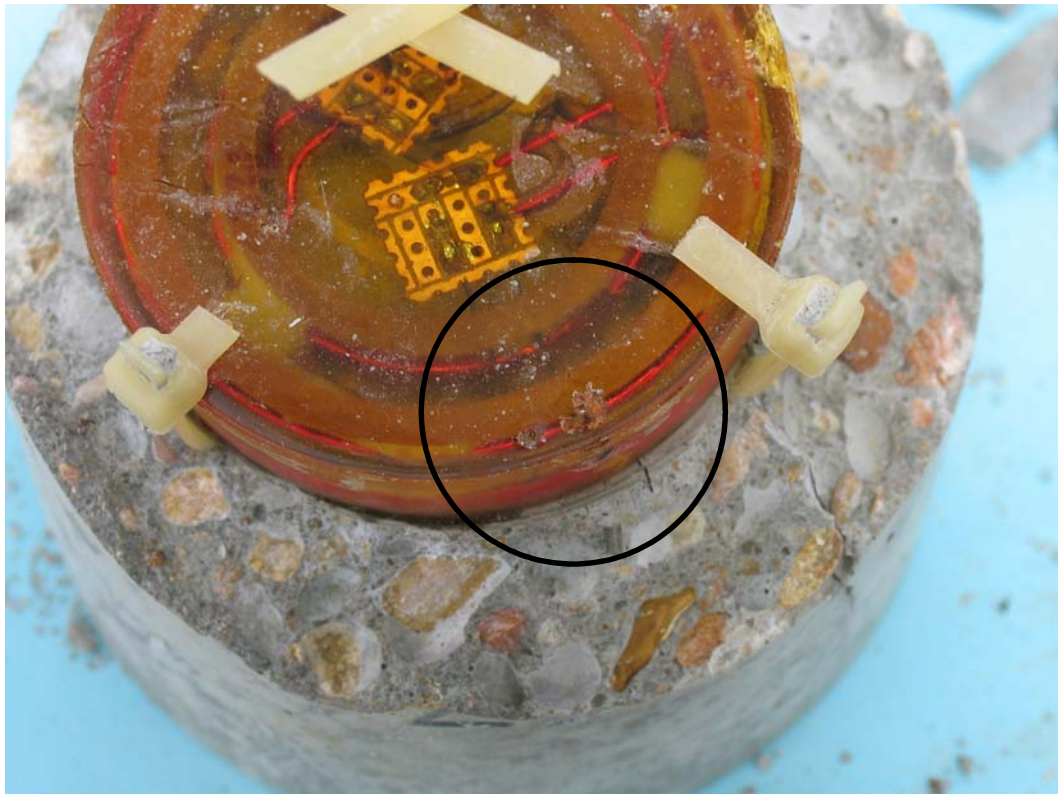


Figure 5-16 Discolored Sensor B25 Showing Corrosion at Wire Exit

5.2.3.5 Statistical Variations in Response

The results from the prism tests provided a large number of sensor readings that can be used to evaluate variations of the measurements with time. Tables 5-6 through 5-8 summarize the means and coefficients of variation for the characteristic frequency, pseudo-quality factor, and phase dip for both the sensing and reference circuits in sensors with intact wires. The same information is summarized in Table 5-9 for the reference circuit in the four sensors with broken wires and multiple readings (A23, A24, A25, and B23).

In general, the characteristic frequencies exhibited the least variation. Among the twelve specimens that were interrogated at room temperature throughout the tests, the largest coefficient of variation was 0.1%. The coefficient of variation did not exceed 1% for any of the ten specimens that were exposed to thermal variations.

The pseudo-quality factors did not vary appreciably during the tests. The coefficient of variation rarely exceeded 1.5% for the twelve specimens interrogated at room temperature or 10% for the ten sensors that were exposed to thermal variations.

The phase dip experienced the largest variations. The coefficient of variation was typically less than 2.5% for the twelve specimens interrogated at room temperature and ranged from 3 to 17% for the sensors that were exposed to thermal variations.

Table 5-6 Variation of Characteristic Frequency for Sensors Embedded in Prisms – Intact Wires

Specimen	Number of Readings	Sensing Circuit		Reference Circuit	
		Mean Char. Freq. (MHz)	Coefficient of Variation (%)	Mean Char. Freq. (MHz)	Coefficient of Variation (%)
A21	12	0.57	0.1%	1.41	0.0%
A22	12	0.56	0.0%	1.41	0.0%
A26	10	0.56	0.7%	1.41	0.1%
A27	12	0.56	0.0%	1.40	0.0%
A28	12	0.57	0.1%	1.42	0.0%
A29	8	0.56	0.1%	1.41	0.0%
A30	10	0.57	0.1%	1.41	0.0%
B19	12	0.46	0.6%	1.53	0.2%
B20	12	0.46	0.4%	1.55	0.2%
B21	12	0.46	0.0%	1.53	0.0%
B22	12	0.46	0.0%	1.54	0.0%
B24	17	0.46	0.8%	1.54	0.3%
B25	11	0.46	0.7%	1.54	0.2%
B26	12	0.46	0.5%	1.52	0.2%
B27	12	0.46	0.0%	1.51	0.0%
B28	12	0.46	0.0%	1.54	0.0%
B29	12	0.46	0.0%	1.54	0.0%
B30	11	0.46	0.1%	1.54	0.0%

Table 5-7 Variation of Pseudo-Quality Factor for Sensors Embedded in Prisms – Intact Wires

Specimen	Number of Readings	Sensing Circuit		Reference Circuit	
		Mean Pseudo-Quality Factor	Coefficient of Variation (%)	Mean Pseudo-Quality Factor	Coefficient of Variation (%)
A21	12	5.4	1.7%	76.3	0.2%
A22	12	5.3	1.2%	75.7	0.4%
A26	10	4.9	11.3%	72.4	4.5%
A27	12	5.8	1.4%	77.4	0.3%
A28	12	5.7	1.6%	75.3	0.3%
A29	8	5.5	1.8%	77.1	0.3%
A30	10	4.9	1.1%	71.2	0.2%
B19	12	7.0	9.0%	32.0	7.2%
B20	12	7.8	5.3%	34.7	4.6%
B21	12	7.6	0.6%	33.6	0.5%
B22	12	7.8	0.8%	34.5	0.7%
B24	17	7.3	10.1%	33.2	8.7%
B25	11	6.8	9.9%	32.2	7.4%
B26	12	7.2	8.7%	32.4	6.6%
B27	12	7.9	0.9%	34.4	0.6%
B28	12	7.6	1.3%	34.5	0.7%
B29	12	7.6	1.6%	34.2	0.6%
B30	11	7.9	1.2%	34.8	0.7%

Table 5-8 Variation of Phase Dip for Sensors Embedded in Prisms – Intact Wires

Specimen	Number of Readings	Sensing Circuit		Reference Circuit	
		Amplitude of Phase Dip (°)	Coefficient of Variation (%)	Amplitude of Phase Dip (°)	Coefficient of Variation (%)
A21	12	0.8	2.1%	16.9	1.0%
A22	12	1.0	1.4%	11.7	1.4%
A26	10	0.6	11.6%	15.7	6.0%
A27	12	0.9	2.6%	14.2	1.4%
A28	12	0.7	2.2%	13.3	1.5%
A29	8	0.7	2.5%	14.8	1.1%
A30	10	0.6	1.8%	31.3	0.7%
B19	12	2.1	12.3%	1.5	6.5%
B20	12	2.8	6.9%	1.4	3.8%
B21	12	2.8	0.6%	1.5	0.4%
B22	12	2.4	0.8%	1.5	0.6%
B24	17	2.4	13.4%	1.5	7.3%
B25	11	5.6	13.2%	3.0	5.5%
B26	12	4.7	11.1%	2.4	5.2%
B27	12	2.6	0.9%	1.5	0.5%
B28	12	2.5	1.5%	1.5	0.6%
B29	12	5.3	2.1%	2.8	0.9%
B30	11	5.6	1.5%	2.8	0.7%

**Table 5-9 Variation of Measured Response of Sensors Embedded in
Prisms – Broken Wires**

Specimen	No.	Characteristic Frequency		Pseudo Quality Factor		Phase Dip	
		Mean (MHz)	Coef. of Variation	Mean	Coef. of Variation	Mean (°)	Coef. of Variation
A23	15	1.41	0.3%	74.9	9.2%	15.2	9.1%
A24	15	1.38	0.2%	76.9	7.8%	9.6	7.8%
A25	8	1.41	0.1%	73.4	1.0%	11.2	2.8%
B23	14	1.42	0.1%	62.9	13.8%	26.6	16.5%

5.2.4 Interpretation and Evaluation

Both concentric and coplanar sensors have responded as designed during environmental exposure tests of the concrete prisms. Control specimens, which should not have any active corrosion or significant variations in temperature, have exhibited stable response, as expected, for an intact steel sensing wire.

The success of sensors in detecting corrosion of the steel sensing wire has been confirmed by corrosion testing. Two concentric sensors and three coplanar sensors that indicated broken steel sensing wires have been visually examined and confirmed to have corrosion-induced breaks. Pitting corrosion, a form of micro-cell corrosion, in the steel wires at a location where the wires crossed cracks in the concrete was the probable cause of broken wires in all five confirmed cases. This is also expected, because at the point where the steel wire crosses a crack, it is exposed to a greater concentration of free chloride ions and moisture, which are known to initiate active corrosion. This type of corrosion results in a very small anodic area of steel that corrodes at a faster rate than generalized corrosion of the

entire wire. As confirmed by visual examination, a substantial length of steel wire acts as the cathode in the electrochemical reaction and does not corrode.

Sensors with broken wires have responded at only the reference characteristic frequency in all cases except one. Using the pseudo-quality factor, for the one case where a sensor with a broken wire responded at both the sensing and reference characteristic frequencies, a clear difference may be established between a sensor with an intact wire and one with a broken wire. This shows that using a combination of characteristic frequency and pseudo-quality factor is a reliable method to establish the state of the steel sensing wire.

Thermal testing indicates that the sensors will be functional and have a stable response for the full range of temperatures expected in a typical reinforced concrete structure. Although the pseudo-quality factor for very hot or very cold sensors is slightly different than those for sensors at room temperature, a distinction may be made between a change due to temperature and a change due to a broken wire.

The thermal variations used to test the concrete prisms identified an obvious problem with second generation sensors: thermal incompatibility with concrete. Differential expansion due to elevated temperatures caused very wide cracks to form in the concrete, which in-turn broke the steel sensing wires prematurely. In a typical reinforced concrete structure, reinforcing steel that crosses cracks prevents cracks from widening. In the case of the prisms, no reinforcing steel crossed the cracks and, therefore, the cracks became very large. Also, the temperature (230 °F) of the oven used for drying specimens is much higher than temperatures expected in typical reinforced concrete structures. This is a problem that requires further careful study before embedding sensors for long-term use in structures exposed to temperature fluctuations. Possible solutions to this problem include using a different potting material for the sensors

that is thermally compatible with concrete, or adding an additional housing that allows expansion of the body of the sensor without direct contact with concrete.

5.3 REINFORCED CONCRETE SLABS

Embedding sensors in large-scale reinforced concrete slabs accommodates the need for corrosion testing in a realistic setting, that is, sensors adjacent to actual reinforcing steel. This practical testing is needed to establish a correlation between corrosion of steel sensing wires and corrosion of reinforcing steel. To be suitable for a controlled laboratory environment, slabs were sized to fit indoors. This way, moisture and chloride exposure could be controlled to minimize the time necessary to initiate corrosion. Because different corrosion thresholds are expected to be detected based on the diameter of steel sensing wire, a separate slab was necessary for each wire diameter used in sensor fabrication. Using separate slabs facilitates interior examination of corrosion at the end of testing at different times.

5.3.1 Construction

Two reinforced concrete slabs were constructed for accelerated corrosion testing of second generation sensors. Slabs are 8-in. deep, 18-in. wide, and 10-ft long and represent a small section of bridge deck. A diagram of the slabs is provided in Fig. 5-17. Slabs were cast on 16 December 2004 and allowed to cure for three weeks. Plastic sheets were draped over the slabs for moist curing. At the end of the curing period, forms were removed and initial readings were taken for the sensors. All of the sensors survived the construction process and responded in the unbroken state. Slabs were cracked and a salt water bath was placed at midspan. The salt water ponds were constructed using a plastic storage box with the bottom cut out. The boxes were attached to the surface of the slab with Sika™ grey construction epoxy. A continuous bead of epoxy was placed on

both the plastic storage box and the concrete surface before setting the boxes in place. Cracks running through the salt water bath area outside the bath on the top surface and sides of the slabs were also covered with construction epoxy to prevent leakage of the salt water from the bath. After waiting 24 hours for the epoxy to cure, the baths were water tested and any leaks or water spots on the concrete surface were marked. After the water dried, silicon sealant was used to seal around the marked areas. Throughout testing to-date, no problems with water leakage have occurred. Testing using alternating wet and dry cycles began on 13 January 2005.

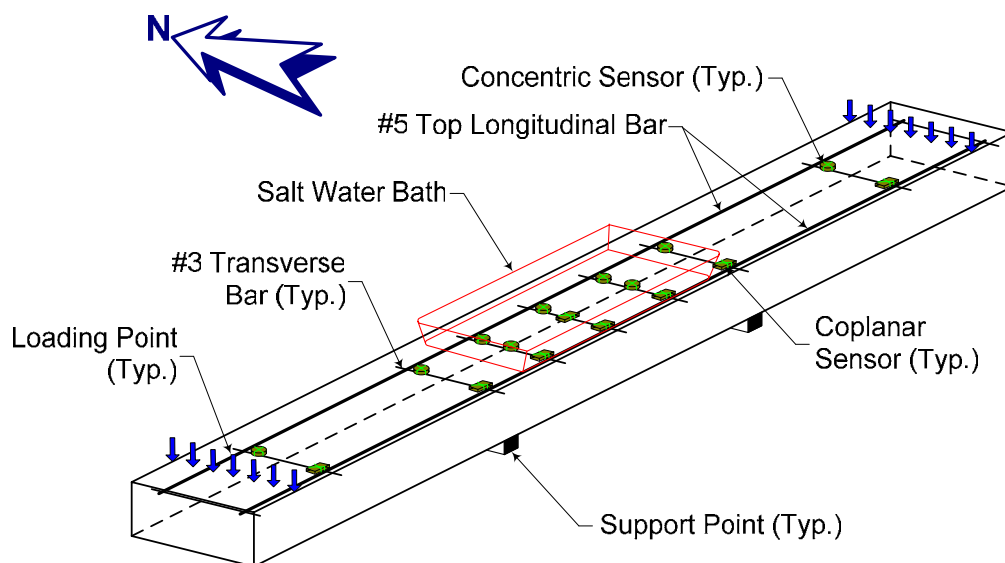


Figure 5-17 Diagram of Reinforced Concrete Slab

The slabs have two layers of reinforcing steel that were supported on plastic chairs prior to placement of concrete as shown in Fig. 5-18 and 5-19. A cross-section showing the arrangement of reinforcing steel is given in Fig. 5-20. The top layer of steel consists of two #5 longitudinal bars and nine #3 transverse bars. An enamel-coated copper wire was silver-soldered to one of the top longitudinal bars to provide an electrical connection to the reinforcement.

Sensors were tied to the top layer of steel at transverse bar locations using plastic zip ties with the orientation of the steel sensing wire toward the interior of the slab, as shown in Fig. 5-21.

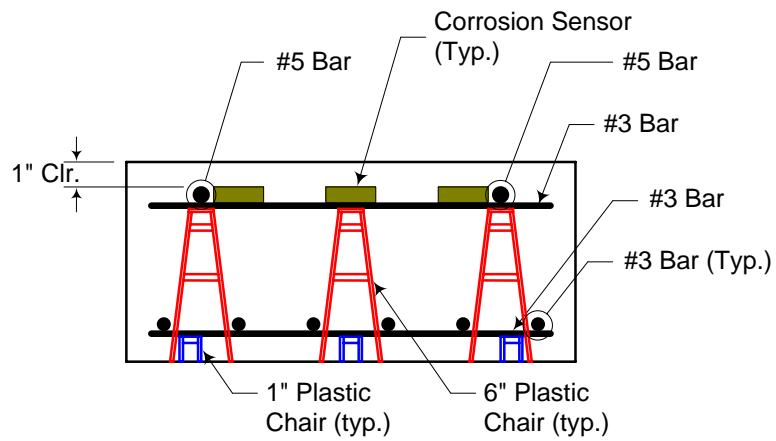


Figure 5-18 Slab Cross-Section Showing Plastic Chairs and Clear Cover



Figure 5-19 Slab #1 Prior to Placing Concrete

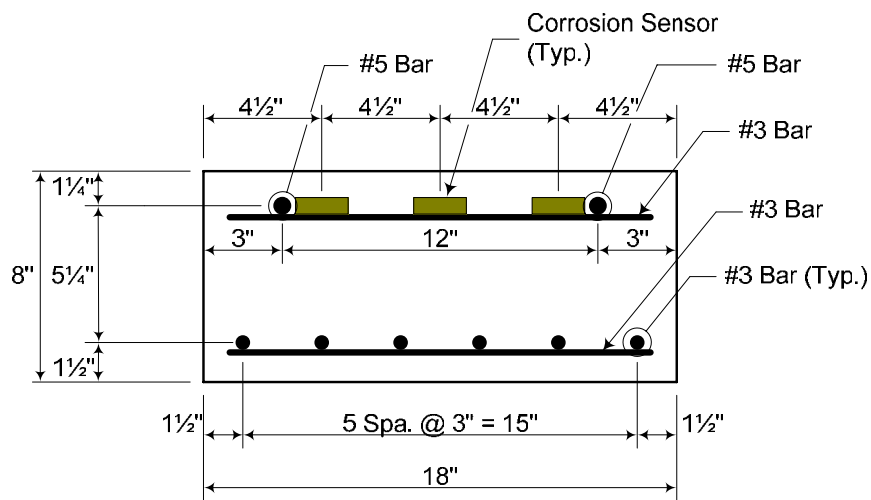


Figure 5-20 Slab Cross-Section Showing Dimensions

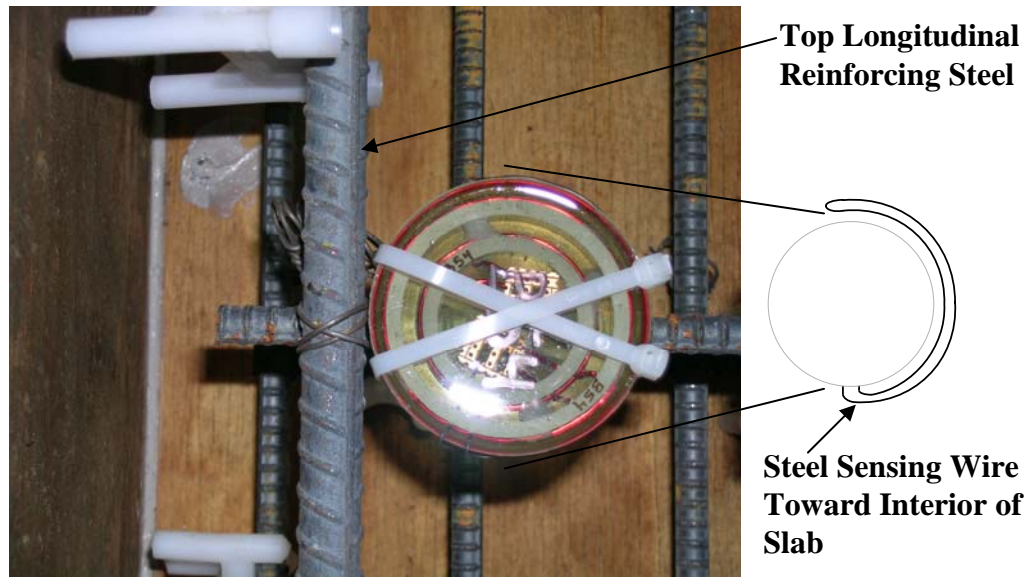


Figure 5-21 Orientation of Sensors Embedded in Slabs

A total of seventeen sensors, nine concentric sensors and eight coplanar sensors, were embedded in each slab. Slab #1 has sensors with 26-gage steel sensing wires and slab #2 has sensors with 21-gage wires. A plan view showing the sensor layout is shown for slab #1 in Fig. 5-22 and for slab #2 in Fig. 5-23.

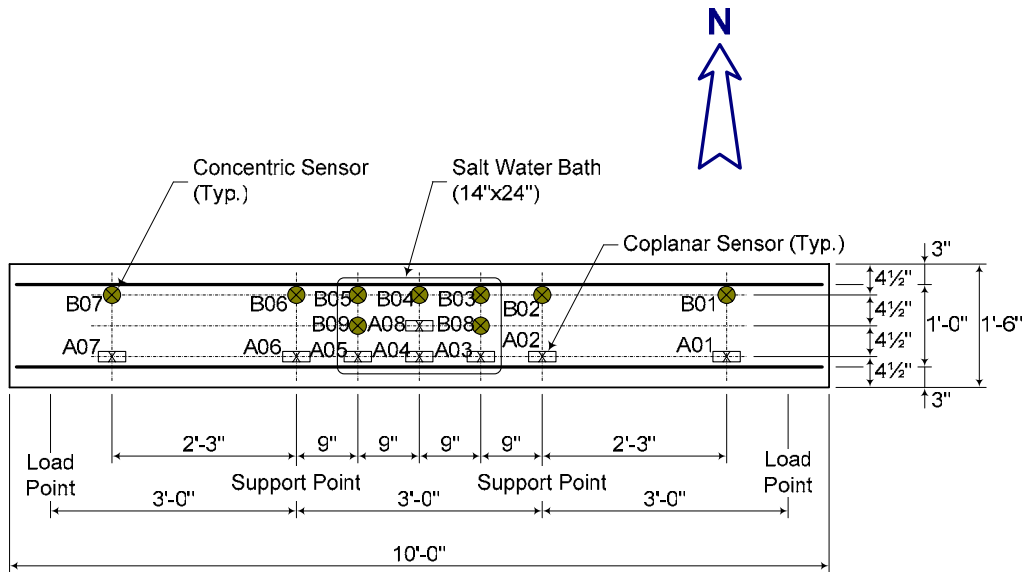


Figure 5-22 Slab #1 Sensor Layout

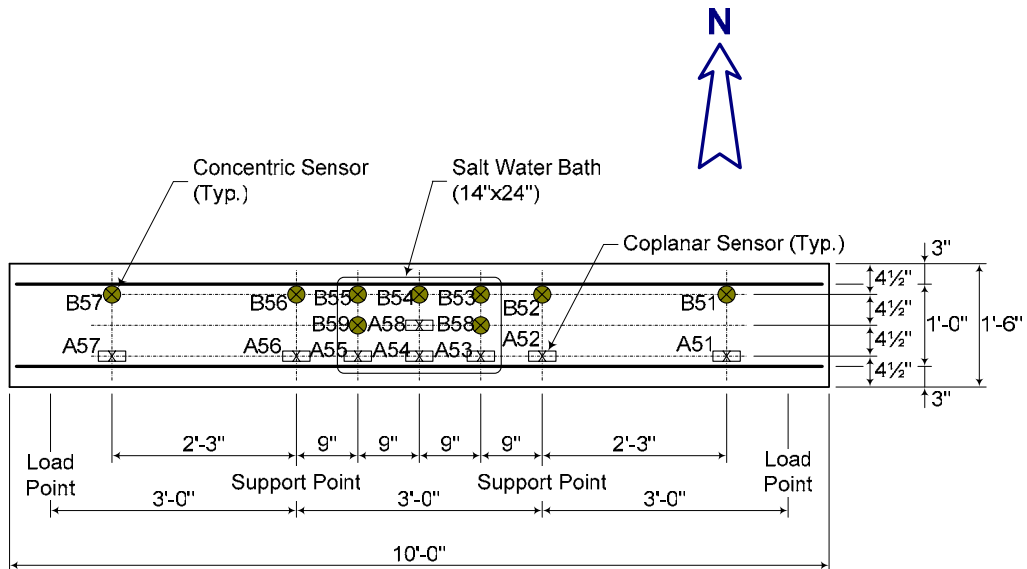


Figure 5-23 Slab #2 Sensor Layout

Five concentric sensors and four coplanar sensors were embedded inside of the salt water bath area in each slab, while four concentric and four coplanar

sensors were embedded outside of the salt water bath area. Embedding sensors outside of the salt water bath area allow the evaluation of sensor reliability in regions where corrosion is not active. Sensors furthest away from the salt water bath should give consistent, stable readings for intact steel sensing wires.

5.3.2 Design of Experiments

Reinforced concrete slabs were used to test sensors under corrosion conditions using wet and dry cycles with salt water. Each wet and dry period has a duration of two weeks. Salt water (3.5% by weight) is ponded over the area shown in Fig. 5-24 at a height of 2 in. above the top surface of slabs during wet periods. While previous tests were conducted outside [15], these tests are being conducted inside to allow complete control of wet and dry cycles.

Slabs were designed to accelerate corrosion of top longitudinal bars and steel sensing wires within the salt water bath area. Top and bottom mats of reinforcement were kept electrically isolated to prevent macrocell corrosion through a direct metal to metal connection. A sustained load was introduced at the ends of the slabs to crack the top surface and maintain the crack width (Fig. 5-24). Reinforcing steel and sensors were placed with only 1-in. of cover to decrease the time for chloride penetration. A crack map, taken 24 hours after loading the slabs, is provided for slab #1 in Fig. 5-25 and for slab #2 in Fig. 5-26. The average crack width for transverse cracks within the salt water bath area was approximately 0.020 in. for both slabs. This crack width has been used on previous corrosion investigations [14] and has shown to be adequate for accelerating the infusion of chlorides into concrete specimens.

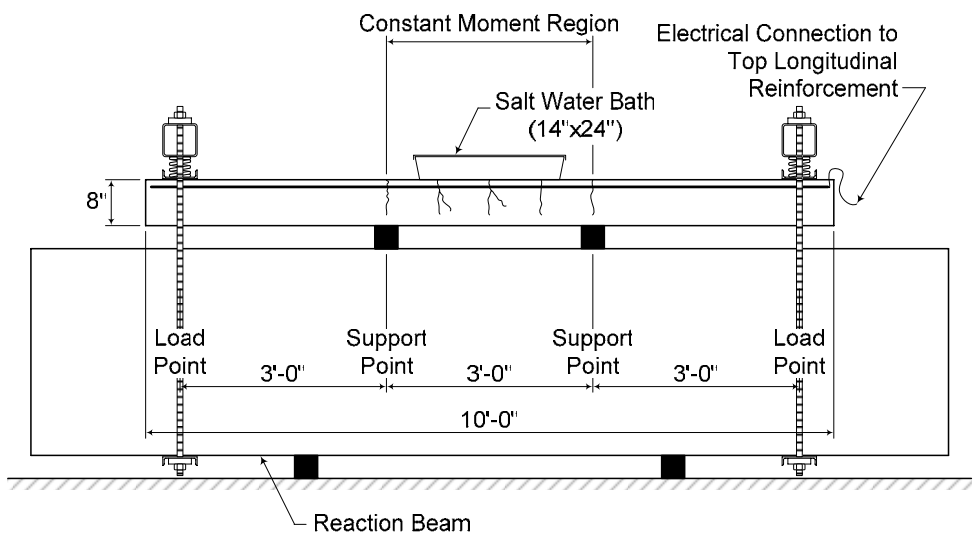


Figure 5-24 Slab Experiment Set-up

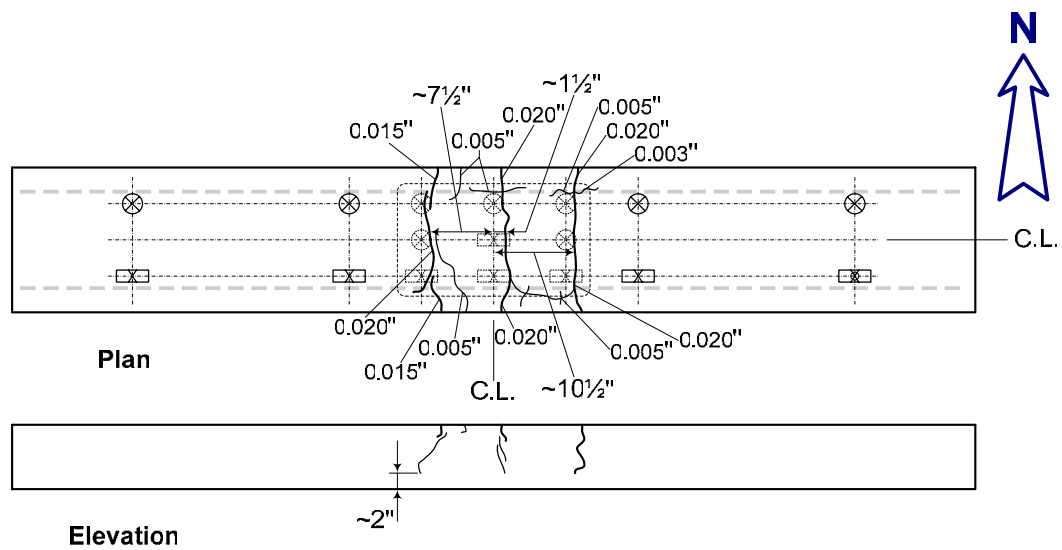


Figure 5-25 Slab #1 Crack Map

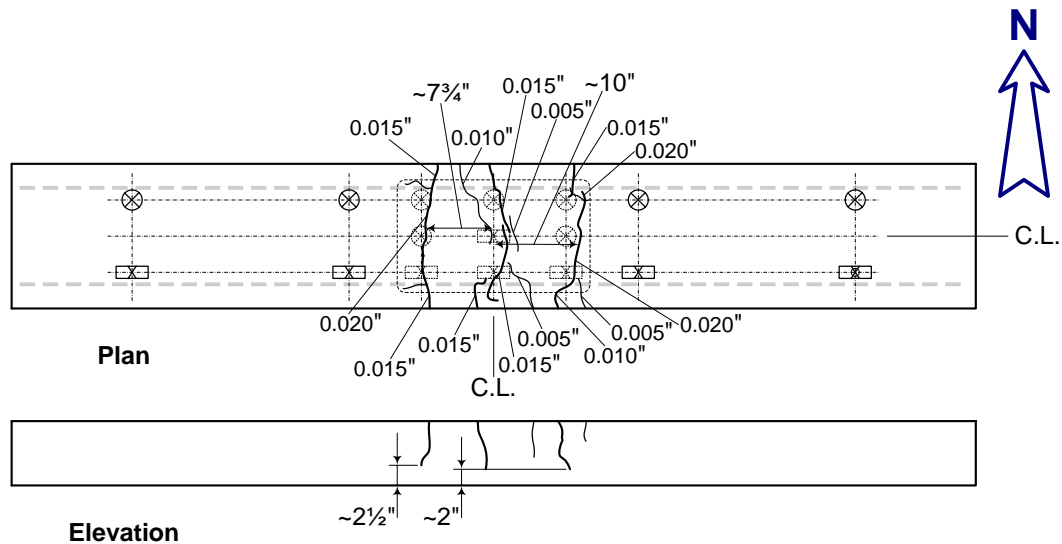


Figure 5-26 Slab #2 Crack Map

Sensors were interrogated every two weeks at the end of each wet or dry period using the Solartron impedance analyzer and a 4-in. diameter reader coil with 5 turns of 18-gage copper magnet wire. The reader was attached to the analyzer using a 3-ft cable. As shown in Chapter 3, this configuration of analyzer and reader coil produced the best readings when using a cable. In addition, the geometry of the salt water bath resulted in a 4 in. maximum reader coil diameter that could be centered over all sensors and also not receive interference from nearby sensors.

In addition to interrogating the sensors at the end of each period, traditional corrosion measurements, including half-cell potential and linear polarization resistance readings are being taken at the same interval. Each slab is monitored at thirty-one points to detect changes in static potential (Fig. 5-27) and twenty points to establish corrosion rates (Fig. 5-28). The standard test method for half-cell potentials of uncoated reinforcing steel in concrete from ASTM C 876 [6] applied to half-cell potential measurements taken on the slabs. Half-cell

measurements were made using a calomel electrode and the results were converted into equivalent copper-copper sulfate electrode potentials. The method outlined in the operational manual of KCC, Inc. for the 3LP device [10], following the standard method of test for rapid determination of corrosion rate of uncoated steel in reinforced concrete from AASHTO TP 11-95 [1], applied to linear polarization resistance measurements. The electrode used for linear polarization resistance measurements was a copper-copper sulfate electrode.

After the corrosion threshold is detected, cover concrete will be removed and the reinforcing steel and sensors will be examined to observe the state of corrosion. The chloride ion content will also be determined from concrete powder taken from the salt water bath area after sensors indicate that the corrosion threshold has been exceeded.

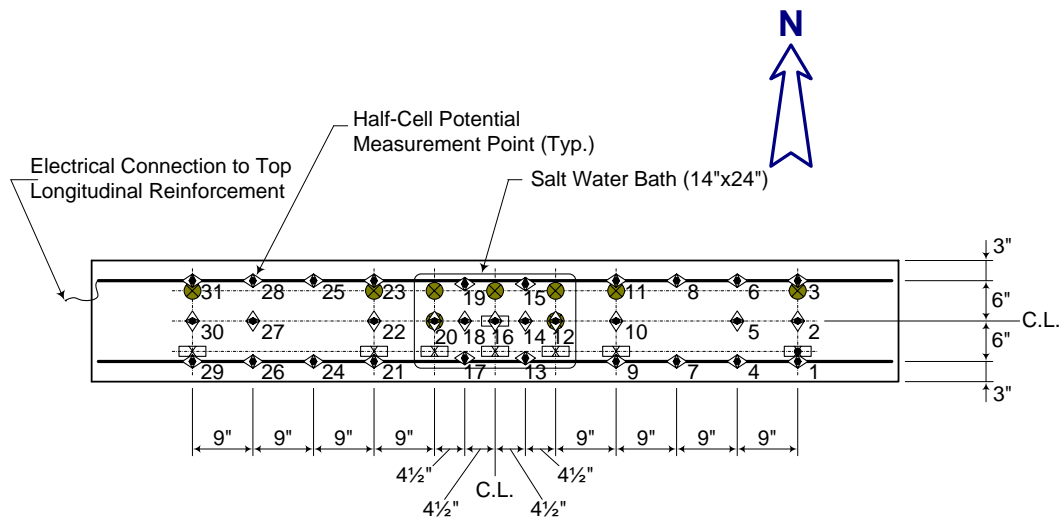


Figure 5-27 Half-Cell Potential Measurement Points

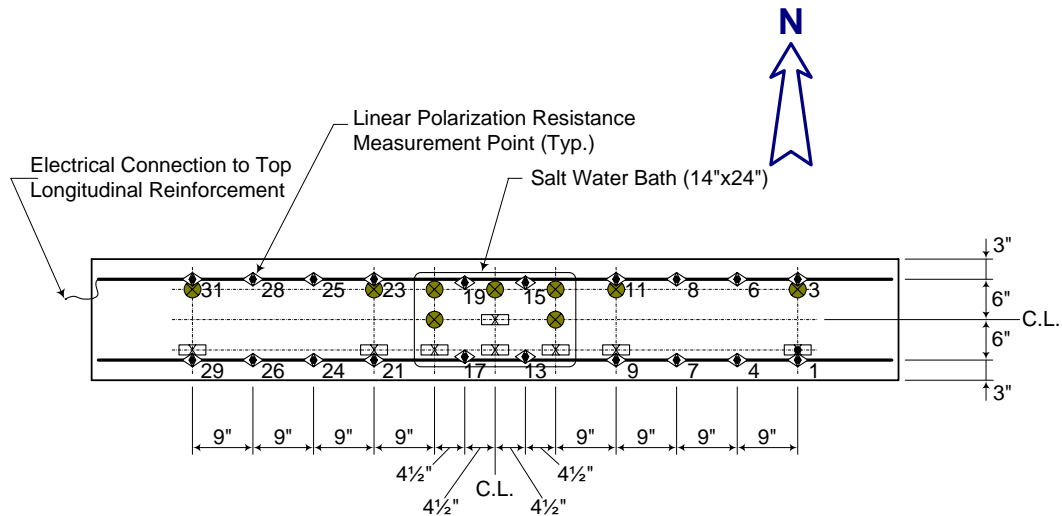


Figure 5-28 Linear Polarization Resistance Measurement Points

5.3.3 Measured Response during First Twelve Weeks

Results obtained between 13 January and 6 April 2005 are provided in Appendix I for slab #1 and Appendix J for slab #2. Results include sensing circuit and reference circuit characteristic frequencies and pseudo-quality factors for all interrogations of each sensor. Corrosion risk histories from half-cell potential measurements and corrosion rate histories calculated from linear polarization resistance measurements are also given for each measurement point corresponding to sensor locations.

5.3.3.1 Half-Cell Potentials

Typically, the half-cell potential is measured only after active corrosion is suspected within a reinforced concrete structure. Because initial measurements were taken on the slabs before corrosion testing began and multiple measurements at regular intervals since, the half-cell potential history may be developed and used for greater insight into corrosion activity.

Figure 5-29 shows surface contour plots of measured half-cell potentials for slab #1 at the end of each period. Figure 5-30 shows the same information for slab #2. Contours were constructed using linear interpolation between measurement points. The potential was assumed to be the same at the sides of the slabs as at the adjacent measurement points and zero potential was assumed at slab ends. The -150 millivolt (mV) contour intervals correspond with recommended corrosion probabilities developed from statistical evaluation of empirical half-cell data for copper-copper sulfate reference electrodes [6]. In general, the more negative the half-cell potential, the greater the probability of active corrosion in the steel embedded within the concrete at the measurement point. However, half-cell measurements do not give a direct indication of the rate that corrosion is occurring.

Initially, half-cell potentials were all more positive than -200 mV, indicating low corrosion risk as would be expected in concrete that has not been exposed to chlorides. Immediately after the first wet period, the potentials in the salt water bath began to rise substantially above the high corrosion risk potential of -350 mV, as shown in Fig. 5-31 for slab #1 and Fig. 5-33 for slab #2. Potentials appear to peak during wet periods and then fall back during dry periods, with each successive cycle producing more negative potentials. In addition, the measurements at points outside of the salt water bath have tended to become less negative after an initial increase during the first wet cycle, as shown in Fig. 5-32 for slab #1 and Fig. 5-34 for slab #2. Because the entire environmental history for each slab is known, an inference can be made that as active corrosion develops in the salt water bath, the steel is becoming more anodic in that region, while the steel outside of the salt water bath is becoming more cathodic in the electrochemical corrosion process. Slab #1 has a slightly more negative average potential in the salt water bath than slab #2, although the

difference is probably not significant enough to infer a difference in corrosion rate between the two slabs.

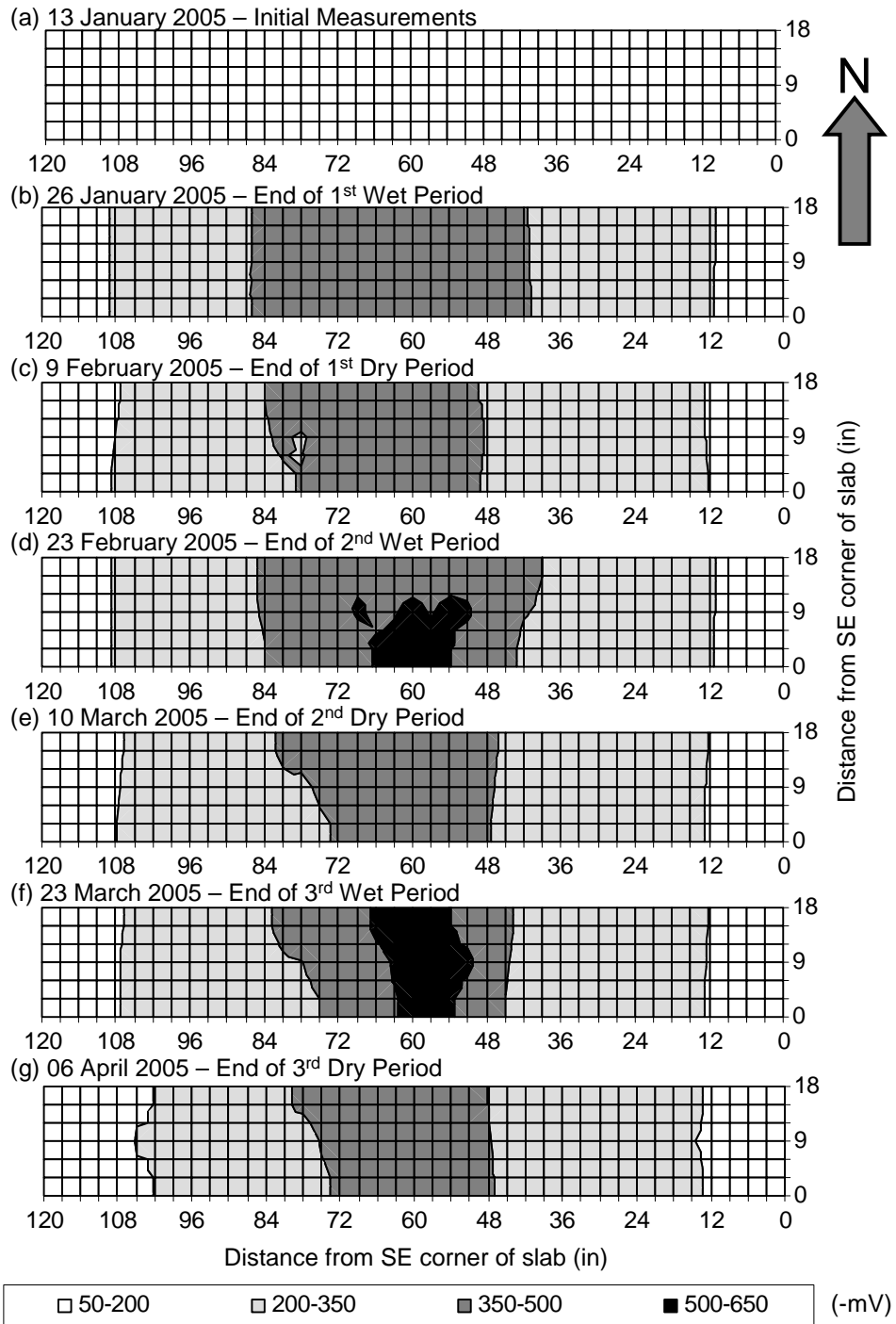


Figure 5-29 Slab #1 Half-Cell Potential Contour Plots

Slab #1 - Salt Water Bath Average

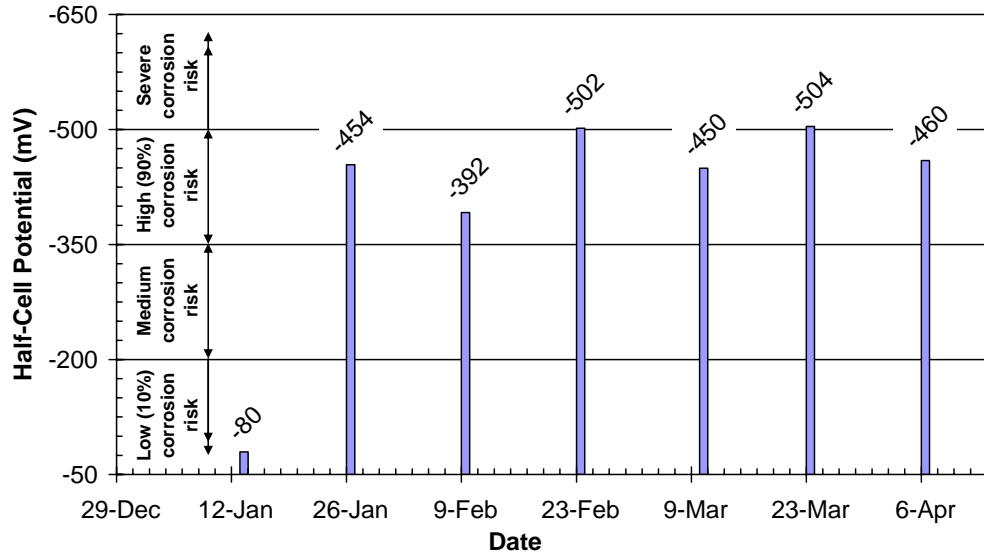


Figure 5-31 Slab #1 Corrosion Risk History Inside of Salt Water Bath

Slab #1 - Outside of Salt Water Bath Average

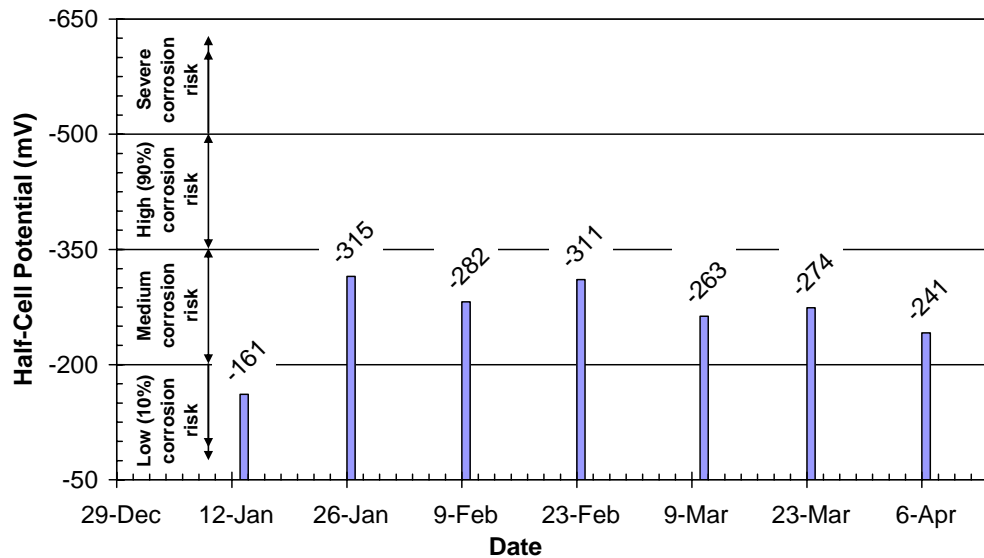


Figure 5-32 Slab #1 Corrosion Risk History Outside of Salt Water Bath

Slab #2 - Salt Water Bath Average

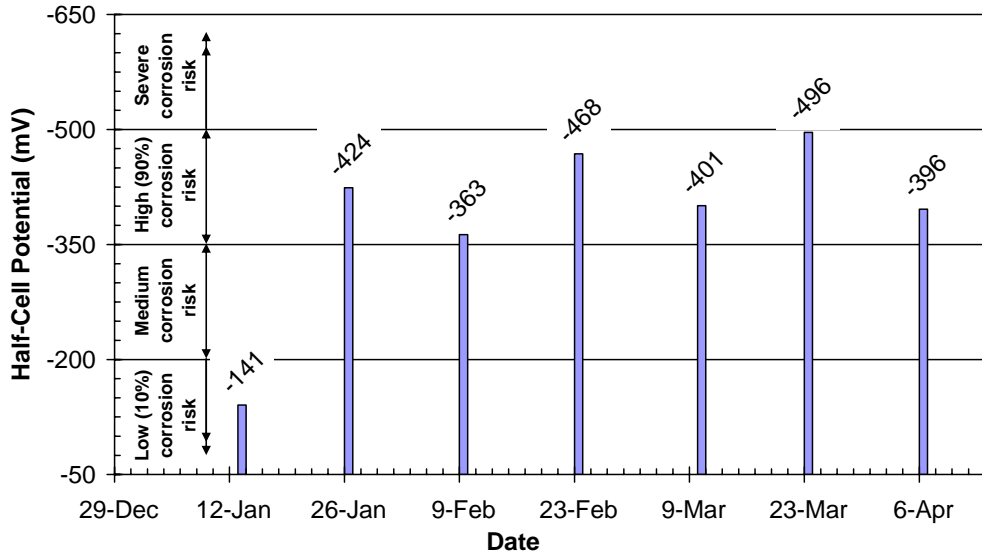


Figure 5-33 Slab #2 Corrosion Risk History Inside of Salt Water Bath

Slab #2 - Outside of Salt Water Bath Average

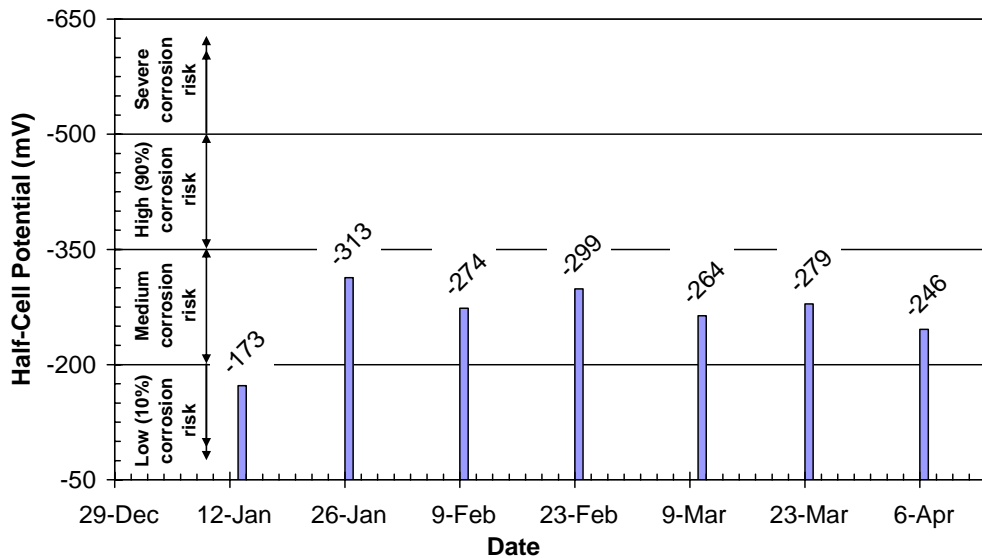


Figure 5-34 Slab #2 Corrosion Risk History Outside of Salt Water Bath

5.3.3.2 *Linear Polarization Resistance*

Linear polarization resistance is a technique used to approximate the instantaneous rate of corrosion for the area of steel being polarized. By using a counter electrode to deliver direct current to the concrete surface, steel embedded in concrete can be polarized, creating a change in potential that is measured using a reference electrode. A linear approximation to the slope of this current-potential relationship gives the polarization resistance of the steel. Corrosion current can then be calculated using the Stern-Geary equation [10] and converted to metal loss over time using Faraday's Law. Although this is an instantaneous measure of corrosion current, if multiple measurements are taken over time, the corrosion rate can be integrated to give the total amount of metal loss for a given length of time.

Type I equipment [1] without a guard ring was used for linear polarization resistance measurements on the slabs. The area of steel being polarized was assumed as the area directly beneath the counter electrode sponge. The sponge used for linear polarization resistance measurements was 3 in. wide and 7 in. long. One drawback of the linear polarization resistance method is the assumption about area of steel subject to polarization. In this case, both transverse and longitudinal bars in the top layer of steel only were used to calculate the affected area. Although the absolute values of corrosion rates obtained using this assumption may be considerably in error, comparison of corrosion rates in time will give very valuable insight into the corrosion activity occurring within the slabs.

Corrosion rate surface contour plots of slab #1 and slab #2 at the end of each period are shown in Figures 5-35 and 5-36, respectively. Contours were constructed using linear interpolation between measurement points, while assuming zero for the corrosion rate at the ends and sides of the slab. A corrosion rate of zero was assumed at the edges of the slab because no steel is present at

those locations. Although the initial contours for the slabs show a corrosion rate above 1 MPY in the middle of the slab, the actual maximum calculated rate in that region was only 1.04 MPY. Like the half-cell potential measurements, at the end of the first wet period, a large increase in corrosion rate in the salt water bath region was already apparent. As shown in Fig. 5-37 for slab #1 and Fig. 5-39 for slab #2, the corrosion rate remained approximately constant inside the salt water bath after the initial increase with only slight changes during the third full cycle. Outside of the salt water bath, no significant change in average corrosion rate is apparent, except for a slight decreasing trend after an initial increase at the end of the first wet period. Average corrosion rate histories for points outside of the salt water bath are given in Fig. 5-38 for slab #1 and Fig. 5-40 for slab #2. Corrosion rates for slab #1 have been slightly larger than rates for slab #2 during the entire test period.

Slab #1 - Salt Water Bath Average

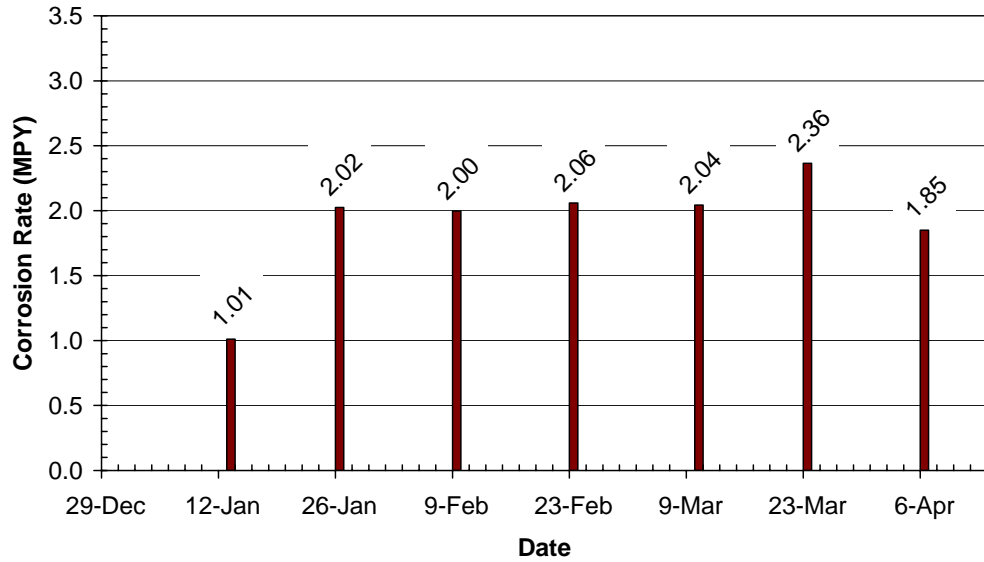


Figure 5-37 Slab #1 Corrosion Rate History Inside of Salt Water Bath

Slab #1 - Outside of Salt Water Bath Average

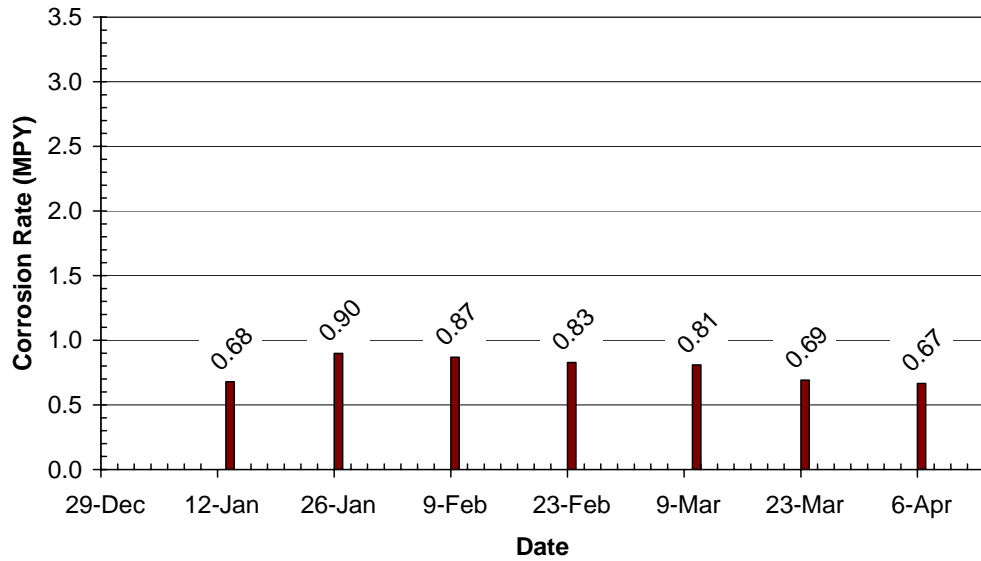


Figure 5-38 Slab #1 Corrosion Rate History Outside of Salt Water Bath

Slab #2 - Salt Water Bath Average

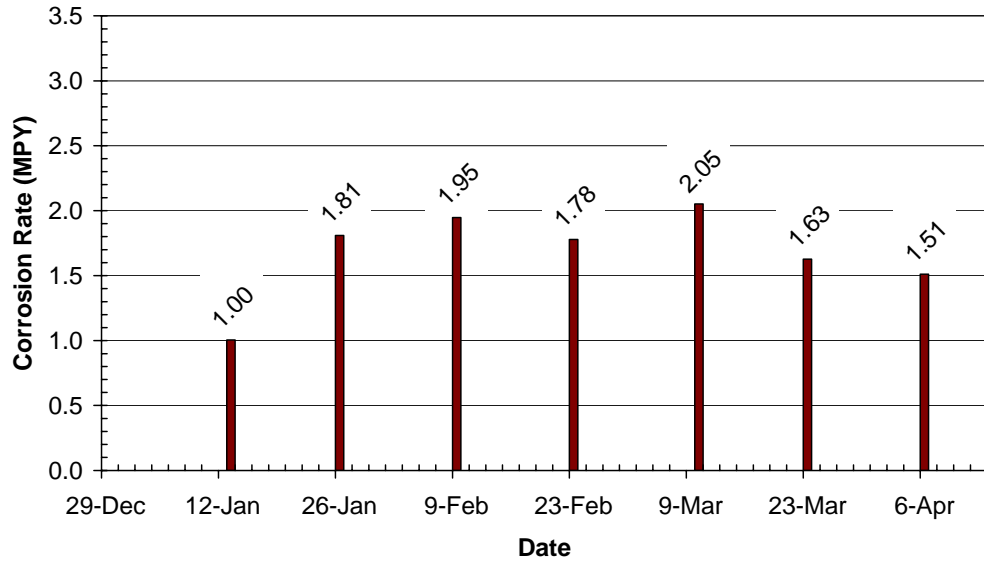


Figure 5-39 Slab #2 Corrosion Rate History Inside of Salt Water Bath

Slab #2 - Outside of Salt Water Bath Average

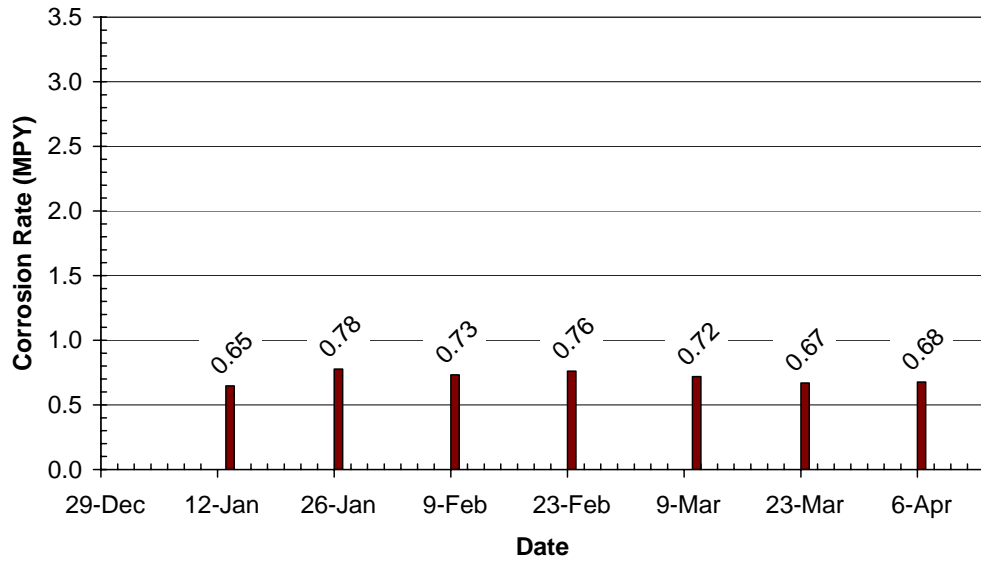


Figure 5-40 Slab #2 Corrosion Rate History Outside of Salt Water Bath

5.3.3.3 Sensor Monitoring

The phase response of each sensor embedded in the slabs has been evaluated using the signal processing routine discussed in Appendix D for all interrogations. Results are provided for each sensor embedded in slab #1 in Appendix I and for slab #2 in Appendix J.

For interrogations of sensors through 6 April 2005, only one sensor has indicated a broken wire, B05, a concentric sensor in slab #1 near the northwest corner of the salt water bath. The broken steel sensing wire in sensor B05 was detected on 9 February 2005 at the end of the first dry period. Since that time, it has responded at the reference characteristic frequency only. No internal investigation was conducted, as it was still very early in the test. Therefore, it is unknown whether the wire broke due to corrosion or for some other reason.

The readings from one other sensor in slab #1, A06, are too weak to be processed. Sensor A06 is a coplanar sensor in slab #1 just outside of the salt water bath on the southwest. Because the phase response of this sensor has been extremely weak since the very first reading, it is likely that the sensor was moved during concrete placement and ended up angled sharply to the surface of the slab. If a sensor is angled more than about 40° from horizontal, coupling between the angled sensor and horizontal reader coil becomes too weak to obtain quality readings. Therefore, the readings for sensor A06 cannot be reliably processed.

The results from the slab tests provided a large number of sensor readings that can be used to evaluate variations of the measurements with time. For Slab #1, Tables 5-10 through 5-12 summarize the means and coefficients of variation for the characteristic frequency, pseudo-quality factor, and phase dip for both the sensing and reference circuits in sensors with intact wires. The same information is summarized in Tables 5-13 through 5-15 for the sensors embedded in slab #2.

In general, variations in the measured responses were least for concentric sensors with 21-gage steel sensing wires. Concentric sensors with 26-gage steel sensing wires and coplanar sensors with 21-gage steel sensing wires also had acceptably small variations. Coplanar sensors with 26-gage steel sensing wires had the poorest response of the sensors tested.

The characteristic frequencies exhibited the least variation. Among the thirty-four sensors embedded in the slabs, the largest coefficient of variation was 0.1% for concentric sensors and 0.6% for coplanar sensors.

The pseudo-quality factors did not vary appreciably during the tests. The coefficient of variation did not exceed 10% for both the sensing and reference circuits for the all of the sensors except coplanar sensors with 26-gage steel sensing wires.

The phase dip experienced the largest variations. The coefficient of variation was typically less than 7% for the concentric sensors, but was typically over 10% for coplanar sensors.

Table 5-10 Variation of Characteristic Frequency for Sensors Embedded in Slab #1 – Intact Wires

Specimen	Number of Readings	Sensing Circuit		Reference Circuit	
		Mean Char. Freq. (MHz)	Coefficient of Variation (%)	Mean Char. Freq. (MHz)	Coefficient of Variation (%)
A01	8	0.56	0.2%	1.43	0.0%
A02	8	0.55	0.2%	1.40	0.0%
A03	8	0.56	0.4%	1.43	0.0%
A04	8	0.56	0.6%	1.44	0.0%
A05	8	0.56	0.4%	1.43	0.0%
A07	8	0.57	0.2%	1.43	0.0%
A08	8	0.56	0.3%	1.44	0.0%
B01	8	0.46	0.0%	1.54	0.0%
B02	8	0.46	0.0%	1.51	0.0%
B03	8	0.46	0.1%	1.52	0.0%
B04	8	0.46	0.1%	1.54	0.0%
B06	8	0.46	0.1%	1.54	0.0%
B07	8	0.47	0.1%	1.56	0.0%
B08	8	0.46	0.1%	1.55	0.0%
B09	8	0.46	0.1%	1.54	0.1%

Table 5-11 Variation of Pseudo-Quality Factor for Sensors Embedded in Slab #1 – Intact Wires

Specimen	Number of Readings	Sensing Circuit		Reference Circuit	
		Mean Pseudo-Quality Factor	Coefficient of Variation (%)	Mean Pseudo-Quality Factor	Coefficient of Variation (%)
A01	8	5.1	14.0%	33.8	0.6%
A02	8	5.7	14.3%	47.0	1.4%
A03	8	6.1	16.1%	32.7	1.4%
A04	8	5.4	19.0%	33.9	1.4%
A05	8	6.0	13.7%	34.6	1.7%
A07	8	6.0	11.7%	34.3	1.4%
A08	8	5.2	6.5%	40.6	1.4%
B01	8	7.3	1.6%	28.9	3.8%
B02	8	7.4	1.9%	29.9	4.5%
B03	8	7.3	2.1%	27.7	6.3%
B04	8	7.6	2.5%	27.9	8.8%
B06	8	7.9	1.9%	30.9	6.3%
B07	8	6.9	2.0%	28.1	5.8%
B08	8	7.6	3.2%	28.2	5.6%
B09	8	7.6	2.5%	26.4	9.8%

**Table 5-12 Variation of Phase Dip for Sensors Embedded in
Slab #1 – Intact Wires**

Specimen	Number of Readings	Sensing Circuit		Reference Circuit	
		Amplitude of Phase Dip (°)	Coefficient of Variation (%)	Amplitude of Phase Dip (°)	Coefficient of Variation (%)
A01	8	0.3	20.1%	9.5	4.7%
A02	8	0.3	23.7%	7.0	8.7%
A03	8	0.2	8.8%	2.7	11.5%
A04	8	0.2	10.3%	2.9	8.0%
A05	8	0.2	13.6%	2.7	9.2%
A07	8	0.2	24.5%	3.1	8.5%
A08	8	0.2	6.5%	3.5	6.1%
B01	8	1.6	5.5%	0.8	5.1%
B02	8	1.6	4.2%	0.8	3.1%
B03	8	1.1	7.6%	0.6	7.6%
B04	8	1.0	5.4%	0.5	6.1%
B06	8	1.1	5.0%	0.6	5.3%
B07	8	1.5	4.6%	0.8	3.9%
B08	8	1.3	15.1%	0.7	15.8%
B09	8	0.9	5.5%	0.5	6.4%

Table 5-13 Variation of Characteristic Frequency for Sensors Embedded in Slab #2 – Intact Wires

Specimen	Number of Readings	Sensing Circuit		Reference Circuit	
		Mean Char. Freq. (MHz)	Coefficient of Variation (%)	Mean Char. Freq. (MHz)	Coefficient of Variation (%)
A51	8	0.59	0.1%	1.41	0.0%
A52	8	0.59	0.3%	1.39	0.0%
A53	8	0.59	0.1%	1.39	0.0%
A54	8	0.59	0.2%	1.42	0.0%
A55	8	0.59	0.1%	1.43	0.1%
A56	8	0.59	0.2%	1.41	0.0%
A57	8	0.59	0.2%	1.42	0.0%
A58	8	0.59	0.1%	1.42	0.0%
B51	8	0.47	0.0%	1.53	0.0%
B52	8	0.47	0.0%	1.54	0.0%
B53	8	0.48	0.1%	1.55	0.0%
B54	8	0.47	0.0%	1.53	0.0%
B55	8	0.48	0.1%	1.54	0.0%
B56	8	0.47	0.0%	1.52	0.0%
B57	8	0.47	0.0%	1.53	0.0%
B58	8	0.48	0.0%	1.53	0.0%
B59	8	0.48	0.0%	1.53	0.0%

Table 5-14 Variation of Pseudo-Quality Factor for Sensors Embedded in Slab #2 – Intact Wires

Specimen	Number of Readings	Sensing Circuit		Reference Circuit	
		Mean Pseudo-Quality Factor	Coefficient of Variation (%)	Mean Pseudo-Quality Factor	Coefficient of Variation (%)
A51	8	8.7	4.8%	34.1	1.0%
A52	8	9.3	5.2%	44.9	1.1%
A53	8	9.3	6.4%	34.2	0.9%
A54	8	9.1	1.7%	32.3	0.4%
A55	8	9.4	4.3%	32.3	1.0%
A56	8	9.3	3.8%	42.7	0.5%
A57	8	8.7	8.8%	32.4	0.9%
A58	8	8.9	1.9%	39.3	0.5%
B51	8	11.7	0.4%	34.7	2.2%
B52	8	11.9	1.0%	36.7	2.0%
B53	8	11.3	1.6%	34.4	1.7%
B54	8	11.7	1.3%	35.1	3.8%
B55	8	11.3	1.0%	34.5	1.7%
B56	8	12.0	1.0%	37.2	2.0%
B57	8	11.3	0.8%	33.9	5.0%
B58	8	11.8	1.2%	33.7	1.6%
B59	8	12.3	1.8%	40.4	2.2%

Table 5-15 Variation of Phase Dip for Sensors Embedded in Slab #2 – Intact Wires

Specimen	Number of Readings	Sensing Circuit		Reference Circuit	
		Amplitude of Phase Dip (°)	Coefficient of Variation (%)	Amplitude of Phase Dip (°)	Coefficient of Variation (%)
A51	8	0.3	17.0%	2.8	8.9%
A52	8	0.2	32.6%	5.8	4.7%
A53	8	0.4	12.8%	2.5	9.2%
A54	8	0.4	26.1%	3.9	5.0%
A55	8	0.4	19.7%	4.2	4.5%
A56	8	0.2	12.3%	7.1	2.4%
A57	8	0.3	35.0%	4.3	6.2%
A58	8	0.6	15.4%	5.3	6.8%
B51	8	2.6	6.5%	0.9	6.8%
B52	8	3.6	5.7%	1.2	4.6%
B53	8	3.6	5.1%	0.9	3.4%
B54	8	3.5	3.2%	1.1	2.5%
B55	8	2.9	3.9%	0.9	0.1%
B56	8	3.3	3.3%	1.2	2.9%
B57	8	2.4	4.1%	0.7	3.9%
B58	8	3.3	3.6%	0.8	2.3%
B59	8	6.2	1.5%	1.7	1.0%

5.3.4 Interpretation and Evaluation

Results from the reinforced concrete slabs are not complete because the tests are still ongoing. All of the monitoring should be continued until broken wires are detected in several sensors. Conclusions may be developed after broken wires are detected, corrosion of the reinforcing steel and steel sensing wires are examined, and chloride contents are obtained. At that time, results from sensor monitoring, half-cell potential measurements, and linear polarization resistance measurements should be evaluated.

CHAPTER 6

Conclusions

6.1 SUMMARY

The second generation wireless corrosion sensors developed through this research fulfill the need for an inexpensive and reliable method for early detection of corrosion in reinforced concrete structures. Tests of sensors embedded in small concrete prisms have confirmed the ability of the sensors to detect a threshold amount of corrosion. Although testing should be continued, results from sensor calibration and testing thus far indicate that the signal processing method used in conjunction with second generation sensors produces a reliable indication of the state of the steel sensing wire in all environmental conditions expected for common reinforced concrete structures. Established corrosion monitoring techniques were used in tests of reinforced concrete slabs to provide even more information on the performance of second generation sensors.

The parameters affecting sensor response have been identified and verified through testing. Conclusions from parametric tests may be applied to future sensor designs. The sensitivity of the sensor response to the conductivity of the environment has been explored and, although the resulting sensors exhibit transition behavior, the sensors are less sensitive than earlier prototypes. Tests confirm that an appropriate sensor circuit model should include a variable resistor for the external steel sensing wire rather than a switch. Both characteristic frequencies and pseudo-quality factors must be used to determine the state of the steel sensing wires.

Although read range has been improved, increased cover depths or readings in areas not directly accessible with the reader coil require substantial further improvements. However, the goals of increased read range and smaller sensor size are contradictory. The size of the second generation sensors should be considered the maximum size for a practical embedded corrosion sensor. Therefore, further increases in read range must be obtained through development of improved interrogation equipment.

6.2 RECOMMENDATIONS

Current testing of the second generation sensors, which includes monitoring of sensors embedded in concrete prisms and reinforced concrete slabs, should continue. Half-cell potentials and corrosion rates from linear polarization resistance measurements on the reinforced concrete slabs should also be collected. After at least half of the sensors embedded within the salt water bath area of a reinforced concrete slab indicate broken steel sensing wires, chloride contents should be determined at the level of the sensors both at cracks and away from cracks and the cover concrete should be removed from the entire slab to examine the state of corrosion on the reinforcement and the steel sensing wires of sensors.

Thermal testing of second generation sensors that are not embedded in concrete should be carried out over the temperature range expected in typical reinforced concrete structures to develop the relationship among characteristic frequencies, pseudo-quality factors, and temperature. More tests of second generation sensors embedded in concrete prisms and reinforced concrete slabs would be useful for further establishing sensor reliability. In future tests, concrete prisms should be constructed with equal cover over the sensors on the top and sides and prisms and slabs should have a uniform and smooth finish on the top surface. Using heat lamps to increase temperatures may be useful for increasing

the rate of corrosion in future tests. Also, to test the sensors in a situation common to many reinforced concrete structures, it would be useful to construct reinforced concrete slabs specifically set up to develop macrocell corrosion. Sensors may behave differently in the macrocell corrosion environment.

Read range must be increased before the sensors can be installed in structures outside of the laboratory for testing. The practical limits explored in Chapter 3 make the interrogation equipment the most likely source of future improvements.

The potting material used for the sensors should be thermally compatible with concrete. If adjustments cannot be made to the coefficient of thermal expansion of the marine epoxy potting material used for second generation sensors, a new potting material may be necessary to ensure that the durability of a structure with embedded sensors is not compromised.

With further research, sensors may be developed to detect more information than just a corrosion threshold. Tuning of sensors to detect a specific resistance of the surrounding environment might be possible, which would enable a broad range of different sensors to be developed. Sensors may provide analog information about the rate of corrosion in the steel sensing wires or about the surrounding environment with further development.

APPENDIX A

Parametric Study I

A.1 INTRODUCTION

In Parametric Study I, 27 completely sealed sensors were constructed using a single inductor with varying diameters and numbers of magnet wire turns. Three different nominal diameters of PVC pipe were used (0.75-in., 1.0-in., and 1.25-in.) and the number of 24-gage copper magnet wire turns varied between 1 and 9. The intent was to keep the characteristic frequency nearly constant at approximately 4 MHz, so different values of capacitance were required in the different sensors. Because different capacitors were used to construct the sensors, the effects of capacitor type could not be eliminated from the results. Sensors were potted with marine epoxy, which bonds to metal and completely seals and protects the sensor components.

Tests were conducted in June 2004. The Solartron Impedance Analyzer was used to interrogate all sensors. Sensors were interrogated using a 2-in. diameter reader coil with a single turn of 24-gage copper magnet wire. This is the same reader coil used in previous tests by Andringa [5], Grizzle [9], and Simonen [15]. Interrogations were conducted with varying read distances in three different environments: air, tap water, and salt water (3.5% sodium chloride by weight). Results of the parametric study showing the effect of inductor diameter, number of turns in the inductor, read distance, and environment are presented in this Appendix. The effect of capacitor type is also discussed. All comparisons are qualitative assessments based on the phase response of the sensors, using the phase dip.

A.2 SENSORS

A diagram of the sensor circuit used for this study is shown in Fig. A-1. In the cases where a single capacitor with the required value of capacitance was available, a single capacitor was used, as shown in the circuit diagram. In some cases, multiple capacitors were needed to obtain the required capacitance and, therefore, capacitors were soldered into the circuit in parallel.

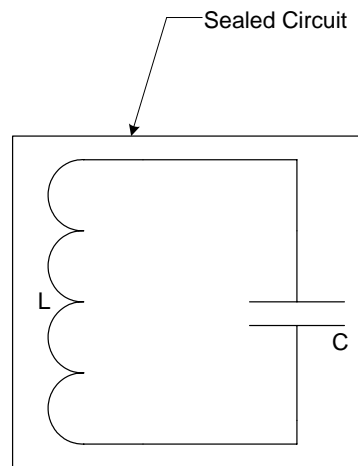


Figure A-1 Sensor Circuit Diagram for Parametric Study I

Sensors were labeled based on diameter and number of magnet wire turns. Labels consist of the number of wire turns followed by a letter signifying the nominal diameter of PVC pipe used for the inductor: “a” for 0.75-in. nominal diameter, “b” for 1.0-in. nominal diameter, and “c” for 1.25-in. nominal diameter. For example, sensor 1a has an inductor with a single turn of 24-gage copper magnet wire around a slice of 0.75-in. nominal diameter PVC pipe.

Table A-1 lists the sensors with 0.75-in. nominal diameter inductors along with the value of capacitance and the approximate inductance used in the circuit. Tables A-2 and A-3 list the same information for sensors with 1.0-in. and 1.25-in. nominal diameter inductors, respectively. All of the sensors were constructed using ceramic capacitors of different grades and classes.

Table A-1 Sensors with 0.75-in. Nominal Diameter Inductors

Sensor	Inductor Diameter (in.)	Number of Turns	Length of Coil (in.)	Approximate Inductance L (μ H)	Capacitance C (pF)
1a	1.055	1	0.02	0.06	27000
2a	1.055	2	0.04	0.23	6600
3a	1.055	3	0.06	0.50	3300
4a	1.055	4	0.08	0.85	1800
5a	1.055	5	0.10	1.30	1150
6a	1.055	6	0.12	1.81	890
7a	1.055	7	0.14	2.40	660
8a	1.055	8	0.16	3.05	560
9a	1.055	9	0.18	3.76	430

Table A-2 Sensors with 1.0-in. Nominal Diameter Inductors

Sensor	Inductor Diameter (in.)	Number of Turns	Length of Coil (in.)	Approximate Inductance L (μ H)	Capacitance C (pF)
1b	1.31	1	0.02	0.07	22000
2b	1.31	2	0.04	0.29	4700
3b	1.31	3	0.06	0.63	2500
4b	1.31	4	0.08	1.09	1500
5b	1.31	5	0.10	1.66	1000
6b	1.31	6	0.12	2.33	660
7b	1.31	7	0.14	3.09	560
8b	1.31	8	0.16	3.95	430
9b	1.31	9	0.18	4.89	330

Table A-3 Sensors with 1.25-in. Nominal Diameter Inductors

Sensor	Inductor Diameter (in.)	Number of Turns	Length of Coil (in.)	Approximate Inductance L (μ H)	Capacitance C (pF)
1c	1.68	1	0.02	0.09	14700
2c	1.68	2	0.04	0.37	3600
3c	1.68	3	0.06	0.82	2000
4c	1.68	4	0.08	1.42	1000
5c	1.68	5	0.10	2.18	650
6c	1.68	6	0.12	3.08	500
7c	1.68	7	0.14	4.12	300
8c	1.68	8	0.16	5.28	250
9c	1.68	9	0.18	6.56	200

A.3 INDUCTOR DIAMETER

In order to check the feasibility of reducing the size of the sensors, two inductor diameters were chosen that were smaller than the inductor diameter used in the first generation sensors. The smallest diameter PVC pipe that still allowed enough room for soldering circuit components inside the pipe was 0.75-in. nominal diameter. As shown in the following results, the magnitude of phase dip generally decreased with smaller inductor diameter and was very poor for the smallest inductor. This is expected because as the effective inductance of the circuit is reduced with decreasing diameter, the coupling efficiency of the sensor with the reader coil is also reduced. In the few cases that phase dips were smaller for larger diameter inductors, the effects of capacitor type are likely at fault. Many different capacitors were used in order to keep the characteristic frequency of the sensor around 4 MHz. Some of these capacitors were not high-quality ceramic capacitors and have an unsatisfactory quality factor for use in the sensors. Capacitor type is discussed in A.7.

In Fig. A-2 through A-10, phase dip is plotted against nominal inductor diameter for each number of turns. All of these results were measured at a constant read distance of 0.5-in. for sensors in air.

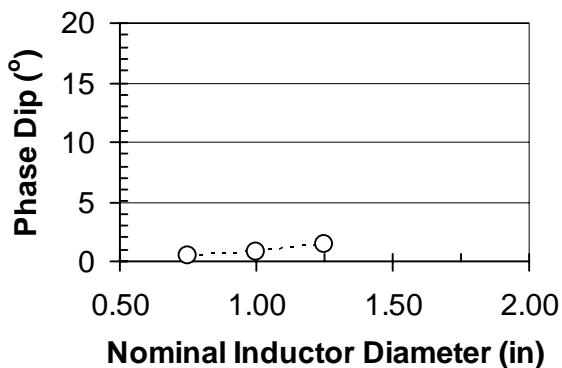


Figure A-2 Phase Dip vs. Inductor Diameter for 1-Turn Inductor

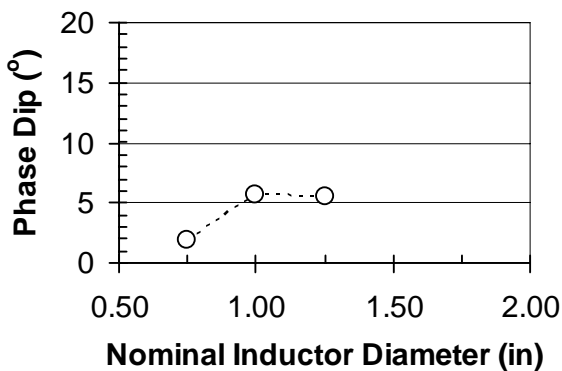


Figure A-3 Phase Dip vs. Inductor Diameter for 2-Turn Inductor

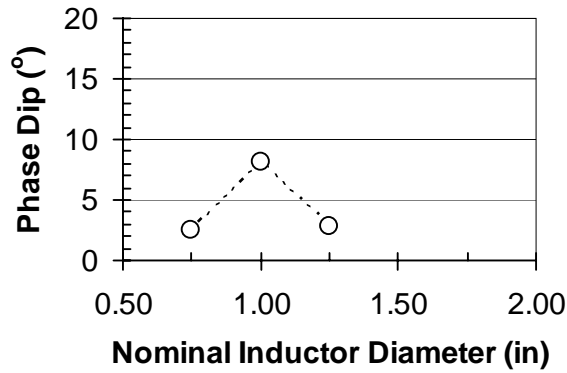


Figure A-4 Phase Dip vs. Inductor Diameter for 3-Turn Inductor

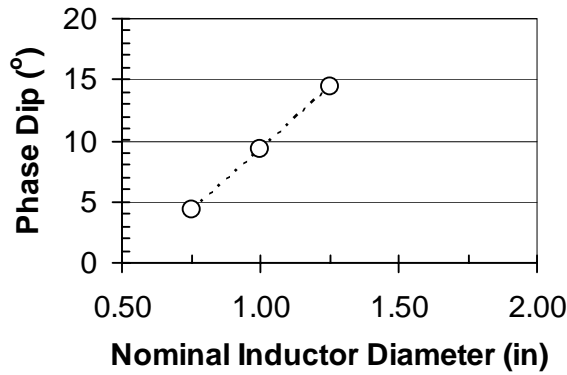


Figure A-5 Phase Dip vs. Inductor Diameter for 4-Turn Inductor

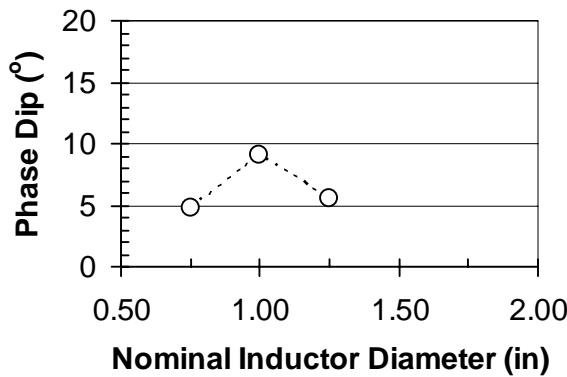


Figure A-6 Phase Dip vs. Inductor Diameter for 5-Turn Inductor

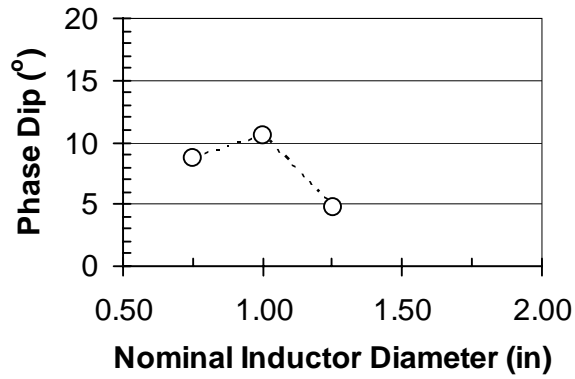


Figure A-7 Phase Dip vs. Inductor Diameter for 6-Turn Inductor

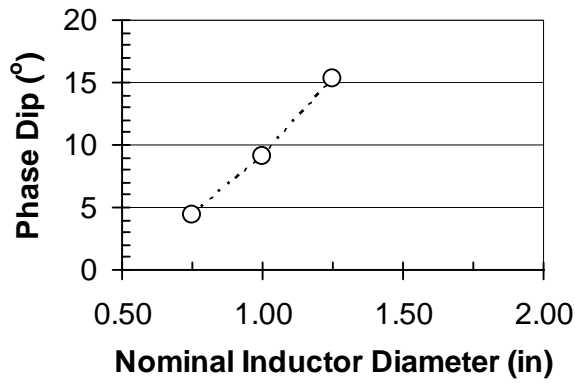


Figure A-8 Phase Dip vs. Inductor Diameter for 7-Turn Inductor

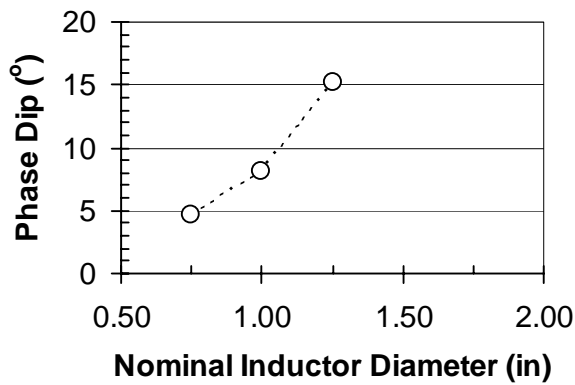


Figure A-9 Phase Dip vs. Inductor Diameter for 8-Turn Inductor

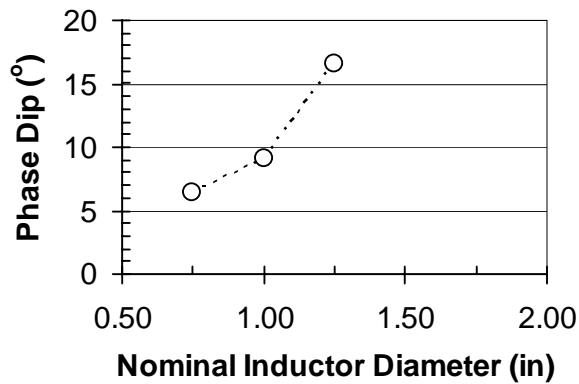


Figure A-10 Phase Dip vs. Inductor Diameter for 9-Turn Inductor

A.4 NUMBER OF TURNS

The number of magnet wire turns was varied between 1 and 9 for all three diameters of inductor coil. In general, phase dip increased with increasing number of turns. However, this trend appears to diminish above 5 turns. Therefore, 5 turns was selected as the optimum in further sensor development to provide a good quality phase dip while also reducing the amount of time required for fabrication of the sensors. In a few cases, sensors with a greater number of turns had smaller phase dips than sensors with fewer turns. Again, the suspected cause of reduced phase dips was the type of capacitor used in the circuit. The effect of capacitor type is discussed in A.7.

In Fig. A-11 through A-13, phase dip is plotted against number of turns for each inductor diameter. All of these results were measured at a constant read distance of 0.5-in. for sensors interrogated in air.

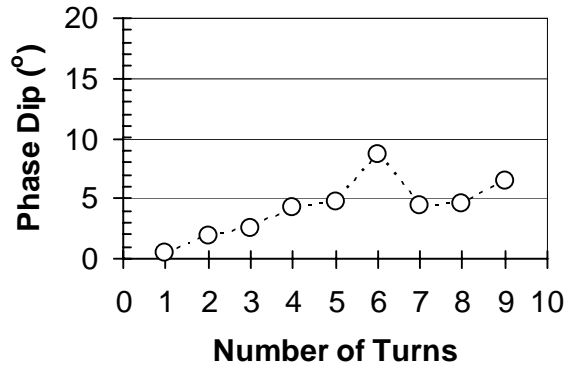


Figure A-11 Phase Dip vs. Number of Turns for 0.75-in. Diameter Inductor

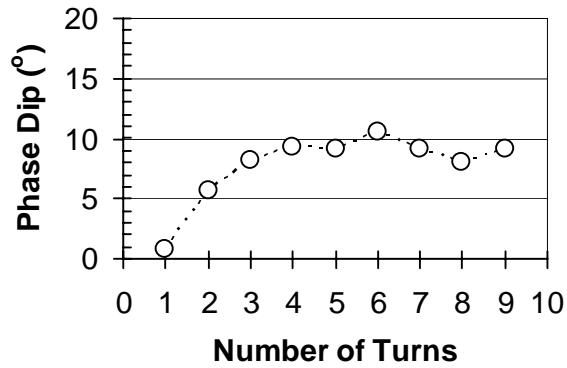


Figure A-12 Phase Dip vs. Number of Turns for 1.0-in. Diameter Inductor

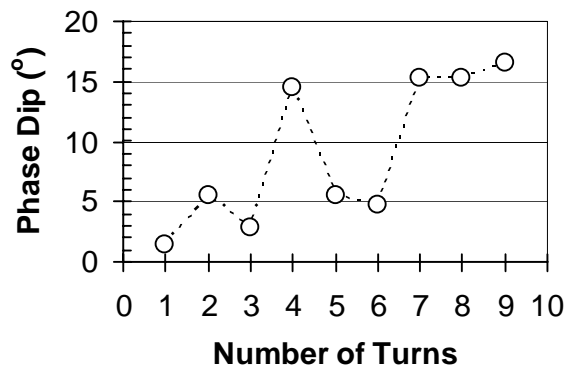


Figure A-13 Phase Dip vs. Number of Turns for 1.25-in. Diameter Inductor

A.5 READ DISTANCE

Read distance has the greatest effect on phase dip of the parameters considered. For this study, sensors were interrogated at six different read distances ranging from 0 to 2.5 in. in 0.5-in. increments. Phase dips are greatly reduced with increasing read distance. For a given reader coil diameter and number of magnet wire turns, and a given inductor diameter and number of turns, phase dip may be reduced by as much as 80% with only 0.5-in. increase in read distance. The maximum read distance was defined as the read distance where phase dips become less than 0.1° . This limit was selected because it is about two times the amplitude of the noise produced in readings with the Solartron Impedance Analyzer. Noise is the variation in baseline phase angle with varying frequency without any external sensor circuit present.

Table A-4 gives the maximum read distance for each sensor. Fig. A-14 shows phase dip plotted against inductor diameter for four different read distances: 0.0-in., 0.5-in., 1.0-in., and 1.5-in. All data shown in Fig. A-14 are for sensors with 7 magnet wire turns interrogated in air. Fig. A-15 shows phase dip on a log scale plotted against number of turns for the same four read distances. In this figure, sensors with a constant 1.25-in. inductor diameter were interrogated in air. Read distances beyond 2.0-in. generally had very small phase dips of just a few tenths of a degree, which would be difficult to interpret in practice. Overall, the 1.25-in. nominal diameter inductor provided the best phase dip over the largest range of read distances. The smaller phase dips shown for 3 turns, 5 turns, and 6-turns with the 1.25-in. nominal diameter inductors are most likely due to low-quality capacitors.

Table A-4 Maximum Read Distance

0.75-in. Diameter Sensor	Maximum Read Distance (in.)	1.0-in. Diameter Sensor	Maximum Read Distance (in.)	1.25-in. Diameter Sensor	Maximum Read Distance (in.)
1a	1.0	1b	1.0	1c	1.5
2a	1.5	2b	2.0	2c	2.0
3a	1.5	3b	2.0	3c	1.5
4a	2.0	4b	2.0	4c	2.5
5a	1.5	5b	2.0	5c	2.0
6a	1.5	6b	2.5	6c	2.0
7a	2.0	7b	2.5	7c	2.5
8a	1.5	8b	2.5	8c	2.5
9a	1.5	9b	2.0	9c	2.5

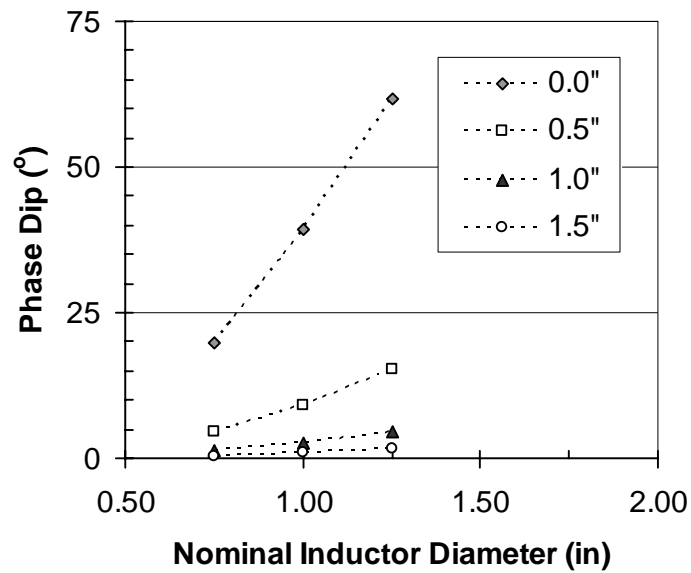


Figure A-14 Phase Dip for 7-Turn Inductor at Different Read Distances

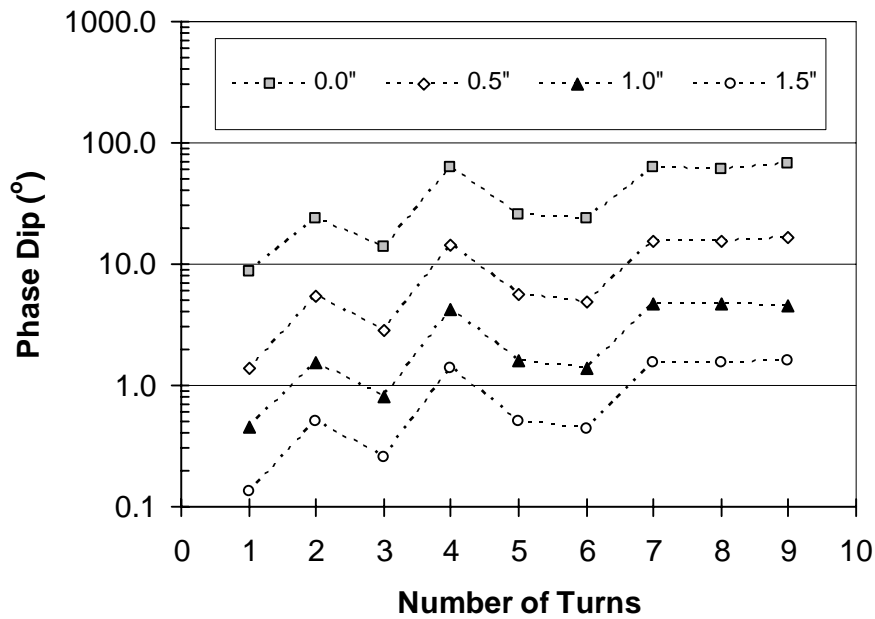


Figure A-15 Phase Dip for 1.25-in. Diameter Inductor at Different Read Distances

A.6 SURROUNDING ENVIRONMENT

To test the effect of surrounding environment that the sensor must be inductively coupled through, sensors were interrogated at varying read distances in air, tap water, and salt water with a 3.5% concentration of sodium chloride by weight.

Based on previous tests by Novak [13], steel in very close proximity with the inductor coil was shown to be parasitic to inductive coupling of the reader with the inductor coil of EAS tags. This parasitic effect reduces the coupling efficiency between the reader and the inductor of the sensor, effectively shielding the characteristic frequency response of the sensor. For example, sensors could not be interrogated if a steel plate is placed between the reader coil and the inductor coil of the sensor. Although sensors could be interrogated through

concrete as shown by Grizzle [9] and Simonen [15], a decrease in resistance due to the presence of moisture and chlorides might lead to a parasitic effect similar to that of steel. This decreasing resistance of the environment was modeled outside of concrete using air, tap water, and salt water.

For sensor circuits that are completely sealed by an impervious potting material, very little difference in phase dip occurs as the conductivity of environment increases. A slight reduction in phase dip occurs with the change from air to tap water. This reduction is generally about 5-10% of the phase dip in air. Although the tap water may have some effect, the small decrease in phase dip may be due to the test method. In order to test the sensors in water, a beaker must be placed over the reader coil to contain the water. The thickness of the glass bottom of the beaker increases the read distance slightly. This increased read distance for readings in tap water probably results in the majority of the reduction in phase dip.

A larger reduction in phase dip occurs with the change from tap water to salt water. This reduction is generally about 20-40% of the phase dip in tap water. So, while the increased conductivity of salt water does have a slightly parasitic effect on readings, the reduction in phase dip is not sufficient to shield sensor response completely. In general, the maximum read distance in salt water was about 0.5-in. less than the maximum read distance in air and tap water.

Fig. A-16 and A-17 show phase dip plotted against inductor diameter for sensors interrogated at 0.5-in. read distance in air, tap water, and salt water. Fig. A-16 is for sensors with 7 turns of magnet wire and Fig. A-17 is for sensors with 4 turns of magnet wire. Clearly, the difference between interrogations in air and tap water is much smaller than the difference between interrogations in tap water and salt water. In Fig. A-18, phase dip is plotted against number of magnet wire turns for sensors with a 1.25-in. nominal diameter inductor coil interrogated at

0.5-in. read distance in air, tap water, and salt water. Points for interrogations in air and tap water fall almost on top of one another, while interrogations in salt water show much smaller phase dips. The effect of a conductive environment appears to have a greater influence on sensors with higher values of inductance.

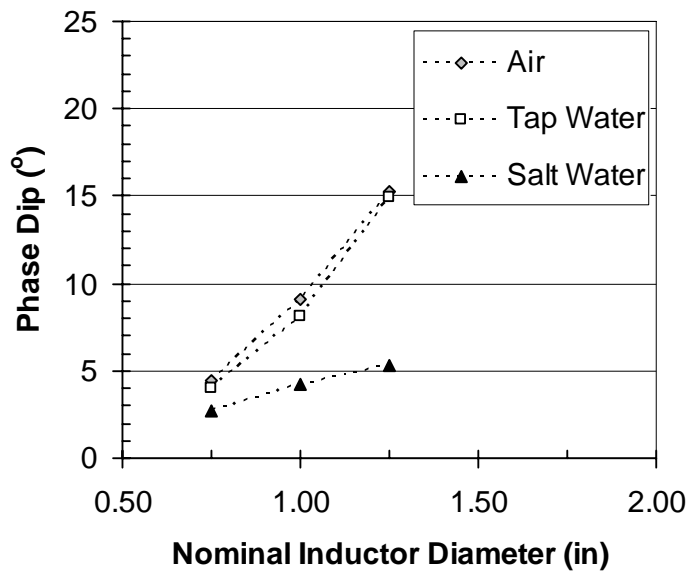


Figure A-16 Phase Dip for 7-Turn Inductor in Different Environments

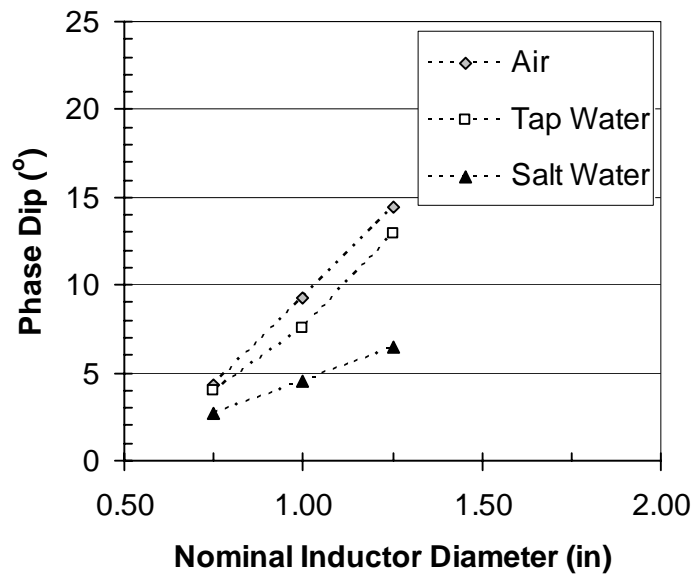


Figure A-17 Phase Dip for 4-Turn Inductor in Different Environments

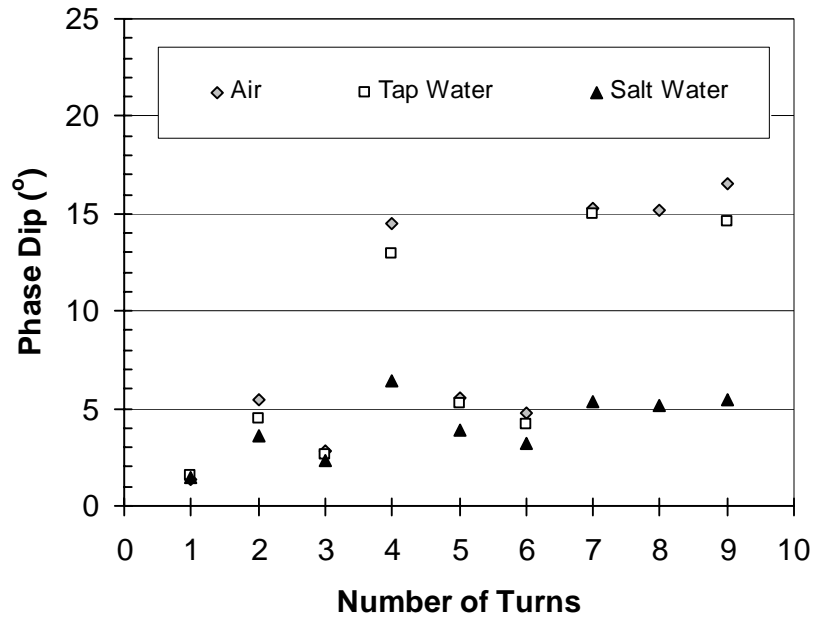


Figure A-18 Phase Dip for 1.25-in Inductor in Different Environments

A.7 CAPACITOR TYPE

The only consideration given to capacitors for sensor fabrication prior to this study was the value of capacitance and the physical size of the capacitor. In the process of fabricating sensors for this study, several different types of capacitors were purchased because a wide range of capacitance values were required. Most of the capacitors produced phase dips of reasonable quality, but a few exhibited very poor behavior. For example, the reduction in phase dip for sensors with 1.25-in. nominal diameter inductors with 3-turns, 5-turns, and 6-turns is likely due to capacitor type (Fig. A-4, A-6, A-7, A-13, A-15 and A-18). The 500-pF capacitors used in the 5 and 6-turn sensors and the 2000-pF capacitor used in the 3-turn sensor were an inferior grade of ceramic capacitor. In addition to being shallow, the phase dips were also wide and rounded for sensors fabricated with these inferior capacitors (Fig. A-19).

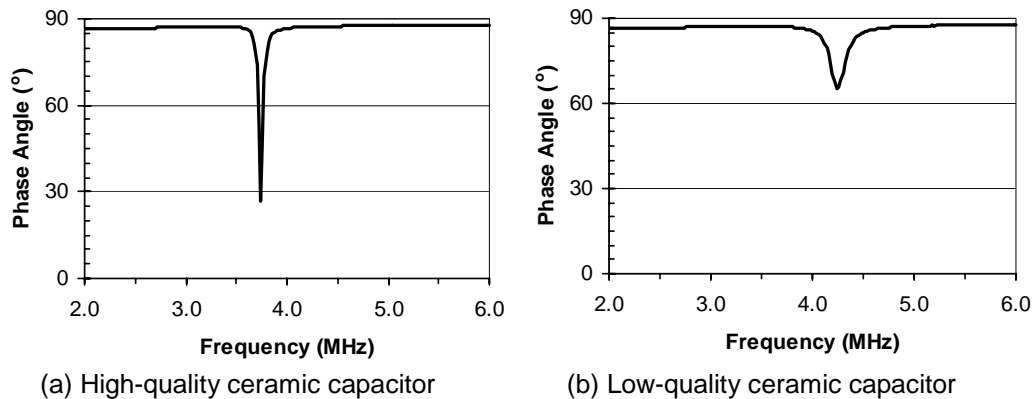


Figure A-19 Effect of Capacitor Type on Phase Response of Sensors

Several types of capacitors are available commercially and used in various electronic products. They are built using various dielectric materials, some for very specific applications, like Teflon® capacitors for guitar amplifiers. The premium-quality capacitors for special uses are much more expensive than mass-

produced capacitors for general purpose electronic applications. Because one requirement of the corrosion sensor is to be inexpensive, standard capacitors are well suited for the application. Capacitors are rated based on variance in capacitance (error), temperature stability or temperature coefficient, frequency range, dielectric constant, and dielectric absorption, among other factors. All of the factors influencing capacitor quality are too numerous to address in this appendix and are outside the scope of this research. However, further information on capacitors, including coding and dielectric material, can be found in References 16 and 17.

Class 1 high-quality ceramic capacitors are best suited for use in the sensors. These are typically labeled NP0 or COG and meet stringent temperature stability requirements. COG capacitors are generally larger than capacitors of lower classes, but remain small enough for use in hand-fabricated corrosion sensors. COG capacitors are produced in the 1 to 47,000-pF range, but may be difficult to find above 10,000 pF. Ceramic capacitors with X7R labels may also be of high enough quality to be used in the sensors, but are generally considered Class 2 capacitors. Other capacitors with plastic, mica, tantalum, and ceramic dielectric materials should be avoided due to their poor error and temperature ratings, dielectric absorption, and frequency instability.

APPENDIX B

Parametric Study II

B.1 INTRODUCTION

In Parametric Study II, four trial sensors were constructed using nominally identical inductors and capacitors, but four different combinations of wire material and gage were used as the sensing mechanism. Two different diameters of steel wire, 21-gage and 26-gage, and two diameters of copper magnet wire, 18-gage and 24-gage were used for sensing wires. The circuit model for the trial sensors was the same as that for the first generation basic sensor. Sensors were potted with marine epoxy, which bonds to metal and completely seals and protects the sensor components, leaving only the sensing wire exposed to the environment.

Tests were conducted in August 2004. The Solartron Impedance Analyzer was used to interrogate all sensors. Sensors were interrogated using a 4-in. diameter reader coil with a single turn of 24-gage copper magnet wire. This reader coil was shown through testing to produce deeper phase dips over a greater range of read distances than the smaller diameter reader coil used in Parametric Study I. Interrogations were conducted with varying read distance in air, tap water, and salt water with varying concentrations of sodium chloride. Results of the parametric study showing the effect of sensing wire material and gage, and surrounding environment are presented in this Appendix. All comparisons are qualitative assessments based on the phase response of the sensors, using characteristic frequency and phase dip.

B.2 SENSORS

A diagram of the sensor circuit used for this study is shown in Fig. B-1. The inductor was fabricated using 2.0-in. nominal diameter PVC pipe with 5 turns of 18-gage copper magnet wire, resulting in an approximate inductance of $3.0\ \mu\text{H}$. High-quality ceramic capacitors of 2,700 and 33,000 pF were used in the sensor circuits. The effective capacitance, as well as the phase response of the sensor, changes depending on the state of the sensing wire. With the sensing wire intact, the sensor has an initial effective circuit capacitance of 35,700 pF and responds at an initial characteristic frequency of approximately 0.4 MHz, as shown in Fig. B-2(a). When the sensing wire is cut, the sensor has a final effective circuit capacitance of 2,700 pF and responds at a final characteristic frequency of approximately 1.8 MHz as shown in Fig. B-2(b).

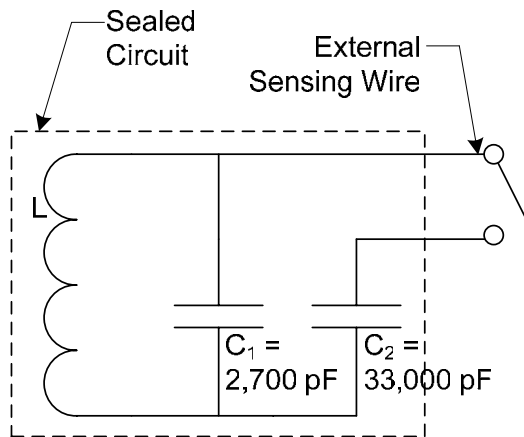


Figure B-1 Sensor Circuit Diagram for Parametric Study II

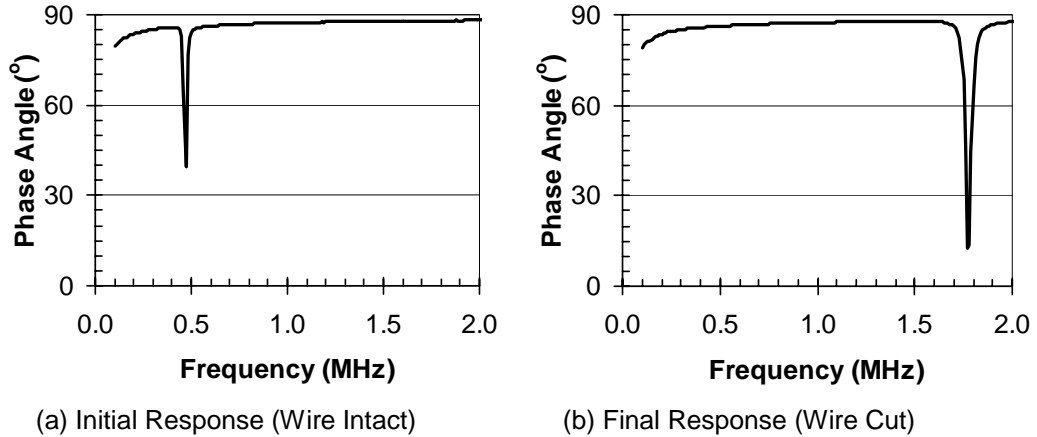


Figure B-2 Phase Response of Sensors used in Parametric Study II

Sensors were labeled as shown in Table B-1. Labels consist of the number of wire turns followed by a letter signifying the nominal diameter of PVC pipe used for the inductor. In this case 5D represents a 5-turn inductor with a 2.0-in. nominal diameter. The trial sensor configuration and capacitance values are represented by the next two characters in the sensor label, with C representing a two-capacitor, single-inductor circuit with the capacitance values given above. The number following C represents the material and wire gage used for the sensing wire. Wires are numbered in order of decreasing resistance.

Table B-1 Sensing Wire Material and Size

Sensor	Wire Type	Wire Gage*	Wire Diameter (in)
5D_C1	Steel	26	0.0180
5D_C2	Steel	21	0.0320
5D_C3	Copper	24	0.0201
5D_C4	Copper	18	0.0403

*Steel wire is sized using the U.S. Steel Wire Gage (USSWG) standard and copper wire is sized using the American Wire Gage (AWG) standard

B.3 SENSING WIRE MATERIAL

For this study, all four sensors were interrogated in air at a read distance of 0.5-in. with both intact sensing wires and cut sensing wires. Fig. B-3 shows the amplitude of the phase dip for each wire material with sensing wires intact. Using a steel wire as the sensing mechanism for the sensors has a tremendous effect on phase response. Sensors with copper wires have phase dips that are 2 to 4 times greater than sensors with steel wires for intact sensing wires. The reduced phase dip for steel wire is expected because of the increased resistance of steel compared with copper. For cut sensing wires, Fig. B-4 shows the phase dip for each wire material. When the sensing wire is cut and the sensor is interrogated in air, the circuits are essentially identical. Therefore, the difference in phase dip for different sensing wire materials is insignificant when the wire is cut. Because the use of steel as the corroding sensing mechanism is central to the corrosion sensor concept, the detrimental effect of using steel wire in the sensor circuit is unavoidable.

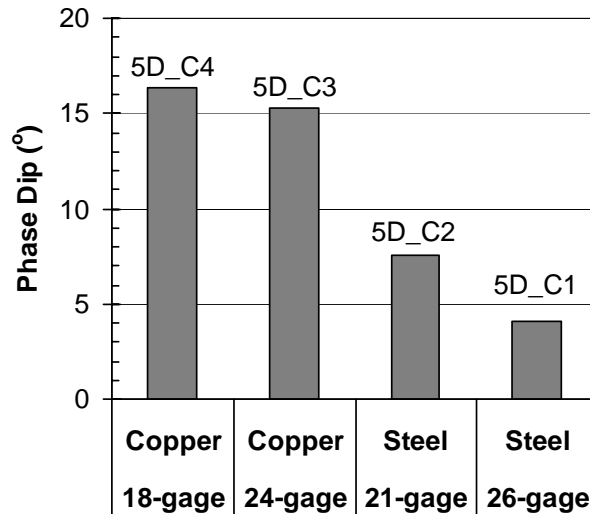


Figure B-3 Phase Dips for Intact Sensing Wires

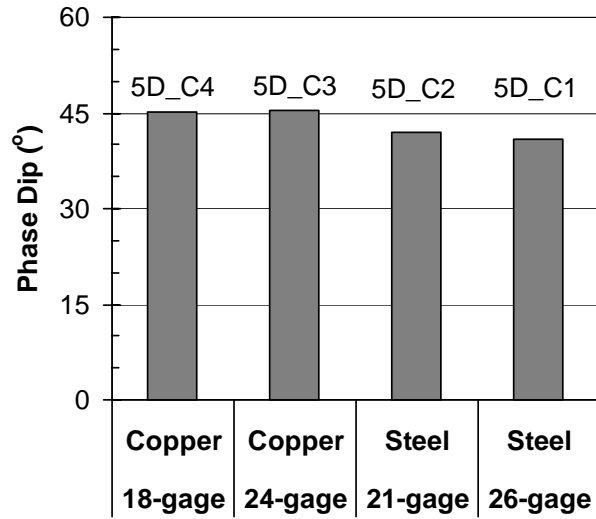


Figure B-4 Phase Dips for Cut Sensing Wires

B.4 SENSING WIRE DIAMETER

Wire diameter does not have as significant an effect as wire material on sensor phase response. The phase dip for 18-gage copper wire was 7% greater than the phase dip for 24-gage copper wire as shown in Fig. B-3. For steel, the difference in response due to wire gage is more pronounced. As shown in Fig. B-3, the phase dip for 26-gage steel wire was 46% less than the phase dip for 21-gage steel wire. This effect is expected because of decreasing resistance with increasing wire cross-sectional area.

B.5 SURROUNDING ENVIRONMENT

Results of first generation sensor testing by Simonen [15] showed that environmental factors such as moisture and chlorides may influence sensor response. Parametric Study I concluded that the effect of a conductive

environment on a completely sealed sensor is minimal. However, the presence of a sensing wire exposed to the environment poses a new problem.

To test the effect of environments for sensors with exposed sensing wires, all four sensors were interrogated at 0.5-in. read distance in air, tap water, and salt water with 3.5% sodium chloride by weight. Each of these materials has a significant increase in conductivity. The phase response of each sensor in all three environments with both intact and cut sensing wires is provided in Fig. B-5 through B-8. Very little change occurs with environment for intact sensing wires, as shown in (a), (c), and (e) in the figures. This is the same behavior noted in Parametric Study I. However, significant changes in phase response are apparent for sensors with cut sensing wires in the three environments. Sensors with steel sensing wires, 5D_C1 and 5D_C2, undergo a complete transition from final characteristic frequency response to initial characteristic frequency response between tap water and 3.5% salt water. This shows that if the environment within concrete is as conductive as 3.5% salt water, the sensor would produce a false negative reading if only the characteristic frequency is used for evaluation of sensor response. Because the phase response (width and amplitude of the resonance) is not exactly the same for an intact sensing wire in 3.5% salt water and a cut sensing wire in 3.5% salt water, further signal processing may be adequate to determine the difference between the intact wire and the cut wire.

Sensors with copper sensing wires, 5D_C3 and 5D_C4, did not exhibit the same complete transition. The response of these sensors remains at the final characteristic frequency in all three environments. However, the phase dip is substantially reduced between tap water and 3.5% salt water. The reason that the more conductive copper sensing wires do not cause the same or even stronger transition behavior as the environment becomes more conductive is because the copper wire used in the study was enamel coated magnet wire. Therefore, for the

cut copper sensing wires, only the cross-sectional area of wire was exposed to the environment at the cut. For cut steel sensing wires, the entire length of wire was exposed to the environment. This shows that the transition behavior of sensors exposed to conductive environments depend on the exposed area of metal. Careful study of the phase responses reveals that sensors with larger diameter sensing wires were more sensitive to the conductivity of the environment than those with smaller diameter sensing wires.

The sensors with cut steel sensing wires were also interrogated at 0.5-in. read distance in varying concentrations of salt water. Figures B-9 and B-10 show the transition behavior of sensors 5D_C1 and 5D_C2, respectively. Salt water concentration increases in increments of 0.1% in (a) through (f) and in increments of 0.5% in (g) through (l). Sensor 5D_C1 exhibits essentially no characteristic frequency response from 0.2% to 0.5% salt water concentration and sensor 5D_C2 behaves similarly for salt concentrations between 0.2% and 0.4%. The phase dips immediately outside this range of concentrations are extremely small and would be difficult to detect outside the laboratory. This response is similar to the transition behavior observed during full-scale slab monitoring of first generation sensors by Simonen [15]. The phase dip reappears at the initial characteristic frequency for both sensors in concentrations of salt water above about 1.0%.

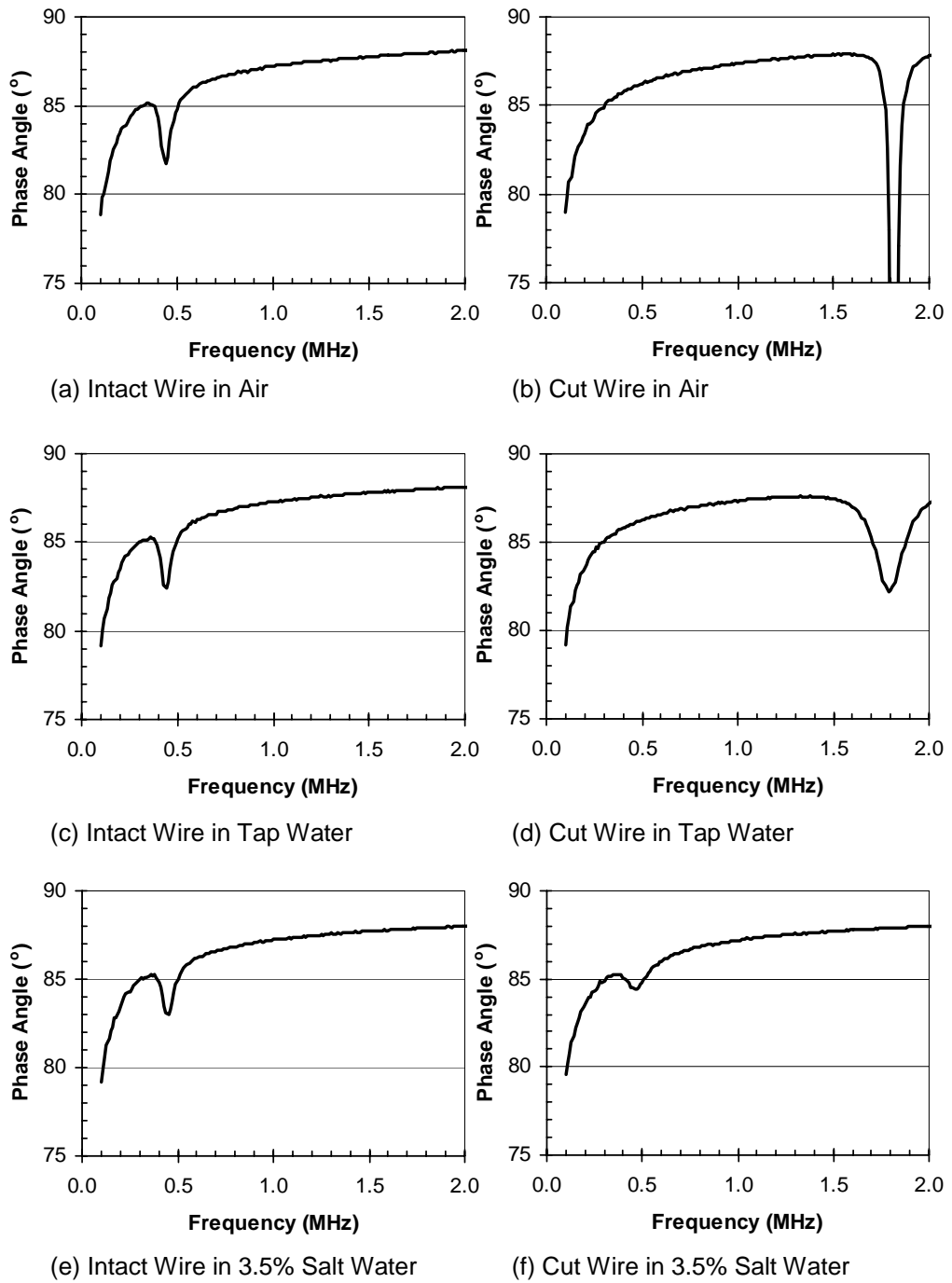


Figure B-5 Phase Response of Sensor 5D_C1 in Different Environments

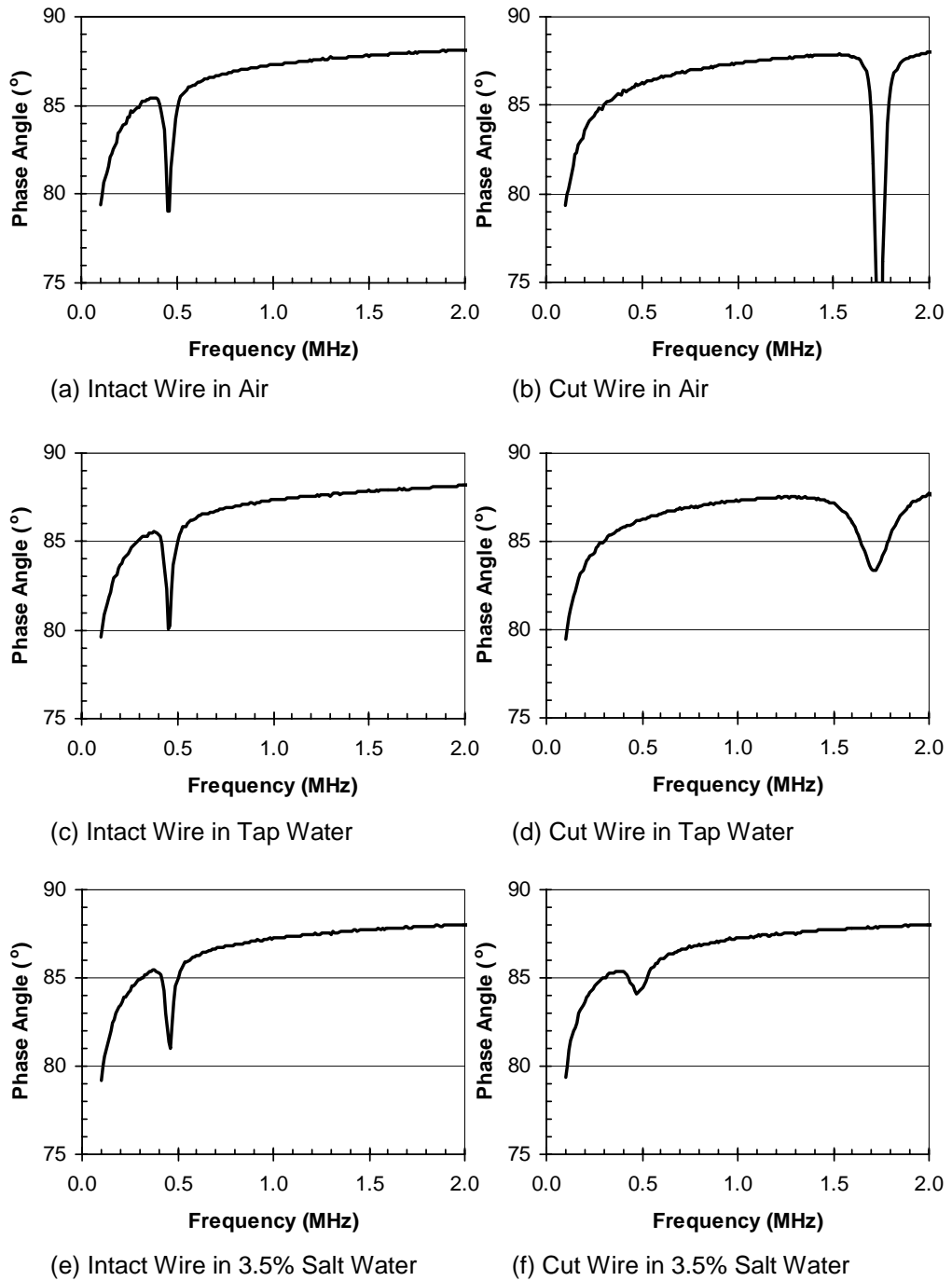


Figure B-6 Phase Response of Sensor 5D_C2 in Different Environments

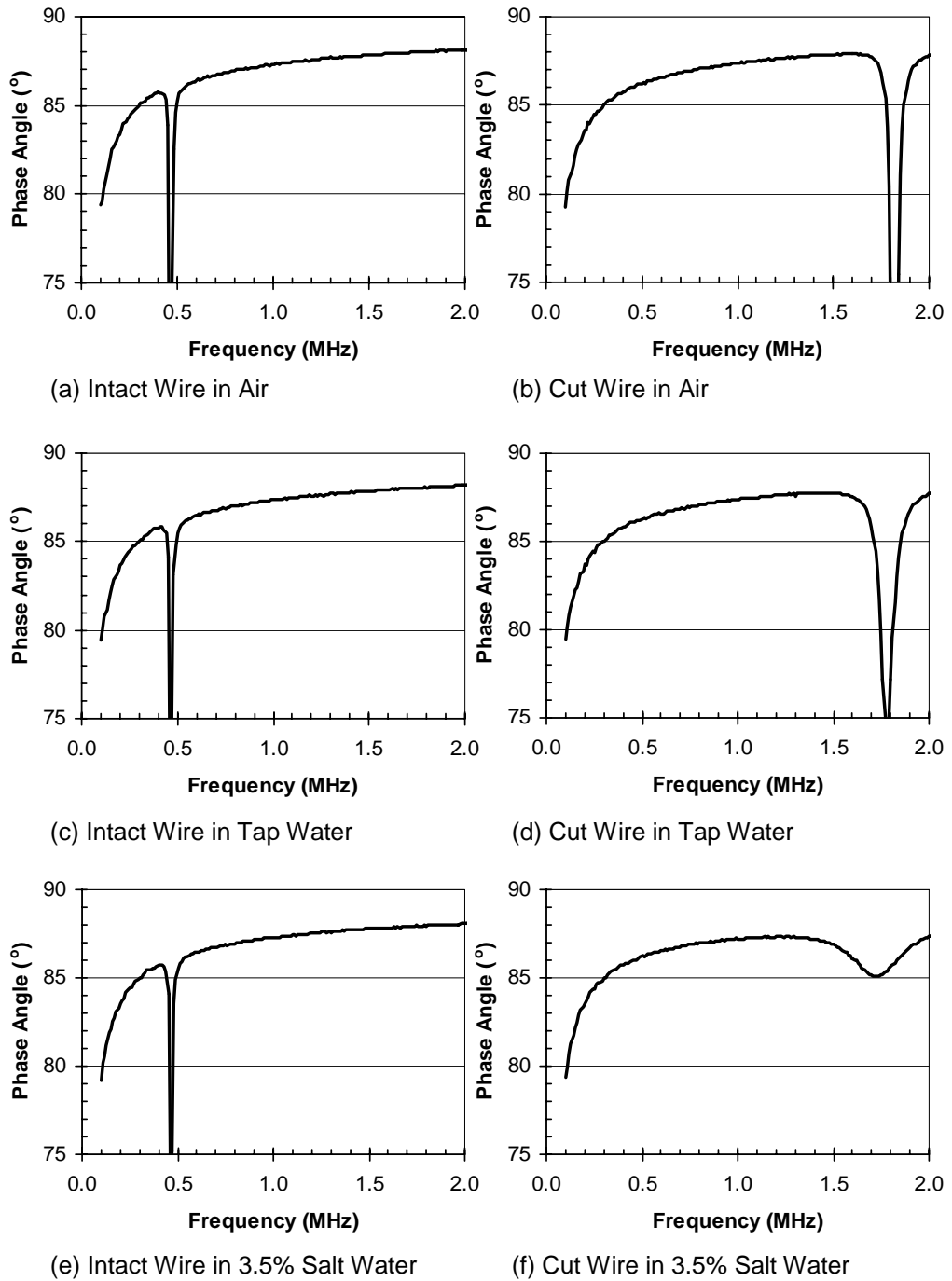


Figure B-7 Phase Response of Sensor 5D_C3 in Different Environments

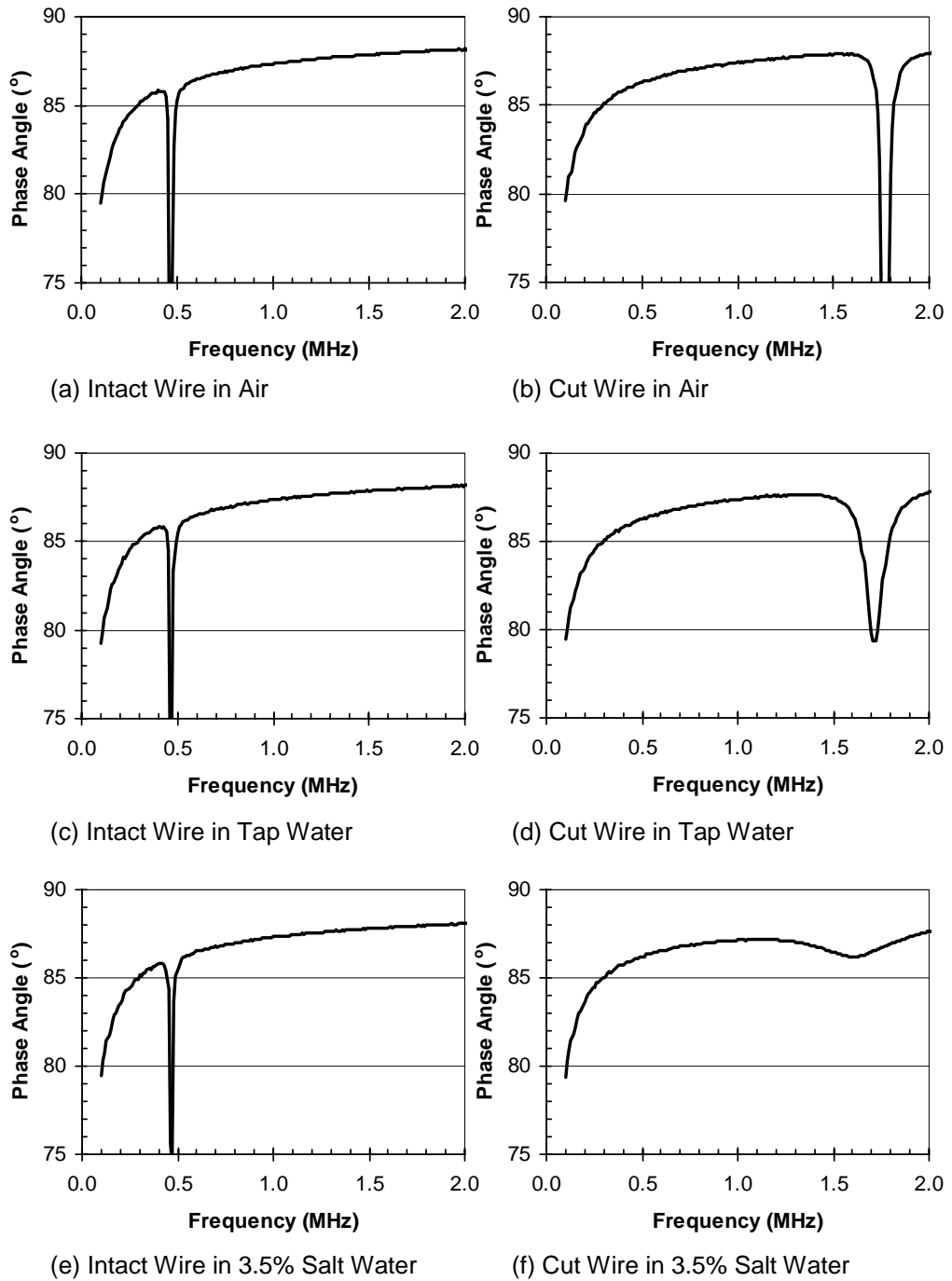


Figure B-8 Phase Response of Sensor 5D_C4 in Different Environments

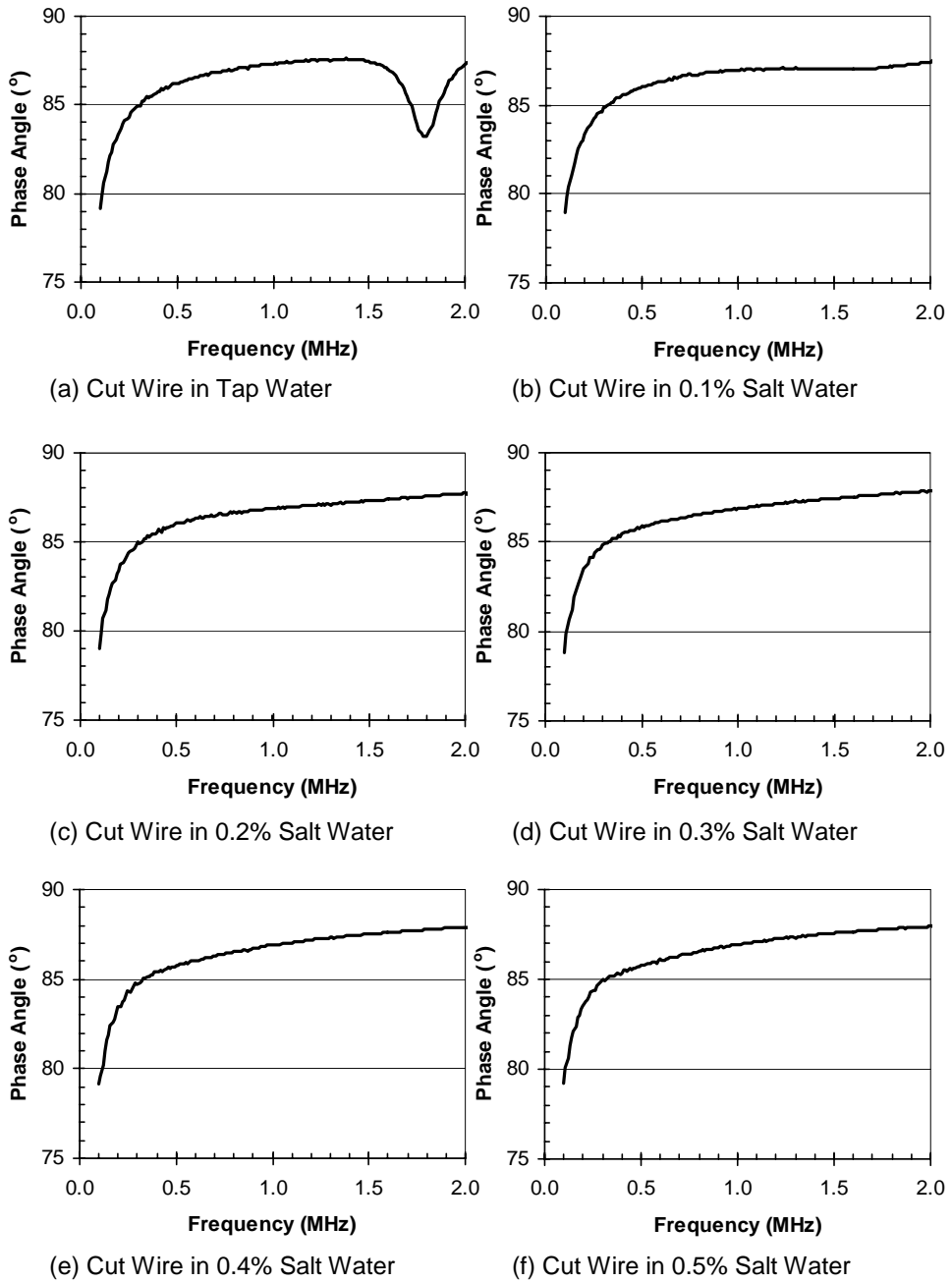
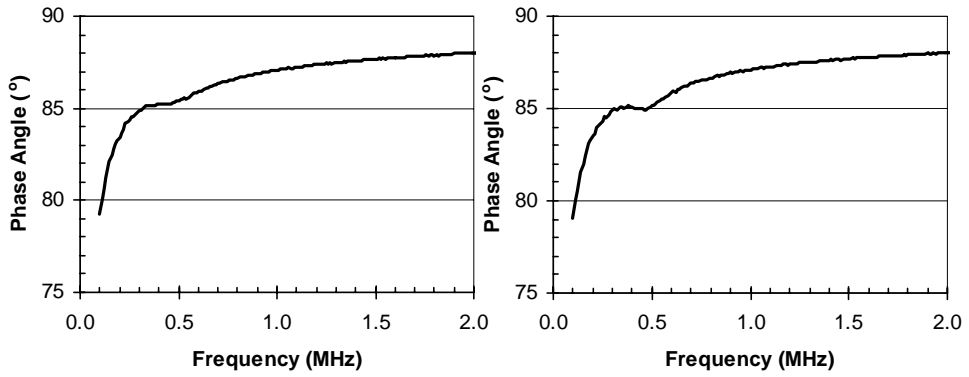
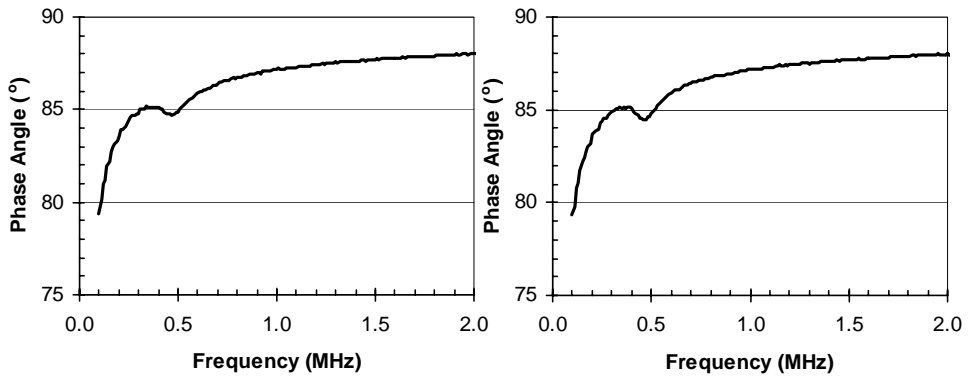


Figure B-9 Phase Response of Sensor 5D_C1 in Varying Concentrations of Salt Water



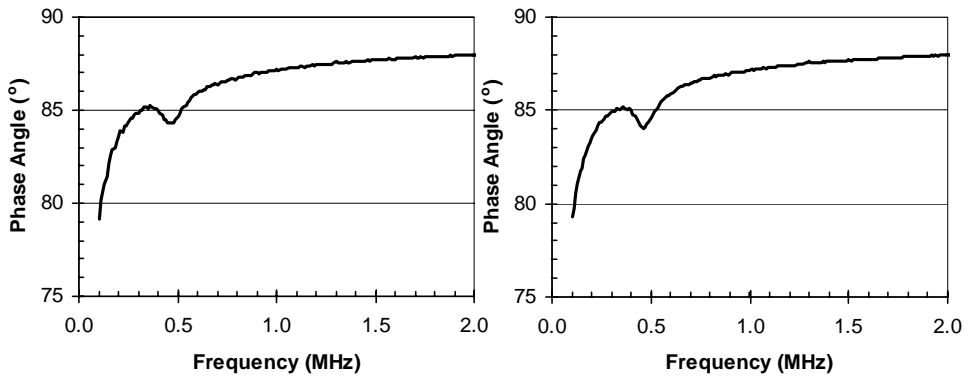
(g) Cut Wire in 1.0% Salt Water

(h) Cut Wire in 1.5% Salt Water



(i) Cut Wire in 2.0% Salt Water

(j) Cut Wire in 2.5% Salt Water



(k) Cut Wire in 3.0% Salt Water

(l) Cut Wire in 3.5% Salt Water

Figure B-9 (Cont.) Phase Response of Sensor 5D_C1 in Varying Concentrations of Salt Water

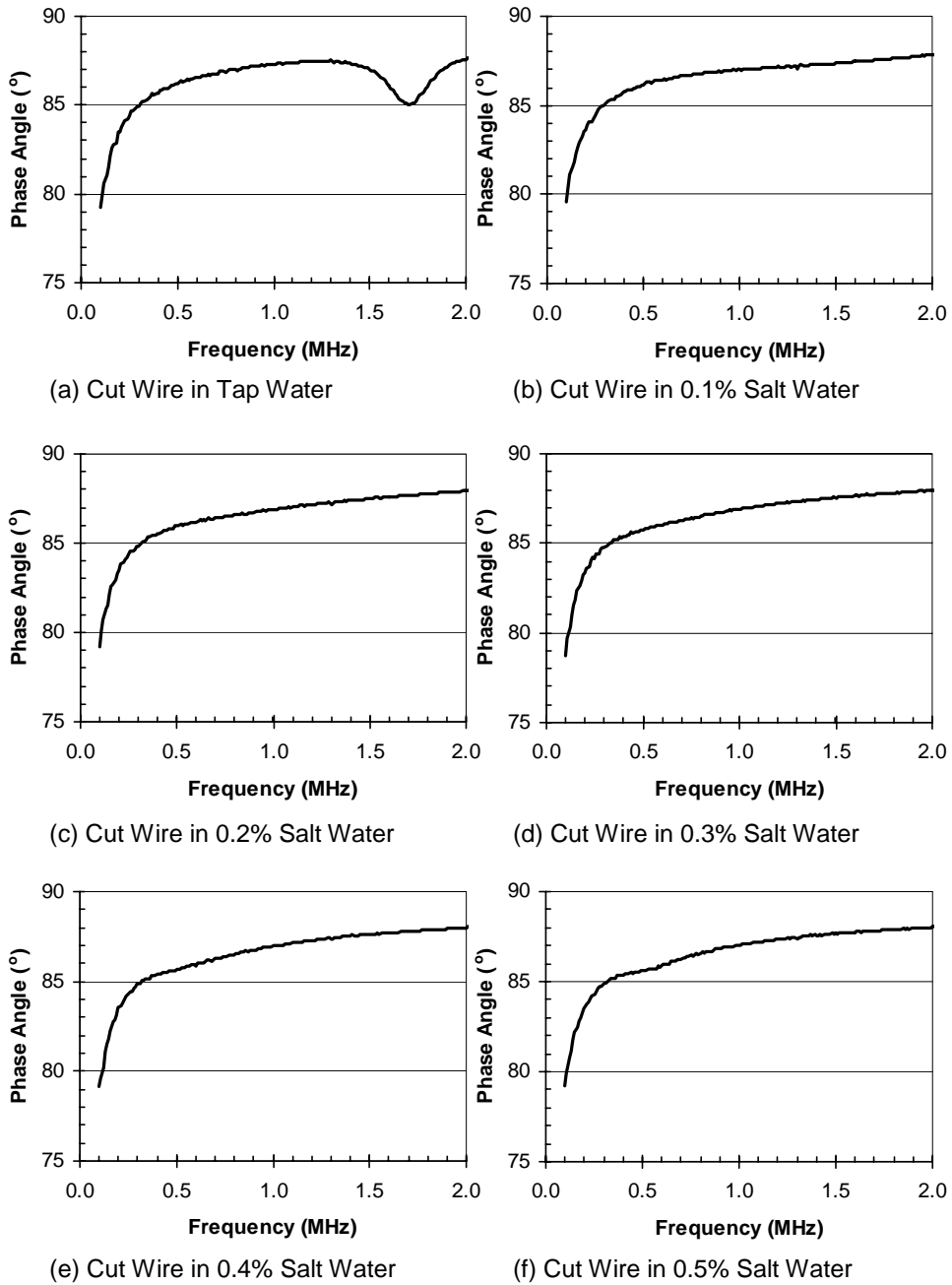
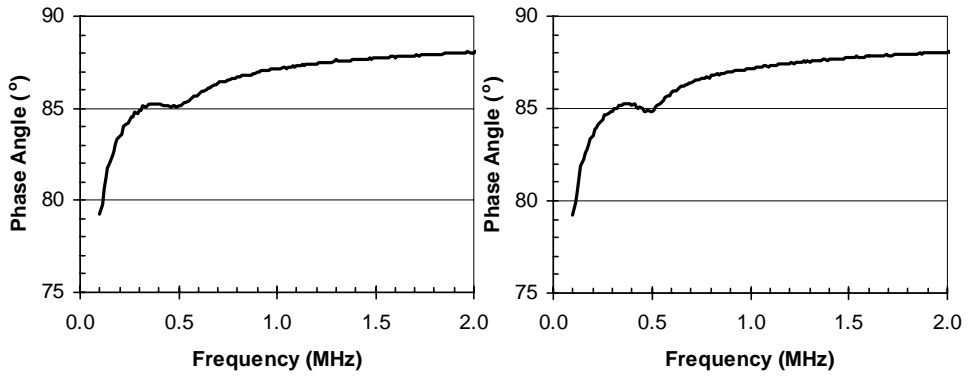
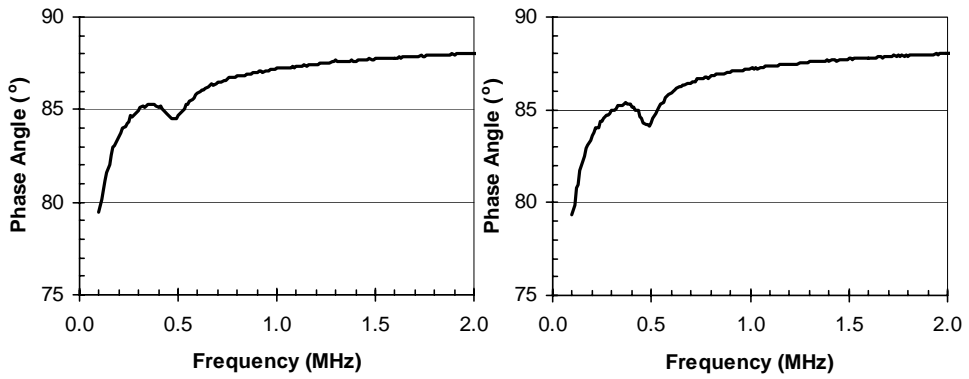


Figure B-10 Phase Response of Sensor 5D_C2 in Varying Concentrations of Salt Water



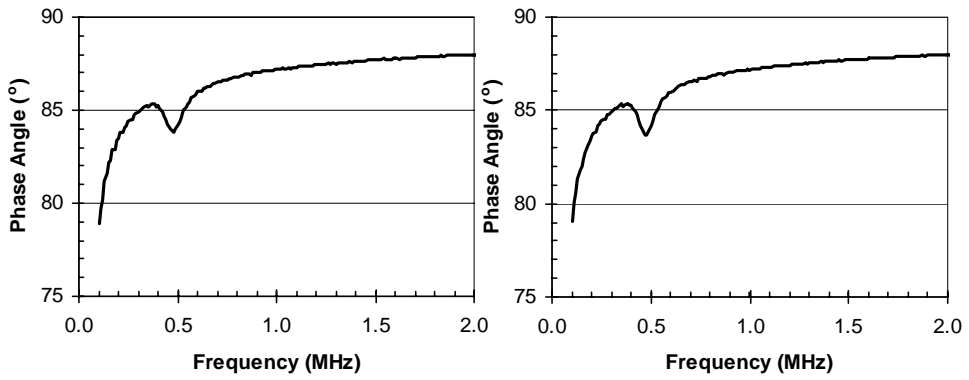
(g) Cut Wire in 1.0% Salt Water

(h) Cut Wire in 1.5% Salt Water



(i) Cut Wire in 2.0% Salt Water

(j) Cut Wire in 2.5% Salt Water



(k) Cut Wire in 3.0% Salt Water

(l) Cut Wire in 3.5% Salt Water

Figure B-10 (Cont.) Phase Response of Sensor 5D_C2 in Varying Concentrations of Salt Water

APPENDIX C

Parametric Study III

C.1 INTRODUCTION

In order to eliminate the possibility of obtaining no characteristic frequency response from sensors exposed to conductive environments – the “transition” behavior discussed in Parametric Study II – a sealed reference circuit was added to the sensor. While this reference circuit is not connected to the sensing circuit, the presence of another resonant circuit complicates sensor response. Adding a reference circuit or multiple sensing circuits with separate inductor coils results in mutual inductance among the reader coil and sensor inductor coils. The geometric arrangement of inductor coils and the characteristic frequency of each circuit influence the behavior of sensors with multiple resonant circuits.

In Parametric Study III, the effect of multiple resonant circuits in a single sensor was examined. Three completely sealed sensors were constructed using nominally identical inductors, but with different values of capacitance. A fourth sensor had a larger diameter inductor. Because each sensor had a different value of capacitance, the characteristic frequency of each sensor was different. Sensors were interrogated separately and in pairs using stacked, side-by-side, and concentric arrangements of inductor coils.

The Solartron Impedance Analyzer was used to interrogate all sensors. Sensors were interrogated using a 4-in. diameter reader coil with 20 turns of 18-gage copper magnet wire. This reader coil was developed experimentally and provides a superior baseline phase response compared with earlier reader coils.

Results of the parametric study, showing the effect of two resonant circuits in various arrangements, are presented in this Appendix.

C.2 SENSOR CIRCUIT

A diagram of the sensor circuit used for this study is shown in Fig. C-1. A single inductor constructed using 1.25-in. nominal diameter PVC pipe and 5 turns of 18-gage copper magnet wire was used for three sensors. A fourth trial sensor with a larger inductor, fabricated using a 2.0-in. nominal diameter PVC pipe, was also included in the study to facilitate the concentric arrangement of inductor coils. Table C-1 gives the value of capacitance, approximate inductance, and label for each sensor used in the study.

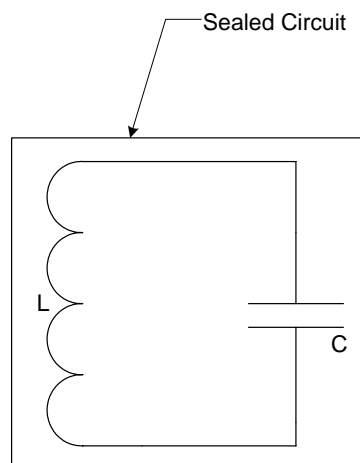


Figure C-1 Sensor Circuit Diagram for Parametric Study III

Sensors were labeled based on the capacitor and diameter and number of magnet wire turns used for the inductor in the sensor circuit. Labels consist of the number of wire turns followed by a letter signifying the nominal diameter of PVC pipe used for the inductor: “C” is 1.25-in. nominal diameter and “D” is 2.0-in. nominal diameter. For example, sensor 5D has an inductor with five turns of 18-gage copper magnet wire around a slice of 2.0-in. nominal diameter PVC pipe.

The next number in the label represents the value of capacitance used in the circuit. Numbers are assigned sequentially with increasing capacitance. All sensors were fabricated using a single, high-quality ceramic capacitor.

Table C-1 Parametric Study III Sensors

Sensor	Inductor Diameter (in.)	Number of Turns	Length of Coil (in.)	Approximate Inductance L (μ H)	Capacitance C (pF)
5C_1	1.68	5	0.20	2.0	1000
5C_2	1.68	5	0.20	2.0	2700
5C_3	1.68	5	0.20	2.0	6800
5D_4	2.40	5	0.20	3.0	33,000

C.3 RESPONSE OF INDIVIDUAL SENSORS

All of the sensors were interrogated individually at two different read distances. The phase response of each individual sensor is shown in Fig. C-2 through C-5. Response at a read distance of 0 in. is given in (a), while the response at a read distance of 0.5 in. is shown in (b). It is necessary to present the response at two different read distances to characterize the baseline response of sensors in the stacked arrangement for testing of sensor pairs. Sensors were 0.5 in. thick, which resulted in a larger read distance for the upper sensor when the sensors were stacked.

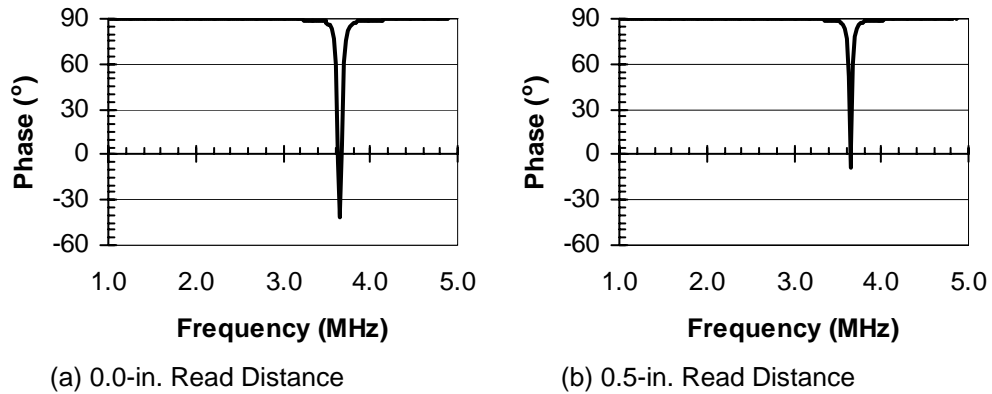


Figure C-2 Sensor 5C_1 Individual Response

Sensor 5C_1 responds at a characteristic frequency of 3.64 MHz with a phase dip of 131.6° at 0-in. read distance and 98.5° at 0.5-in. read distance. This sensor had the highest characteristic frequency of the sensors used in the study.

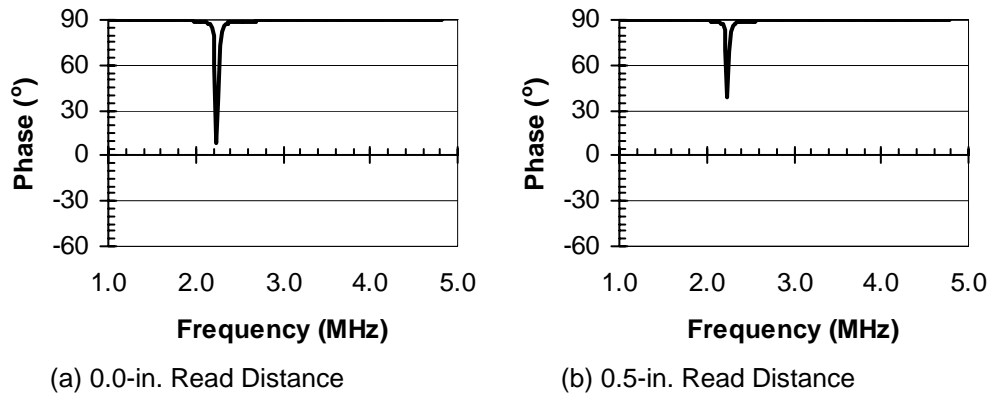


Figure C-3 Sensor 5C_2 Individual Response

Sensor 5C_2 responds at a characteristic frequency of 2.24 MHz with a phase dip of 81.4° at 0-in. read distance and 51.9° at 0.5-in. read distance. The characteristic frequency of this sensor falls between that of 5C_1 and 5C_3.

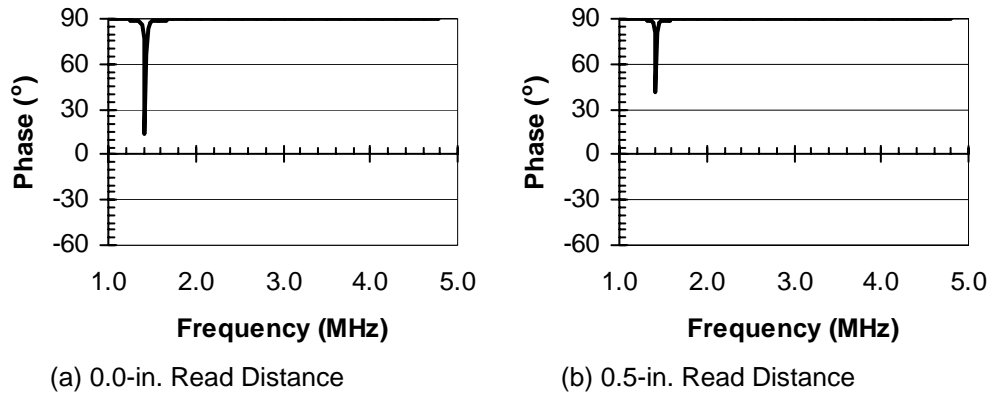


Figure C-4 Sensor 5C_3 Individual Response

Sensor 5C_3 responds at a characteristic frequency of 1.42 MHz with a phase dip of 76.5° at 0-in. read distance and 49.2° at 0.5-in. read distance. The characteristic frequency of this sensor is the smallest among the three sensors with the same inductor diameter.

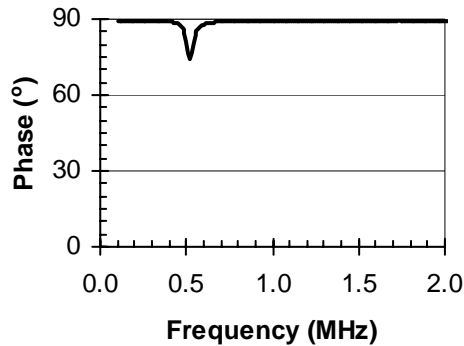


Figure C-5 Sensor 5D_4 Individual Response at 0-in. Read Distance

Sensor 5D_4 responds at a characteristic frequency of 0.52 MHz with a phase dip of 15.7° at 0-in. read distance. The response at 0.5-in. read distance was not necessary for the study, as this sensor was used only for the concentric arrangement of inductor coils. The reduced phase dip for this sensor compared with the others used in this study is due to the presence of a steel sensing wire in

the circuit. The characteristic frequency of this sensor is the smallest of all sensors tested for this study.

C.4 RESPONSE OF SENSOR PAIRS

Four different arrangements of sensors were tested: (a) stacked with the lower characteristic frequency sensor closer to the reader coil, (b) stacked with the higher characteristic frequency sensor closer to the reader coil, (c) side-by-side, and (d) concentric. Sensors 5C_1, 5C_2, and 5C_3 were used in stacked and side-by-side arrangements, while sensors 5D_4 and 5C_3 were used for the concentric arrangement. Results are presented by sensor pair in sections C.4.1 through C.4.4.

C.4.1 Sensor Pair 1: 5C_1 and 5C_2

A summary of interrogation results is provided in Table C-2 for sensor pair 1. The table includes the characteristic frequency and phase dip of each sensor in all of the different arrangements. As shown in Fig. C-6, with sensor 5C_2 closer to the reader coil and sensor 5C_1 stacked on top, phase dips occur at two characteristic frequencies. The lower characteristic frequency corresponds to the circuit in 5C_2 and the higher frequency corresponds to the circuit in 5C_1. The larger phase dip at the lower frequency is due to the proximity of the reader coil with sensor 5C_2 and is actually slightly larger than the phase dip obtained when interrogating sensor 5C_2 individually at a read distance of 0-in. (Fig. C-3a). The phase dip for the higher characteristic frequency of sensor 5C_1 is only about 25% of the phase dip obtained when interrogating that sensor individually at a read distance of 0.5-in. (Fig. C-2b). A slight frequency shift is apparent for both circuits. The characteristic frequency of sensor 5C_1 stacked on top of sensor 5C_2 is higher than its individual response, while the characteristic frequency of sensor 5C_2 is slightly lower than its individual response. When the

sensor pair is interrogated in this stacked arrangement, the characteristic frequencies appear to be pushed away from each other compared with the individual sensor responses. In addition, the sensor closer to the reader coil appears to shield the sensor farther away.

The response of sensor pair 1 with the higher characteristic frequency sensor, 5C_1, closer to the reader coil and sensor 5C_2 stacked on top is shown in Fig. C-7. Once again, the characteristic frequency of the sensor closer to the reader coil responds with the larger phase dip. However, the phase dip for the lower frequency circuit of 5C_2 is only reduced by about 5% from the phase dip obtained from interrogating that sensor at a read distance of 0.5-in (Fig. C-3b). The phase dip for the higher frequency circuit of 5C_1 is reduced by about 17% from the phase dip obtained from interrogating that sensor at a read distance of 0-in. (Fig. C-2a). The same trend of shifting characteristic frequencies away from each other appears for this sensor arrangement. For sensor 5C_2, the characteristic frequency shifts slightly lower when interrogated in this stacked arrangement. For sensor 5C_1, the shift to a higher frequency is more pronounced. Unlike the previous stacked arrangement, the lower-frequency phase dip is not significantly shielded when the higher-frequency circuit is closer to the reader coil.

For sensor pair 1 interrogated in a side-by-side arrangement, each sensor circuit responds in very nearly the same way as sensors interrogated individually. For sensor 5C_1, the characteristic frequency was just slightly higher than the frequency under individual interrogation and the phase dip increased about 4% compared to the individual response. Sensor 5C_2 responded at exactly the same characteristic frequency obtained during individual interrogation of the sensor and the phase dip was only about 6% smaller.

Table C-2 Summary of Interrogation Results for Sensor Pair 1: 5C_1 and 5C_2

Description	Characteristic Frequencies (MHz)		Phase Dips (°)			
	5C_1	5C_2	5C_1		5C_2	
			0 in.	0.5 in.	0 in.	0.5 in.
Interrogated Separately	3.64	2.24	131.6	98.5	81.4	51.9
Stacked with 5C_2 Closer to Reader Coil	3.76	2.22	—	25.3	88.0	—
Stacked with 5C_1 Closer to Reader Coil	3.78	2.22	108.6	—	—	49.0
Side-by-Side	3.66	2.24	136.6	—	76.5	—

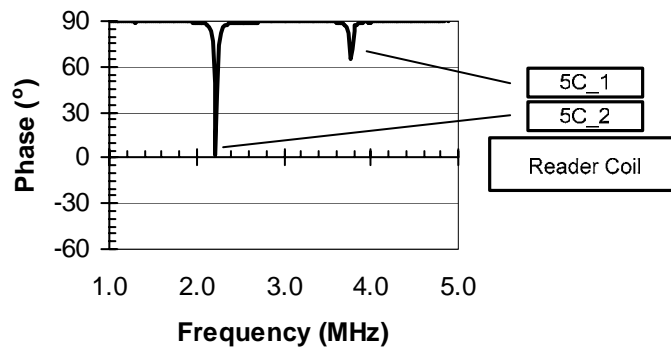


Figure C-6 Response of Sensor Pair 1 in Stacked Arrangement with Lower-Frequency Sensor Closer to Reader Coil

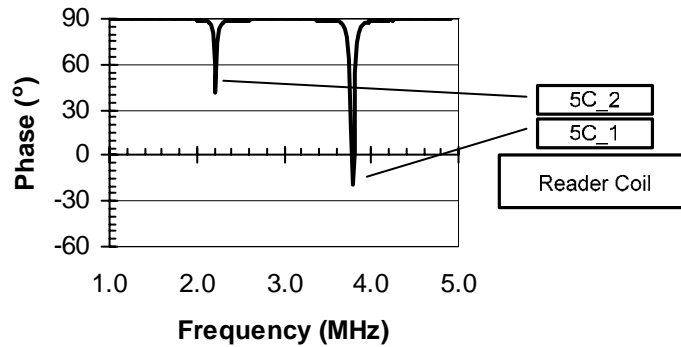


Figure C-7 Response of Sensor Pair 1 in Stacked Arrangement with Higher Frequency Sensor Closer to Reader Coil

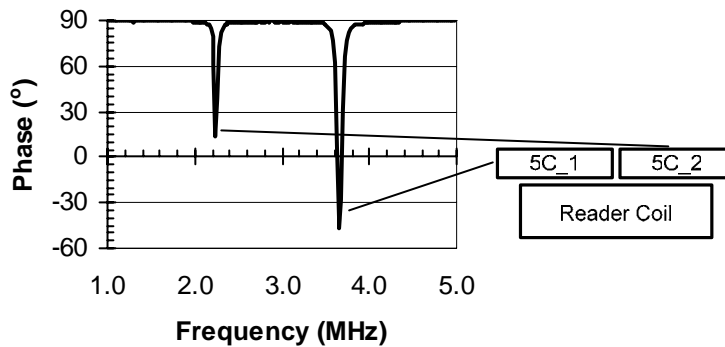


Figure C-8 Response of Sensor Pair 1 in Side-by-Side Arrangement

C.4.2 Sensor Pair 2: 5C_2 and 5C_3

A summary of interrogation results is provided in Table C-3 for sensor pair 2. The table includes the characteristic frequency and phase dip of each sensor in all of the different arrangements. As shown in Fig. C-9, with sensor 5C_3 closer to the reader coil and sensor 5C_2 stacked on top, phase dips occur at two characteristic frequencies. The lower characteristic frequency corresponds to the circuit in 5C_3 and the higher corresponds to the circuit in 5C_2. The larger phase dip at the lower frequency is due to the proximity of the reader coil with

sensor 5C_3 and is just slightly smaller than the phase dip obtained when interrogating sensor 5C_3 individually at a read distance of 0-in. (Fig. C-4a). The phase dip for the higher characteristic frequency of sensor 5C_2 is only about 22% of the phase dip obtained when interrogating that sensor individually at a read distance of 0.5-in. (Fig. C-3b). A slight frequency shift is apparent for both circuits. The characteristic frequency of sensor 5C_2 stacked on top of sensor 5C_3 is higher than its individual response, while the characteristic frequency of sensor 5C_3 is slightly lower than its individual response. When the sensor pair is interrogated in this stacked arrangement, the characteristic frequencies appear to be pushed away from each other compared to the individual sensor responses. In addition, the sensor closer to the reader coil appears to shield the sensor farther away.

The response of sensor pair 2 with the higher characteristic frequency sensor, 5C_2, closer to the reader coil and sensor 5C_3 stacked on top is shown in Fig. C-11. Once again, the characteristic frequency of the sensor closer to the reader coil gives the larger phase dip. However, the phase dip for the lower frequency circuit of 5C_3 is only reduced by about 10% from the phase dip obtained from interrogating that sensor at a read distance of 0.5-in (Fig. C-4b). The phase dip for the higher frequency circuit of 5C_2 is reduced by about 29% from the phase dip obtained from interrogating that sensor at a read distance of 0-in (Fig. C-3a). The same trend of shifting characteristic frequencies away from each other appears for this sensor arrangement. However, in this stacked arrangement, the lower-frequency phase dip is not significantly shielded when the higher-frequency circuit is closer to the reader coil.

For sensor pair 2 interrogated in a side-by-side arrangement, each sensor circuit responds in very nearly the same way as sensors interrogated individually. For sensor 5C_2, the characteristic frequency was exactly the same as the

frequency under individual interrogation and the phase dip only decreased about 2% compared to the individual response. Sensor 5C_3 responded at exactly the same characteristic frequency obtained during individual interrogation of the sensor and the phase dip was only about 8% smaller.

Table C-3 Summary of Interrogation Results for Sensor Pair 2: 5C_2 and 5C_3

Description	Characteristic Frequencies (MHz)		Phase Dips (°)			
	5C_2	5C_3	5C_2		5C_3	
			0 in.	0.5 in.	0 in.	0.5 in.
Interrogated Separately	2.24	1.42	81.4	51.9	76.5	49.2
Stacked with 5C_3 Closer to Reader Coil	2.32	1.40	—	11.2	70.1	—
Stacked with 5C_2 Closer to Reader Coil	2.32	1.40	57.7	—	—	44.0
Side-by-Side	2.24	1.42	80.2	—	70.0	—

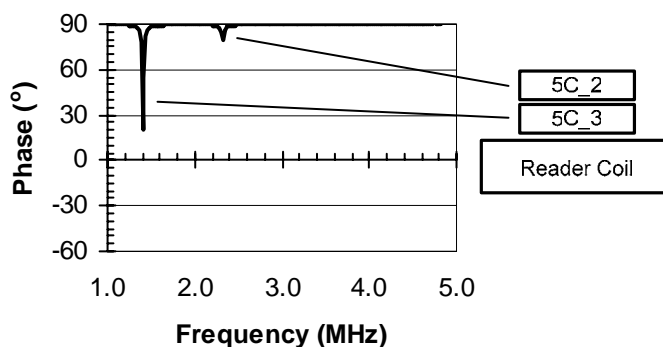


Figure C-9 Response of Sensor Pair 2 in Stacked Arrangement with Lower Frequency Sensor Closer to Reader Coil

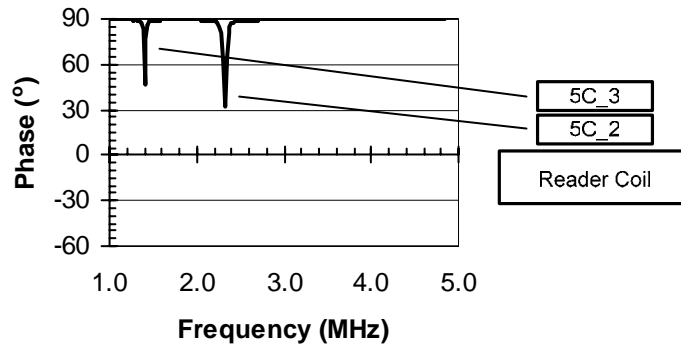


Figure C-10 Response of Sensor Pair 2 in Stacked Arrangement with Higher Frequency Sensor Closer to Reader Coil

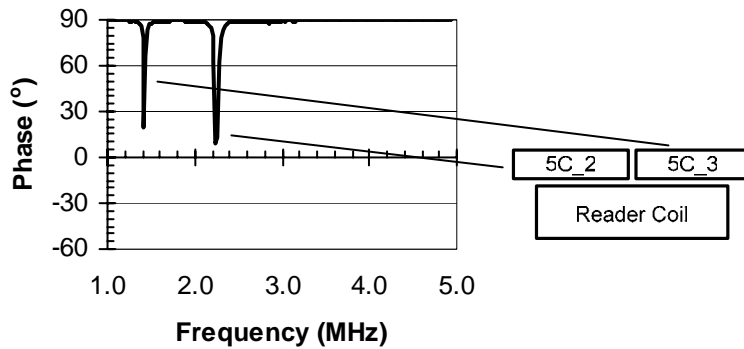


Figure C-11 Response of Sensor Pair 2 in Side-by-Side Arrangement

C.4.3 Sensor Pair 3: 5C_1 and 5C_3

A summary of interrogation results is provided in Table C-4 for sensor pair 3. The table includes the characteristic frequency and phase dip of each sensor in all of the different arrangements. As shown in Fig. C-12, with sensor 5C_3 closer to the reader coil and sensor 5C_1 stacked on top, phase dips occur at two characteristic frequencies. The lower characteristic frequency corresponds to the circuit in 5C_3 and the higher frequency corresponds to the circuit in 5C_1. The larger phase dip at the lower frequency is due to the proximity of the reader

coil with sensor 5C_3 and is actually slightly larger than the phase dip obtained when interrogating sensor 5C_3 individually at a read distance of 0-in. (Fig. C-4a). The phase dip for the higher characteristic frequency of sensor 5C_1 is about 45% of the phase dip obtained when interrogating that sensor individually at a read distance of 0.5-in. (Fig. C-2b). The characteristic frequency for sensor 5C_3 is the same for the stacked arrangement as for the individual interrogation of the sensor. Only sensor 5C_1 shows a slightly higher frequency compared to individual interrogation. When the sensor pair is interrogated in this stacked arrangement, only the higher characteristic frequency appears to be pushed away from its individual sensor response. Again, the sensor closer to the reader coil appears to shield the sensor farther away, but this effect is much less than that for sensor pairs 1 and 2.

The response of sensor pair 3 with the higher characteristic frequency sensor, 5C_1, closer to the reader coil and sensor 5C_3 stacked on top is shown in Fig. C-13. Once again, the characteristic frequency of the sensor closer to the reader coil gives the larger phase dip. However, the phase dip for the lower frequency circuit of 5C_3 is reduced by about 29% from the phase dip obtained from interrogating that sensor at a read distance of 0.5-in (Fig. C-4b). The phase dip for the higher frequency circuit of 5C_1 is reduced by about 14% from the phase dip obtained from interrogating that sensor at a read distance of 0-in (Fig. C-2a). The same trend of shifting characteristic frequencies away from each other appears for this sensor arrangement, although the shift occurs for the higher frequency circuit only. As seen with sensor pairs 1 and 2, the lower-frequency phase dip is not significantly shielded when the higher-frequency circuit is closer to the reader coil in this stacked arrangement.

For sensor pair 3 interrogated in a side-by-side arrangement, each sensor circuit responds in very nearly the same way as sensors interrogated individually.

For sensor 5C_1, the characteristic frequency was exactly the same as the frequency under individual interrogation, and the phase dip decreased by about 4% compared to the individual response. Sensor 5C_3 also responded at exactly the same characteristic frequency obtained during individual interrogation of the sensor and the phase dip was also only about 4% smaller.

Table C-4 Summary of Interrogation Results for Sensor Pair 3: 5C_1 and 5C_3

Description	Characteristic Frequencies (MHz)		Phase Dips (°)			
	5C_1	5C_3	5C_1		5C_3	
			0 in.	0.5 in.	0 in.	0.5 in.
Interrogated Separately	3.64	1.42	131.6	98.5	76.5	49.2
Stacked with 5C_3 Closer to Reader Coil	3.74	1.42	—	44.4	80.0	—
Stacked with 5C_1 Closer to Reader Coil	3.74	1.42	112.8	—	—	35.1
Side-by-Side	3.64	1.42	126.3	—	73.4	—

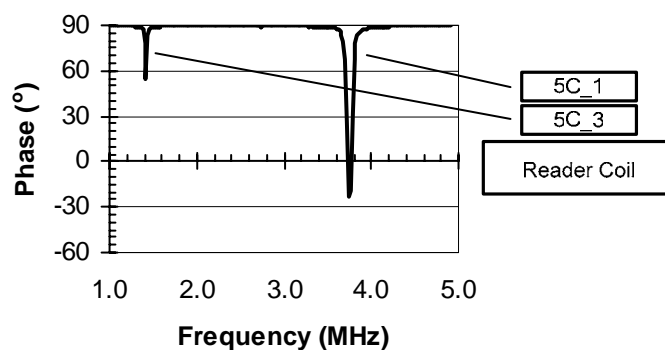


Figure C-12 Response of Sensor Pair 3 in Stacked Arrangement with Lower Frequency Sensor Closer to Reader Coil

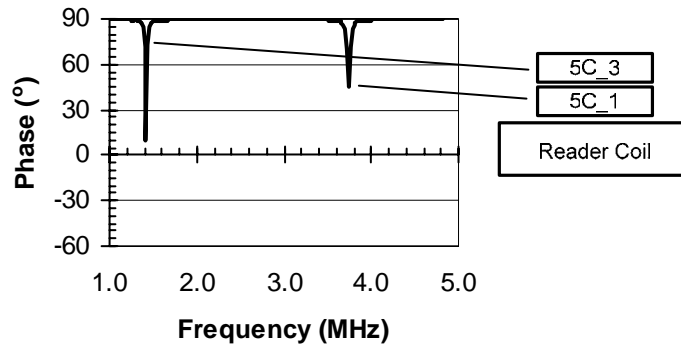


Figure C-13 Response of Sensor Pair 3 in Stacked Arrangement with Higher Frequency Sensor Closer to Reader Coil

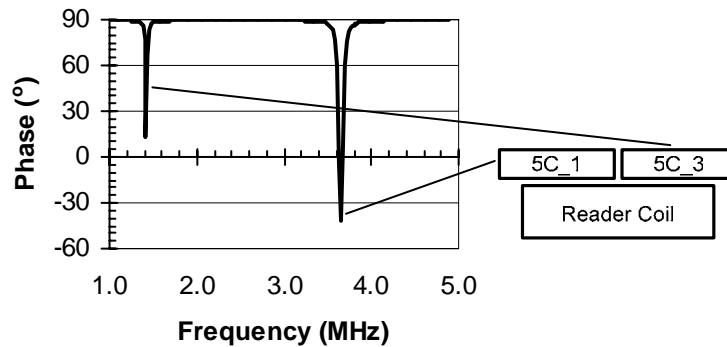


Figure C-14 Response of Sensor Pair 3 in Side-by-Side Arrangement

C.4.4 Sensor Pair 4: 5C_3 and 5D_4

A summary of interrogation results is provided in Table C-5 for sensor pair 4. The table includes the characteristic frequency and phase dip of each sensor in all of the different arrangements. For sensor pair 4, the lower characteristic frequency corresponds to sensor 5D_4. The concentric arrangement of sensor circuits produced a shift in characteristic frequency lower than that for sensor 5D_4 interrogated individually. Also, the concentric arrangement resulted in a small reduction in phase dip of about 13% compared with the individual

response of sensor 5D_4. For sensor 5C_3, the characteristic frequency shifted higher and the phase dip was substantially reduced from the individual interrogation. This shows that the lower frequency, larger inductance circuit of sensor 5D_4 shielded the response of sensor 5C_3 because of the strong mutual inductance in the concentric arrangement.

Table C-5 Summary of Interrogation Results for Sensor Pair 1: 5C_1 and 5C_2

Description	Characteristic Frequencies (MHz)		Phase Dips (°)			
	5C_3	5D_4	5C_3		5D_4	
			0 in.	0.5 in.	0 in.	0.5 in.
Interrogated Separately	1.42	0.52	76.5	49.2	15.7	—
Concentric	1.55	0.46	5.7	—	13.5	—

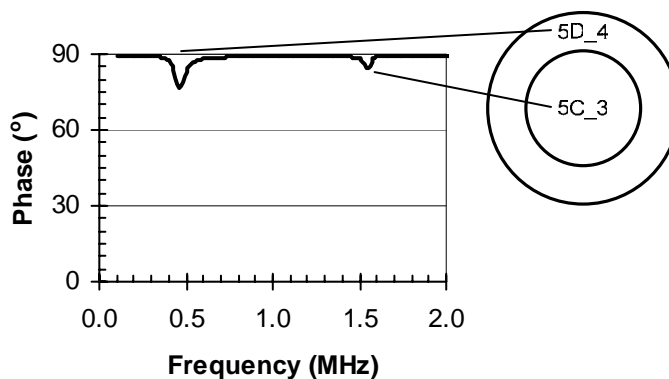


Figure C-15 Response of Sensor Pair 4 in Concentric Arrangement

C.5 CONCLUSIONS

The concentric arrangement of inductor coils resulted in the greatest amount of mutual inductance and shielding of the higher frequency circuit. The side-by-side arrangement of inductor coils results in virtually no mutual

inductance or shielding. In the stacked arrangements, the lower frequency circuit had a much larger shielding effect on the higher frequency circuit when it was closer to the reader coil than the higher frequency had on the lower frequency. Therefore, the sensing circuit is best suited for lower frequencies when a reference circuit is present and the sensing circuit should always be closer to the reader coil for best response.

APPENDIX D

Signal Processing

D.1 INTRODUCTION

Visually, evaluating the phase response of corrosion sensors is very simple. During interrogation of the sensors, phase is plotted versus frequency. The locations of dips in the phase plot indicate the characteristic frequency response of the sensor. This is shown in Fig. D-1. The strength of the coupling efficiency between the reader coil and the sensor can be evaluated by comparing the amplitude of the phase dip. Better coupling efficiency results in larger phase dips.

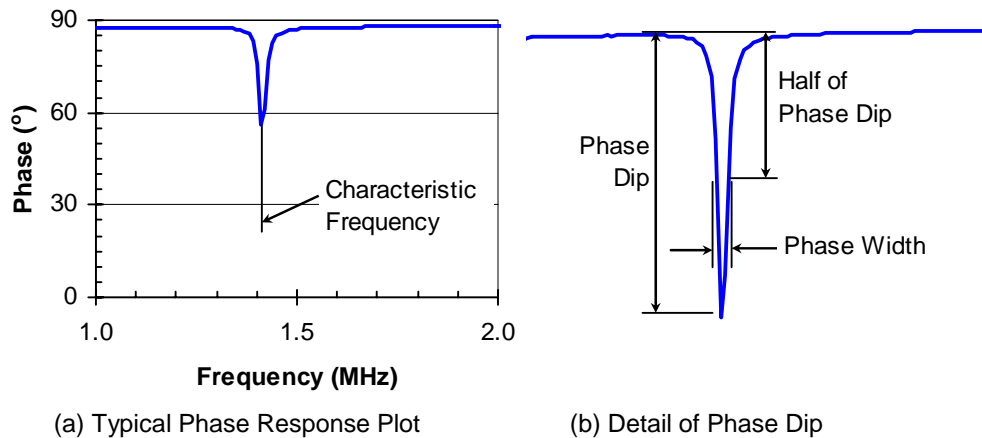


Figure D-1 Definition of Terms for Signal Processing

The state of the steel sensing wire in a corrosion sensor is determined in two ways: (1) the phase dip shifts from one characteristic frequency to another frequency when the sensing wire breaks (Fig. D-2), or (2) the phase dip appears at both the sensing characteristic frequency and the reference characteristic frequency with the steel sensing wire intact, but only the phase dip at the

reference characteristic frequency is present with the steel wire broken (Fig. D-3). The method of using the shifting characteristic frequency was used to detect a wire break in first generation sensor design. For second generation sensors, the second method was used.

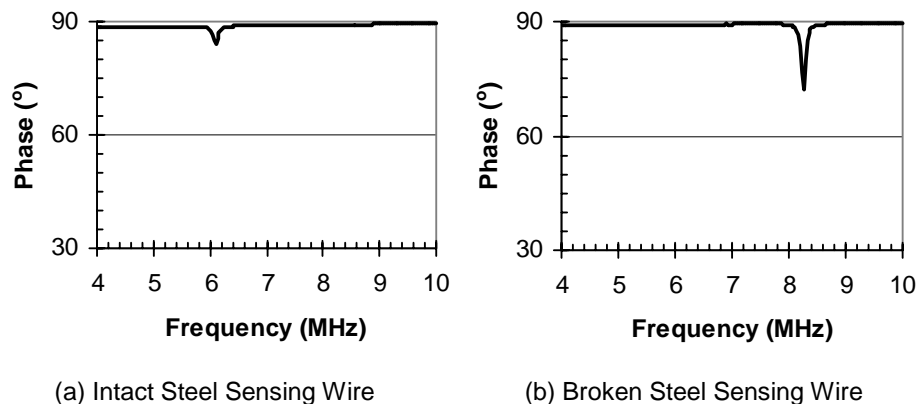


Figure D-2 First Generation Basic Sensor Phase Response

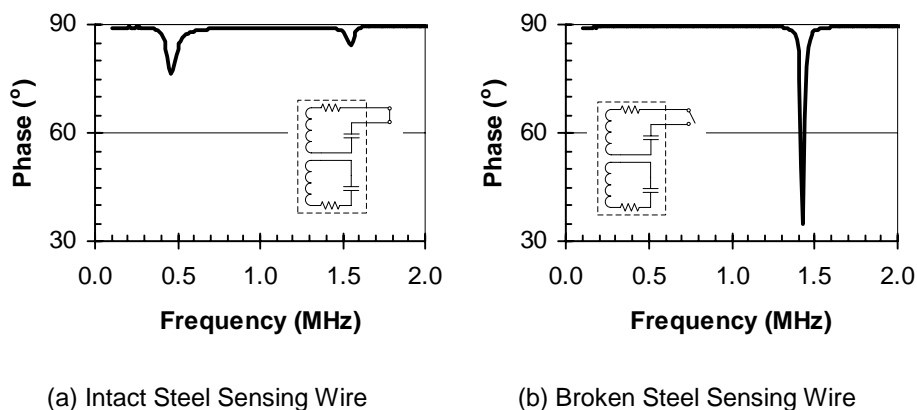


Figure D-3 Second Generation Concentric Sensor Phase Response

Tests of first generation sensors showed that identification of a characteristic frequency alone was not adequate to determine the state of the sensing wire. Transition behavior was observed, in which a very weak signal or no signal could be detected from sensors with broken sensing wires exposed to

conductive environments. Sensors used in Parametric Study II (Appendix B) also exhibited this behavior. Second generation sensors are also susceptible to transition behavior as shown in Chapter 4 and Appendix F. Because the response of the sensor changes with the environmental conditions, read distance, and interrogation equipment, a numerical technique is required to identify the difference between changes due to the state of the sensing wire and changes due to other factors. The pseudo-quality factor was proposed as a single number that could be used, along with the characteristic frequency, to identify the state of the sensing wire with varying environmental conditions and interrogation configurations. The pseudo-quality factor is defined as:

$$\bar{Q} = \frac{f}{\Delta f} \quad (D-1)$$

where \bar{Q} is the unitless pseudo-quality factor, f is the characteristic frequency in Hertz, and Δf is the width of the resonance at half of the maximum amplitude of the phase dip in Hertz.

Using a computer algorithm to fit a curve to the measured phase response and using the fitted curve to determine the characteristic frequency and pseudo-quality factor permits signal processing without human intervention. This appendix describes the method used to calculate the pseudo-quality factor for interrogations of second generation sensors for this thesis. The curve-fitting method and computer algorithms were developed by Andringa [4]. Extensive testing of the method is needed before conclusions can be made about the effectiveness of the pseudo-quality factor.

D.2 CURVE FITTING

The first step in calculation of the pseudo-quality factor is fitting mathematical functions to the measured phase response. Two types of curve-

fitting routines are necessary to define the measured phase response: baseline fitting and phase dip fitting.

D.2.1 Baseline

Because the baseline phase response depends on the impedance analyzer and reader coil configuration used to take the reading and includes the signal noise as shown in Chapter 3, no single function with constant coefficients can fit the baseline response. Fitting a baseline curve to the measured data removes the noise and permits the accurate calculation of phase dip parameters. A fifth-order inverse polynomial was selected to fit the baseline response. The baseline fitting function is given by:

$$y(x) = A + \frac{B}{x} + \frac{C}{x^2} + \frac{D}{x^3} + \frac{E}{x^4} \quad (\text{D-2})$$

where $y(x)$ represents the phase of the impedance in degrees, x is frequency in Hertz, and A through E are fitting coefficients.

Points on the baseline curve at frequencies outside the expected ranges of the phase dips are required for a proper fit. Therefore, frequency ranges to include in the fit must be specified for frequencies lower and higher than all possible phase dips for a single measurement. An additional frequency corresponding to a point between phase dips (if there are two phase dips in the response) must also be specified.

A computer algorithm is used to find the best fit for the polynomial, seeking to minimize the square-root of the sum of squares error. An initial guess for coefficients is included in the algorithm to begin the error minimizing process. Further increases in the order of the polynomial used to fit the baseline did not result in significant reductions in error.

D.2.2 Phase Dip

Phase dips can have a diverse range of depths, widths, and curvatures, so a flexible function is required to fit the phase response. The fit of the phase dip is critical because all of the factors used in evaluating sensor response stem from the fitting parameters. A Lorentzian function was chosen to fit the phase dips, which is given by:

$$y(x) = \frac{a}{(x-b)^2 + c^2} \quad (D-3)$$

where $y(x)$ represents the phase of the impedance in degrees, x is frequency in Hertz, and a through c are fitting coefficients.

The form of the Lorentzian function is convenient, because the fitting coefficients are directly related to the parameters necessary for evaluation of sensor response. The minimum in the phase (or maximum amplitude of phase dip) occurs at $x=b$, making b the characteristic frequency in Hertz. The maximum amplitude of the phase dip is $y(b) = \frac{a}{c^2}$, and the width of the resonance at half of the maximum amplitude (phase width) is $2c$. Therefore, the pseudo-quality factor is given by $\bar{Q} = \frac{b}{2c}$.

The Lorentzian function is fit to the phase dips using an iterative process developed by Andringa [4]. First, the baseline for the measured response is shifted to 90° . Then, by searching between the limits provided for the baseline fit, the phase minima are located and the amplitude of the phase dip is calculated. The points on the measured phase response curve closest to the phase angle at half of the phase dip are located and linear interpolation is used to find the phase width. Using the frequency at the phase minimum, the phase dip, and the phase width, the coefficients for a trial Lorentzian function are calculated. The initial

Lorentzian functions are combined with the baseline polynomial and a weighted error is calculated for the combined function against the measured response using a higher weight for points on the phase dip. Coefficients for the Lorentzian functions and the inverse polynomial function are recalculated and errors are checked again until the combined best fit is achieved.

D.3 EXAMPLE

An example of the curve-fitting process and a calculation of important phase response parameters is shown below for a measured response from a second generation sensor. Here, the weighted error calculation steps have been neglected to simplify the example.

D.3.1 Measured Response

The measured response for sensor B10, a concentric sensor with 26-gage wire, is shown in Fig. D-4. The reading was taken in air with the steel sensing wire intact at a read distance of 0.5 in. The reading was taken using a 4-in. diameter reader coil with five turns of 18-gage magnet wire attached to the Solartron Impedance Analyzer with a 3-ft cable. The phase response was measured between 0.1 MHz and 2.1 MHz using an increment of 0.01 MHz. Therefore, a total of 200 data points are available from a typical sensor interrogation.

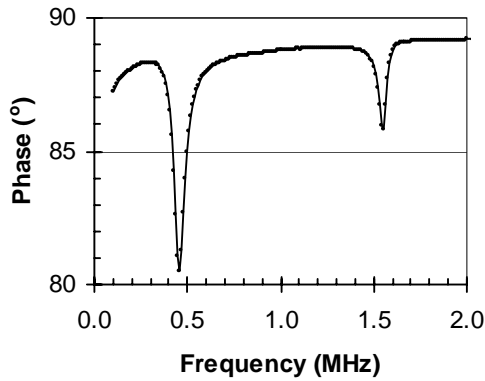


Figure D-4 Measured Phase Response of Sensor B10

D.3.2 Baseline

The algorithm uses two frequency ranges, which are not influenced by the characteristic frequencies, to establish the baseline response: the 0.1 to 0.3-MHz range is below the characteristic frequency of the sensing circuit and the 1.8 to 2.1-MHz range is above the characteristic frequency of the reference circuit. In addition, the baseline curve was tied to the measured response at a frequency of 1.0 MHz, which is between the two characteristic frequencies. The initial and final values of the coefficients for the inverse polynomial are given in Table D-1.

Table D-1 Fitting Coefficients for Baseline

	A	B	C	D	E
Initial	89.00	$-2.00 \cdot 10^6$	$3.00 \cdot 10^{11}$	$-4.00 \cdot 10^{16}$	$1.50 \cdot 10^{21}$
Final	89.84	$-1.59 \cdot 10^6$	$6.33 \cdot 10^{11}$	$-9.74 \cdot 10^{16}$	$4.78 \cdot 10^{21}$

The final baseline fit is shown in Fig. D-5 and the corresponding equation of the inverse polynomial is:

$$y(x) = 89.84 - \frac{1.59 \cdot 10^6}{x} + \frac{6.33 \cdot 10^{11}}{x^2} - \frac{9.74 \cdot 10^{16}}{x^3} + \frac{4.78 \cdot 10^{21}}{x^4}$$

The strange curvature at the lower frequencies is due to the combined fitting process that gives a greater weight to the fit of the phase dips. When the phase dip fits are added to the baseline, the resulting curve fit will be very good.

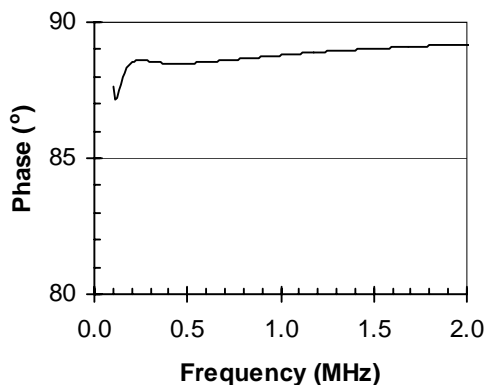


Figure D-5 Baseline Curve Fit

D.3.3 Phase Dips

Coefficients for the final Lorentzian functions used to fit the sensing and reference circuit phase dips are shown in Table D-2. Because the Lorentzian function alone gives positive values from zero for the fit as shown in Fig. D-6, the function must be subtracted from 90° to give the actual phase values.

Table D-2 Fitting Coefficients for Phase Dips

	a	b	c
Sensing Circuit	$8.52 \cdot 10^9$	$0.46 \cdot 10^6$	$32.62 \cdot 10^3$
Reference Circuit	$1.69 \cdot 10^9$	$1.54 \cdot 10^6$	$22.57 \cdot 10^3$

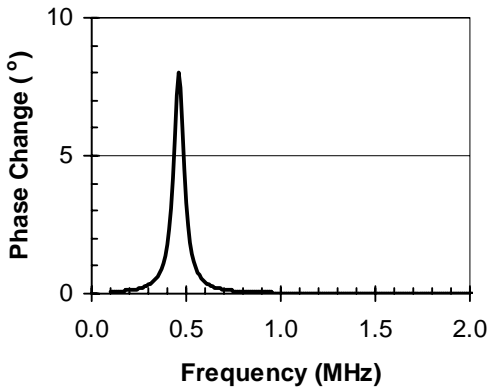


Figure D-6 Lorentzian Function for Sensing Circuit Phase Dip

D.3.3.1 Sensing Circuit Phase Dip

The fitted curve for the sensing phase dip is shown in Fig. D-7 and the corresponding equation is:

$$y(x) = 90 - \frac{8.52 \cdot 10^9}{(x - 0.46 \cdot 10^6)^2 + (32.62 \cdot 10^3)^2}$$

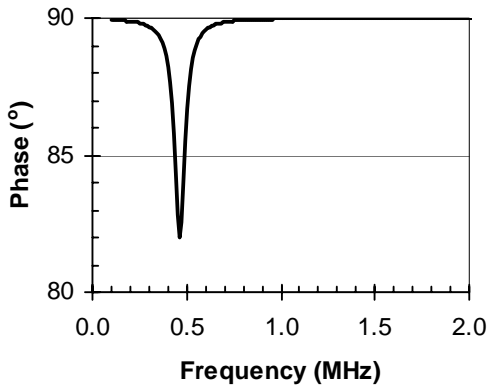


Figure D-7 Curve Fit of Sensing Circuit Phase Dip

The important parameters calculated for the sensing circuit include:

- (1) Characteristic Frequency: $f = b = 0.46$ MHz
- (2) Phase Dip: $\theta = \frac{a}{c^2} = 8.0^\circ$

(3) Phase Width: $\Delta f = 2c = 0.065 \text{ MHz}$

(4) Pseudo-Quality Factor: $\bar{Q} = \frac{f}{\Delta f} = \frac{b}{2c} = 7.07$

D.3.3.2 Reference Circuit Phase Dip

The fitted curve for the reference phase dip is shown in Fig. D-8 and the corresponding equation is:

$$y(x) = 90 - \frac{1.69 \cdot 10^9}{(x - 1.54 \cdot 10^6)^2 + (22.57 \cdot 10^3)^2}$$

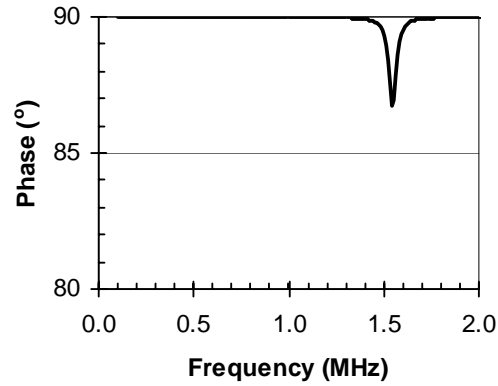


Figure D-8 Curve Fit of Reference Circuit Phase Dip

The important parameters calculated for the reference circuit include:

(1) Characteristic Frequency: $f = b = 1.54 \text{ MHz}$

(2) Phase Dip: $\theta = \frac{a}{c^2} = 3.3^\circ$

(3) Phase Width: $\Delta f = 2c = 0.045 \text{ MHz}$

(4) Pseudo-Quality Factor: $\bar{Q} = \frac{f}{\Delta f} = \frac{b}{2c} = 34.20$

D.3.4 Complete Curve Fit

The final fitted curve is achieved by merely adding the equations of the baseline and each phase dip together. The fitted curve is shown by itself in Fig. D-9 and is also plotted with the measured data in Fig. D-10. It is evident from Fig. D-10 that, while the fitted curve is not perfect, it is very good. The minor differences near the edges of the phase dips do not affect the calculation of important sensor response parameters. The curve-fitting routine was used on all measured data from second generation sensors with very good results. However, further testing and evaluation is necessary before the pseudo-quality factor can be considered a reliable method of determining the state of the steel sensing wire. Further discussion of pseudo-quality factor is presented in Chapter 4. It may be possible to obtain even more analog information about the state of the sensor or its surrounding environment with further study of curve-fitting phase response.

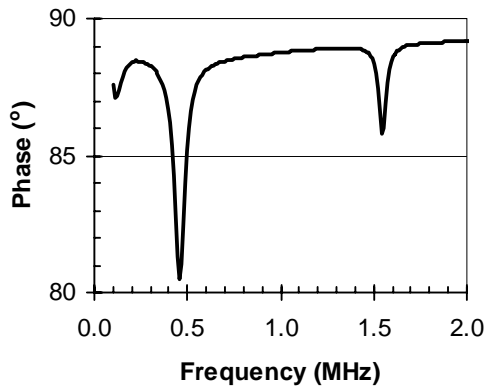


Figure D-9 Completed Curve Fit

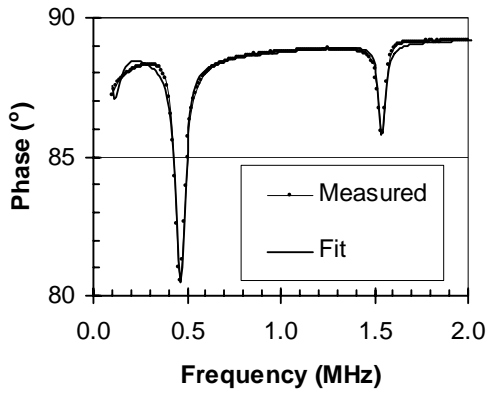


Figure D-10 Comparison of Measured Phase Response and Fitted Curve

APPENDIX E

Second Generation Sensor Fabrication

E.1 CONCENTRIC SENSOR

Before beginning fabrication of concentric sensors, 1.25-in. and 2.0-in. nominal diameter PVC pipes should be cut using a miter saw or other appropriate cutting tool into 0.5-in. slices (Fig. E-1). Also, PC component boards should be broken into small enough pieces to fit easily inside the smaller PVC pipe, but with enough holes and exposed copper to complete soldering of circuits (Fig. E-2). A 4x4 pattern of holes is suitable.

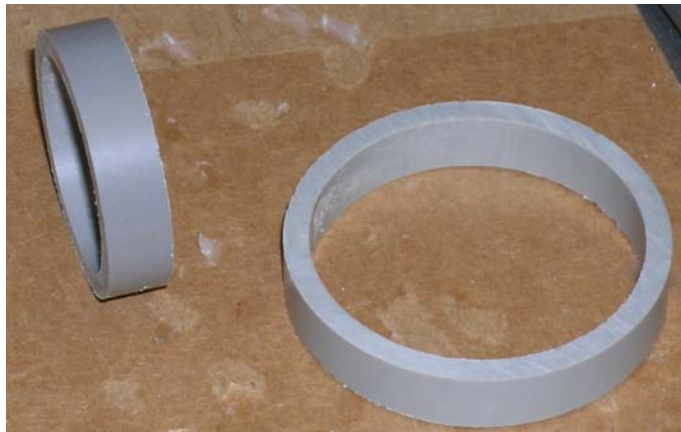


Figure E-1 Slices of PVC Pipe



Figure E-2 Piece of PC Component Board



Figure E-3 Holes Drilled in PVC Slices



Figure E-4 Winding Inductor Coil – Wind Toward Open Hole

Fabrication of the concentric sensor starts with winding the inductor coils. Holes are drilled in both slices of PVC pipe as shown in Fig. E-3 with enough space between them to fit five turns of copper magnet wire. Using a spool of magnet wire, the free end is inserted through one of the holes from the outside. Winding begins in the nearest direction of the other hole, such that the turns overlap between holes (Fig. E-4). The wire is wound tightly around the slice of

PVC for five turns (Fig. E-5) and secured at several locations with hot glue (Fig. E-6). After the hot glue cools, the magnet wire is cut and the cut end is inserted through the remaining open hole (Fig. E-7). Wires should be cut with two sections of wire of approximately the same length extending inside the PVC slice. The enamel coating should be stripped from the surface of the wire for a length of approximately 0.5 in. along each section (Fig. E-8).



Figure E-5 Winding Inductor Coil – Wind Five Complete Turns



Figure E-6 Winding Inductor Coil – Secure Wire with Hot Glue



Figure E-7 Winding Inductor Coil – Cut and Insert Wire

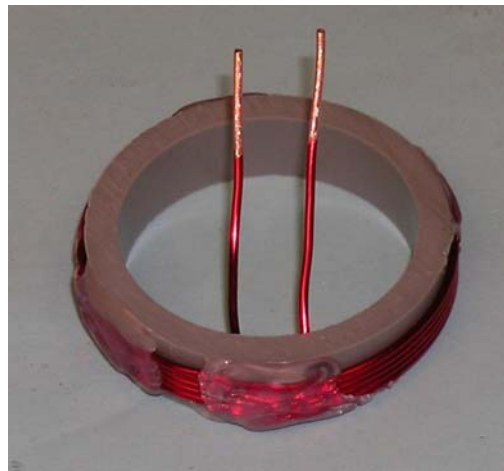


Figure E-8 Winding Inductor Coil – Cut Wires to Length and Strip Ends

The next step in sensor fabrication is soldering of capacitors to PC component boards. A vice is necessary to hold the PC component boards. For the reference circuit, the two lead wires extending from the 6,800-pF capacitor should be inserted through the side of the PC board without exposed copper and

bent to keep them in place. It may be helpful to place an object behind the capacitor to hold it in place (Fig. E-9).

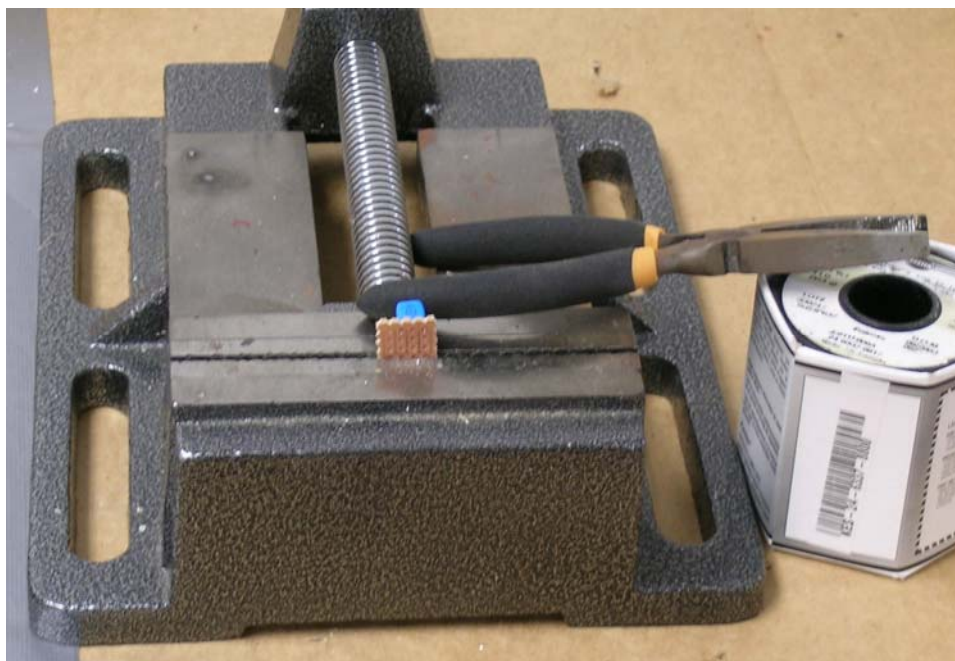


Figure E-9 Preparation for Soldering Reference Circuit

After heating and tinning, the soldering iron tip should be placed so that it is touching both the PC board copper and the capacitor lead wire and kept in place for a few seconds (Fig. E-10). Once the wires and board are heated sufficiently, hold the free end of solder wire to the tip of the soldering iron briefly to melt solder in place, and pull the soldering iron off of the circuit components. Solder should fill the entire area of the hole around the wire and extend a short distance up the wire and along the exposed copper of the PC board. Allow the solder to cool and then check to make sure that the wire and circuit board connection is solid. Repeat this process for the other wire extending from the capacitor. Kester™ 0.031-in. diameter solder wire was used for all soldered connections in the sensors.

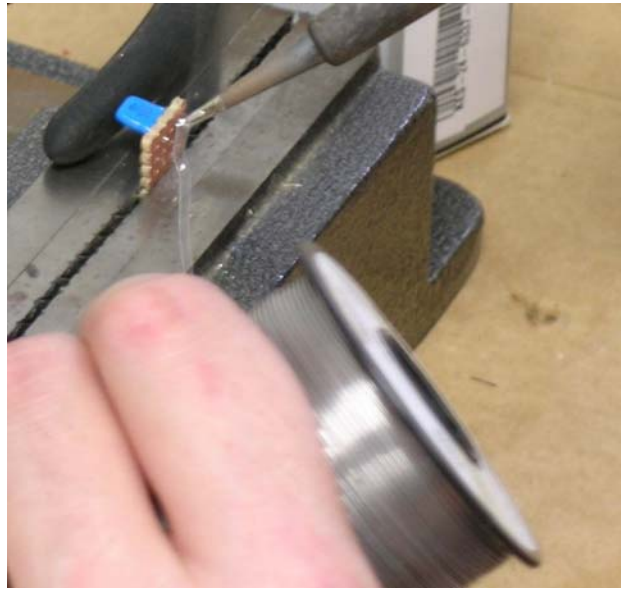


Figure E-10 Soldering Reference Circuit Capacitor

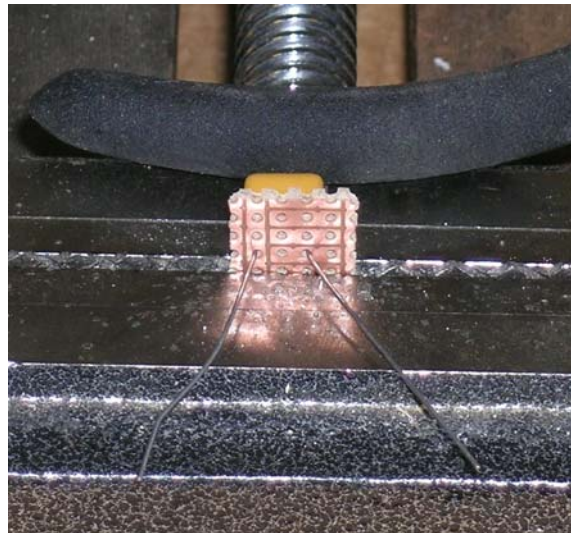


Figure E-11 Arrangement of Sensing Circuit Capacitor Before Soldering

The same steps are repeated for the sensing circuit using a 33,000-pF capacitor with the arrangement on the PC board shown in Fig. E-11. Once the soldering is complete, wires should be cut flush with the top of the solder (Fig. E-

12). The soldering locations must be carefully placed to result in the proper circuit for the final sensor.

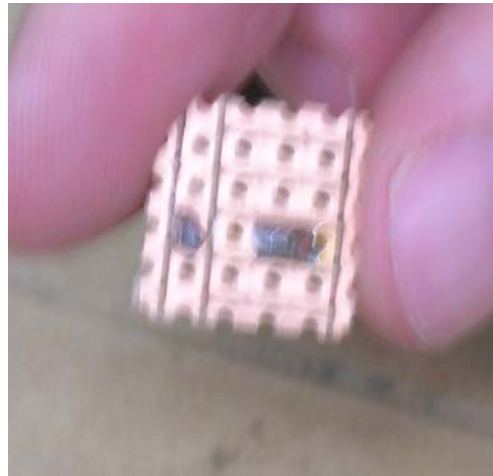


Figure E-12 Finished Soldering of Sensing Circuit Capacitor

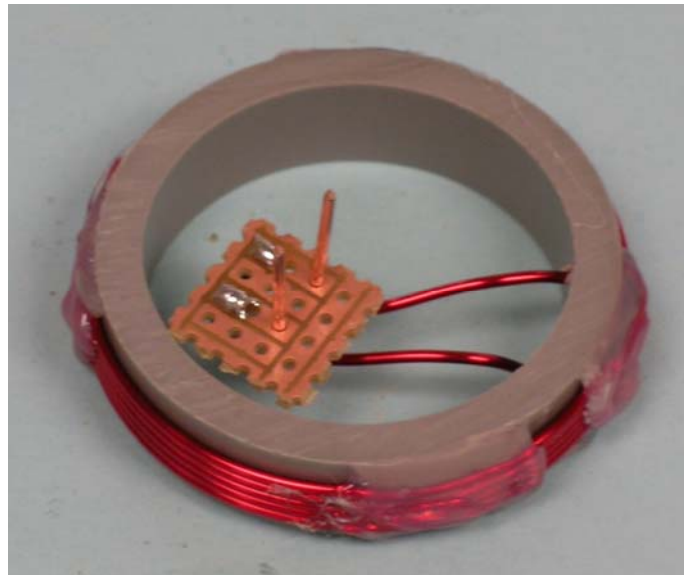


Figure E-13 Reference Inductor and PC Component Board Connected Before Soldering

To complete the reference circuit, the reference circuit inductor coil is soldered to the PC board. Inductor coil wires should be bent at the appropriate distance apart before connecting to the PC board. Fig. E-13 shows the PC board on the inductor coil wires before soldering. The finished reference circuit is shown in Fig. E-14. Care should be taken to ensure that no solder remains on the PC board that could short out the circuit. The solder balls at each connection do not need to be in contact because the copper strips on the PC component board connect the circuit.

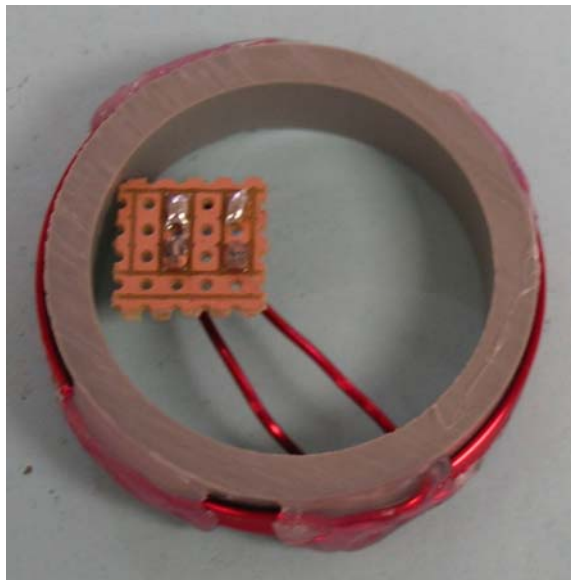


Figure E-14 Finished Reference Circuit

With the reference circuit complete, two more holes should be drilled in the PVC slice used to form the reference circuit (Fig. E-15). Insert the completed reference circuit over the sensing circuit inductor coil wire (Fig. E-16) and bend the sensing circuit wires into place (Fig. E-17). After the PC board is in place on the sensing circuit wires, complete soldering of wires from the sensing circuit inductor coil to the sensing circuit PC board (Fig. E-18). At this point, the sensor

should be interrogated for the first time to check that it responds at the reference characteristic frequency only.

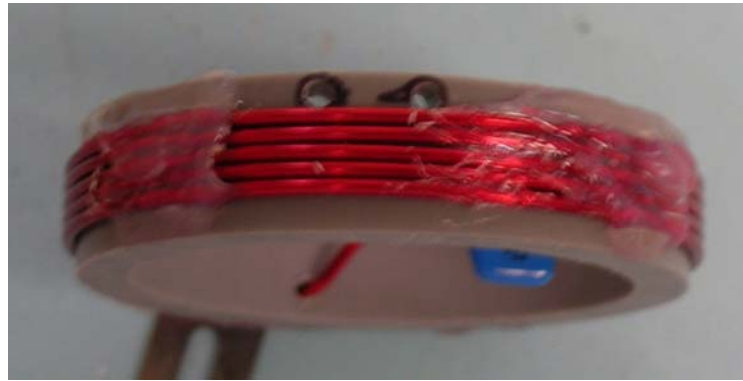


Figure E-15 Holes in Reference Circuit Inductor for Sensing Circuit Wires

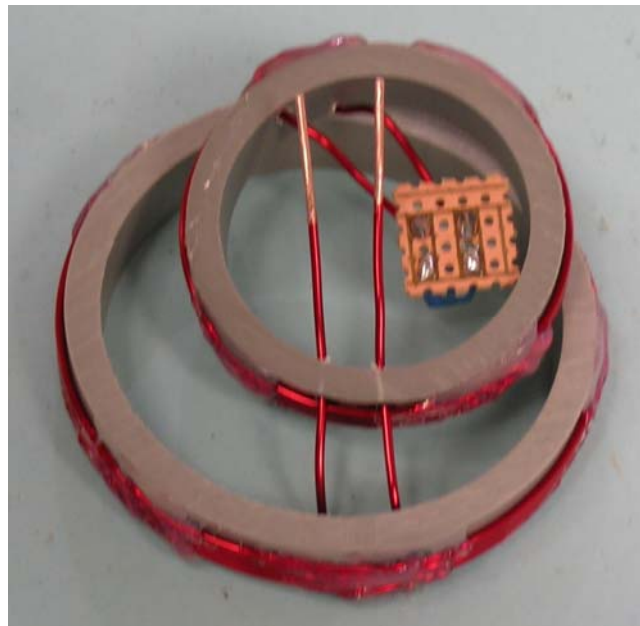


Figure E-16 Placing Reference Circuit Over Sensing Circuit Inductor Wires

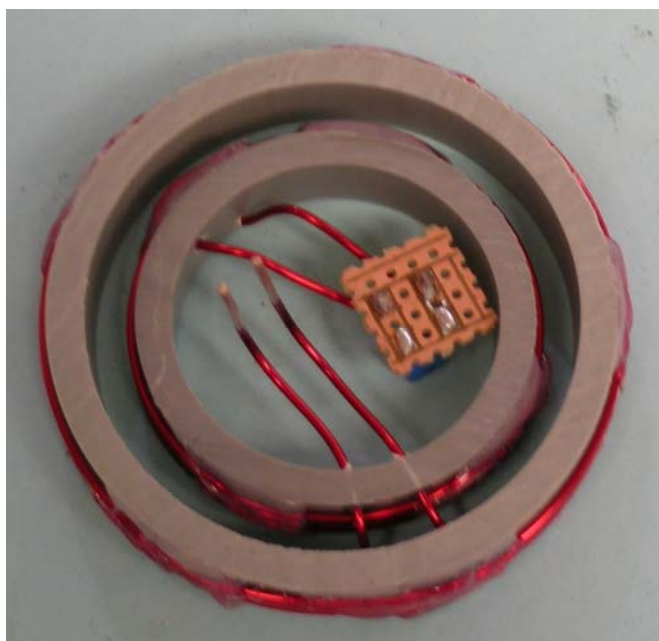


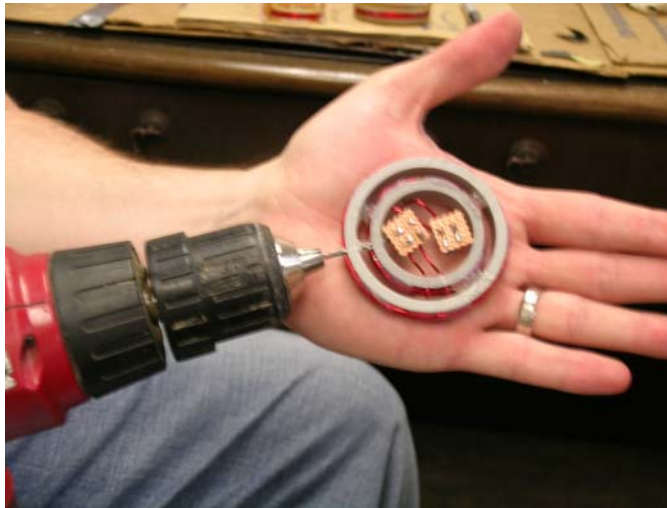
Figure E-17 Inductor Wires of Sensing Circuit Ready for PC Component Board



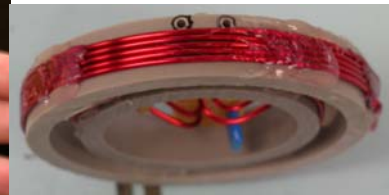
Figure E-18 Soldering Sensing Circuit Inductor Wires to PC Component Board

The last step before potting the sensor is to add the steel sensing wire. It may be helpful if the two coils are held in position on a flat surface while hot glue is placed between them to hold the inductor coils for the remaining steps. Two more holes should be drilled through each of the PVC slices (Fig. E-19). Cut a length of steel wire that is approximately 10 in. long. Both ends of the wire

should be cleaned by scraping or sanding for lengths of approximately 0.5 in. This step is extremely important to obtain a high-quality soldered connection to the steel sensing wire. The wire should then be bent in half to form two parallel segments (Fig. E-20). After the steel wire is inserted through the inductor coils and the proper holes in the sensing circuit PC component board (Fig. E-21), the steel wire should be cleaned with flux (Fig. E-22). The connection between the steel wire and the PC component board should be soldered immediately and cleaned again with isopropyl alcohol. Harris Stay-Clean™ flux was used for the soldered connections of the steel wires. The sensor should be interrogated again at this point to check that it responds at both the sensing and reference characteristic frequencies prior to potting.



(a) Drilling Through Both Inductor Coils



(b) Hole Locations For Steel Sensing Wire

Figure E-19 Holes for Steel Sensing Wire

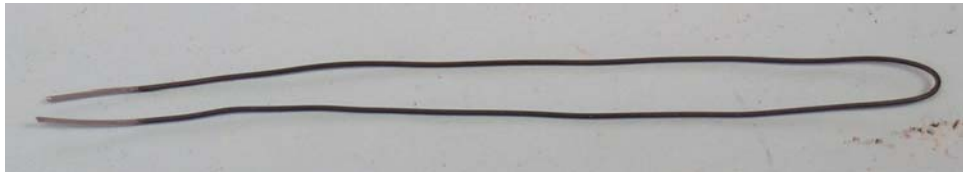


Figure E-20 Steel Sensing Wire

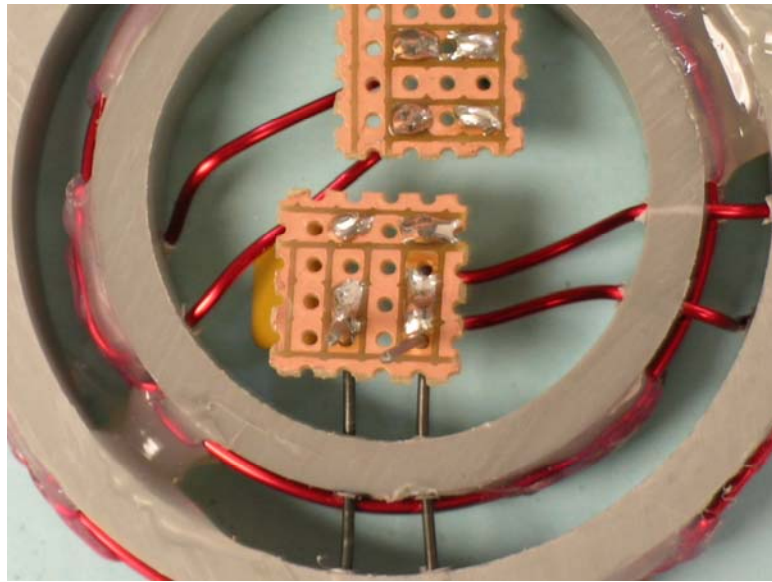


Figure E-21 Steel Sensing Wire in Position and Ready for Soldering

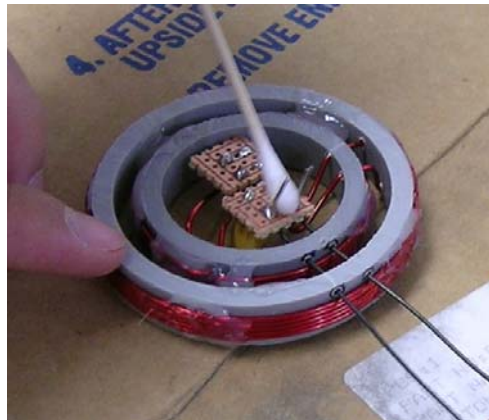


Figure E-22 Cleaning Steel Sensing Wires Before Soldering

The final step in sensor fabrication is potting with marine epoxy. Plastic cups that are just slightly larger in diameter than the completed sensor circuits work best for potting with epoxy. Cups should be cut to a height of approximately 1 in. to facilitate placement of epoxy. Steel sensing wires should be bent upward with an angle of 90° and sensors should be placed in the cup with the soldered side up (Fig. E-23). It is important to ensure that the inductor coils are parallel to the bottom of the cup. Typically, hot glue is used to attach the PVC slices to the bottom of the cup. For best results, cups should be placed on a level surface before placing the epoxy. Because the epoxy does not bond to plastic, the potted sensors can be easily removed from the cups after the epoxy cures. Styrofoam or paper cups should not be used to pot the sensors or mix the epoxy.

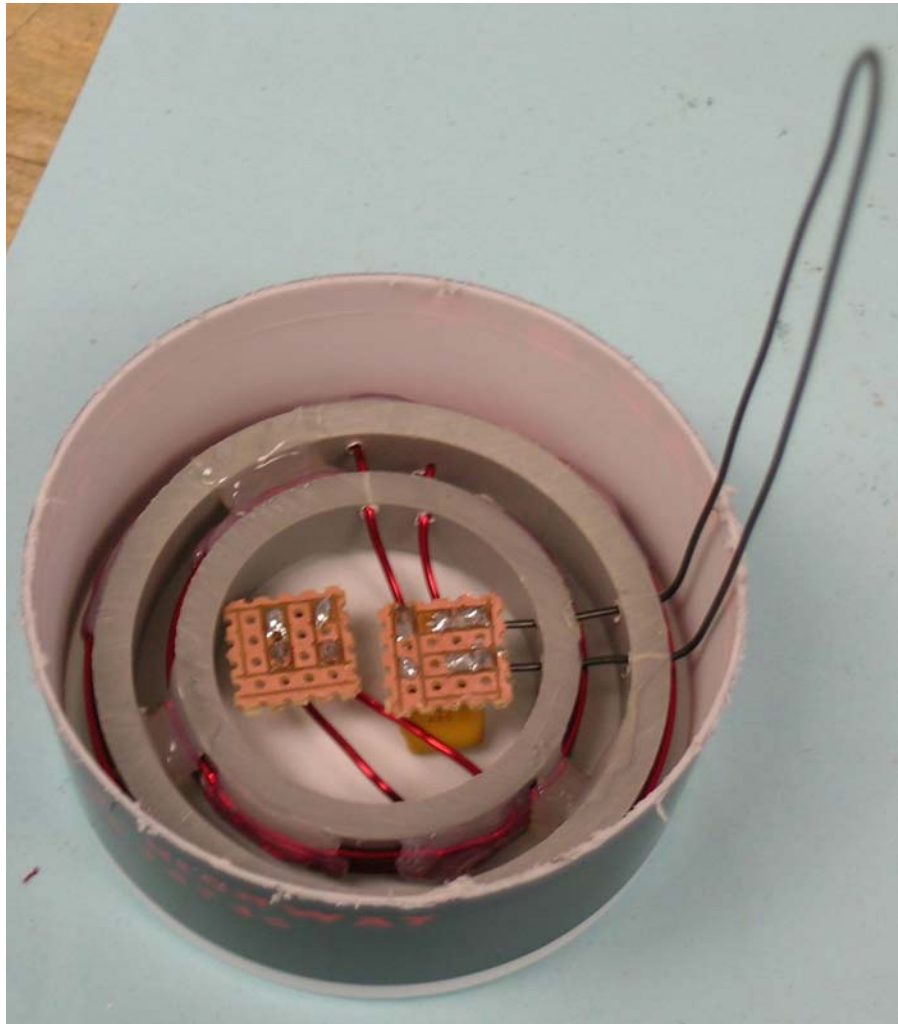


Figure E-23 Completed Sensor Circuits Ready for Potting with Epoxy

Bondo™ marine epoxy, which is a two-part fluid epoxy, has been used successfully to pot the sensors. It has a low viscosity, so it is easy to pour into the cup, forms a level surface along the top of the sensor without agitation, and cures to form an extremely hard and durable potting material. Extreme care should be taken to measure the two parts of epoxy in equal volumes and mix them together very thoroughly. If the proportioning of the epoxy mix is not correct, the epoxy

will not harden and the sensor will be ruined. A completed concentric sensor is shown in Fig. E-24.

As discussed in Chapter 5, the coefficient of expansion for marine epoxy is larger than that for concrete. Therefore, future work is needed to modify this material, or select a different material, to reduce these differences.

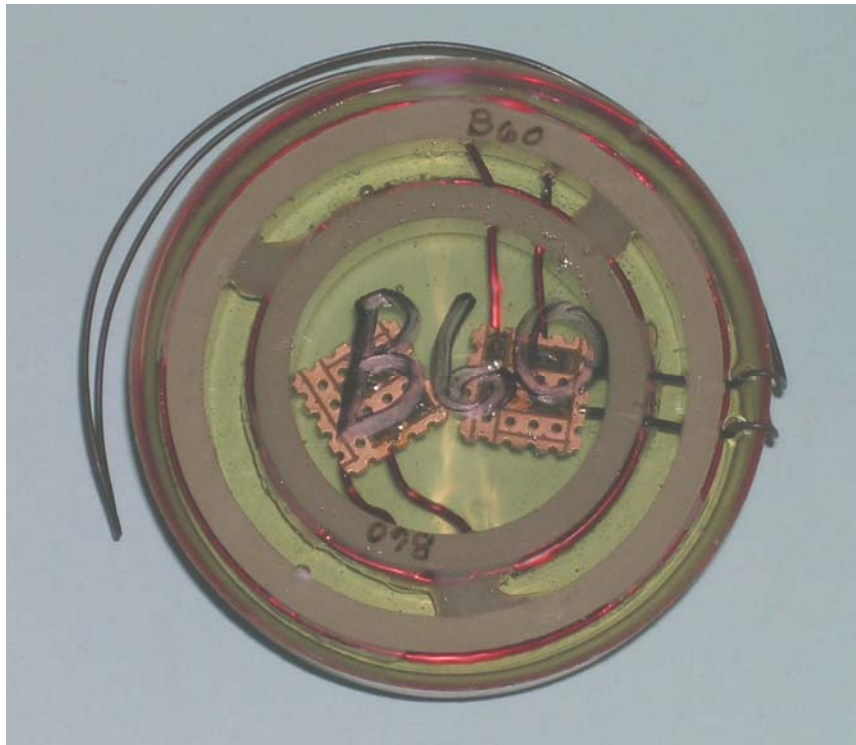


Figure E-24 Completed Concentric Sensor

E.2 COPLANAR SENSOR

The process of fabricating a coplanar sensor is essentially the same as a concentric sensor, but slightly less complicated because the two sensor circuits may be constructed independently of one another. Two slices of 1.25-in. nominal diameter PVC pipe are used and the finished circuits are potted in a rectangular

plastic dish rather than a round plastic cup. A completed coplanar sensor is shown in Fig. E-25.

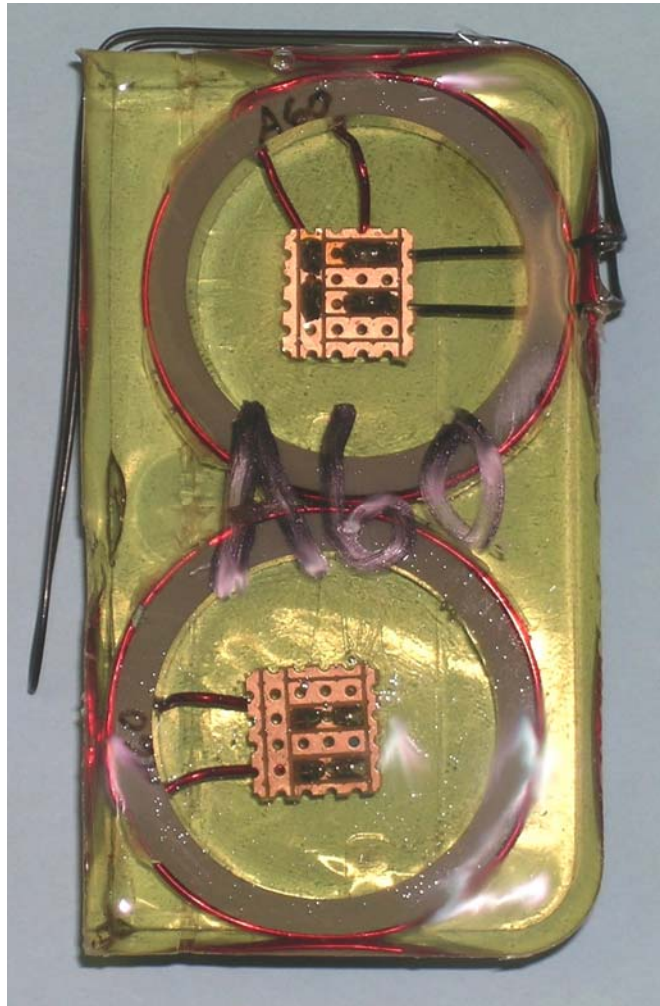


Figure E-25 Completed Coplanar Sensor

APPENDIX F

Second Generation Sensor Calibration

F.1 INTRODUCTION

Tests of sensors not embedded in concrete were used to calibrate the response of second generation sensors in preparation for the environmental exposure tests. In Chapter 5, the response of sensors embedded in concrete prisms and reinforced concrete slabs were evaluated using the data from calibration tests. Four second generation sensors were used for the calibration tests. Tests were performed using two concentric sensors, one with a 26-gage steel sensing wire (B10) and one with a 21-gage steel sensing wire (B60). Two coplanar sensors were also tested, one with a 26-gage steel sensing wire (A10) and one with a 21-gage steel sensing wire (A60).

Sensors were tested with both intact and cut steel sensing wires. Tests were conducted in air, tap water, and salt water with 3.5% sodium chloride by weight at seven different read distances. Salt water with a 3.5% concentration of sodium chloride provides an environment with a much higher conductivity than environments likely to be encountered within concrete structures. Therefore, this concentration was selected as the upper bound for testing. In addition, tests were conducted in air at four read distances with seven different reader coil configurations. For sensors with cut steel sensing wires, additional tests were performed in varying concentrations of salt water at three different read distances. The Solartron Impedance Analyzer was used for all interrogations. This elaborate testing plan was necessary to establish the behavior of sensors under controlled conditions so that conclusions could be drawn about sensor response in test conditions that are not controlled.

All of the results of second generation sensor calibration testing are presented in this appendix. The sensor phase response is plotted for selected cases only. All of the interrogation data, including characteristic frequency, phase dip, and pseudo-quality factor for both the sensing circuit response and reference circuit response, are presented in tables or figures. The signal processing method outlined in Appendix D was used for all of the data reduction. For the purposes of comparing data, the response of a sensor at a 1.0-in. read distance in air is used as the baseline, or standard, response of the sensor. The standard reader configuration consists of a 4-in. diameter reader coil with 5 turns of 18-gage magnet wire connected to the impedance analyzer with a 3-ft cable (reader coil 4t05 with a cable). Additional statistical analyses were performed on portions of the data and are also presented in this appendix.

F.2 CONCENTRIC SENSOR B10

Sensor B10 is a concentric sensor with a 26-gage steel sensing wire. The phase response of this sensor is shown in Fig. F-1 for an intact sensing wire (a) and for a cut sensing wire (b). This is the baseline response of the sensor in air with a read distance of 1.0 in. A 4-in. diameter reader coil with 5 turns of 18-gage magnet wire connected to the impedance analyzer with a 3-ft cable was used for this interrogation (reader coil 4t05 with a cable). With the steel sensing wire intact, the sensor responds at both the sensing circuit characteristic frequency and the reference circuit characteristic frequency. The reference circuit is heavily shielded when the sensing circuit response is present due to the sensing circuit inductor surrounding the reference circuit inductor. The change in phase response due to fracture of the steel sensing wire is significant. The sensing circuit phase dip disappears and the reference circuit is no longer shielded, resulting an 8%

characteristic frequency shift down from 1.54 MHz to 1.42 MHz and a much larger phase dip.

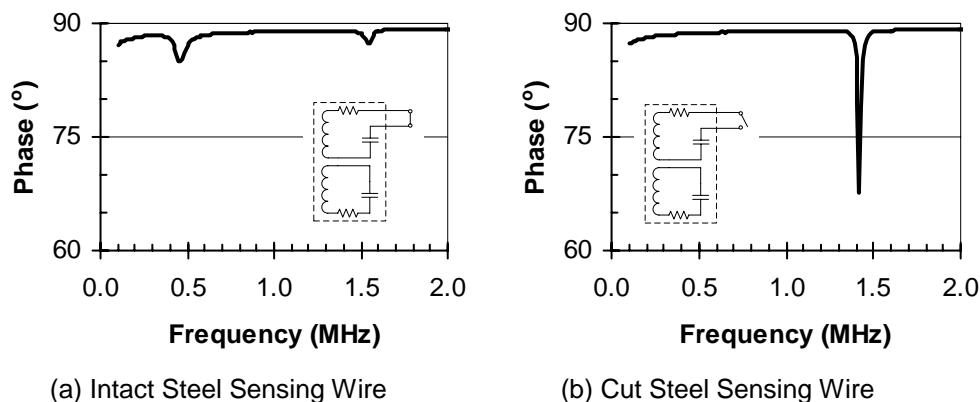


Figure F-1 Phase Response of Sensor B10

F.2.1 Surrounding Environment

To gauge the effect of the surrounding environment on the performance of sensor B10, the sensor was interrogated in air, tap water, and salt water using reader coil 4t05 attached to the impedance analyzer with a 3-ft cable. Interrogations were taken with intact and cut steel sensing wires. In addition to those three environments, sensor B10 with a cut sensing wire was also interrogated using the same reader configuration in varying concentrations of salt water. Salt water concentrations of 0.0%, 0.01%, 0.02%, 0.05%, 0.1%, 0.2%, 0.3%, 0.4%, 0.5%, 1.0%, and 3.5% were selected to provide a well-defined transition behavior for the sensor.

F.2.1.1 Intact Steel Sensing Wire

Interrogation results at a read distance of 1.0 in. were used to compare the response of sensor B10 in air, tap water, and 3.5% salt water. Table F-1 shows the effect of surrounding environment on sensor B10 with an intact steel sensing

wire. The characteristic frequencies and pseudo-quality factors remain approximately constant with the change from air to tap water. Only a 7-8% reduction in pseudo-quality factor occurs with the change from tap water to 3.5% salt water. Phase dips are more sensitive to the surrounding environments, with reductions of approximately 30% for the change from air to tap water and approximately another 10-25% for the change from tap water to 3.5% salt water. As discussed in Chapter 3, the reduction in phase dip for the change from air to tap water may be due to the test method. The thickness of glass on the bottom of the beaker used to contain the water increases the read distance slightly, which probably results in most of the reduction in phase dip.

Table F-1 Effect of Surrounding Environment on Sensor B10 with Intact Sensing Wire

Environment	Sensing Circuit			Reference Circuit		
	Char. Freq. (MHz)	Phase Dip (°)	Pseudo-Quality Factor	Char. Freq. (MHz)	Phase Dip (°)	Pseudo-Quality Factor
Air	0.46	3.7	7.1	1.54	1.8	33.6
Tap Water	0.46	2.6	7.3	1.54	1.3	33.5
3.5% Salt Water	0.47	2.5	6.6	1.55	1.0	31.2

F.2.1.2 Cut Steel Sensing Wire

Table F-2 shows the effect of surrounding environment on sensor B10 with a cut steel sensing wire. The reference characteristic frequency remains constant with the change from air to tap water, while the sensing characteristic frequency is not present. The reference pseudo-quality factor falls approximately

50% and the reference phase dip decreases by almost 70% with the change from air to tap water. Sensor behavior is even more drastic for the change from tap water to 3.5% salt water. The sensing circuit characteristic frequency reappears with a phase dip and pseudo-quality factor approximately 30% less than those for the same sensor with an intact steel sensing wire interrogated in 3.5% salt water. The reference circuit characteristic frequency shifts back to the value with the wire intact due to shielding from the sensing circuit resonance. The phase dip decreases by almost 90% with the change from tap water to 3.5% salt water. The pseudo-quality factor also decreases by 26%. Compared with the phase dip of the reference circuit in sensor B10 with the steel sensing wire intact, the phase dip is reduced by 9% with the steel sensing wire cut. The pseudo-quality factor for the reference circuit of sensor B10 with a cut steel sensing wire in 3.5% salt water is also reduced by 7% compared with the sensor with an intact wire.

Table F-2 Effect of Surrounding Environment on Sensor B10 with Cut Sensing Wire

Environment	Sensing Circuit			Reference Circuit		
	Char. Freq. (MHz)	Phase Dip (°)	Pseudo-Quality Factor	Char. Freq. (MHz)	Phase Dip (°)	Pseudo-Quality Factor
Air	-	-	-	1.42	21.4	76.9
Tap Water	-	-	-	1.42	6.8	39.3
3.5% Salt Water	0.49	1.7	4.6	1.55	0.9	29.1

Table F-3 shows the effect of varying salt water concentration on sensor B10 with a cut steel sensing wire. Interrogation results are shown for 1.0-in. read distance. The reference circuit phase dip decreases with increasing salt water

concentration to a minimum at 0.5% and then increases slightly with increasing concentration. The reference characteristic frequency shifts higher as the sensing circuit characteristic frequency begins to reappear and shield the reference circuit response. At a concentration of 0.5% and above, the sensing circuit response is present with a phase dip of 0.1° or more. Fig. F-2 shows the phase response of the sensor with varying concentrations of salt water. The transition response of sensor B10 is evident with increasing conductivity of the surrounding environment. The phase response of the sensor with a cut sensing wire immersed in 3.5% salt water (k) is very close to the response of the sensor with an intact sensing wire immersed in 3.5% salt water (l). However, the difference in pseudo-quality factors may still provide the information needed to determine the state of the steel sensing wire. Further discussion on use of the pseudo-quality factor is provided in Section F.2.2.

Table F-3 Effect of Varying Concentration of Salt Water on Sensor B10 with Cut Sensing Wire

Salt Water Concentration	Sensing Circuit			Reference Circuit		
	Char. Freq. (MHz)	Phase Dip (°)	Pseudo-Quality Factor	Char. Freq. (MHz)	Phase Dip (°)	Pseudo-Quality Factor
0.0%	-	-	-	1.42	6.8	39.3
0.01%	-	-	-	1.42	4.7	28.1
0.02%	-	-	-	1.42	3.4	22.7
0.05%	-	-	-	1.42	2.2	14.1
0.1%	-	-	-	1.42	1.5	10.8
0.2%	-	-	-	1.44	0.9	9.1
0.3%	-	-	-	1.46	0.7	9.6
0.4%	-	-	-	1.49	0.6	10.7
0.5%	0.57	0.6	0.4	1.50	0.6	11.5
1.0%	0.52	0.5	2.4	1.53	0.6	16.5
3.5%	0.49	1.7	4.6	1.55	0.9	29.1

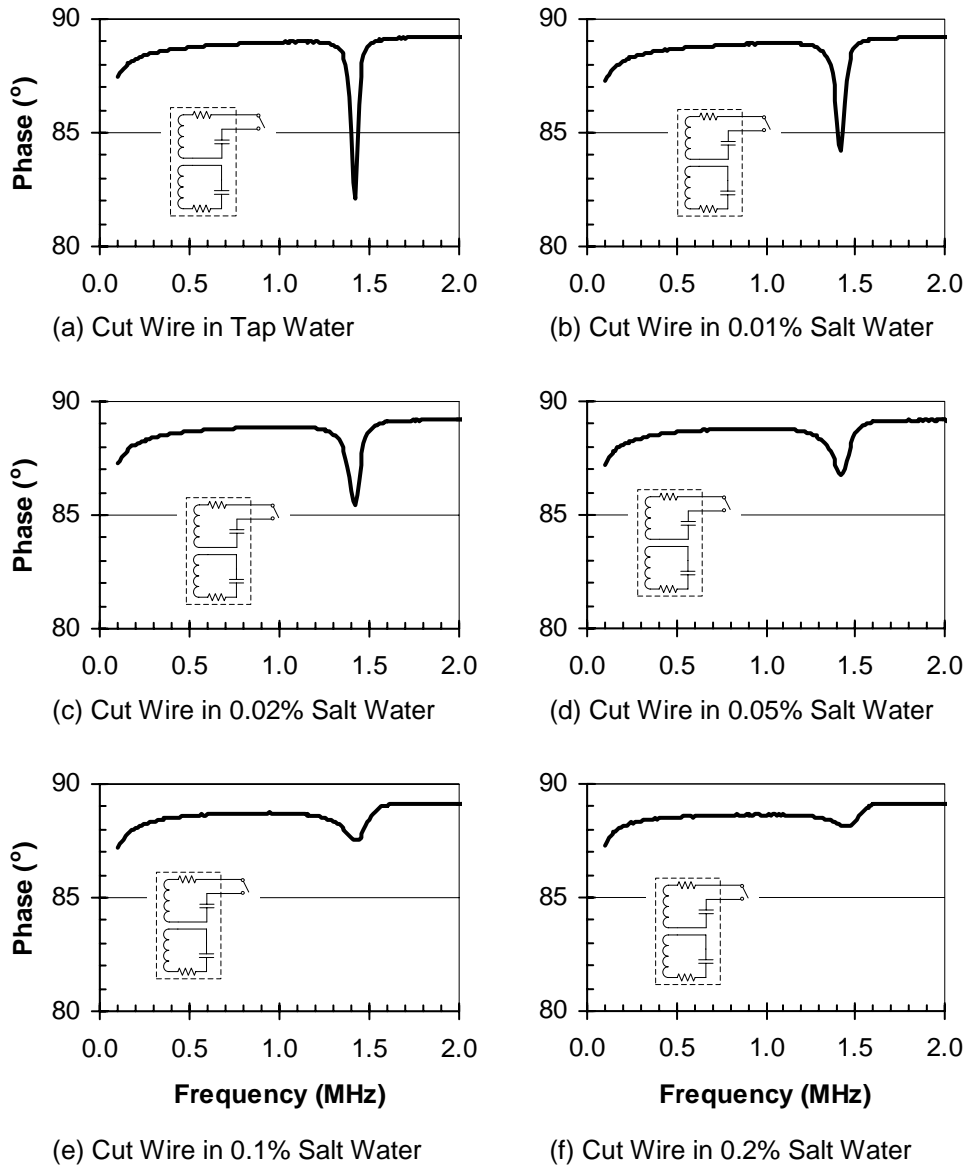
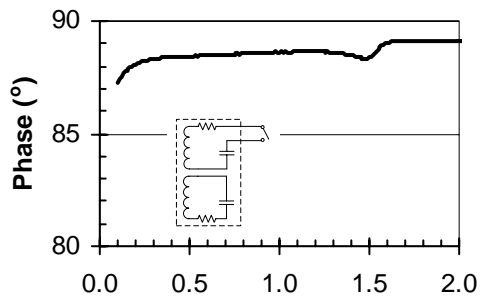
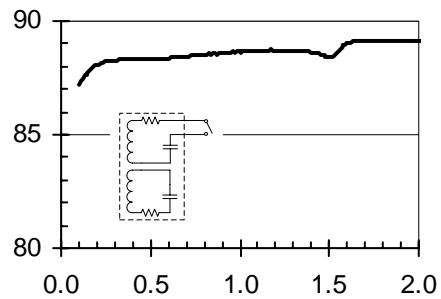


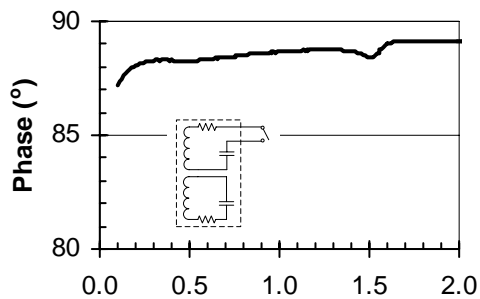
Figure F-2 Phase Response of Sensor B10 in Varying Concentrations of Salt Water



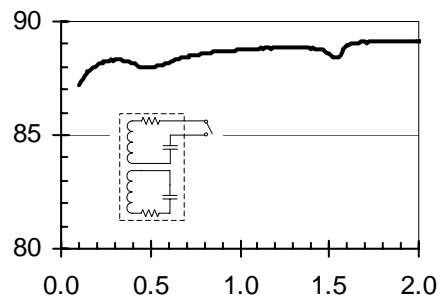
(g) Cut Wire in 0.3% Salt Water



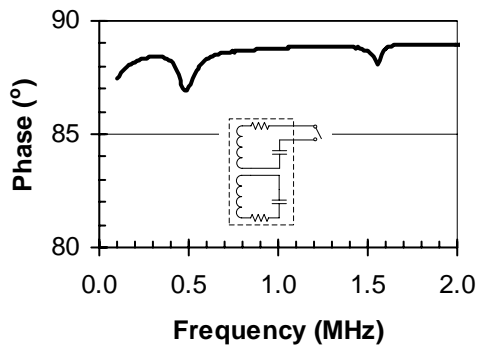
(h) Cut Wire in 0.4% Salt Water



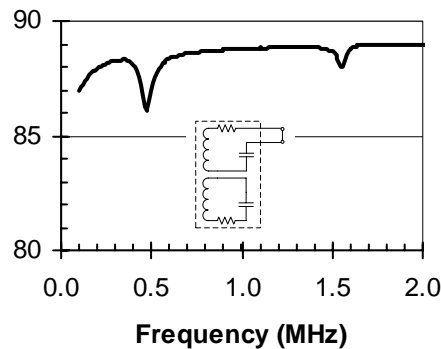
(i) Cut Wire in 0.5% Salt Water



(j) Cut Wire in 1.0% Salt Water



(k) Cut Wire in 3.5% Salt Water



(l) Intact Wire in 3.5% Salt Water

Figure F-2 (Cont.) Phase Response of Sensor B10 in Varying Concentrations of Salt Water

F.2.2 Read Distance

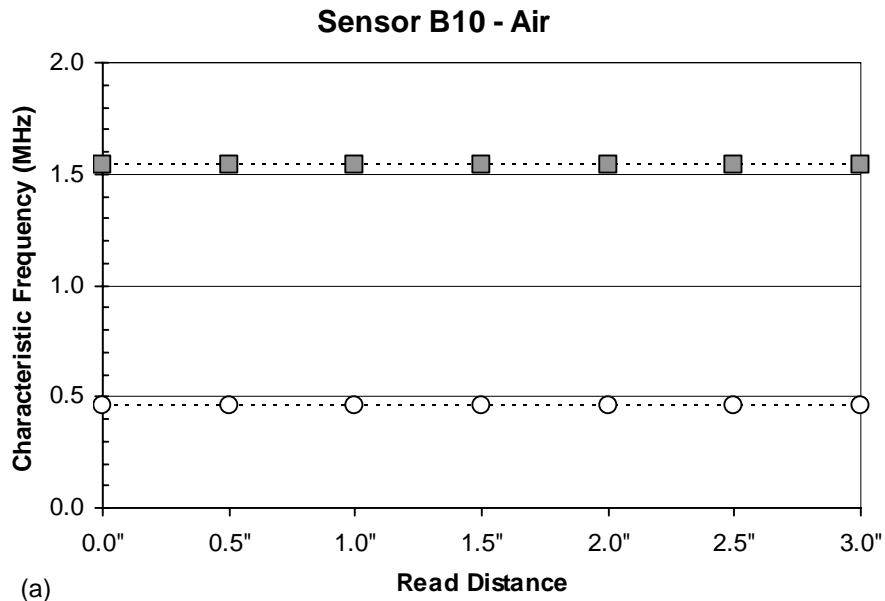
Because read distance also affects the performance of sensors, sensor B10 was interrogated at read distances from 0.0 in. to 3.0 in. at 0.5-in increments in air, tap water, and 3.5% salt water using reader coil 4t05 attached to the impedance analyzer with a 3-ft cable. Interrogations were taken with intact and cut steel sensing wires. In addition to those three environments, sensor B10 was also interrogated using the same reader configuration in varying concentrations of salt water at read distances of 0.0 in., 1.0 in., and 2.0 in.

F.2.2.1 Intact Steel Sensing Wire

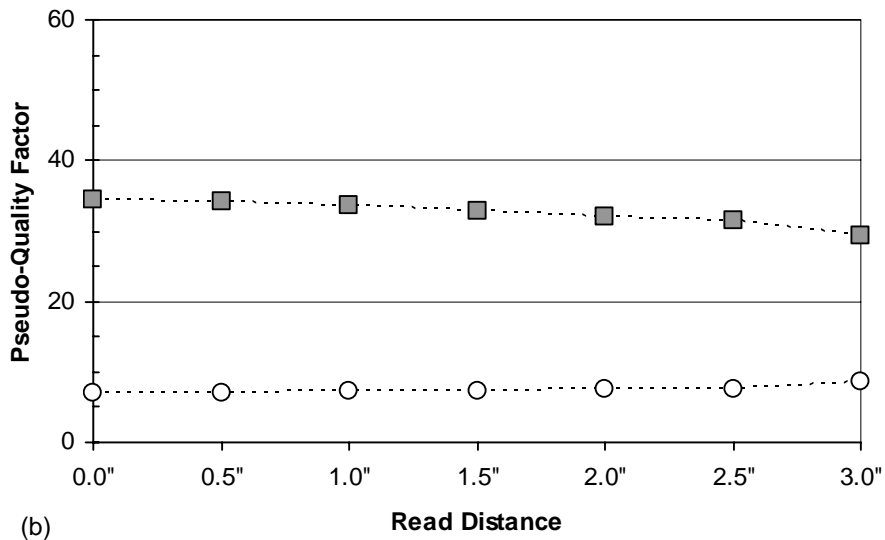
Table F-4 shows the effect of read distance on sensor B10 with an intact steel sensing wire. Interrogation results are shown in the table for readings in air. While phase dips are significantly reduced with increasing read distance, the characteristic frequency of each circuit remains the same. The pseudo-quality factor only increases slightly for the sensing circuit and decreases slightly for the reference circuit with increasing read distance. The characteristic frequencies and pseudo-quality factors are plotted versus read distance in Fig. F-3 for interrogations in air, Fig. F-4 for tap water, and Fig. F-5 for 3.5% salt water. A statistical summary of the characteristic frequency, phase dip, and pseudo-quality factor for the sensing circuit is provided in Table F-5. The same information for the reference circuit is provided in Table F-6. The coefficients of variation for characteristic frequencies of both the sensing and reference circuits are very small (<0.5%). Because phase dips are highly dependent on read distance, the coefficients of variation for phase dips are quite large (>100%). The coefficients of variation for pseudo-quality factors are very good, ranging from 4.1% to 8.2%.

Table F-4 Effect of Read Distance on Sensor B10 with Intact Sensing Wire

Read Distance (in.)	Sensing Circuit			Reference Circuit		
	Char. Freq. (MHz)	Phase Dip (°)	Pseudo- Quality Factor	Char. Freq. (MHz)	Phase Dip (°)	Pseudo- Quality Factor
0.0	0.46	15.3	6.9	1.54	4.7	34.5
0.5	0.46	8.0	7.1	1.54	3.3	34.2
1.0	0.46	3.7	7.1	1.54	1.8	33.6
1.5	0.46	1.7	7.2	1.54	0.9	32.9
2.0	0.46	0.8	7.4	1.54	0.4	32.1
2.5	0.46	0.4	7.6	1.54	0.2	31.5
3.0	0.46	0.2	8.7	1.54	0.1	29.3



(a)



(b)



Figure F-3 Effect of Read Distance on Response of Sensor B10 with an Intact Sensing Wire for Readings in Air

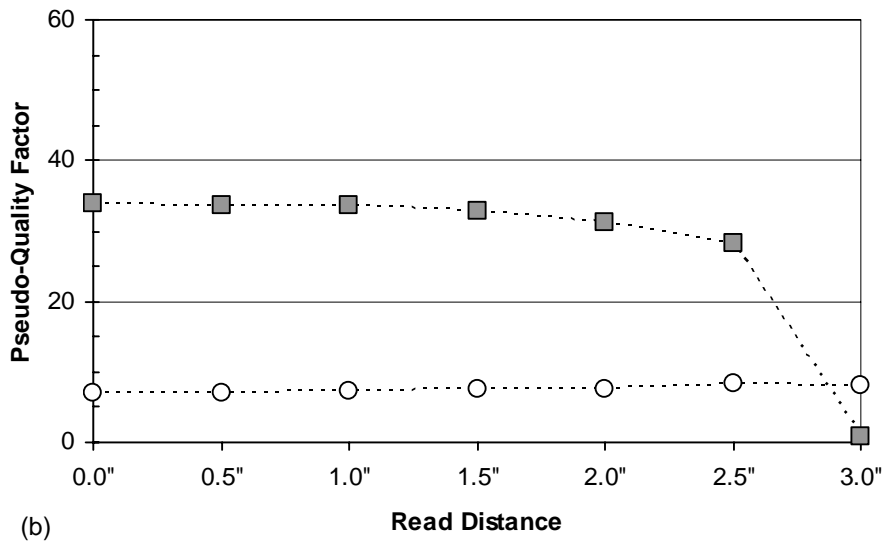
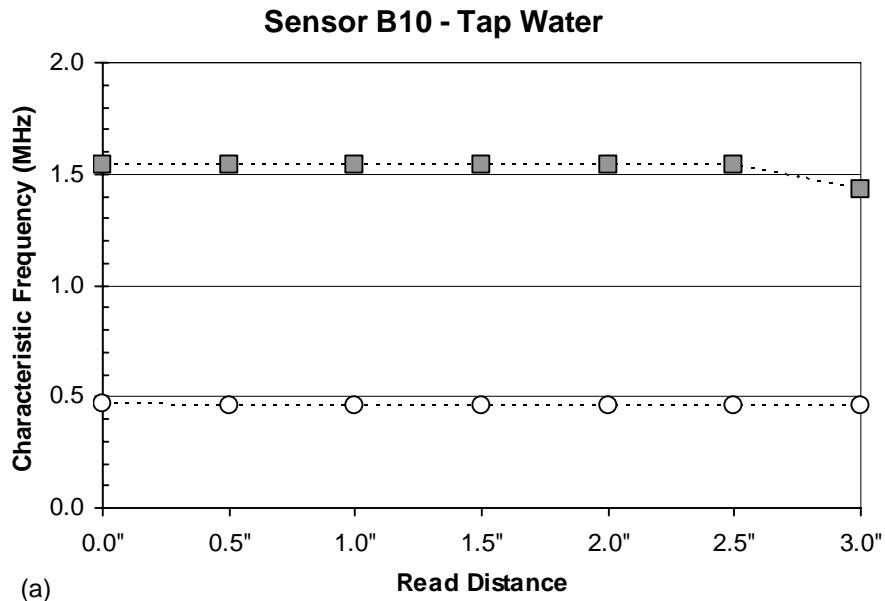


Figure F-4 Effect of Read Distance on Response of Sensor B10 with an Intact Sensing Wire for Readings in Tap Water

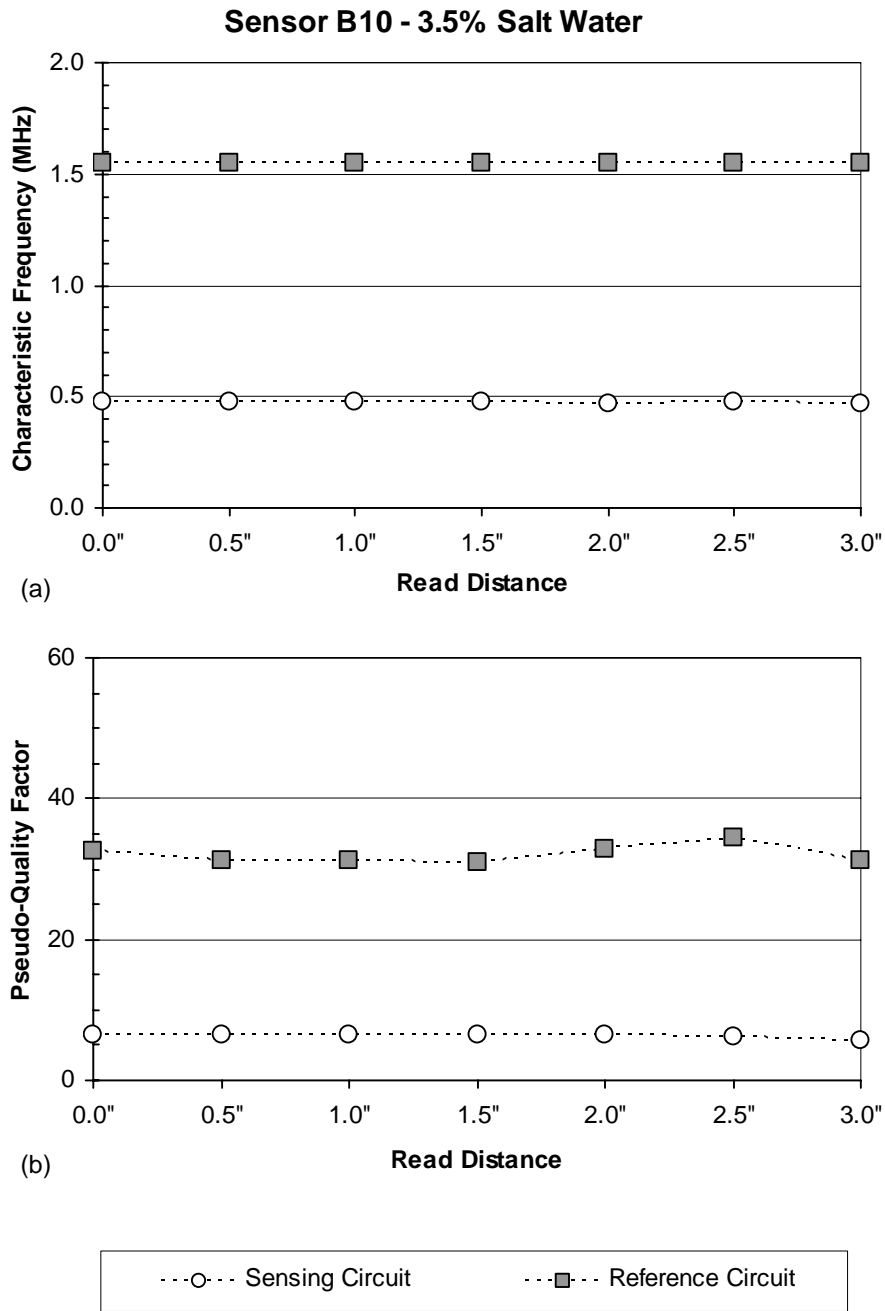


Figure F-5 Effect of Read Distance on Response of Sensor B10 with an Intact Sensing Wire for Readings in 3.5% Salt Water

**Table F-5 Variation of Measured Response of Sensor B10 with Intact Sensing
Wire for Sensing Circuit with Varying Read Distance**

Environment	Number of Readings	Characteristic Frequency		Pseudo-Quality Factor		Phase Dip	
		Mean (MHz)	Coef. of Variation	Mean	Coef. of Variation	Mean (°)	Coef. of Variation
Air	7	0.46	0.4%	7.4	8.2%	4.3	129.4%
Tap Water	7	0.46	0.4%	7.5	6.3%	3.7	120.2%
3.5% Salt Water	7	0.47	0.4%	6.4	5.3%	3.1	133.2%

**Table F-6 Variation of Measured Response of Sensor B10 with Intact Sensing
Wire for Reference Circuit with Varying Read Distance**

Environment	Number of Readings	Characteristic Frequency		Pseudo-Quality Factor		Phase Dip	
		Mean (MHz)	Coef. of Variation	Mean	Coef. of Variation	Mean (°)	Coef. of Variation
Air	7	1.54	0.0%	32.6	5.5%	1.6	107.2%
Tap Water*	6	1.54	0.0%	32.2	6.9%	1.5	120.2%
3.5% Salt Water	7	1.55	0.0%	32.0	4.1%	1.0	117.6%

* Data from read distance of 3 in. were not included

F.2.2.2 Cut Steel Sensing Wire

The effect of read distance on sensor B10 with a cut steel sensing wire is shown in Table F-7. Interrogation results are shown in the table for readings in air. Again, phase dips are substantially reduced with increasing read distance. Characteristic frequencies do not change and the variations in pseudo-quality

factors are small. The characteristic frequencies and pseudo-quality factors are plotted versus read distance in Fig. F-6 for interrogations in air, Fig. F-7 for tap water, and Fig. F-8 for 3.5% salt water. A statistical summary of the characteristic frequency, phase dip, and pseudo-quality factor for the reference circuit is provided in Table F-8. The same information for the sensing circuit is provided in Table F-9. The sensing circuit only responded in the 3.5% salt water environment. Coefficients of variation are very small for characteristic frequencies and very large for phase dips.

While the coefficients of variation for pseudo-quality factors are small, ranging from 5.1% to 6.9% for the reference circuit, the values change substantially with increasing conductivity of the surrounding environment. In 3.5% salt water, the reference circuit mean pseudo-quality factor is 30.0 for a cut steel sensing wire, while it is 32.0 for an intact wire. The sensing circuit mean pseudo-quality factor is 4.3 for a cut steel sensing wire and 6.4 for an intact wire. Therefore, the pseudo-quality factor may give a reliable indication of the state of the steel sensing wire in the presence of a conductive environment.

Table F-7 Effect of Read Distance on Sensor B10 with Cut Sensing Wire

Read Distance (in.)	Sensing Circuit			Reference Circuit		
	Char. Freq. (MHz)	Phase Dip (°)	Pseudo- Quality Factor	Char. Freq. (MHz)	Phase Dip (°)	Pseudo- Quality Factor
0.0	-	-	-	1.42	70.3	67.5
0.5	-	-	-	1.42	42.4	74.4
1.0	-	-	-	1.42	21.4	76.9
1.5	-	-	-	1.42	10.3	77.7
2.0	-	-	-	1.42	5.1	78.0
2.5	-	-	-	1.42	2.5	78.9
3.0	-	-	-	1.42	1.3	78.8

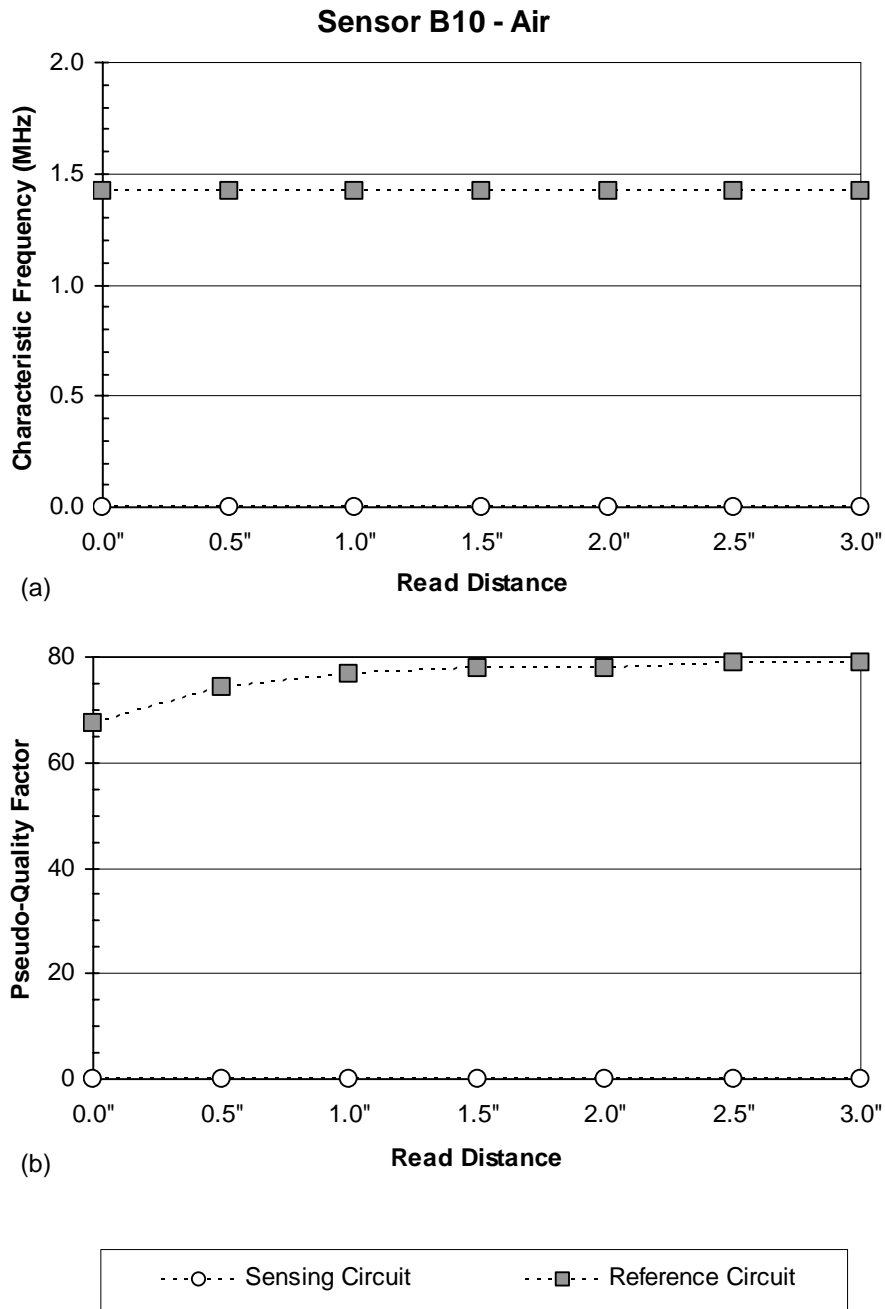


Figure F-6 Effect of Read Distance on Response of Sensor B10 with a Cut Sensing Wire for Readings in Air

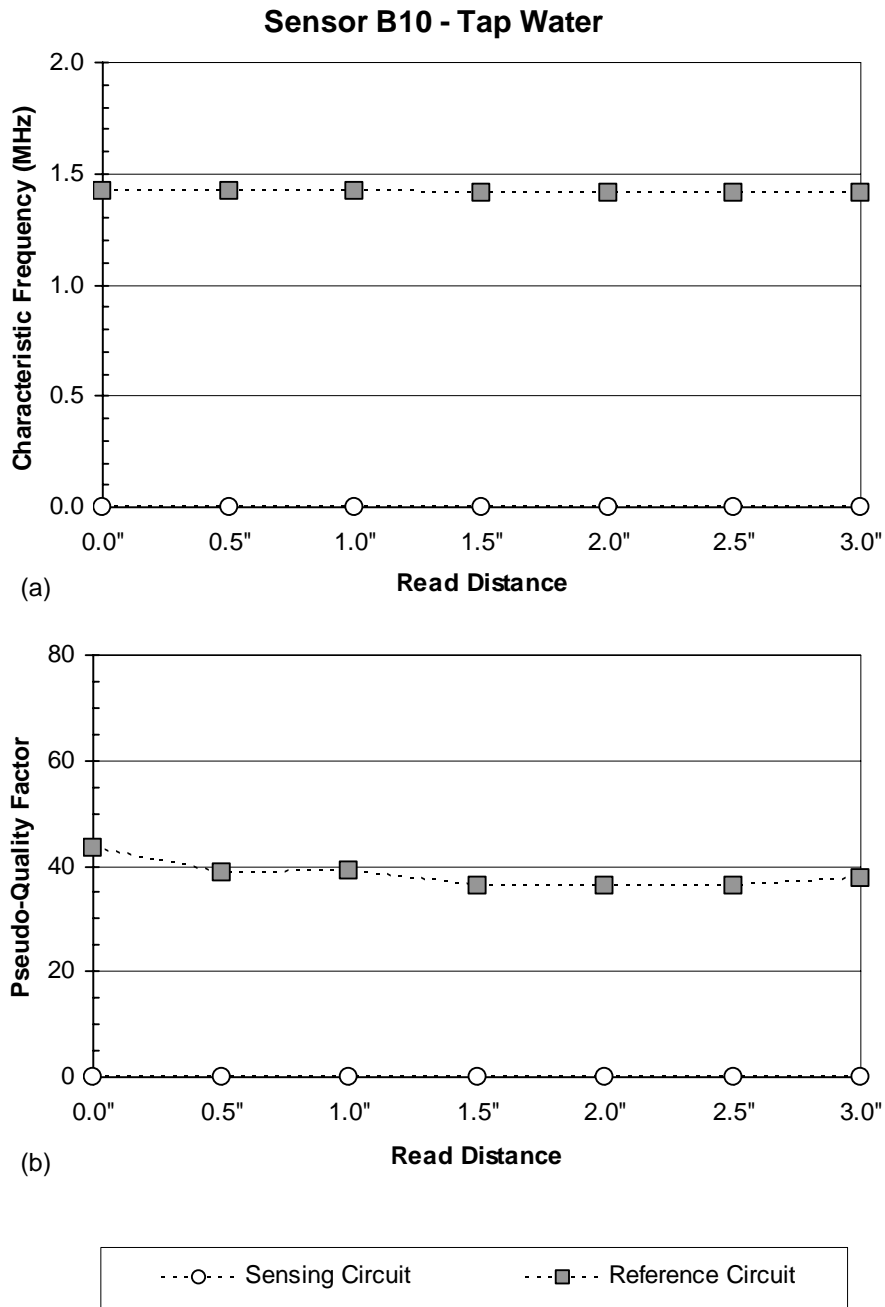


Figure F-7 Effect of Read Distance on Response of Sensor B10 with a Cut Sensing Wire for Readings in Tap Water

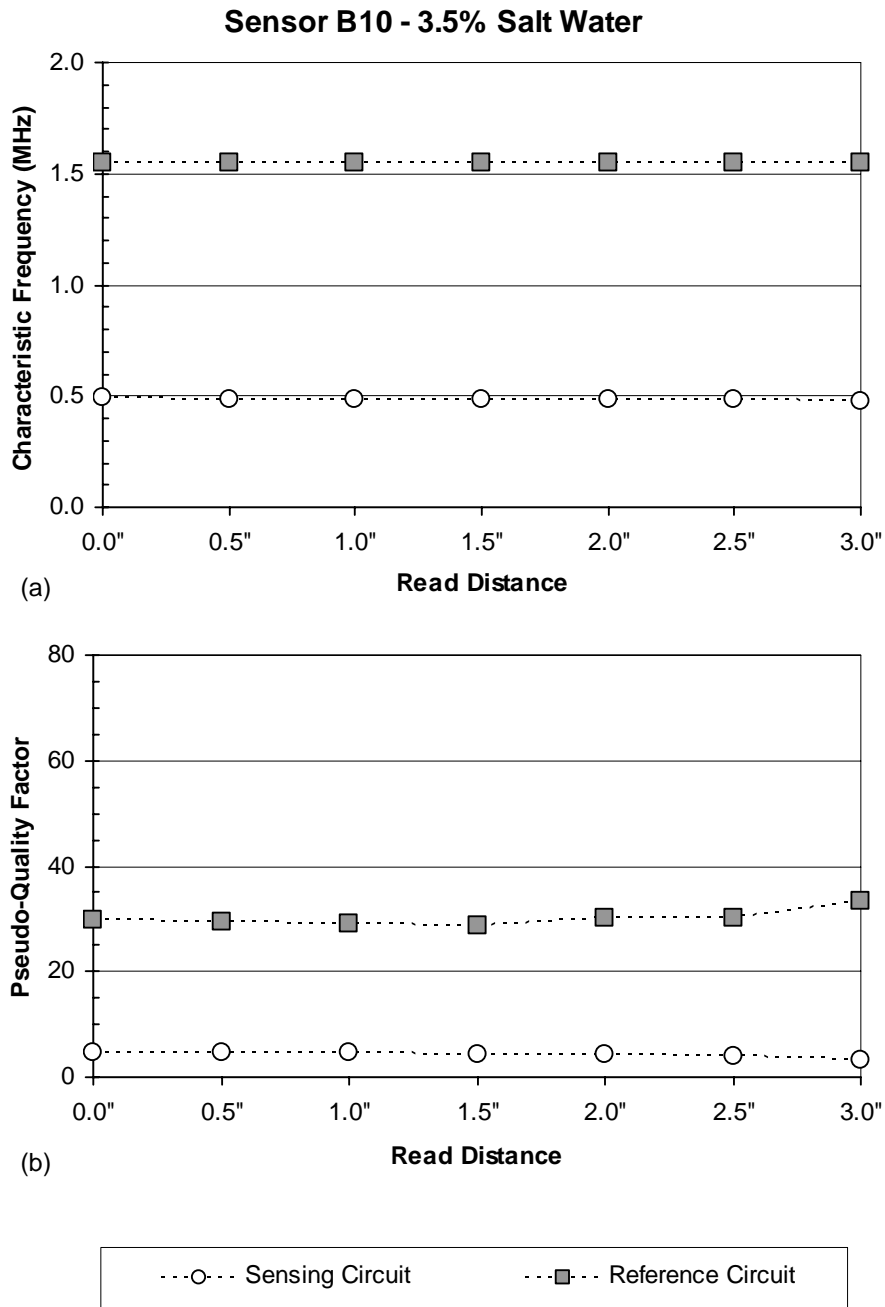


Figure F-8 Effect of Read Distance on Response of Sensor B10 with a Cut Sensing Wire for Readings in 3.5% Salt Water

**Table F-8 Variation of Measured Response of Sensor B10 with Cut Sensing
Wire for Reference Circuit with Varying Read Distance**

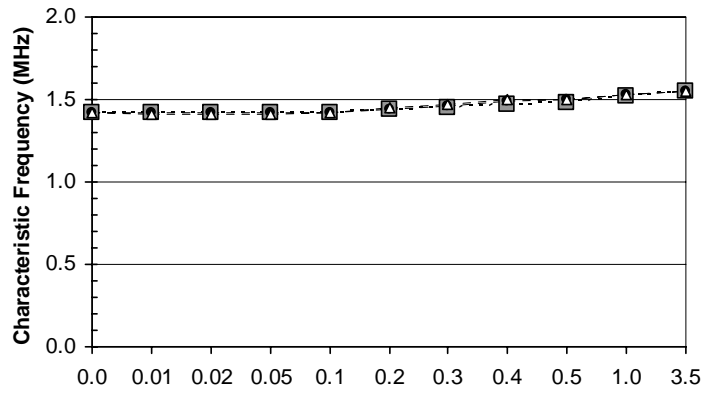
Environment	Number of Readings	Characteristic Frequency		Pseudo-Quality Factor		Phase Dip	
		Mean (MHz)	Coef. of Variation	Mean	Coef. of Variation	Mean (°)	Coef. of Variation
Air	7	1.42	0.1%	76.0	5.3%	21.9	117.7%
Tap Water	7	1.42	0.2%	38.3	6.9%	6.9	112.8%
3.5% Salt Water	7	1.55	0.1%	30.0	5.1%	0.9	115.5%

**Table F-9 Variation of Measured Response of Sensor B10 with Cut Sensing
Wire for Sensing Circuit with Varying Read Distance**

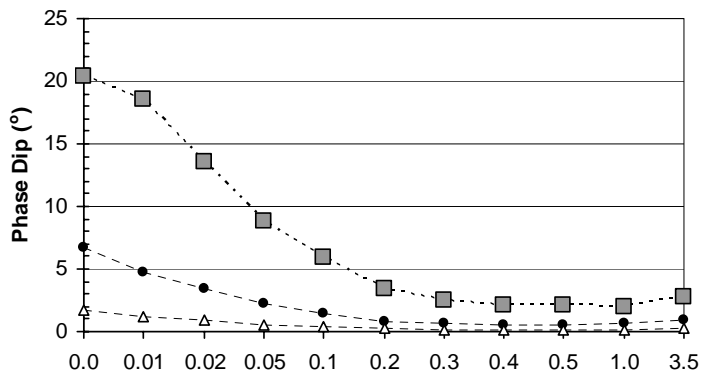
Environment	Number of Readings	Characteristic Frequency		Pseudo-Quality Factor		Phase Dip	
		Mean (MHz)	Coef. of Variation	Mean	Coef. of Variation	Mean (°)	Coef. of Variation
3.5% Salt Water	7	0.49	0.9%	4.3	12.7%	2.1	131.3%

Plots of characteristic frequency, phase dip, and pseudo-quality factor versus salt water concentration are shown for three different read distances, 0.0 in., 1.0 in., and 2.0 in. in Fig. F-9 for the reference circuit and Fig. F-10 for the sensing circuit. When the sensing circuit response is present ($\geq 0.5\%$ salt water), the pseudo-quality factors of the sensing circuit and the reference circuit can be compared with values for both intact and cut wire. This information can be used to determine the state of the steel sensing wire for embedded sensors. With an intact steel sensing wire, the pseudo-quality factor of the sensing circuit should always be greater than 6. When the steel sensing wire is broken (or cut), the state of the wire can be determined two ways: (1) if the sensing circuit phase dip is not

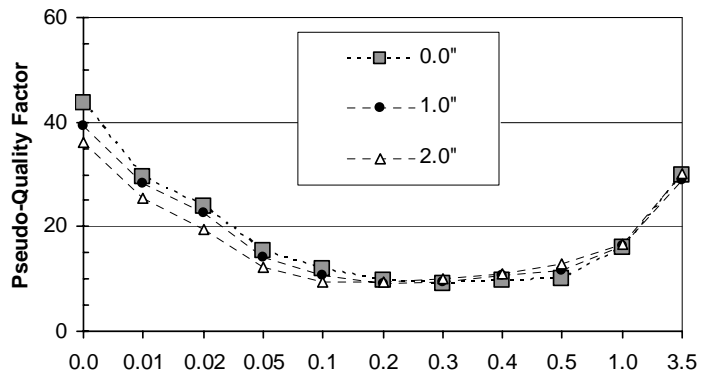
present, then the wire is broken, or (2) if the sensing circuit phase dip is present and the pseudo-quality factor of the sensing circuit is less than 5, then the wire is broken.



(a) Salt Concentration (%)



(b) Salt Concentration (%)



(c) Salt Concentration (%)

Figure F-9 Sensor B10 Reference Circuit Response for a Cut Sensing Wire with Increasing Concentration of Salt Water at Three Read Distances

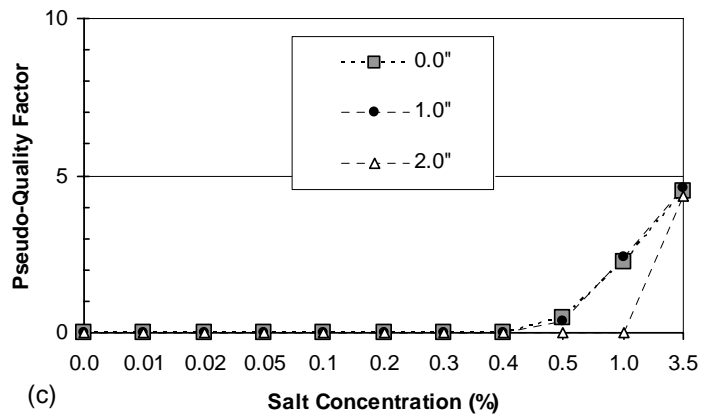
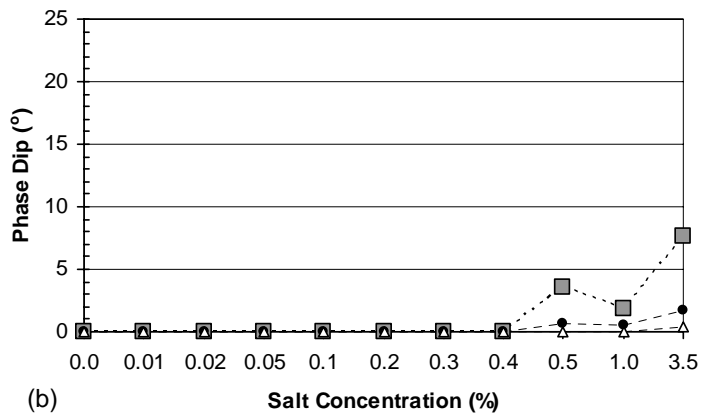
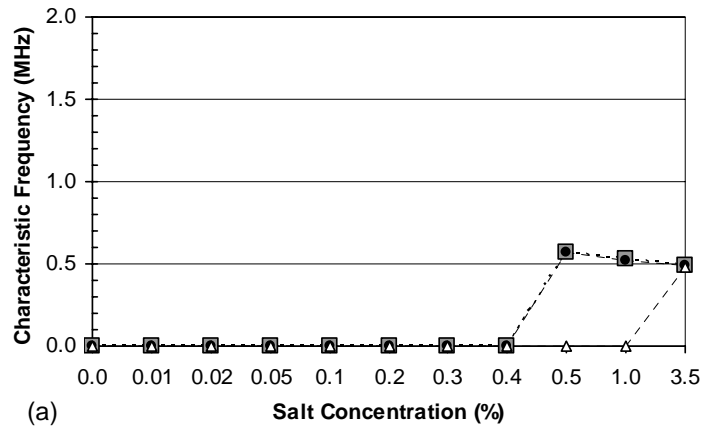


Figure F-10 Sensor B10 Sensing Circuit Response for a Cut Sensing Wire with Increasing Concentration of Salt Water at Three Read Distances

F.2.3 Reader Configuration

In order to assess the sensitivity of phase response to reader configuration, sensor B10 was interrogated using seven different reader coils. The Solartron Impedance Analyzer was used for all of the interrogations. The sensor was interrogated in air at read distances of 0.0 in., 1.0 in., 2.0 in., and 3.0 in.

Table F-10 gives the details for each reader coil. Reader coils were labeled based on diameter and number of magnet wire turns, where the first number is the nominal diameter of the form in inches, the next letter designates the type of reader coil: “t” for constant diameter coils and “s” for flat spiral coils, and the last digits indicate the number of magnet wire turns and magnet wire gage, if necessary. More details are provided for the reader coils in Chapter 3.

Table F-10 Experimental Reader Coils used in Calibration Testing

Reader Coil	Diameter (in.)	Number of Turns	Magnet Wire Gage
4t01-24	4	1	24
4t01-18	4	1	18
4t05	4	5	18
4t20	4	20	18
6t10	6	10	18
3s	3	*	18

* Flat spiral configuration

Results from interrogations of sensor B10 with an intact steel sensing wire at a read distance of 1.0 in. are shown in Table F-11 for all of the reader configurations used in this study. Table F-12 shows the same results for sensor B10 with a cut steel sensing wire. Despite the large variations in phase dip with different reader coils, the characteristic frequencies remain nearly constant and

the variation in pseudo-quality factors is small. The maximum read distance for sensor B10 with an intact steel sensing wire is shown for each reader configuration in Table F-13. Maximum read distance is defined as the read distance at which the phase dip is at least 0.1° for interrogations in air. As shown in Chapter 3, reader coils 4t05, 4t20, and 6t10 provide the flattest baseline response and also the best maximum read distance. When reader coils are connected to the impedance analyzer with a cable, reader coil 4t05 provides the best response. Statistical summaries that show the variation in characteristic frequency, pseudo-quality factor, and phase dip for all reader configurations used in this study are provided in Table F-14 for the sensing circuit with an intact sensing wire, Table F-15 for the reference circuit with an intact sensing wire, and Table F-16 for the reference circuit with a cut sensing wire.

Table F-11 Effect of Reader Configuration on Sensor B10 with Intact Sensing Wire for a 1-in. Read Distance

Reader Coil	Sensing Circuit			Reference Circuit		
	Char. Freq. (MHz)	Phase Dip ($^\circ$)	Pseudo-Quality Factor	Char. Freq. (MHz)	Phase Dip ($^\circ$)	Pseudo-Quality Factor
4t01-24	0.46	2.6	7.4	1.54	1.2	34.3
4t01-18	0.46	2.8	7.5	1.54	1.2	34.0
4t05	0.46	4.0	7.3	1.54	1.8	34.8
4t05 w/ cable	0.46	3.7	7.1	1.54	1.8	33.6
4t20	0.46	3.9	7.2	1.54	2.0	35.2
6t10	0.46	2.6	7.3	1.54	1.0	34.7
3s	0.46	5.5	7.3	1.55	4.8	34.5

Table F-12 Effect of Reader Configuration on Sensor B10 with Cut Sensing Wire for a 1-in. Read Distance

Reader Coil	Sensing Circuit			Reference Circuit		
	Char. Freq. (MHz)	Phase Dip (°)	Pseudo-Quality Factor	Char. Freq. (MHz)	Phase Dip (°)	Pseudo-Quality Factor
4t01-24	-	-	-	1.42	14.6	77.2
4t01-18	-	-	-	1.42	15.5	77.4
4t05	-	-	-	1.42	21.7	77.0
4t05 w/ cable	-	-	-	1.42	21.4	76.9
4t20	-	-	-	1.42	22.6	76.0
6t10	-	-	-	1.42	13.7	77.6
3s	-	-	-	1.42	39.1	74.2

Table F-13 Maximum Read Distances for Sensor B10 with Intact Sensing Wire

Reader Coil	Maximum Read Distance (in.)
4t01-24	2
4t01-18	2
4t05	3
4t05 w/ cable	3
4t20	3
6t10	3
3s	2

**Table F-14 Variation of Measured Response of Sensor B10 with Intact Sensing
Wire for Sensing Circuit with Different Reader Coils**

Read Distance (in.)	Number of Readings	Characteristic Frequency		Pseudo-Quality Factor		Phase Dip	
		Mean (MHz)	Coef. of Variation	Mean	Coef. of Variation	Mean (°)	Coef. of Variation
0.0	7	0.47	1.9%	6.9	8.6%	20.2	102.3%
1.0	7	0.46	0.2%	7.3	1.6%	3.6	28.8%
2.0	7	0.46	0.3%	7.5	2.2%	0.8	22.2%
3.0	4	0.46	0.1%	8.2	5.1%	0.3	25.7%
All	25	0.46	1.2%	7.4	7.5%	6.9	194.1%

**Table F-15 Variation of Measured Response of Sensor B10 with Intact Sensing
Wire for Reference Circuit with Different Reader Coils**

Read Distance (in.)	Number of Readings	Characteristic Frequency		Pseudo-Quality Factor		Phase Dip	
		Mean (MHz)	Coef. of Variation	Mean	Coef. of Variation	Mean (°)	Coef. of Variation
0.0	7	1.55	0.9%	33.2	11.4%	18.8	210.5%
1.0	7	1.54	0.1%	34.4	1.5%	2.0	65.9%
2.0	7	1.54	0.0%	34.6	4.8%	0.4	16.3%
3.0	4	1.54	0.0%	36.7	17.0%	0.1	20.9%
All	25	1.55	0.5%	34.5	9.4%	6.0	360.7%

Table F-16 Variation of Measured Response of Sensor B10 with Cut Sensing Wire for Reference Circuit with Different Reader Coils

Read Distance (in.)	Number of Readings	Characteristic Frequency		Pseudo-Quality Factor		Phase Dip	
		Mean (MHz)	Coef. of Variation	Mean	Coef. of Variation	Mean (°)	Coef. of Variation
0.0	7	1.43	1.7%	61.3	39.2%	130.0	146.9%
1.0	7	1.42	0.1%	76.6	1.5%	21.2	41.0%
2.0	7	1.42	0.0%	77.8	0.4%	4.7	18.0%
3.0	4	1.42	0.0%	78.1	1.3%	1.5	21.7%
All	25	1.42	0.9%	72.9	19.4%	43.9	251.6%

Coefficients of variation for characteristic frequencies are very small for readings at all read distances with all reader coils, ranging from 0.0% to 1.9%. Therefore, characteristic frequency response of sensors is very reliable with varying read distances and with different reader configurations. Pseudo-quality factors also give small coefficients of variation for varying read distances and different reader coils. Therefore, especially if the read distance is known, the calculation of pseudo-quality factors provides reliable values for use in determining the state of the steel sensing wire. Because phase dips are severely affected by both read distance and reader coil, the coefficients of variation in phase dips are large. Although the amplitude of the phase dip must be determined to calculate the pseudo-quality factor for a sensor reading, phase dip alone is not a reliable number for evaluating the state of the sensor.

F.3 CONCENTRIC SENSOR B60

Sensor B60 is a concentric sensor with a 21-gage steel sensing wire. The phase response of this sensor is shown in Fig. F-11 for an intact sensing wire (a) and for a cut sensing wire (b). This is the baseline response of the sensor in air

with a read distance of 1.0 in. A 4-in. diameter reader coil with 5 turns of 18-gage magnet wire connected to the impedance analyzer with a 3-ft cable was used for this interrogation (reader coil 4t05 with a cable). With the steel sensing wire intact, the sensor responds at both the sensing circuit characteristic frequency and the reference circuit characteristic frequency. The reference circuit is heavily shielded when the sensing circuit response is present due to the sensing circuit inductor surrounding the reference circuit inductor. The sensing circuit phase dip is slightly larger than sensor B10 due to the larger sensing wire and corresponding smaller effective resistance of the sensing circuit. The change in phase response due to a fracture of the steel sensing wire is significant. The sensing circuit phase dip disappears and the reference circuit is no longer shielded, resulting an 8% characteristic frequency shift down from 1.52 MHz to 1.39 MHz and a much larger phase dip.

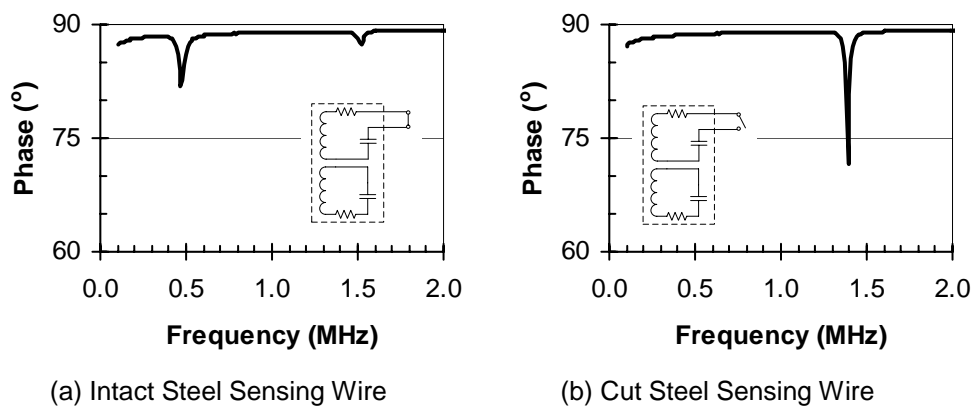


Figure F-11 Phase Response of Sensor B60

F.3.1 Surrounding Environment

To gauge the effect of the surrounding environment on the performance of sensor B60, the sensor was interrogated in air, tap water, and salt water using reader coil 4t05 attached to the impedance analyzer with a cable. Interrogations

were taken with intact and cut steel sensing wires. In addition to those three environments, sensor B60 with a cut sensing wire was also interrogated using the same reader configuration in varying concentrations of salt water. Salt water concentrations of 0.0%, 0.01%, 0.02%, 0.05%, 0.1%, 0.2%, 0.3%, 0.4%, 0.5%, 1.0%, and 3.5% were selected to provide a well-defined transition behavior for the sensor.

F.3.1.1 Intact Steel Sensing Wire

Interrogation results at a read distance of 1.0 in. were used to compare the response of sensor B60 in air, tap water, and 3.5% salt water. Table F-17 shows the effect of surrounding environment on sensor B60 with an intact steel sensing wire. The characteristic frequencies and pseudo-quality factors remain approximately constant with the change from air to tap water. A 10-18% reduction in pseudo-quality factor occurs with the change from tap water to 3.5% salt water. Phase dips are more sensitive to the surrounding environments, with reductions of approximately 30% for the change from air to tap water and approximately another 10-25% for the change from tap water to 3.5% salt water. As discussed in Chapter 3, the reduction in phase dip for the change from air to tap water may be due to the test method. The thickness of glass on the bottom of the beaker used to contain the water increases the read distance slightly, which probably results in most of the reduction in phase dip.

Table F-17 Effect of Surrounding Environment on Sensor B60 with Intact Sensing Wire

Environment	Sensing Circuit			Reference Circuit		
	Char. Freq. (MHz)	Phase Dip (°)	Pseudo-Quality Factor	Char. Freq. (MHz)	Phase Dip (°)	Pseudo-Quality Factor
Air	0.47	7.0	12.5	1.52	1.7	40.5
Tap Water	0.47	4.8	12.6	1.52	1.2	40.6
3.5% Salt Water	0.48	4.1	10.4	1.52	1.0	36.3

F.3.1.2 Cut Steel Sensing Wire

Table F-18 shows the effect of surrounding environment on sensor B60 with a cut steel sensing wire. The reference characteristic frequency remains constant with the change from air to tap water, while the sensing characteristic frequency is not present. The reference pseudo-quality factor falls approximately 50% and the reference phase dip decreases by 70% with the change from air to tap water. Sensor behavior is even more drastic for the change from tap water to 3.5% salt water. The sensing circuit characteristic frequency reappears with a phase dip and pseudo-quality factor approximately 45% less than those for the same sensor with an intact steel sensing wire interrogated in 3.5% salt water. The reference circuit characteristic frequency shifts back to the value with the wire intact due to shielding from the sensing circuit resonance. The phase dip decreases by 85% with the change from tap water to 3.5% salt water. The pseudo-quality factor actually increases by 4%. Compared with the phase dip of the reference circuit in sensor B60 with the steel sensing wire intact, the phase dip is reduced by 20% with the steel sensing wire cut. The pseudo-quality factor for

the reference circuit of sensor B60 with a cut steel sensing wire in 3.5% salt water is reduced by 12% compared with the sensor with an intact wire.

Table F-18 Effect of Surrounding Environment on Sensor B60 with Cut Sensing Wire

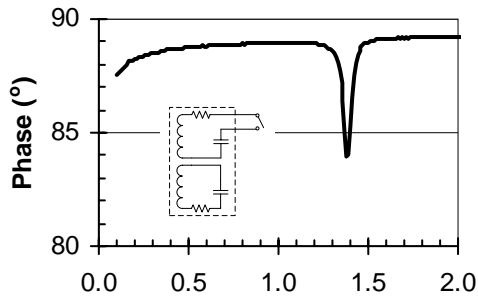
Environment	Sensing Circuit			Reference Circuit		
	Char. Freq. (MHz)	Phase Dip (°)	Pseudo-Quality Factor	Char. Freq. (MHz)	Phase Dip (°)	Pseudo-Quality Factor
Air	-	-	-	1.39	17.7	66.2
Tap Water	-	-	-	1.39	5.2	30.7
3.5% Salt Water	0.50	2.3	5.8	1.52	0.8	32.0

Table F-19 shows the effect of varying salt water concentration on sensor B60 with a cut steel sensing wire. Interrogation results are shown for 1.0-in. read distance. The reference circuit phase dip decreases with increasing salt water concentration to a minimum at 0.4% and then increases slightly with increasing concentration. The reference characteristic frequency shifts higher as the sensing circuit characteristic frequency begins to reappear and shield the reference circuit response. At a concentration of 0.4% and above, the sensing circuit response is present with a phase dip of 0.1° or more. Fig. F-12 shows the phase response of the sensor with varying concentrations of salt water. The transition response of sensor B60 is evident with increasing conductivity of the surrounding environment. The phase response of the sensor with a cut sensing wire immersed in 3.5% salt water (k) is very close to the response of the sensor with an intact sensing wire immersed in 3.5% salt water (l). However, the difference in pseudo-quality factors may still provide the information needed to determine the state of

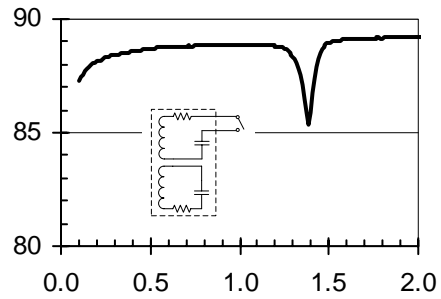
the steel sensing wire. Further discussion on use of the pseudo-quality factor is provided in Section F.3.2.

Table F-19 Effect of Varying Concentration of Salt Water on Sensor B60 with Cut Sensing Wire

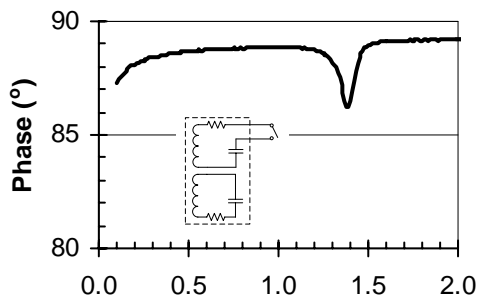
Salt Water Concentration	Sensing Circuit			Reference Circuit		
	Char. Freq. (MHz)	Phase Dip (°)	Pseudo-Quality Factor	Char. Freq. (MHz)	Phase Dip (°)	Pseudo-Quality Factor
0.0%	-	-	-	1.39	5.2	30.7
0.01%	-	-	-	1.39	3.5	24.4
0.02%	-	-	-	1.38	2.8	17.8
0.05%	-	-	-	1.39	1.6	11.6
0.1%	-	-	-	1.40	0.9	9.0
0.2%	-	-	-	1.42	0.6	8.4
0.3%	-	-	-	1.45	0.5	10.2
0.4%	0.59	0.7	0.6	1.47	0.5	10.4
0.5%	0.55	0.8	0.7	1.48	0.5	12.4
1.0%	0.51	0.8	2.8	1.51	0.6	20.6
3.5%	0.50	2.3	5.8	1.52	0.8	32.0



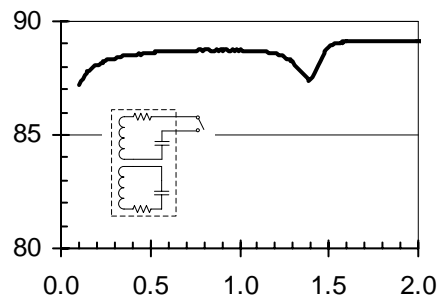
(a) Cut Wire in Tap Water



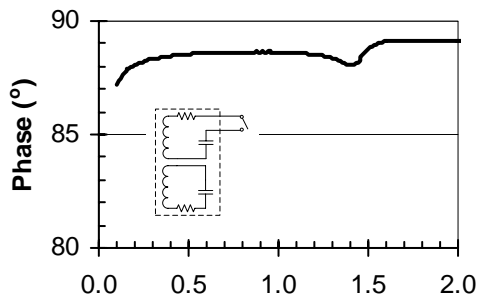
(b) Cut Wire in 0.01% Salt Water



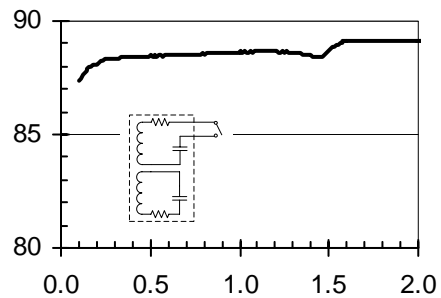
(c) Cut Wire in 0.02% Salt Water



(d) Cut Wire in 0.05% Salt Water

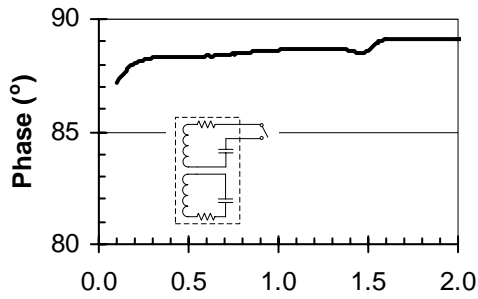


(e) Cut Wire in 0.1% Salt Water

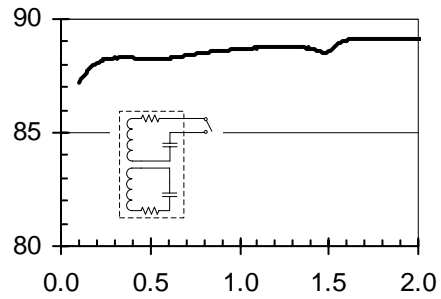


(f) Cut Wire in 0.2% Salt Water

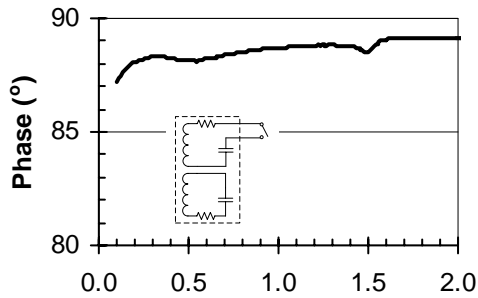
Figure F-12 Phase Response of Sensor B60 in Varying Concentrations of Salt Water



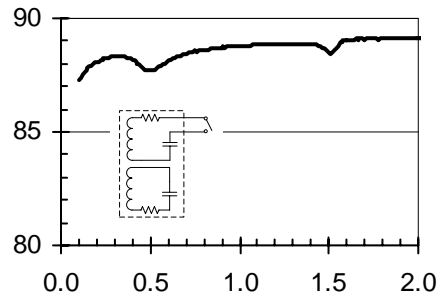
(g) Cut Wire in 0.3% Salt Water



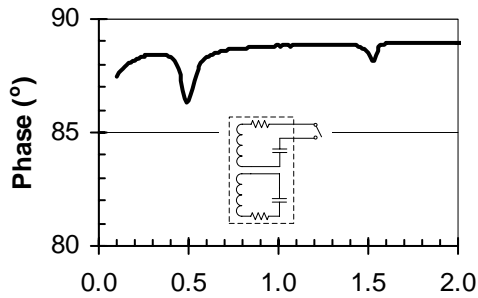
(h) Cut Wire in 0.4% Salt Water



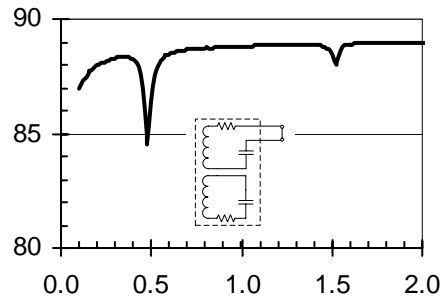
(i) Cut Wire in 0.5% Salt Water



(j) Cut Wire in 1.0% Salt Water



(k) Cut Wire in 3.5% Salt Water



(l) Intact Wire in 3.5% Salt Water

Figure F-12 (Cont.) Phase Response of Sensor B60 in Varying Concentrations of Salt Water

F.3.2 Read Distance

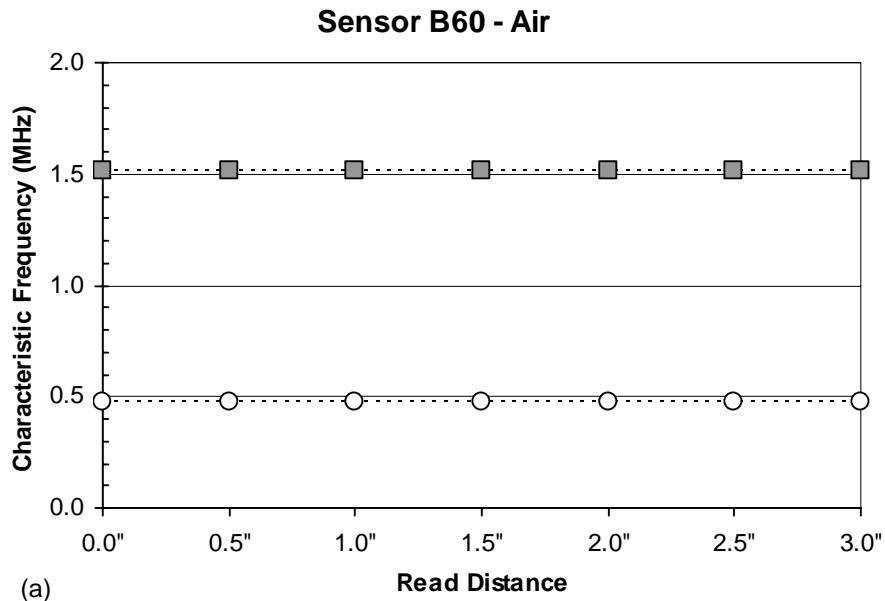
Because read distance also affects the performance of sensors, sensor B60 was interrogated at read distances from 0.0-in. to 3.0-in. at 0.5-in increments in air, tap water, and 3.5% salt water using reader coil 4t05 attached to the impedance analyzer with a 3-ft cable. Interrogations were taken with intact and cut steel sensing wires. In addition to those three environments, sensor B60 was also interrogated using the same reader configuration in varying concentrations of salt water at read distances of 0.0 in., 1.0 in., and 2.0 in.

F.3.2.1 Intact Steel Sensing Wire

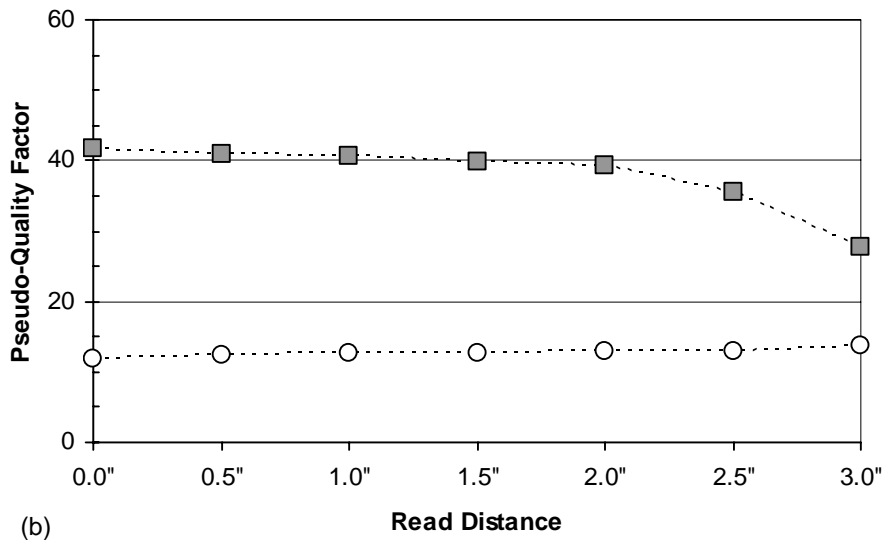
Table F-20 shows the effect of read distance on sensor B60 with an intact steel sensing wire. Interrogation results are shown in the table for readings in air. While phase dips are significantly reduced with increasing read distance, the characteristic frequency of each circuit remains the same. The pseudo-quality factor only increases slightly for the sensing circuit and decreases slightly for the reference circuit with increasing read distance. The characteristic frequencies and pseudo-quality factors are plotted versus read distance in Fig. F-13 for interrogations in air, Fig. F-14 for tap water, and Fig. F-15 for 3.5% salt water. A statistical summary of the characteristic frequency, phase dip, and pseudo-quality factor for the sensing circuit is provided in Table F-21. The same information for the reference circuit is provided in Table F-22. The coefficients of variation for characteristic frequencies of both the sensing and reference circuits are very small (<0.5%). Because phase dips are highly dependent on read distance, the coefficients of variation for phase dips are quite large (>100%). The coefficients of variation for pseudo-quality factors are very good, ranging from 2.8% to 14.8%.

Table F-20 Effect of Read Distance on Sensor B60 with Intact Sensing Wire

Read Distance (in.)	Sensing Circuit			Reference Circuit		
	Char. Freq. (MHz)	Phase Dip (°)	Pseudo- Quality Factor	Char. Freq. (MHz)	Phase Dip (°)	Pseudo- Quality Factor
0.0	0.48	28.5	11.9	1.52	4.3	41.7
0.5	0.48	15.1	12.3	1.52	3.1	40.9
1.0	0.47	7.0	12.5	1.52	1.7	40.5
1.5	0.47	3.3	12.6	1.52	0.9	39.8
2.0	0.47	1.6	13.1	1.52	0.4	39.2
2.5	0.47	0.8	13.0	1.52	0.2	35.5
3.0	0.47	0.4	13.7	1.52	0.1	27.8



(a)



(b)



Figure F-13 Effect of Read Distance on Response of Sensor B60 with an Intact Sensing Wire for Readings in Air

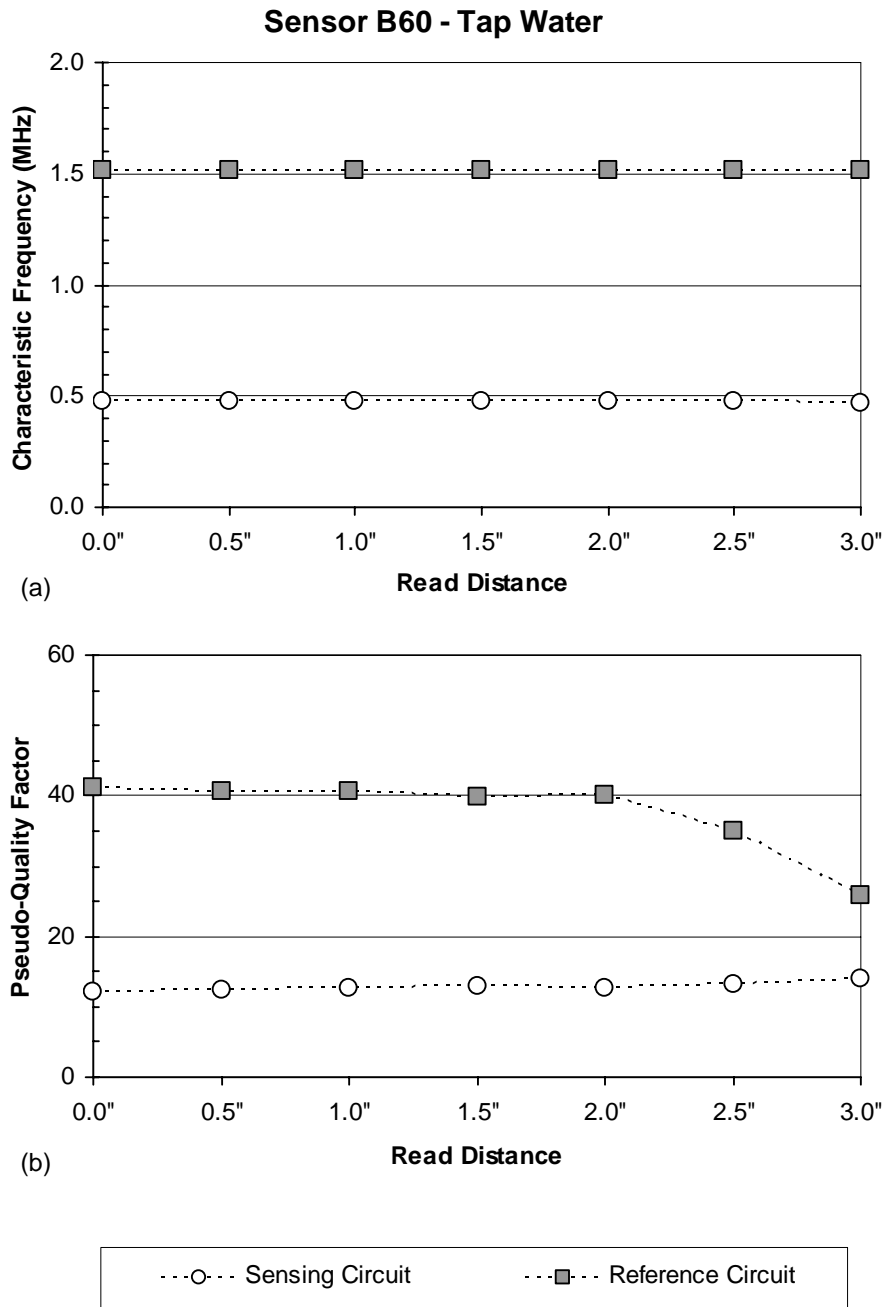


Figure F-14 Effect of Read Distance on Response of Sensor B60 with an Intact Sensing Wire for Readings in Tap Water

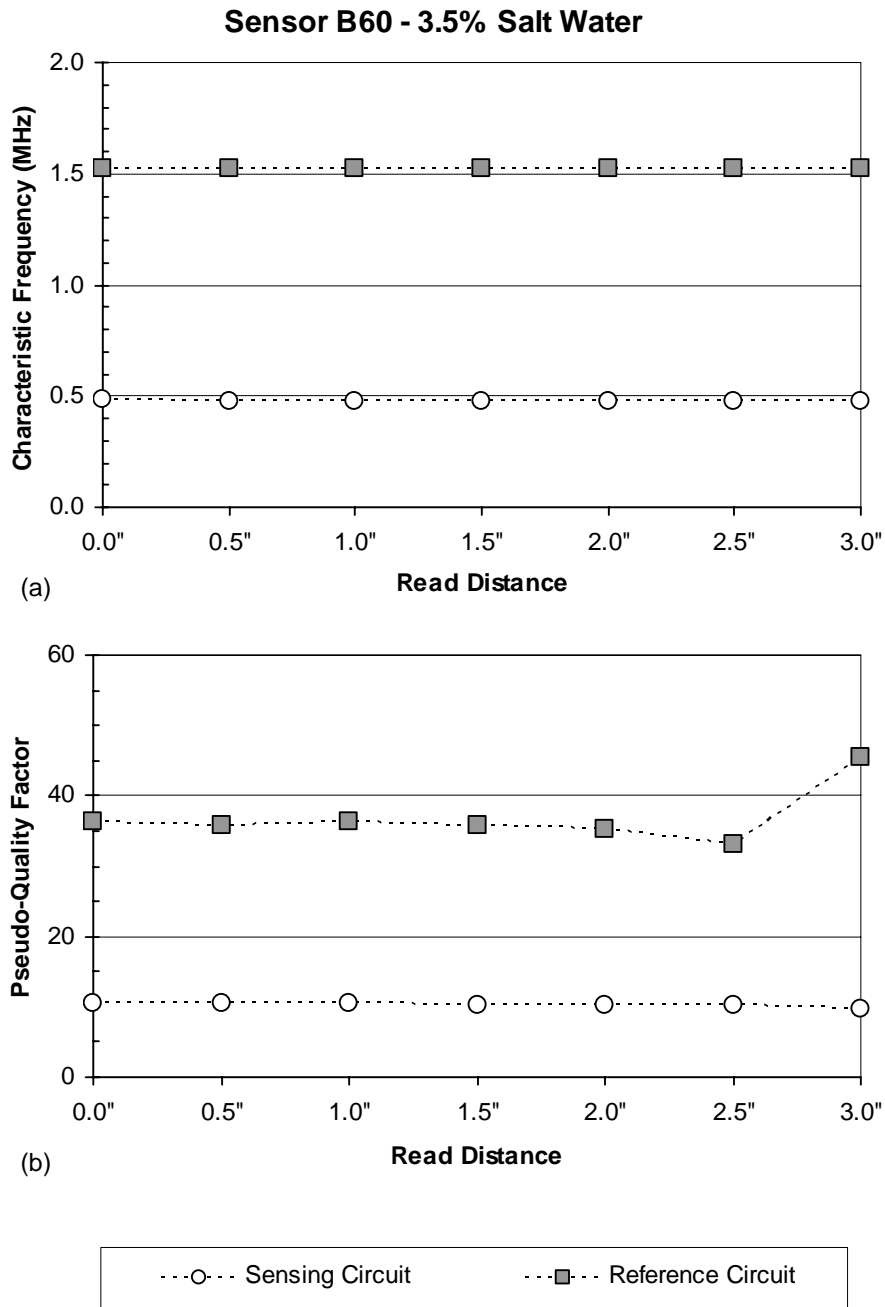


Figure F-15 Effect of Read Distance on Response of Sensor B60 with an Intact Sensing Wire for Readings in 3.5% Salt Water

Table F-21 Variation of Measured Response of Sensor B60 with Intact Sensing Wire for Sensing Circuit with Varying Read Distance

Environment	Number of Readings	Characteristic Frequency		Pseudo-Quality Factor		Phase Dip	
		Mean (MHz)	Coef. of Variation	Mean	Coef. of Variation	Mean (°)	Coef. of Variation
Air	7	0.47	0.4%	12.8	4.5%	8.1	128.1%
Tap Water	7	0.47	0.4%	12.8	4.3%	5.9	133.0%
3.5% Salt Water	7	0.48	0.3%	10.2	2.8%	5.1	133.6%

Table F-22 Variation of Measured Response of Sensor B60 with Intact Sensing Wire for Reference Circuit with Varying Read Distance

Environment	Number of Readings	Characteristic Frequency		Pseudo-Quality Factor		Phase Dip	
		Mean (MHz)	Coef. of Variation	Mean	Coef. of Variation	Mean (°)	Coef. of Variation
Air	7	1.52	0.0%	37.9	12.9%	1.5	105.9%
Tap Water	7	1.52	0.0%	37.6	14.8%	1.2	114.5%
3.5% Salt Water	7	1.52	0.1%	36.9	10.7%	1.0	115.1%

F.3.2.2 Cut Steel Sensing Wire

The effect of read distance on sensor B60 with a cut steel sensing wire is shown in Table F-23. Interrogation results are shown in the table for readings in air. Again, phase dips are substantially reduced with increasing read distance. Characteristic frequencies do not change and the variations in pseudo-quality

factors are small. The characteristic frequencies and pseudo-quality factors are plotted versus read distance in Fig. F-16 for interrogations in air, Fig. F-17 for tap water, and Fig. F-18 for 3.5% salt water. A statistical summary of the characteristic frequency, phase dip, and pseudo-quality factor for the reference circuit is provided in Table F-24. The same information for the sensing circuit is provided in Table F-25. The sensing circuit only responded in the 3.5% salt water environment. Coefficients of variation are very small for characteristic frequencies and very large for phase dips.

While the coefficients of variation for pseudo-quality factors are small, ranging from 4.9% to 5.8% for the reference circuit, the values change substantially with increasing conductivity of the surrounding environment. In 3.5% salt water, the reference circuit mean pseudo-quality factor is 32.8 for a cut steel sensing wire, while it is 36.9 for an intact wire. The sensing circuit mean pseudo-quality factor is 5.5 for a cut steel sensing wire and 10.2 for an intact wire. Therefore, the pseudo-quality factor may give a reliable indication of the state of the steel sensing wire in the presence of a conductive environment.

Table F-23 Effect of Read Distance on Sensor B60 with Cut Sensing Wire

Read Distance (in.)	Sensing Circuit			Reference Circuit		
	Char. Freq. (MHz)	Phase Dip (°)	Pseudo- Quality Factor	Char. Freq. (MHz)	Phase Dip (°)	Pseudo- Quality Factor
0.0	-	-	-	1.39	60.7	57.2
0.5	-	-	-	1.39	35.6	63.0
1.0	-	-	-	1.39	17.7	66.2
1.5	-	-	-	1.39	8.5	66.7
2.0	-	-	-	1.39	4.1	66.9
2.5	-	-	-	1.39	2.1	67.4
3.0	-	-	-	1.39	1.1	67.7

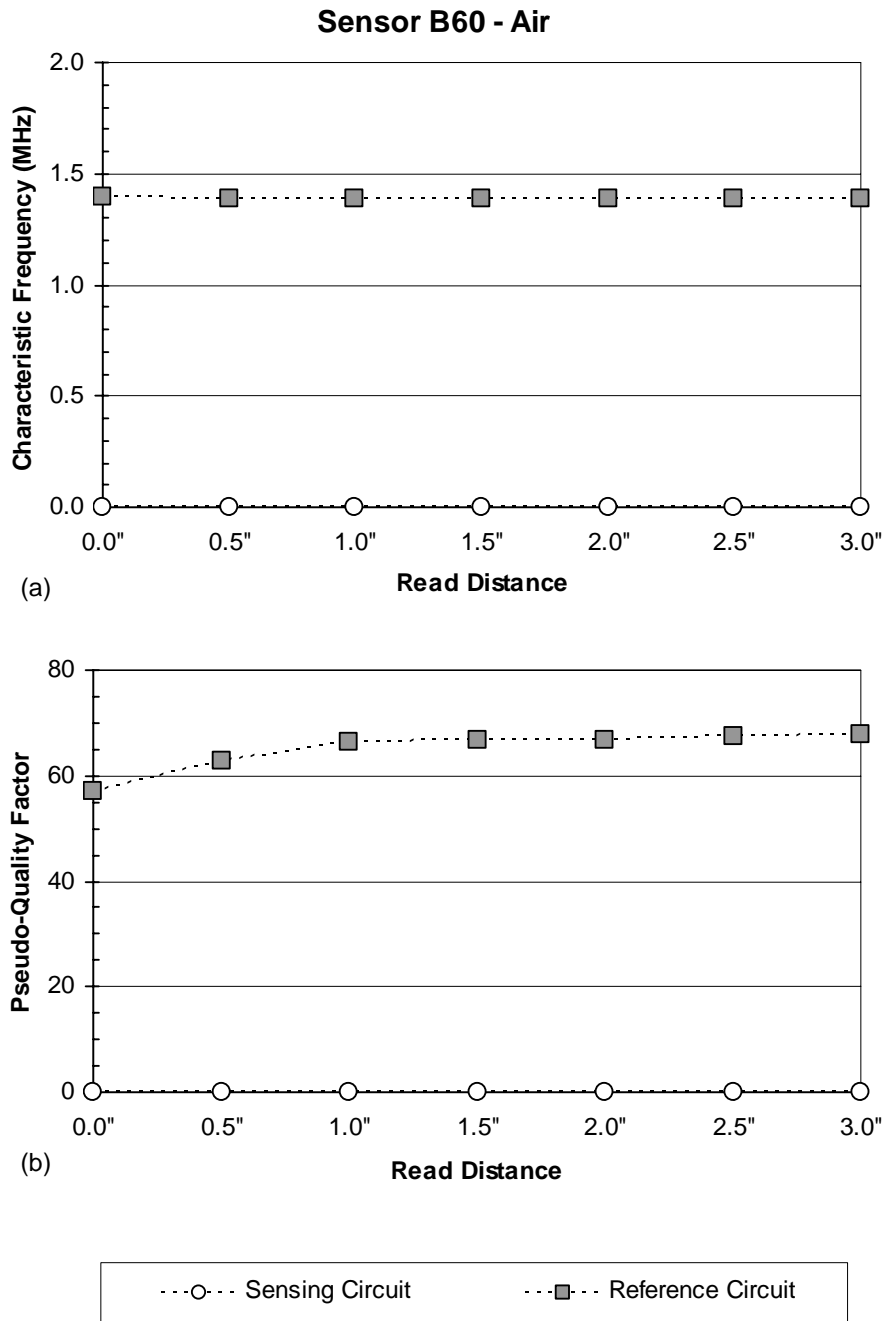


Figure F-16 Effect of Read Distance on Response of Sensor B60 with a Cut Sensing Wire for Readings in Air

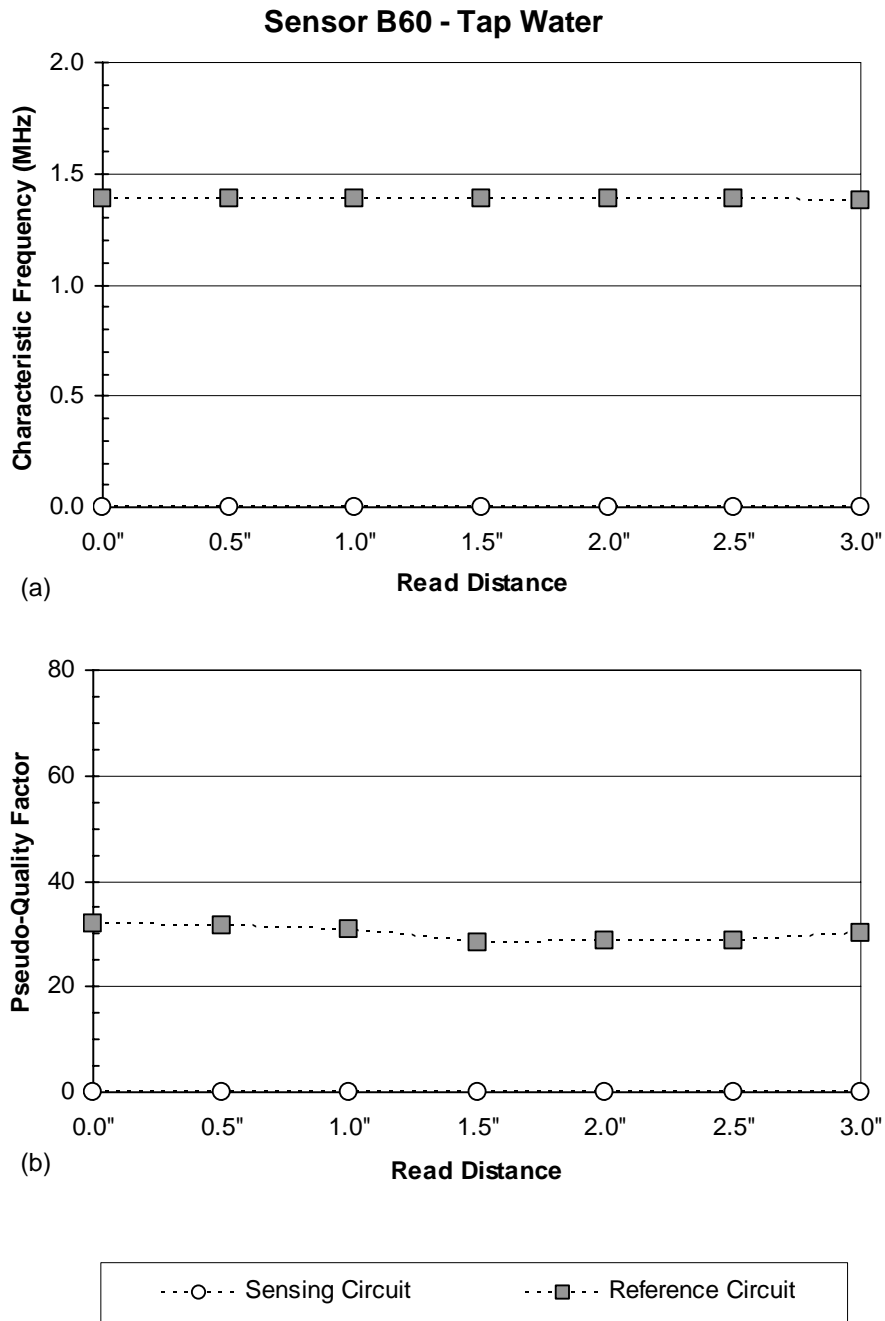


Figure F-17 Effect of Read Distance on Response of Sensor B60 with a Cut Sensing Wire for Readings in Tap Water

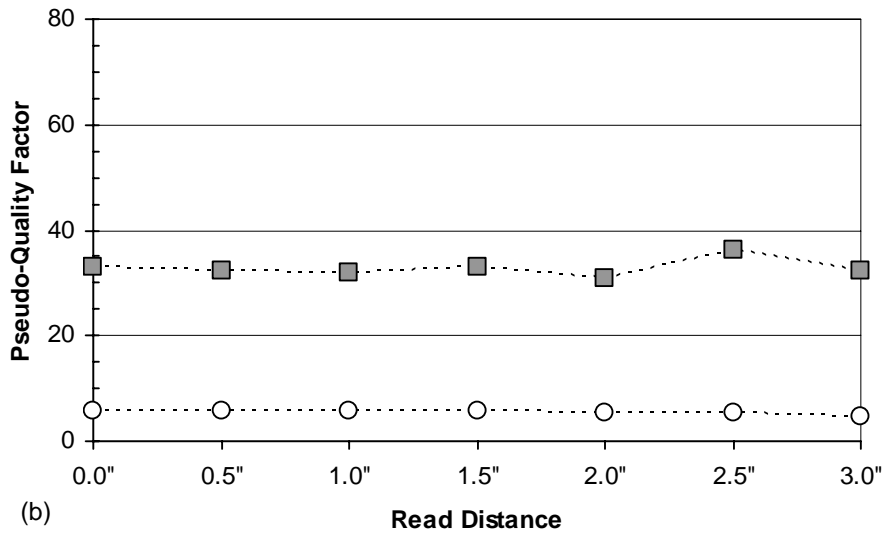
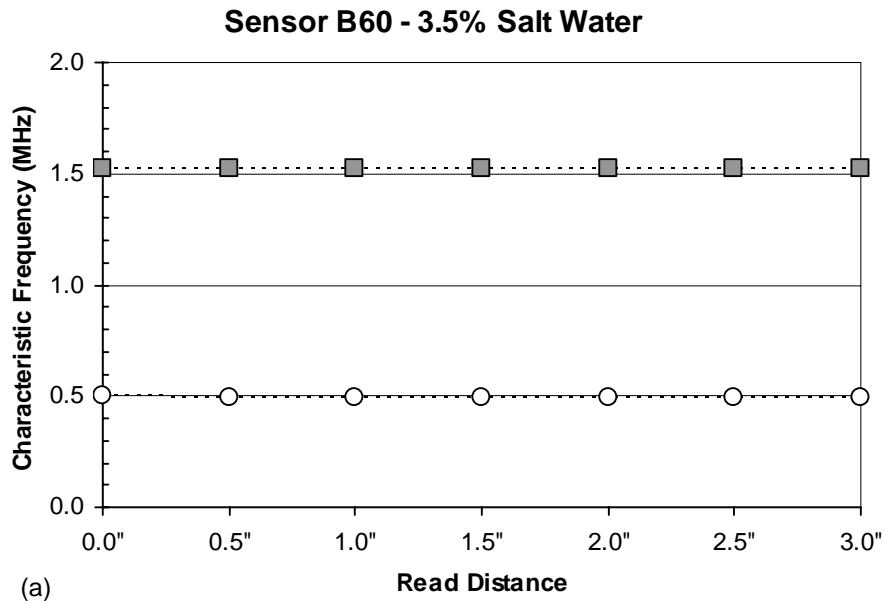


Figure F-18 Effect of Read Distance on Response of Sensor B60 with a Cut Sensing Wire for Readings in 3.5% Salt Water

**Table F-24 Variation of Measured Response of Sensor B60 with Cut Sensing
Wire for Reference Circuit with Varying Read Distance**

Environment	Number of Readings	Characteristic Frequency		Pseudo-Quality Factor		Phase Dip	
		Mean (MHz)	Coef. of Variation	Mean	Coef. of Variation	Mean (°)	Coef. of Variation
Air	7	1.39	0.1%	65.0	5.8%	18.5	119.7%
Tap Water	7	1.38	0.2%	30.0	4.9%	5.8	125.3%
3.5% Salt Water	7	1.52	0.1%	32.8	4.9%	0.8	114.8%

**Table F-25 Variation of Measured Response of Sensor B60 with Cut Sensing
Wire for Sensing Circuit with Varying Read Distance**

Environment	Number of Readings	Characteristic Frequency		Pseudo-Quality Factor		Phase Dip	
		Mean (MHz)	Coef. of Variation	Mean	Coef. of Variation	Mean (°)	Coef. of Variation
3.5% Salt Water	7	0.49	0.6%	5.5	7.4%	2.9	132.6%

Plots of characteristic frequency, phase dip, and pseudo-quality factor versus salt water concentration are shown for three different read distances, 0.0 in., 1.0 in., and 2.0 in. in Fig. F-19 for the reference circuit and Fig. F-20 for the sensing circuit. When the sensing circuit response is present ($\geq 0.4\%$ salt water), the pseudo-quality factors of the sensing circuit and the reference circuit can be compared with values for both intact and cut wire. This information can be used to determine the state of the steel sensing wire for embedded sensors. With an intact steel sensing wire, the pseudo-quality factor of the sensing circuit should always be greater than 10. When the steel sensing wire is broken (or cut), the state of the wire can be determined two ways: (1) if the sensing circuit phase dip

is not present, then the wire is broken, or (2) if the sensing circuit phase dip is present and the pseudo-quality factor of the sensing circuit is less than 6, then the wire is broken.

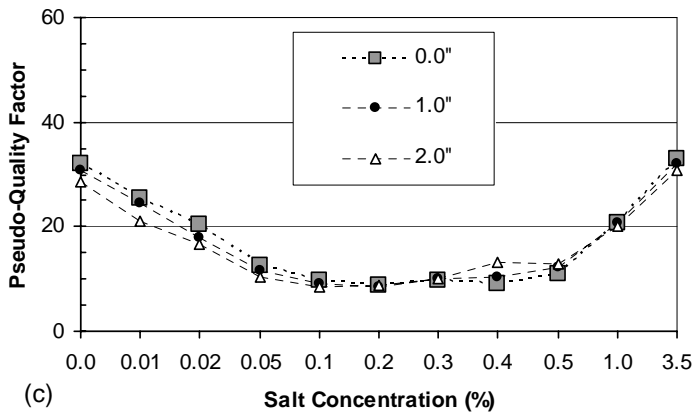
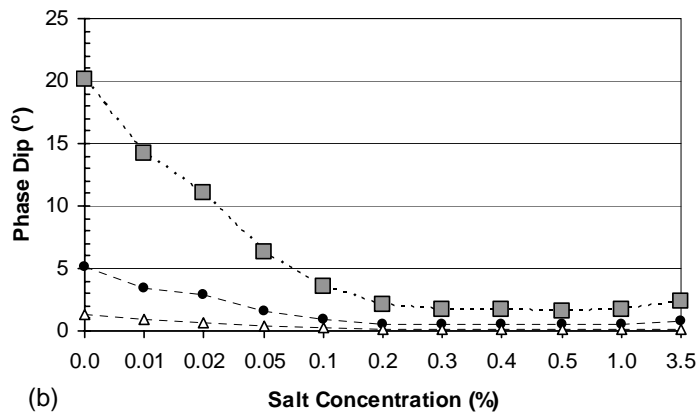
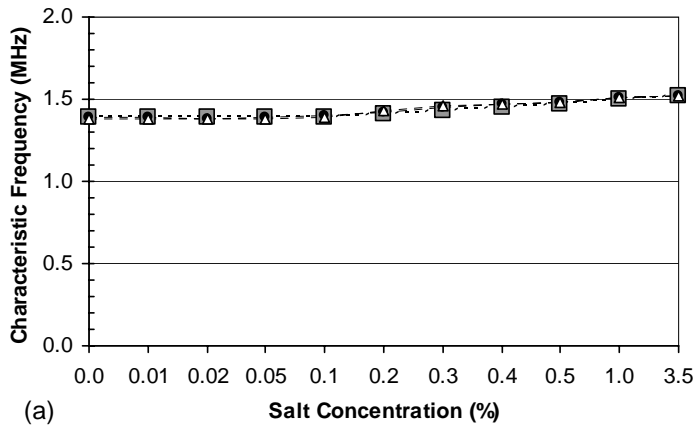
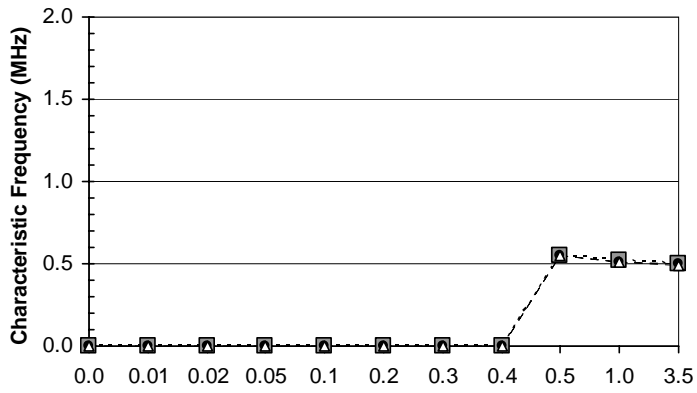
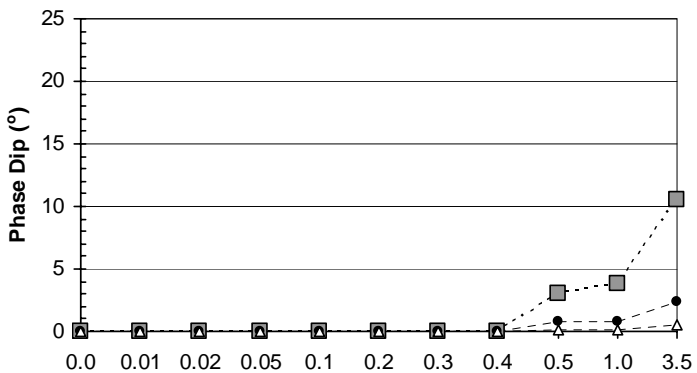


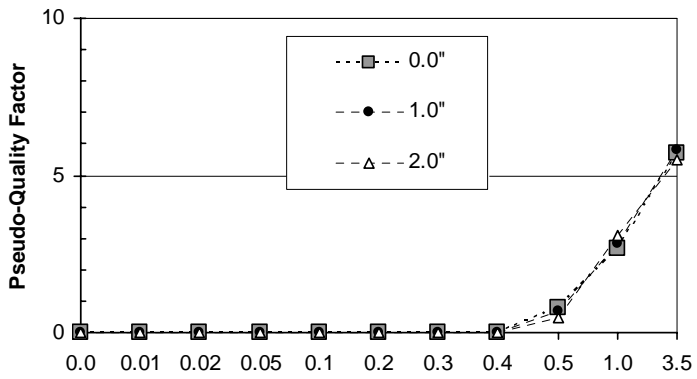
Figure F-19 Sensor B60 Reference Circuit Response for a Cut Sensing Wire with Increasing Concentration of Salt Water at Three Read Distances



(a)



(b)



(c)

Figure F-20 Sensor B60 Sensing Circuit Response for a Cut Sensing Wire with Increasing Concentration of Salt Water at Three Read Distances

F.3.3 Reader Configuration

In order to assess the sensitivity of phase response to reader configuration, sensor B60 was interrogated using seven different reader coils. The Solartron Impedance Analyzer was used for all of the interrogations. The sensor was interrogated in air at read distances of 0.0 in., 1.0 in., 2.0 in., and 3.0 in. Table F-10 gives the details for each reader coil.

Results from interrogations of sensor B60 with an intact steel sensing wire at a read distance of 1.0 in. are shown in Table F-26 for all of the reader configurations used in this study. Table F-27 shows the same results for sensor B60 with a cut steel sensing wire. Despite the large variations in phase dip with different reader coils, the characteristic frequencies remain nearly constant and the variation in pseudo-quality factors is small. The maximum read distance for sensor B60 with an intact steel sensing wire is shown for each reader configuration in Table F-28. Maximum read distance is defined as the read distance at which the phase dip is at least 0.1° for interrogations in air. As shown in Chapter 3, reader coils 4t05, 4t20, and 6t10 provide the flattest baseline response and also the best maximum read distance. When reader coils are connected to the impedance analyzer with a cable, reader coil 4t05 provides the best response. Statistical summaries that show the variation in characteristic frequency, pseudo-quality factor, and phase dip for all reader configurations used in this study are provided in Table F-29 for the sensing circuit with an intact sensing wire, Table F-30 for the reference circuit with an intact sensing wire, and Table F-31 for the reference circuit with a cut sensing wire.

**Table F-26 Effect of Reader Configuration on Sensor B60 with Intact Sensing
Wire for a 1-in. Read Distance**

Reader Coil	Sensing Circuit			Reference Circuit		
	Char. Freq. (MHz)	Phase Dip (°)	Pseudo-Quality Factor	Char. Freq. (MHz)	Phase Dip (°)	Pseudo-Quality Factor
4t01-24	0.47	5.0	12.8	1.52	1.1	39.9
4t01-18	0.47	5.3	12.6	1.52	2.8	41.0
4t05	0.47	7.4	12.6	1.52	1.7	41.5
4t05 w/ cable	0.47	7.0	12.5	1.52	1.7	40.5
4t20	0.47	7.2	12.5	1.52	1.8	41.2
6t10	0.47	4.8	12.6	1.52	1.0	42.3
3s	0.47	10.2	12.5	1.52	4.7	41.1

**Table F-27 Effect of Reader Configuration on Sensor B60 with Cut Sensing
Wire for a 1-in. Read Distance**

Reader Coil	Sensing Circuit			Reference Circuit		
	Char. Freq. (MHz)	Phase Dip (°)	Pseudo-Quality Factor	Char. Freq. (MHz)	Phase Dip (°)	Pseudo-Quality Factor
4t01-24	-	-	-	1.39	12.0	65.8
4t01-18	-	-	-	1.39	12.8	66.9
4t05	-	-	-	1.39	17.9	66.3
4t05 w/ cable	-	-	-	1.39	17.7	66.2
4t20	-	-	-	1.39	18.7	66.2
6t10	-	-	-	1.39	11.4	66.6
3s	-	-	-	1.39	31.7	64.6

Table F-28 Maximum Read Distances for Sensor B60 with Intact Sensing Wire

Reader Coil	Maximum Read Distance (in.)
4t01-24	2
4t01-18	2
4t05	3
4t05 w/ cable	3
4t20	3
6t10	3
3s	2

Table F-29 Variation of Measured Response of Sensor B60 with Intact Sensing Wire for Sensing Circuit with Different Reader Coils

Read Distance (in.)	Number of Readings	Characteristic Frequency		Pseudo-Quality Factor		Phase Dip	
		Mean (MHz)	Coef. of Variation	Mean	Coef. of Variation	Mean (°)	Coef. of Variation
0.0	7	0.48	2.0%	11.4	15.6%	35.0	92.0%
1.0	7	0.47	0.1%	12.6	0.8%	6.7	28.5%
2.0	7	0.47	0.2%	13.0	2.5%	1.5	17.9%
3.0	4	0.47	0.1%	13.1	4.2%	0.5	22.4%
All	25	0.48	1.3%	12.4	9.2%	12.2	179.3%

**Table F-30 Variation of Measured Response of Sensor B60 with Intact Sensing
Wire for Reference Circuit with Different Reader Coils**

Read Distance (in.)	Number of Readings	Characteristic Frequency		Pseudo-Quality Factor		Phase Dip	
		Mean (MHz)	Coef. of Variation	Mean	Coef. of Variation	Mean (°)	Coef. of Variation
0.0	7	1.52	0.7%	40.0	12.7%	18.3	212.7%
1.0	7	1.52	0.0%	41.1	1.9%	1.9	67.8%
2.0	7	1.52	0.0%	40.5	9.5%	0.4	18.2%
3.0	4	1.52	0.1%	40.4	27.7%	0.1	16.2%
All	25	1.52	0.4%	40.5	11.5%	6.0	357.1%

**Table F-31 Variation of Measured Response of Sensor B60 with Cut Sensing
Wire for Reference Circuit with Different Reader Coils**

Read Distance (in.)	Number of Readings	Characteristic Frequency		Pseudo-Quality Factor		Phase Dip	
		Mean (MHz)	Coef. of Variation	Mean	Coef. of Variation	Mean (°)	Coef. of Variation
0.0	7	1.40	1.6%	53.5	34.3%	73.6	73.7%
1.0	7	1.39	0.0%	66.1	1.1%	17.5	40.1%
2.0	7	1.39	0.0%	67.0	1.0%	3.8	18.4%
3.0	4	1.39	0.0%	66.8	1.8%	1.3	21.4%
All	25	1.39	0.9%	62.9	17.5%	26.8	152.9%

Coefficients of variation for characteristic frequencies are very small for readings at all read distances with all reader coils, ranging from 0.0% to 2.0%. Therefore, characteristic frequency response of sensors is very reliable with varying read distances and with different reader configurations. Pseudo-quality factors also give small coefficients of variation for varying read distances and different reader coils. Therefore, especially if the read distance is known, the calculation of pseudo-quality factors provides reliable values for use in

determining the state of the steel sensing wire. Because phase dips are severely affected by both read distance and reader coil, the coefficients of variation in phase dips are large. Although the amplitude of the phase dip must be determined to calculate the pseudo-quality factor for a sensor reading, phase dip alone is not a reliable number for evaluating the state of the sensor.

F.4 COPLANAR SENSOR A10

Sensor A10 is a coplanar sensor with a 26-gage steel sensing wire. The phase response of this sensor is shown in Fig. F-21 for an intact sensing wire (a) and for a cut sensing wire (b). This is the baseline response of the sensor in air with a read distance of 1.0 in. A 4-in. diameter reader coil with 5 turns of 18-gage magnet wire connected to the impedance analyzer with a 3-ft cable was used for this interrogation (reader coil 4t05 with a cable). With the steel sensing wire intact, the sensor responds at both the sensing circuit characteristic frequency and the reference circuit characteristic frequency. The reference circuit is not shielded when the sensing circuit response is present because the mutual inductance between the sensing circuit inductor and reference circuit inductor is negligible in the side-by-side arrangement. The sensing circuit phase dip disappears due to fracture of the steel sensing wire, but the response of the reference circuit remains essentially unchanged. This makes the response of the sensor entirely dependent on the sensing circuit, which must be readable to determine the state of the steel sensing wire.

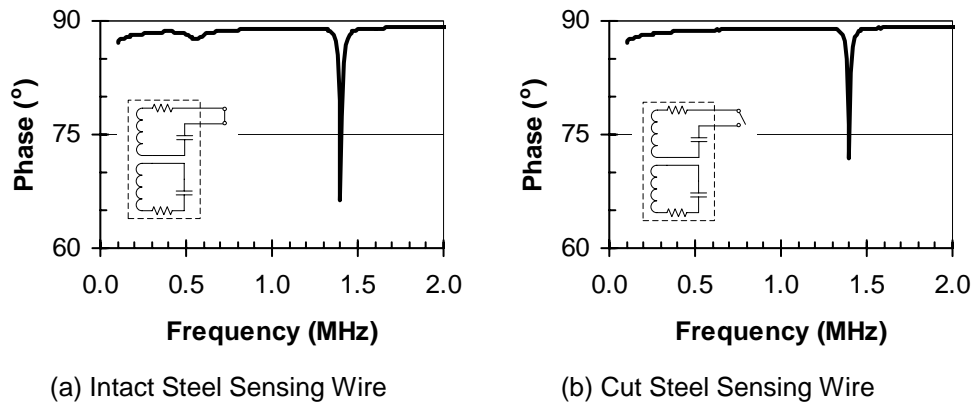


Figure F-21 Phase Response of Sensor A10

F.4.1 Surrounding Environment

To gauge the effect of the surrounding environment on the performance of sensor A10, the sensor was interrogated in air, tap water, and salt water using reader coil 4t05 attached to the impedance analyzer with a cable. Interrogations were taken with intact and cut steel sensing wires. In addition to those three environments, sensor A10 with a cut sensing wire was also interrogated using the same reader configuration in varying concentrations of salt water. Salt water concentrations of 0.0%, 0.01%, 0.02%, 0.05%, 0.1%, 0.2%, 0.3%, 0.4%, 0.5%, 1.0%, and 3.5% were selected to provide a well-defined transition behavior for the sensor.

F.4.1.1 Intact Steel Sensing Wire

Interrogation results at a read distance of 1.0 in. were used to compare the response of sensor A10 in air, tap water, and 3.5% salt water. Table F-32 shows the effect of surrounding environment on sensor A10 with an intact steel sensing wire. The characteristic frequencies and pseudo-quality factors remain approximately constant with the change from air to tap water. A 8-21% reduction

in pseudo-quality factor occurs with the change from tap water to 3.5% salt water. Phase dips are more sensitive to the surrounding environments, with reductions of approximately 30-35% for the change from air to tap water and approximately another 10-20% for the change from tap water to 3.5% salt water. As discussed in Chapter 3, the reduction in phase dip for the change from air to tap water may be due to the test method. The thickness of glass on the bottom of the beaker used to contain the water increases the read distance slightly, which probably results in most of the reduction in phase dip.

Table F-32 Effect of Surrounding Environment on Sensor A10 with Intact Sensing Wire

Environment	Sensing Circuit			Reference Circuit		
	Char. Freq. (MHz)	Phase Dip (°)	Pseudo-Quality Factor	Char. Freq. (MHz)	Phase Dip (°)	Pseudo-Quality Factor
Air	0.56	1.1	5.2	1.40	23.0	76.1
Tap Water	0.56	0.8	5.3	1.40	14.8	76.5
3.5% Salt Water	0.58	0.7	4.9	1.40	12.2	60.6

F.4.1.2 Cut Steel Sensing Wire

Table F-33 shows the effect of surrounding environment on sensor A10 with a cut steel sensing wire. The reference characteristic frequency remains constant with the change from air to tap water, while the sensing characteristic frequency is not present. The reference pseudo-quality factor only decreases by 3%, while the reference phase dip decreases by 32% with the change from air to tap water. The change in sensor behavior is significant for the change from tap

water to 3.5% salt water. The sensing circuit characteristic frequency reappears with a phase dip and pseudo-quality factor approximately 25% less than those for the same sensor with an intact steel sensing wire interrogated in 3.5% salt water. The reference circuit characteristic frequency does not change and the phase dip decreases by 10% with the change from tap water to 3.5% salt water. The pseudo-quality factor also decreases by 23%. Compared with the phase dip of the reference circuit in sensor A10 with the steel sensing wire intact, the phase dip is essentially unchanged with the steel sensing wire cut. The pseudo-quality factor for the reference circuit of sensor A10 with a cut steel sensing wire in 3.5% salt water is also the same as that for the sensor with an intact wire.

Table F-33 Effect of Surrounding Environment on Sensor A10 with Cut Sensing Wire

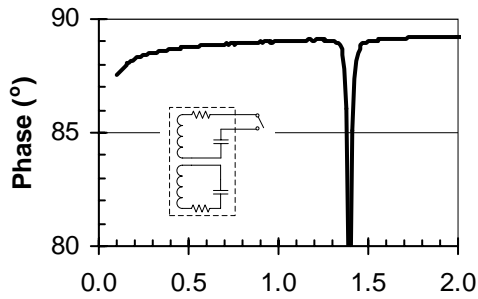
Environment	Sensing Circuit			Reference Circuit		
	Char. Freq. (MHz)	Phase Dip (°)	Pseudo-Quality Factor	Char. Freq. (MHz)	Phase Dip (°)	Pseudo-Quality Factor
Air	-	-	-	1.40	19.9	80.0
Tap Water	-	-	-	1.40	13.5	77.6
3.5% Salt Water	0.61	0.5	3.6	1.40	12.1	59.8

Table F-34 shows the effect of varying salt water concentration on sensor A10 with a cut steel sensing wire. Interrogation results are shown for 1.0-in. read distance. The reference circuit phase dip decreases with increasing salt water concentration to a minimum at 0.3% and then increases slightly with increasing concentration. The reference characteristic frequency remains constant with increasing salt water concentration. At a concentration of 0.5% and above, the

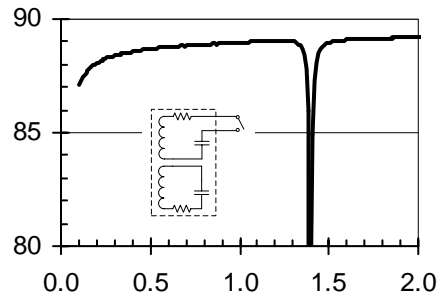
sensing circuit response is present with a phase dip of 0.1° or more. Fig. F-22 shows the phase response of the sensor with varying concentrations of salt water. The transition response of sensor A10 is evident with increasing conductivity of the surrounding environment. The phase response of the sensor with a cut sensing wire immersed in 3.5% salt water (k) is very close to the response of the sensor with an intact sensing wire immersed in 3.5% salt water (l). However, the difference in pseudo-quality factors may still provide the information needed to determine the state of the steel sensing wire. Further discussion on use of the pseudo-quality factor is provided in Section F.4.2.

Table F-34 Effect of Varying Concentration of Salt Water on Sensor A10 with Cut Sensing Wire

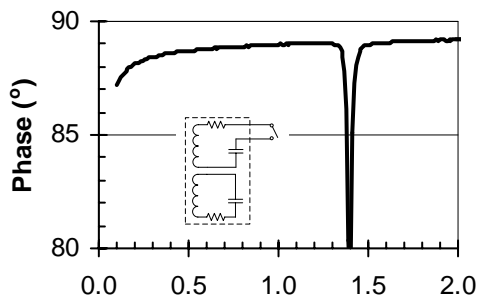
Salt Water Concentration	Sensing Circuit			Reference Circuit		
	Char. Freq. (MHz)	Phase Dip (°)	Pseudo-Quality Factor	Char. Freq. (MHz)	Phase Dip (°)	Pseudo-Quality Factor
0.0%	-	-	-	1.40	13.5	77.6
0.01%	-	-	-	1.40	13.5	76.9
0.02%	-	-	-	1.40	12.6	75.0
0.05%	-	-	-	1.40	12.5	71.3
0.1%	-	-	-	1.40	11.6	61.5
0.2%	-	-	-	1.40	11.7	62.8
0.3%	-	-	-	1.40	11.1	61.9
0.4%	-	-	-	1.40	11.2	61.9
0.5%	0.65	0.2	1.1	1.40	11.7	62.2
1.0%	0.63	0.3	1.1	1.40	12.8	63.7
3.5%	0.61	0.5	3.6	1.40	12.1	59.8



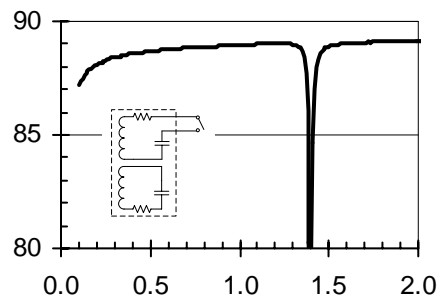
(a) Cut Wire in Tap Water



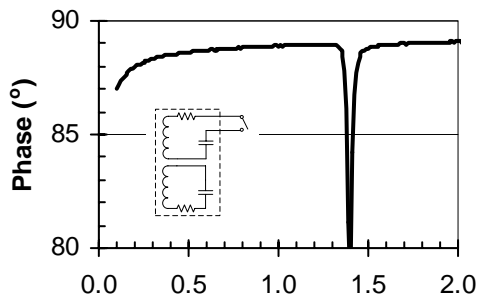
(b) Cut Wire in 0.01% Salt Water



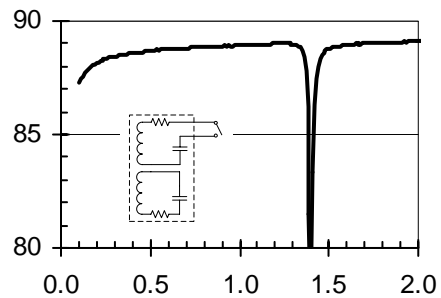
(c) Cut Wire in 0.02% Salt Water



(d) Cut Wire in 0.05% Salt Water

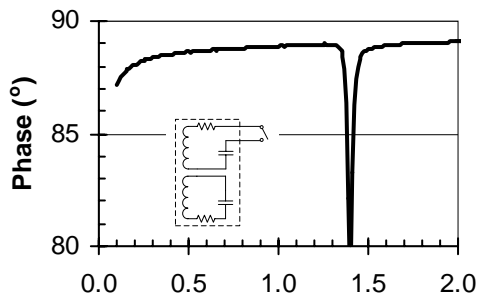


(e) Cut Wire in 0.1% Salt Water

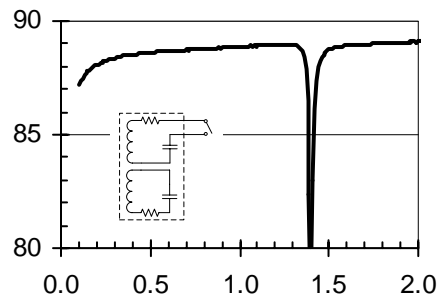


(f) Cut Wire in 0.2% Salt Water

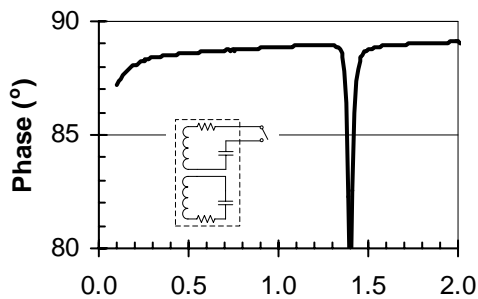
Figure F-22 Phase Response of Sensor A10 in Varying Concentrations of Salt Water



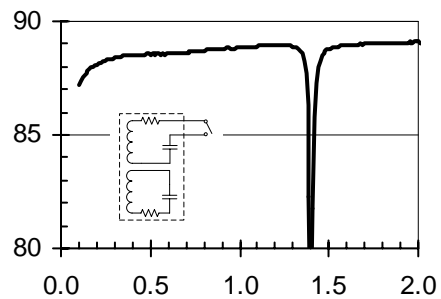
(g) Cut Wire in 0.3% Salt Water



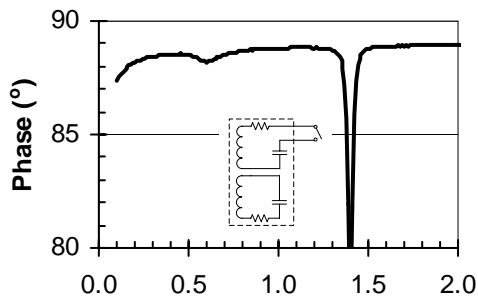
(h) Cut Wire in 0.4% Salt Water



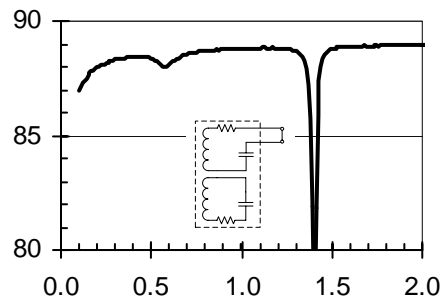
(i) Cut Wire in 0.5% Salt Water



(j) Cut Wire in 1.0% Salt Water



(k) Cut Wire in 3.5% Salt Water



(l) Intact Wire in 3.5% Salt Water

Figure F-22 (Cont.) Phase Response of Sensor A10 in Varying Concentrations of Salt Water

F.4.2 Read Distance

Because read distance also affects the performance of sensors, sensor A10 was interrogated at read distances from 0.0-in. to 3.0-in. at 0.5-in increments in air, tap water, and 3.5% salt water using reader coil 4t05 attached to the impedance analyzer with a 3-ft cable. Interrogations were taken with intact and cut steel sensing wires. In addition to those three environments, sensor A10 was also interrogated using the same reader configuration in varying concentrations of salt water at read distances of 0.0 in., 1.0 in., and 2.0 in.

F.4.2.1 Intact Steel Sensing Wire

Table F-35 shows the effect of read distance on sensor A10 with an intact steel sensing wire. Interrogation results are shown in the table for readings in air. While phase dips are significantly reduced with increasing read distance, the characteristic frequency of each circuit remains the same. The pseudo-quality factor only increases slightly for both the sensing circuit and the reference circuit with increasing read distance. The characteristic frequencies and pseudo-quality factors are plotted versus read distance in Fig. F-23 for interrogations in air, Fig. F-24 for tap water, and Fig. F-25 for 3.5% salt water. A statistical summary of the characteristic frequency, phase dip, and pseudo-quality factor for the sensing circuit is provided in Table F-36. The same information for the reference circuit is provided in Table F-37. The coefficients of variation for characteristic frequencies of both the sensing and reference circuits are very small ($\leq 0.2\%$). Because phase dips are highly dependent on read distance, the coefficient of variation for phase dips are quite large ($>100\%$). The coefficients of variation for pseudo-quality factors are very good, ranging from 2.9% to 9.6%.

Table F-35 Effect of Read Distance on Sensor A10 with Intact Sensing Wire

Read Distance (in.)	Sensing Circuit			Reference Circuit		
	Char. Freq. (MHz)	Phase Dip (°)	Pseudo- Quality Factor	Char. Freq. (MHz)	Phase Dip (°)	Pseudo- Quality Factor
0.0	0.56	5.5	4.7	1.41	92.1	58.0
0.5	0.56	2.5	5.1	1.40	51.1	73.0
1.0	0.56	1.1	5.2	1.40	23.0	76.1
1.5	0.56	0.5	5.3	1.40	10.4	76.8
2.0	0.56	0.2	5.5	1.40	5.1	77.0
2.5	0.56	0.1	5.7	1.40	2.5	77.3
3.0	N/A	N/A	N/A	1.40	1.4	77.2

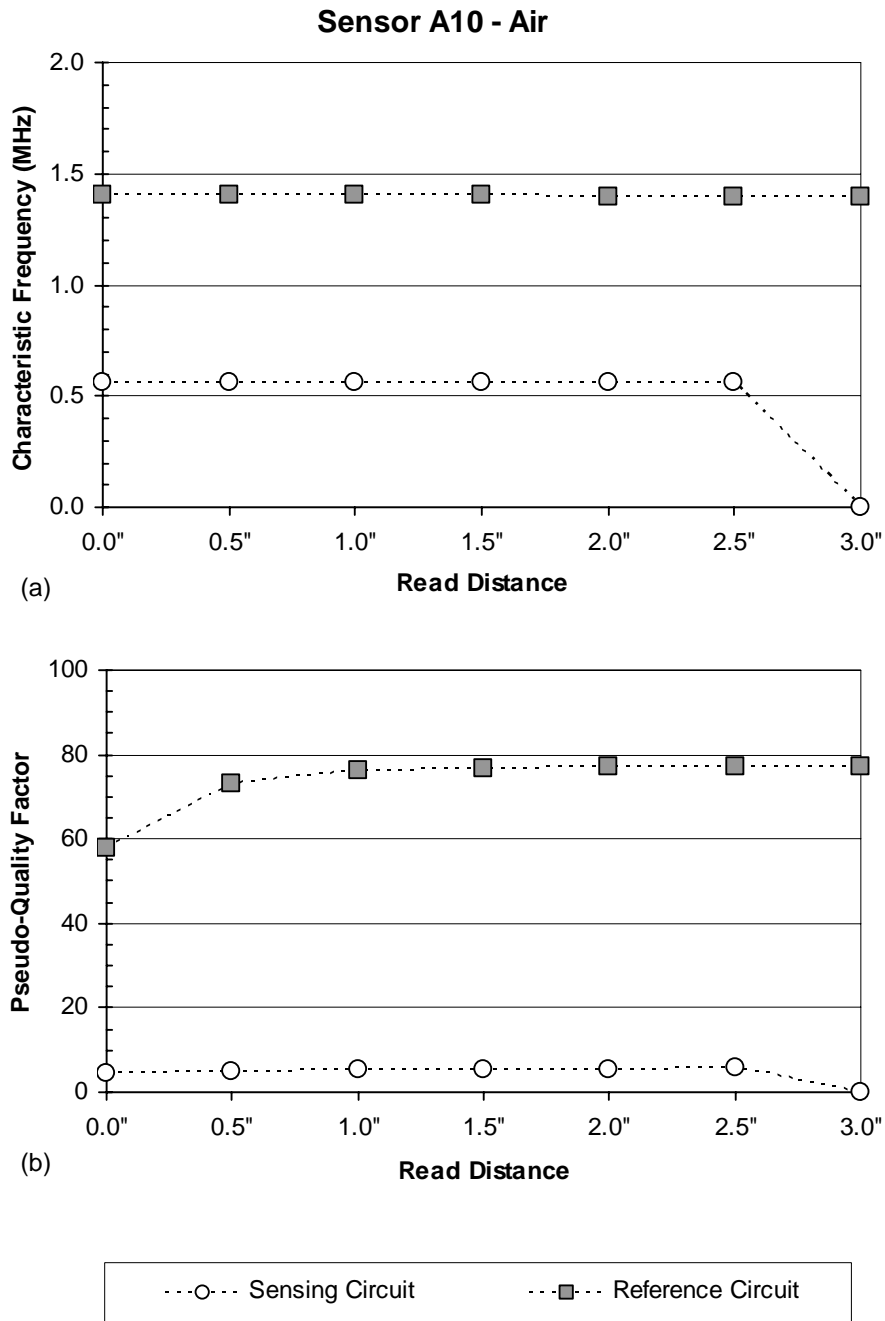


Figure F-23 Effect of Read Distance on Response of Sensor A10 with an Intact Sensing Wire for Readings in Air

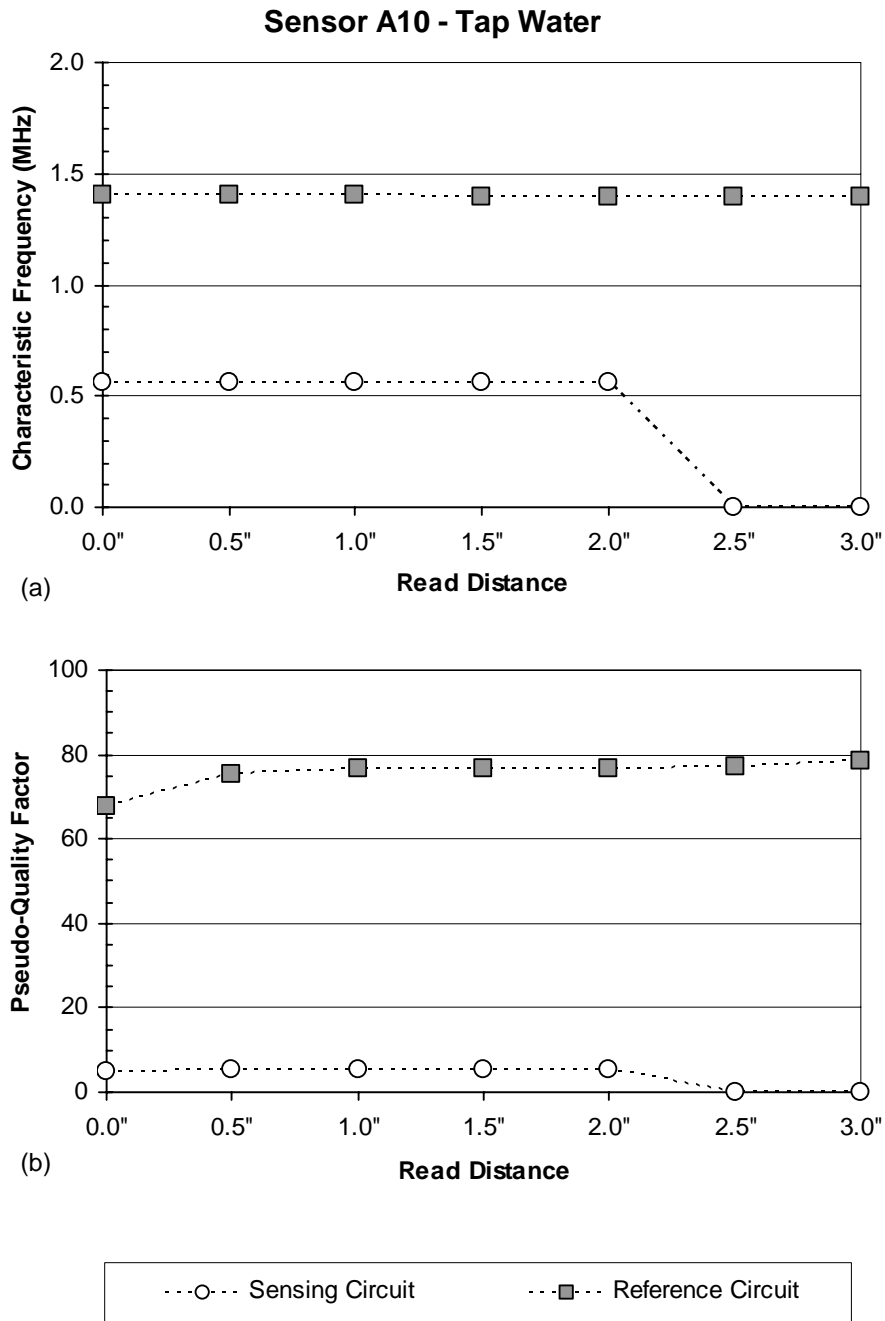


Figure F-24 Effect of Read Distance on Response of Sensor A10 with an Intact Sensing Wire for Readings in Tap Water

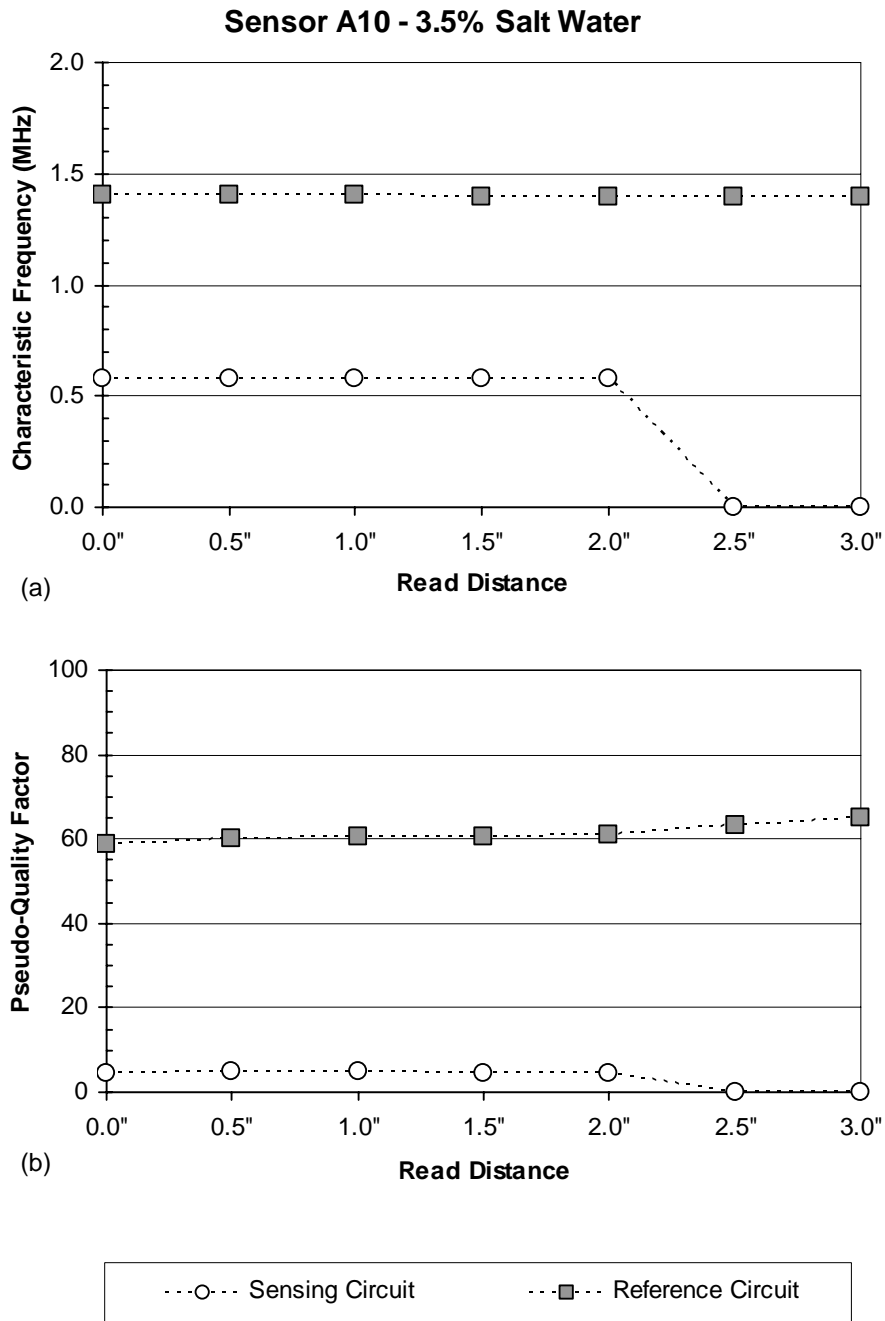


Figure F-25 Effect of Read Distance on Response of Sensor A10 with an Intact Sensing Wire for Readings in 3.5% Salt Water

Table F-36 Variation of Measured Response of Sensor A10 with Intact Sensing Wire for Sensing Circuit with Varying Read Distance

Environment	Number of Readings	Characteristic Frequency		Pseudo-Quality Factor		Phase Dip	
		Mean (MHz)	Coef. of Variation	Mean	Coef. of Variation	Mean (°)	Coef. of Variation
Air	6	0.56	0.1%	5.2	6.6%	1.7	125.5%
Tap Water	5	0.56	0.1%	5.3	4.1%	1.4	110.8%
3.5% Salt Water	5	0.58	0.1%	4.7	2.9%	1.3	114.2%

Table F-37 Variation of Measured Response of Sensor A10 with Intact Sensing Wire for Reference Circuit with Varying Read Distance

Environment	Number of Readings	Characteristic Frequency		Pseudo-Quality Factor		Phase Dip	
		Mean (MHz)	Coef. of Variation	Mean	Coef. of Variation	Mean (°)	Coef. of Variation
Air	6	1.40	0.2%	73.6	9.6%	26.5	127.5%
Tap Water	5	1.40	0.2%	75.6	4.7%	19.2	138.7%
3.5% Salt Water	5	1.40	0.2%	61.4	3.5%	16.4	139.0%

F.4.2.2 Cut Steel Sensing Wire

The effect of read distance on sensor A10 with a cut steel sensing wire is shown in Table F-38. Interrogation results are shown in the table for readings in air. Again, phase dips are substantially reduced with increasing read distance. Characteristic frequencies do not change and the variations in pseudo-quality

factors are small. The characteristic frequencies and pseudo-quality factors are plotted versus read distance in Fig. F-26 for interrogations in air, Fig. F-27 for tap water, and Fig. F-28 for 3.5% salt water. A statistical summary of the characteristic frequency, phase dip, and pseudo-quality factor for the reference circuit is provided in Table F-39. The same information for the sensing circuit is provided in Table F-40. The sensing circuit only responded in the 3.5% salt water environment. Coefficients of variation are very small for characteristic frequencies and very large for phase dips.

While the coefficients of variation for pseudo-quality factors are small, ranging from 2.0% to 9.5% for the reference circuit, the values change slightly with increasing conductivity of the surrounding environment. In 3.5% salt water, the reference circuit mean pseudo-quality factor is 59.8 for a cut steel sensing wire, while it is 61.4 for an intact wire. The sensing circuit mean pseudo-quality factor is 3.3 for a cut steel sensing wire and 4.7 for an intact wire. Therefore, the pseudo-quality factor may give a reliable indication of the state of the steel sensing wire in the presence of a conductive environment.

Table F-38 Effect of Read Distance on Sensor A10 with Cut Sensing Wire

Read Distance (in.)	Sensing Circuit			Reference Circuit		
	Char. Freq. (MHz)	Phase Dip (°)	Pseudo- Quality Factor	Char. Freq. (MHz)	Phase Dip (°)	Pseudo- Quality Factor
0.0	-	-	-	1.40	83.8	65.6
0.5	-	-	-	1.40	43.8	76.0
1.0	-	-	-	1.40	19.9	80.0
1.5	-	-	-	1.40	9.3	80.9
2.0	-	-	-	1.40	4.5	81.4
2.5	-	-	-	1.40	2.4	82.6
3.0	-	-	-	1.40	1.2	84.3

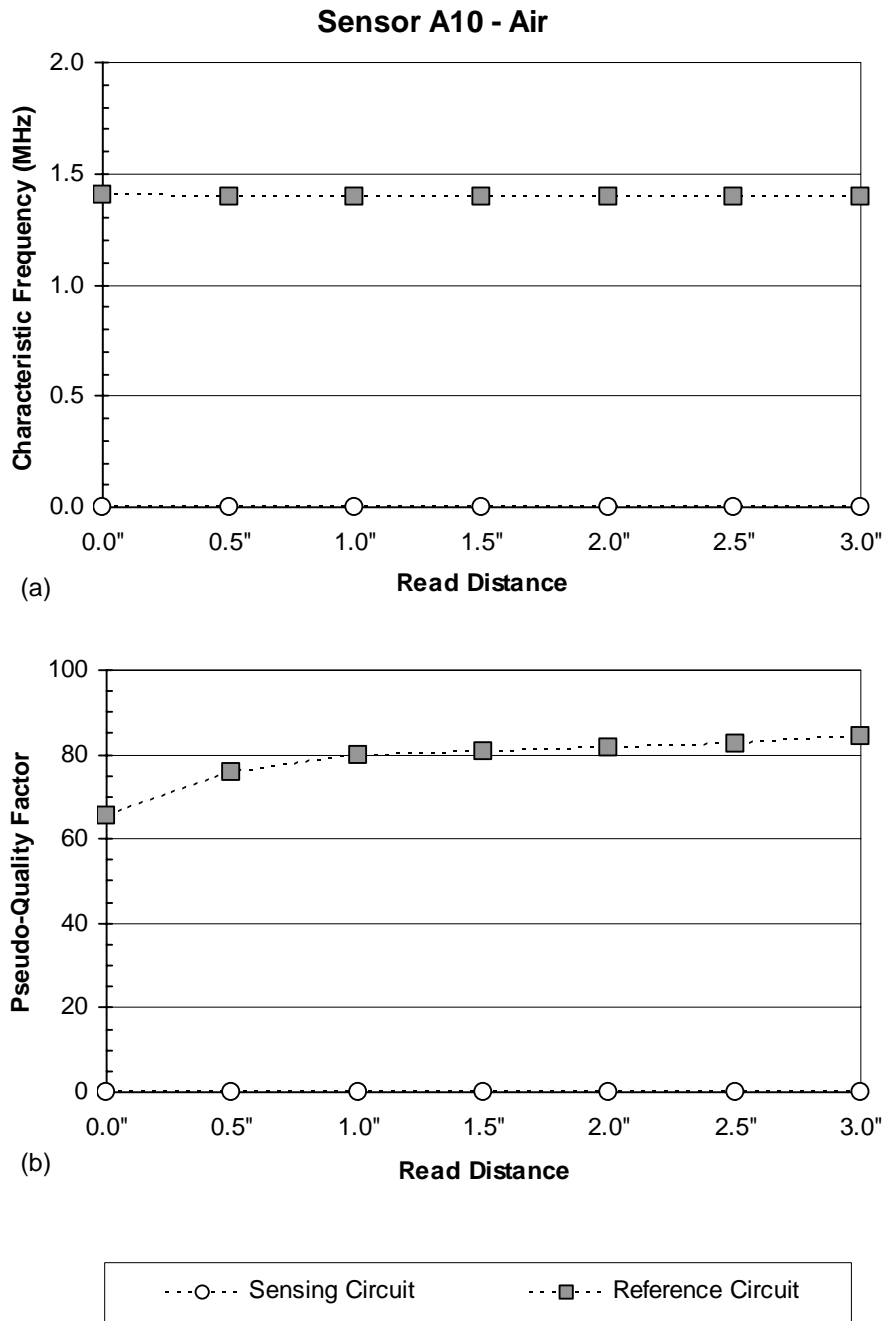


Figure F-26 Effect of Read Distance on Response of Sensor A10 with a Cut Sensing Wire for Readings in Air

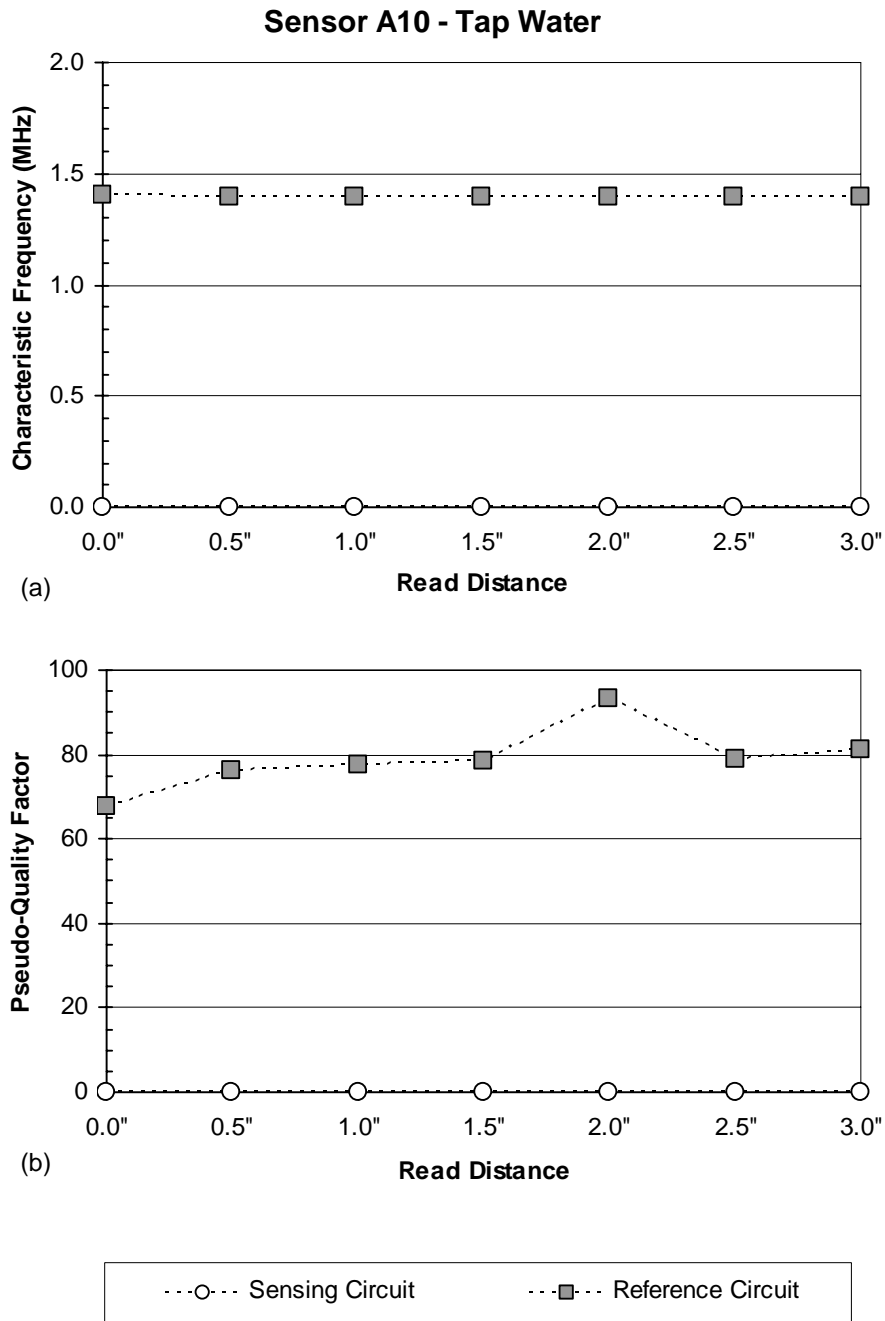
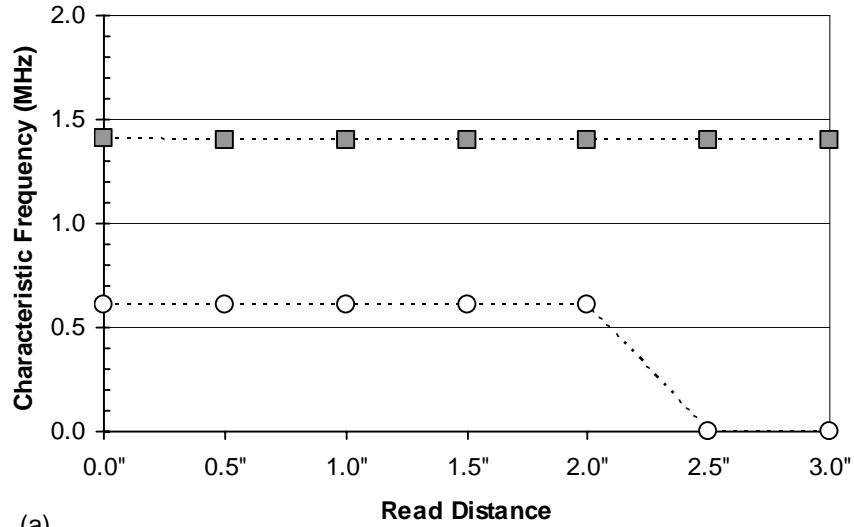
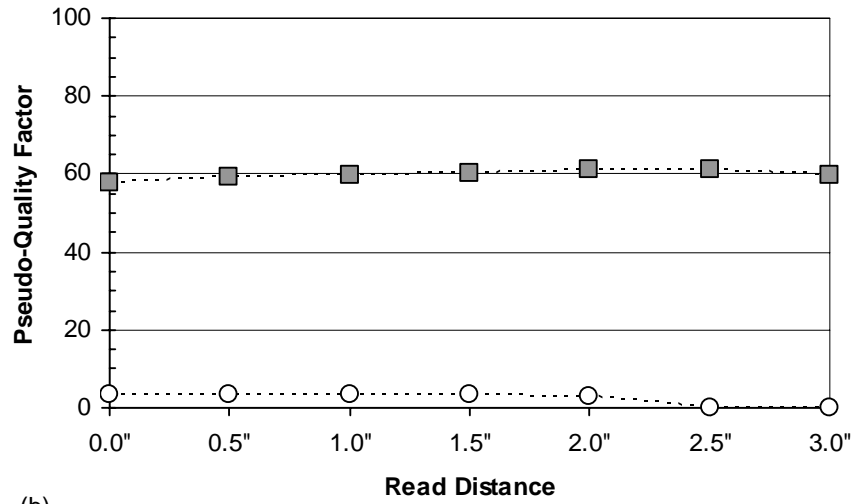


Figure F-27 Effect of Read Distance on Response of Sensor A10 with a Cut Sensing Wire for Readings in Tap Water

Sensor A10 - 3.5% Salt Water



(a)



(b)



Figure F-28 Effect of Read Distance on Response of Sensor A10 with a Cut Sensing Wire for Readings in 3.5% Salt Water

**Table F-39 Variation of Measured Response of Sensor A10 with Cut Sensing
Wire for Reference Circuit with Varying Read Distance**

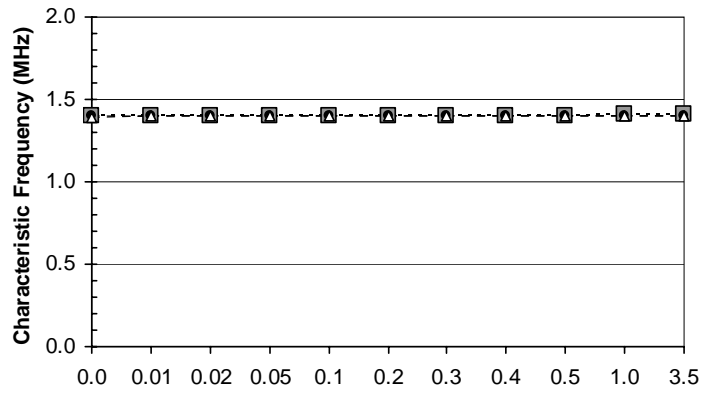
Environment	Number of Readings	Characteristic Frequency		Pseudo-Quality Factor		Phase Dip	
		Mean (MHz)	Coef. of Variation	Mean	Coef. of Variation	Mean (°)	Coef. of Variation
Air	7	1.40	0.2%	78.7	8.0%	23.6	129.3%
Tap Water	7	1.40	0.2%	79.0	9.5%	16.8	139.3%
3.5% Salt Water	7	1.40	0.2%	59.8	2.0%	15.8	138.9%

**Table F-40 Variation of Measured Response of Sensor A10 with Cut Sensing
Wire for Sensing Circuit with Varying Read Distance**

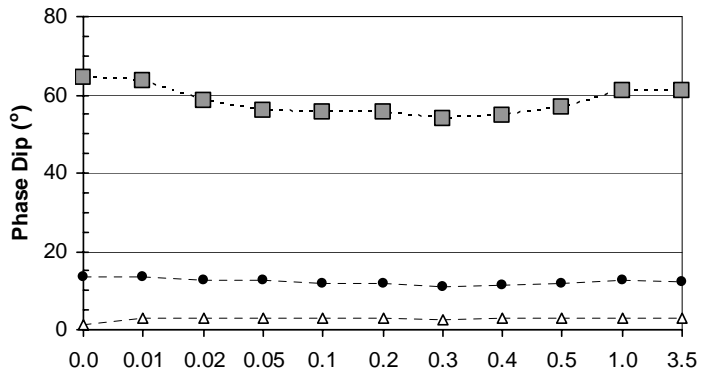
Environment	Number of Readings	Characteristic Frequency		Pseudo-Quality Factor		Phase Dip	
		Mean (MHz)	Coef. of Variation	Mean	Coef. of Variation	Mean (°)	Coef. of Variation
3.5% Salt Water	5	0.61	0.4%	3.3	6.1%	1.0	112.6%

Plots of characteristic frequency, phase dip, and pseudo-quality factor versus salt water concentration are shown for three different read distances, 0.0 in., 1.0 in., and 2.0 in. in Fig. F-29 for the reference circuit and Fig. F-30 for the sensing circuit. When the sensing circuit response is present ($\geq 0.5\%$ salt water), the pseudo-quality factors of the sensing circuit and the reference circuit can be compared with values for both intact and cut wire. This information can be used to determine the state of the steel sensing wire for embedded sensors. With an intact steel sensing wire, the pseudo-quality factor of the sensing circuit should always be greater than 4.5. When the steel sensing wire is broken (or cut), the state of the wire can be determined two ways: (1) if the sensing circuit phase dip

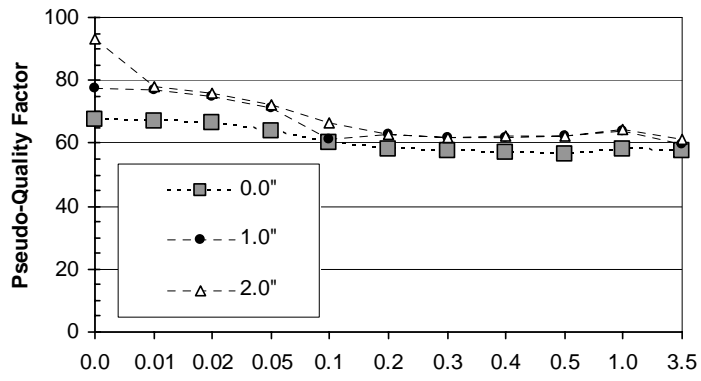
is not present, then the wire is broken, or (2) if the sensing circuit phase dip is present and the pseudo-quality factor of the sensing circuit is less than 4, then the wire is broken.



(a)



(b)



(c)

Figure F-29 Sensor A10 Reference Circuit Response for a Cut Sensing Wire with Increasing Concentration of Salt Water at Three Read Distances

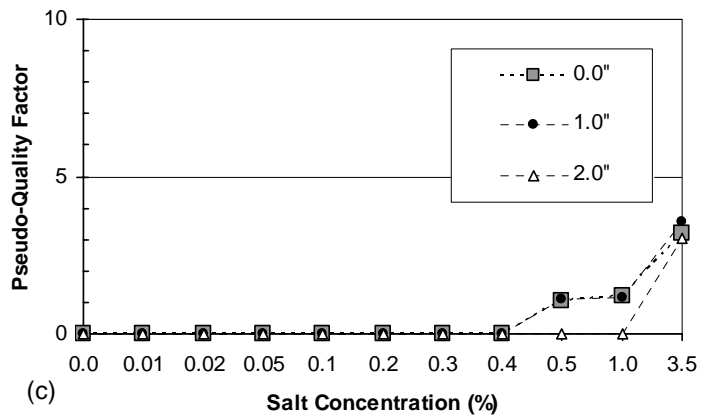
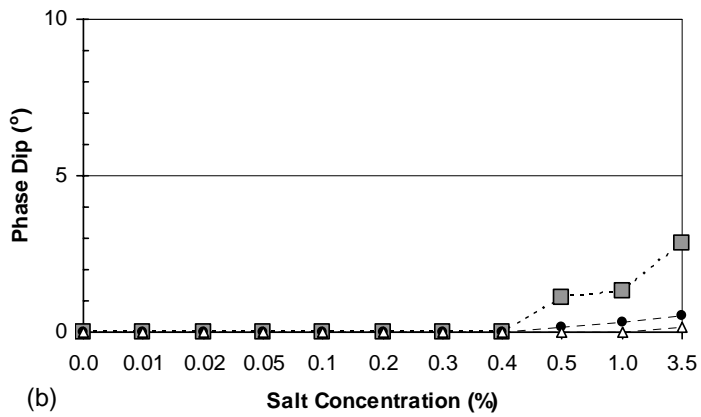
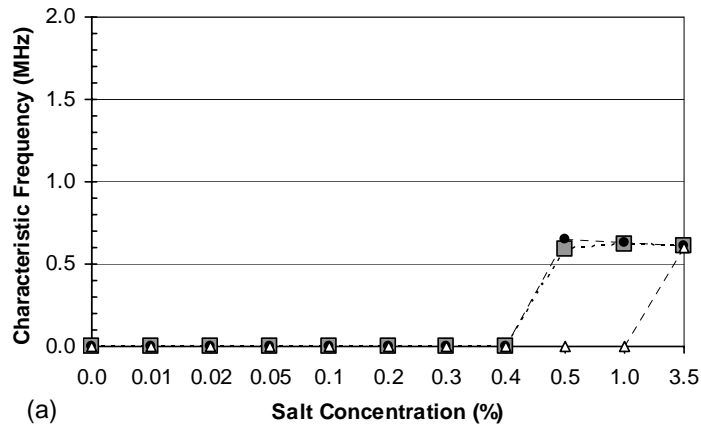


Figure F-30 Sensor A10 Sensing Circuit Response for a Cut Sensing Wire with Increasing Concentration of Salt Water at Three Read Distances

F.4.3 Reader Configuration

In order to assess the sensitivity of phase response to reader configuration, sensor A10 was interrogated using seven different reader coils. The Solartron Impedance Analyzer was used for all of the interrogations. The sensor was interrogated in air at read distances of 0.0 in., 1.0 in., 2.0 in., and 3.0 in. Table F-10 gives the details for each reader coil.

Results from interrogations of sensor A10 with an intact steel sensing wire at a read distance of 1.0 in. are shown in Table F-41 for all of the reader configurations used in this study. Table F-42 shows the same results for sensor A10 with a cut steel sensing wire. Despite the large variations in phase dip with different reader coils, the characteristic frequencies remain nearly constant and the variation in pseudo-quality factors is small. The maximum read distance for sensor A10 with an intact steel sensing wire is shown for each reader configuration in Table F-43. Maximum read distance is defined as the read distance at which the phase dip is at least 0.1° for interrogations in air. In this case, the sensor gives a maximum read distance of only 2-in., even with the reader coils shown to give the flattest baseline response in Chapter 3. When reader coils are connected to the impedance analyzer with a cable, reader coil 4t05 provides the best response. Statistical summaries that show the variation in characteristic frequency, pseudo-quality factor, and phase dip for all reader configurations used in this study are provided in Table F-44 for the sensing circuit with an intact sensing wire, Table F-45 for the reference circuit with an intact sensing wire, and Table F-46 for the reference circuit with a cut sensing wire.

**Table F-41 Effect of Reader Configuration on Sensor A10 with Intact Sensing
Wire for a 1-in. Read Distance**

Reader Coil	Sensing Circuit			Reference Circuit		
	Char. Freq. (MHz)	Phase Dip (°)	Pseudo-Quality Factor	Char. Freq. (MHz)	Phase Dip (°)	Pseudo-Quality Factor
4t01-24	0.56	0.8	5.3	1.40	15.5	76.8
4t01-18	0.56	0.9	5.5	1.40	16.0	76.8
4t05	0.56	1.2	5.3	1.40	22.7	76.3
4t05 w/ cable	0.56	1.1	5.2	1.40	23.0	76.1
4t20	0.56	1.1	5.3	1.40	23.3	76.0
6t10	0.56	0.8	5.4	1.40	16.3	76.6
3s	0.56	1.3	5.5	1.40	25.6	75.1

**Table F-42 Effect of Reader Configuration on Sensor A10 with Cut Sensing
Wire for a 1-in. Read Distance**

Reader Coil	Sensing Circuit			Reference Circuit		
	Char. Freq. (MHz)	Phase Dip (°)	Pseudo-Quality Factor	Char. Freq. (MHz)	Phase Dip (°)	Pseudo-Quality Factor
4t01-24	-	-	-	1.40	13.7	79.1
4t01-18	-	-	-	1.40	14.5	80.3
4t05	-	-	-	1.40	20.7	80.2
4t05 w/ cable	-	-	-	1.40	19.9	80.0
4t20	-	-	-	1.40	20.7	80.0
6t10	-	-	-	1.40	14.6	80.8
3s	-	-	-	1.40	20.8	79.7

Table F-43 Maximum Read Distances for Sensor A10 with Intact Sensing Wire

Reader Coil	Maximum Read Distance (in.)
4t01-24	2
4t01-18	2
4t05	2
4t05 w/ cable	2
4t20	2
6t10	2
3s	2

Table F-44 Variation of Measured Response of Sensor A10 with Intact Sensing Wire for Sensing Circuit with Different Reader Coils

Read Distance (in.)	Number of Readings	Characteristic Frequency		Pseudo-Quality Factor		Phase Dip	
		Mean (MHz)	Coef. of Variation	Mean	Coef. of Variation	Mean (°)	Coef. of Variation
0.0	7	0.56	0.6%	4.8	5.9%	5.8	68.0%
1.0	7	0.56	0.2%	5.3	2.0%	1.0	20.3%
2.0	7	0.56	0.6%	5.0	38.5%	0.2	21.4%
All	22	0.56	2.2%	4.8	30.2%	2.3	145.5%

**Table F-45 Variation of Measured Response of Sensor A10 with Intact Sensing
Wire for Reference Circuit with Different Reader Coils**

Read Distance (in.)	Number of Readings	Characteristic Frequency		Pseudo-Quality Factor		Phase Dip	
		Mean (MHz)	Coef. of Variation	Mean	Coef. of Variation	Mean (°)	Coef. of Variation
0.0	7	1.41	0.9%	58.5	25.3%	82.9	35.3%
1.0	7	1.40	0.0%	76.2	0.8%	20.3	20.7%
2.0	7	1.40	0.0%	76.5	0.9%	4.7	21.8%
3.0	4	1.40	0.0%	77.0	0.6%	1.6	25.1%
All	25	1.40	0.6%	71.5	15.5%	30.5	122.1%

**Table F-46 Variation of Measured Response of Sensor A10 with Cut Sensing
Wire for Reference Circuit with Different Reader Coils**

Read Distance (in.)	Number of Readings	Characteristic Frequency		Pseudo-Quality Factor		Phase Dip	
		Mean (MHz)	Coef. of Variation	Mean	Coef. of Variation	Mean (°)	Coef. of Variation
0.0	7	1.40	0.7%	60.4	28.9%	107.0	72.9%
1.0	7	1.40	0.0%	80.0	0.6%	17.8	19.0%
2.0	7	1.40	0.0%	80.6	1.5%	4.2	22.4%
3.0	4	1.40	0.0%	82.3	1.9%	1.5	24.5%
All	25	1.40	0.5%	75.1	17.1%	36.3	164.8%

Coefficients of variation for characteristic frequencies are very small for readings at all read distances with all reader coils, ranging from 0.0% to 2.2%. Therefore, characteristic frequency response of sensors is very reliable with varying read distance and with different reader configurations. Pseudo-quality factors also give small coefficients of variation for varying read distances and different reader coils. Therefore, especially if the read distance is known, the calculation of pseudo-quality factors provides reliable values for use in

determining the state of the steel sensing wire. Because phase dips are severely affected by both read distance and reader coil, the coefficients of variation in phase dips are large. Although the amplitude of the phase dip must be determined to calculate the pseudo-quality factor for a sensor reading, phase dip alone is not a reliable number for evaluating the state of the sensor.

F.5 COPLANAR SENSOR A60

Sensor A60 is a coplanar sensor with a 21-gage steel sensing wire. The phase response of this sensor is shown in Fig. F-31 for an intact sensing wire (a) and for a cut sensing wire (b). This is the baseline response of the sensor in air with a read distance of 1.0 in. A 4-in. diameter reader coil with 5 turns of 18-gage magnet wire connected to the impedance analyzer with a 3-ft cable was used for this interrogation (reader coil 4t05 with a cable). With the steel sensing wire intact, the sensor responds at both the sensing circuit characteristic frequency and the reference circuit characteristic frequency. The reference circuit is not shielded when the sensing circuit response is present because the mutual inductance between the sensing circuit inductor and the reference circuit inductor is negligible for the side-by-side arrangement. The sensing circuit phase dip disappears due to fracture of the steel sensing wire, but the response of the reference circuit remains essentially unchanged. This makes the response of the sensor entirely dependent on the sensing circuit, which must be readable to determine the state of the steel sensing wire.

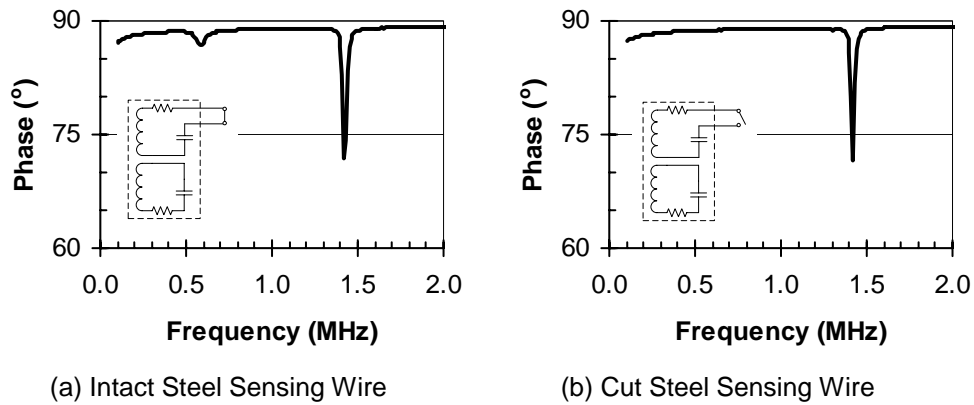


Figure F-31 Phase Response of Sensor A60

F.5.1 Surrounding Environment

To gauge the effect of the surrounding environment on the performance of sensor A60, the sensor was interrogated in air, tap water, and salt water using reader coil 4t05 attached to the impedance analyzer with a cable. Interrogations were taken with intact and cut steel sensing wires. In addition to those three environments, sensor A60 with a cut sensing wire was also interrogated using the same reader configuration in varying concentrations of salt water. Salt water concentrations of 0.0%, 0.01%, 0.02%, 0.05%, 0.1%, 0.2%, 0.3%, 0.4%, 0.5%, 1.0%, and 3.5% were selected to provide a well-defined transition behavior for the sensor.

F.5.1.1 Intact Steel Sensing Wire

Interrogation results at a read distance of 1.0 in. were used to compare the response of sensor A60 in air, tap water, and 3.5% salt water. Table F-47 shows the effect of surrounding environment on sensor A60 with an intact steel sensing wire. The characteristic frequencies and pseudo-quality factors remain approximately constant with the change from air to tap water. A 14-24%

reduction in pseudo-quality factor occurs with the change from tap water to 3.5% salt water. Phase dips are more sensitive to the surrounding environments, with reductions of approximately 30% for the change from air to tap water and approximately another 15-25% for the change from tap water to 3.5% salt water. As discussed in Chapter 3, the reduction in phase dip for the change from air to tap water may be due to the test method. The thickness of glass on the bottom of the beaker used to contain the water increases the read distance slightly, which probably results in most of the reduction in phase dip.

Table F-47 Effect of Surrounding Environment on Sensor A60 with Intact Sensing Wire

Environment	Sensing Circuit			Reference Circuit		
	Char. Freq. (MHz)	Phase Dip (°)	Pseudo-Quality Factor	Char. Freq. (MHz)	Phase Dip (°)	Pseudo-Quality Factor
Air	0.59	2.0	9.6	1.42	20.5	75.6
Tap Water	0.59	1.4	9.6	1.42	14.5	75.7
3.5% Salt Water	0.60	1.1	8.2	1.42	11.1	57.4

F.5.1.2 Cut Steel Sensing Wire

Table F-48 shows the effect of surrounding environment on sensor A60 with a cut steel sensing wire. The reference characteristic frequency remains constant with the change from air to tap water, while the sensing characteristic frequency is not present. The reference pseudo-quality factor only decreases by 4%, while the reference phase dip decreases by 37% with the change from air to tap water. The change in sensor behavior is significant for the change from tap

water to 3.5% salt water. The sensing circuit characteristic frequency reappears with a phase dip and pseudo-quality factor approximately 25% less than those for the same sensor with an intact steel sensing wire interrogated in 3.5% salt water. The reference circuit characteristic frequency does not change and the phase dip decreases by 6% with the change from tap water to 3.5% salt water. The pseudo-quality factor also decreases by 25%. Compared with the phase dip of the reference circuit in sensor A60 with the steel sensing wire intact, the phase dip is only reduced by 5% with the steel sensing wire cut. The pseudo-quality factor for the reference circuit of sensor A60 with a cut steel sensing wire in 3.5% salt water is only reduced by 3% than that for the sensor with an intact wire.

Table F-48 Effect of Surrounding Environment on Sensor A60 with Cut Sensing Wire

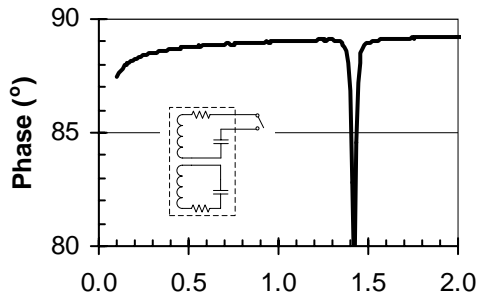
Environment	Sensing Circuit			Reference Circuit		
	Char. Freq. (MHz)	Phase Dip (°)	Pseudo-Quality Factor	Char. Freq. (MHz)	Phase Dip (°)	Pseudo-Quality Factor
Air	-	-	-	1.42	17.8	77.1
Tap Water	-	-	-	1.42	11.2	73.9
3.5% Salt Water	0.62	0.6	4.4	1.42	10.5	55.5

Table F-49 shows the effect of varying salt water concentration on sensor A60 with a cut steel sensing wire. Interrogation results are shown for 1.0-in. read distance. The reference circuit phase dip decreases with increasing salt water concentration to a minimum at 0.1% and then increases slightly with increasing concentration. The reference characteristic frequency remains constant with increasing salt water concentration. At a concentration of 0.5% and above, the

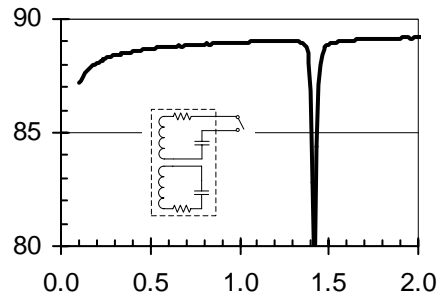
sensing circuit response is present with a phase dip of 0.1° or more. Fig. F-32 shows the phase response of the sensor with varying concentrations of salt water. The transition response of sensor A60 is evident with increasing conductivity of the surrounding environment. The phase response of the sensor with a cut sensing wire immersed in 3.5% salt water (k) is very close to the response of the sensor with an intact sensing wire immersed in 3.5% salt water (l). However, the difference in pseudo-quality factors may still provide the information needed to determine the state of the steel sensing wire. Further discussion on use of the pseudo-quality factor is provided in Section F.5.2.

Table F-49 Effect of Varying Concentration of Salt Water on Sensor A60 with Cut Sensing Wire

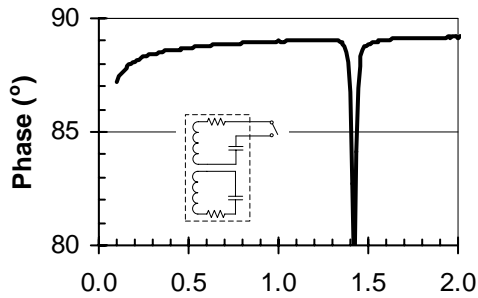
Salt Water Concentration	Sensing Circuit			Reference Circuit		
	Char. Freq. (MHz)	Phase Dip (°)	Pseudo-Quality Factor	Char. Freq. (MHz)	Phase Dip (°)	Pseudo-Quality Factor
0.0%	-	-	-	1.42	11.2	73.9
0.01%	-	-	-	1.42	11.0	72.2
0.02%	-	-	-	1.42	11.1	70.2
0.05%	-	-	-	1.42	10.2	63.5
0.1%	-	-	-	1.42	10.1	61.9
0.2%	-	-	-	1.42	10.4	60.2
0.3%	-	-	-	1.42	10.4	60.1
0.4%	-	-	-	1.42	11.1	60.8
0.5%	0.68	0.2	1.3	1.42	11.1	60.9
1.0%	0.65	0.3	1.5	1.42	11.5	62.1
3.5%	0.62	0.6	4.4	1.42	10.5	55.5



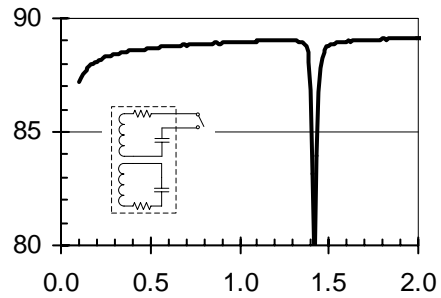
(a) Cut Wire in Tap Water



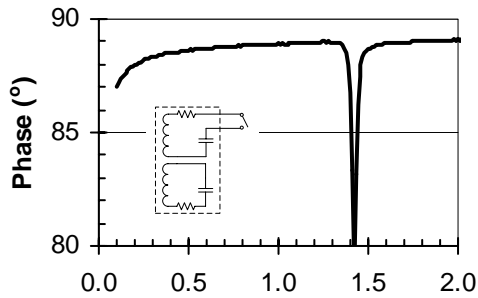
(b) Cut Wire in 0.01% Salt Water



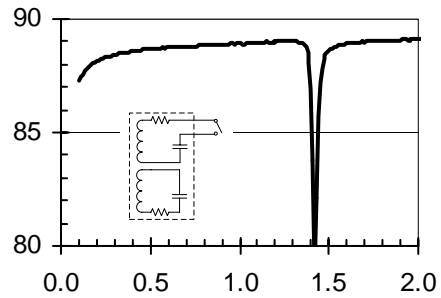
(c) Cut Wire in 0.02% Salt Water



(d) Cut Wire in 0.05% Salt Water

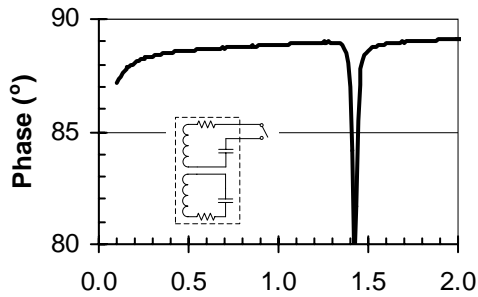


(e) Cut Wire in 0.1% Salt Water

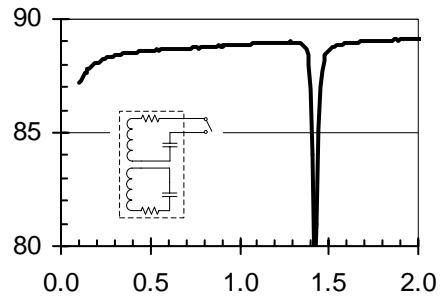


(f) Cut Wire in 0.2% Salt Water

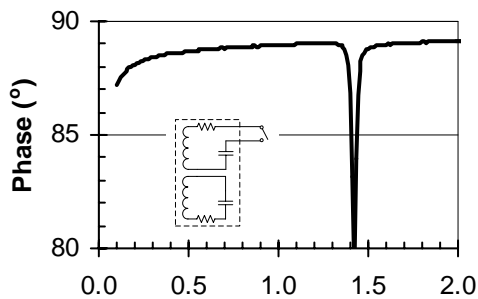
Figure F-32 Phase Response of Sensor A60 in Varying Concentrations of Salt Water



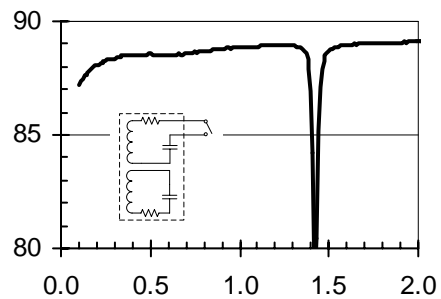
(g) Cut Wire in 0.3% Salt Water



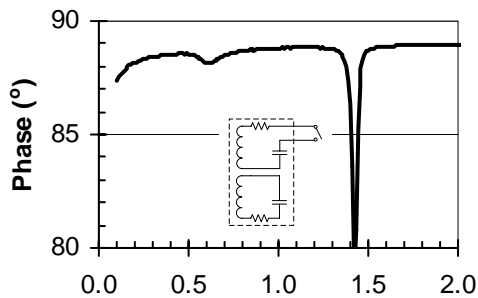
(h) Cut Wire in 0.4% Salt Water



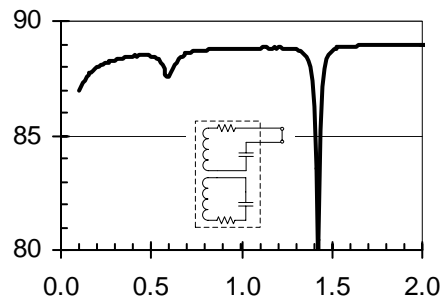
(i) Cut Wire in 0.5% Salt Water



(j) Cut Wire in 1.0% Salt Water



(k) Cut Wire in 3.5% Salt Water



(l) Intact Wire in 3.5% Salt Water

Figure F-32 (Cont.) Phase Response of Sensor A60 in Varying Concentrations of Salt Water

F.5.2 Read Distance

Because read distance also affects the performance of sensors, sensor A60 was interrogated at read distances from 0.0-in. to 3.0-in. at 0.5-in increments in air, tap water, and 3.5% salt water using reader coil 4t05 attached to the impedance analyzer with a 3-ft cable. Interrogations were taken with intact and cut steel sensing wires. In addition to those three environments, sensor A60 was also interrogated using the same reader configuration in varying concentrations of salt water at read distances of 0.0 in., 1.0 in., and 2.0 in.

F.5.2.1 Intact Steel Sensing Wire

Table F-50 shows the effect of read distance on sensor A60 with an intact steel sensing wire. Interrogation results are shown in the table for readings in air. While phase dips are significantly reduced with increasing read distance, the characteristic frequency of each circuit remains the same. The pseudo-quality factor only increases slightly for both the sensing circuit and the reference circuit with increasing read distance. The characteristic frequencies and pseudo-quality factors are plotted versus read distance in Fig. F-33 for interrogations in air, Fig. F-34 for tap water, and Fig. F-35 for 3.5% salt water. A statistical summary of the characteristic frequency, phase dip, and pseudo-quality factor for the sensing circuit is provided in Table F-51. The same information for the reference circuit is provided in Table F-52. The coefficients of variation for characteristic frequencies of both the sensing and reference circuits are very small ($\leq 0.2\%$). Because phase dips are highly dependent on read distance, the coefficient of variation for phase dips are quite large ($>100\%$). The coefficients of variation for pseudo-quality factors are very good, ranging from 3.1% to 12.5%.

Table F-50 Effect of Read Distance on Sensor A60 with Intact Sensing Wire

Read Distance (in.)	Sensing Circuit			Reference Circuit		
	Char. Freq. (MHz)	Phase Dip (°)	Pseudo- Quality Factor	Char. Freq. (MHz)	Phase Dip (°)	Pseudo- Quality Factor
0.0	0.59	10.0	9.1	1.43	86.5	57.4
0.5	0.59	4.5	9.4	1.43	46.4	71.2
1.0	0.59	2.0	9.6	1.42	20.5	75.6
1.5	0.59	0.9	9.6	1.42	9.5	76.5
2.0	0.59	0.4	10.5	1.42	4.8	76.5
2.5	0.59	0.2	10.1	1.42	2.4	76.5
3.0	0.59	0.1	10.4	1.42	1.2	77.5

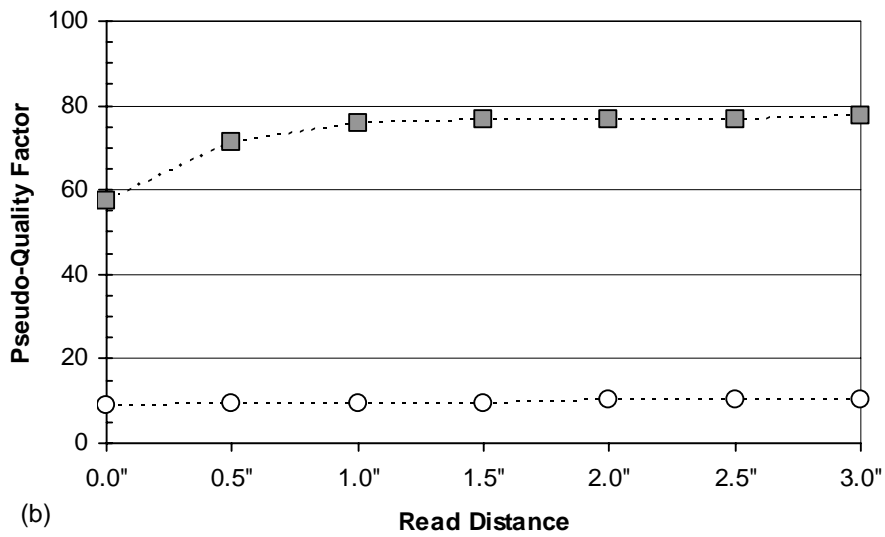
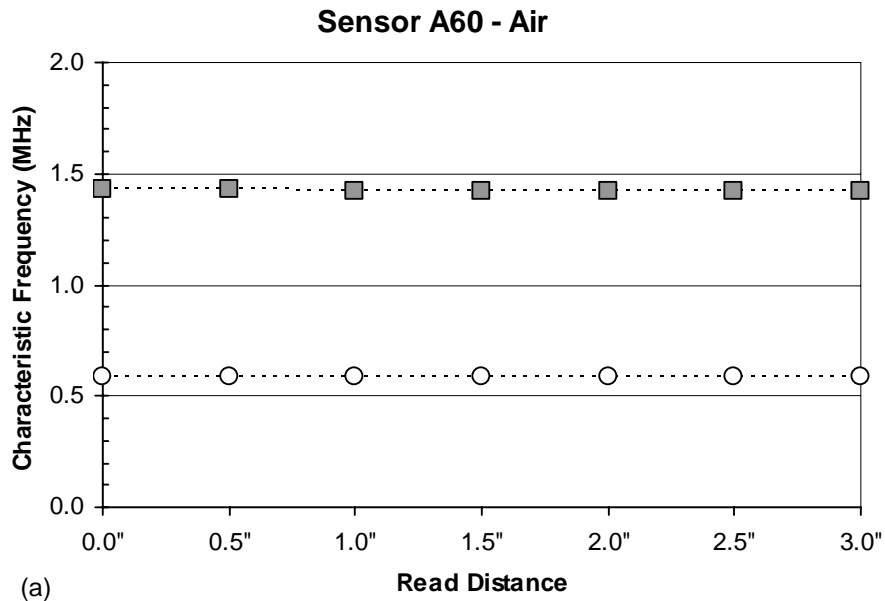


Figure F-33 Effect of Read Distance on Response of Sensor A60 with an Intact Sensing Wire for Readings in Air

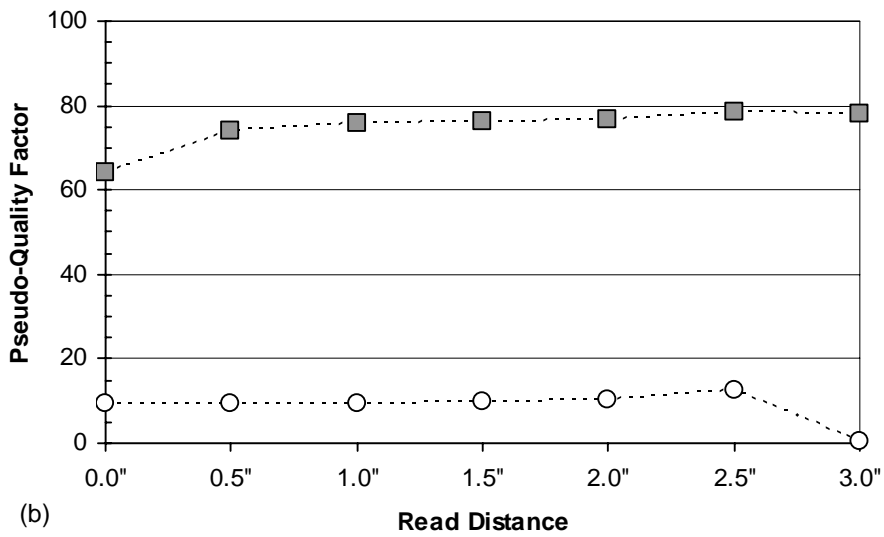
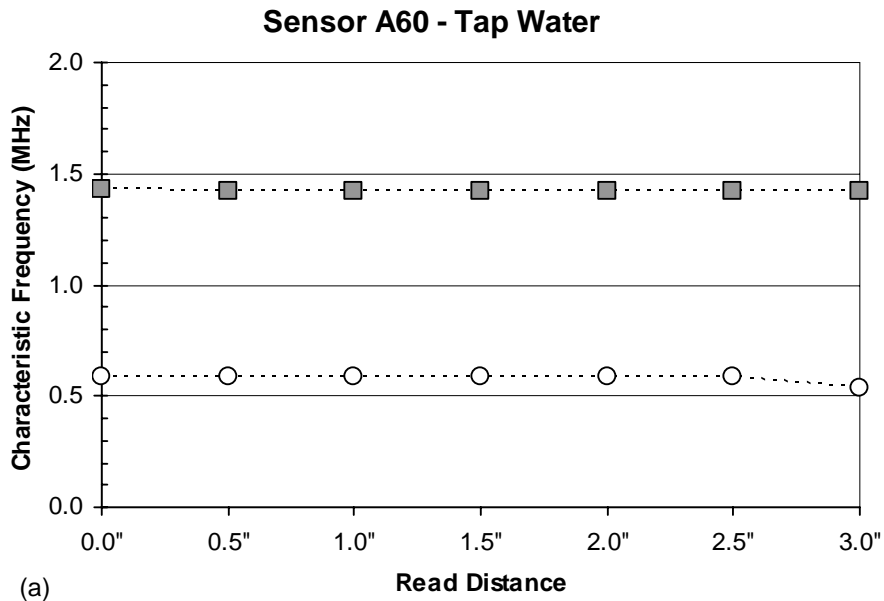


Figure F-34 Effect of Read Distance on Response of Sensor A60 with an Intact Sensing Wire for Readings in Tap Water

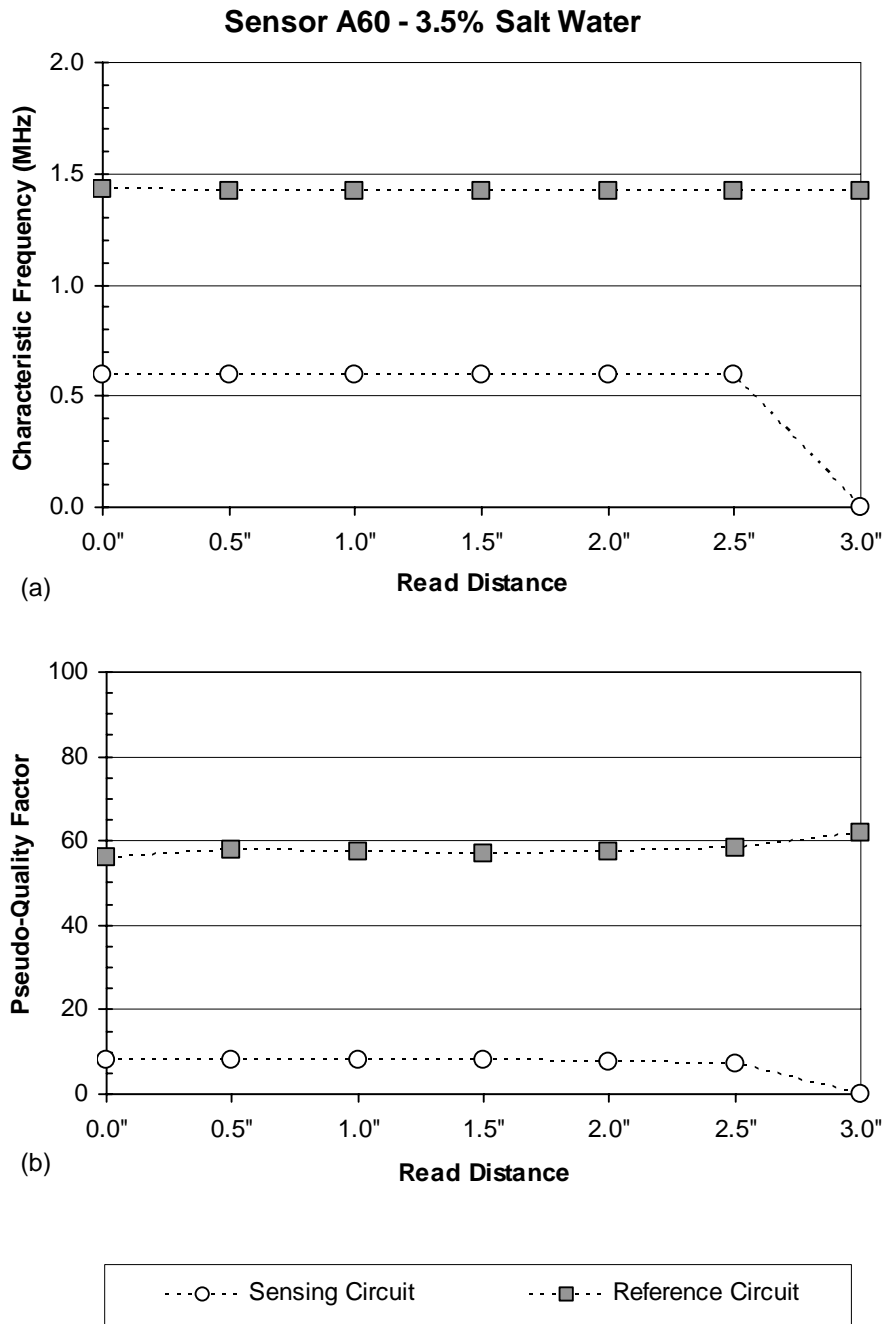


Figure F-35 Effect of Read Distance on Response of Sensor A60 with an Intact Sensing Wire for Readings in 3.5% Salt Water

Table F-51 Variation of Measured Response of Sensor A60 with Intact Sensing Wire for Sensing Circuit with Varying Read Distance

Environment	Number of Readings	Characteristic Frequency		Pseudo-Quality Factor		Phase Dip	
		Mean (MHz)	Coef. of Variation	Mean	Coef. of Variation	Mean (°)	Coef. of Variation
Air	7	0.59	0.2%	9.8	5.4%	2.6	138.3%
Tap Water*	6	0.59	0.1%	10.2	12.5%	2.1	127.7%
3.5% Salt Water*	6	0.60	0.2%	7.9	5.7%	1.9	129.7%

* Data from read distance of 3 in. were not included

Table F-52 Variation of Measured Response of Sensor A60 with Intact Sensing Wire for Reference Circuit with Varying Read Distance

Environment	Number of Readings	Characteristic Frequency		Pseudo-Quality Factor		Phase Dip	
		Mean (MHz)	Coef. of Variation	Mean	Coef. of Variation	Mean (°)	Coef. of Variation
Air	7	1.42	0.2%	73.0	9.8%	24.5	129.0%
Tap Water	7	1.42	0.1%	74.7	6.6%	18.1	132.7%
3.5% Salt Water	7	1.42	0.2%	58.0	3.1%	14.5	139.1%

F.5.2.2 Cut Steel Sensing Wire

The effect of read distance on sensor A60 with a cut steel sensing wire is shown in Table F-53. Interrogation results are shown in the table for readings in air. Again, phase dips are substantially reduced with increasing read distance. Characteristic frequencies do not change and the variations in pseudo-quality

factors are small. The characteristic frequencies and pseudo-quality factors are plotted versus read distance in Fig. F-36 for interrogations in air, Fig. F-37 for tap water, and Fig. F-38 for 3.5% salt water. A statistical summary of the characteristic frequency, phase dip, and pseudo-quality factor for the reference circuit is provided in Table F-54. The same information for the sensing circuit is provided in Table F-55. The sensing circuit only responded in the 3.5% salt water environment. Coefficients of variation are very small for characteristic frequencies and very large for phase dips.

While the coefficients of variation for pseudo-quality factors are small, ranging from 2.7% to 4.9% for the reference circuit, the values change slightly with increasing conductivity of the surrounding environment. In 3.5% salt water, the reference circuit mean pseudo-quality factor is 56.4 for a cut steel sensing wire, while it is 58.0 for an intact wire. The sensing circuit mean pseudo-quality factor is 4.3 for a cut steel sensing wire and 7.9 for an intact wire. Therefore, the pseudo-quality factor may give a reliable indication of the state of the steel sensing wire in the presence of a conductive environment.

Table F-53 Effect of Read Distance on Sensor A60 with Cut Sensing Wire

Read Distance (in.)	Sensing Circuit			Reference Circuit		
	Char. Freq. (MHz)	Phase Dip (°)	Pseudo- Quality Factor	Char. Freq. (MHz)	Phase Dip (°)	Pseudo- Quality Factor
0.0	-	-	-	1.42	79.4	68.3
0.5	-	-	-	1.42	38.7	74.4
1.0	-	-	-	1.42	17.8	77.1
1.5	-	-	-	1.42	8.1	77.7
2.0	-	-	-	1.42	4.1	78.3
2.5	-	-	-	1.42	2.0	78.9
3.0	-	-	-	1.42	1.1	77.4

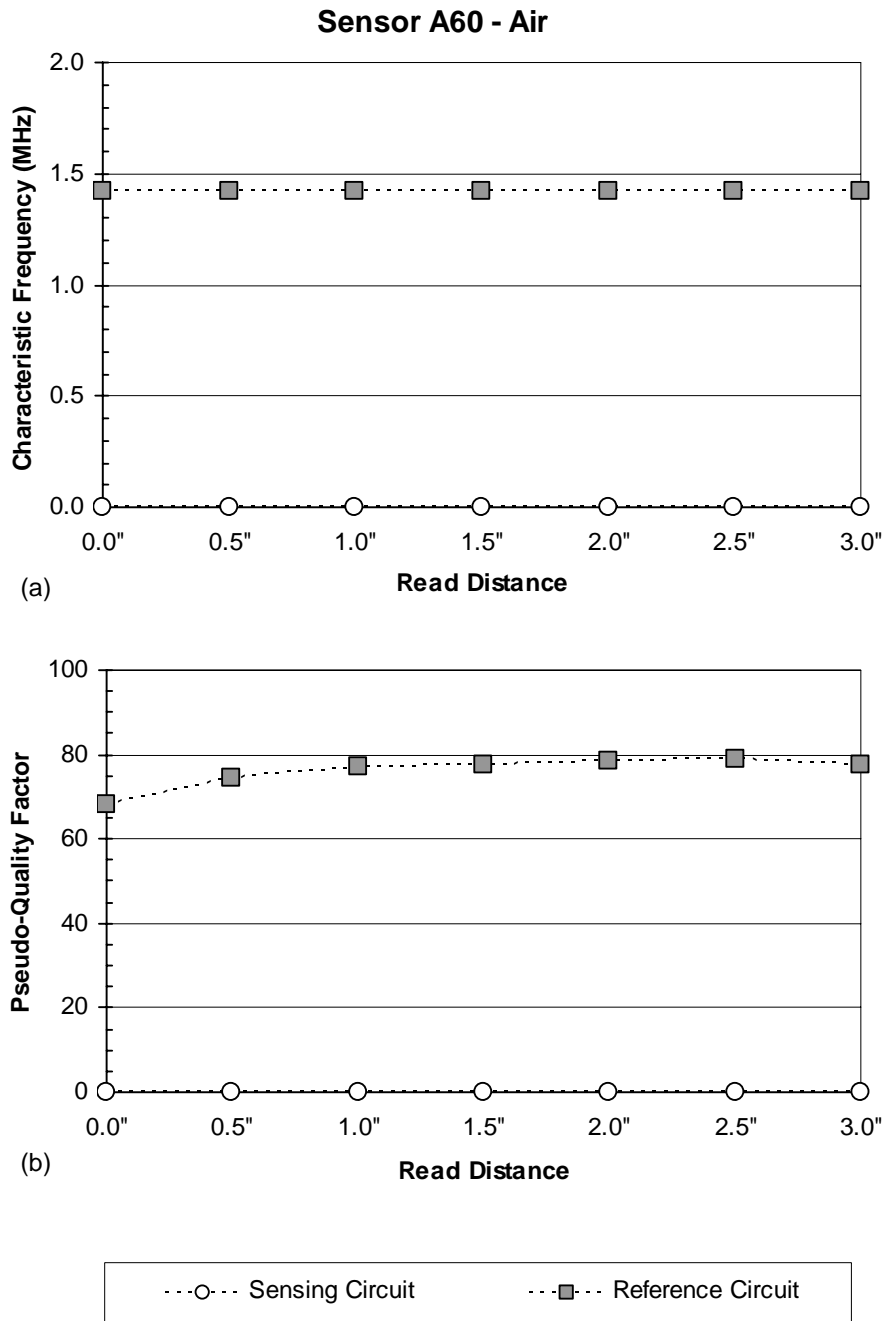


Figure F-36 Effect of Read Distance on Response of Sensor A60 with a Cut Sensing Wire for Readings in Air

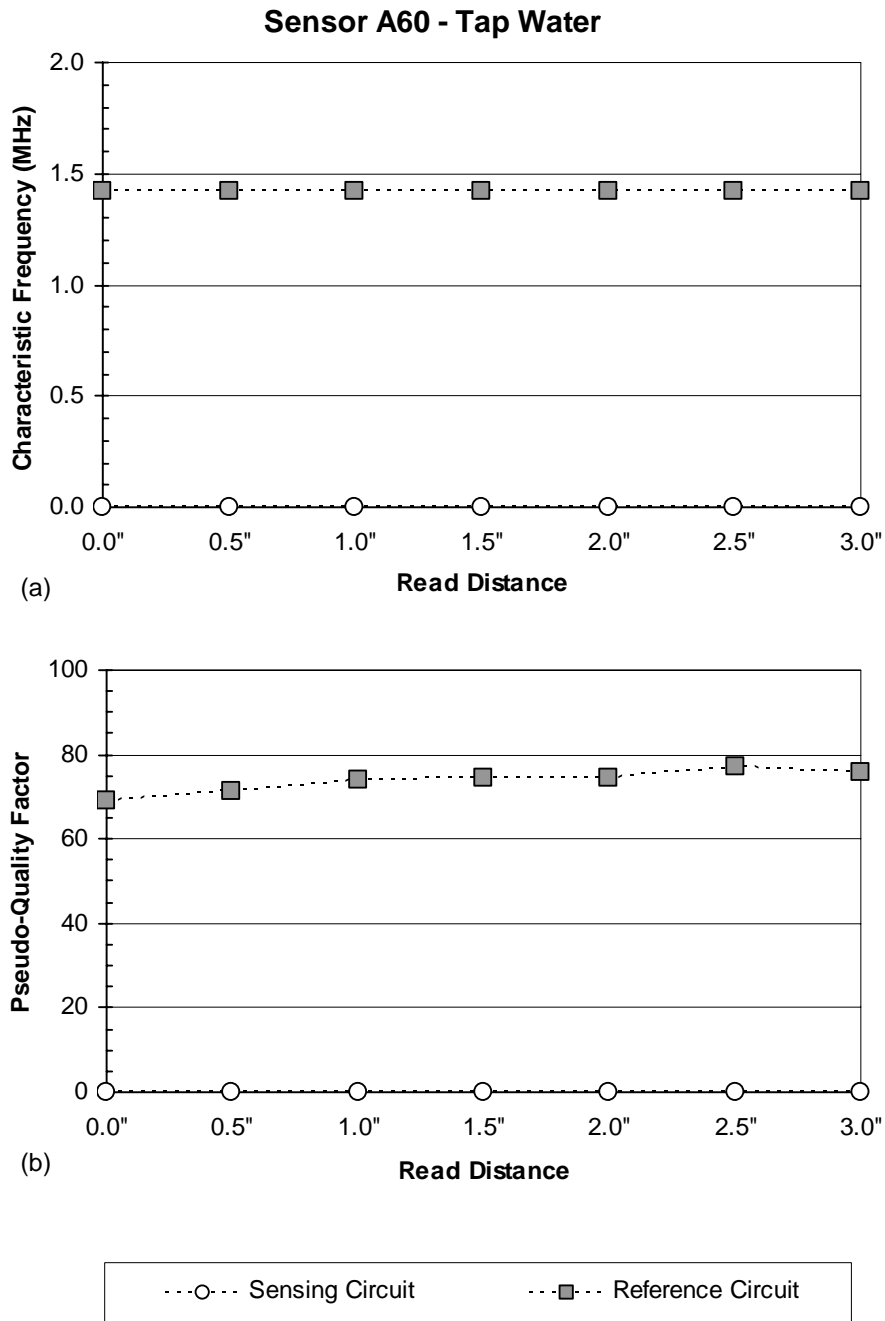
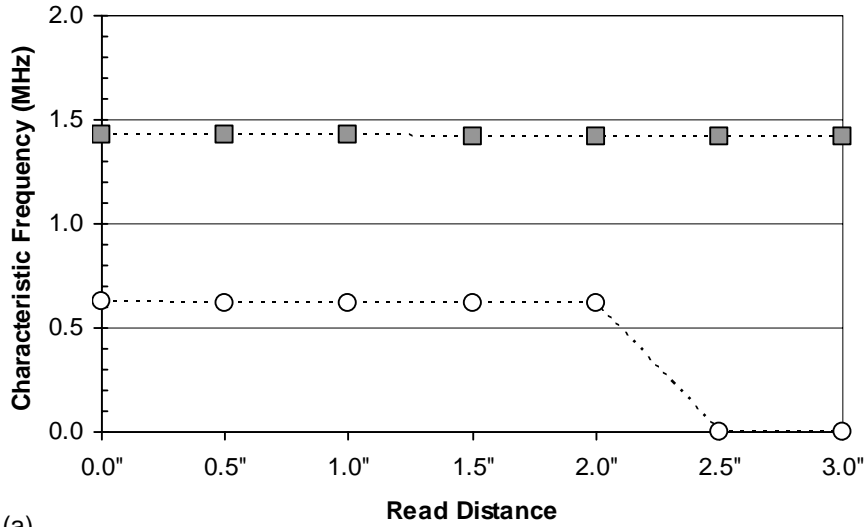
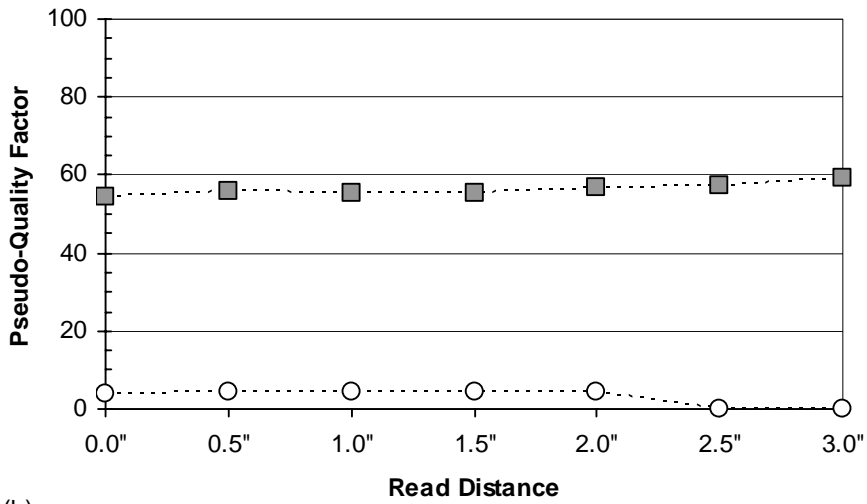


Figure F-37 Effect of Read Distance on Response of Sensor A60 with a Cut Sensing Wire for Readings in Tap Water

Sensor A60 - 3.5% Salt Water



(a)



(b)



Figure F-38 Effect of Read Distance on Response of Sensor A60 with a Cut Sensing Wire for Readings in 3.5% Salt Water

**Table F-54 Variation of Measured Response of Sensor A60 with Cut Sensing
Wire for Reference Circuit with Varying Read Distance**

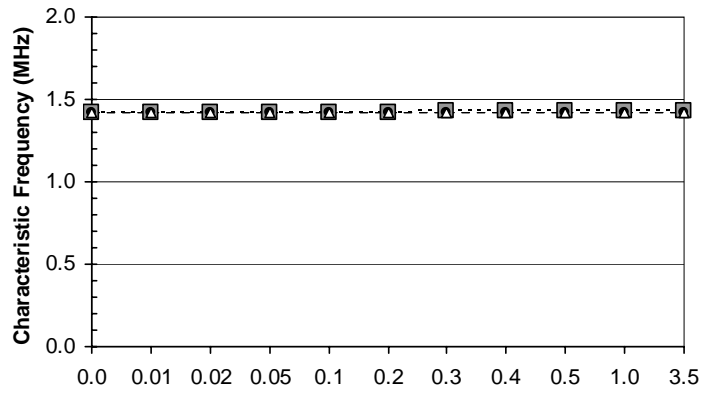
Environment	Number of Readings	Characteristic Frequency		Pseudo-Quality Factor		Phase Dip	
		Mean (MHz)	Coef. of Variation	Mean	Coef. of Variation	Mean (°)	Coef. of Variation
Air	7	1.42	0.2%	76.0	4.9%	21.6	133.0%
Tap Water	7	1.42	0.1%	73.7	3.7%	14.4	135.6%
3.5% Salt Water	7	1.42	0.2%	56.4	2.7%	13.8	139.7%

**Table F-55 Variation of Measured Response of Sensor A60 with Cut Sensing
Wire for Sensing Circuit with Varying Read Distance**

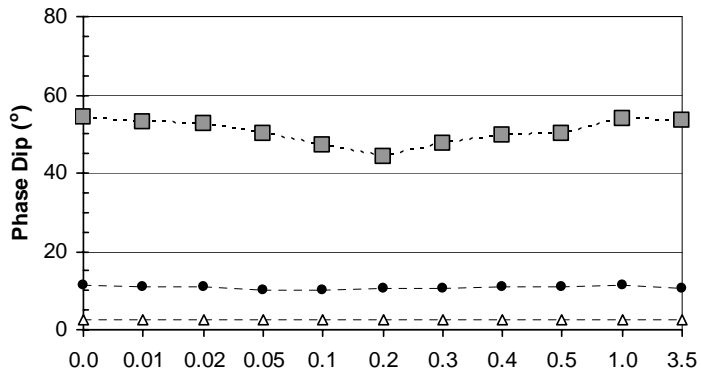
Environment	Number of Readings	Characteristic Frequency		Pseudo-Quality Factor		Phase Dip	
		Mean (MHz)	Coef. of Variation	Mean	Coef. of Variation	Mean (°)	Coef. of Variation
3.5% Salt Water	5	0.62	0.4%	4.3	4.7%	1.1	110.8%

Plots of characteristic frequency, phase dip, and pseudo-quality factor versus salt water concentration are shown for three different read distances, 0.0 in., 1.0 in., and 2.0 in. in Fig. F-39 for the reference circuit and Fig. F-40 for the sensing circuit. When the sensing circuit response is present ($\geq 0.5\%$ salt water), the pseudo-quality factors of the sensing circuit and the reference circuit can be compared with values for both intact and cut wire. This information can be used to determine the state of the steel sensing wire for embedded sensors. With an intact steel sensing wire, the pseudo-quality factor of the sensing circuit should always be greater than 7. When the steel sensing wire is broken (or cut), the state of the wire can be determined two ways: (1) if the sensing circuit phase dip is not

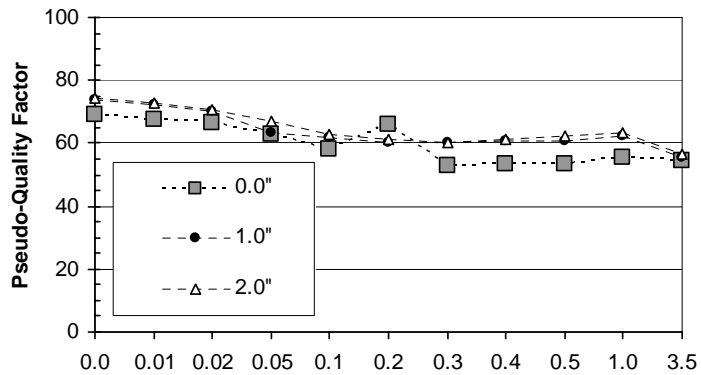
present, then the wire is broken, or (2) if the sensing circuit phase dip is present and the pseudo-quality factor of the sensing circuit is less than 5, then the wire is broken.



(a) Salt Concentration (%)



(b) Salt Concentration (%)



(c) Salt Concentration (%)

Figure F-39 Sensor A60 Reference Circuit Response for a Cut Sensing Wire with Increasing Concentration of Salt Water at Three Read Distances

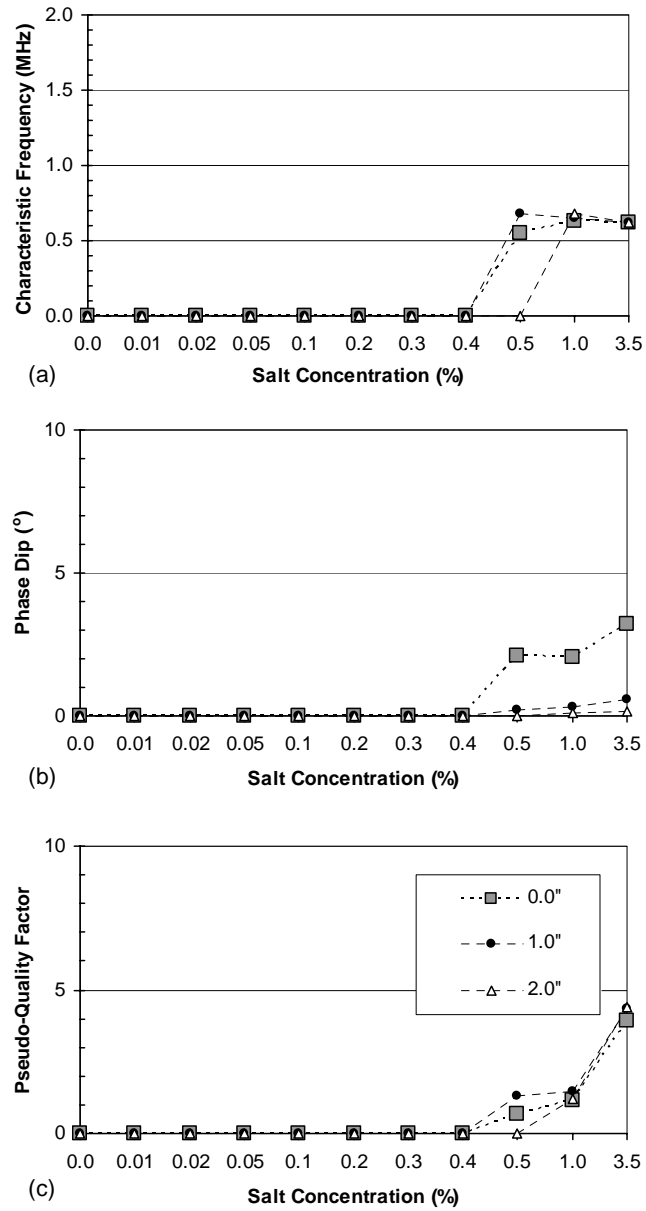


Figure F-40 Sensor A60 Sensing Circuit Response for a Cut Sensing Wire with Increasing Concentration of Salt Water at Three Read Distances

F.5.3 Reader Configuration

In order to assess the sensitivity of phase response to reader configuration, sensor A60 was interrogated using seven different reader coils. The Solartron Impedance Analyzer was used for all of the interrogations. The sensor was interrogated in air at read distances of 0.0 in., 1.0 in., 2.0 in., and 3.0 in. Table F-10 gives the details for each reader coil.

Results from interrogations of sensor A60 with an intact steel sensing wire at a read distance of 1.0 in. are shown in Table F-56 for all of the reader configurations used in this study. Table F-57 shows the same results for sensor A60 with a cut steel sensing wire. Despite the large variations in phase dip with different reader coils, the characteristic frequencies remain nearly constant and the variation in pseudo-quality factors is small. The maximum read distance for sensor A60 with an intact steel sensing wire is shown for each reader configuration in Table F-58. Maximum read distance is defined as the read distance at which the phase dip is at least 0.1° for interrogations in air. As shown in Chapter 3, reader coils 4t05, 4t20, and 6t10 provide the flattest baseline response and also the best maximum read distance. When reader coils are connected to the impedance analyzer with a cable, reader coil 4t05 provides the best response. Statistical summaries that show the variation in characteristic frequency, pseudo-quality factor, and phase dip for all reader configurations used in this study are provided in Table F-59 for the sensing circuit with an intact sensing wire, Table F-60 for the reference circuit with an intact sensing wire, and Table F-61 for the reference circuit with a cut sensing wire.

**Table F-56 Effect of Reader Configuration on Sensor A60 with Intact Sensing
Wire for a 1-in. Read Distance**

Reader Coil	Sensing Circuit			Reference Circuit		
	Char. Freq. (MHz)	Phase Dip (°)	Pseudo-Quality Factor	Char. Freq. (MHz)	Phase Dip (°)	Pseudo-Quality Factor
4t01-24	0.59	1.4	10.0	1.42	14.0	76.4
4t01-18	0.59	1.5	8.9	1.42	15.1	76.1
4t05	0.59	2.1	9.6	1.42	20.6	75.6
4t05 w/ cable	0.59	2.0	9.6	1.42	20.5	75.6
4t20	0.59	2.1	9.5	1.42	21.1	75.6
6t10	0.59	1.5	9.7	1.42	15.7	76.2
3s	0.59	2.4	9.8	1.42	22.5	74.6

**Table F-57 Effect of Reader Configuration on Sensor A60 with Cut Sensing
Wire for a 1-in. Read Distance**

Reader Coil	Sensing Circuit			Reference Circuit		
	Char. Freq. (MHz)	Phase Dip (°)	Pseudo-Quality Factor	Char. Freq. (MHz)	Phase Dip (°)	Pseudo-Quality Factor
4t01-24	-	-	-	1.42	12.0	76.6
4t01-18	-	-	-	1.42	12.8	77.1
4t05	-	-	-	1.42	17.4	77.4
4t05 w/ cable	-	-	-	1.42	17.8	77.1
4t20	-	-	-	1.42	18.0	77.1
6t10	-	-	-	1.42	13.2	77.6
3s	-	-	-	1.42	18.6	76.7

Table F-58 Maximum Read Distances for Sensor A60 with Intact Sensing Wire

Reader Coil	Maximum Read Distance (in.)
4t01-24	2
4t01-18	2
4t05	3
4t05 w/ cable	3
4t20	3
6t10	3
3s	2

Table F-59 Variation of Measured Response of Sensor A60 with Intact Sensing Wire for Sensing Circuit with Different Reader Coils

Read Distance (in.)	Number of Readings	Characteristic Frequency		Pseudo-Quality Factor		Phase Dip	
		Mean (MHz)	Coef. of Variation	Mean	Coef. of Variation	Mean (°)	Coef. of Variation
0.0	7	0.59	0.6%	9.1	3.9%	10.7	67.7%
1.0	7	0.59	0.2%	9.6	3.3%	1.9	21.7%
2.0	7	0.59	0.2%	10.7	8.8%	0.4	18.3%
3.0	4	0.59	0.3%	10.7	18.0%	0.1	18.5%
All	25	0.59	0.5%	9.9	11.2%	3.7	366.5%

**Table F-60 Variation of Measured Response of Sensor A60 with Intact Sensing
Wire for Reference Circuit with Different Reader Coils**

Read Distance (in.)	Number of Readings	Characteristic Frequency		Pseudo-Quality Factor		Phase Dip	
		Mean (MHz)	Coef. of Variation	Mean	Coef. of Variation	Mean (°)	Coef. of Variation
0.0	7	1.43	0.7%	58.2	21.4%	77.7	36.4%
1.0	7	1.42	0.0%	75.7	0.8%	18.5	18.6%
2.0	7	1.42	0.0%	76.7	1.4%	4.3	21.8%
3.0	4	1.42	0.0%	77.5	1.9%	1.5	25.8%
All	25	1.43	0.5%	71.4	14.7%	28.4	123.6%

**Table F-61 Variation of Measured Response of Sensor A60 with Cut Sensing
Wire for Reference Circuit with Different Reader Coils**

Read Distance (in.)	Number of Readings	Characteristic Frequency		Pseudo-Quality Factor		Phase Dip	
		Mean (MHz)	Coef. of Variation	Mean	Coef. of Variation	Mean (°)	Coef. of Variation
0.0	7	1.43	0.6%	64.6	19.3%	72.1	38.4%
1.0	7	1.42	0.0%	77.1	0.5%	15.7	18.3%
2.0	7	1.42	0.0%	77.5	1.4%	3.7	22.4%
3.0	4	1.42	0.0%	77.7	1.2%	1.3	24.2%
All	25	1.42	0.4%	73.8	11.6%	25.8	127.9%

Coefficients of variation for characteristic frequencies are very small for readings at all read distances with all reader coils, ranging from 0.0% to 0.7%. Therefore, characteristic frequency response of sensors is very reliable with varying read distances and with different reader configurations. Pseudo-quality factors also give small coefficients of variation for varying read distances and different reader coils. Therefore, especially if the read distance is known, the calculation of pseudo-quality factors provides reliable values for use in

determining the state of the steel sensing wire. Because phase dips are severely affected by both read distance and reader coil, the coefficients of variation in phase dips are large. Although the amplitude of the phase dip must be determined to calculate the pseudo-quality factor for a sensor reading, phase dip alone is not a reliable number for evaluating the state of the sensor.

APPENDIX G

Concrete Prism Sensor Monitoring Results

Results from monitoring concrete prisms with embedded sensors are presented in this appendix. Plots of characteristic frequencies and pseudo-quality factors at each interrogation are provided through 4 April 2005 for each prism. In addition, Table G-1 provides the change in moisture content for each prism at interrogation times. The relative change in moisture content was determined by weighing the prisms at the end of each stage of the cycle. Initial weights are given in Table G-2.

Table G-1 Change in Moisture Content of Concrete Prisms with Time

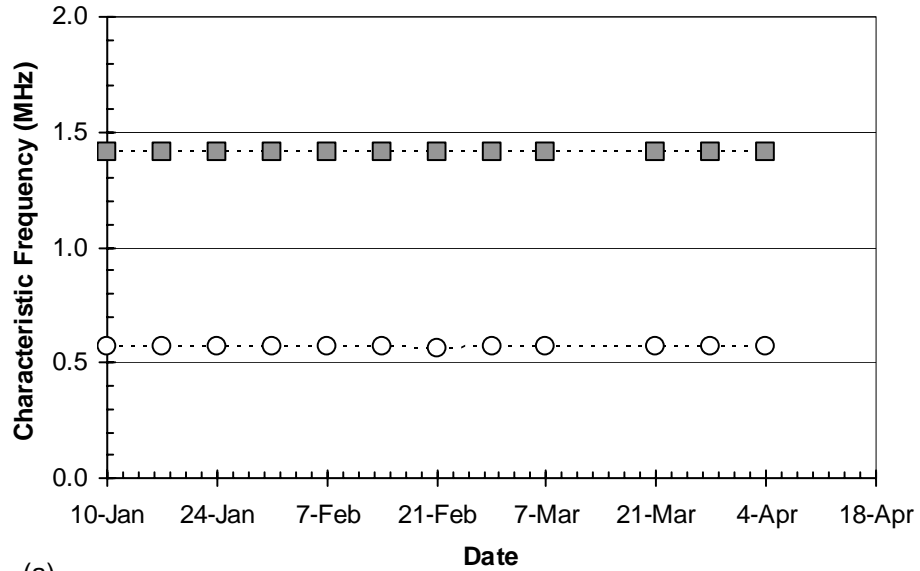
Prism	17-Jan	24-Jan	31-Jan	7-Feb	14-Feb	21-Feb	28-Feb	7-Mar	21-Mar	28-Mar	4-Apr
A21	-0.5%	-0.2%	-0.2%	-0.1%	-0.1%	0.0%	-0.1%	0.0%	-0.1%	0.0%	-0.1%
A22	-0.6%	-0.3%	-0.1%	-0.1%	-0.1%	-0.1%	0.0%	0.0%	-0.1%	-0.1%	0.0%
A23*	1.7%	-5.3%	5.7%	-5.3%	5.7%	-5.2%	5.5%	-5.0%	5.4%	-5.1%	5.3%
A24*	1.7%	-5.4%	5.6%	-5.4%	5.8%	-5.4%	5.6%	-5.2%	5.6%	-5.2%	5.4%
A25	1.7%	-5.8%	6.2%	-5.7%	6.0%	-5.5%	5.8%	-5.3%	5.7%	-5.1%	5.3%
A26	1.8%	-5.8%	6.2%	-5.6%	6.0%	-5.5%	5.8%	-5.3%	5.7%	-5.2%	5.4%
A27	1.8%	-1.5%	1.4%	-1.2%	1.2%	-1.1%	1.1%	-1.0%	1.1%	-1.0%	1.1%
A28	1.8%	-1.4%	1.4%	-1.2%	1.2%	-1.1%	1.1%	-1.0%	1.1%	-1.0%	1.0%
A29	1.7%	-1.3%	1.2%	-1.1%	1.1%	-0.9%	0.9%	-0.8%	0.9%	-	-
A30	1.7%	-1.2%	1.2%	-1.1%	1.0%	-0.9%	0.9%	-0.8%	0.9%	-0.9%	-
B19	-0.5%	-4.0%	0.4%	-0.4%	0.4%	-0.4%	0.4%	-0.4%	0.5%	-0.4%	0.3%
B20	-0.6%	0.0%	-0.3%	0.1%	-0.2%	0.0%	0.0%	0.0%	-0.1%	0.0%	0.0%
B21	-0.6%	-0.2%	-0.2%	-0.1%	-0.1%	0.0%	-0.1%	0.0%	-0.1%	0.0%	-0.1%
B22	-0.6%	-0.3%	-0.1%	-0.1%	-0.1%	-0.1%	0.0%	0.0%	-0.1%	0.0%	0.0%
B23*	1.4%	-5.1%	5.6%	-5.3%	5.7%	-5.2%	5.5%	-5.0%	5.5%	-5.2%	5.3%
B24*	1.5%	-5.3%	5.6%	-5.3%	5.7%	-5.3%	5.5%	-5.2%	5.5%	-5.1%	5.3%
B25	1.4%	-5.7%	6.2%	-5.7%	6.1%	-5.5%	5.9%	-5.4%	5.8%	-5.1%	5.3%
B26	1.5%	-5.7%	6.2%	-5.7%	6.0%	-5.4%	5.8%	-5.3%	5.7%	-5.0%	5.2%
B27	1.7%	-1.4%	1.4%	-1.2%	1.2%	-1.1%	1.1%	-1.0%	1.1%	-1.0%	1.0%
B28	1.6%	-1.4%	1.4%	-1.2%	1.2%	-1.1%	1.1%	-1.0%	1.1%	-1.0%	1.0%
B29	1.5%	-1.2%	1.3%	-1.1%	1.1%	-1.0%	1.0%	-0.9%	1.0%	-0.9%	0.9%
B30	1.6%	-1.2%	1.3%	-1.1%	1.1%	-1.0%	1.0%	-0.8%	1.0%	-0.9%	0.9%

* Moisture content change of prisms between oven cycles and freezer cycles was negligible

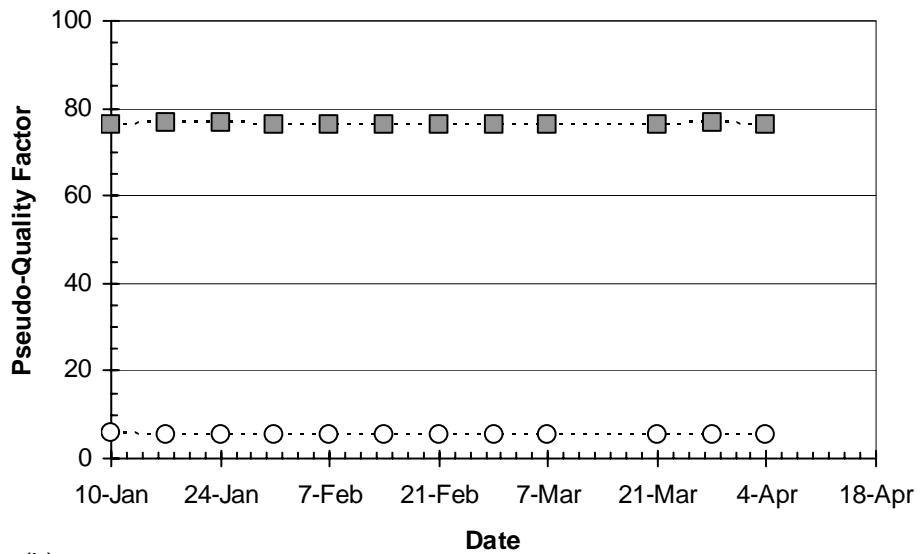
Table G-2 Initial Weight of Concrete Prisms

Prism	Initial Weight Measured 10 Jan 2005 (g)
A21	1412.1
A22	1409.1
A23	1428.3
A24	1455.2
A25	1411.9
A26	1384.6
A27	1368.4
A28	1414.2
A29	1416.9
A30	1417.6
B19	1416.3
B20	1396.5
B21	1406.2
B22	1418.5
B23	1420.6
B24	1414.7
B25	1405.2
B26	1415.9
B27	1422.0
B28	1417.5
B29	1405.2
B30	1422.1

Prism A21



(a)

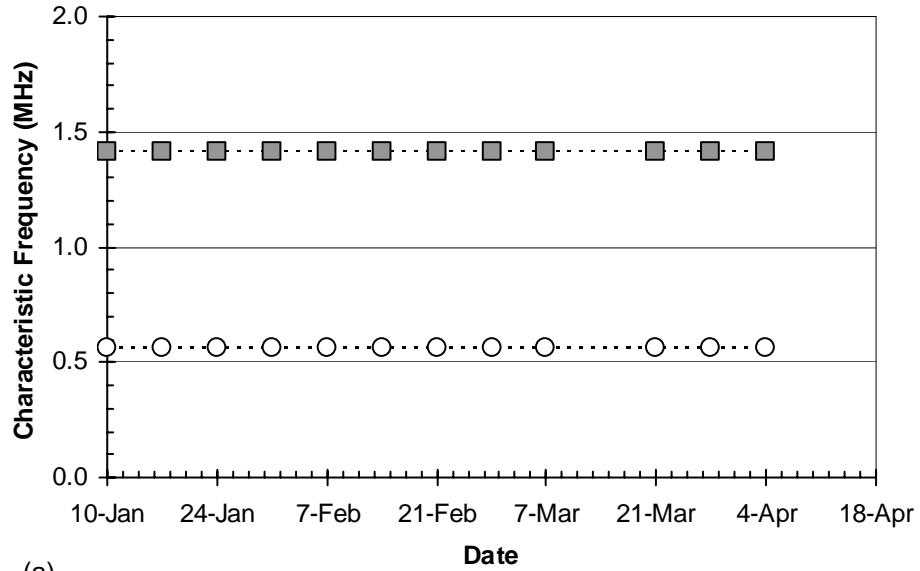


(b)

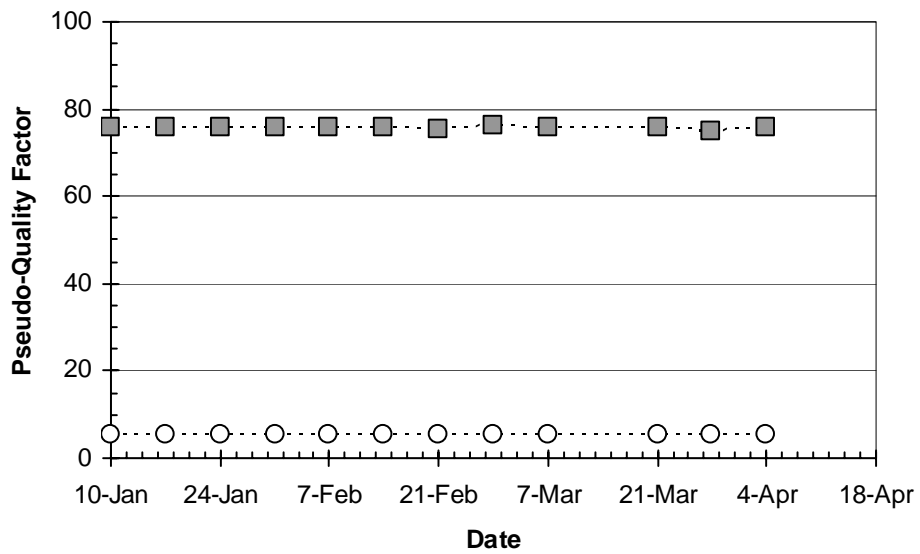


Figure G-1 Prism A21 Sensor Interrogation History

Prism A22



(a)

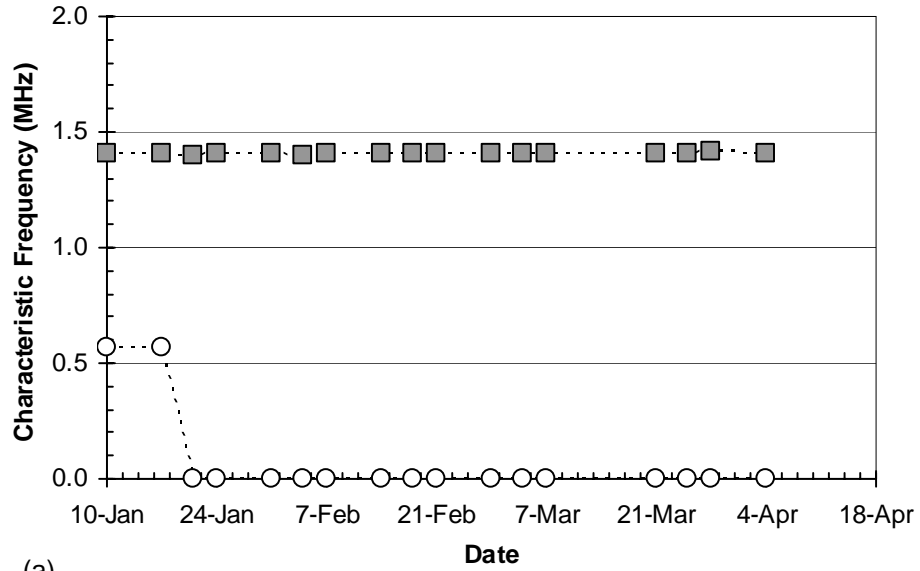


(b)

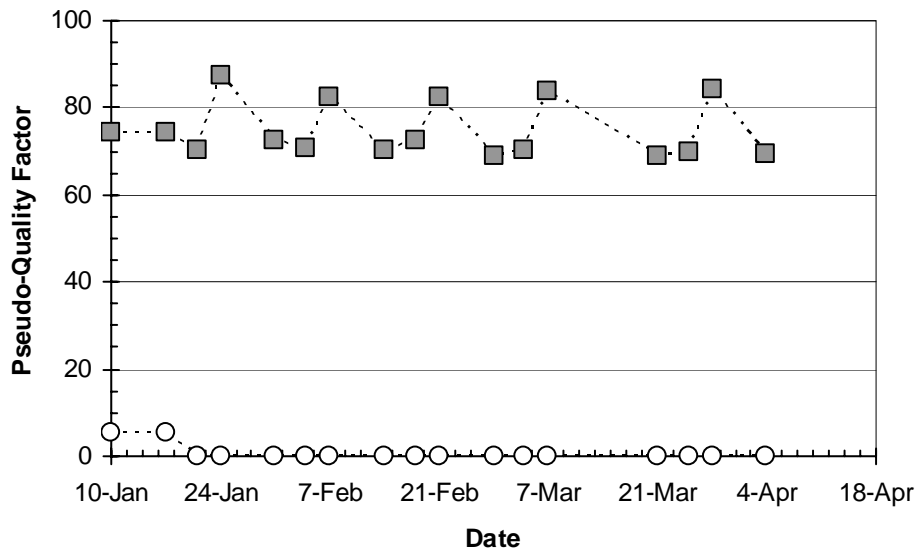


Figure G-2 Prism A22 Sensor Interrogation History

Prism A23



(a)

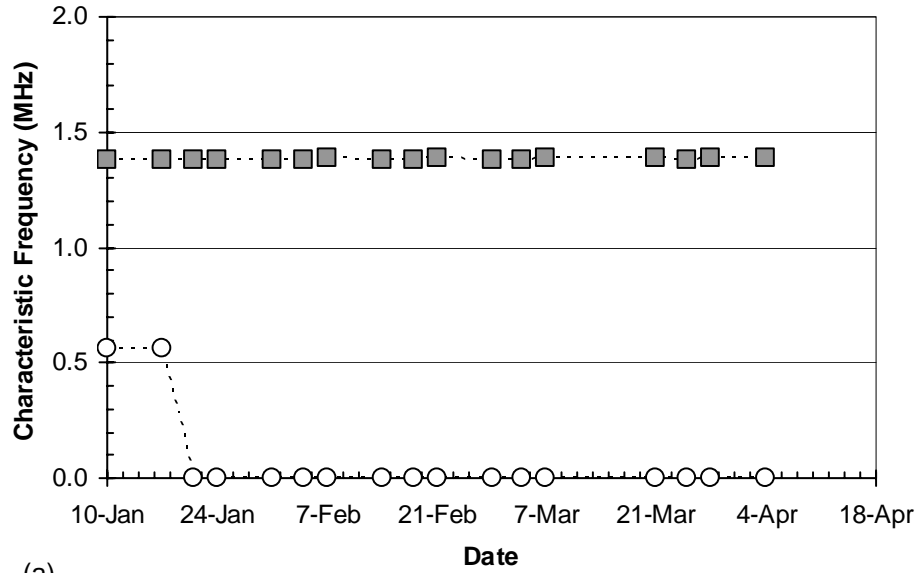


(b)

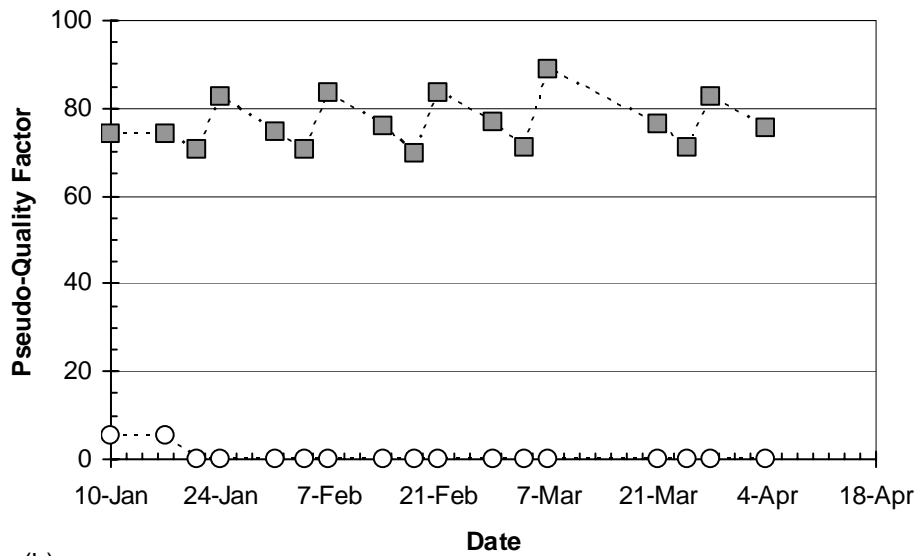


Figure G-3 Prism A23 Sensor Interrogation History

Prism A24



(a)

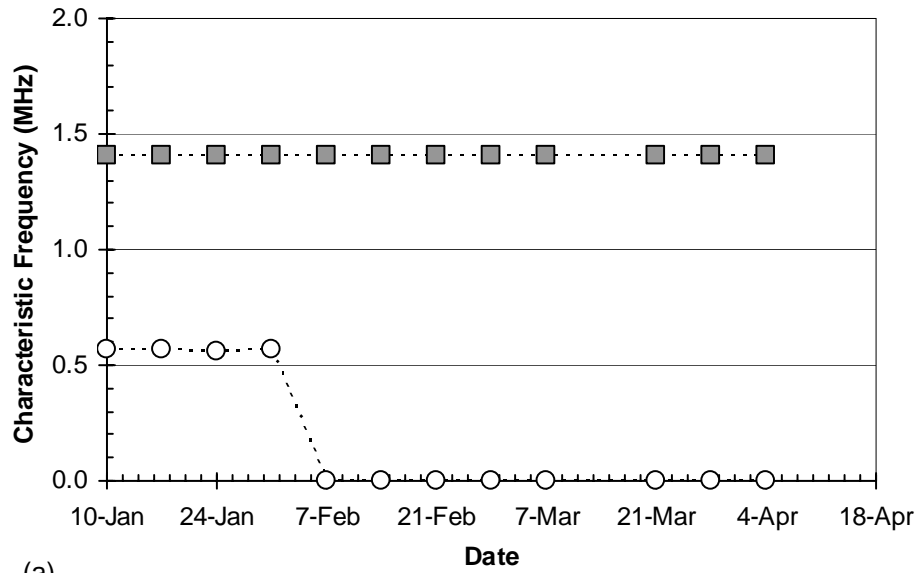


(b)

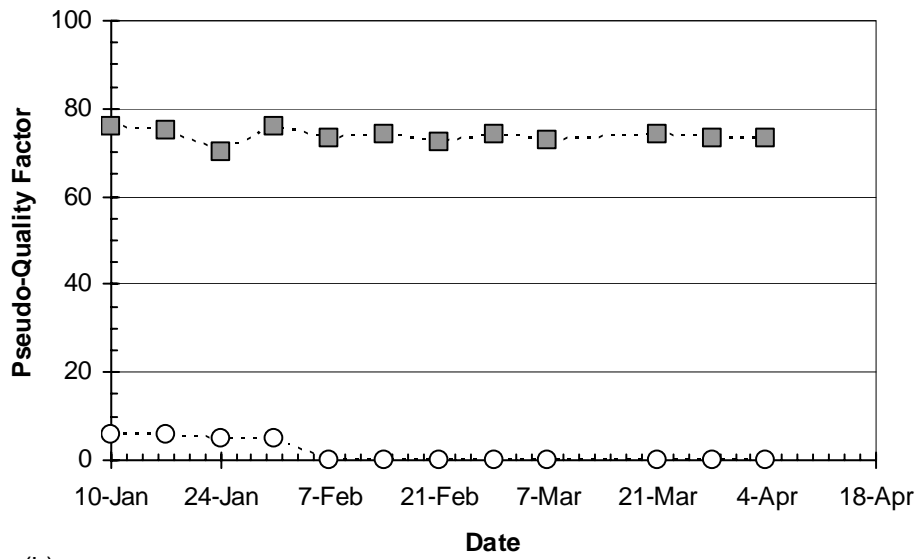


Figure G-4 Prism A24 Sensor Interrogation History

Prism A25



(a)

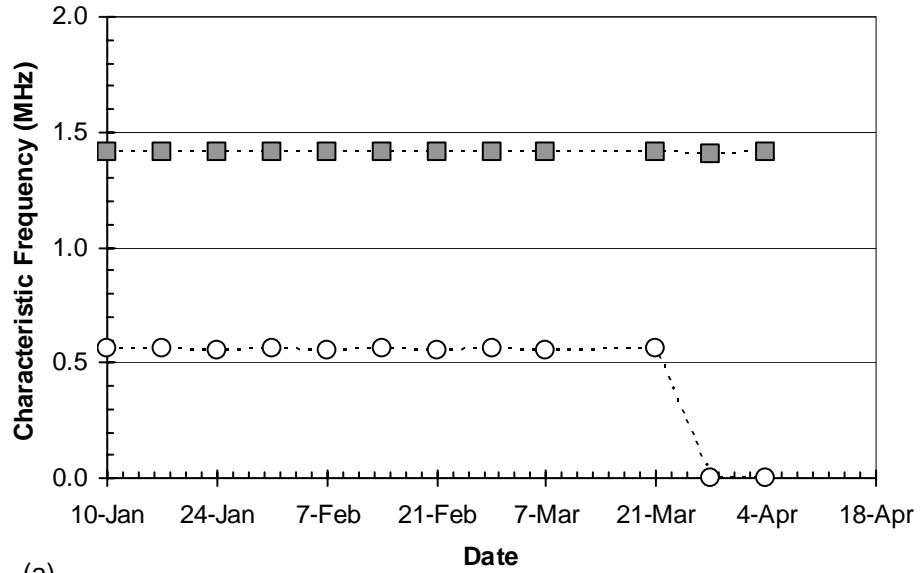


(b)

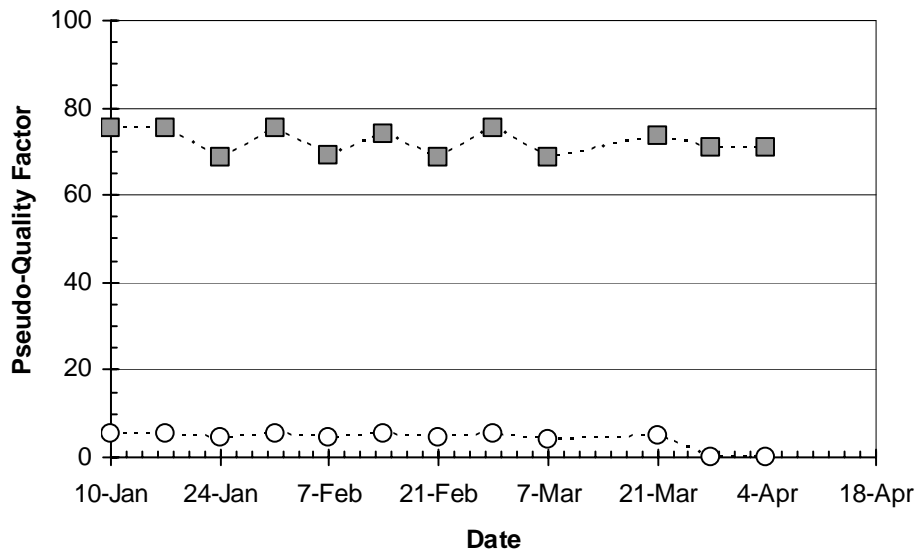


Figure G-5 Prism A25 Sensor Interrogation History

Prism A26



(a)

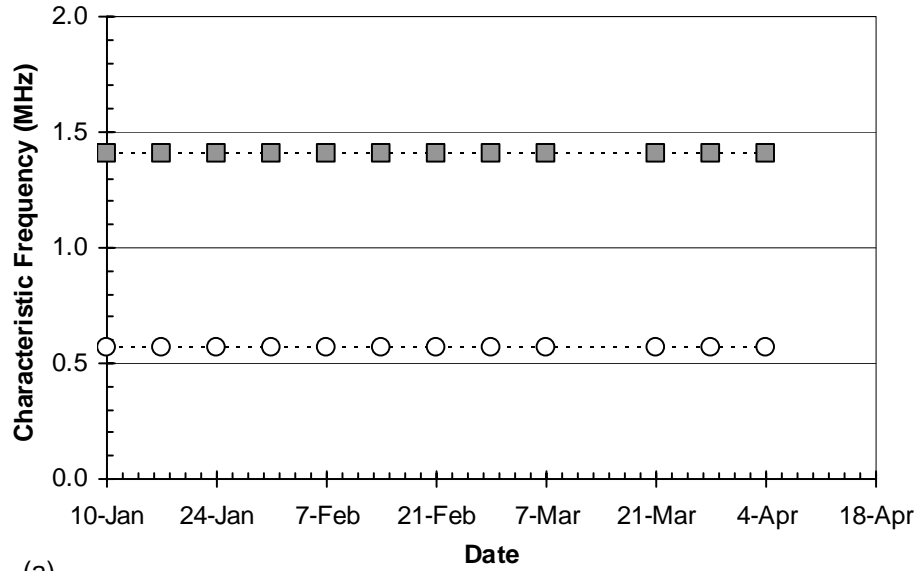


(b)

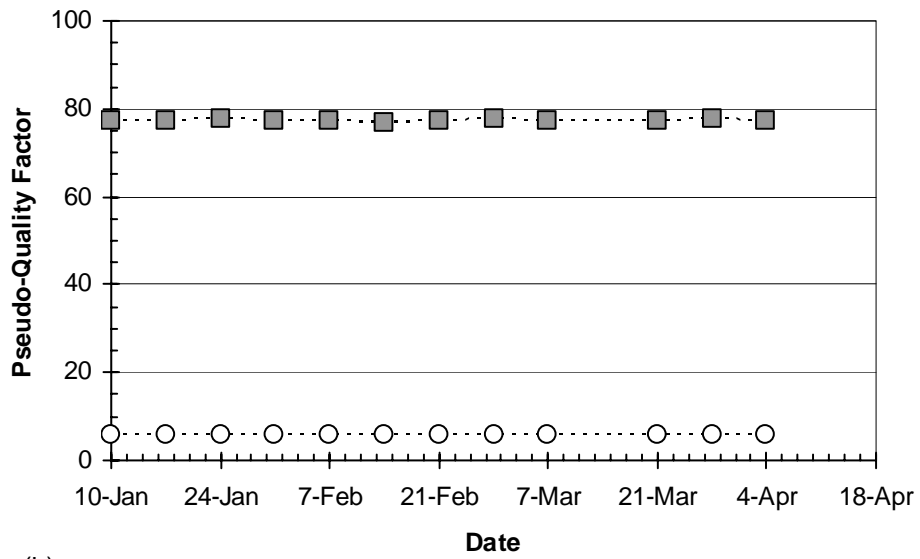


Figure G-6 Prism A26 Sensor Interrogation History

Prism A27



(a)

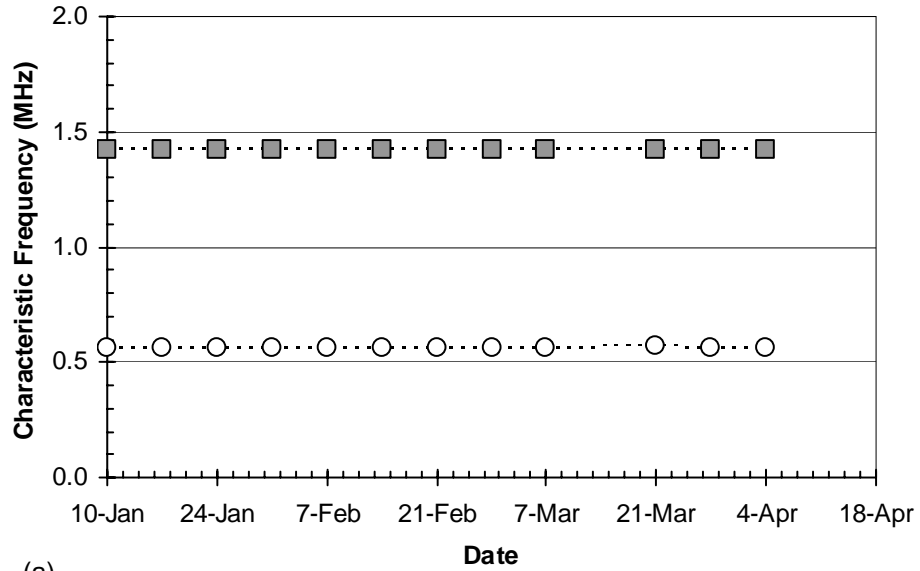


(b)

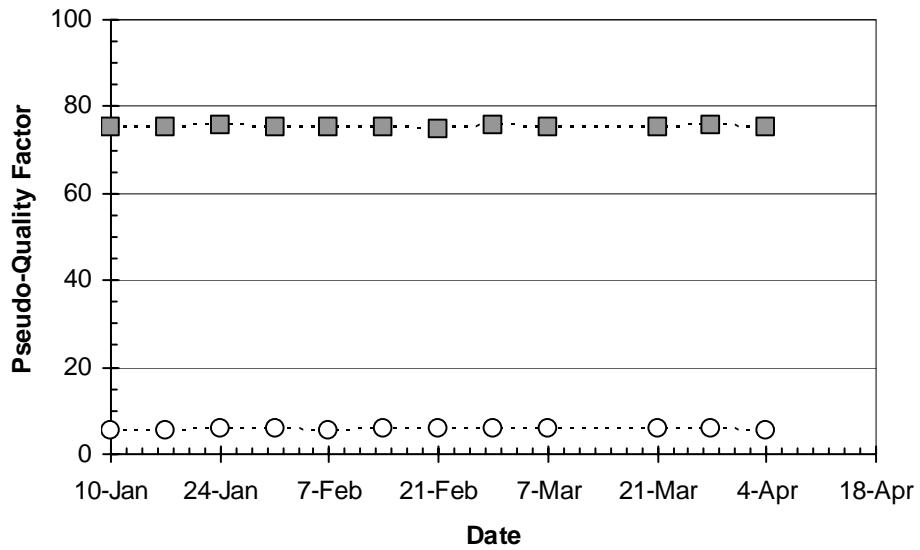


Figure G-7 Prism A27 Sensor Interrogation History

Prism A28



(a)

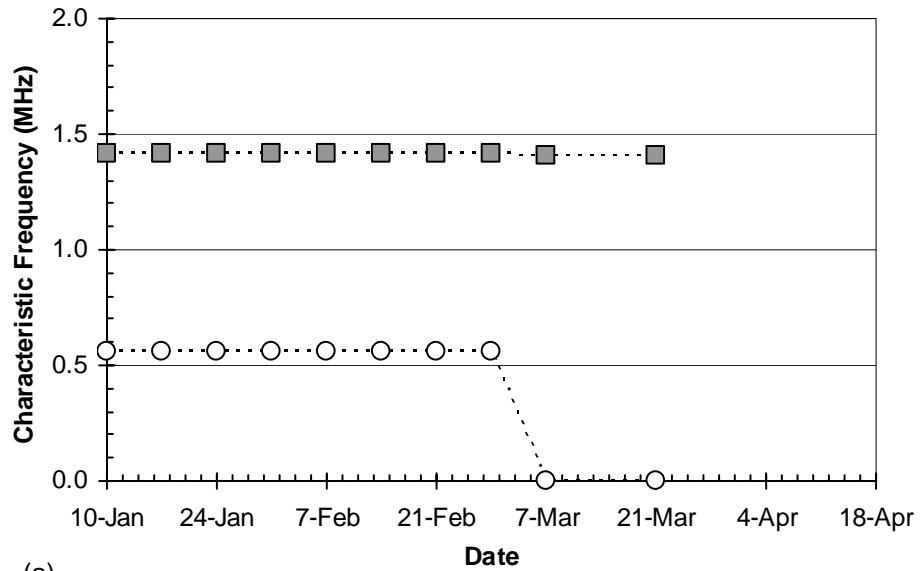


(b)

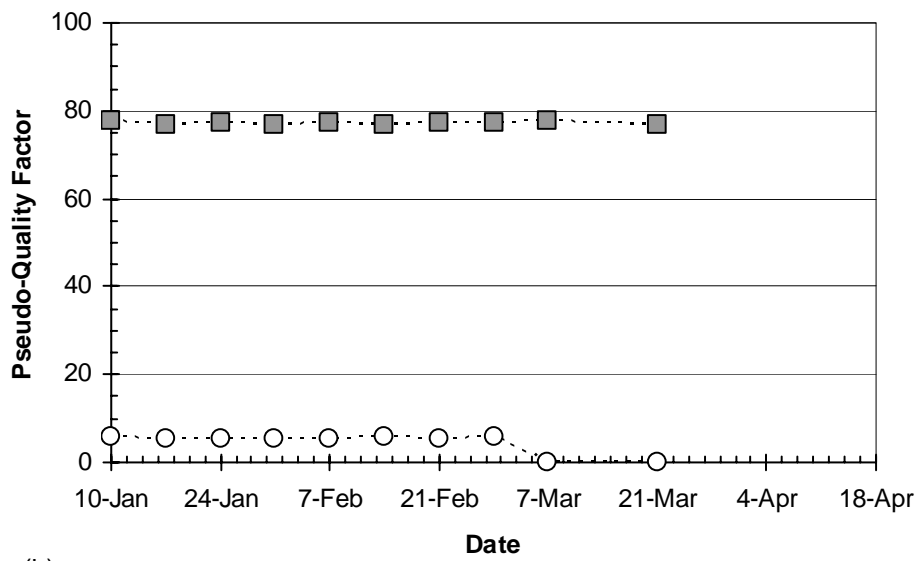


Figure G-8 Prism A28 Sensor Interrogation History

Prism A29



(a)

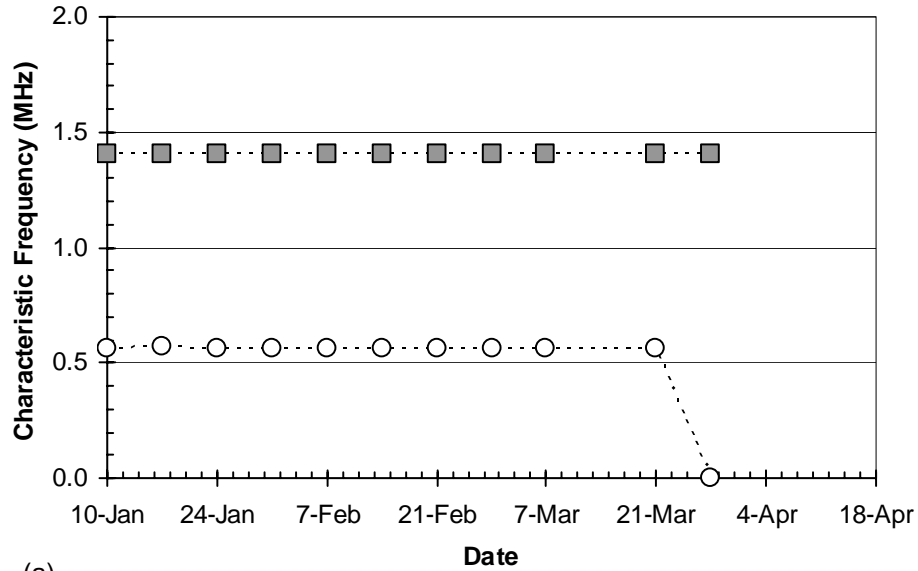


(b)

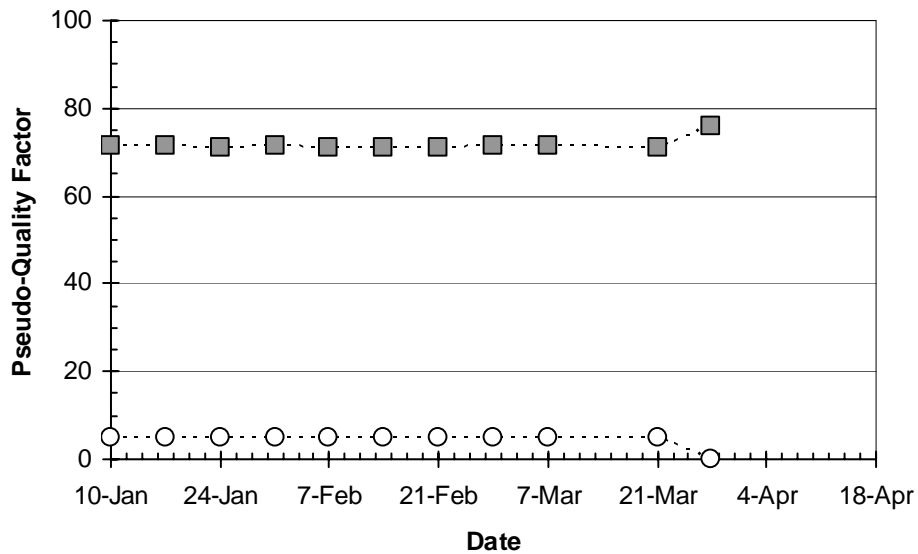


Figure G-9 Prism A29 Sensor Interrogation History

Prism A30



(a)

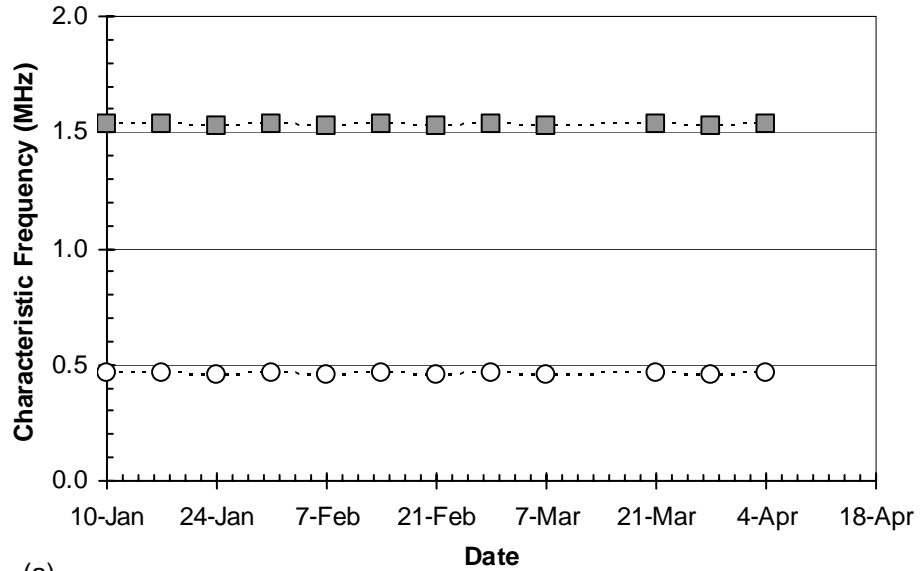


(b)

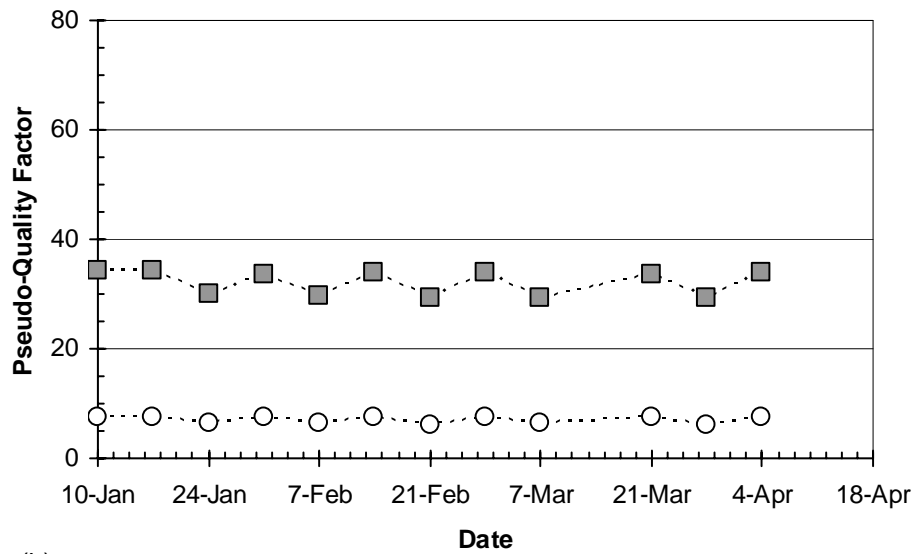


Figure G-10 Prism A30 Sensor Interrogation History

Prism B19



(a)



(b)

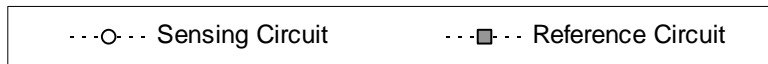
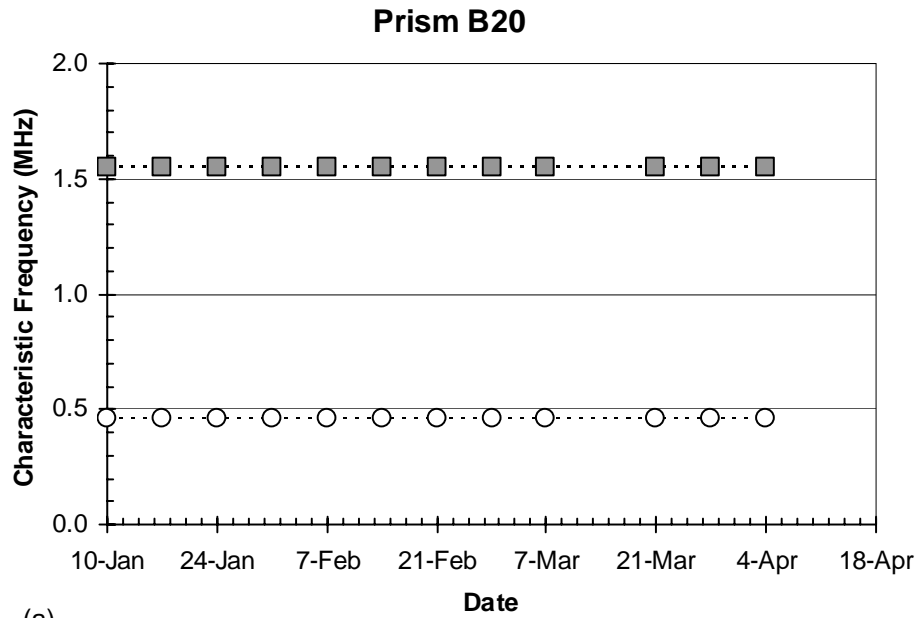
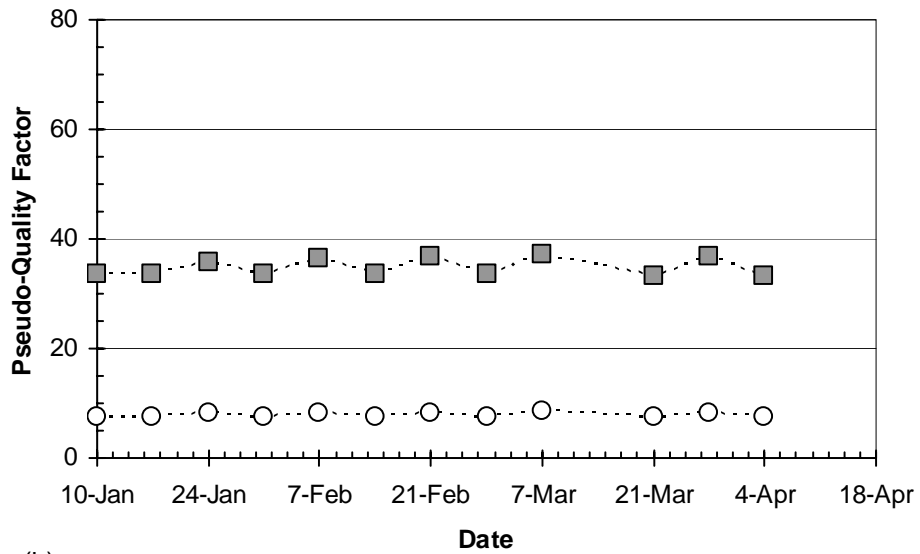


Figure G-11 Prism B19 Sensor Interrogation History



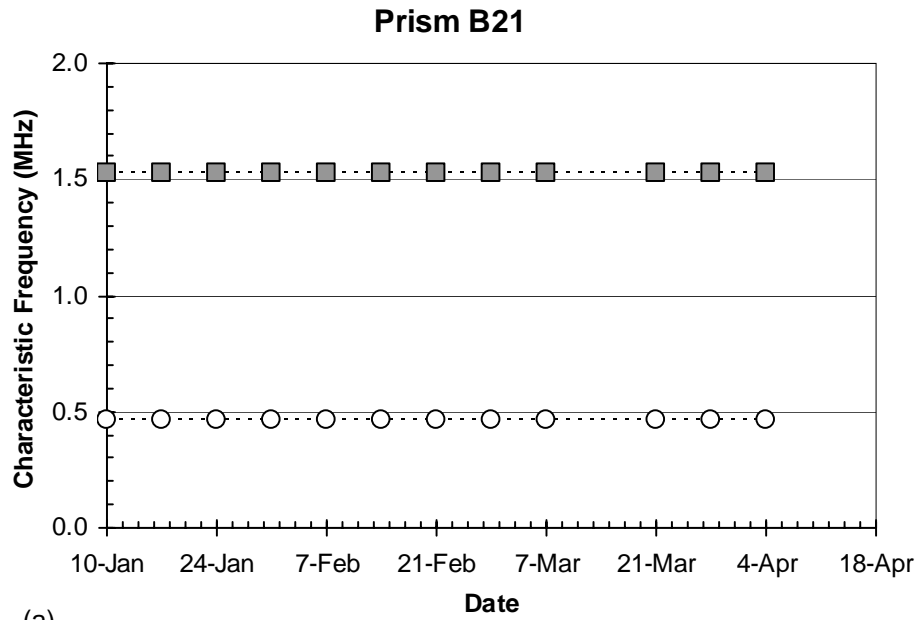
(a)



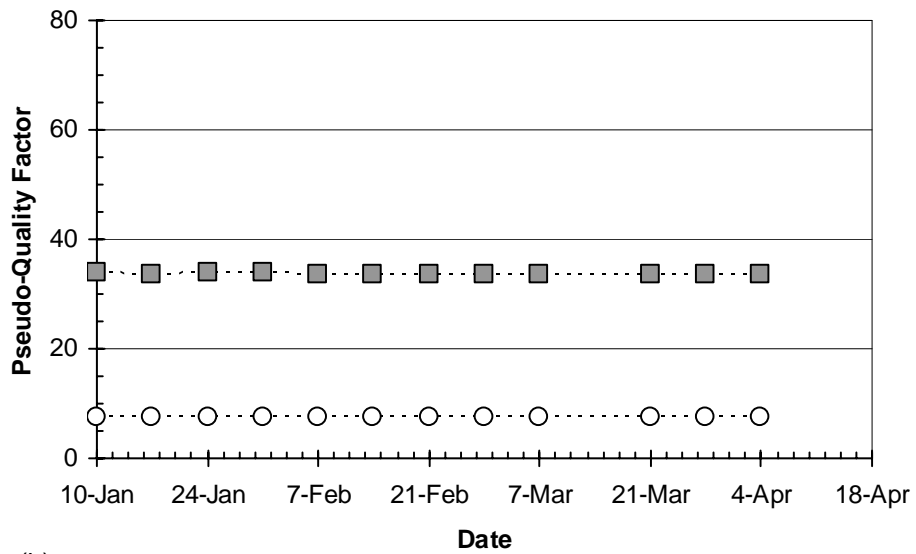
(b)



Figure G-12 Prism B20 Sensor Interrogation History



(a)



(b)

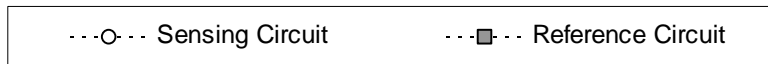
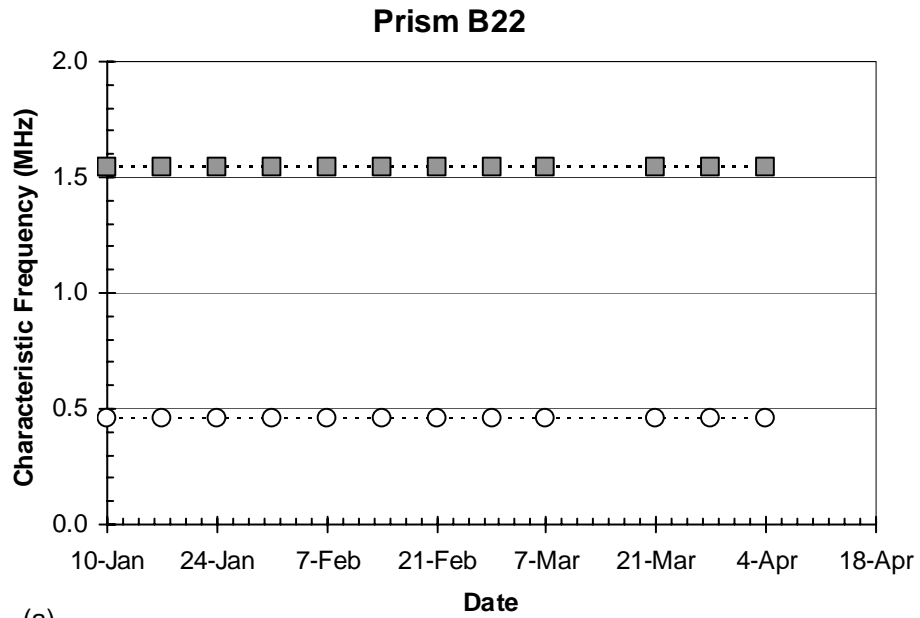
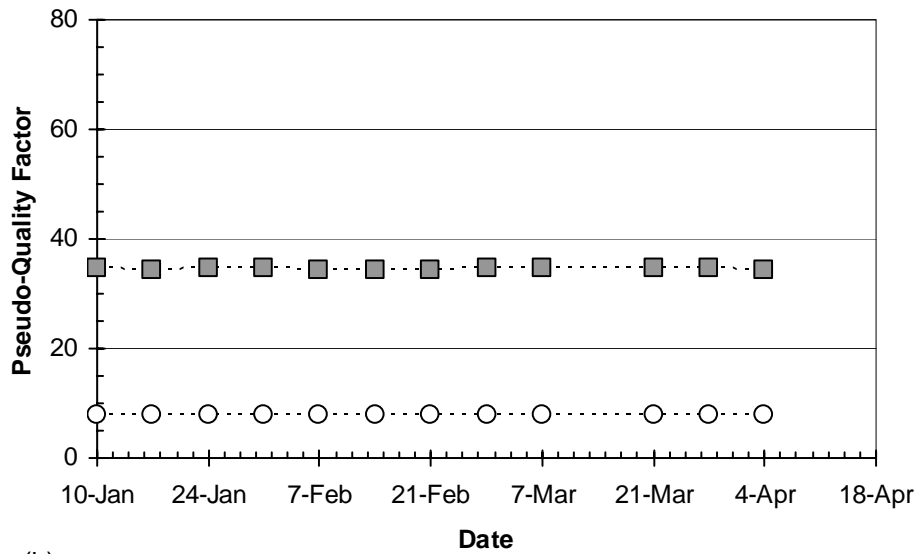


Figure G-13 Prism B21 Sensor Interrogation History



(a)

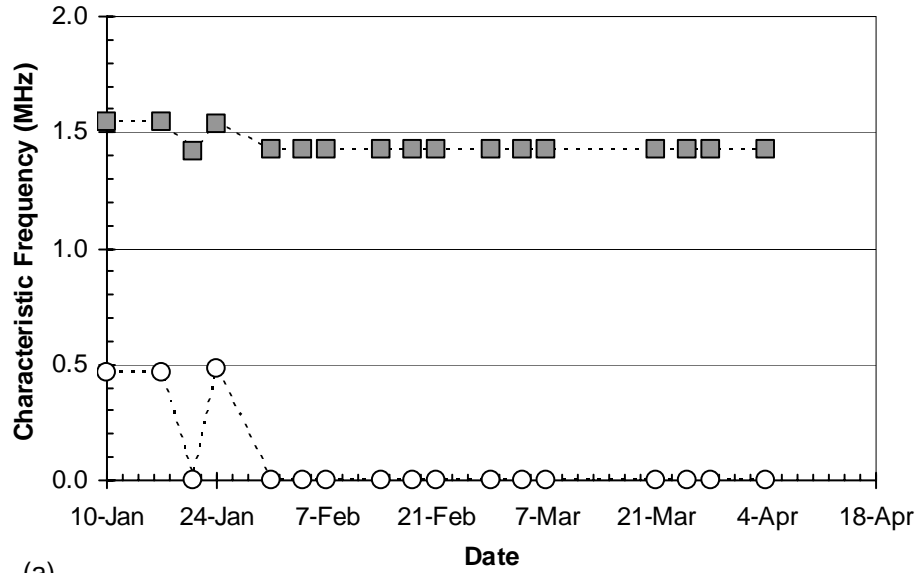


(b)

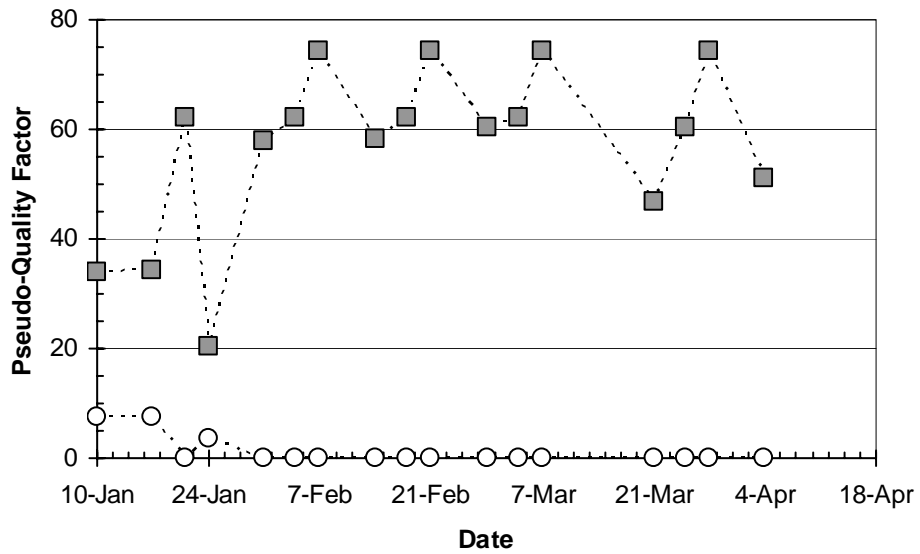


Figure G-14 Prism B22 Sensor Interrogation History

Prism B23



(a)

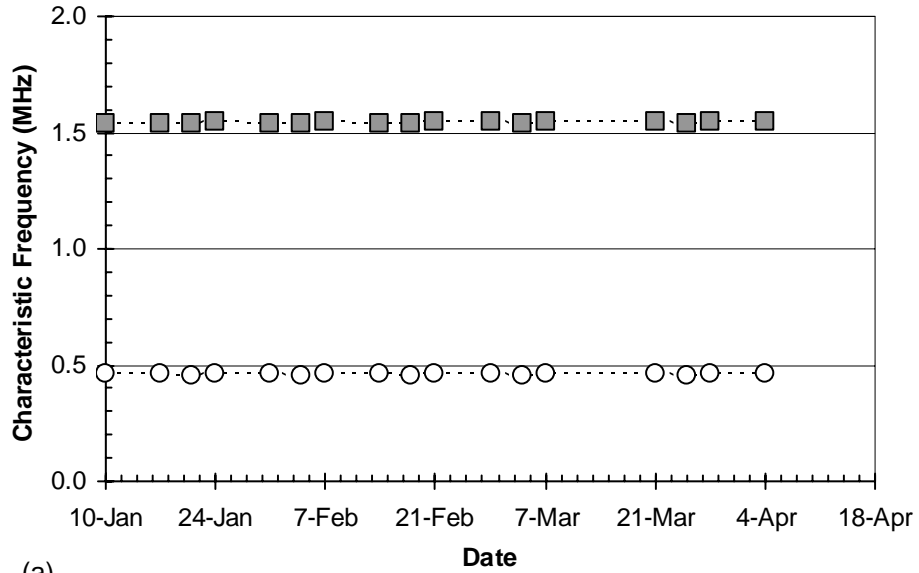


(b)

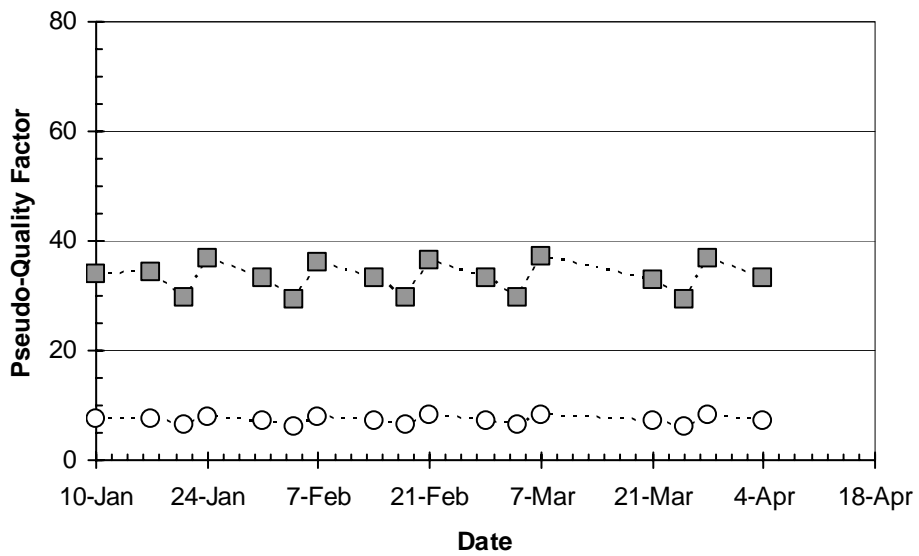


Figure G-15 Prism B23 Sensor Interrogation History

Prism B24



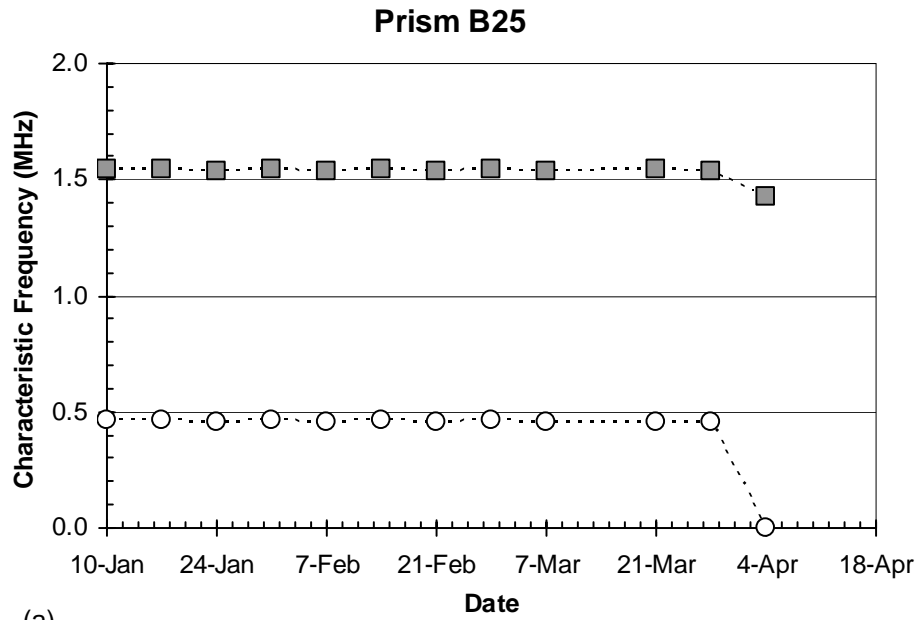
(a)



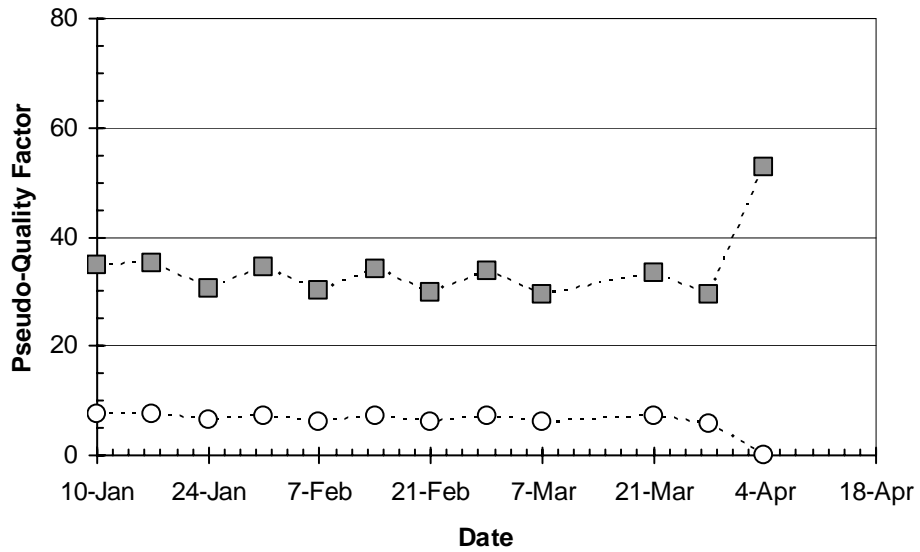
(b)



Figure G-16 Prism B24 Sensor Interrogation History



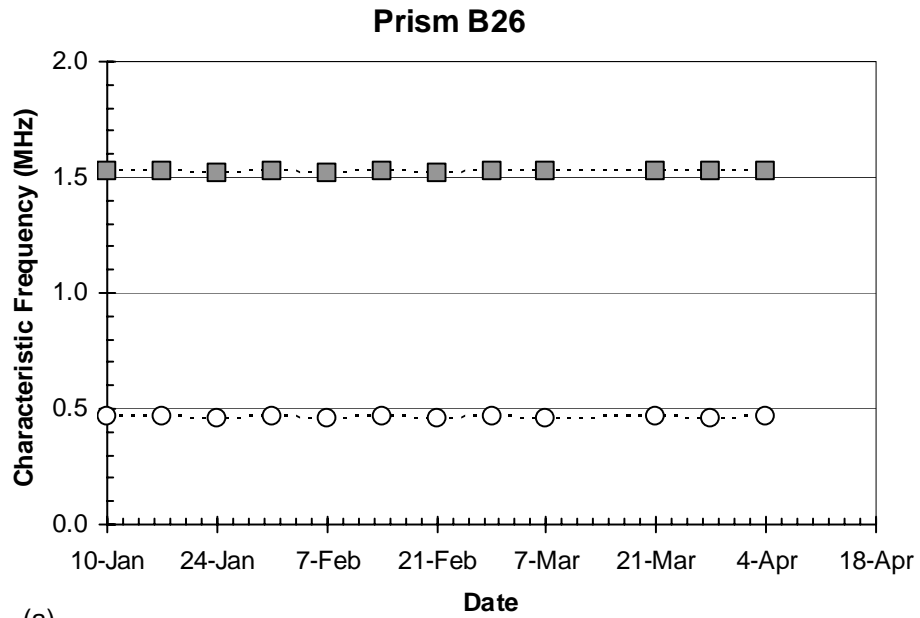
(a)



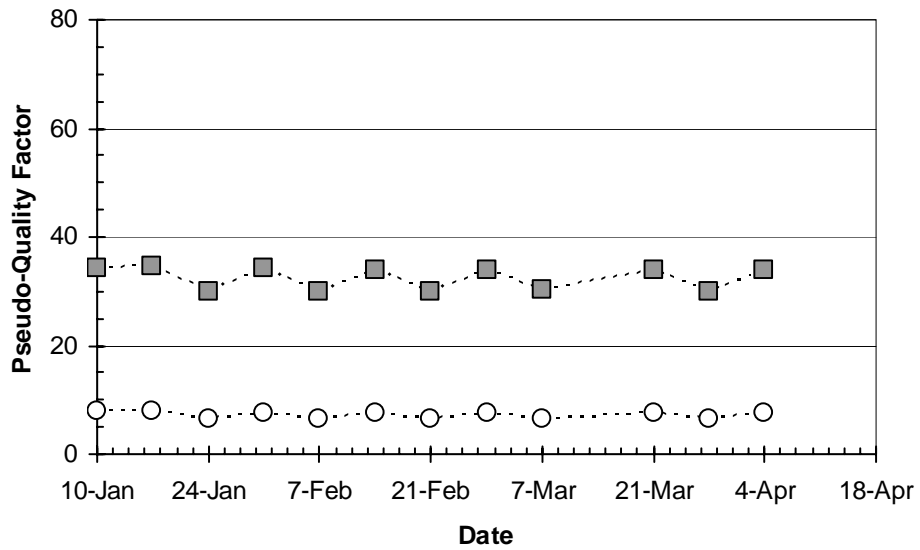
(b)



Figure G-17 Prism B25 Sensor Interrogation History



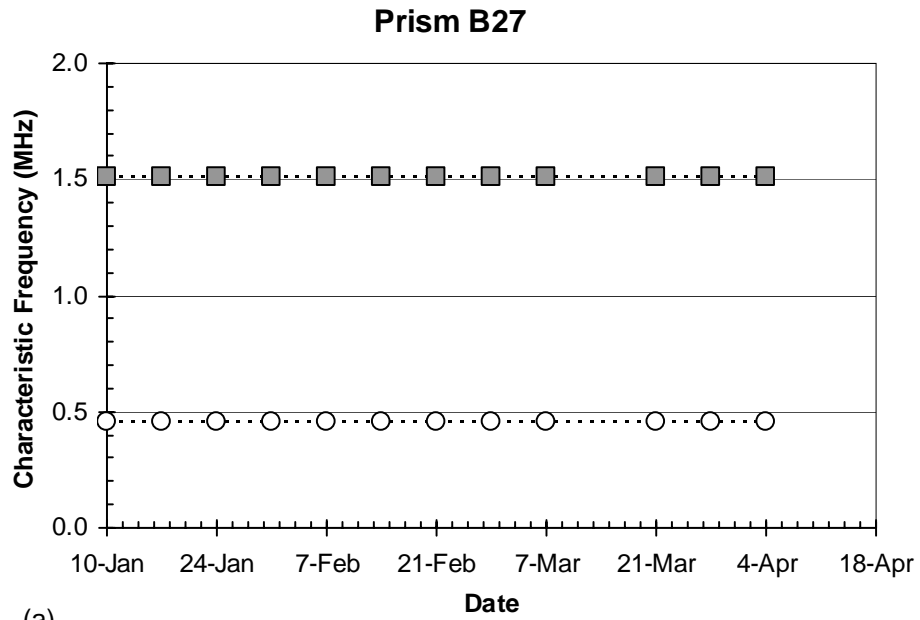
(a)



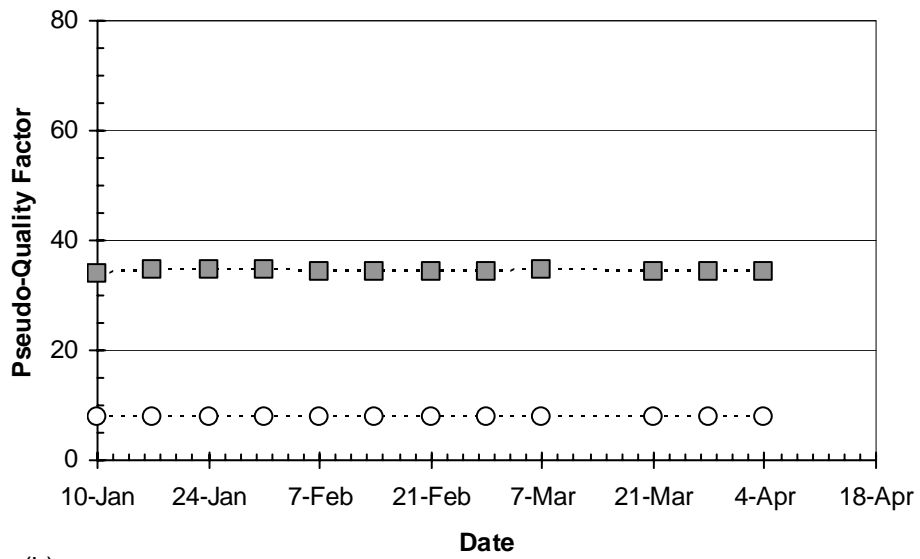
(b)



Figure G-18 Prism B26 Sensor Interrogation History



(a)

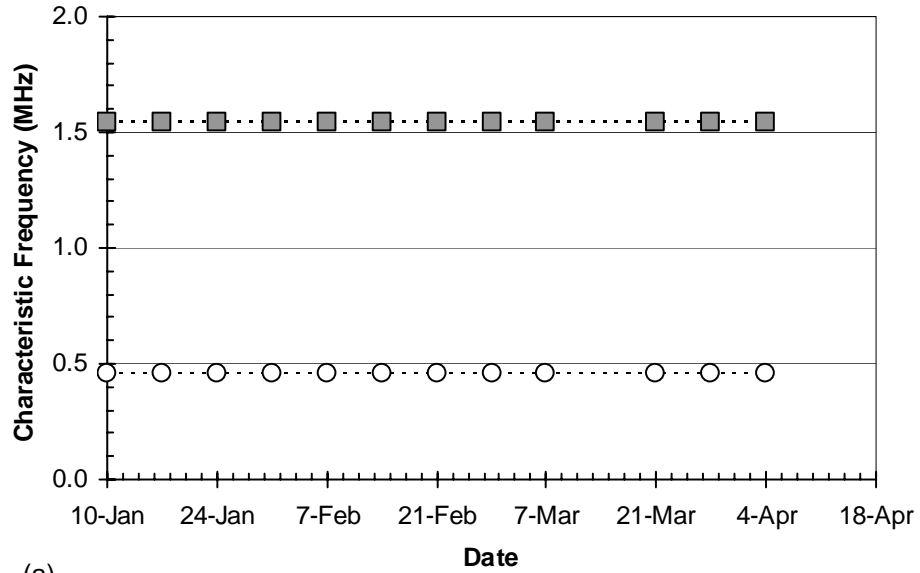


(b)

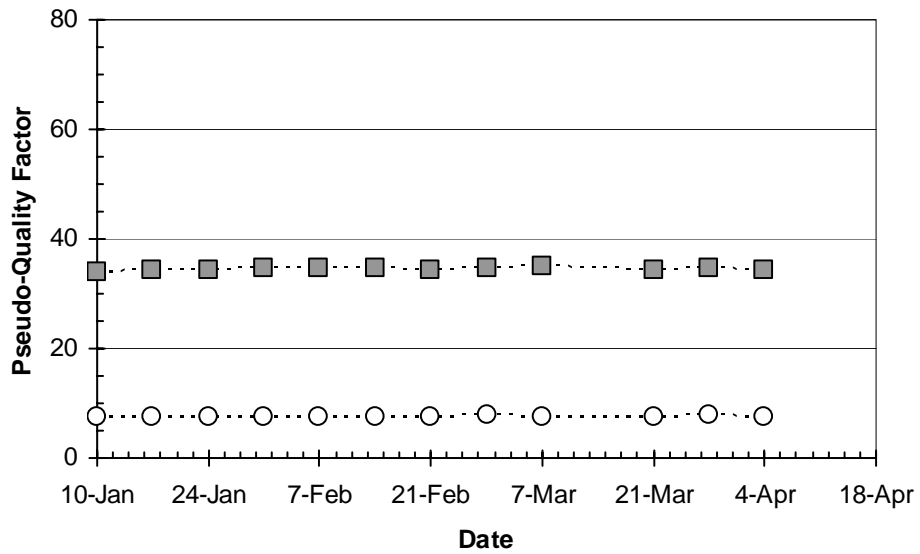


Figure G-19 Prism B27 Sensor Interrogation History

Prism B28



(a)

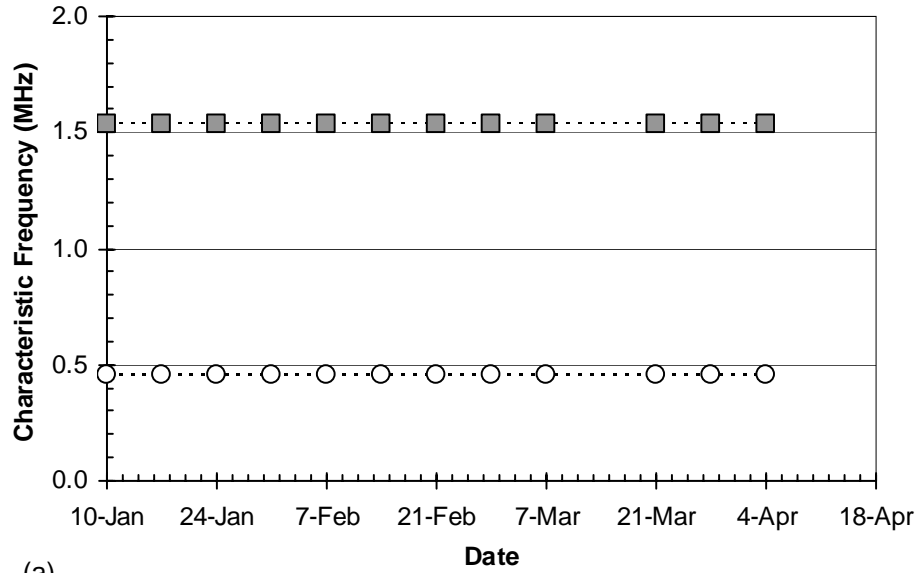


(b)

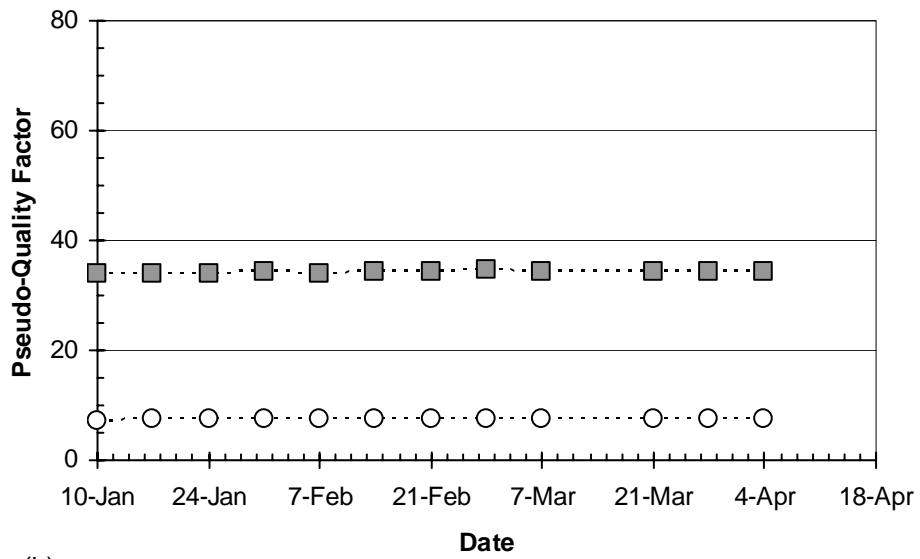


Figure G-20 Prism B28 Sensor Interrogation History

Prism B29



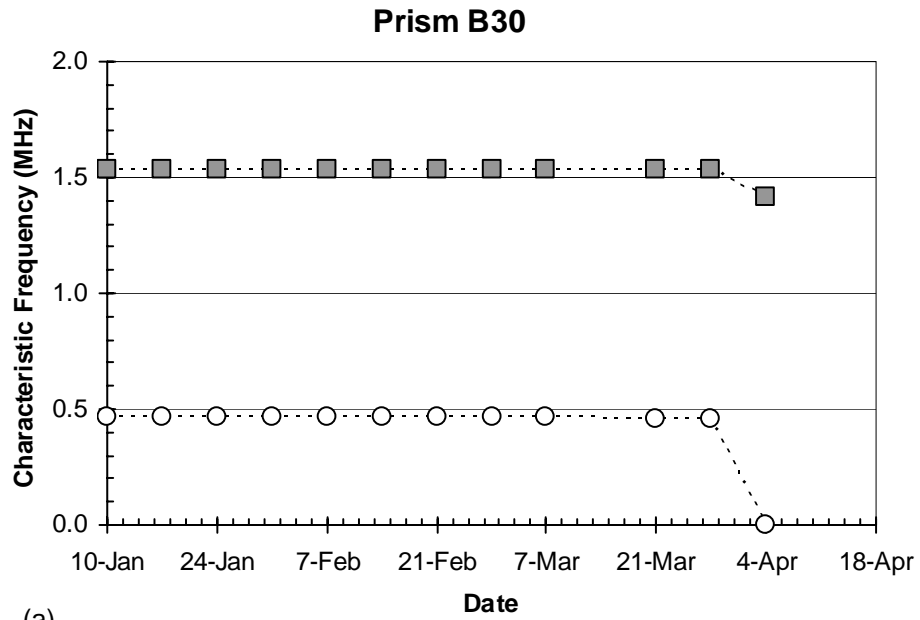
(a)



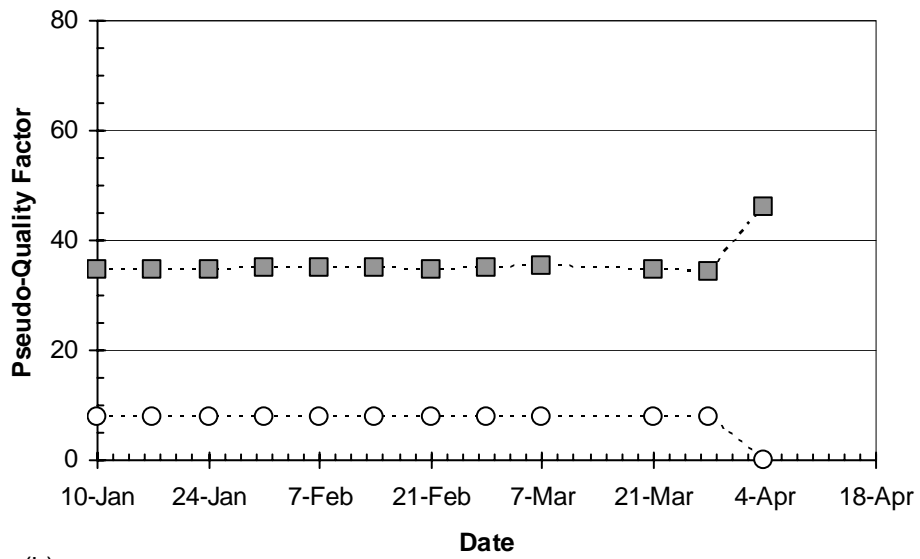
(b)



Figure G-21 Prism B29 Sensor Interrogation History



(a)



(b)



Figure G-22 Prism B30 Sensor Interrogation History

APPENDIX H

Concrete Prism Examinations

Twenty-two concrete prisms with embedded sensors were subjected to various environmental cycles. Cycles shown in Table H-1 began on 10 January 2005. Results from sensor monitoring are presented in Chapter 5 and Appendix G. As of 4 April 2005, nine of the concrete prisms had sensors with broken steel sensing wires. Table H-2 gives the date, cycle, and likely cause of the broken wire for all nine sensors. Because the sensing wires in prisms A23, B23, A24, and A25 broke early in the test, environmental cycles were continued on those prisms. Five of the prisms with broken steel sensing wires (A26, A29, A30, B25, and B30) were examined after sensor interrogations indicated broken wires.

During the examinations, specimens were photographed, cover concrete was removed, and the steel wires and sensors were completely removed. Locations of possible wire breaks and corrosion were documented. Cover concrete was removed carefully using a very small chisel and hammer. Concrete was either broken off in small pieces or pulled apart at existing cracks. Although care was taken to prevent the destruction of the steel sensing wires during removal, some were broken as a result of the examinations. In general, the location of wire breaks due to the examination did not coincide with locations of corrosion. All of the sensors that were examined were confirmed to have broken wires in at least one location due to corrosion. Descriptions and photographs of concrete prism examinations are presented in this appendix.

Table H-1 Environmental Cycles for Concrete Prisms

Concentric Sensors	Coplanar Sensors	First Week	Second Week
Control Conditions			
B21 B22	A21 A22	Air / 68-72 °F / 7 days	Air / 68-72 °F / 7 days
Varying Moisture Conditions			
B27 B28	A27 A28	Tap Water / 68-72 °F / 7 days	Air / 68-72 °F / 7 days
B29 B30	A29 A30	Salt Water / 68-72 °F / 7 days	Air / 68-72 °F / 7 days
Varying Thermal Conditions			
B19	-	Air / 68-72 °F / 7 days	Oven / 230 °F / 7 days
B20	-	Air / 68-72 °F / 7 days	Freezer / -15 °F / 7 days
Varying Moisture and Thermal Conditions			
B23	A23	Salt Water / 68-72 °F / 7 days	Oven / 230 °F / 4 days Freezer / -15 °F / 3 days
B24	A24	Tap Water / 68-72 °F / 7 days	Oven / 230 °F / 4 days Freezer / -15 °F / 3 days
B25 B26	A25 A26	Salt Water / 68-72 °F / 7 days	Oven / 230 °F / 7 days

Table H-2 Prisms with Broken Sensing Wires

Specimen	Date of Detection	Cycle Stage*	Likely Cause of Wire Break
A23	21 Jan	1b	Concrete cracking due to differential thermal expansion
A24	21 Jan	1b	Concrete cracking due to differential thermal expansion
A25	7 Feb	2c	Concrete cracking due to differential thermal expansion
A26	28 Mar	5c	Corrosion of steel sensing wire
A29	7 Mar	4c	Corrosion of steel sensing wire
A30	28 Mar	5c	Corrosion of steel sensing wire
B23	21 Jan	1b	Concrete cracking due to differential thermal expansion
B25	4 Apr	6a	Corrosion of steel sensing wire
B30	4 Apr	6a	Corrosion of steel sensing wire

* a - end of first week (all specimens)

b - end of oven dry stage (specimens A23, A24, B23, and B24)

c - end of second week (all specimens)

H.1 PRISM A26

Prism A26 contained the only coplanar sensor that experienced a sufficient number of moisture and thermal cycles such that the wire break was caused by corrosion. The broken wire was detected in the interrogation at the end of the fifth oven drying period (11 weeks into testing). Photographs of prism A26 prior to removal of concrete cover are provided in Fig. H-1. Large cracks formed due to differential thermal expansion during oven exposure.

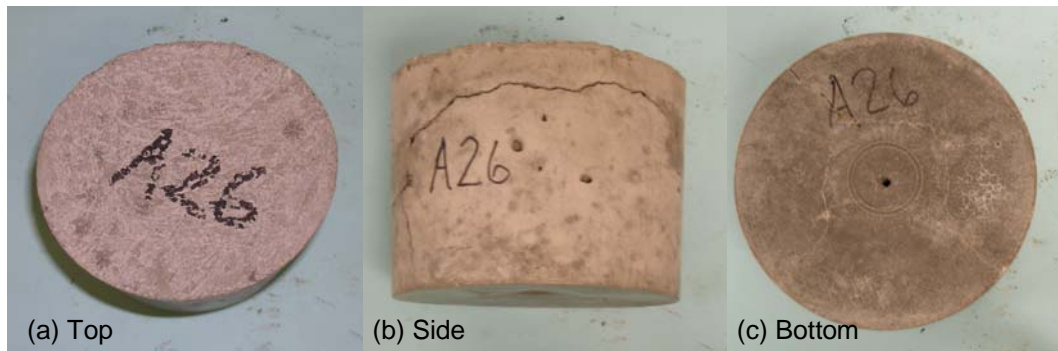


Figure H-1 Prism A26 Before Internal Examination

Internal examination of the specimen revealed the location of the break in the steel sensing wire, near the 180° bend near the end of the wire loop (Fig. H-2) and localized rust staining at that location (Fig. H-3). Some corrosion was also visible where the wires exit the epoxy enclosure, but the wire was not broken at that location. When the remainder of the steel wire was removed, no other corrosion was observed. The sensor epoxy and PVC were discolored due to high temperature exposure during the oven drying period (Fig. H-2).

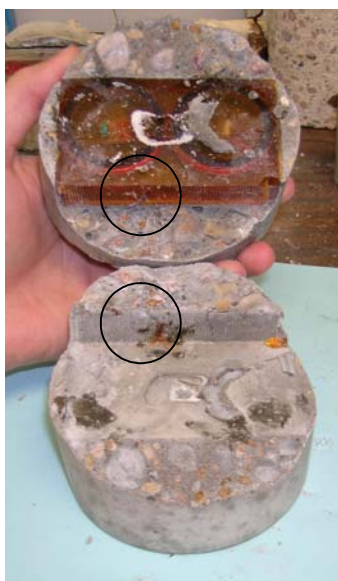


Figure H-2 Interior of Prism A26 Showing Location of Broken Wire

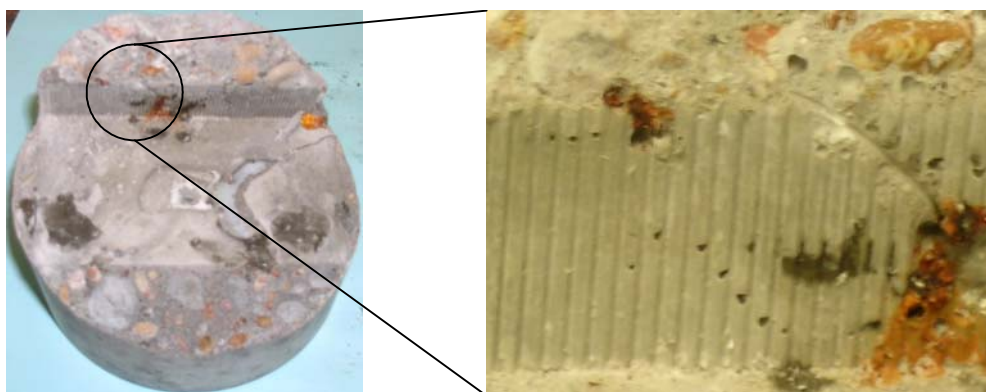


Figure H-3 Corrosion in Prism A26

H.2 PRISM A29

At the end of the fourth air drying period (8 weeks into testing) a broken wire was detected in prism A29. A photograph of prism A29 before removal of the concrete cover is shown in Fig. H-4. Only a small crack was visible on one side of the prism at the level of the sensor.



Figure H-4 Prism A29 Before Internal Examination

Internal examination of the specimen revealed some salt residue near the middle of the bottom of the sensor at a small air void in the concrete (Fig. H-5). The break in the steel sensing wire occurred near the 180° bend at the end of the wire loop (Fig. H-6a) and a very small amount of rust staining was visible at that location. Corrosion was also observed on the portion of intact wire parallel to the broken area (Fig. H-6b). When the remainder of the steel wire was removed, no other corrosion was observed.



Figure H-5 Interior of Prism A29

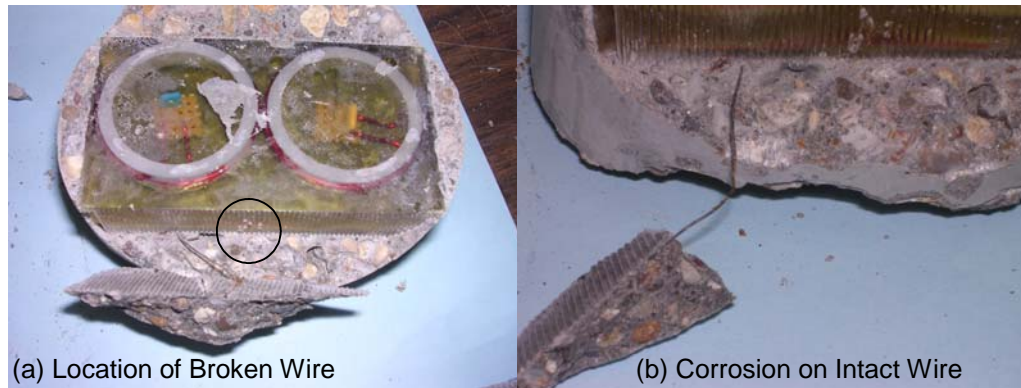


Figure H-6 Prism A29 Corrosion

H.3 PRISM A30

A broken wire was detected in sensor A30 at the end of the fifth dry period (11 weeks into testing). A photograph of prism A30 before removal of the concrete cover is shown in Fig. H-7. Only a small crack is visible at the level of the sensor.



Figure H-7 Prism A30 Before Internal Examination

Internal examination of the specimen revealed the location of the break in the steel sensing wire (Fig. H-8) and localized rust staining at that location. The wire break occurred in both parallel wires near the 180° bend at the end of the

wire loop. The remaining steel wire was examined and no other corrosion was observed.



Figure H-8 Interior of Prism A30 Showing Location of Broken Wire

H.4 PRISM B25

A broken wire was detected in prism B25 at the end of the sixth wet period in salt water (12 weeks into testing). Photographs of the prism prior to examination are provided in Fig. H-9. Wide cracks formed as a result of differential thermal expansion during oven drying periods.

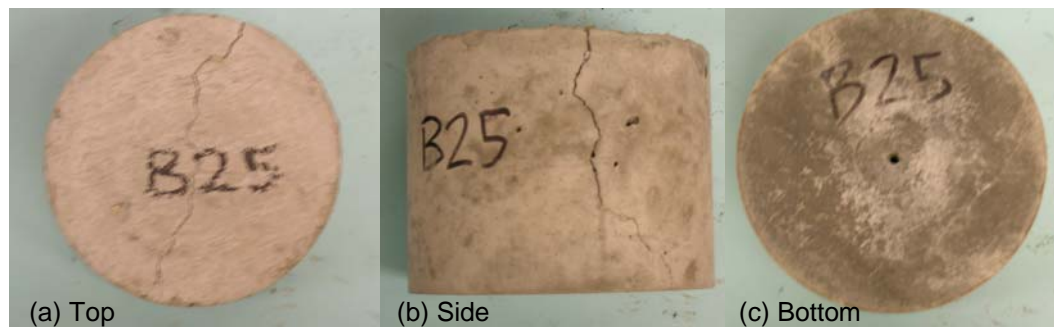


Figure H-9 Prism B25 Before Internal Examination

Internal examination of the specimen revealed more extensive corrosion than in any other prisms discussed in Sections H.1 through H.3. Fig. H-10 shows the locations with the most corrosion on the interior of the prism cover concrete. As shown in Fig. H-11, corrosion product is visible migrating away from the steel sensing wire at the 180° bend near the end of the wire loop and along the length of the wire for roughly one-third of the total loop length. The probable location of the broken wire was the end of the wire loop, but enough corrosion occurred elsewhere along the wire to cause a break in other locations as well. The examination also showed corrosion at the location where the steel sensing wires exit the epoxy enclosure and the discoloration of the epoxy and PVC due to high temperature exposure during the oven drying period (Fig. H-12).

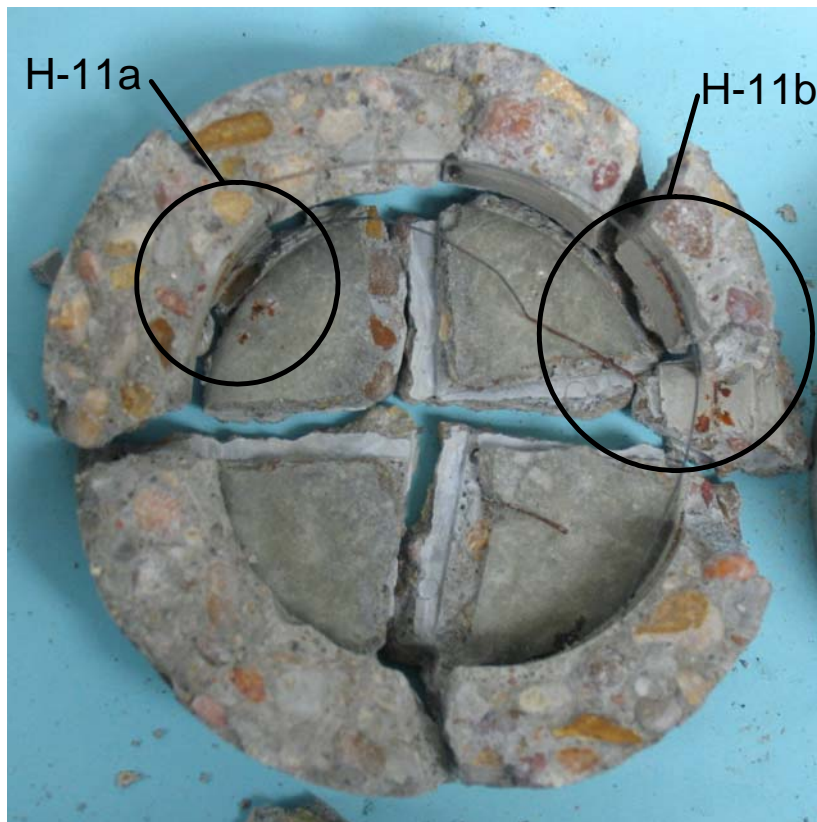
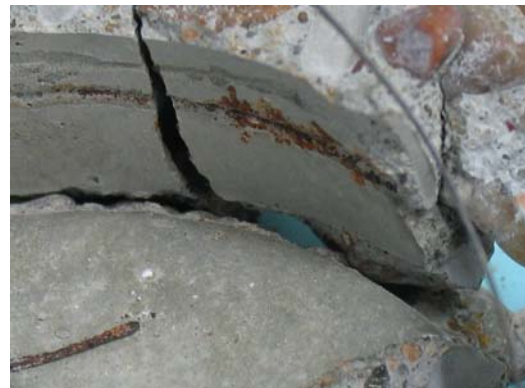


Figure H-10 Interior of Cover Concrete of Prism B25



(a) Corrosion at 180° Bend in Wire



(b) Corrosion Along Wire

Figure H-11 Corrosion of Steel Sensing Wire in Prism B25

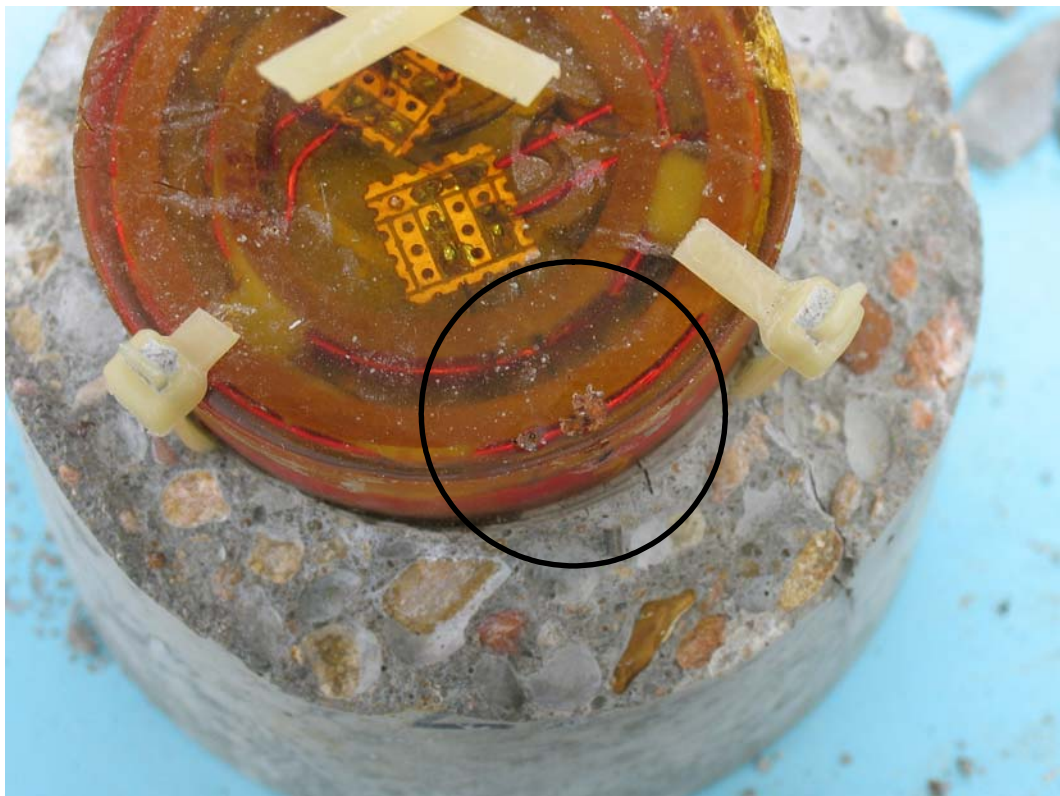


Figure H-12 Discoloration of Sensor B25 and Corrosion at Wire/Epoxy Interface

H.5 PRISM B30

At the end of the sixth wet period in salt water (12 weeks into testing), a broken wire was detected in prism B30. A photograph of prism B30 before removal of the concrete cover is shown in Fig. H-13. Internal examination of the specimen revealed the location of the break in the steel sensing wire (Fig. H-14) and localized rust staining at that location. The wire break occurred near the 180° bend at the end of the wire loop. Corrosion was also observed on one wire at the location where the steel sensing wires exit the epoxy enclosure (Fig. H-15). The remaining steel wire was examined and no other corrosion was observed.

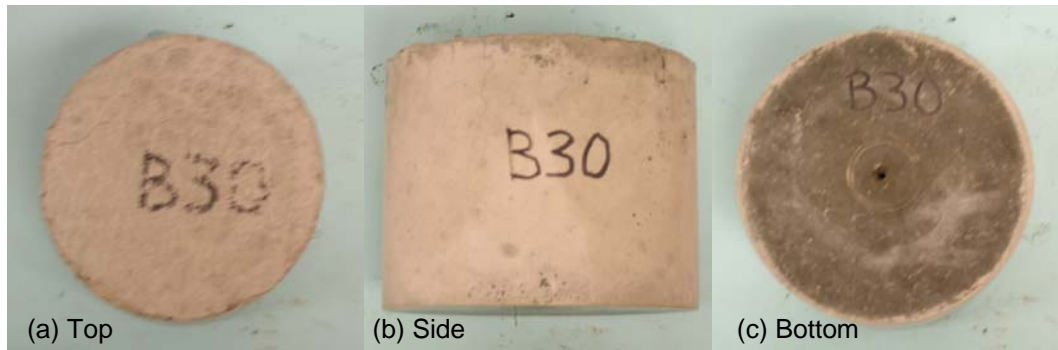


Figure H-13 Prism B30 Before Internal Examination

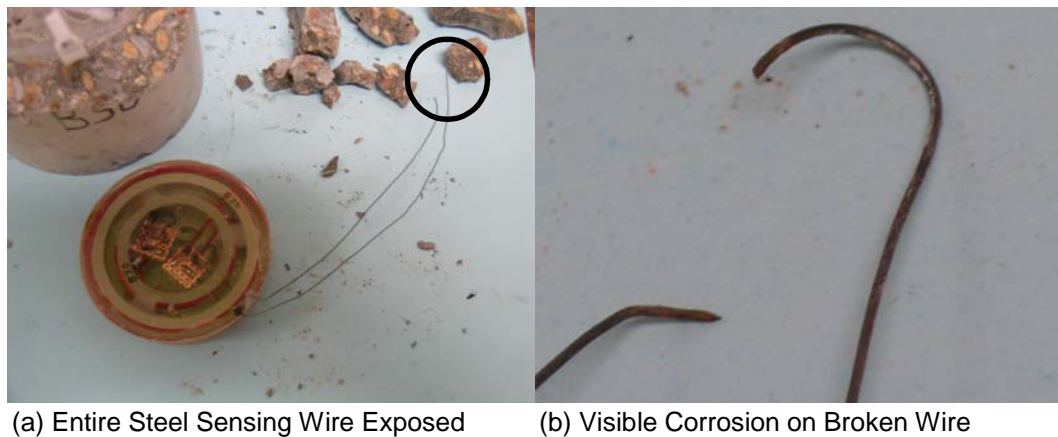


Figure H-14 Location of Broken Wire of Sensor B30

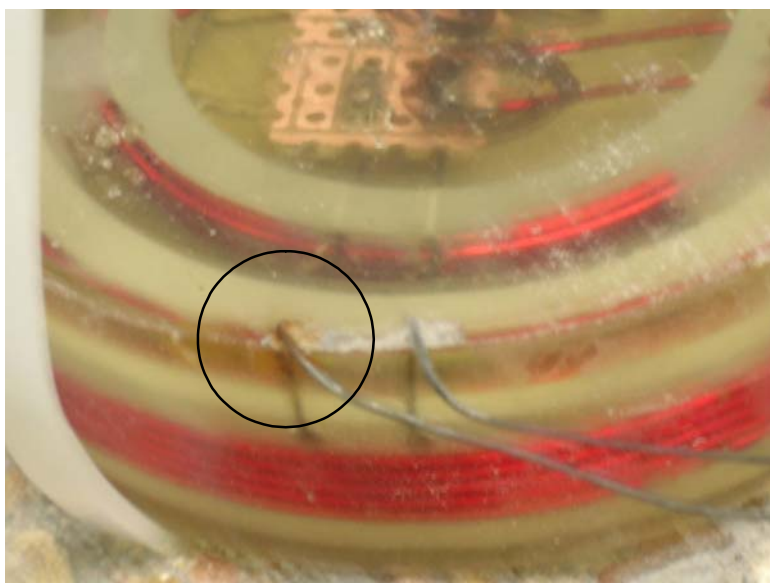


Figure H-15 Corrosion at Wire/Epoxy Interface of Sensor B30

APPENDIX I

Reinforced Concrete Slab #1 Monitoring Results

Results from monitoring reinforced concrete slab #1 with embedded sensors are presented in this appendix. Plots of characteristic frequency and pseudo-quality factors at each interrogation are provided through 6 April 2005 for each sensor. Plots of half-cell potentials and instantaneous corrosion rates are also provided at each interrogation through 6 April 2005 for points on the surface of the slab corresponding to sensor locations. Fig. I-1 shows the temperature at each interrogation.

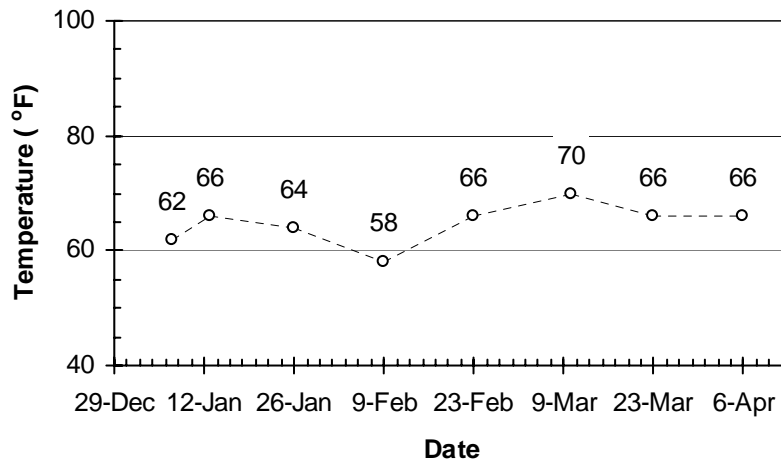
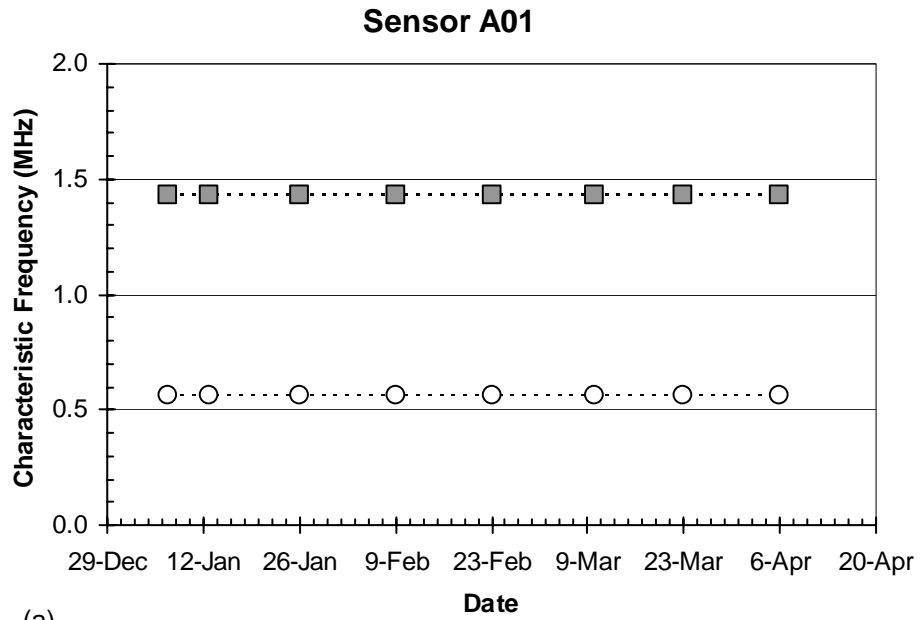
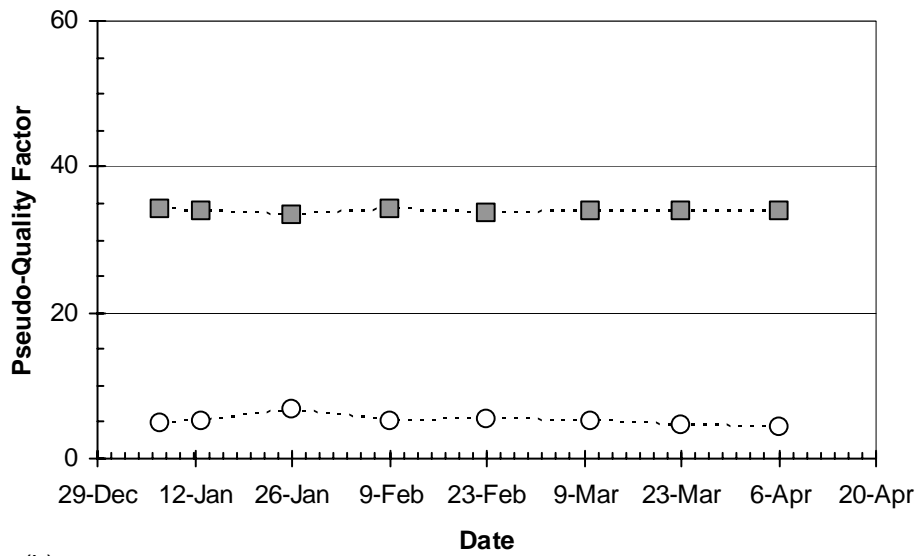


Figure I-1 Temperature Data at Sensor Interrogations for Slab #1



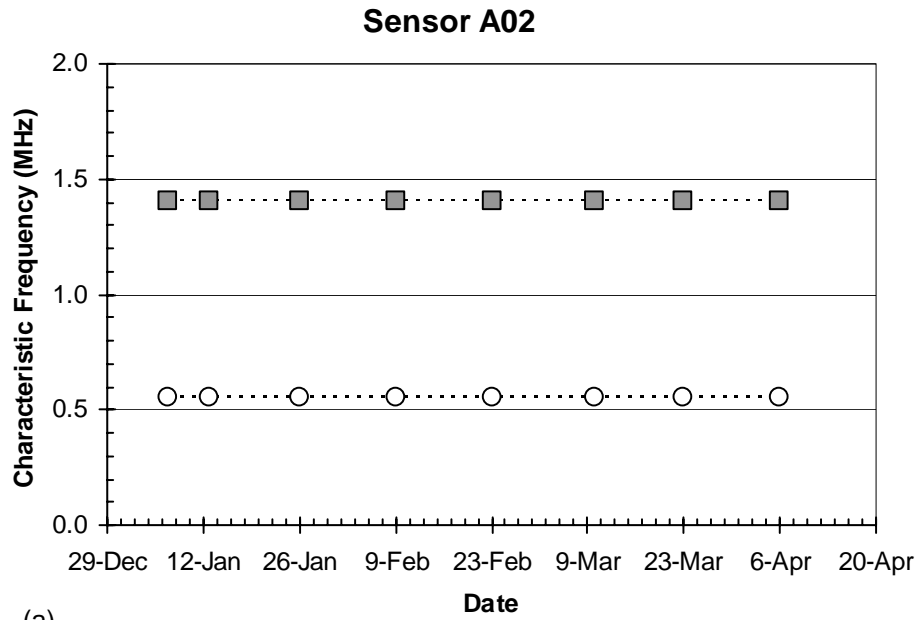
(a)



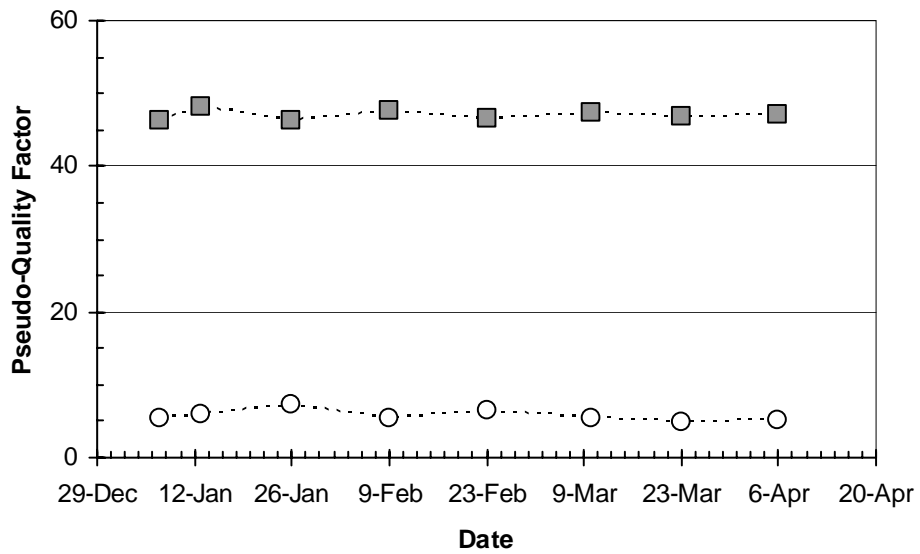
(b)



Figure I-2 Sensor A01 Interrogation History



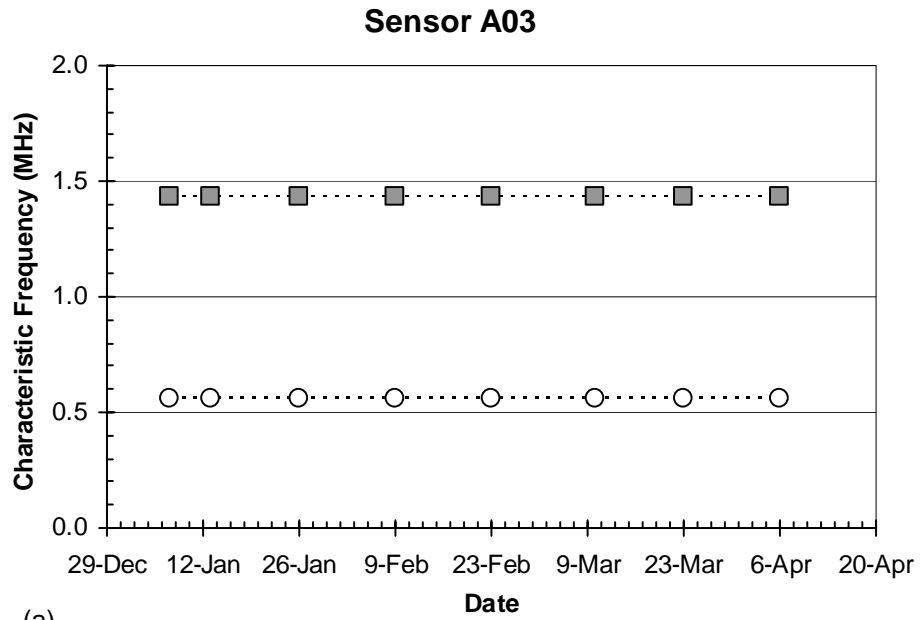
(a)



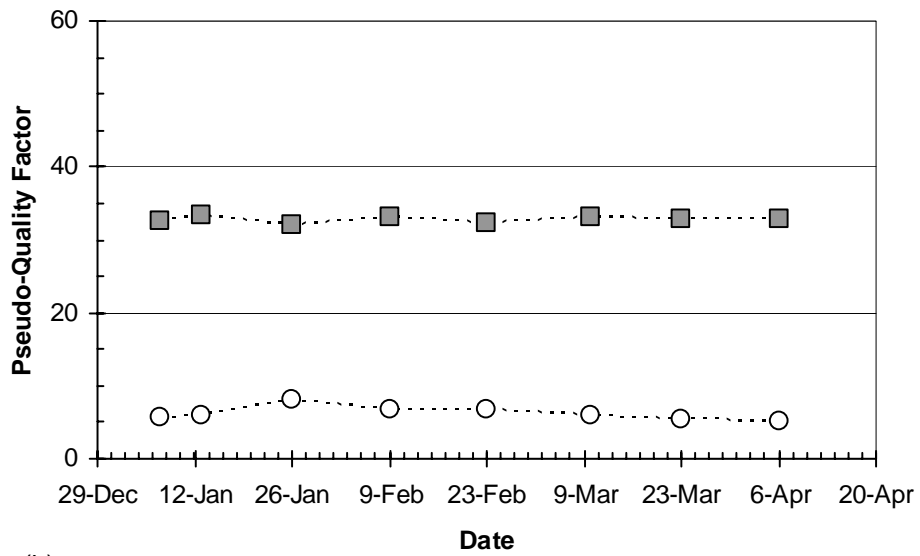
(b)



Figure I-3 Sensor A02 Interrogation History



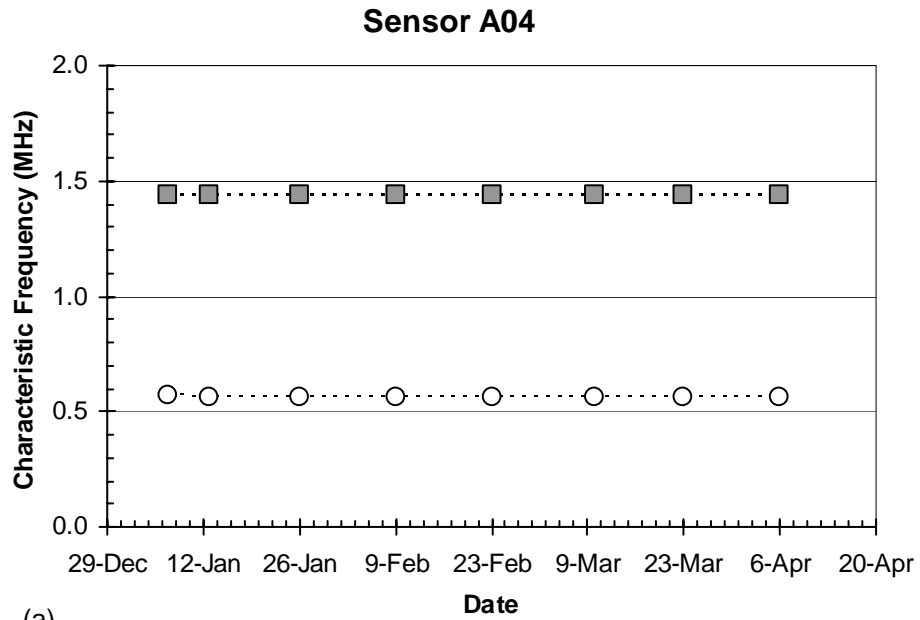
(a)



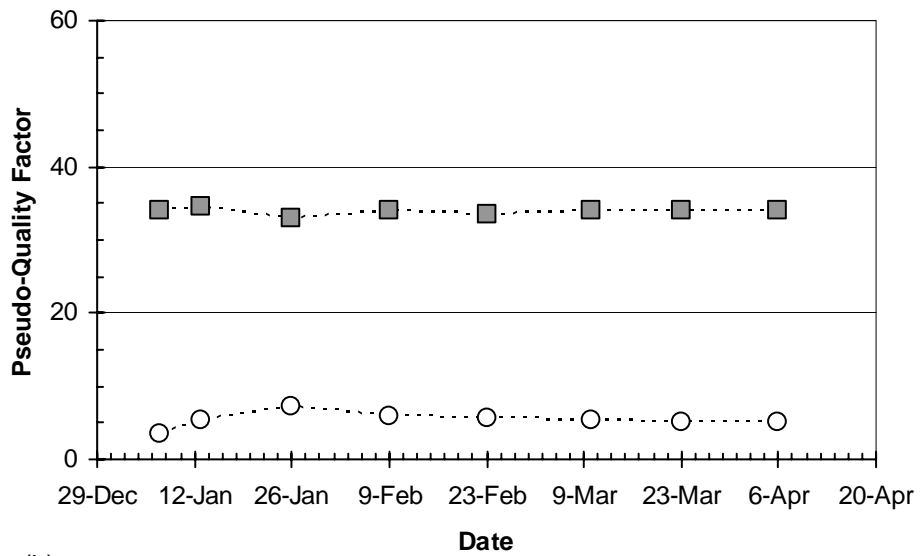
(b)



Figure I-4 Sensor A03 Interrogation History



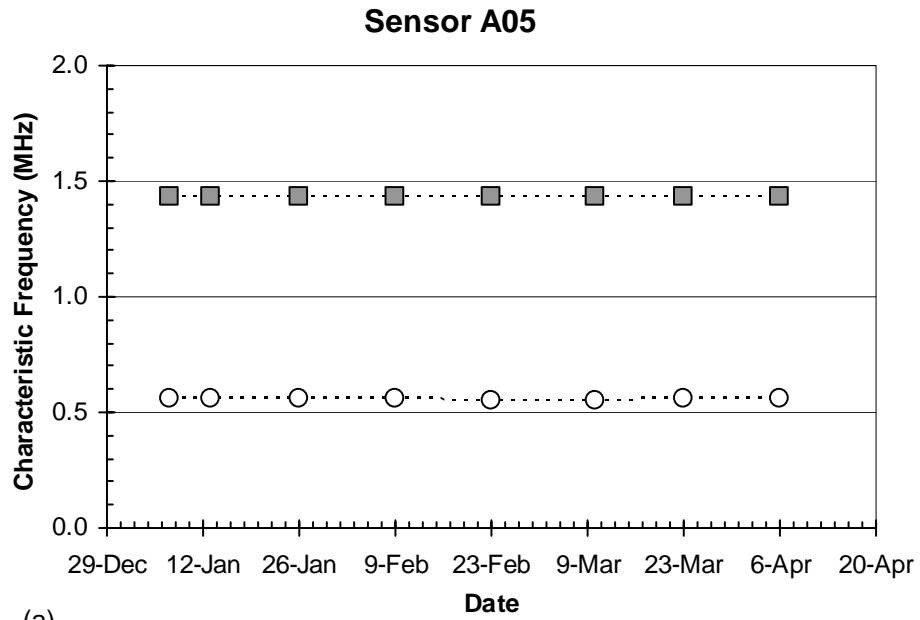
(a)



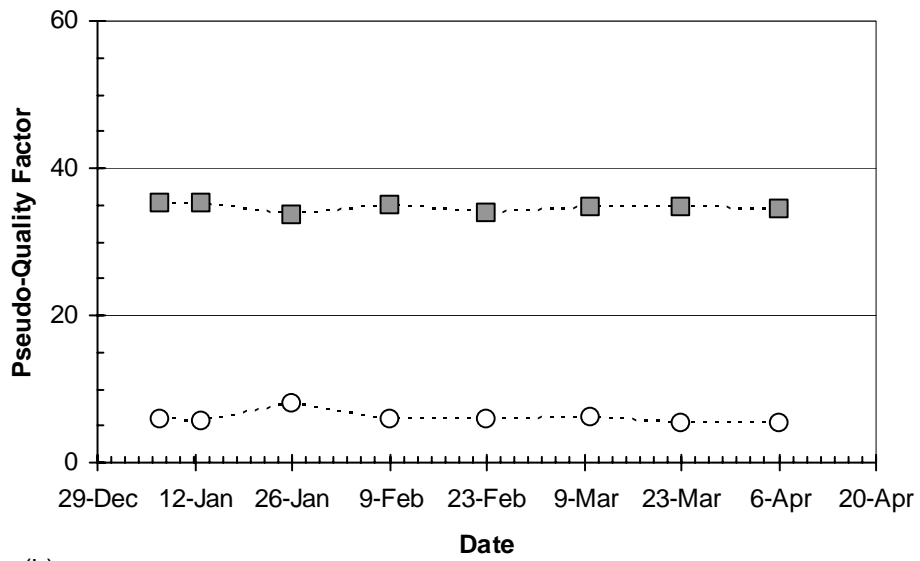
(b)



Figure I-5 Sensor A04 Interrogation History



(a)

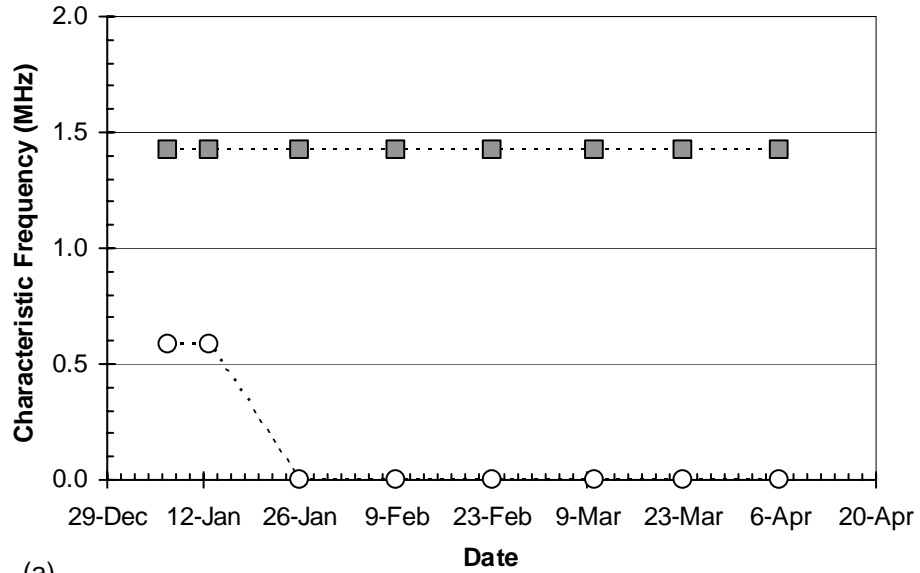


(b)

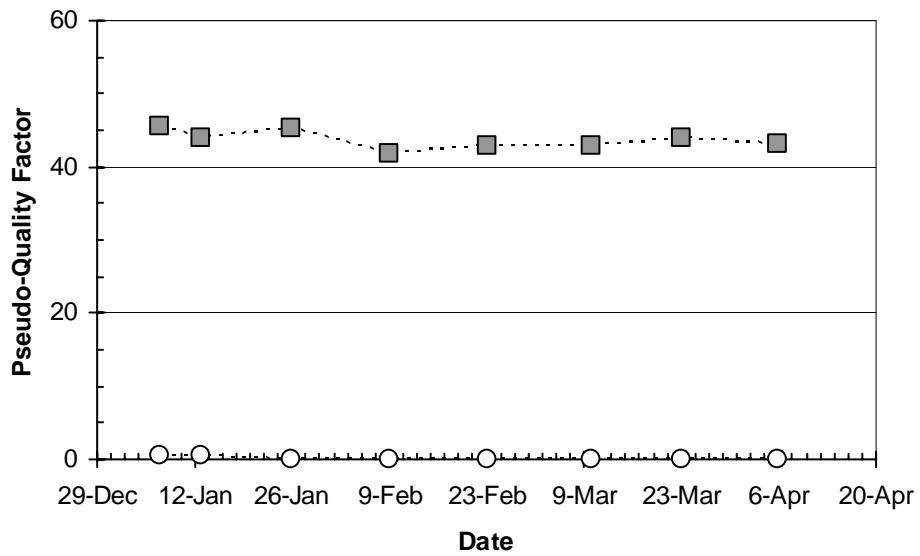


Figure I-6 Sensor A05 Interrogation History

Sensor A06



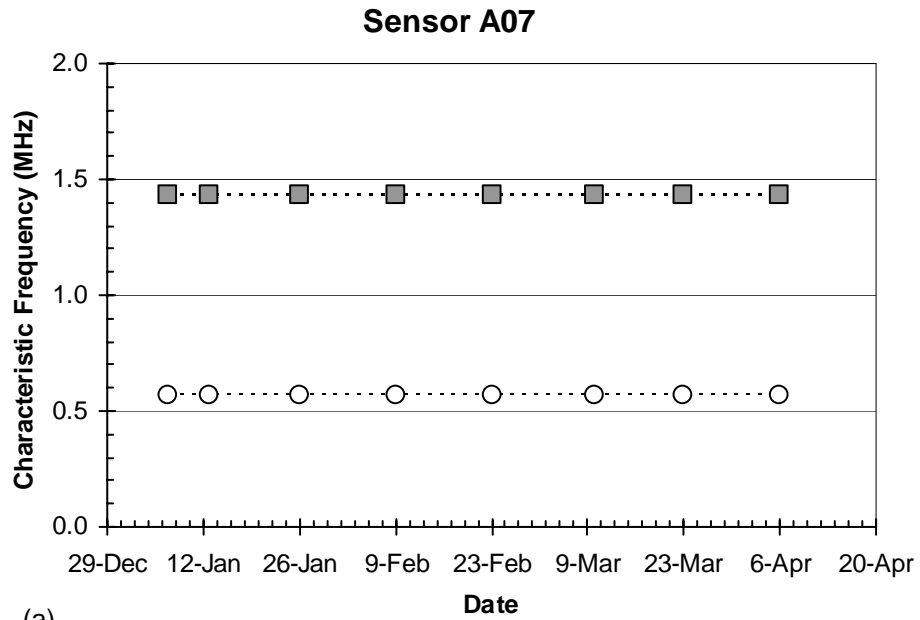
(a)



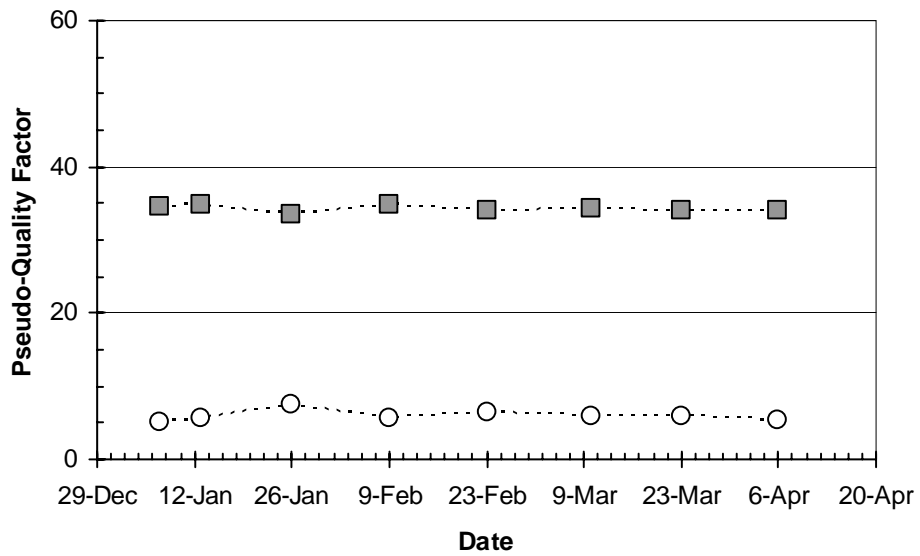
(b)



Figure I-7 Sensor A06 Interrogation History



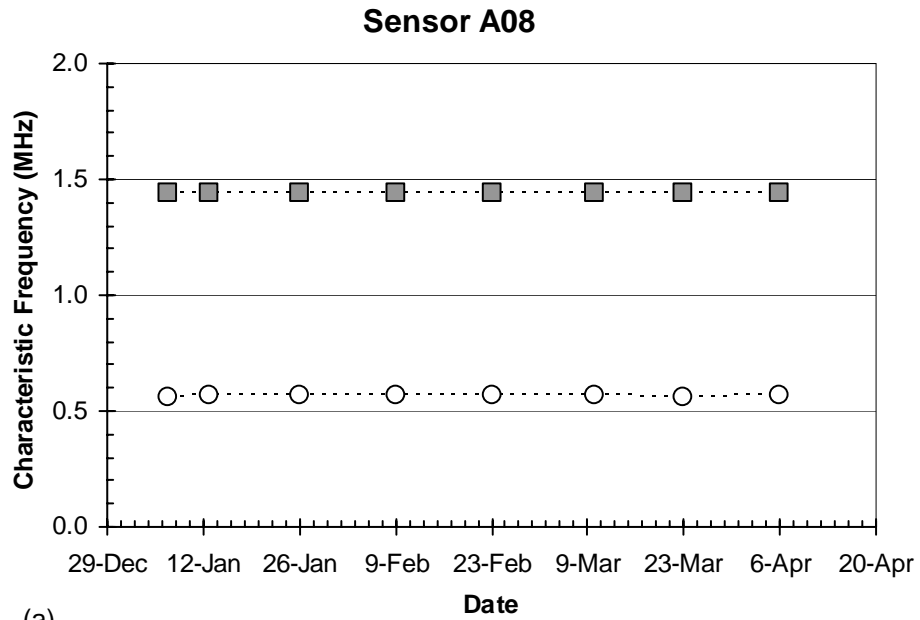
(a)



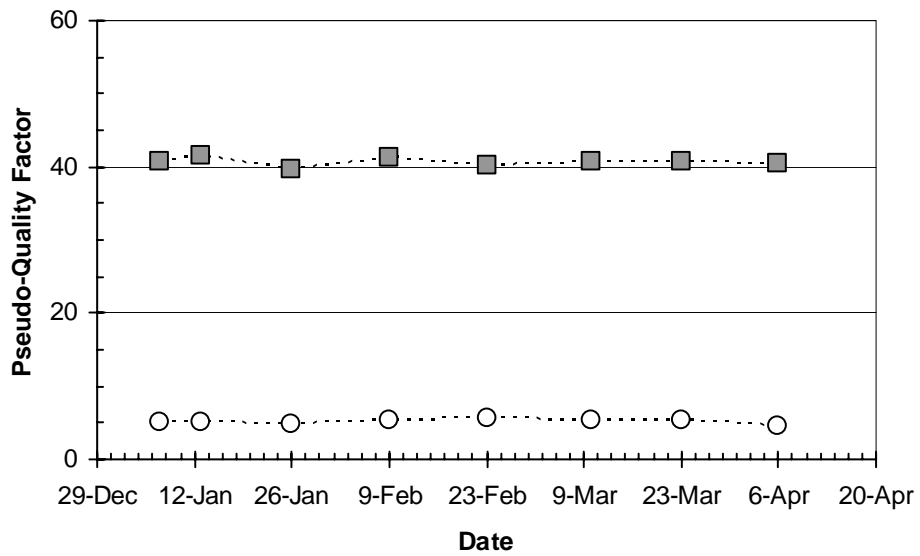
(b)



Figure I-8 Sensor A07 Interrogation History



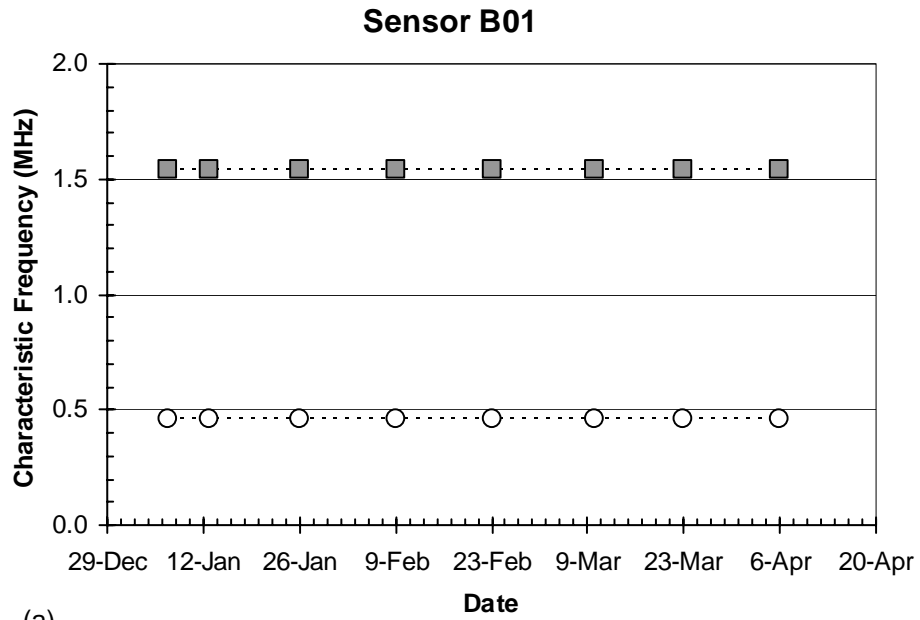
(a)



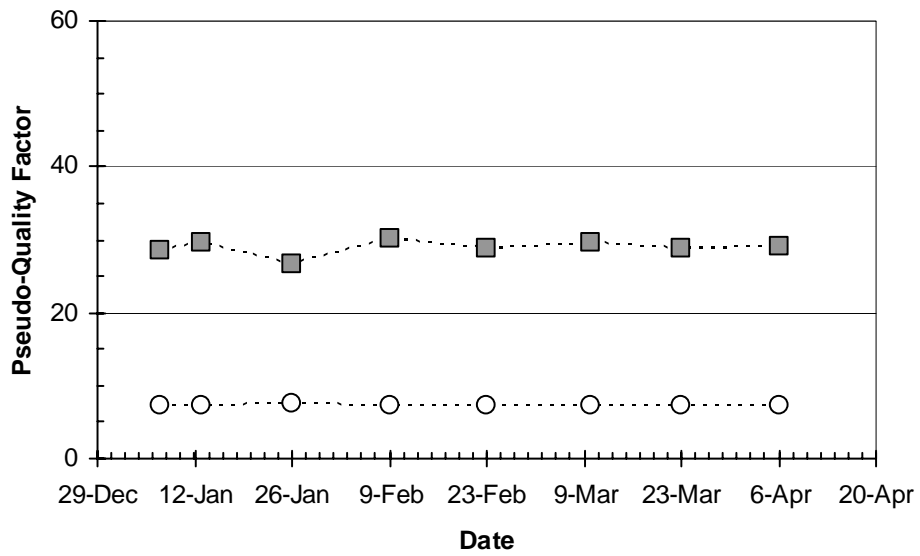
(b)



Figure I-9 Sensor A08 Interrogation History



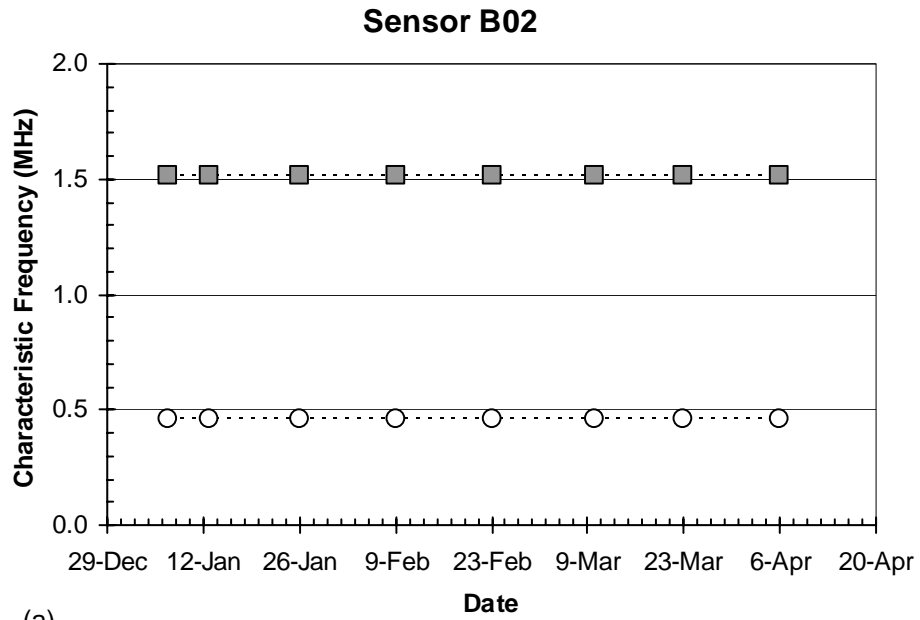
(a)



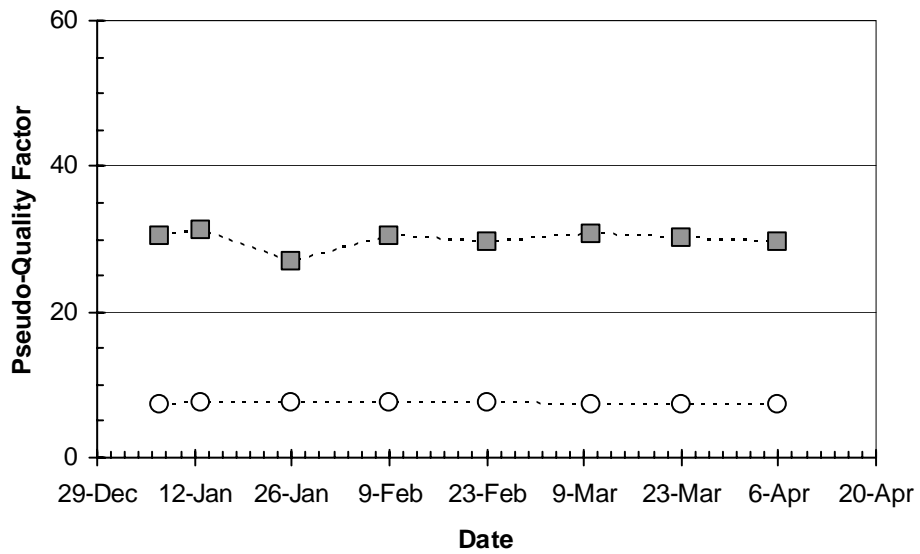
(b)



Figure I-10 Sensor B01 Interrogation History



(a)

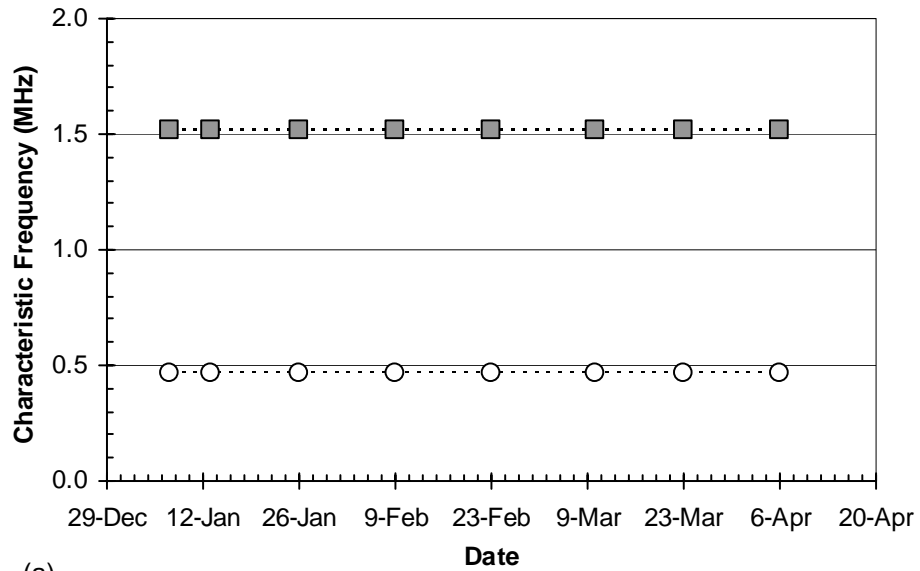


(b)

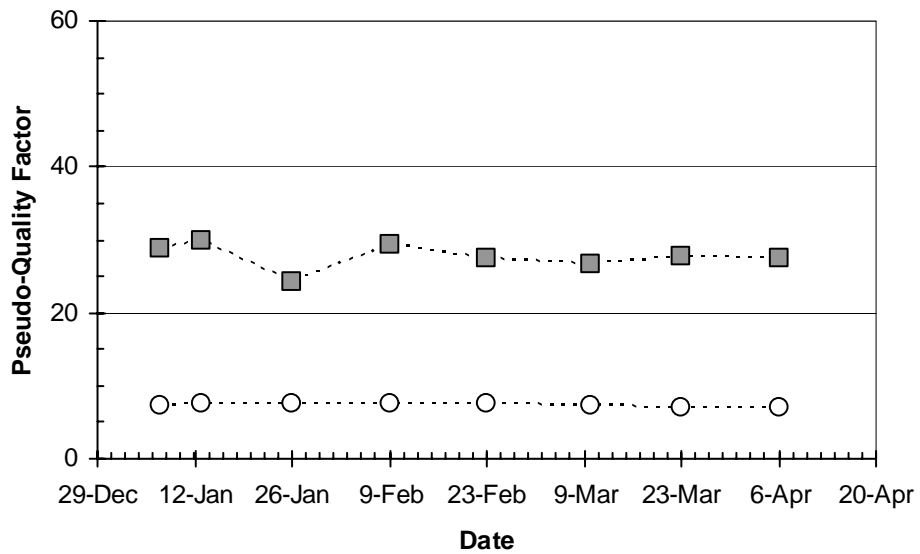


Figure I-11 Sensor B02 Interrogation History

Sensor B03



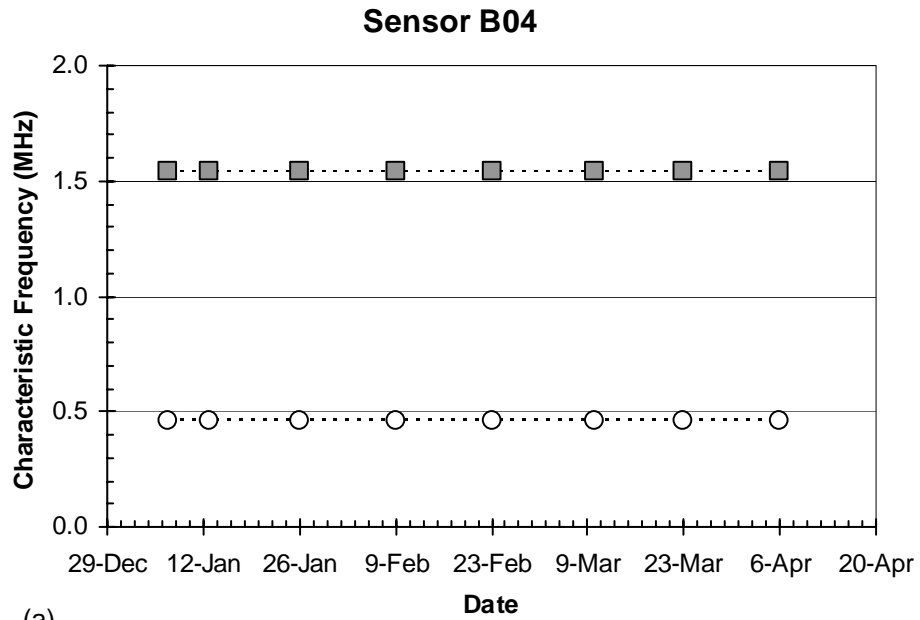
(a)



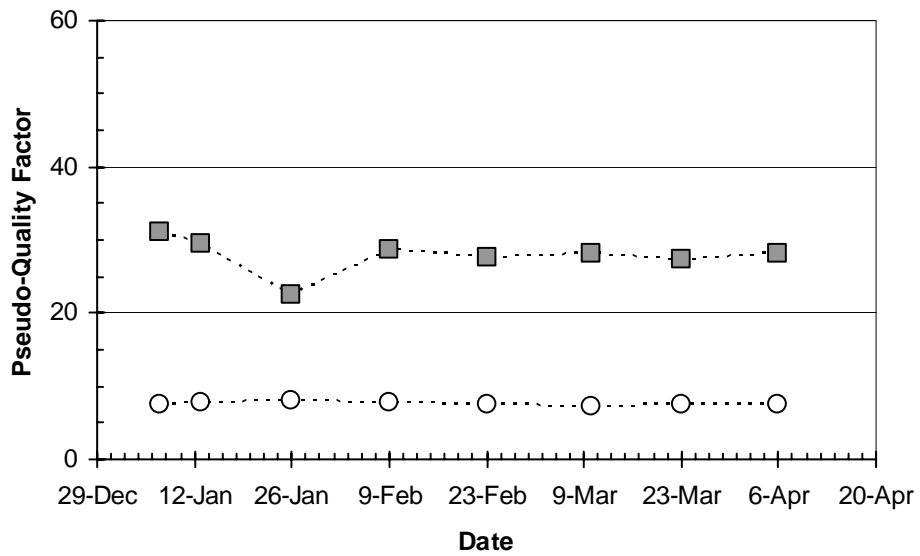
(b)



Figure I-12 Sensor B03 Interrogation History



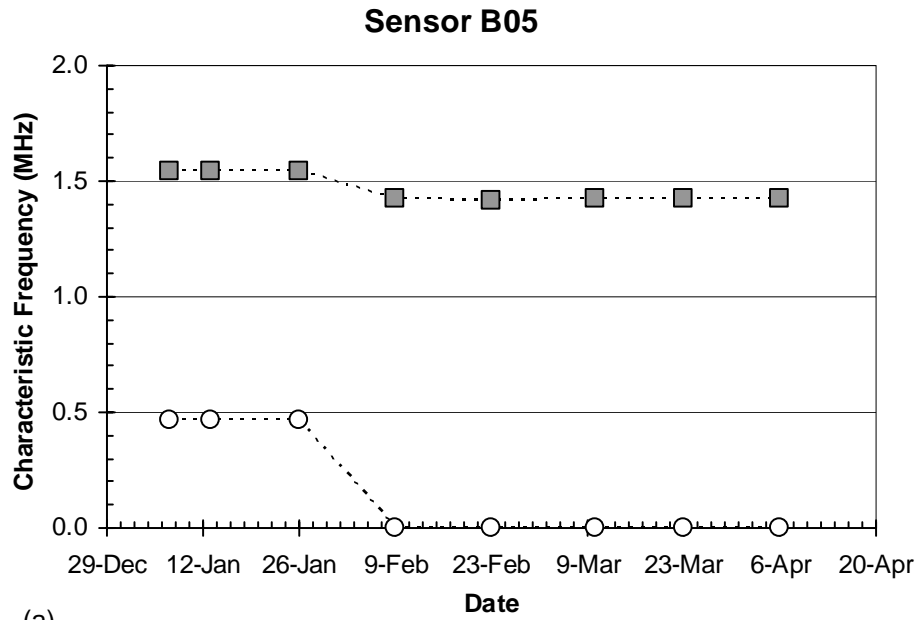
(a)



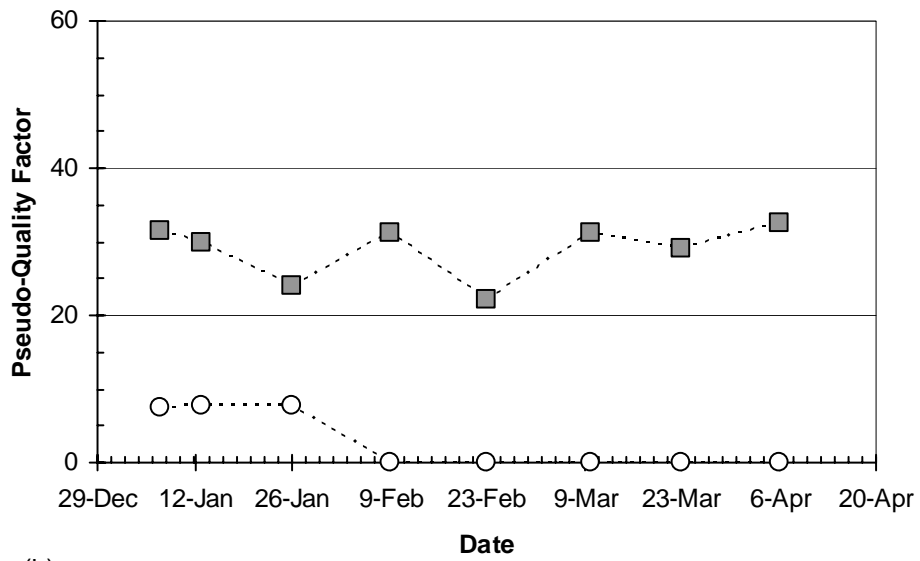
(b)



Figure I-13 Sensor B04 Interrogation History



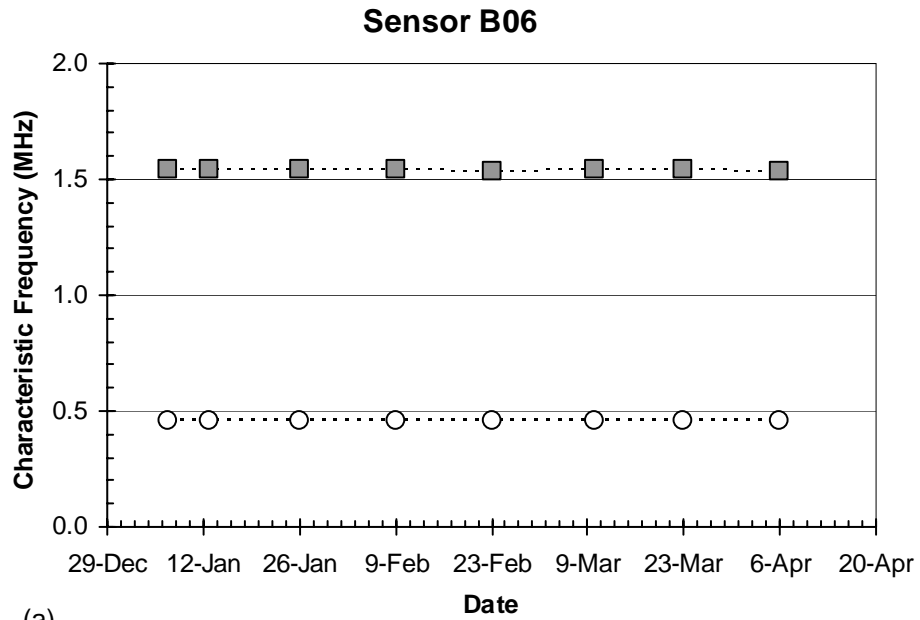
(a)



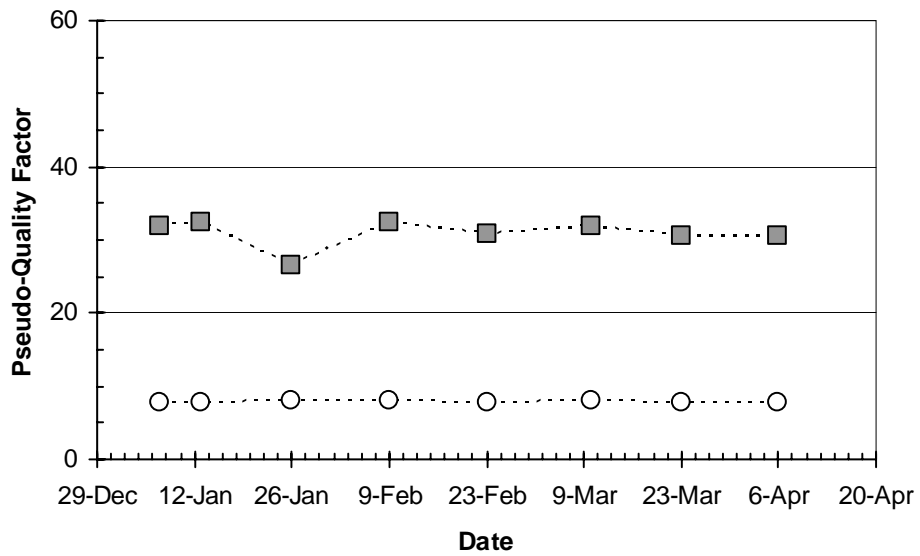
(b)



Figure I-14 Sensor B05 Interrogation History



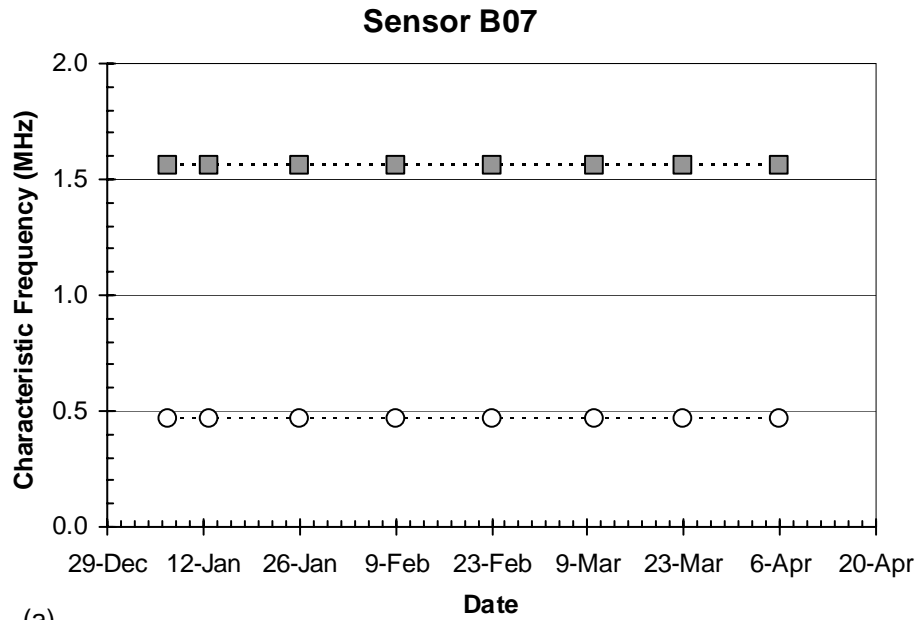
(a)



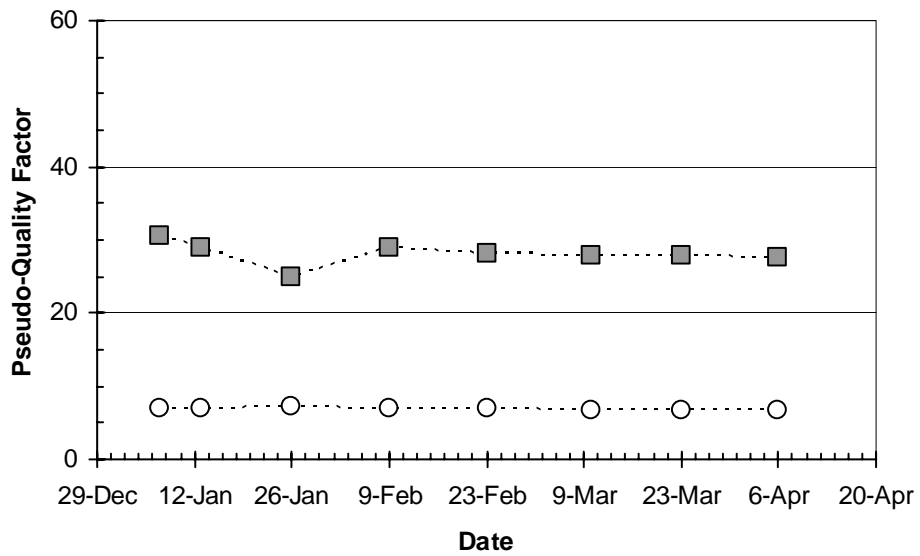
(b)



Figure I-15 Sensor B06 Interrogation History



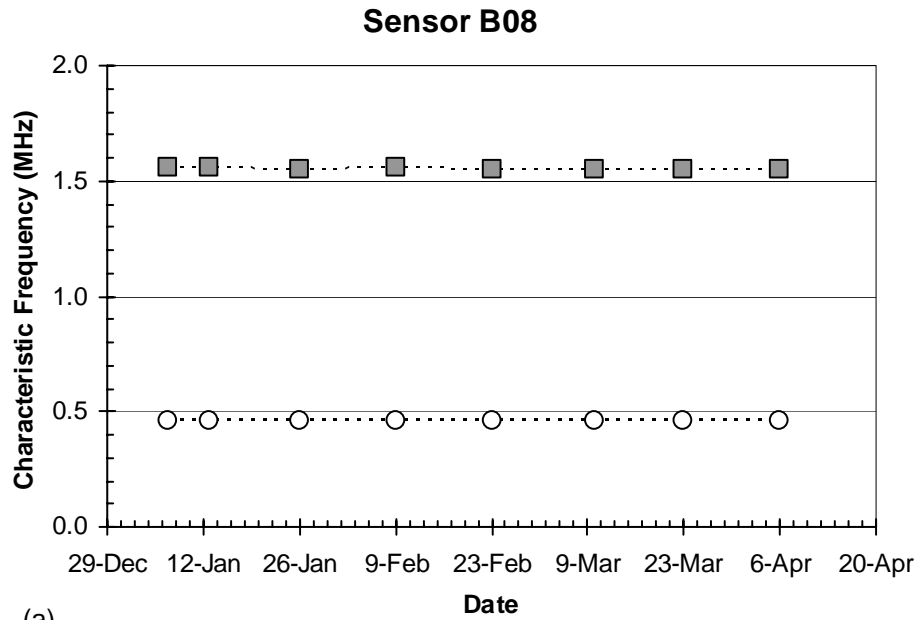
(a)



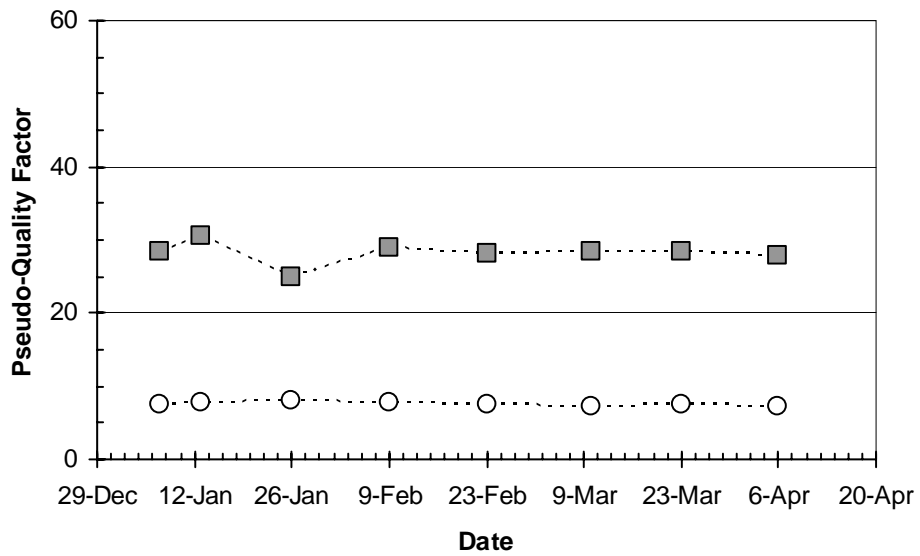
(b)



Figure I-16 Sensor B07 Interrogation History



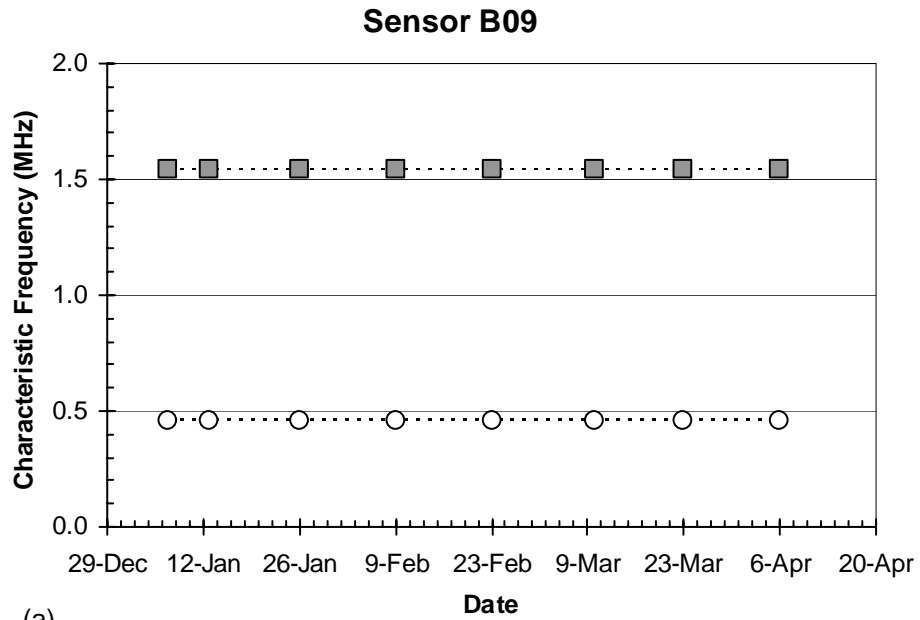
(a)



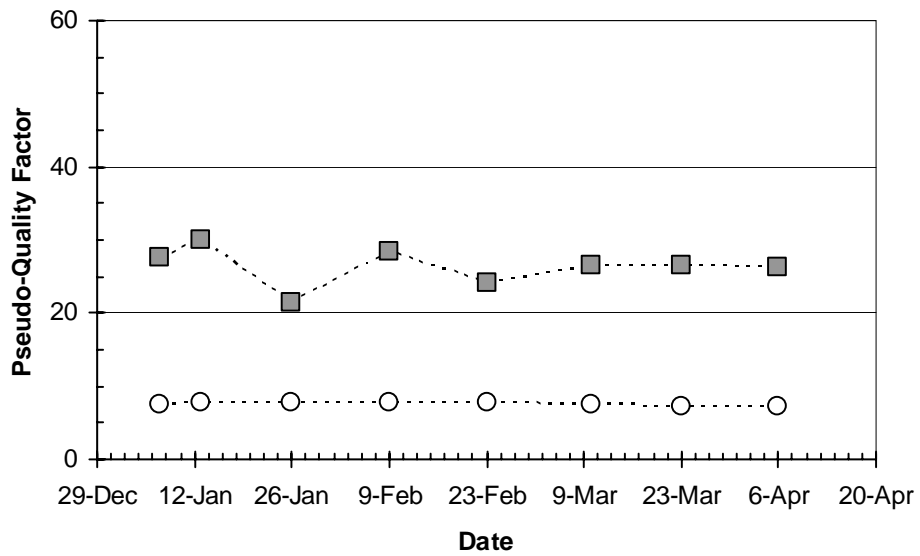
(b)



Figure I-17 Sensor B08 Interrogation History



(a)



(b)



Figure I-18 Sensor B09 Interrogation History

Slab #1 - Point 1 (Sensor A01)

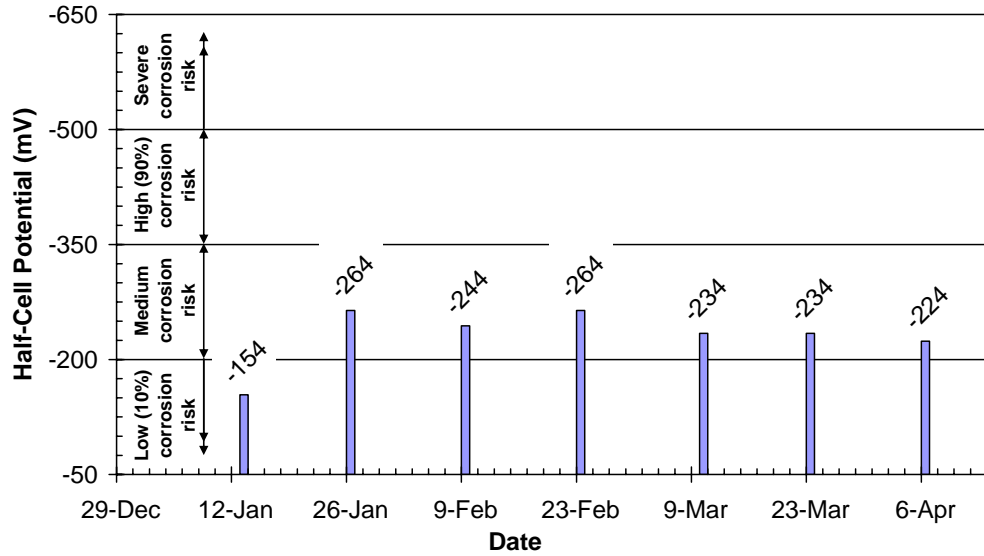


Figure I-19 Point 1 Corrosion Risk History

Slab #1 - Point 1 (Sensor A01)

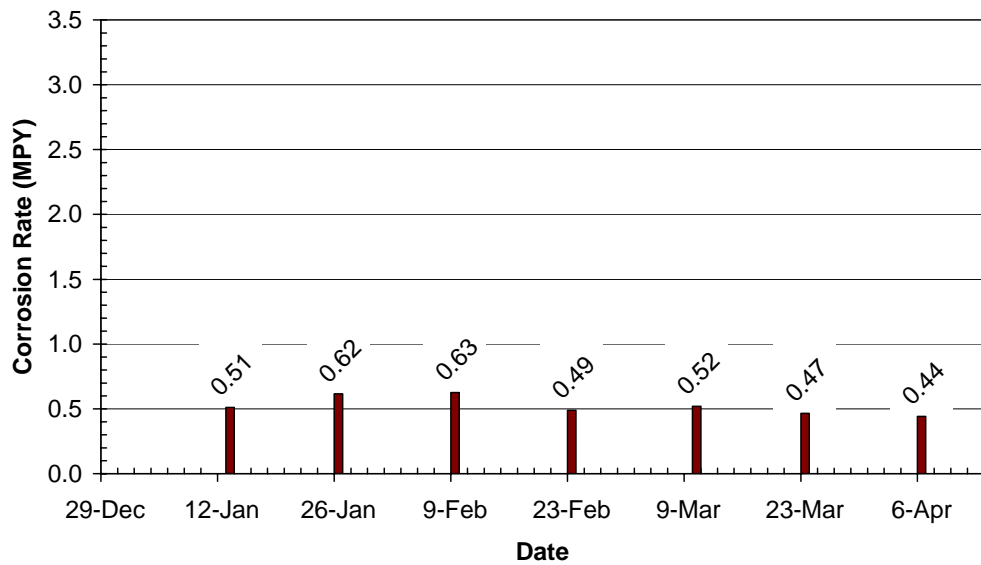


Figure I-20 Point 1 Corrosion Rate History

Slab #1 - Point 3 (Sensor B01)

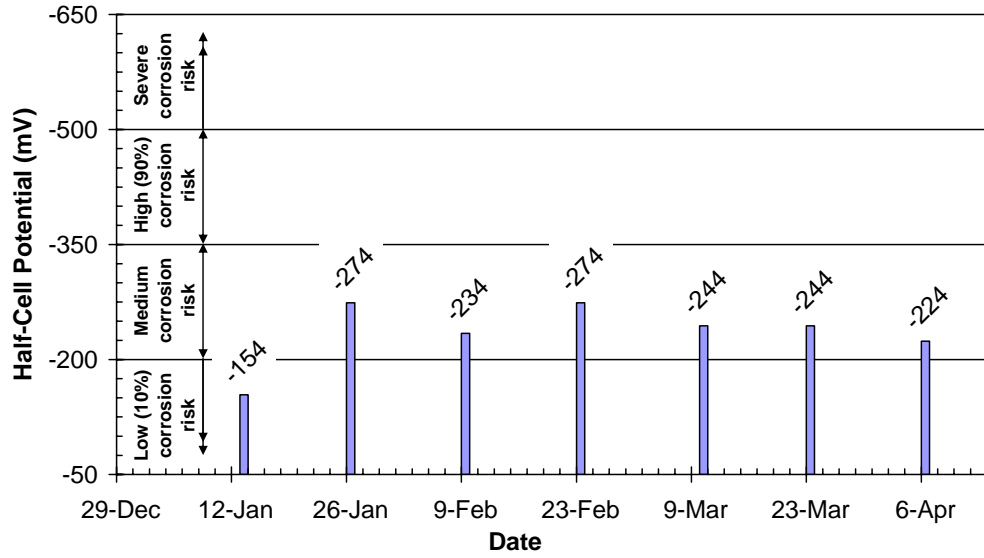


Figure I-21 Point 3 Corrosion Risk History

Slab #1 - Point 3 (Sensor B01)

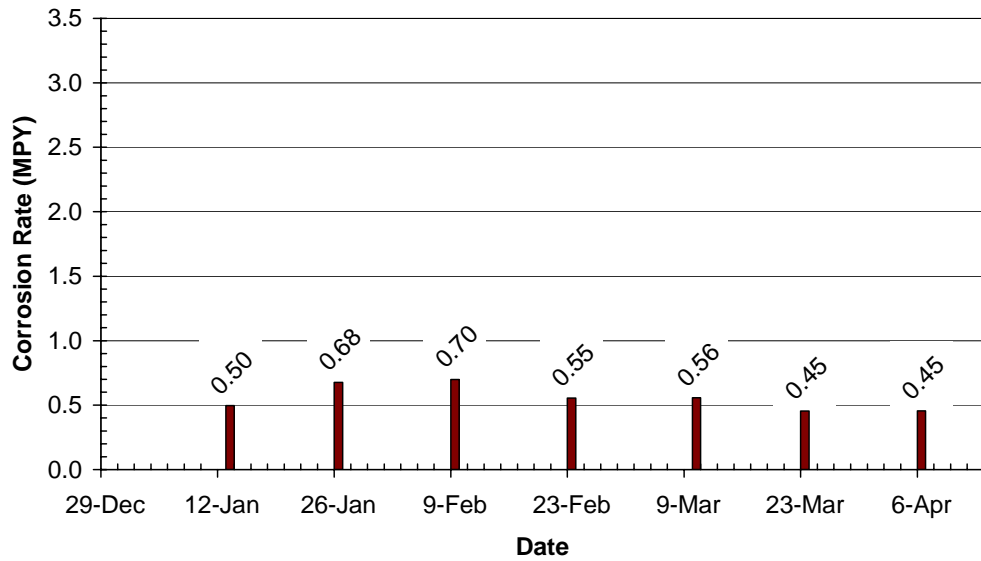


Figure I-22 Point 3 Corrosion Rate History

Slab #1 - Point 9 (Sensor A02)

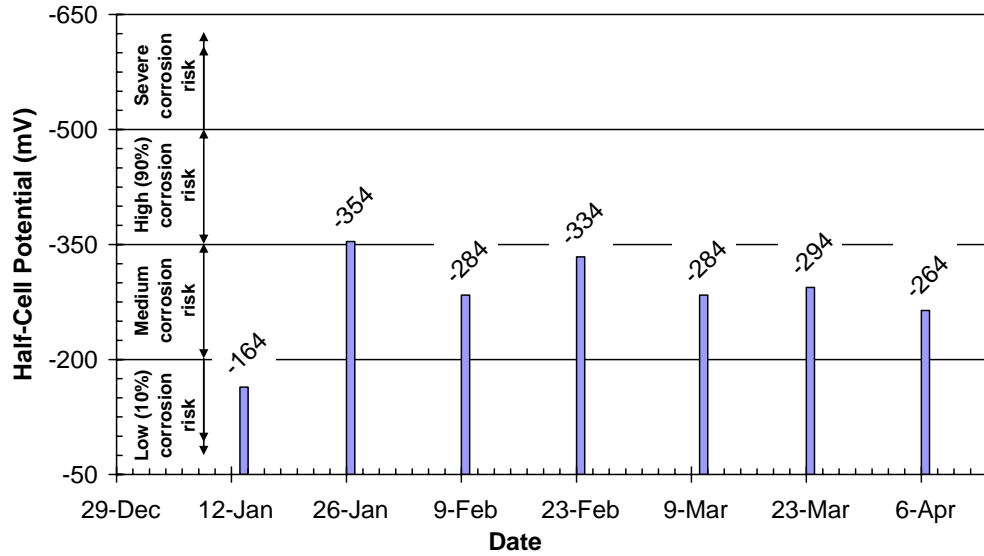


Figure I-23 Point 9 Corrosion Risk History

Slab #1 - Point 9 (Sensor A02)

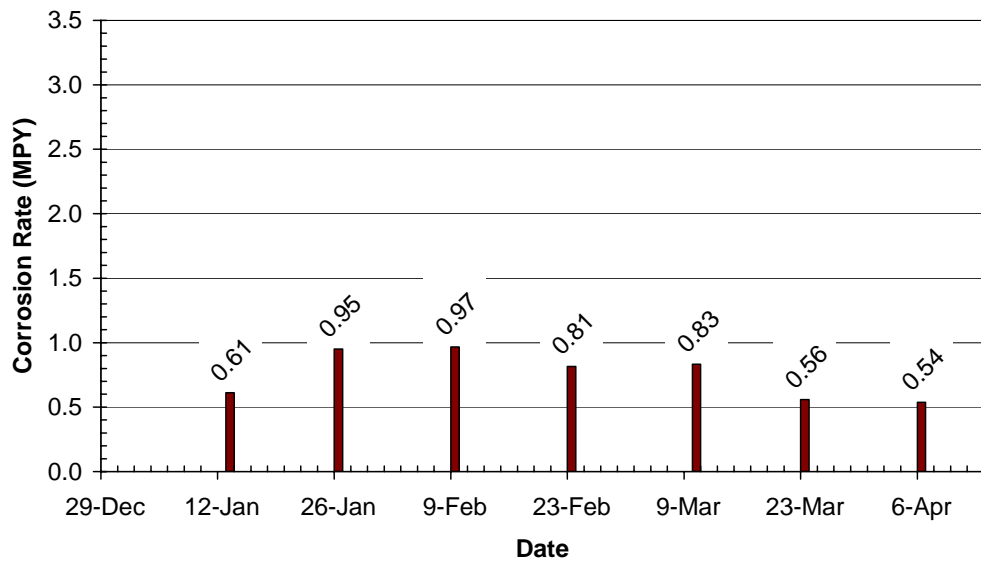


Figure I-24 Point 9 Corrosion Rate History

Slab #1 - Point 11 (Sensor B02)

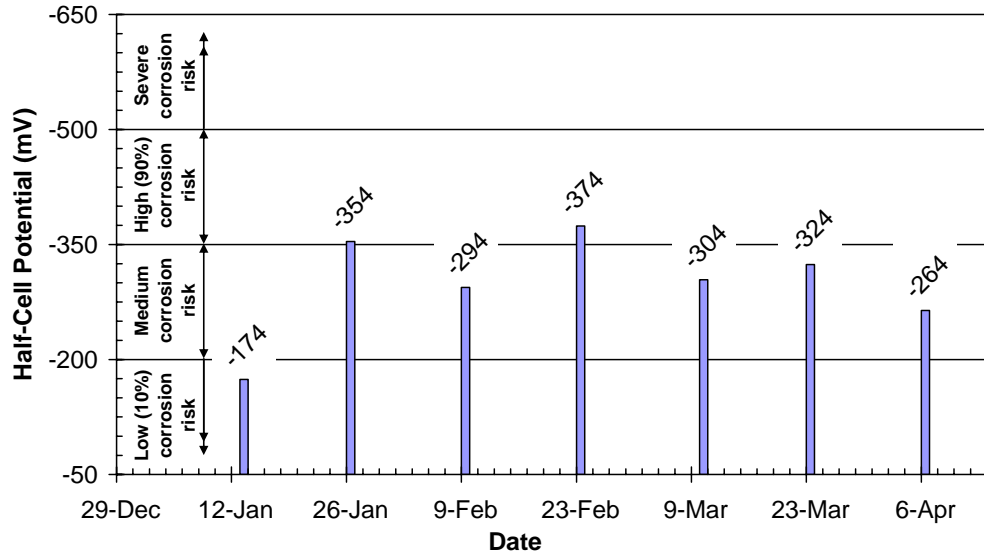


Figure I-25 Point 11 Corrosion Risk History

Slab #1 - Point 11 (Sensor B02)

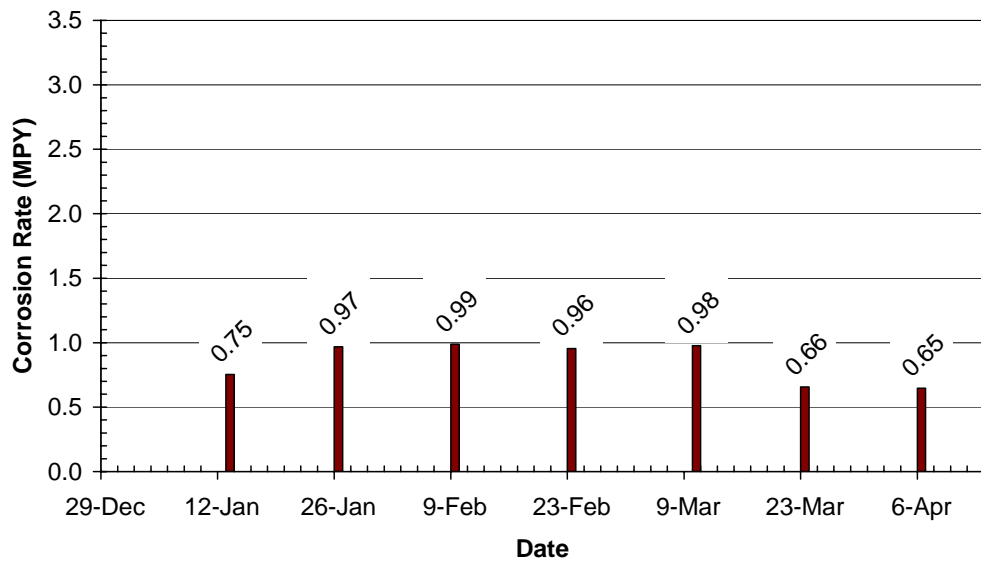


Figure I-26 Point 11 Corrosion Rate History

Slab #1 - Point 13 (Sensors A03 & A04)

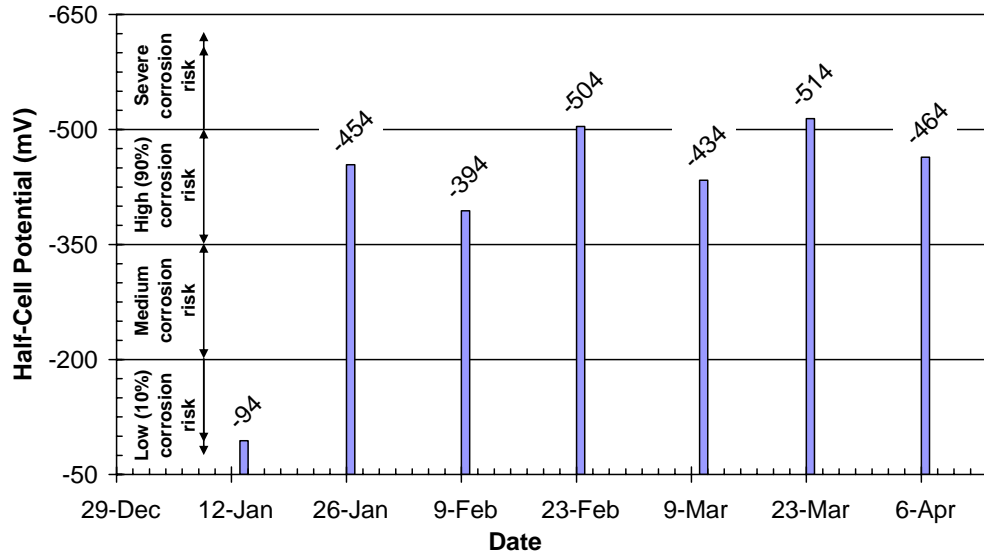


Figure I-27 Point 13 Corrosion Risk History

Slab #1 - Point 13 (Sensors A03 & A04)

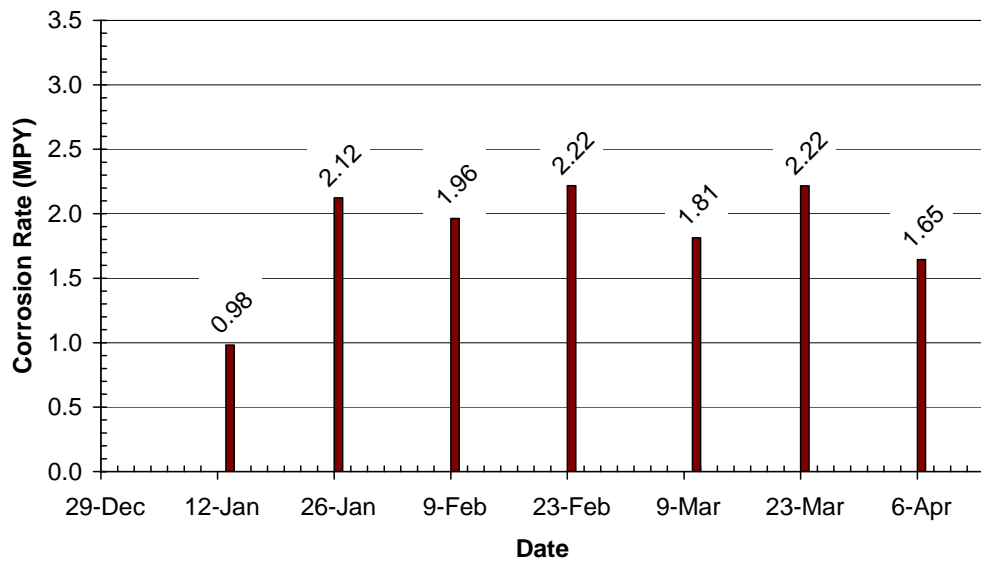


Figure I-28 Point 13 Corrosion Rate History

Slab #1 - Point 15 (Sensors B03 & B04)

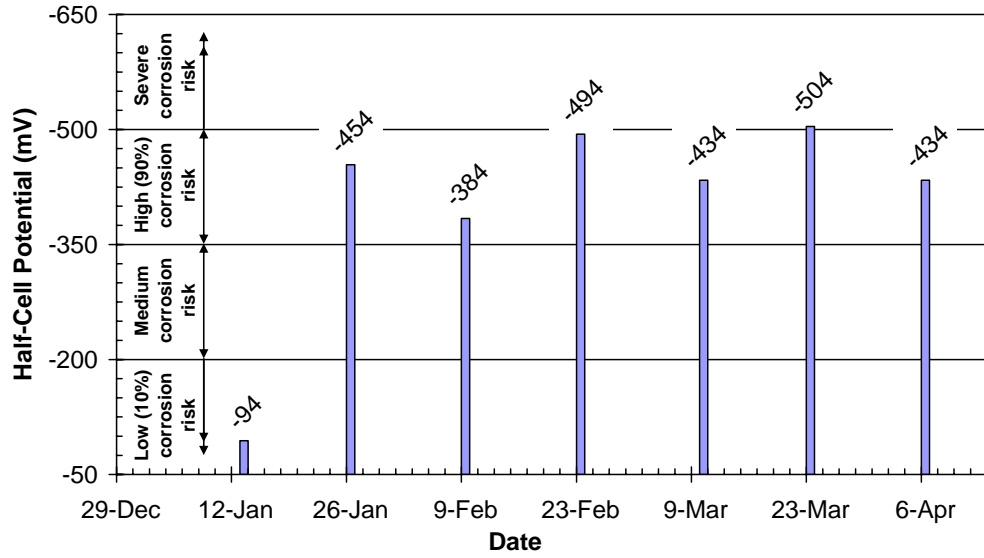


Figure I-29 Point 15 Corrosion Risk History

Slab #1 - Point 15 (Sensors B03 & B04)

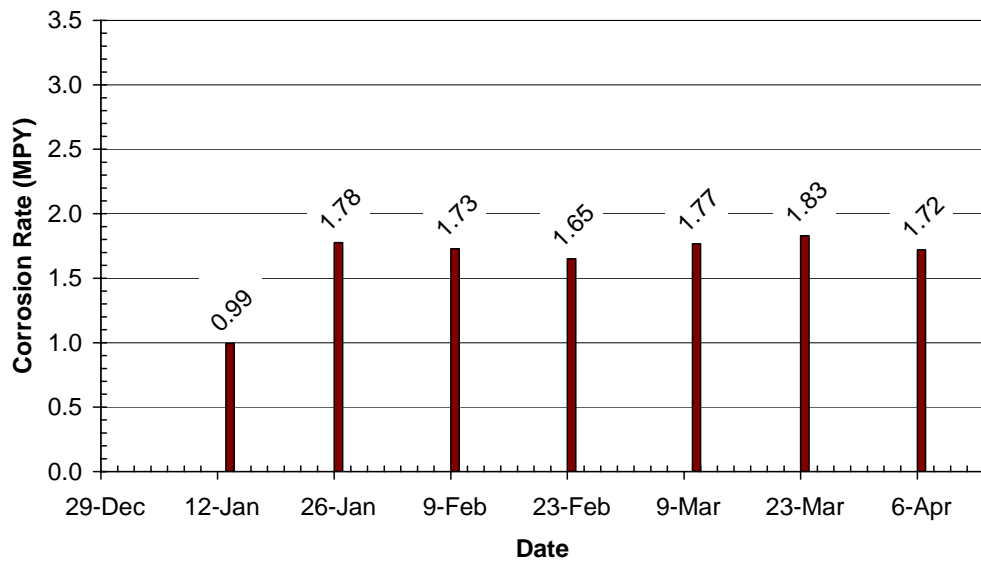


Figure I-30 Point 15 Corrosion Rate History

Slab #1 - Point 17 (Sensors A04 & A05)

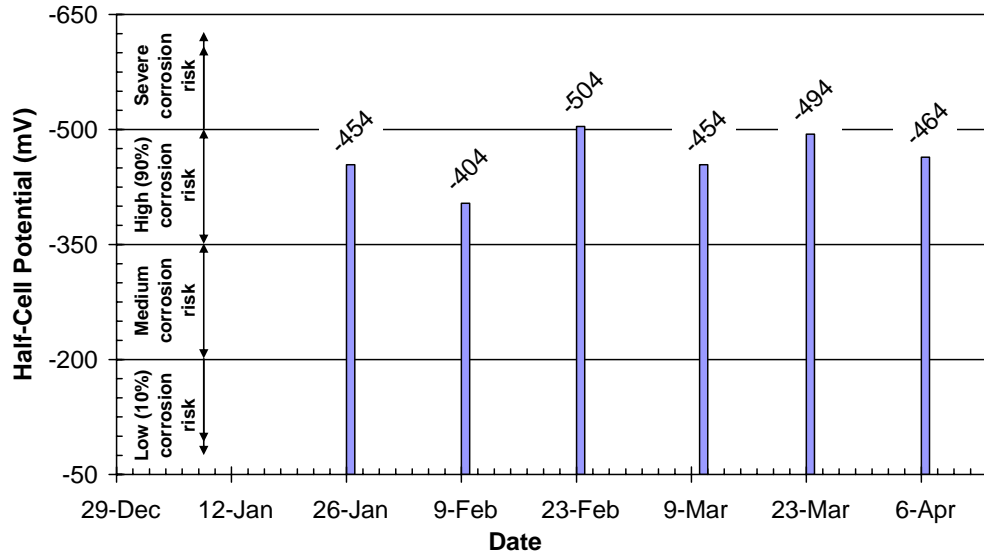


Figure I-31 Point 17 Corrosion Risk History

Slab #1 - Point 17 (Sensors A04 & A05)

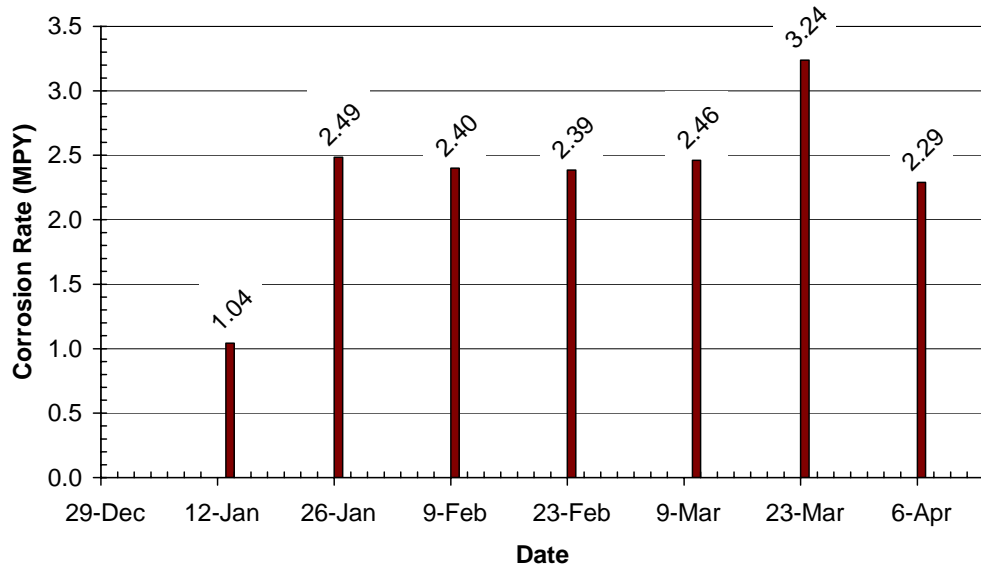


Figure I-32 Point 17 Corrosion Rate History

Slab #1 - Point 19 (Sensors B04 & B05)

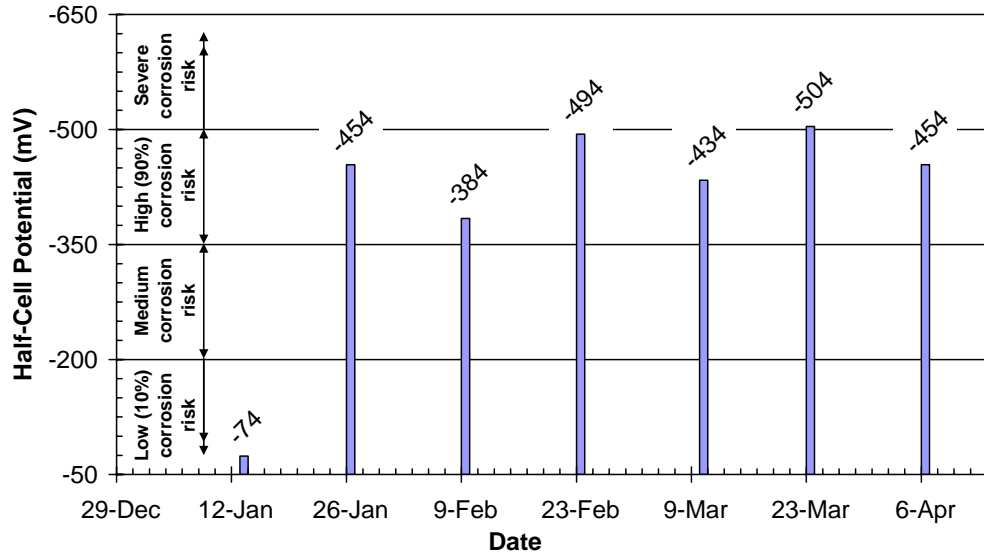


Figure I-33 Point 19 Corrosion Risk History

Slab #1 - Point 19 (Sensors B04 & B05)

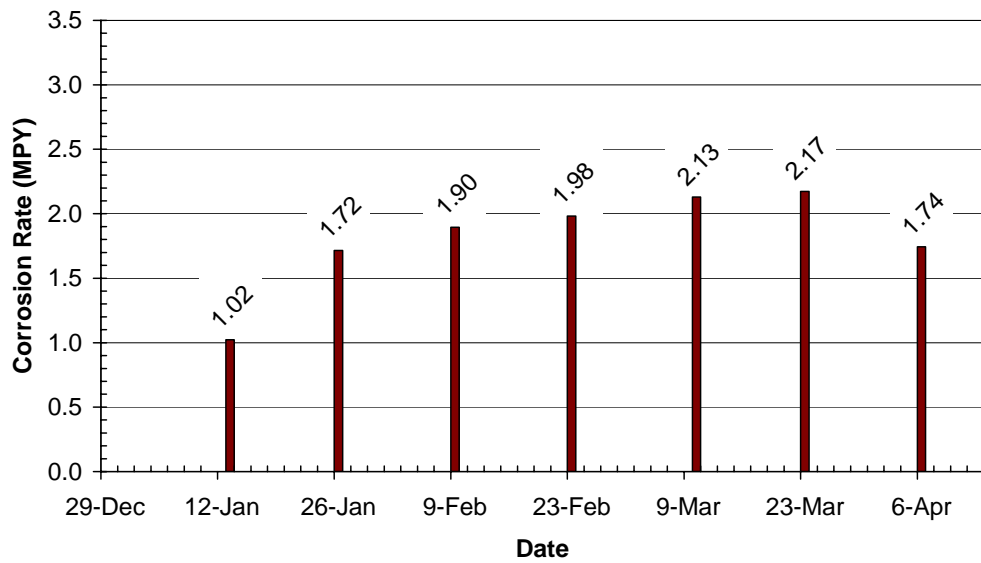


Figure I-34 Point 19 Corrosion Rate History

Slab #1 - Point 21 (Sensor A06)

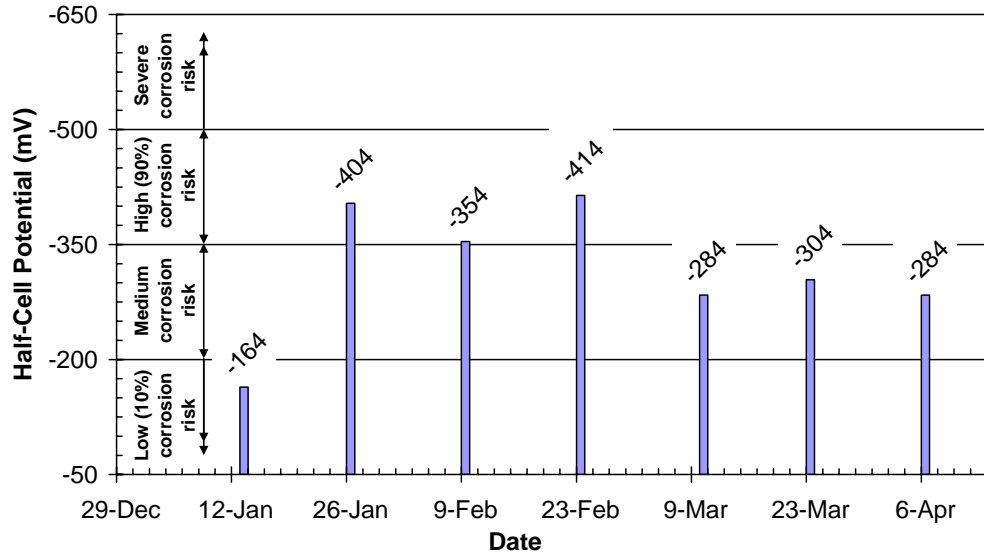


Figure I-35 Point 21 Corrosion Risk History

Slab #1 - Point 21 (Sensor A06)

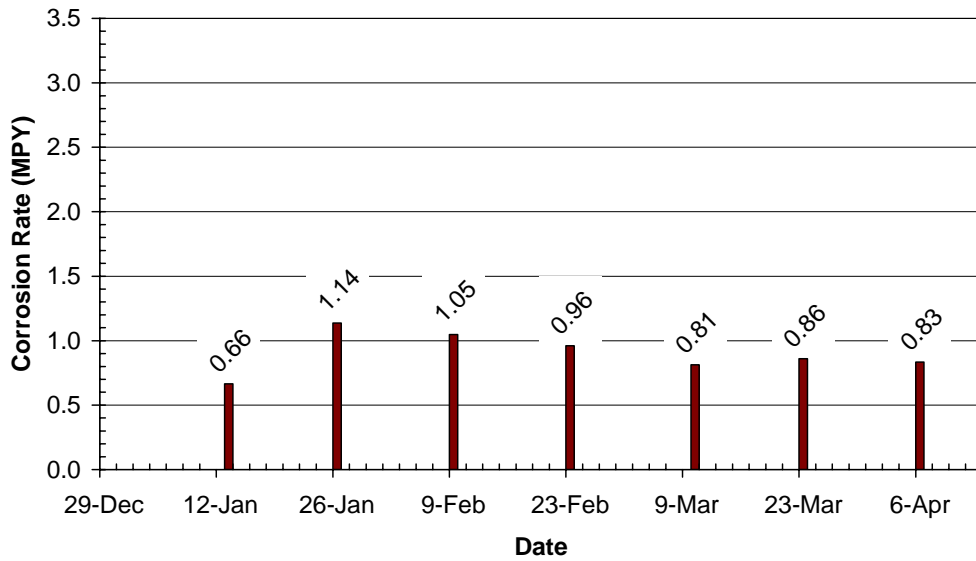


Figure I-36 Point 21 Corrosion Rate History

Slab #1 - Point 23 (Sensor B06)

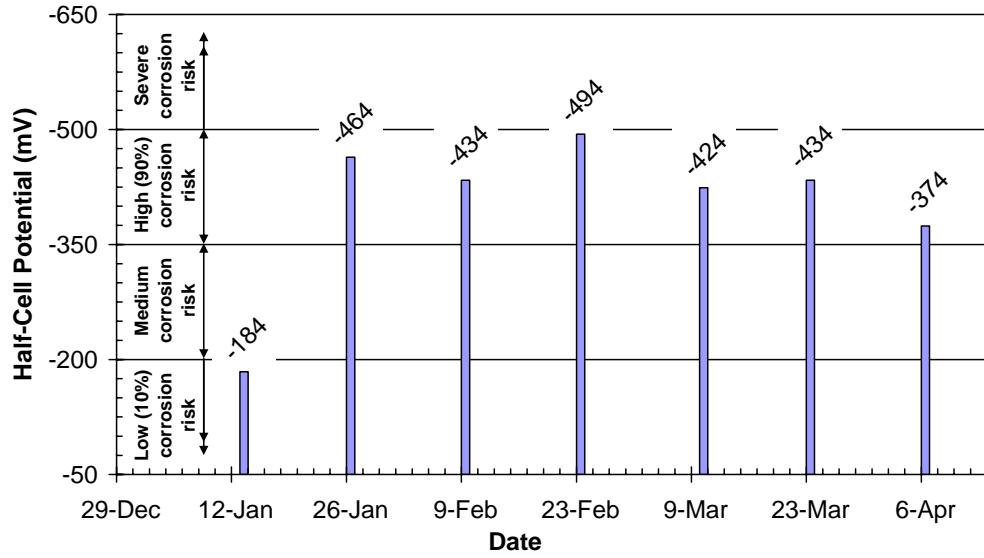


Figure I-37 Point 23 Corrosion Risk History

Slab #1 - Point 23 (Sensor B06)

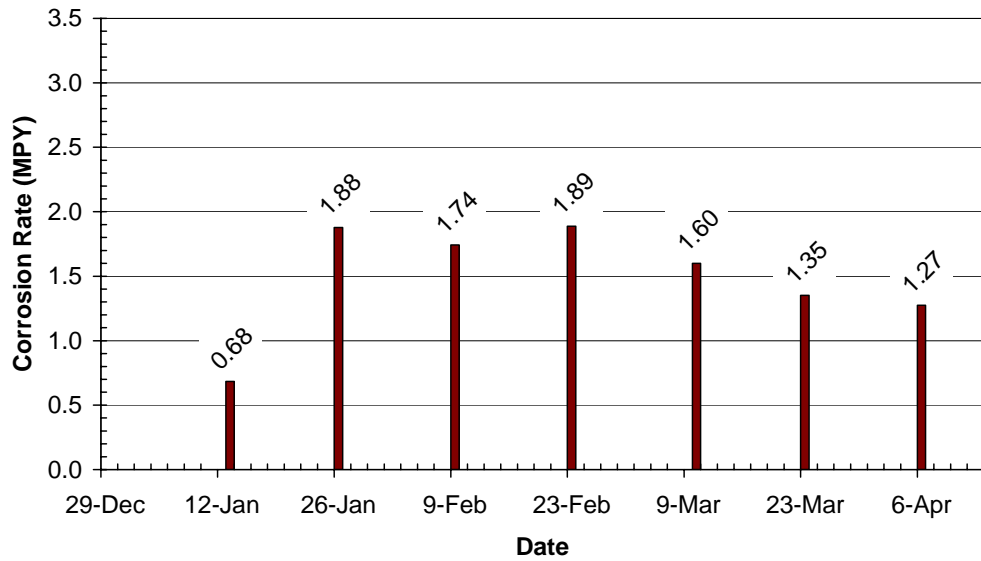


Figure I-38 Point 23 Corrosion Rate History

Slab #1 - Point 29 (Sensor A07)

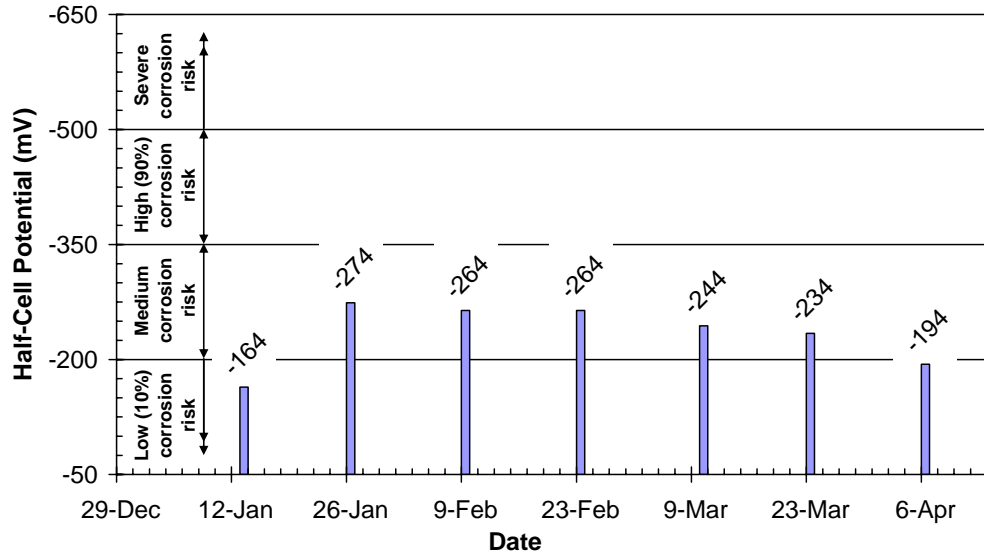


Figure I-39 Point 29 Corrosion Risk History

Slab #1 - Point 29 (Sensor A07)

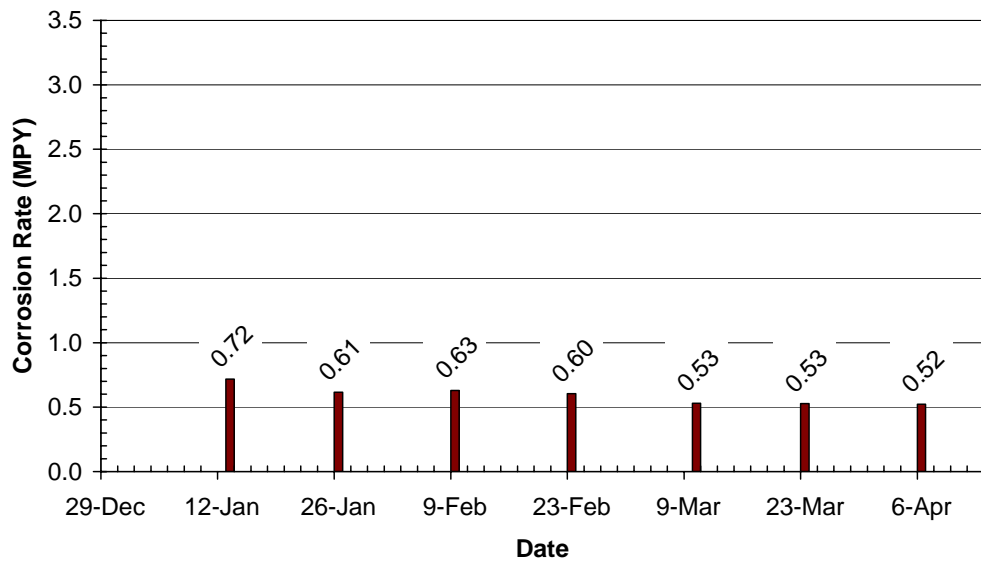


Figure I-40 Point 29 Corrosion Rate History

Slab #1 - Point 31 (Sensor B07)

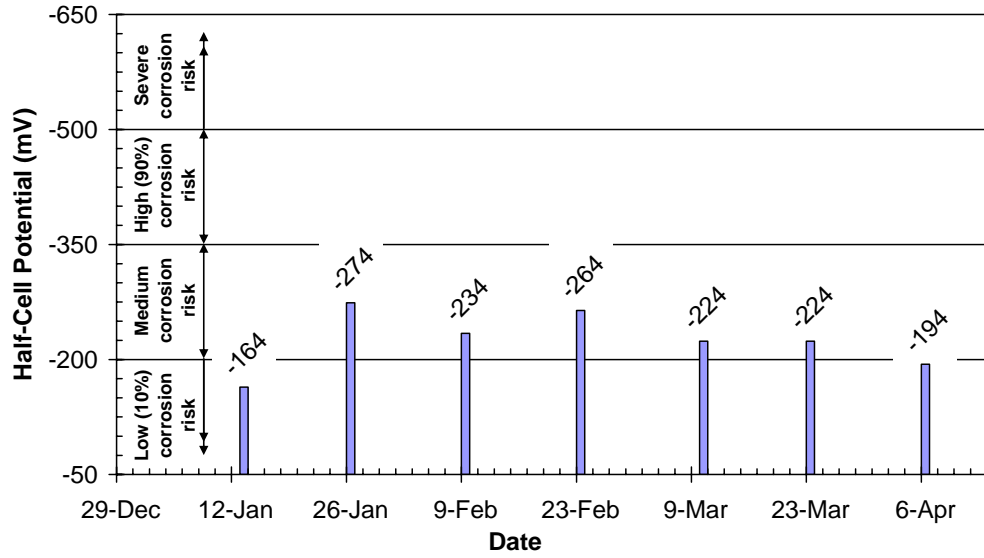


Figure I-41 Point 31 Corrosion Risk History

Slab #1 - Point 31 (Sensor B07)

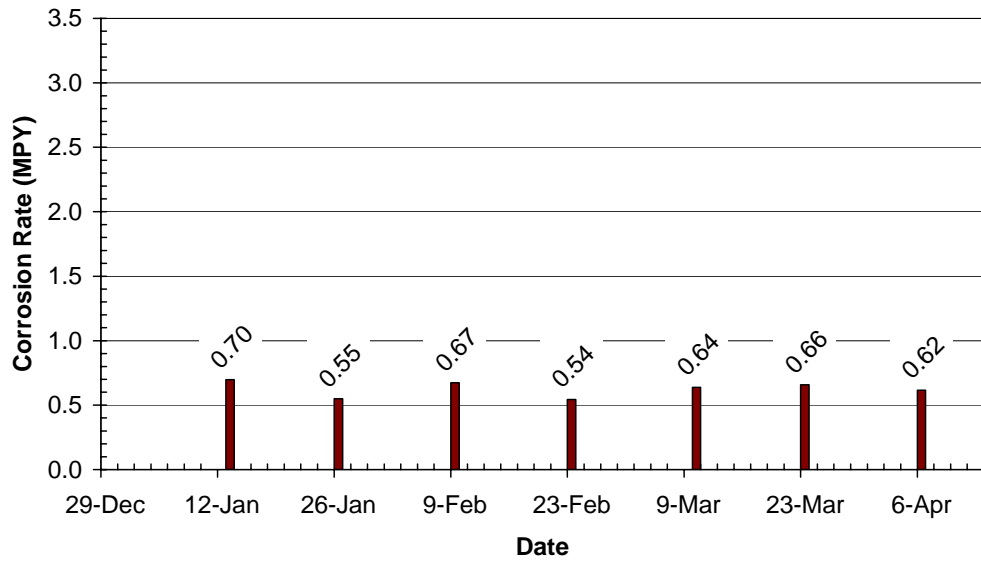


Figure I-42 Point 31 Corrosion Rate History

APPENDIX J

Reinforced Concrete Slab #2 Monitoring Results

Results from monitoring reinforced concrete slab #2 with embedded sensors are presented in this appendix. Plots of characteristic frequency and pseudo-quality factors at each interrogation are provided through 6 April 2005 for each sensor. Plots of half-cell potentials and instantaneous corrosion rates are also provided at each interrogation through 6 April 2005 for points on the surface of the slab corresponding to sensor locations. Fig. J-1 shows the temperature at each interrogation.

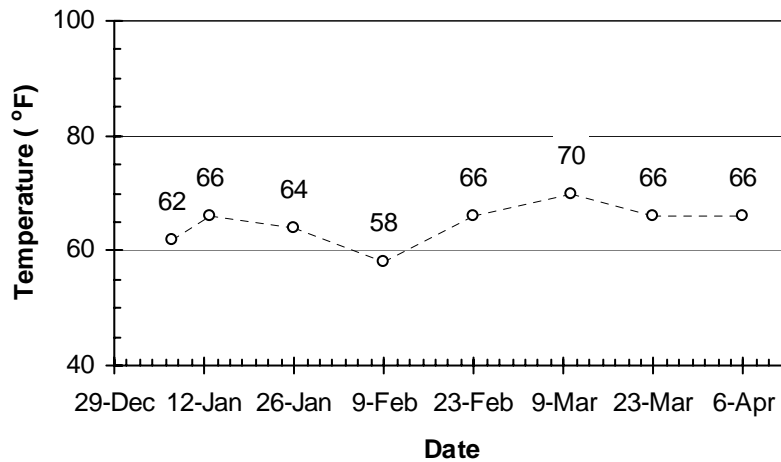
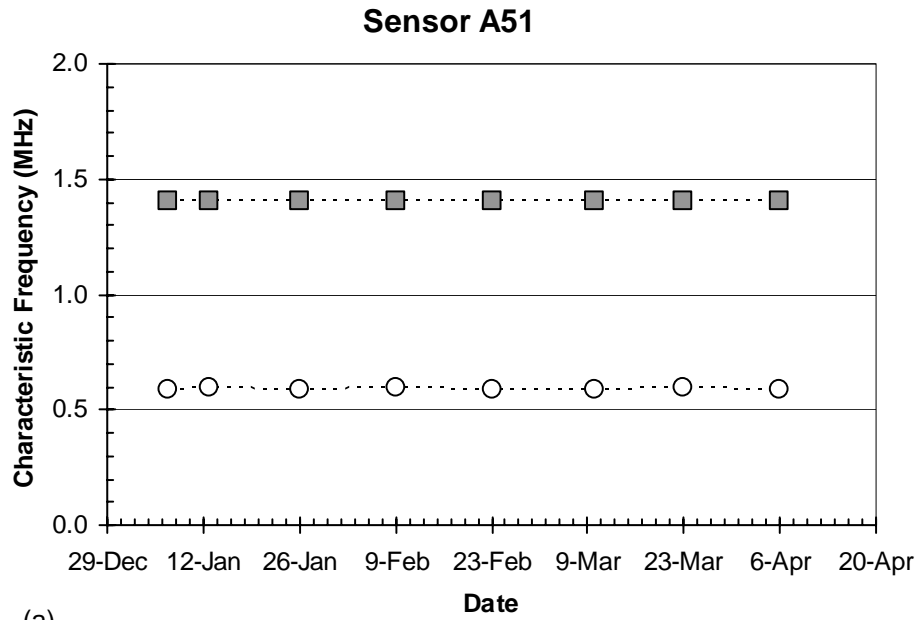
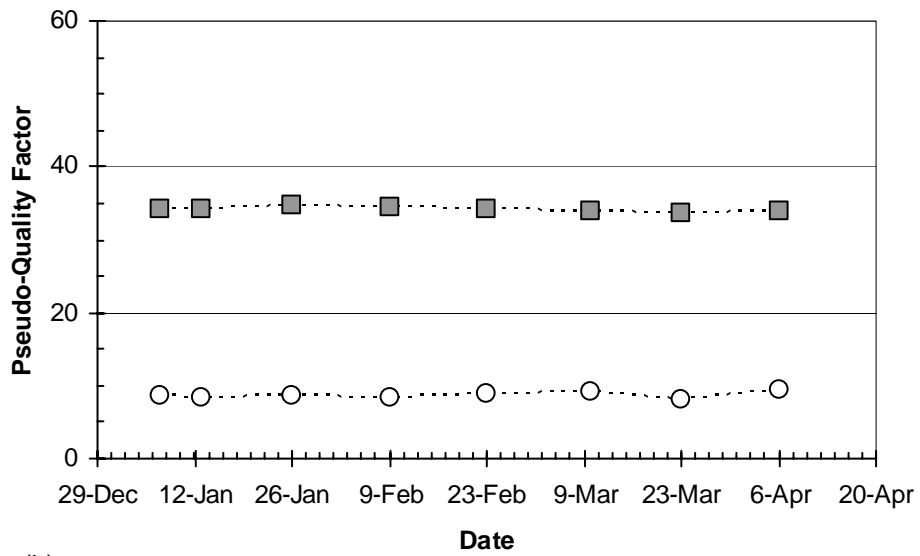


Figure J-1 Temperature Data at Sensor Interrogations for Slab #2



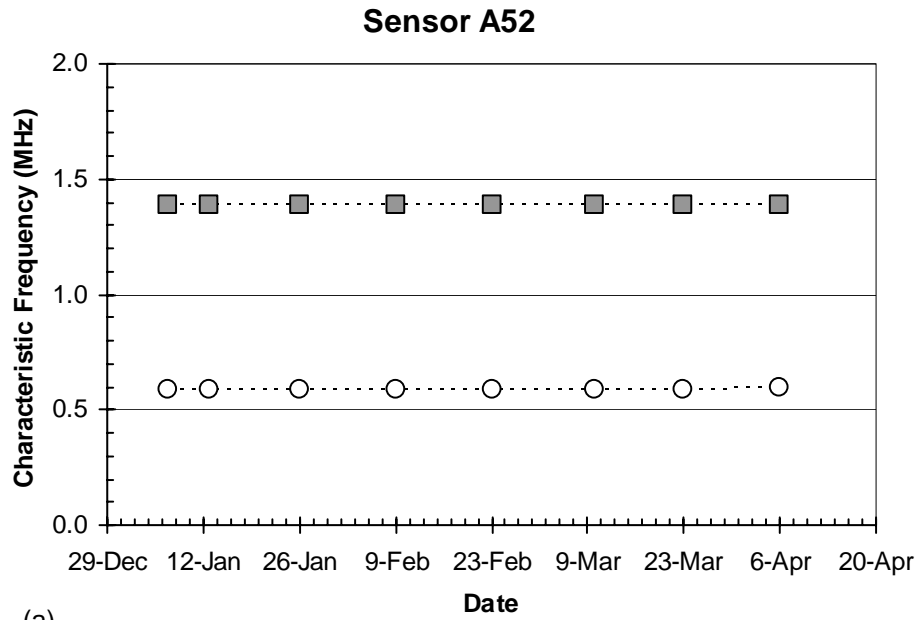
(a)



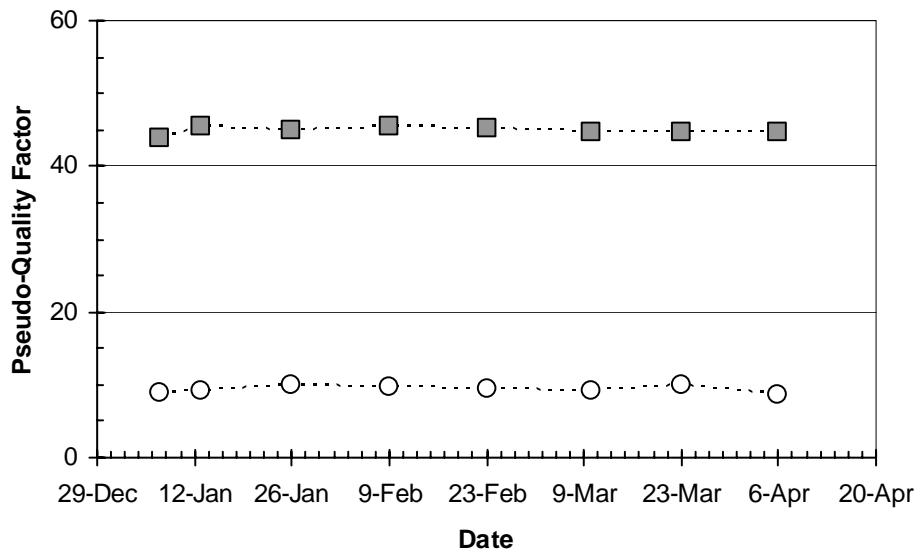
(b)



Figure J-2 Sensor A51 Interrogation History



(a)

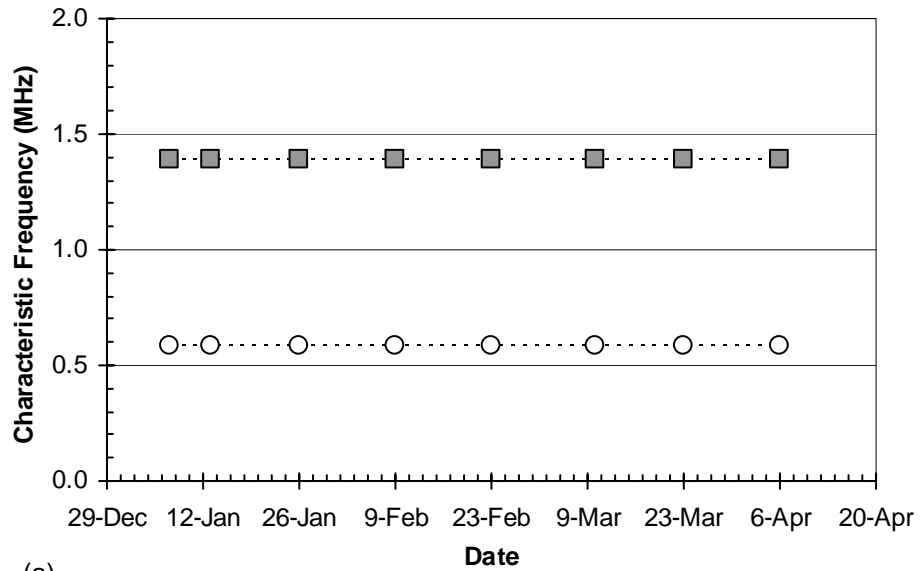


(b)

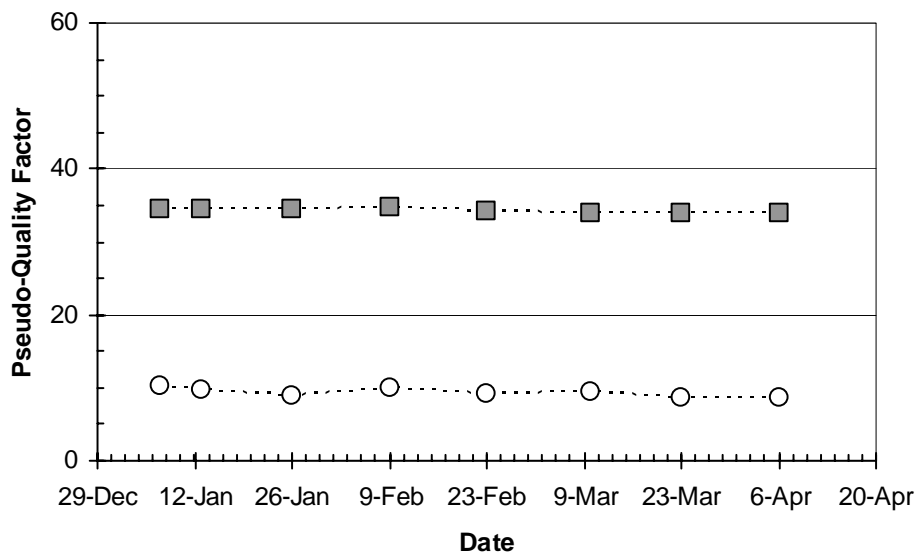


Figure J-3 Sensor A52 Interrogation History

Sensor A53



(a)

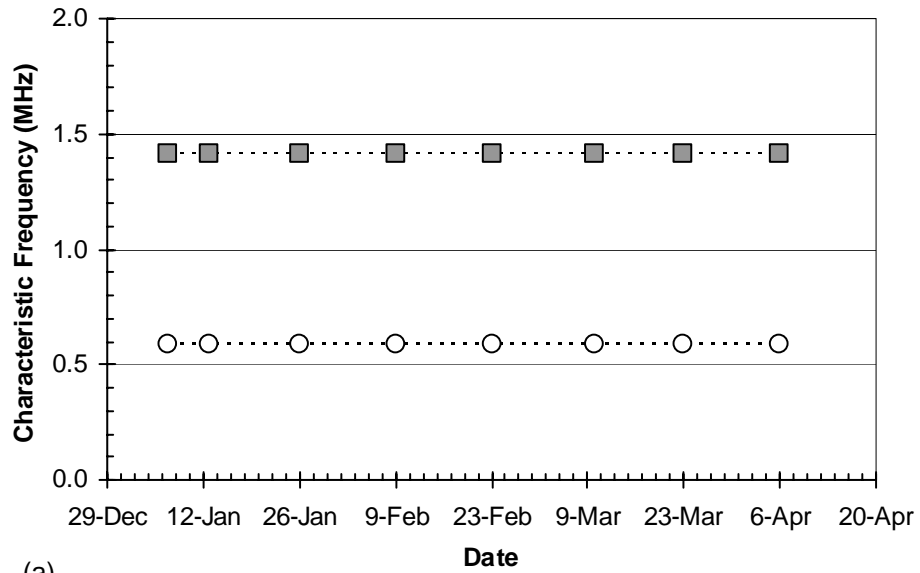


(b)

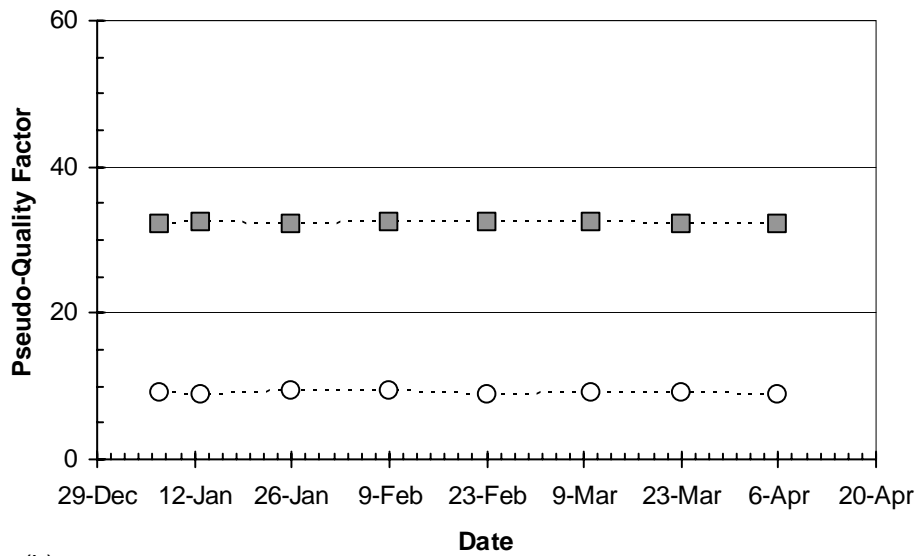


Figure J-4 Sensor A53 Interrogation History

Sensor A54



(a)

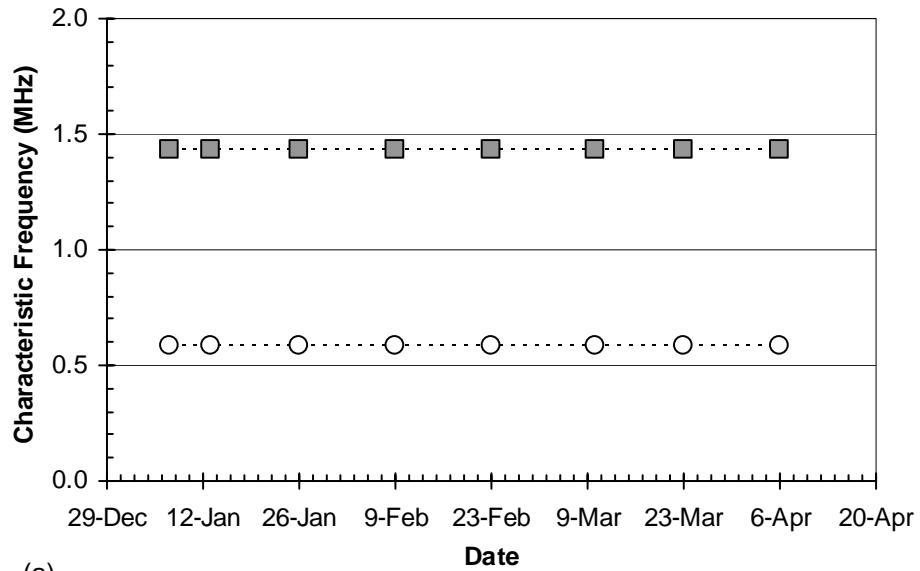


(b)

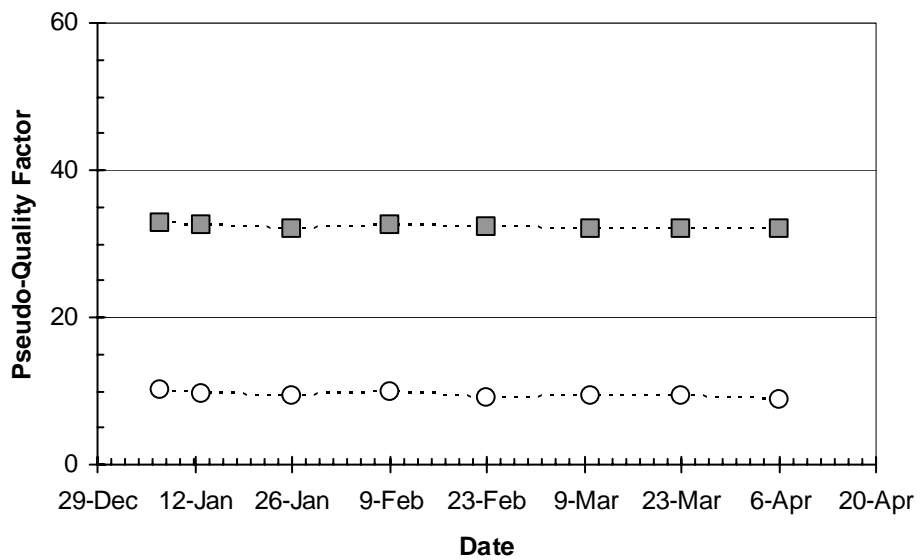


Figure J-5 Sensor A54 Interrogation History

Sensor A55



(a)

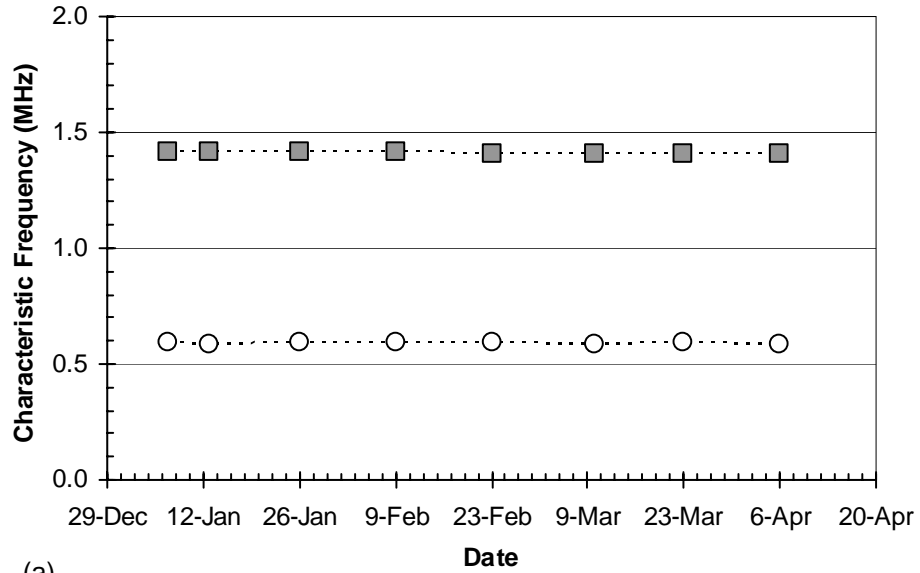


(b)

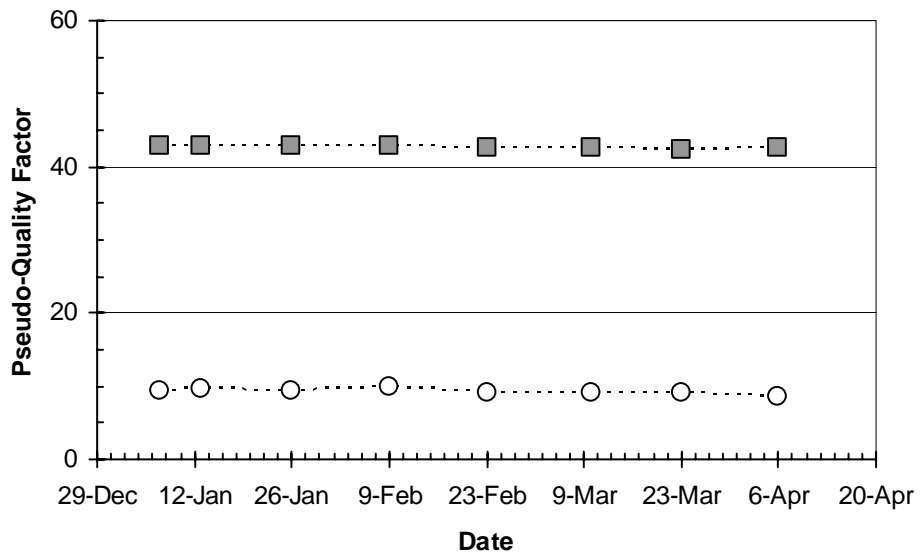


Figure J-6 Sensor A55 Interrogation History

Sensor A56



(a)

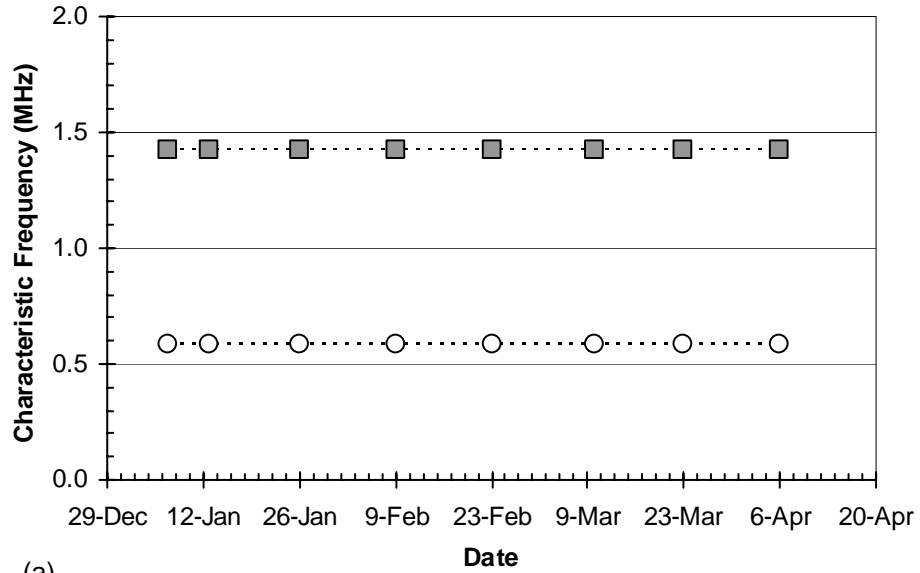


(b)

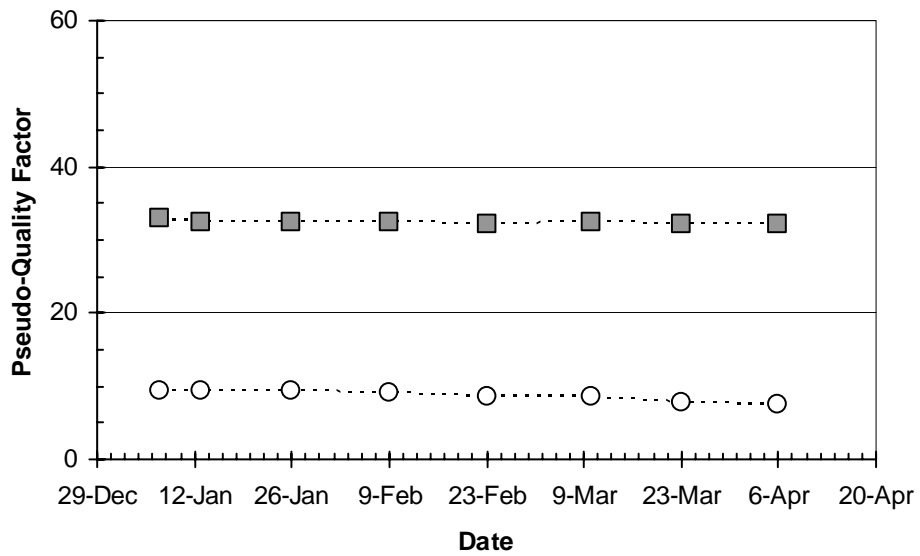


Figure J-7 Sensor A56 Interrogation History

Sensor A57



(a)

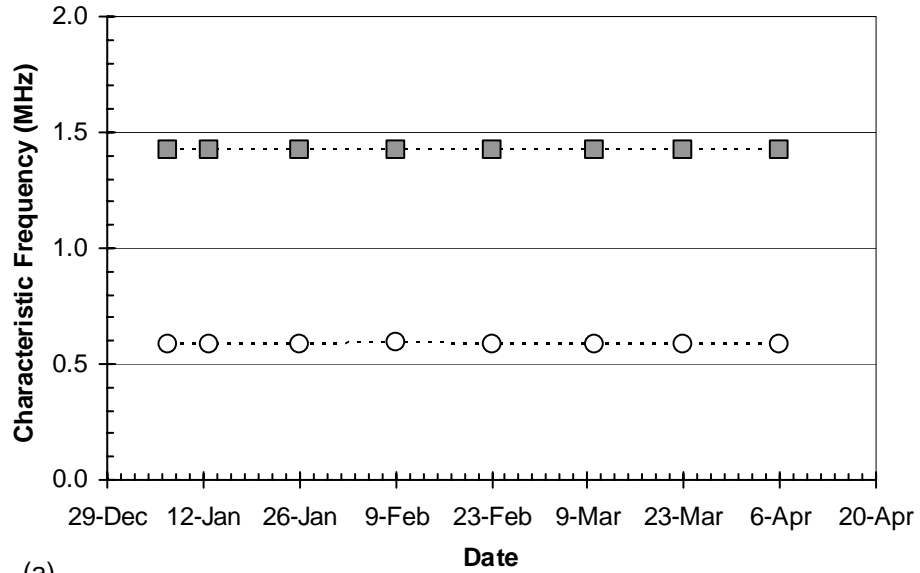


(b)

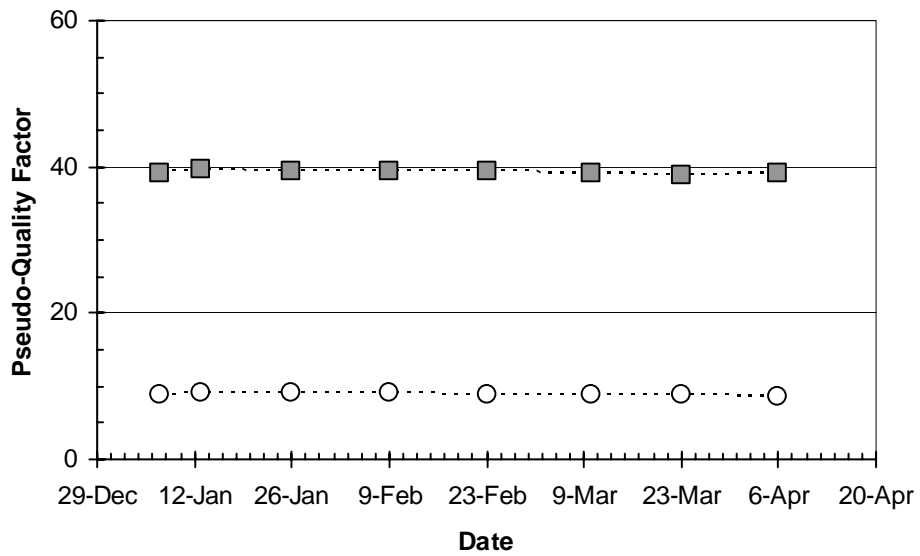


Figure J-8 Sensor A57 Interrogation History

Sensor A58



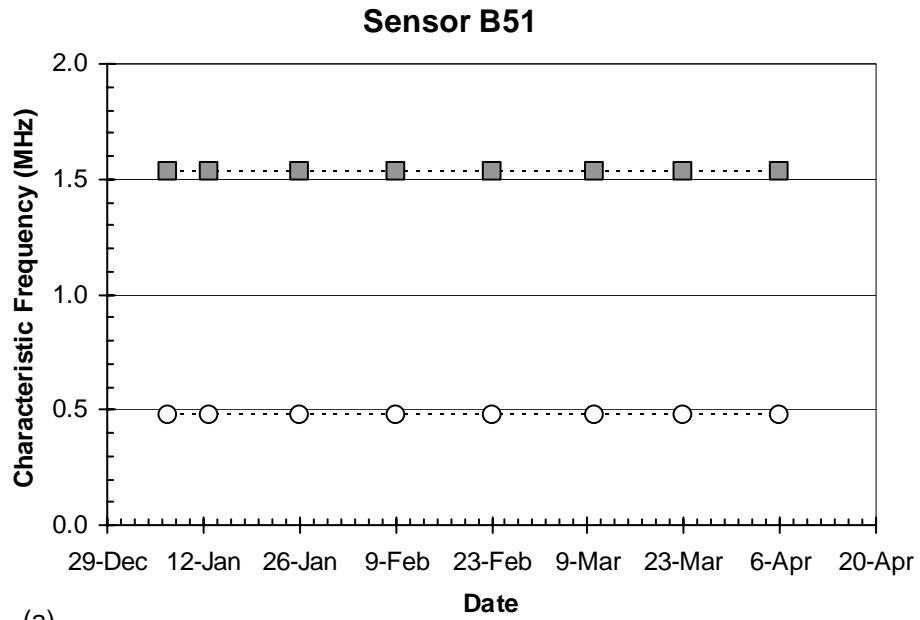
(a)



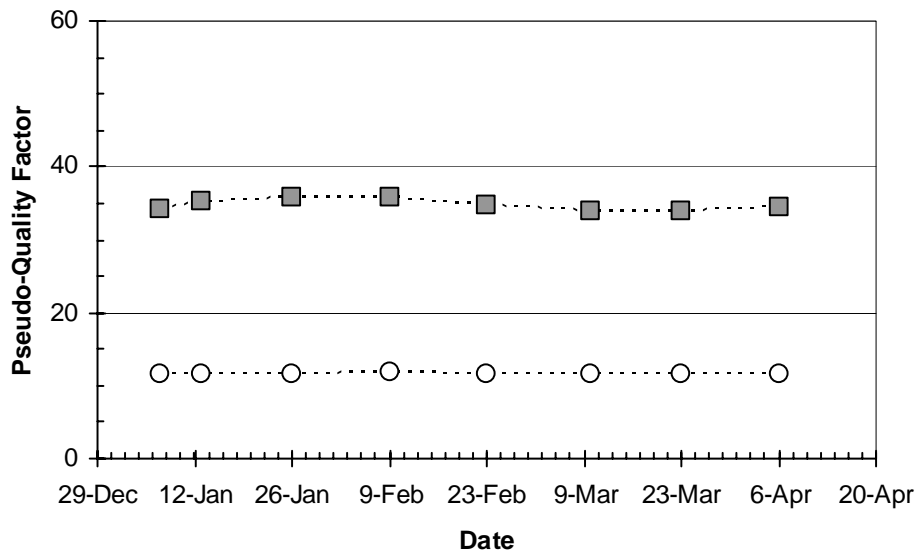
(b)



Figure J-9 Sensor A58 Interrogation History



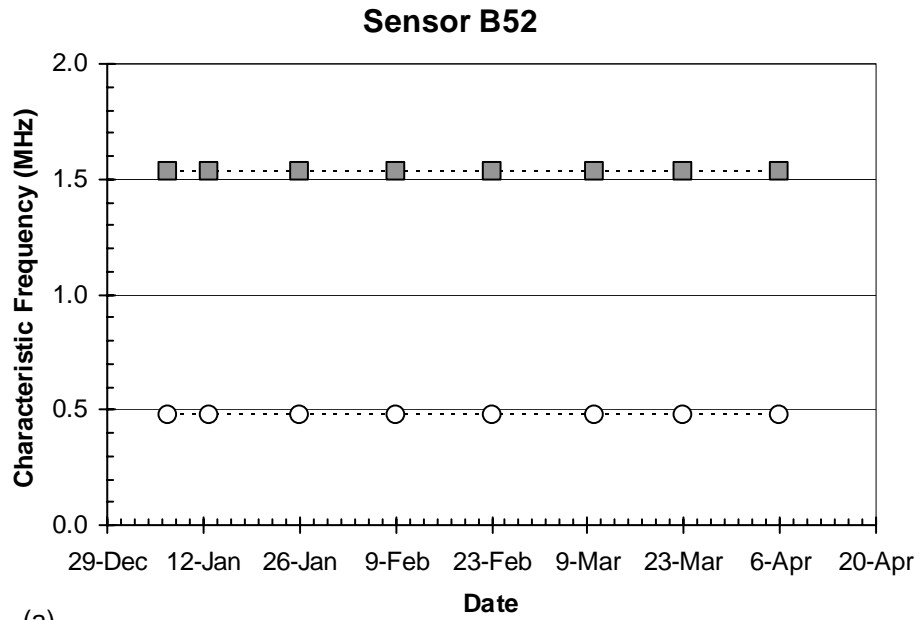
(a)



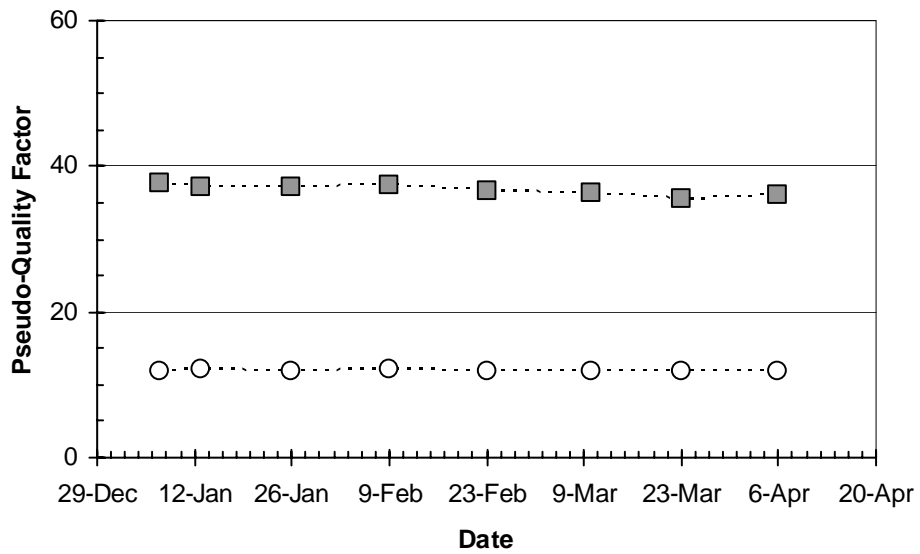
(b)



Figure J-10 Sensor B51 Interrogation History



(a)

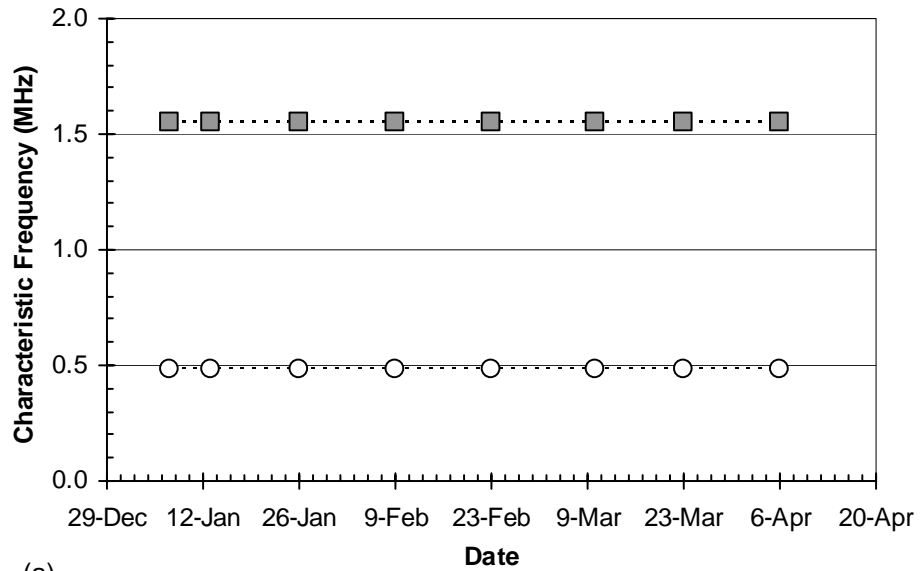


(b)

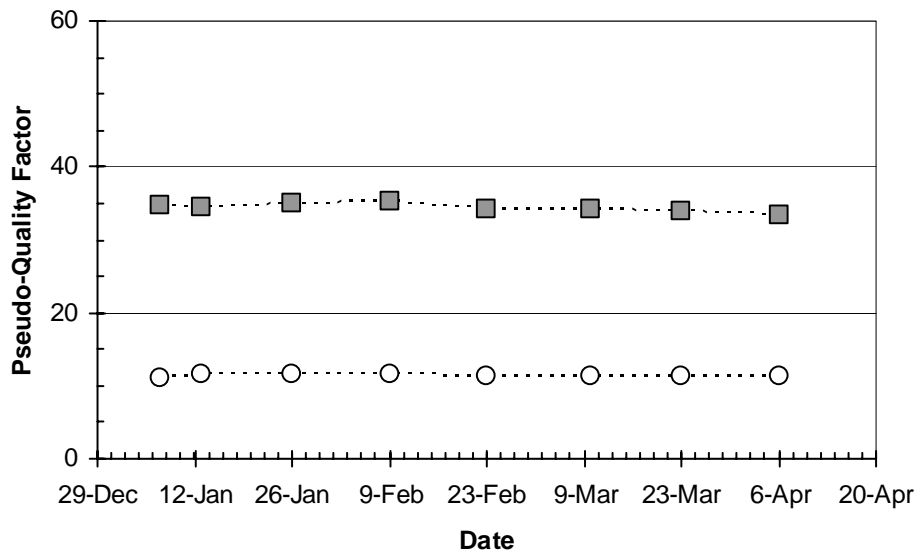


Figure J-11 Sensor B52 Interrogation History

Sensor B53



(a)



(b)

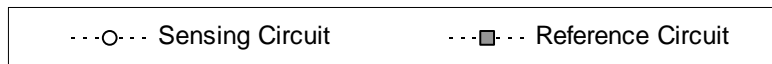
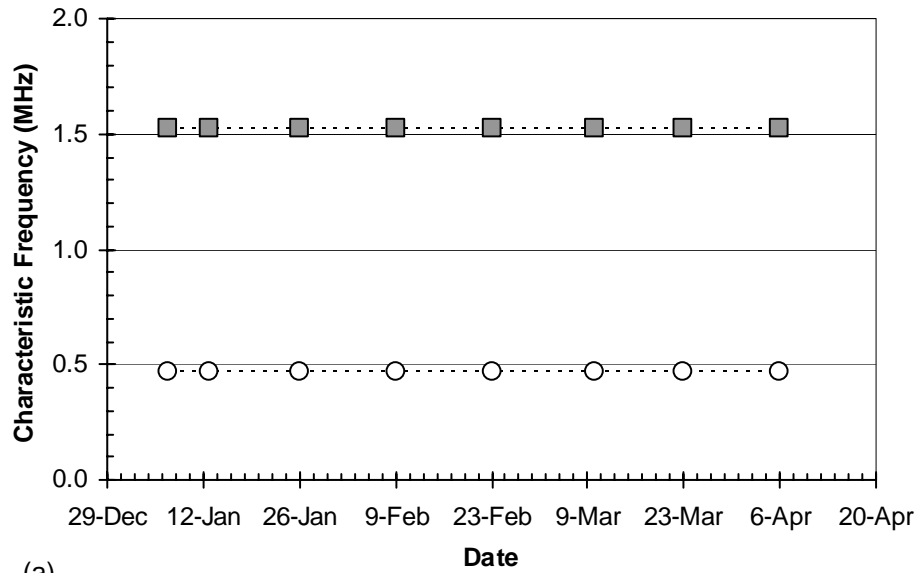
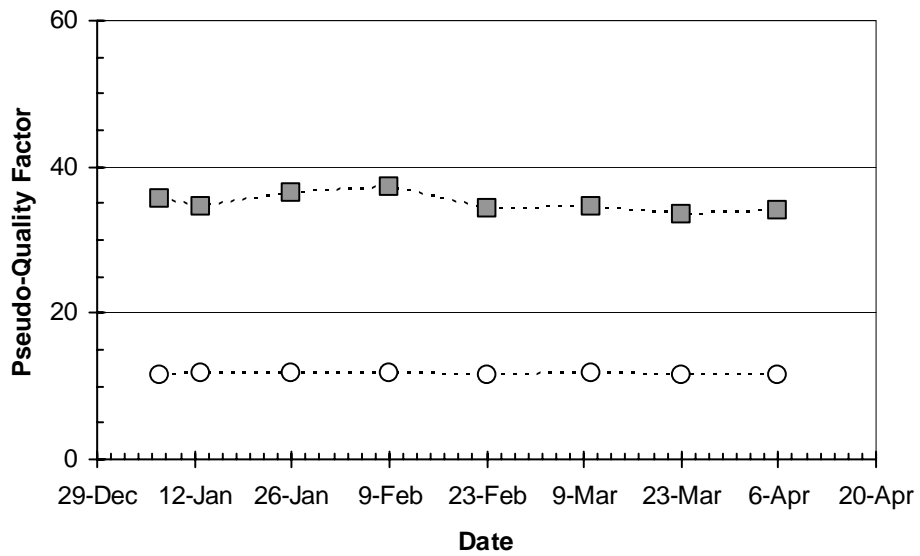


Figure J-12 Sensor B53 Interrogation History

Sensor B54



(a)

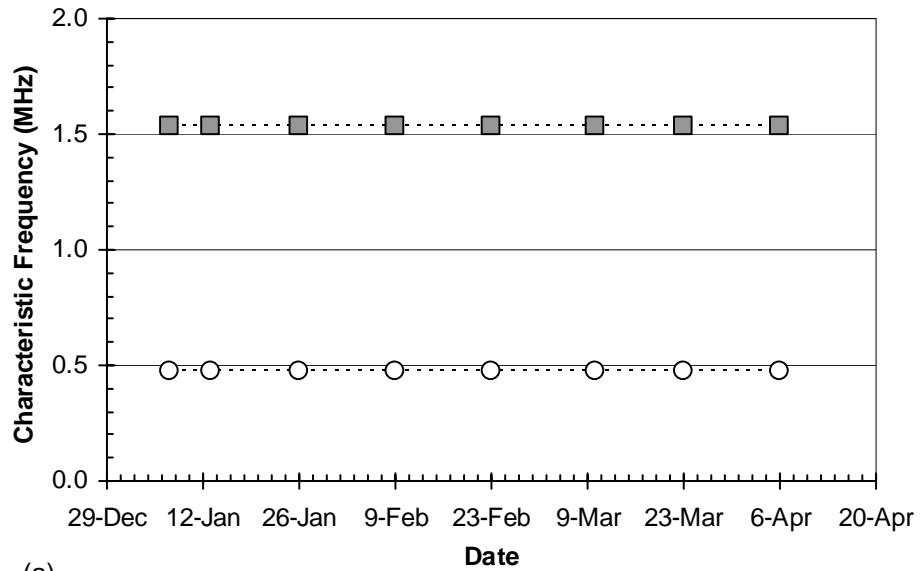


(b)

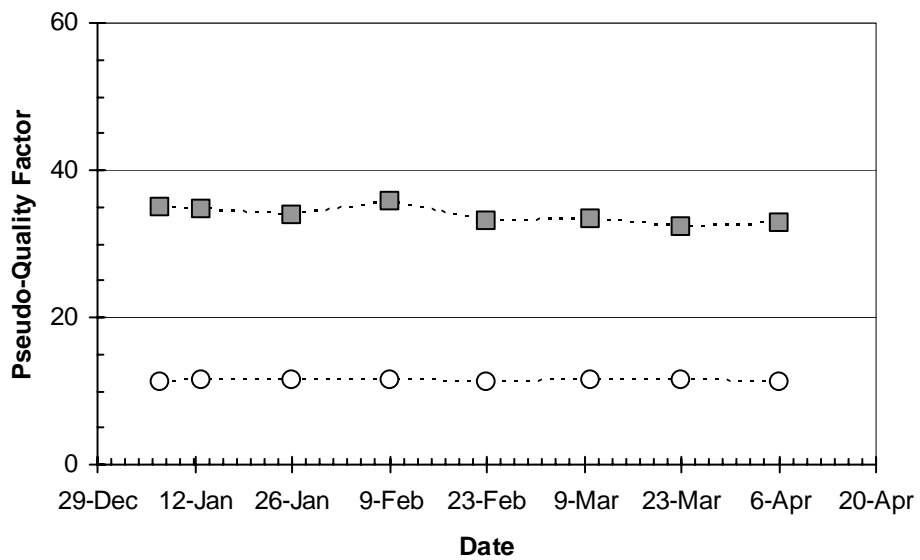


Figure J-13 Sensor B54 Interrogation History

Sensor B55



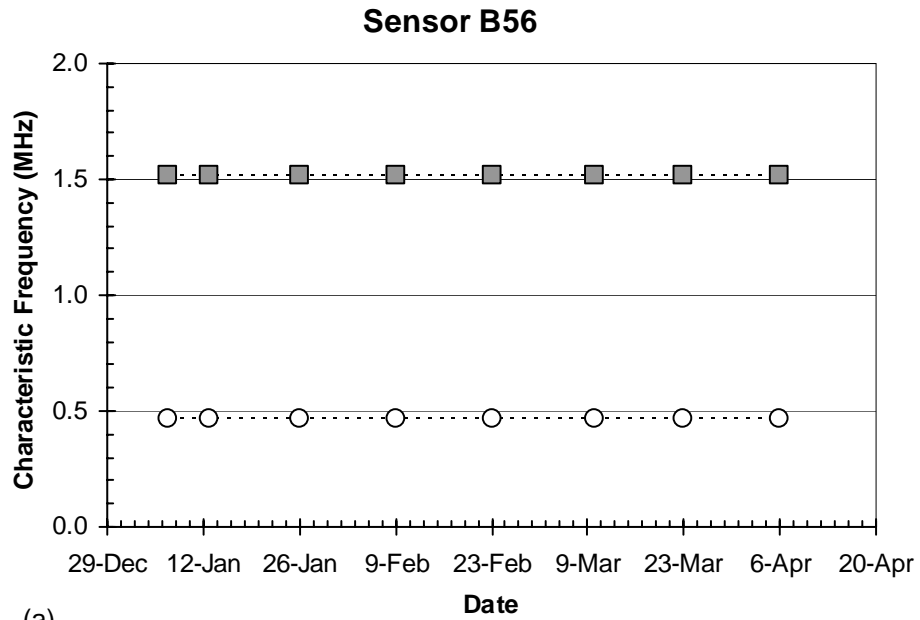
(a)



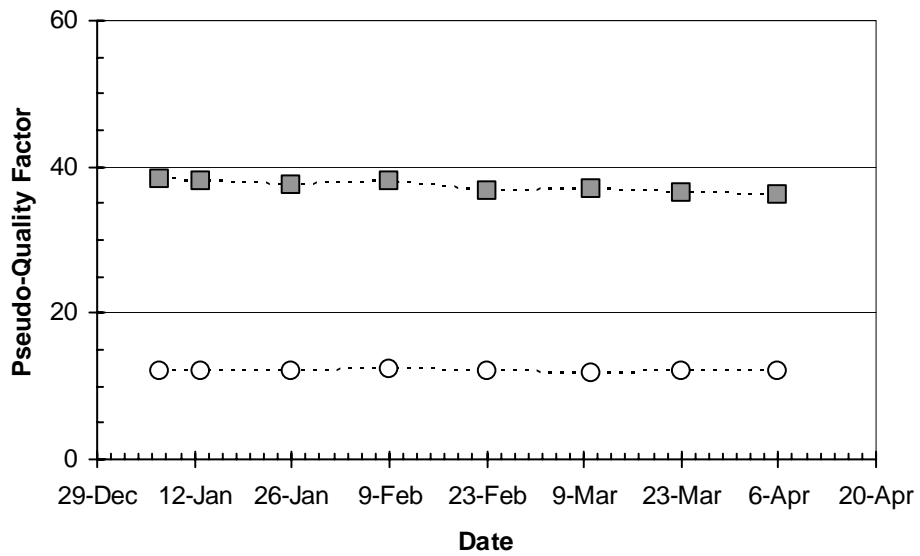
(b)



Figure J-14 Sensor B55 Interrogation History



(a)

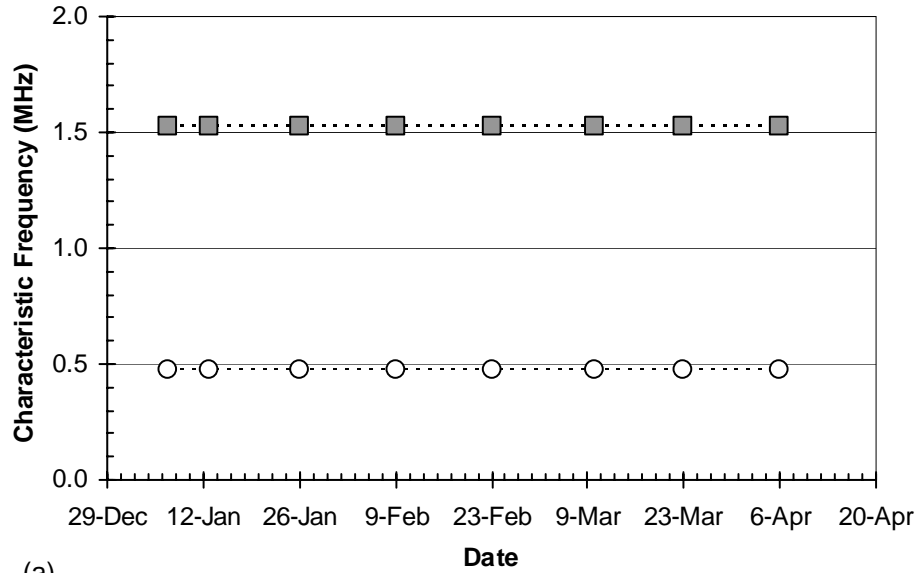


(b)

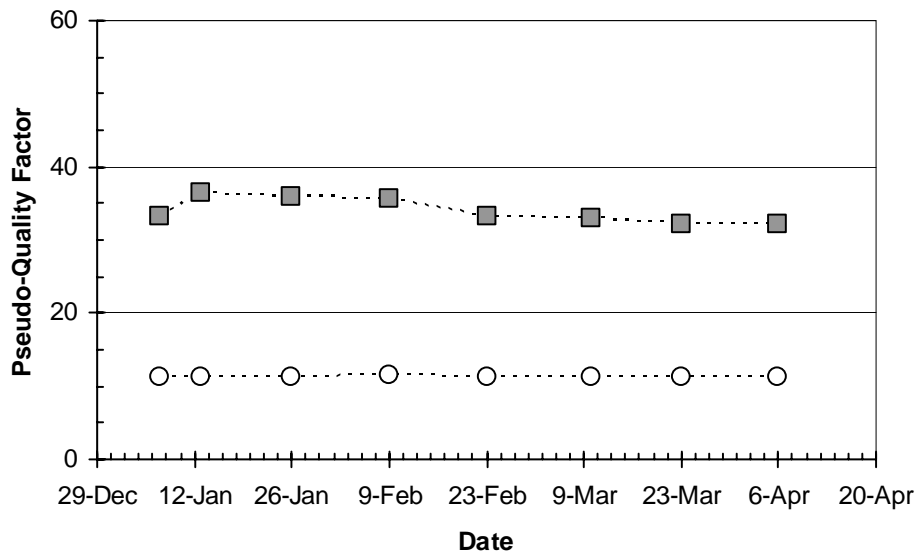


Figure J-15 Sensor B56 Interrogation History

Sensor B57



(a)

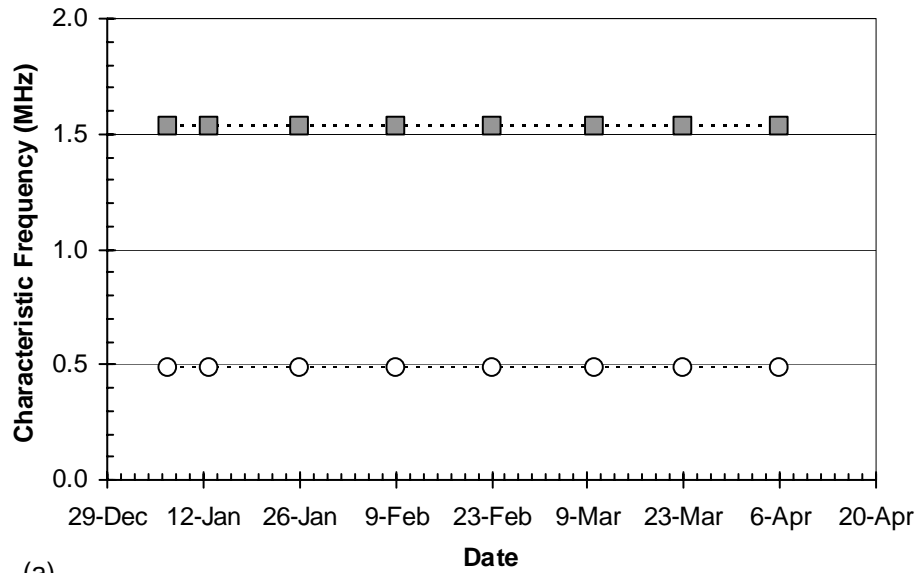


(b)

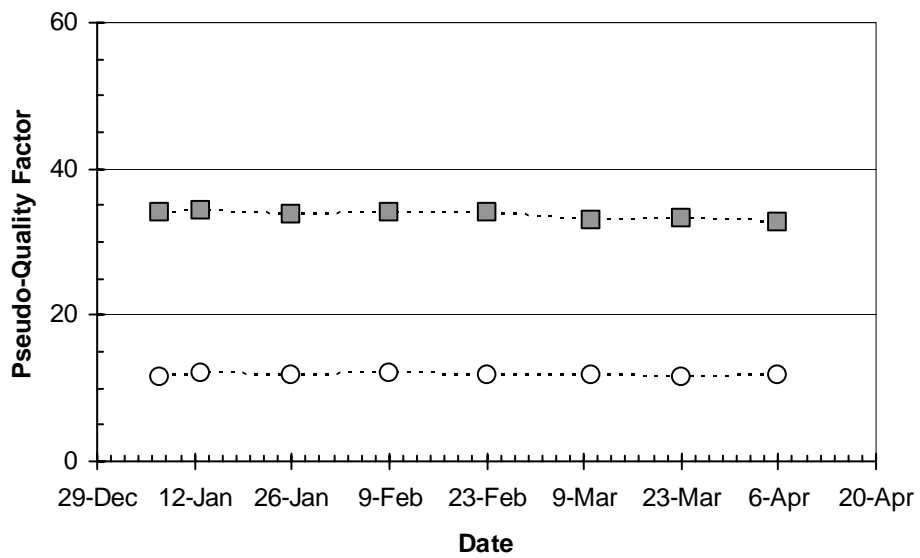


Figure J-16 Sensor B57 Interrogation History

Sensor B58



(a)

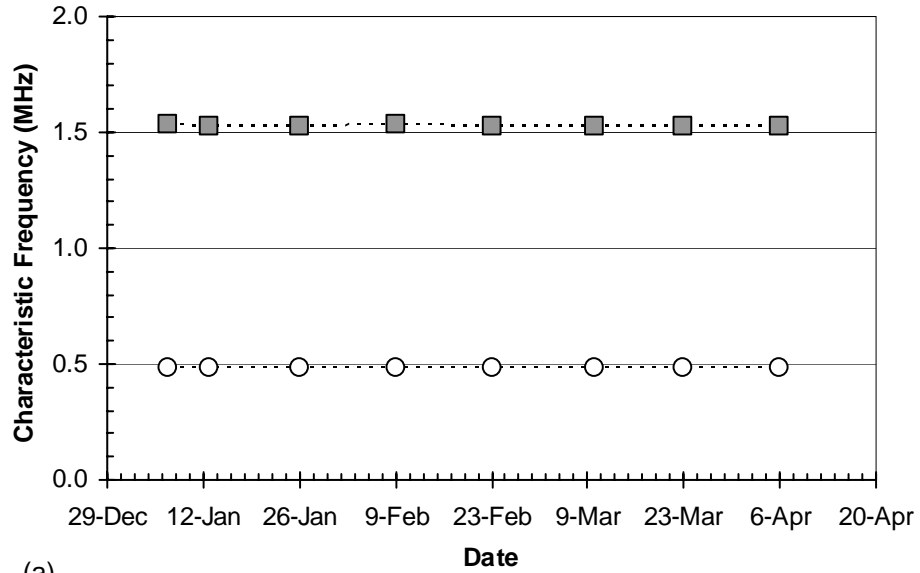


(b)

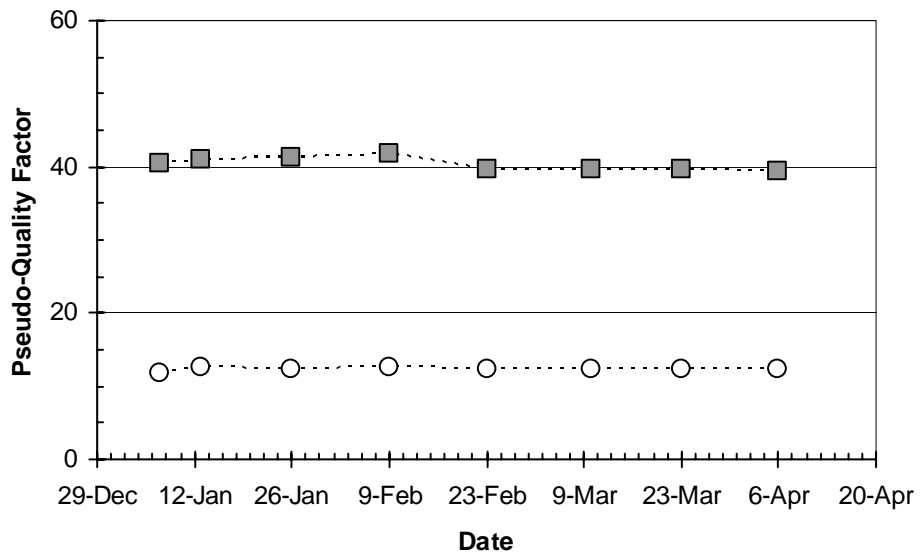


Figure J-17 Sensor B58 Interrogation History

Sensor B59



(a)



(b)



Figure J-18 Sensor B59 Interrogation History

Slab #2 - Point 1 (Sensor A51)

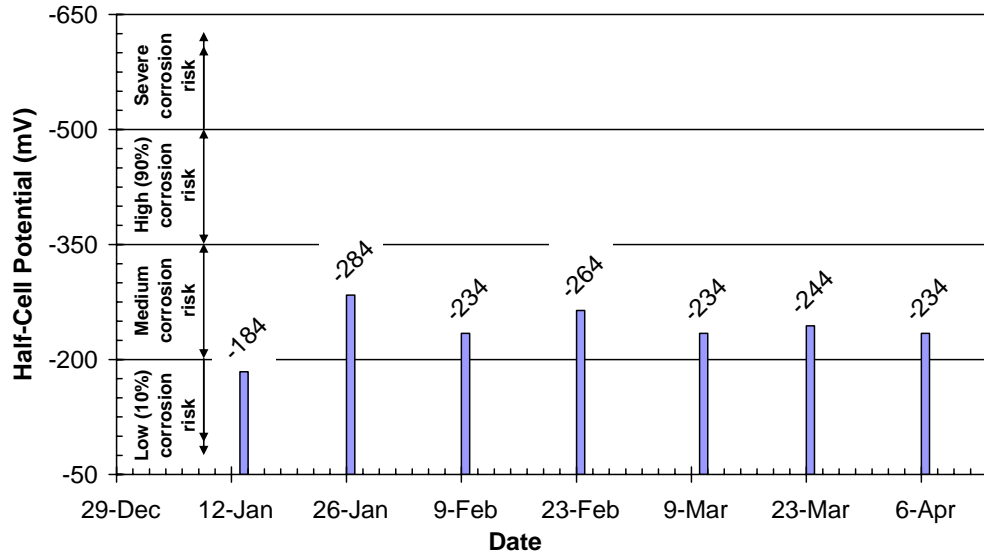


Figure J-19 Point 1 Corrosion Risk History

Slab #2 - Point 1 (Sensor A51)

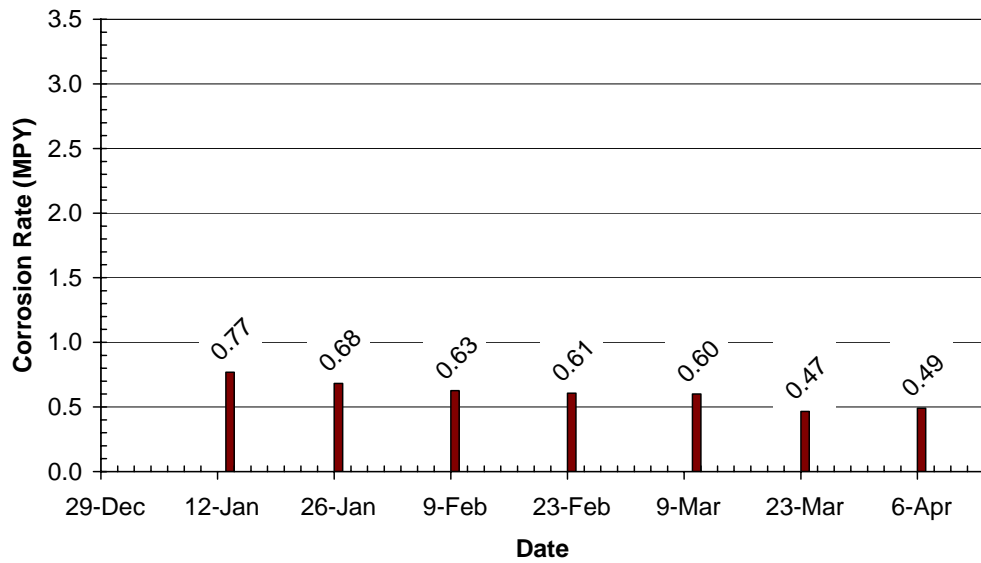


Figure J-20 Point 1 Corrosion Rate History

Slab #2 - Point 3 (Sensor B51)

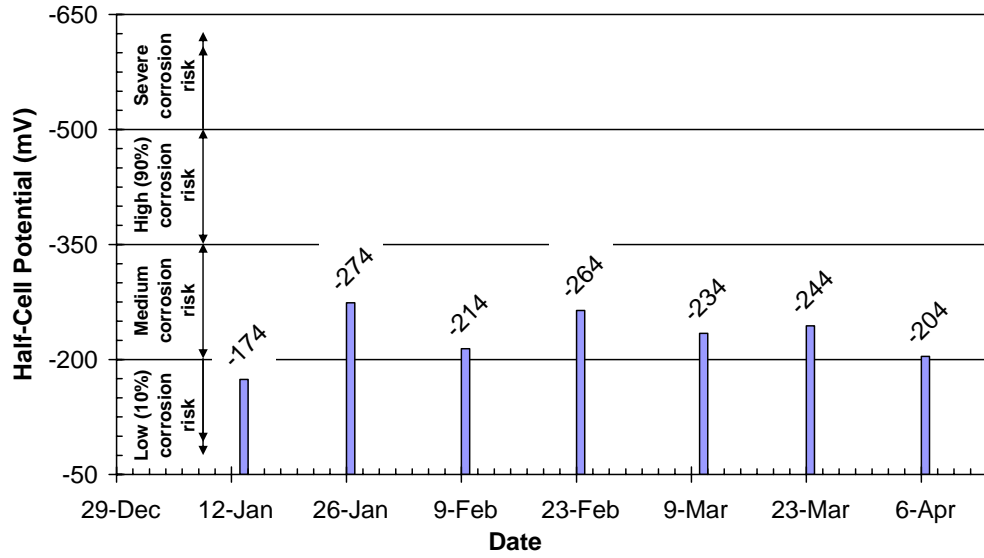


Figure J-21 Point 3 Corrosion Risk History

Slab #2 - Point 3 (Sensor B51)

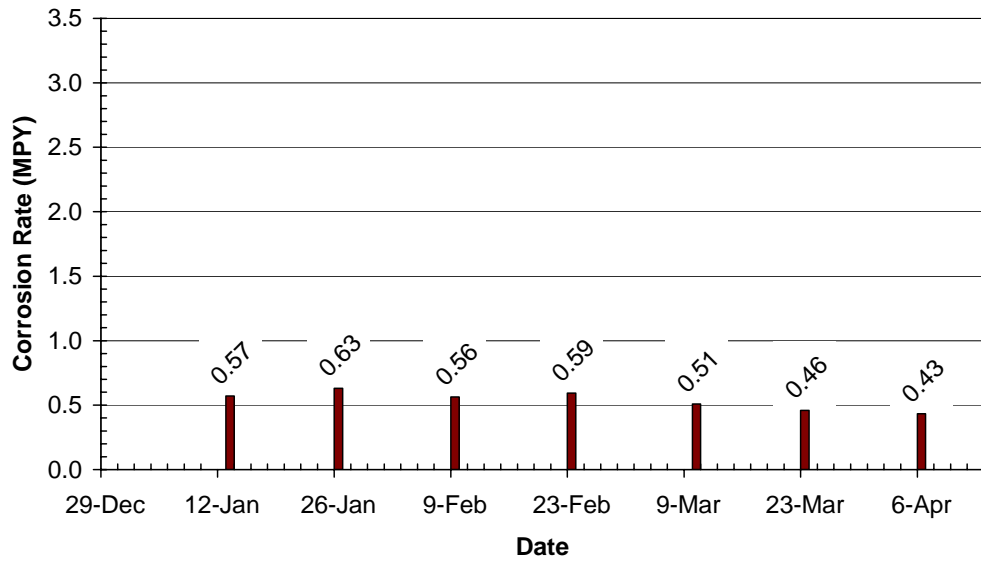


Figure J-22 Point 3 Corrosion Rate History

Slab #2 - Point 9 (Sensor A52)

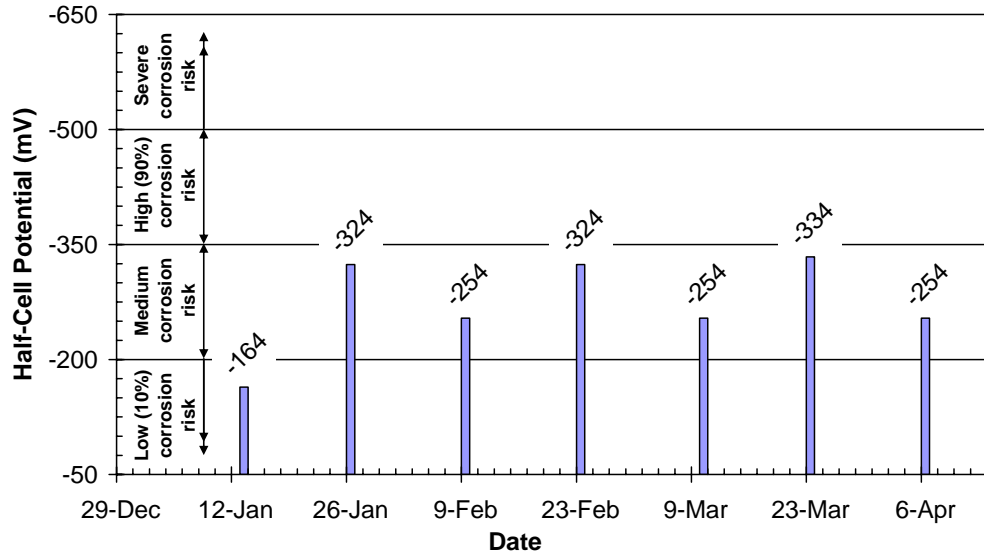


Figure J-23 Point 9 Corrosion Risk History

Slab #2 - Point 9 (Sensor A52)

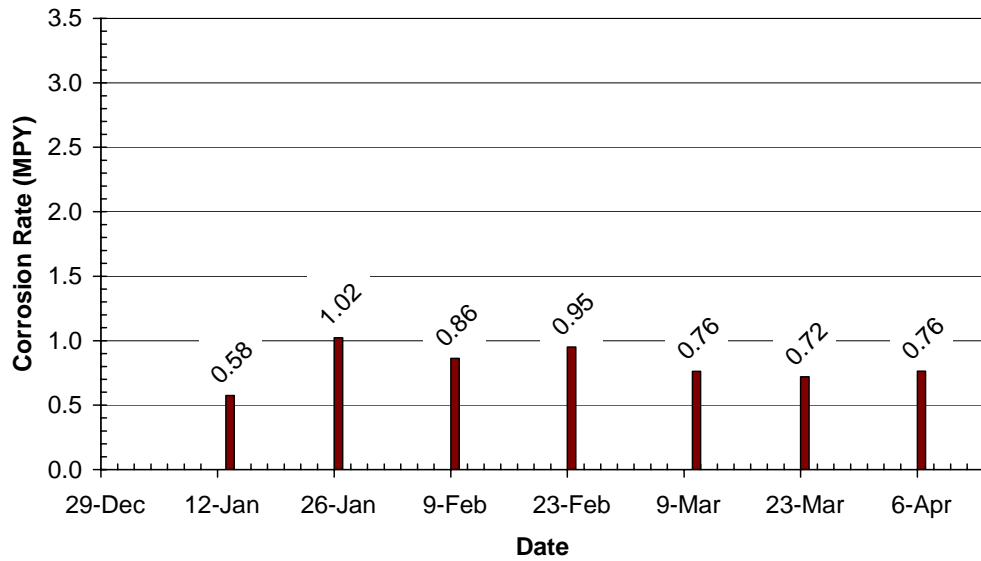


Figure J-24 Point 9 Corrosion Rate History

Slab #2 - Point 11 (Sensor B52)

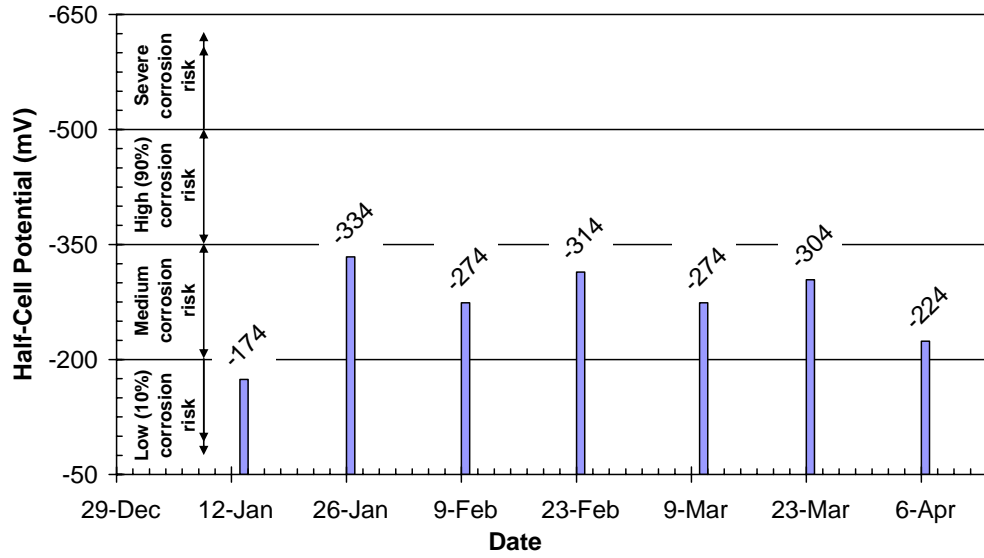


Figure J-25 Point 11 Corrosion Risk History

Slab #2 - Point 11 (Sensor B52)

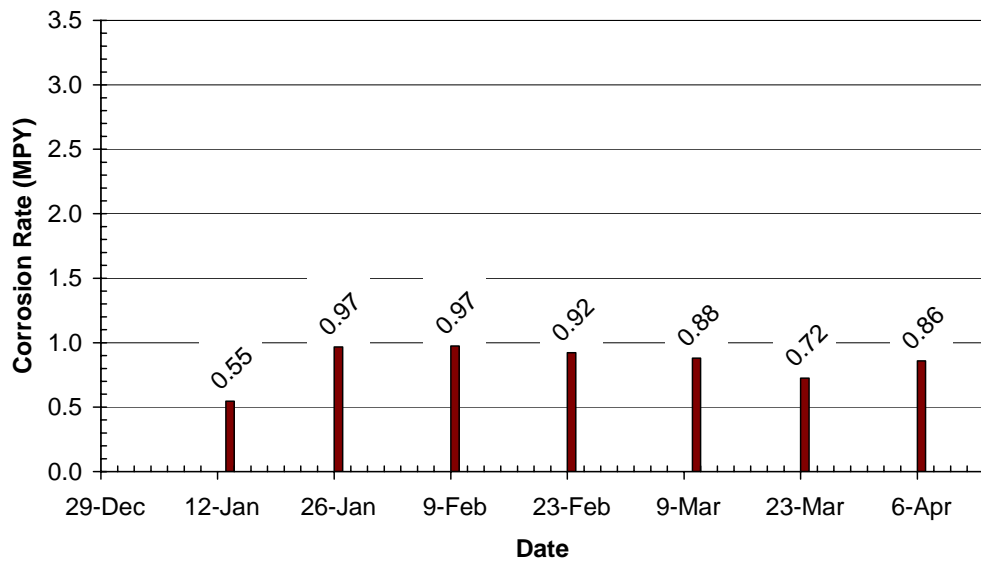


Figure J-26 Point 11 Corrosion Rate History

Slab #2 - Point 13 (Sensors A53 & A54)

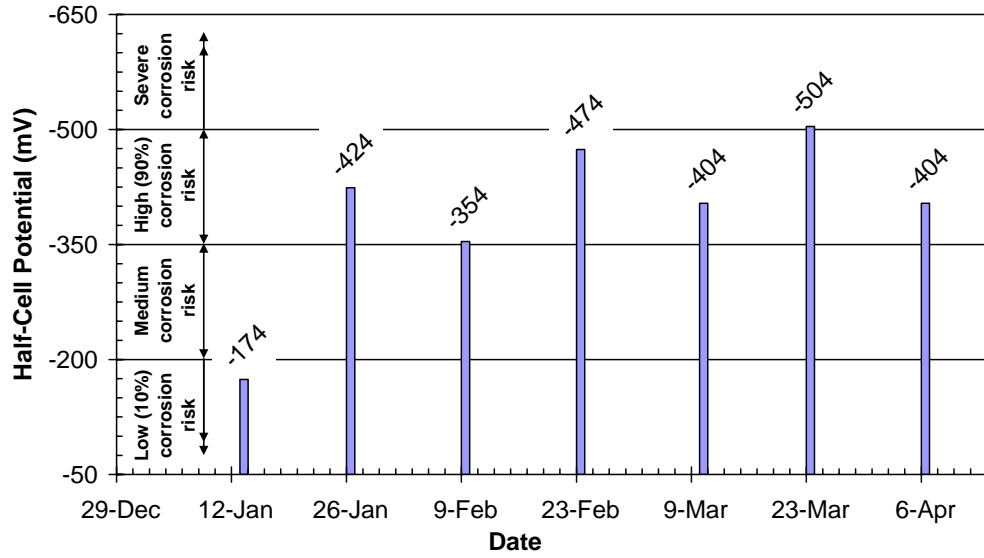


Figure J-27 Point 13 Corrosion Risk History

Slab #2 - Point 13 (Sensors A53 & A54)

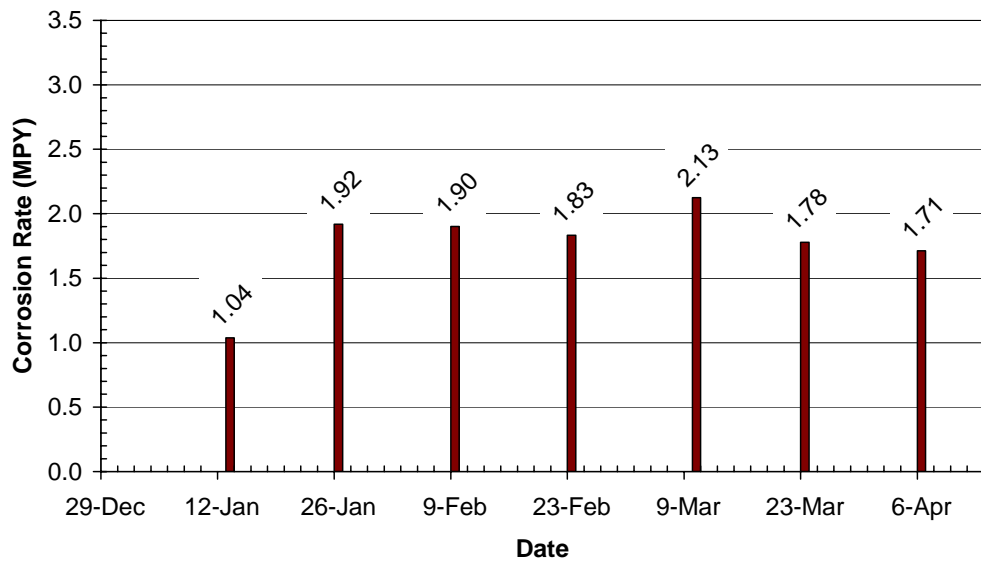


Figure J-28 Point 13 Corrosion Rate History

Slab #2 - Point 15 (Sensors B53 & B54)

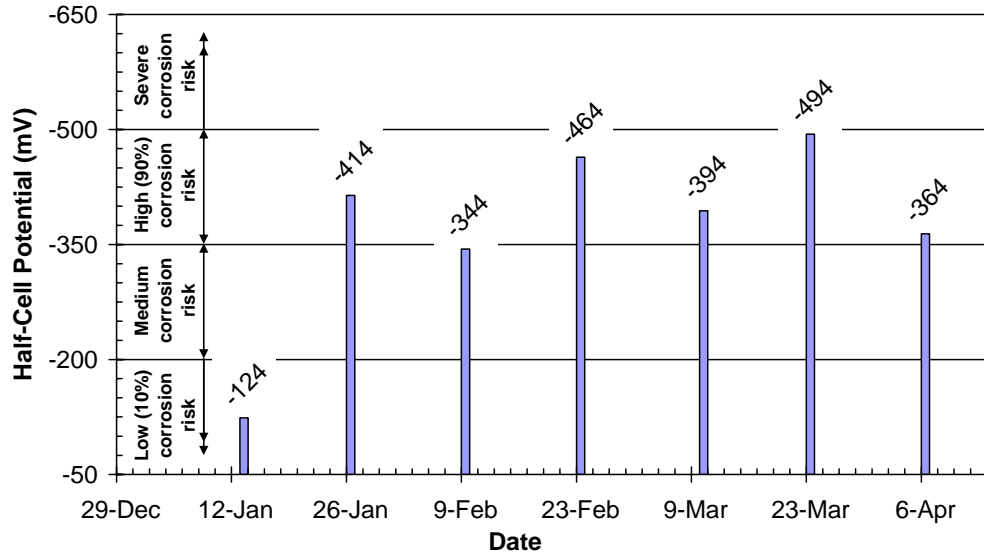


Figure J-29 Point 15 Corrosion Risk History

Slab #2 - Point 15 (Sensors B53 & B54)

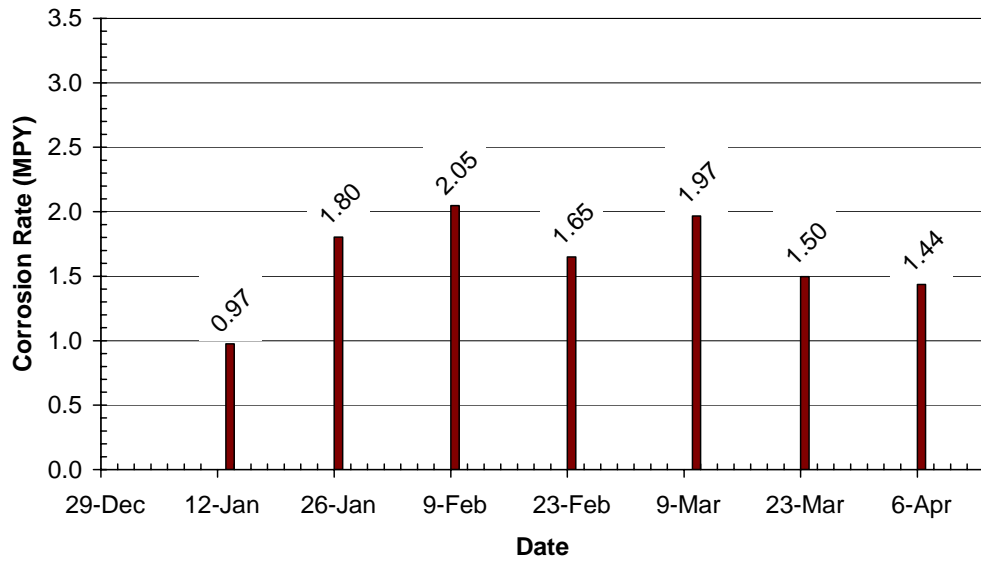


Figure J-30 Point 15 Corrosion Rate History

Slab #2 - Point 17 (Sensors A54 & A55)

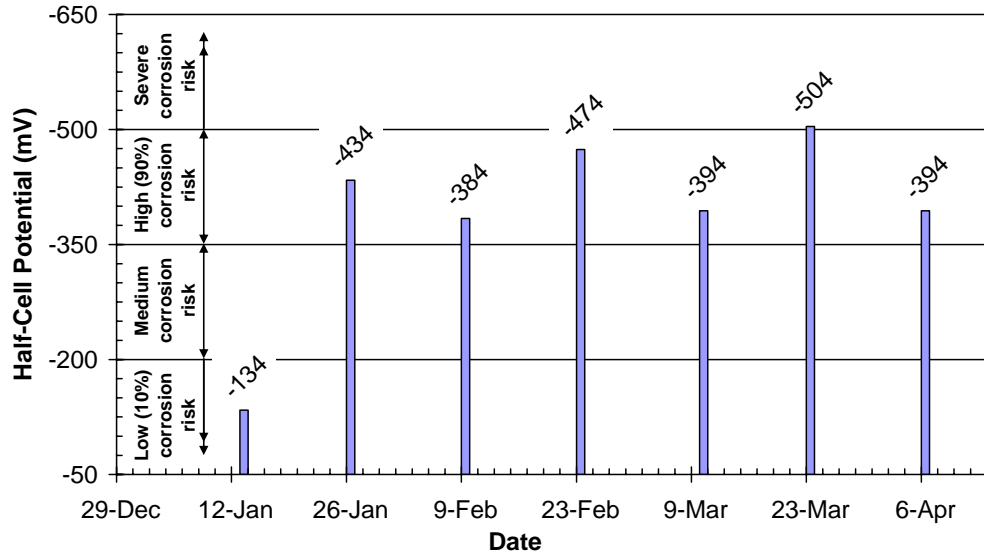


Figure J-31 Point 17 Corrosion Risk History

Slab #2 - Point 17 (Sensors A54 & A55)

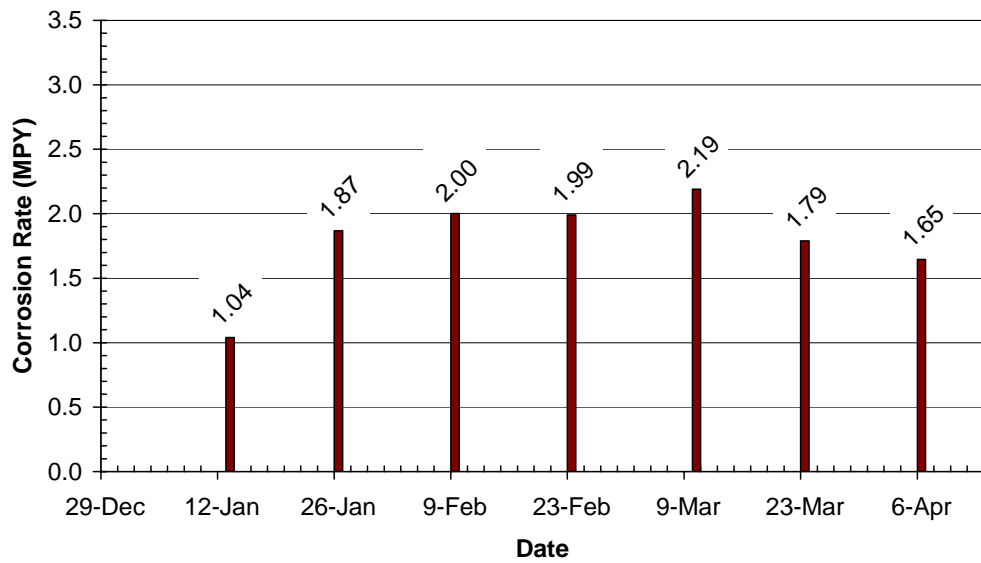


Figure J-32 Point 17 Corrosion Rate History

Slab #2 - Point 19 (Sensors B54 & B55)

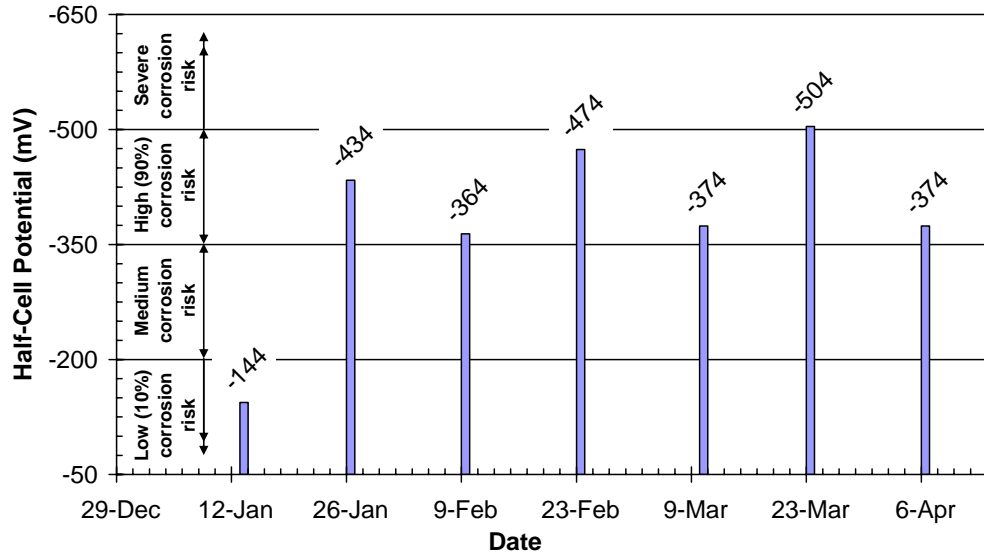


Figure J-33 Point 19 Corrosion Risk History

Slab #2 - Point 19 (Sensors B54 & B55)

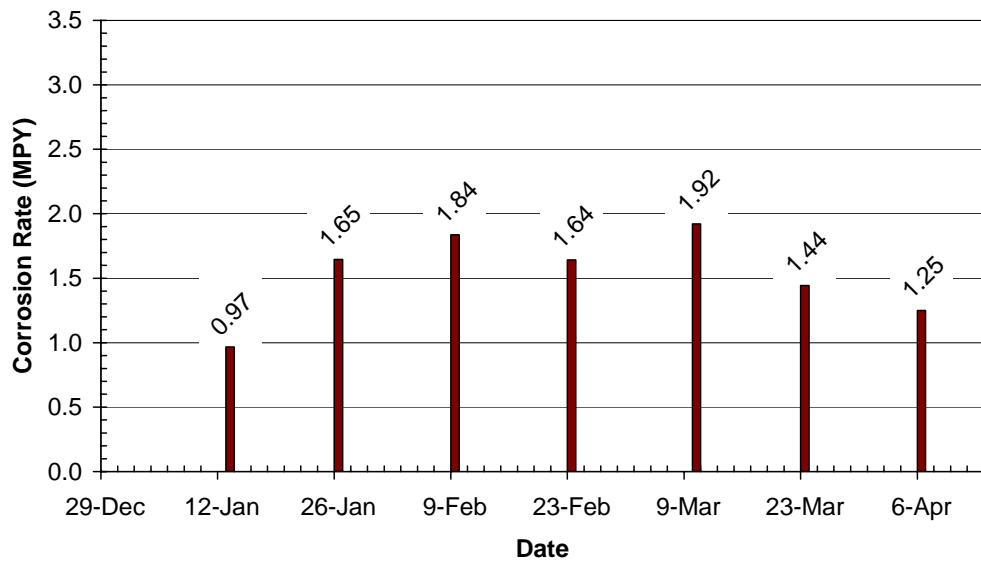


Figure J-34 Point 19 Corrosion Rate History

Slab #2 - Point 21 (Sensor A56)

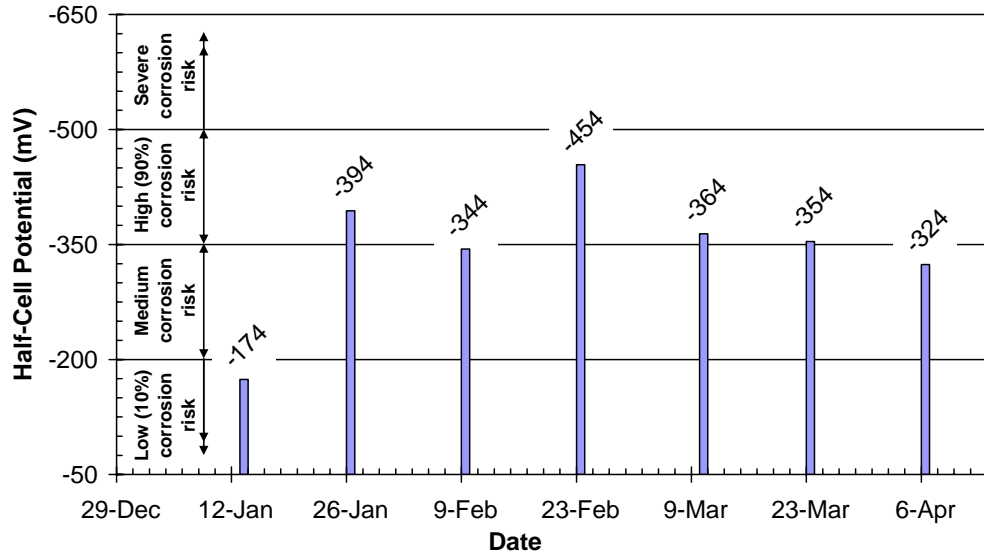


Figure J-35 Point 21 Corrosion Risk History

Slab #2 - Point 21 (Sensor A56)

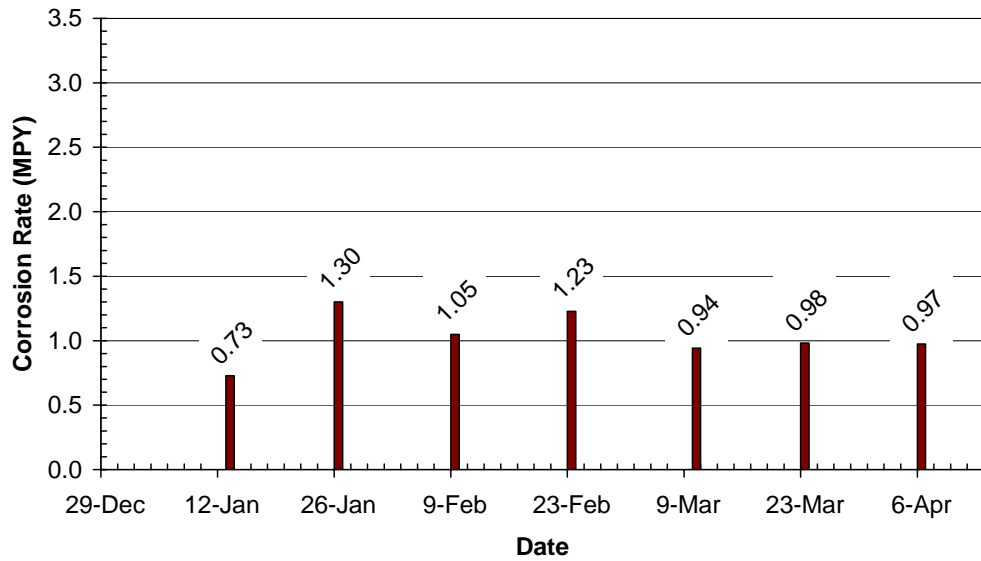


Figure J-36 Point 21 Corrosion Rate History

Slab #2 - Point 23 (Sensor B56)

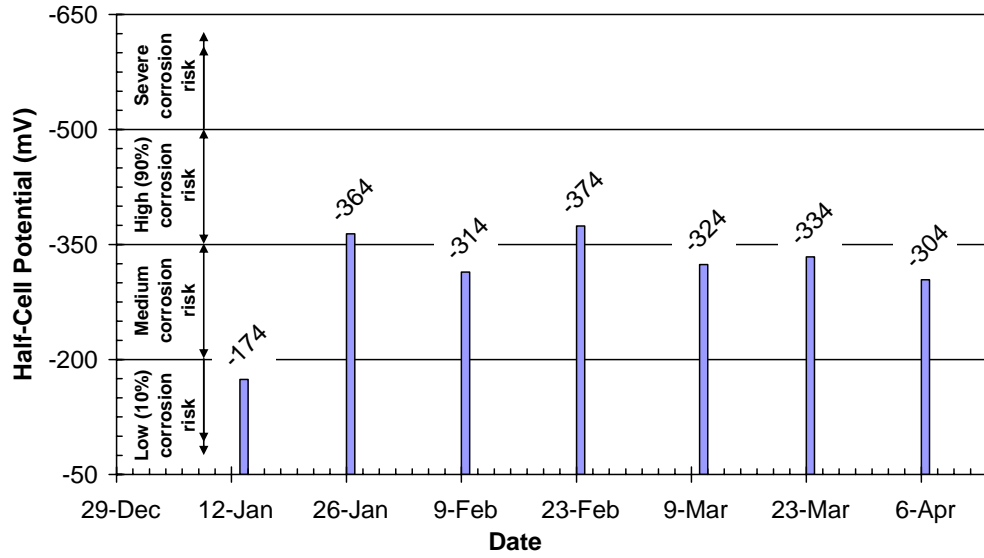


Figure J-37 Point 23 Corrosion Risk History

Slab #2 - Point 23 (Sensor B56)

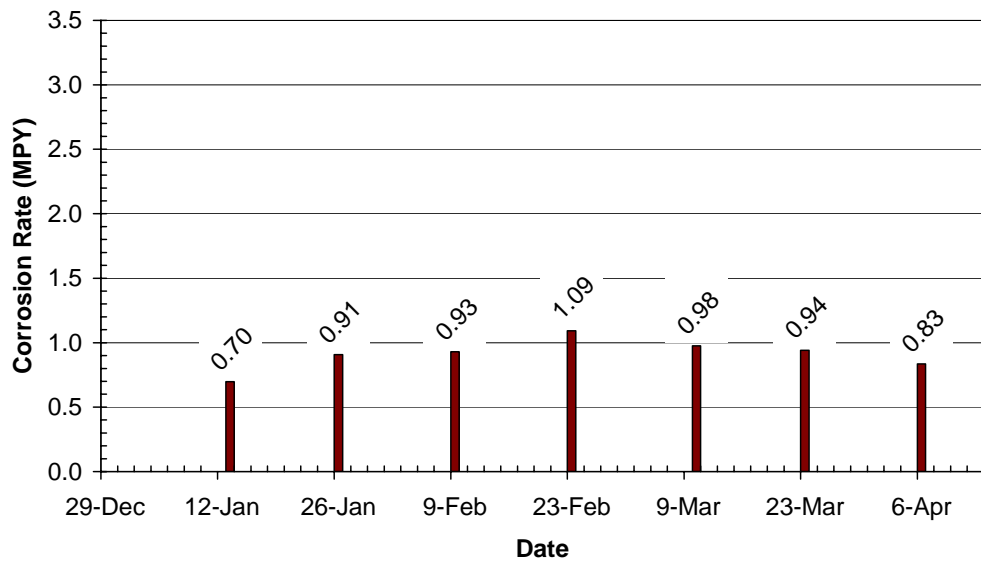


Figure J-38 Point 23 Corrosion Rate History

Slab #2 - Point 29 (Sensor A57)

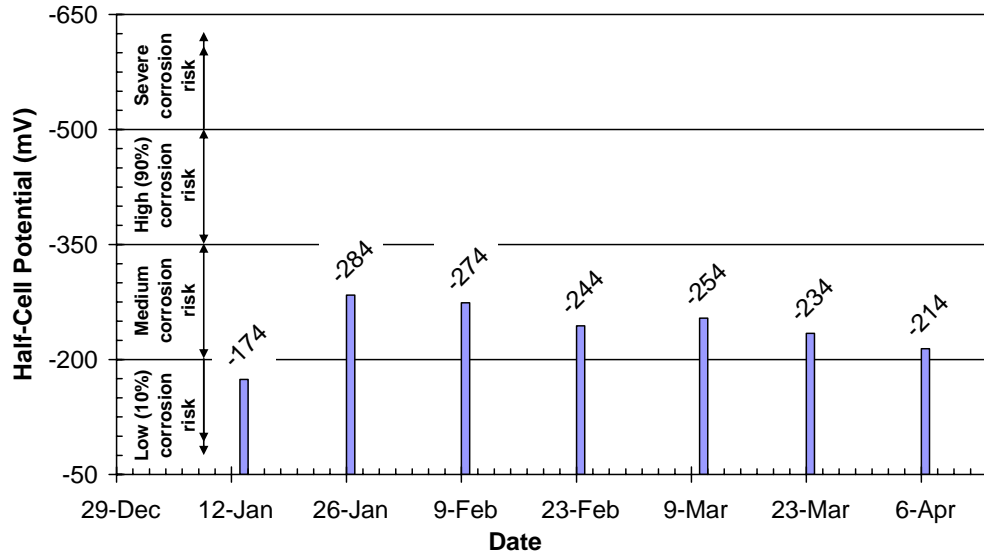


Figure J-39 Point 29 Corrosion Risk History

Slab #2 - Point 29 (Sensor A57)

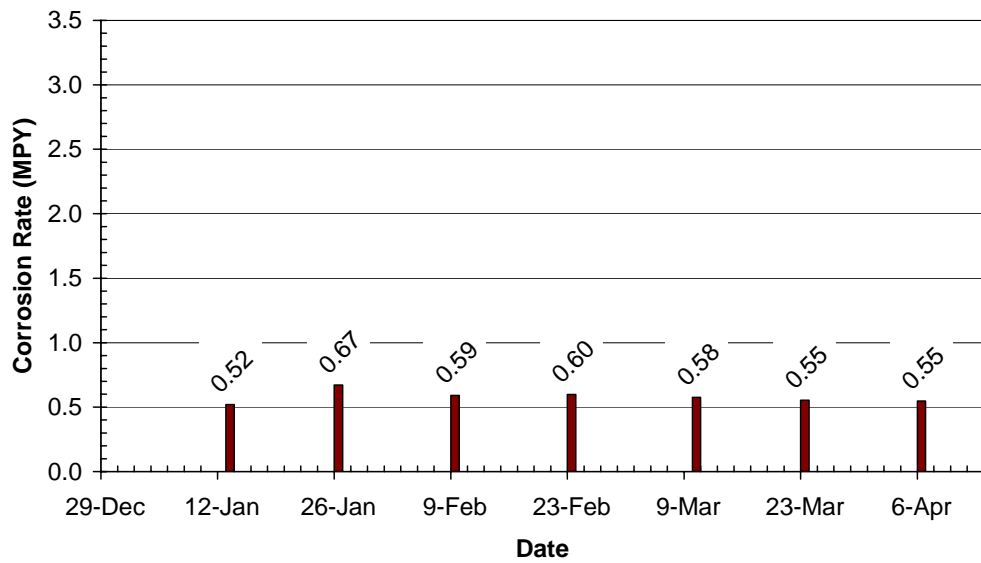


Figure J-40 Point 29 Corrosion Rate History

Slab #2 - Point 31 (Sensor B57)

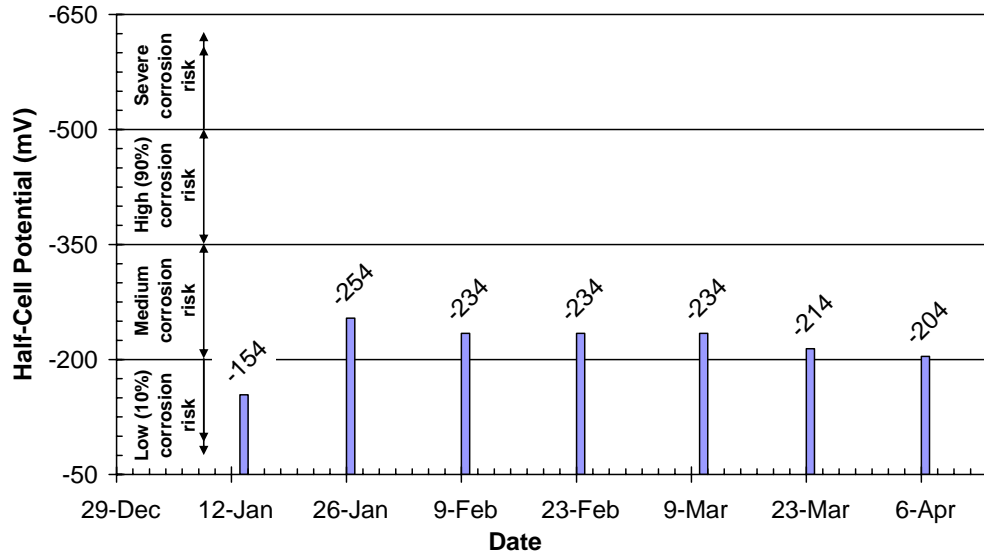


Figure J-41 Point 31 Corrosion Risk History

Slab #2 - Point 31 (Sensor B57)

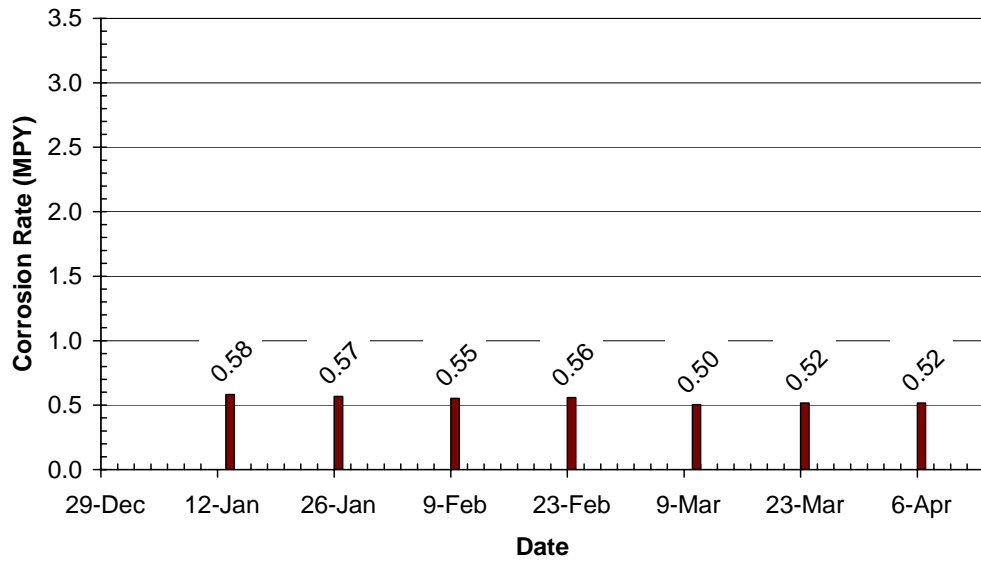


Figure J-42 Point 31 Corrosion Rate History

References

1. AASHTO TP 11-95 (2002). "Rapid Determination of Corrosion Rate of Uncoated Steel in Reinforced Concrete." American Association of State Highway and Transportation Officials, Washington, D.C.
2. ACI 222 (2001). "Protection of Metals in Concrete Against Corrosion (ACI222R-01)." Committee 222, American Concrete Institute, Farmington Hills, MI.
3. ACI 318 (2002). "Building Code and Commentary for Structural Concrete (ACI 318-02) and Commentary (ACI 318R-02)." Committee 318, American Concrete Institute, Farmington Hills, MI.
4. Andringa, Matthew M. (2005). Personal Communication.
5. Andringa, Matthew M. (2003). "Development of a passive wireless analog resistance sensor." M.S. Thesis, Dept. of Electrical and Computer Engineering, University of Texas at Austin.
6. ASTM C 876 (1999). "Standard Test Method for Half-Cell Potentials of Uncoated Reinforcing Steel in Concrete." American Society for Testing and Materials, West Conshohocken, PA.
7. ASTM G 109 (1992). "Standard Test Method for Determining the Effects of Chemical Admixtures on the Corrosion of Embedded Steel Reinforcement in Concrete Exposed to Chloride Environments." American Society for Testing and Materials, West Conshohocken, PA.
8. Broomfield, John P. (1997). "Corrosion of Steel in Concrete: Understanding, investigation and repair." E & FN Spon, 2-6 Boundary Row, London SE1 8HN, UK.
9. Grizzle, Kristi M. (2003). "Development of a Wireless Sensor Used to Monitor Corrosion in Reinforced Concrete Structures." M.S. Thesis, Dept. of Civil Engineering, University of Texas at Austin.
10. KCC Inc. (1990). "3LP Package: Test Procedures, Data Analysis Procedures and General Information." Kenneth C. Clear, Inc., Sterling, VA.

11. Lee, Youbok (1998). "microID™ 125 kHz RFID System Design Guide." Microchip Technology, Inc., Mountain View, CA.
12. Nainani, Prem R. (2004). "Optimization of Passive Wireless Concrete Corrosion Sensors Using the Genetic Algorithm." M.S. Thesis, Dept. of Electrical and Computer Engineering, University of Texas at Austin.
13. Novak, Lisa J. (2002). "Development of a Wireless Sensor to Detect Cracks in Welded Steel Connections." M.S. Thesis, Dept. of Civil Engineering, University of Texas at Austin.
14. Salas, Ruben M. (2003). "Accelerated Corrosion Testing, Evaluation and Durability Design of Bonded Post-Tensioned Concrete Tendons." Ph.D. Dissertation, Dept. of Civil Engineering, University of Texas at Austin.
15. Simonen, Jarkko T. (2004). "Development of an Embedded Wireless Corrosion Sensor for Monitoring Corrosion in Reinforced Concrete Members." M.S. Thesis, Dept. of Civil Engineering, University of Texas at Austin.
16. Transtronics, Inc. (2005). "How to Read Capacitor Codes." <http://xtronics.com/kits/ccode.htm>.
17. Endl, Robert (2005). "Introduction to Capacitors." *CapSite 2005 Release 3.6*. <http://my.execpc.com/~endlr/>.

VITA

Nathan Paul Dickerson was born on November 15, 1977 in Albion, Nebraska to James E. and Julianne K. Dickerson. Nathan was raised in Elgin, Nebraska and graduated from Elgin Public High School in May of 1996. He attended the University of Nebraska-Lincoln in Lincoln, Nebraska from August of 1996 until graduating with a Bachelor of Science in Civil Engineering degree in May of 2000. After graduation, Nathan worked for HDR Engineering, Inc. in Omaha, Nebraska as a project engineer in the railroad structures section for three years. In August of 2003, Nathan moved to Austin, Texas to attend graduate school in structural engineering at the University of Texas at Austin. There, he worked as a graduate research assistant at Ferguson Structural Engineering Laboratory and conducted research work under the supervision of Dr. Sharon L. Wood. Nathan graduated in August of 2005 with a Master of Science in Civil Engineering degree. After finishing his work at UT, he moved back to Omaha, Nebraska, where he accepted a position with his former employer, HDR Engineering, Inc.

Publications

Nathan P. Dickerson, Jarkko T. Simonen, Matthew M. Andringa, Sharon L. Wood, and Dean P. Neikirk, "Wireless low-cost corrosion sensors for reinforced concrete structures," Proceedings of SPIE, *Smart Structures and Materials 2005: Sensors and Smart Structures Technologies for Civil, Mechanical, and Aerospace Systems*, Vol. 5765, Paper 52, 2005.

Permanent Address: 2345 South 80th Avenue
Omaha, Nebraska 68124
United States of America

This thesis was typed by the author.